PREDICTING THE EFFECT OF DRUG-GENE AND DRUG-DRUG-GENE INTERACTIONS ON THE PHARMACOKINETICS OF CYP2D6 SUBSTRATES

LEVERAGING THE CYP2D6 ACTIVITY SCORE SYSTEM IN PHYSIOLOGICALLY BASED PHARMACOKINETIC MODELING

DISSERTATION

Zur Erlangung des Grades des Doktors der Naturwissenschaften
der Naturwissenschaftlich-Technischen Fakultät
der Universität des Saarlandes

von

Simeon Matthias Rüdesheim

Apotheker, M.Sc.

Saarbrücken

2023

Die vorliegende Arbeit wurde von Januar 2020 bis August 2023 unter Anleitung von Herrn Professor Dr. Thorsten Lehr in der Fachrichtung Klinische Pharmazie der Naturwissenschaftlich-Technischen Fakultät der Universität des Saarlandes angefertigt.

Tag des Kolloquiums:	18. Januar 2024
Dekan:	Prof. Dr. Ludger Santen
Berichterstatter:	Prof. Dr. Thorsten Lehr Prof. Dr. Markus R. Meyer Prof. Dr. Matthias Schwab
Akad. Mitglied:	Dr. Agnes-Valencia Weiß
Vorsitz:	Prof. Dr. Andriy Luzhetskyy

All models are wrong; some models are useful.

– George E. P. Box

The digitization of human beings will make
a parody out of 'doctor knows best'.

– Eric Topol

PUBLICATIONS & CONTRIBUTIONS

PUBLICATIONS

This thesis includes the following publications [1–5]:

1. Rüdesheim, S.; Wojtyniak, J.-G.; Selzer, D.; Hanke, N.; Mahfoud, F.; Schwab, M.; Lehr, T. Physiologically Based Pharmacokinetic Modeling of Metoprolol Enantiomers and α-Hydroxymetoprolol to Describe CYP2D6 Drug-Gene Interactions. *Pharmaceutics* **2020**, *12*, 1200, DOI: 10.3390/pharmaceutics12121200.
2. Rüdesheim, S.; Selzer, D.; Fuhr, U.; Schwab, M.; Lehr, T. Physiologically-based pharmacokinetic modeling of dextromethorphan to investigate interindividual variability within CYP2D6 activity score groups. *CPT: pharmacometrics & systems pharmacology* **2022**, *11*, 494–511, DOI: 10.1002/psp4.12776.
3. Rüdesheim, S.; Selzer, D.; Mürdter, T.; Igel, S.; Kerb, R.; Schwab, M.; Lehr, T. Physiologically Based Pharmacokinetic Modeling to Describe the CYP2D6 Activity Score-Dependent Metabolism of Paroxetine, Atomoxetine and Risperidone. *Pharmaceutics* **2022**, *2022*, 1734, DOI: 10.3390/pharmaceutics14081734.
4. Kovar, C.; Kovar, L.; Rüdesheim, S.; Selzer, D.; Ganchev, B.; Kröner, P.; Igel, S.; Kerb, R.; Schaeffeler, E.; Mürdter, T. E.; Schwab, M.; Lehr, T. Prediction of Drug–Drug–Gene Interaction Scenarios of (*E*)-Clomiphene and Its Metabolites Using Physiologically Based Pharmacokinetic Modeling. *Pharmaceutics* **2022**, *14*, 2604, DOI: 10.3390/pharmaceutics14122604.
5. Feick, D.; Rüdesheim, S.; Marok, F. Z.; Selzer, D.; Loer, H. L. H.; Teutonico, D.; Frechen, S.; van der Lee, M.; Moes, D. J. A. R.; Swen, J. J.; Schwab, M.; Lehr, T. Physiologically-based pharmacokinetic modeling of quinidine to establish a CYP3A4, P-gp, and CYP2D6 drug-drug-gene interaction network. *CPT: pharmacometrics & systems pharmacology* **2023**, 1–14, DOI: 10.1002/psp4.12981.

CONTRIBUTION REPORT

The author of this thesis has contributed to the listed publications according to the contributor roles taxonomy (CRediT) [6].

1. Conceptualization, Investigation, Writing–Original Draft, Writing–Review & Editing
2. Conceptualization, Investigation, Visualization, Writing–Original Draft, Writing–Review & Editing
3. Conceptualization, Investigation, Visualization, Writing–Original Draft, Writing–Review & Editing
4. Formal Analysis, Methodology, Writing–Review & Editing
5. Conceptualization, Investigation, Visualization, Writing–Original Draft, Writing–Review & Editing

ABSTRACT

Personalized medicine and precision dosing aim to tailor drug therapy to individual needs, improving patient outcomes and reducing healthcare costs. A key component of precision dosing is pharmacogenomics (PGx) as variants in pharmacogenes are thought to be responsible for a significant fraction of variability in drug response. PGx guidelines provide clinicians with recommendations, integrating PGx information into clinical decision making processes. These guidelines are developed based on knowledge generated in dedicated clinical PGx trials, typically conducted in small, homogeneous patient populations. However, adverse drug reactions (ADRs) often occur as a result of complex drug-drug-gene interactions (DDGIs), observed in patients taking multiple drugs simultaneously.

Here, physiologically based pharmacokinetic (PBPK) modeling shows great potential in extending the findings from DDGI trials to real-world patient populations. In this thesis, new whole-body PBPK models for substrates and inhibitors of the polymorphically expressed CYP subfamily 2D6 (CYP2D6) enzyme are presented. These models integrate current knowledge on CYP2D6 drug-gene interactions (DGIs) by incorporating the activity score-dependent metabolism of CYP2D6 substrates. This thesis showcases the various applications of DGI PBPK models to facilitate a more personalized drug therapy.

ZUSAMMENFASSUNG

Die *Personalisierte Medizin* und *Präzisionsdosierung* verfolgen das Ziel, die Arzneimitteltherapie an die Bedürfnisse des Patienten anzupassen, um so den Therapieerfolg zu sichern. Da Varianten in Pharmakogenen für große interindividuelle Unterschiede in der Pharmakologie von Arzneistoffen verantwortlich sind, stellt die Pharmakogenomik (PGx) ein Schlüsselelement der Präzisionsdosierung dar. PGx Leitlinien bieten Handlungsempfehlungen auf Grundlage klinischer Studien, um PGx Informationen in Entscheidungsprozesse einzubeziehen. Unerwünschte Arzneimittelwirkungen treten häufig als Folge komplexer Arzneimittel-Arzneimittel-Gen Interaktionen (DDGIs) auf, die bei Patienten beobachtet werden, welche oft mehrere Arzneimittel gleichzeitig einnehmen – Szenarien, die aus ethischen Gründen nicht in klinischen Studien abgebildet werden können.

Hier bedarf es innovativer Ansätze, wie der Verwendung mathematischer Modelle, um den Effekt von DDGIs vorherzusagen. In dieser Arbeit werden physiologie-basierte pharmakokinetische (PBPK) Modelle für Substrate und Inhibitoren des CYP2D6 Enzyms vorgestellt. Die Modelle wurden auf der Grundlage des aktuellen Wissenstands über CYP2D6 Arzneimittel-Gen Interaktionen (DGIs) entwickelt, indem der Metabolismus in Abhängigkeit vom *activity score* modelliert wurde. Außerdem werden mögliche Anwendungen von DGI Modellen präsentiert und die Notwendigkeit von PBPK Modellen zur Verbesserung der personalisierten Arzneimitteltherapie verdeutlicht.

GRAPHICAL ABSTRACT

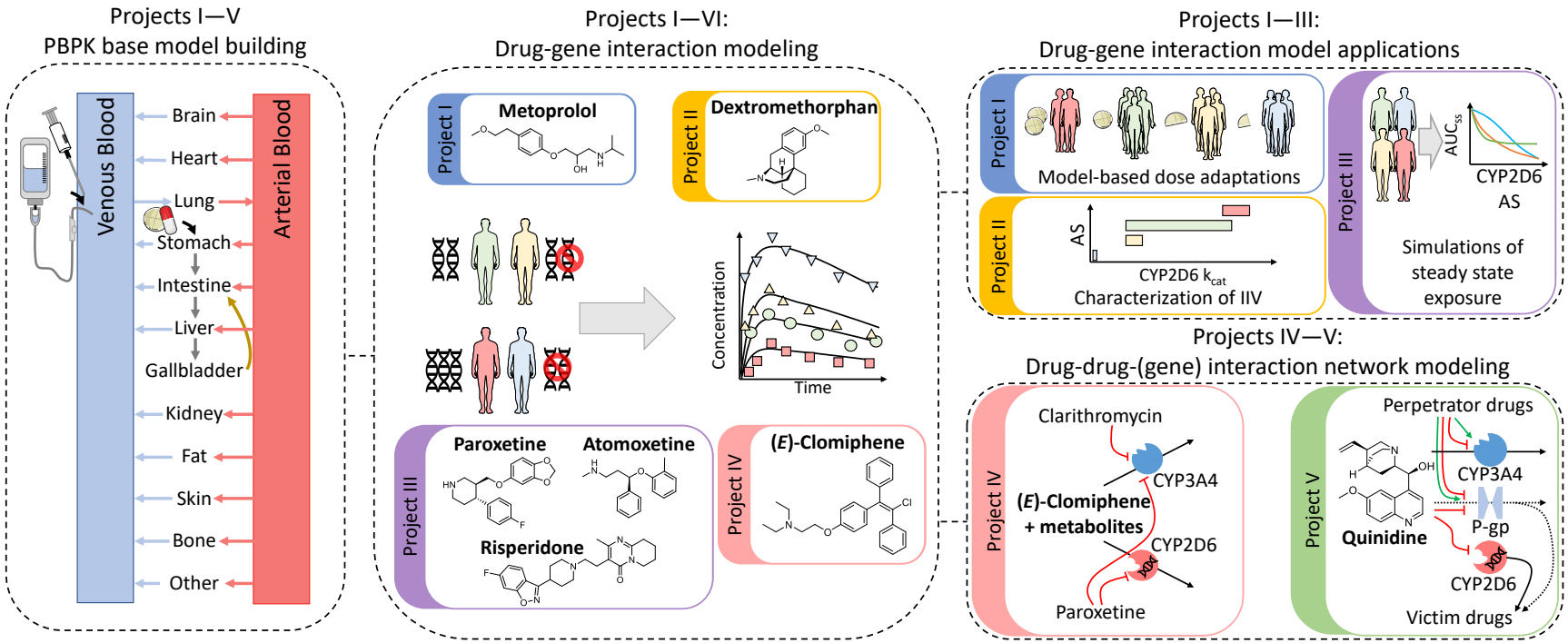

Figure 1: **Graphical Abstract.** Illustrations of tablets, capsules and people were taken from Servier [7], licensed under CC BY 3.0 (https://creativecommons.org/licenses/by/3.0/). AUC_{ss}, area under the plasma concentration-time curve (AUC) during steady state; AS, activity score; IIV, interindividual variability; CYP2D6, CYP subfamily 2D6; CYP3A4, CYP subfamily 3A4; k_{cat}, catalytic rate constant; P-gp, P-glycoprotein.

CONTENTS

ACRONYMS

ADME	Absorption, distribution, metabolism and excretion
ADHD	Attention deficit hyperactivity disorder
ADR	Adverse drug reaction
ADRB1	Adrenoceptor β_1
ADRB2	Adrenoceptor β_2
AUC	Area under the plasma concentration-time curve
AUC_{0-24h}	AUC from 0 to 24 hours
AUC_{last}	AUC from the time of the first concentration measurement to the time of the last concentration measurement
AUC_{ss}	AUC during steady state
AS	Activity score
BSV	Between-subject variability
CAR	Constitutive androstane receptor
CDSS	Clinical decision support systems
CPIC	Clinical Pharmacogenetics Implementation Consortium
CKD	Chronic kidney disease
C_{max}	Maximum plasma concentration
CNV	Copy number variation
COMT	Catechol-O-methyltransferase
CRediT	Contributor roles taxonomy
CYP	Cytochrome P450
CYP1A2	CYP subfamily 1A2
CYP2B6	CYP subfamily 2B6
CYP2C19	CYP subfamily 2C19
CYP2C9	CYP subfamily 2C9
CYP2D6	CYP subfamily 2D6
CYP2E1	CYP subfamily 2E1
CYP3A4	CYP subfamily 3A4
CYP3A5	CYP subfamily 3A5
DDI	Drug-drug interaction
DDGI	Drug-drug-gene interaction
DDGDI	Drug-drug-gene-disease interaction

DGI	Drug-gene interaction
DPYD	Dihydropyrimidine dehydrogenase
DPWG	Dutch Pharmacogenetics Working Group
EHR	Electronic health record
EMA	European Medicines Agency
FSH	Follicle-stimulating hormone
indels	Insertions or deletions
IIV	Interindividual variability
IPV	Interpatient variability
iv	Intravenous
IVSF	In vitro scaling factor
FDA	US Food and Drug Administration
GMFE	Geometric mean fold error
GnRH	Gonadotropin-releasing hormone
GNB3	Guanine nucleotide-binding protein subunit β_3
GWAS	Genome-wide association studies
HCSC	Health Canada (Santé Canada)
k_{cat}	Catalytic rate constant
$k_{cat,\ rel}$	Catalytic rate constant relative to activity score 2
KLF9	Krüppel-like factor 9
K_M	Michaelis-Menten constant
LH	Luteinizing hormone
md	Multiple dose
MDMA	Methylendioxymethamphetamine
MID3	Model-informed drug discovery and development
MIPD	Model-informed precision dosing
mRNA	Messenger ribonucleic acid
MRD	Mean relative deviation
NDA	New drug application
NLME	Nonlinear mixed effects
ODE	Ordinary differential equation
OLS	Ordinary least squares
PBPK	Physiologically based pharmacokinetic
PCOS	Polycystic ovary syndrome
PD	Pharmacodynamics
PDUFA	Prescription Drug User Fee Act Reauthorization

P-gp	P-glycoprotein
PGx	Pharmacogenomics
PGRN	Pharmacogenetics Research Network
PharmGKB	Pharmacogenomics Knowledge Base (pharmgkb.org)
PK	Pharmacokinetics
PMDA	Pharmaceuticals and Medical Device Agency
PopPK	Population pharmacokinetic
PXR	Pregnane X receptor
QSAR	Quantity structure-activity relationship
RUV	Residual unexplained variability
SHP	Small heterodimer partner
sd	Single dose
SD	Standard deviation
SERM	Selective estrogen receptor modulator
SNP	Single nucleotide polymorphism
SSRI	Selective serotonin reuptake inhibitor
Swissmedic	Swiss Agency for Therapeutic Products
TDM	Therapeutic drug monitoring
UGT	Uridine 5′-diphospho-glucuronosyltransferase
UGT2B4	UGT subfamily 2B4
UGT2B7	UGT subfamily 2B7
UGT2B15	UGT subfamily 2B15
UGT2B17	UGT subfamily 2B17
V_{max}	Maximum reaction velocity

1 INTRODUCTION

1.1 PERSONALIZED MEDICINE AND PRECISION DOSING

Personalized medicine describes the concept of tailoring drug therapy to the individual's needs, therefore maximizing treatment efficacy while minimizing the risk of ADRs and, consequently, reducing overall health care costs. Precision dosing is a key component of personalized medicine and is mainly concerned with drug dosing [8]. Contrary to the prevalent "generalized approach", often referred to as "One Treatment Fits All", precision dosing explicitly takes individual patient characteristics, such as genetic predisposition, underlying diseases and co-medication into account [9] (see Figure 1.1). These influences are widely recognized to be major contributors to the variability in the response of patients to drugs and, by extension, in the individual risk-benefit ratio for the respective therapy [10].

Precision Dosing vs. "One Treatment Fits All"

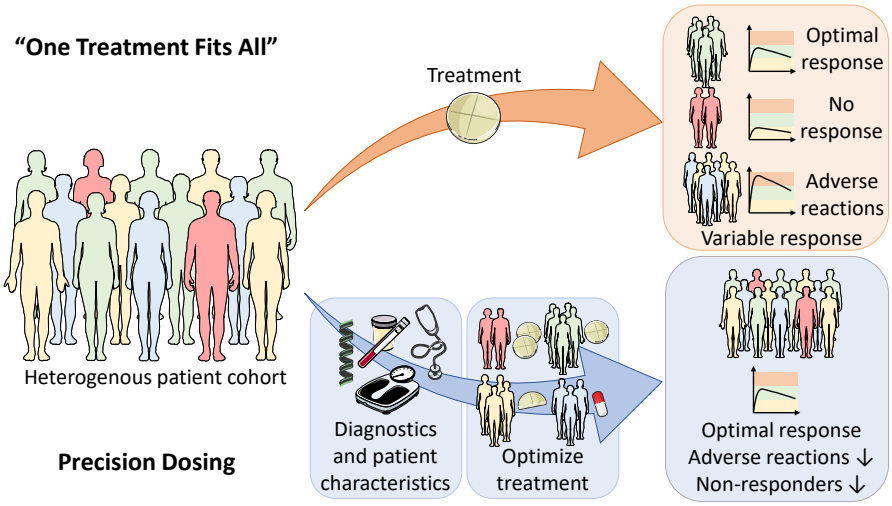

Figure 1.1: **Precision Dosing vs. "One Treatment Fits All".** The "One Treatment Fits All" approach is based on the assumption that all patients respond to a drug in the same way. In contrast, precision dosing explicitly takes individual patient characteristics, such as genetic predisposition, underlying diseases and co-medication into account and aims to optimize the efficacy and safety of drug therapy. Illustrations of tablets, capsules, medical equipment, DNA, arrows and people were taken from Servier [7], licensed under CC BY 3.0 (https://creativecommons.org/licenses/by/3.0/).

ADRs are a considerable threat to patient health as they have been estimated to account for 2 million hospitalizations per year in the US alone, while simultaneously being one of the leading causes of in-

Implications for Patient Safety and Economics

hospital mortality [11]. Annual costs of patient hospitalizations caused by ADRs have been estimated to exceed $177 billion in the US [10, 12], placing an enormous financial burden on health care providers. These costs could be considerably reduced by shifting from the paradigm of "trial and error" drug prescriptions to a personalized approach, as an estimated 40% of ADRs resulting in emergency department visits or hospitalizations are thought to be preventable [13].

Diagnostic Tests

Diagnostic tests are important cornerstones of personalized medicine and precision dosing [12], as they enable adapting drug therapy based on an individual's features. The patient's genotype is estimated to account for up to 95% of variability in drug response, as indicated by twin studies [14], highlighting the particular importance of genetic tests. Hence, studying the role of the genetic makeup of an individual to optimize drug response is an integral component of personalized medicine and precision dosing [15]. Here, the terms *pharmacogenetics* and *PGx* are regularly used in the context of precision dosing. While often used interchangeably, *pharmacogenetics* describes the effect of genetic polymorphisms on drug response whereas *PGx* also encompasses drug development driven by new findings in the field of genetics [16].

Implementation of PGx in Clinical Practice

Despite rapidly growing knowledge generated by PGx studies, its overall impact on clinical practice has been relatively small outside of some select fields such as oncology and psychiatry. Extensive knowledge of pharmacology is a prerequisite for the interpretation of findings obtained from PGx studies, aggravating the implementation of PGx into clinical practice [17]. To tackle these issues, several working groups, such as the Dutch Pharmacogenetics Working Group (DPWG) and the Clinical Pharmacogenetics Implementation Consortium (CPIC) have put increasing efforts into developing actionable PGx guidelines.

PGx Guidelines

These guidelines aim to provide evidence-based suggestions for the use of specific drugs and their optimal dosage based on an individual's genetic makeup [17]. In 2000, the Pharmacogenetics Research Network (PGRN) established the Pharmacogenomics Knowledge Base (pharmgkb.org) (PharmGKB) to provide a publicly accessible platform condensing the PGx knowledge generated in the past decades [18].

PharmGKB

This platform serves as a knowledge repository with curated information and annotations tailored towards clinicians on drugs affected by PGx, drug labels containing PGx information and, importantly, PGx guidelines [19].

Limitations of PGx Trials

Most PGx data is typically generated in phase I clinical DGI trials, where subjects are selected and stratified based on their genotype for one or more genes of interest. Here, the term DGI is used to describe the effect of variants in pharmacogenes on the pharmacokinetics (PK) and pharmacodynamics (PD) of a drug [20]. Additionally to their genotypes for one or multiple pharmacogenes of interest, participants of DGI trials are generally homogeneous regarding demographic

parameters and typically consist of healthy, young and often only male volunteers. However, the number of study participants is often too small to detect statistically significant phenotypical differences in the pharmacology of the studied drug [21]. Overall, these limitations of PGx trials make it difficult to extrapolate their results to *real-world* patients, as these are often elderly, fragile and typically receive co-medication [20].

Dedicated clinical trials simultaneously investigating the effect of genetic polymorphisms, co-medication and co-morbidities on drug response in a sufficiently large study population would not only entail enormous costs but would also put study participants at a considerable risk of experiencing ADRs [22]. Here, PK modeling presents a promising approach to augment existing PGx knowledge and provide predictions for highly complex scenarios, including DDGIs, organ impairment and involving special populations such as pediatric, geriatric, pregnant or obese patients. Finally, these models hold enormous potential in the context of precision dosing, as they can be used for dose recommendations, safety monitoring, drug development and clinical trial design [9].

PK Modeling as a Tool to Augment PGx Knowledge

1.2 CYP2D6

1.2.1 *Overview*

CYP2D6 is involved in the metabolism of 15–25% of clinically used drugs, while only making up approximately 1–4% of the hepatic cytochrome P450 (CYP) pool [23]. This enzyme is mainly expressed in the liver, and to a lesser extent in lung and heart tissue. Here, it is involved in the biosynthesis and metabolism of various endogenous amines, such as serotonin [24]. Exogenous CYP2D6 substrates are represented in most therapeutic drug classes, such as antidepressants, antipsychotics, oncologic drugs and opioid analgesics as well as antiarrhythmic and antihypertensive drugs [23]. Both endogenous and exogenous substrates bear structural similarities – they typically are organic bases showing optimal distances of 0.25–0.45 nm from their positively charged amine function to both the metabolic oxidation site and the anionic site of the enzyme [25, 26]. Commonly catalyzed pathways include *O*-demethylation, *N*-demethylation and aromatic hydroxylation [24]. Importantly, CYP2D6 enzymatic activity displays considerable interindividual variability (IIV) with up to 40-fold differences in drug clearance and substrate plasma concentrations [27]. This variability is primarily attributed to genetic polymorphisms in the *CYP2D6* gene [24]. Interindividual differences in CYP2D6 activity have first been described in 1977 when a bimodal distribution of the metabolic ratio of the antihypertensive drug debrisoquine was observed in a study population of 94 Caucasian volunteers [28]. Two

Endogenous and Exogenous Substrates of CYP2D6

Variability in CYP2D6 Activity

years later, similar observations were reported in a study cohort of 360 volunteers, where 5% of participants were found to be *non-metabolizers* of the antiarrhythmic drug sparteine. [29]. The authors of both studies independently identified genetic polymorphisms as the main cause of debrisoquine- and sparteine metabolizer phenotypes, respectively [28, 29]. Moreover, higher occurrences of ADRs, such as hypotension during debrisoquine therapy, had been reported in patients displaying the sparteine/debrisoquine poor metabolizer phenotype [30]. In 1987, the identity of the *CYP2D6* gene, which encodes a new CYP enzyme, was confirmed and its link to the sparteine/debrisoquine metabolizer phenotype was validated [31].

Debrisoquine and Sparteine Oxidation Phenotypes

1.2.2 *The CYP2D6 Gene*

The *CYP2D6* gene is located on the long arm of chromosome 22 [31] and the only gene of the CYP2D family encoding for a functional protein in humans [23]. Today, more than 140 allelic variants (not counting various subvariants) have been identified [32], highlighting the highly polymorphic nature of *CYP2D6* and the enormous clinical interest in his gene.

Allelic variants are typically caused by single nucleotide polymorphisms (SNPs) and insertions or deletions (indels) and can have varying effects on the activity of the encoded enzyme. For instance, allelic variants can cause a change in the amino acid sequence of the translated protein which typically reduces either the biochemical activity of the enzyme or its expression levels compared to the wild type **1* allele [33]. Conversely, so-called *silent polymorphisms* occur, when the change in the nucleic acid sequence of the allele does not infer a change in the amino acid sequence of the translated protein.

Allelic Variants of CYP2D6

The *CYP2D6* gene is prone to structural variants, such as copy number variations (CNVs) [32]. These structural variants, have been observed to result in zero to up to 13 copies of a given allele in an individual and can have a dramatic effect on the activity of CYP2D6 [34]. For instance, homozygous carriers of the *CYP2D6*5* gene deletion allele express no functional CYP2D6 enzymes, rendering them CYP2D6 poor metabolizers [35]. Conversely, CNVs of the **1* allele, such as *CYP2D6*1x2*, can lead to increased expression of the encoded protein, resulting in increased CYP2D6 activity [34].

Structural Variants of CYP2D6

CYP2D6 alleles are not equally distributed across world populations [36]. For instance, the loss-of-function **4* allele and the **5* gene deletion allele are found in >20% of Europeans resulting in more than 5% of Europeans being categorized as CYP2D6 poor metabolizer phenotype, whereas less than 1% of East Asian populations were found to be CYP2D6 poor metabolizers [36]. Conversely, the reduced-function **10* allele occurring in less than 5% of Europeans, has been observed to be the most frequently expressed allele in East Asians, resulting in an

Ethnicities and CYP2D6 Alleles

overall decrease of CYP2D6 activity compared to other populations [1, 33]. Allele multiplications due to CNVs occur in 2–3% of Europeans, whereas 40% of Mozabites, an Amazigh population in northern Algeria, were found to be ultrarapid metabolizers, carrying more than 3 active gene copies of CYP2D6 [37].

1.2.3 *CYP2D6 Phenotypes*

Phenotyping describes the process of quantifying the *in vivo* activity of a given enzyme or transporter in an individual [38]. Determination of the phenotype for a specific enzyme typically involves the administration of a phenotyping probe, i.e., a substrate that is known to be metabolized by the enzyme. Subsequently, the parent compound and one of its metabolites, which is ideally specifically formed via the enzyme of interest, are quantified in plasma or urine and a metabolic ratio is calculated (see Figure 1.2).

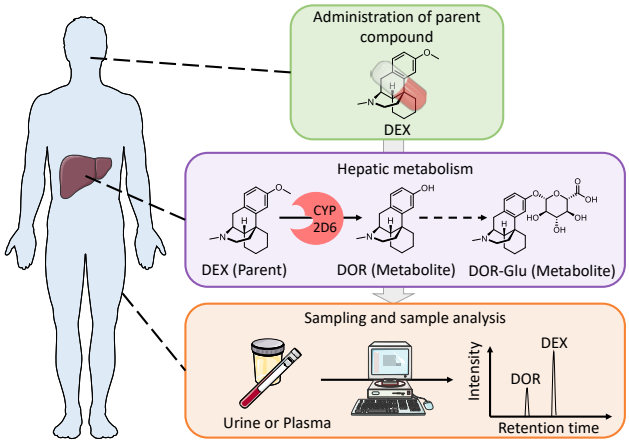

Figure 1.2: **Schematic illustration of the phenotyping process.** The CYP2D6 phenotyping probe dextromethorphan (DEX) is typically administered as a single oral dose. DEX undergoes extensive metabolism by CYP2D6 resulting in the formation of dextrorphan (DOR). Subsequent glucuronidation via uridine 5'-diphosphoglucuronosyltransferases (UGTs) results in the formation of dextrorphan *O*-glucuronide (DOR-Glu). Plasma or urine samples are collected at one or multiple time points and the concentrations of dextromethorphan and total dextrorphan (DOR + DOR-glu) are quantified. Illustrations of capsules, medical equipment, organs and people were taken from Servier [7], licensed under CC BY 3.0 (https://creativecommons.org/licenses/by/3.0/).

Overall, urinary metabolic ratios are considered the gold standard for CYP2D6 phenotyping due to their minimal invasiveness and good correlation with CYP2D6 activity [27]. Frequently used CYP2D6 phe-

notyping probes include debrisoquine, sparteine, dextromethorphan, metoprolol, bufuralol and tramadol [27].

CYP2D6 Phenotyping Probes and Urinary Metabolic Ratios

Historically, phenotyping has been predominately used to discriminate between CYP2D6 poor metabolizers and extensive metabolizers in a given population. However, since the advent of genotyping and the subsequent characterization of allelic and structural variants of CYP2D6, the definition of CYP2D6 phenotypes has been extended to include additional categories, such as intermediate metabolizers and ultrarapid metabolizers [39]. More recently, the CPIC has suggested using the term *normal metabolizer* instead of *extensive metabolizer*, to reflect the determined *normal* enzyme activity [40].

Phenotype Categories

1.2.4 *Genotype-to-Phenotype Translation*

CYP2D6 phenotyping may provide the most accurate estimate of CYP2D6 activity for an individual, however, phenotyping entails relatively high costs, is time-consuming and uncomfortable for the subjects, as they are required to collect their urine for a given period or have plasma samples taken [27]. Conversely, costs for PGx testing has been decreasing steadily over the last decades and these tests are becoming increasingly available [41]. Thus, increasing efforts have been put into developing methods for estimating an individual's phenotype based on their genotype. Inferring CYP2D6 activity from a given genotype is highly challenging due to the vast number (> 10,000) of potential CYP2D6 genotypes and often incomplete data on the *in vitro* and *in vivo* consequences of a given allele [42]. Therefore, translation methods typically involve categorizing CYP2D6 alleles based on the activity of the expressed protein as determined through *in vitro* and *in vivo* experiments [43].

Concept and Challenges

Here, Steimer et al. proposed to assign *semiquantitative gene doses* for each allele, reflecting no (0), reduced (0.5) and normal (1) activity based on the observed amitriptyline and nortriptyline exposure in their clinical study [44]. This concept was later extended and renamed to the *activity score system* by Gaedigk et al., which provides an intuitive system to translate genotype data into traditional CYP2D6 phenotype categories [43]. Activity values are assigned to both haplotypes of an individual. These reflect no (0), reduced (0.25 or 0.5) or normal (1) CYP2D6 activity compared to the wild-type **1* allele, as well as multiple copies of a normal activity allele (2). The sum of activity values represents the activity score, which can be translated into the CYP2D6 poor metabolizer (0), intermediate metabolizer (0.5–1), normal metabolizer (1.25–2.25) and ultrarapid metabolizer (>2.25) categories (see Table 1.1) [45].

Activity Score Assignment

Table 1.1: CYP2D6 activity assignment [45] reproduced according to [1].

Activity Score	Projected Phenotype	Examples of Relevant *CYP2D6* Genotypes
0	Poor Metabolizer	*3/*3, *3/*4, *4/*4, *5/*6
0.25	Intermediate Metabolizer	*4/*10, *5/*10
0.5		*4/*41, *5/*17, *10/*10
0.75		*17/*10, *41/*10
1		*1/*4, *2/*5, *17/*17, *17/*41
1.25	Normal Metabolizer	*1/*10, *2/*10, *35/*10
1.5		*1/*41, *2/*17, *35/*41
2		*1/*1, *1/*2, *2/*35
2.25		*1x2/*10, *35x2/*10
> 2.25	Ultrarapid Metabolizer	*1/*1x3, *1/*35x2, *2x2/*9

CYP2D6: CYP subfamily 2D6.

Recently, this system has been harmonized between CPIC, DPWG and major working groups in the field of PGx. This facilitates the integration of the activity score into existing and future PGx guidelines and increases comparability of study results and guideline recommendations [45]. The activity score system has been validated in numerous clinical studies over the past decade and has widely been adapted in the context of PGx testing. However, the activity score system is not without limitations. For instance, interindividual differences in CYP2D6 activity in a population sharing the same CYP2D6 phenotype, activity score or even genotype, have been found to be substantial [42]. Moreover, the activity score system disregards substrate-dependent differences in CYP2D6 activity for specific alleles observed *in vitro* [46].

Limitations of the Activity Score System

1.2.5 *Factors affecting CYP2D6 Activity*

Interindividual differences in populations sharing the same CYP2D6 genotype are thought to be caused by both genetic variation outside of the *CYP2D6* gene locus and environmental factors (see Figure 1.3). Currently, these factors are not captured by the activity score approach [42].

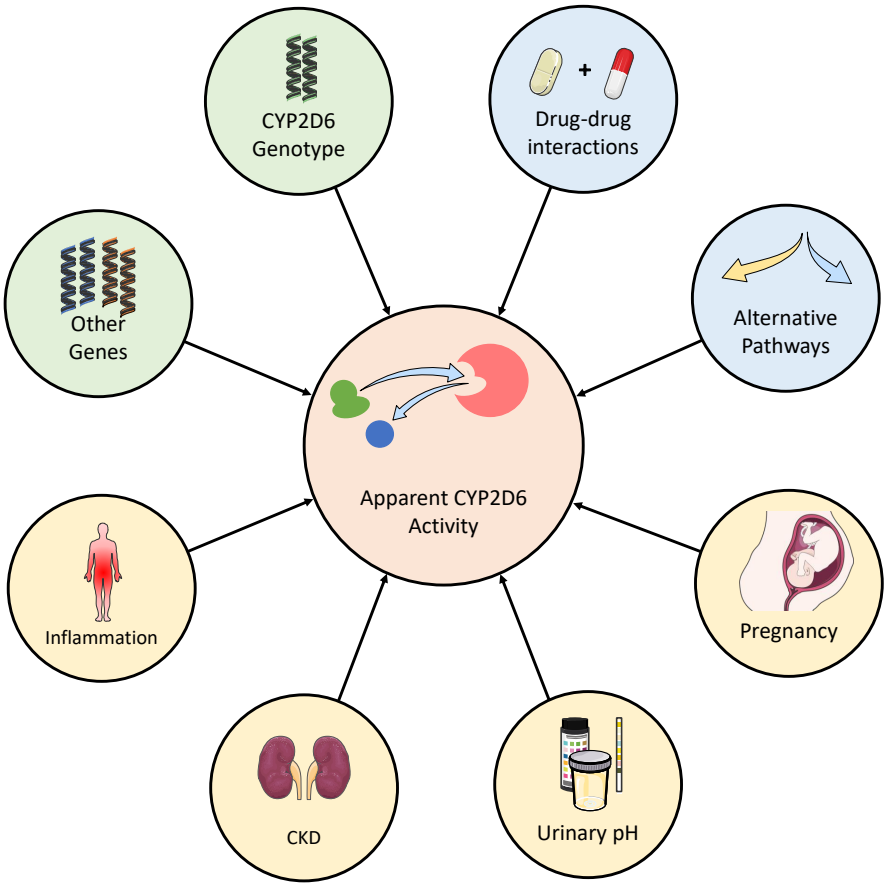

Figure 1.3: **Factors affecting apparent CYP2D6 activity and causing interindividual/interpatient variability.** CYP2D6 activity is influenced by genetic (green), (patho-)physiological (yellow) and other factors (blue). CKD: chronic kidney disease. Illustrations of capsules, tablets, medical equipment, organs, genes and people were taken from Servier [7], licensed under CC BY 3.0 (https://creativecommons.org/licenses/by/3.0/).

1.2.5.1 *Genetic Factors Affecting CYP2D6 Activity*

Although the *CYP2D6* gene is the major determinant of CYP2D6 activity, it may also be affected by other genes [33, 42]. These genes typically modulate CYP2D6 activity by altering the transcription of the *CYP2D6* gene to messenger ribonucleic acid (mRNA) and the subsequent translation to CYP2D6 protein, primarily affecting CYP2D6

expression levels [42]. Here, genome-wide association studies (GWAS) have identified 30 SNPs outside of the *CYP2D6* gene that may affect the activity of CYP2D6. These SNPs were predominately located in close proximity (200 kb) to the *CYP2D6* gene locus, suggesting self-regulation of CYP2D6 translation [47].

Modulation of CYP2D6 Expression

SNPS

Studies have found normal CYP2D6 activity in Caucasian individuals genotyped as *CYP2D6**2/*2, whereas African American subjects with the same genotype showed a considerably decreased CYP2D6 activity compared to wild-type individuals [43]. Here, a link to the *rs5758850* SNP has been established, which is located in the *CYP2D6* enhancer region and has been observed to amplify gene expression [48]. The *rs5758850* SNP occurs in significantly higher frequency in Caucasian carriers of the *CYP2D6**2 allele compared to African Americans [48–50]. Although a combined assessment of the *CYP2D6* and *rs5758850* has been proposed to categorize CYP2D6 activity, a recent study found only a modest overall effect of *rs5758850* SNP on CYP2D6 expression [51].

*rs5758850 and CYP2D6*2*

TRANSCRIPTION FACTORS

Unlike other CYP enzymes such as CYP subfamily 3A4 (CYP3A4), CYP2D6 is considered essentially non-inducible by activation of the pregnane X receptor (PXR) and constitutive androstane receptor (CAR) transcription factors [42]. However, numerous studies have found a considerable effect of pregnancy on CYP2D6 activity with up to 4-fold increases of oral metoprolol clearance and 2-fold decreases of dextromethorphan/dextrorphan metabolic ratios found in pregnant women compared to postpartum [52–54]. Here, two transcription factors, small heterodimer partner (SHP) and Krüppel-like factor 9 (KLF9) have been identified as a repressor and an activator of CYP2D6 transcription during pregnancy, respectively [55]. Consequently, activation of these transpription factors due to pregnancy results in an increase in CYP2D6 activity compared to postpartum.

CYP2D6 Transcription and Pregnancy

1.2.5.2 *Non-genetic Factors Affecting CYP2D6 Activity*

An individual's CYP2D6 activity is generally considered to be fairly stable to changes in environmental conditions, even over multiple years. For instance, smoking, alcohol consumption, intake of oral contraceptives, sex and age have been known to affect the activity of various other CYP enzymes, whereas the effect on CYP2D6 activity is considered negligible [23]. However, other factors have been shown to affect CYP2D6 activity or impede accurate assessment thereof [42].

DRUG-DRUG INTERACTIONS

Drug-drug interactions (DDIs) occur, when the co-administration of

a drug alters the PK and PD of another drug. Here, CYP2D6 DDIs are typically caused by inhibitory processes, as CYP2D6 is considered non-inducible by prototypical inducers of other CYP enzymes such as rifampicin and phenobarbital [55]. Most inhibitors of CYP2D6 can be classified based on the mechanism of inhibition into competitive, non-competitive and irreversible inhibition. Reversible inhibition of CYP enzymes is caused by a compound competitively binding to the active site of an enzyme (competitive inhibition) or allosteric modulation of enzyme activity by binding to a site different from the active site of the enzyme (non-competitive inhibition). Irreversible inhibition is caused by a compound covalently binding to either its active site or prosthetic groups integral to the enzyme's function, consequently permanently inactivating it (mechanism-based inhibition) [56]. Here, the new synthesis of CYP2D6 is required to restore baseline enzyme activity [57].

Mechanisms of CYP2D6 Inhibition

Overall, CYP2D6 inhibitors can significantly affect the biotransformation of CYP2D6 substrates, which may either result in increased exposure to the substrate or decreased exposure to the substrate's active metabolite. Here, the US Food and Drug Administration (FDA) lists fluoxetine, quinidine, terbinafine (reversible inhibitors), paroxetine (irreversible inhibitor) and bupropion as strong inhibitors of CYP2D6 [58, 59]. Interestingly, bupropion has been found to interact uniquely with CYP2D6. It acts as a competitive inhibitor of CYP2D6 while simultaneously causing down-regulation of CYP2D6 expression [60, 61].

Inhibitors of CYP2D6

Depending on the inherent CYP2D6 activity, concomitant administration of CYP2D6 inhibitors can have differing effects on the PK of a CYP2D6 substrate. For instance, dextromethorphan/dextrorphan metabolic ratios have been observed to be affected by the co-administration of quinidine in normal and intermediate metabolizers of CYP2D6, while there was no effect on the metabolic ratio of poor metabolizers of CYP2D6 [62, 63]. Similarly, pretreatment with paroxetine resulted in substantial increases in the dextromethorphan/dextrorphan metabolic ratio of subjects originally phenotyped as normal or intermediate metabolizers, rendering a substantial fraction of these subjects poor metabolizers of CYP2D6 [64]. This phenomenon is typically referred to as *phenoconversion* and its effect is thought to be highly dependent on the inherent CYP2D6 activity. Taking the initial CYP2D6 activity of an individual into account, poor metabolizers of CYP2D6 are not prone to phenoconversion due to DDIs, whereas intermediate and normal metabolizers are at an increased risk of being converted to poor or intermediate metabolizers, respectively [65].

Phenoconversion due to CYP2D6 Inhibition

Phenotype-dependent Risk of Phenoconversion

ALTERNATIVE PATHWAYS

While CYP2D6 is considered the primary enzyme responsible for the metabolism of many clinically used drugs, a compound's biotransfor-

mation is often mediated by more than one enzyme. Relative contributions of CYP2D6 to the metabolism of a compound may vary substantially based on both the mass balance of the compound and the inherent CYP2D6 activity of an individual. For instance, CYP2D6 has been found to mediate >96% of the dextromethorphan N-demethylation, producing its major metabolite dextrorphan, in normal metabolizers [62]. Despite no residual CYP2D6 activity, dextrorphan is detectable, albeit in very small amounts, in the urine of CYP2D6 poor metabolizers [62, 63]. These observations from *in vivo* studies are well in line with findings of *in vitro* experiments, which have identified CYP subfamily 2C9 (CYP2C9) and CYP subfamily 2C19 (CYP2C19) as minor contributors to dextromethorphan N-demethylation [66]. Hence, with decreasing CYP2D6 activity, the importance of CYP2C9 and CYP2C19 for dextromethorphan N-demethylation increases substantially. As both CYP2C9 and CYP2C19 are also polymorphically expressed [67], their activity may also vary between individuals and consequently affect dextrorphan formation [2, 42].

Contributions of Alternative Pathways

PHYSIOLOGICAL AND PATHOPHYSIOLOGICAL FACTORS

Urinary metabolic ratios are typically used to assess an individual's CYP2D6 activity and while these are highly accurate in discriminating poor metabolizers from normal metabolizers, they have been observed to be highly variable even between subjects within the same activity score category [43]. Renal excretion of a given compound is dependent on the renal function of an individual and can be affected by pathophysiological conditions such as chronic kidney disease (CKD) [68]. Moreover, renal excretion may also be affected by urinary pH, as CYP2D6 substrates are typically basic compounds [27]. Here, approximately 80% of IIV in urinary metabolic ratios of CYP2D6 phenotyping probes dextromethorphan and metoprolol have been attributed to differences in urinary pH within the physiological range [69]. Consequently, urinary metabolic ratios should be interpreted with great caution and both urinary pH and renal function should be taken into account [42].

Chronic Kidney Disease and Urinary pH

Finally, inflammatory processes have been found to heavily affect the expression of CYP enzymes. Here, pro-inflammatory cytokines typically cause down-regulation of CYP mRNA, consequently reducing enzyme activity [70]. Pathophysiological inflammatory conditions have been shown to affect CYP2D6 activity, for instance in patients with hepatitis C or HIV [71]. While the body of evidence for cytokine-induced CYP2D6 down-regulation is still relatively small, especially compared to other CYP enzymes, cytokine-induced CYP regulation is likely to affect the metabolism of CYP2D6 substrates by shifting relative contributions of alternative pathways [42].

Inflammation

RANDOM EFFECTS

Pharmacokinetic measurements are typically subject to random fluctuations, which are often referred to as *random effects* [72]. Random effects are typically attributed to IIV (often also referred to as interpatient variability (IPV) or between-subject variability (BSV)) and residual unexplained variability (RUV). These terms are typically used in a very technical context, i.e., in nonlinear mixed effects (NLME) modeling, to describe the variability of PK or PD parameters in a population (IIV) and the residual variability of the model (RUV) not covered by the models, its covariates, and the IPV [73]. Apparent variability in CYP2D6 activity may also be partially attributable to sources of IPV such as genetic and non-genetic factors or demographic differences, such as age, weight and height. Moreover, RUV may also contribute to apparent variability in CYP2D6 activity, as differences in manufacturing processes can affect the amount of active compound in a drug product or its release rate and therefore affect the PK of a phenotyping probe.

Between Subject Variability and Residual Unexplained Variability

Additionally, differences in clinical trial execution such as time of drug administration and blood sampling may also contribute to apparent variability in CYP2D6 activity.

1.2.6 *Substrates and Inhibitors of CYP2D6*

In 2022, 76 FDA-approved drug labels and 22 drug labels approved by the European Medicines Agency (EMA) contained CYP2D6 PGx annotations, either requiring or recommending genetic testing prior to drug treatment or containing actionable information regarding treatment adjustments based on CYP2D6 genotypes [74, 75]. The following sections provide information on the CYP2D6 substrates and inhibitors that were selected to be included in this thesis. The selection of substrates and inhibitors was based on the following criteria: (1) The compound is a substrate or inhibitor of CYP2D6 according to the FDA Table of Substrates, Inhibitors and Inducers [58, 59] and/or (2) a sufficient number of *in vivo* clinical study data in healthy volunteers was available from the published literature, including studies that investigated the effect of genetic variation in CYP2D6 on the pharmacokinetics of the compound and/or (3) an adequate amount of *in vivo* clinical DDGI study data in healthy volunteers was available from the published literature. Figure 1.4 provides a network representation of the seven compounds modeled in this work.

Rationale for Selection of Substrates and Inhibitors

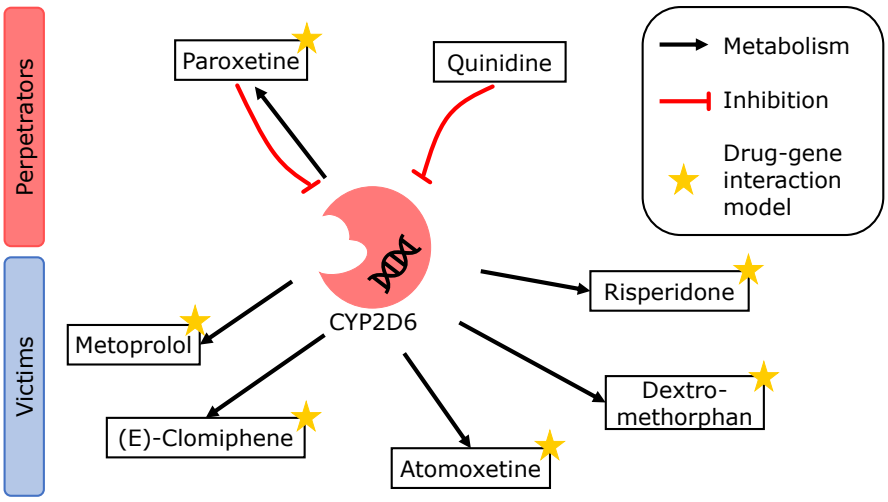

Figure 1.4: **Compounds modeled in this work in a DDGI network representation** Of the seven compounds modeled in this work, six compounds (metoprolol, dextromethorphan, atomoxetine, paroxetine, risperidone and (*E*)-clomiphene are substrates of CYP2D6 as indicated by the black arrows. Additionally, paroxetine and quinidine are inhibitors of the CYP2D6 enzyme as indicated by red blunt arrows. Paroxetine and quinidine are typically used as *perpetrator* drugs in CYP2D6 DDI scenarios (although paroxetine can also be a *victim* drug, as it is metabolized by CYP2D6). Metoprolol, dextromethorphan, atomoxetine, risperidone and (*E*)-clomiphene are considered *victim* drugs in CYP2D6 DDI scenarios. Yellow stars indicate that the respective compound PBPK model was extended to include CYP2D6 DGIs.

METOPROLOL

Metoprolol is a β_1-selective adrenergic receptor blocker that is used in the treatment of hypertension, angina pectoris and heart failure [76]. Among the most frequently prescribed drugs in the United States, metoprolol ranked 6th in 2020 with more than 60 million total prescriptions [77]. While metoprolol is administered as a racemic mixture, the *(S)*-enantiomer is thought to be predominately responsible for the pharmacological effects of metoprolol [78]. Similar to many other beta-blockers, such as nebivolol [79], propranolol [80] and bufuralol [81], metoprolol is extensively metabolized by CYP2D6. Principal pathways of metoprolol metabolism include α-hydroxylation and *O*-demethylation [82]. Here, other CYP enzymes such as CYP2C9, CYP subfamily 2B6 (CYP2B6) and CYP3A4 have been identified to contribute to the metabolism of metoprolol, albeit to a lesser extent [83]. Of note, CYP2D6 shows enantio-preference towards the *(R)*-enantiomer of metoprolol, resulting in a higher ratio of *(S)*- to *(R)*-metoprolol plasma concentrations in ultrarapid, normal and intermediate metabolizers of CYP2D6, whereas the effect normalizes in CYP2D6 poor metabolizers [78]. Metoprolol is still used in some phenotyping cocktails to assess CYP2D6 activity [38]. However, metoprolol α-hydroxylation is gen-

Metoprolol Metabolism

Metoprolol ADRs and Use in Clinical DDI Trials

erally considered a less specific marker reaction for CYP2D6 activity than dextromethorphan *O*-demethylation and administration of metoprolol may cause ADRs such as bradycardia, fatigue and dizziness [38, 84]. Regardless, the FDA recommends the use of metoprolol in clinical DDI trials as a moderate sensitive substrate of CYP2D6 activity [59].

PGx Information in Metoprolol Drug Labels

While there are currently no explicit dosing recommendations for metoprolol based on *CYP2D6* genotype in drug labels approved by FDA or EMA, informative PGx information is available in the FDA drug labels and actionable PGx annotations are contained in metoprolol drug labels of the Health Canada (Santé Canada) (HCSC) and Swiss Agency for Therapeutic Products (Swissmedic) [85]. These drug labels generally denote that the *CYP2D6* genotype may have a significant impact on the pharmacokinetics of metoprolol, resulting in several-fold increases in metoprolol exposure in CYP2D6 poor metabolizers compared to extensive metabolizers, reducing metoprolol cardioselectivity [86]. Response to metoprolol treatment and the risk of ADRs is presumably not solely determined by the CYP2D6 genotype but also other pharmacogenes, such as *adrenoceptor β_1 (ADRB1)*, *adrenoceptor β_2 (ADRB2)* and *guanine nucleotide-binding protein subunit β_3 (GNB3)* [48, 87, 88].

DEXTROMETHORPHAN

Dextromethorphan has been widely used as an over-the-counter cough suppressant since the 1950s and is part of many cough-and-cold remedies [89]. In recent years, dextromethorphan has been approved by the FDA in fixed drug combinations for the treatment of pseudobulbar affect (NUEDEXTA®, dextromethorphan/quinidine) [90] and major depressive disorder (AUVELITY®, dextromethorphan/bupropion) [91]. While dextromethorphan bears many structural similarities to opioids, it does not bind to opioid receptors and consequently has no analgesic properties [92]. Instead, dextromethorphan and its major metabolite dextrorphan act as non-selective N-methyl-D-aspartate receptor antagonists and exhibit strong serotonergic effects [89]. Dextromethorphan is extensively metabolized by CYP2D6 to its major metabolite dextrorphan with only minor contributions from CYP2C9 and CYP2C19. Alternatively, *N*-demethylation of dextromethorphan results in the formation of 3-methoxymorphinan, mainly catalyzed by CYP3A4 [62, 66]. Subsequently, 3-hydroxymorphinan is formed via *N*-demethylation of dextrorphan and *O*-demethylation of 3-methoxymorphinan. Both 3-hydroxymorphinan and dextrorphan are glucuronidated via UGT isozymes including UGT subfamily 2B15 (UGT2B15), UGT2B7, UGT2B17 and UGT2B4 [93]. As dextromethorphan *O*-demethylation is predominately mediated by CYP2D6 [62] and dextromethorphan is both readily available and well tolerated, it has become the standard phenotyping probe for CYP2D6 activity [27] and is part of many established phenotyping cocktails [38]. Accord-

Dextromethorphan Metabolism

ingly, the FDA recommends the use of dextromethorphan both in *in vitro* studies of CYP-mediated drug metabolism as well as in clinical DDI trials as a sensitive substrate of CYP2D6 activity [58, 59].

Dextromethorphan as a Probe Substrate in Clinical DDI Trials

Various drug labels contain PGx information for dextromethorphan in fixed combinations, including the FDA labels for NUEDEXTA® (dextromethorphan/quinidine) and AUVELITY® (dextromethorphan/bupropion) [94]. Here, the FDA recommends testing patients for variants in the *CYP2D6* gene prior to the use of NUEDEXTA® and discourages its use in poor metabolizers of CYP2D6 [95]. For AUVELITY®, the FDA label contains dosing recommendations based on the *CYP2D6* genotype, i.e., dose reduction for poor metabolizers of CYP2D6 [96].

PGx Information in Dextromethorphan Drug Labels

PAROXETINE

Paroxetine is a selective serotonin reuptake inhibitor (SSRI) used in the treatment of major depressive disorder, generalized anxiety disorder, obsessive-compulsive disorder, panic disorder and social anxiety disorder [97]. Paroxetine ranks 82nd among the most frequently prescribed drugs in the United States with more than 9 million total prescriptions in 2020 [77]. The principal pathway of paroxetine is its demethylation to a catechol intermediate, which is rapidly metabolized to various metabolites by catechol-O-methyltransferase (COMT) and UGTs [97, 98]. CYP2D6 is the major enzyme responsible for the metabolism of paroxetine to paroxetine-catechol, with minor contributions from CYP3A4, CYP subfamily 1A2 (CYP1A2), CYP2C19 and CYP subfamily 3A5 (CYP3A5) [99]. Interestingly, paroxetine is a potent mechanism-based inhibitor of CYP2D6 and consequently inhibits its metabolism. Analogous to methylendioxymethamphetamine (MDMA) [100], the methylendioxy moiety of paroxetine has been proposed to form covalent bonds with the heme complex of CYP2D6, either through carbene intermediates or ortho-quinone intermediates, effectively inactivating the enzyme [101]. Consequently, multiple administrations of paroxetine may result in pronounced CYP2D6 phenoconversion and significantly reduce the clearance of paroxetine itself and other CYP2D6 substrates [102]. The FDA recommends the use of paroxetine in clinical DDI trials as a strong inhibitor of CYP2D6 and as a selective inhibitor for CYP2D6-mediated reactions *in vitro* [58, 59]. PharmGKB lists no drug labels containing PGx information on paroxetine itself [103]. However, the FDA label for paroxetine notes that paroxetine is both a substrate and inhibitor of paroxetine and may increase exposure of other CYP2D6 substrates, such as atomoxetine [104].

Paroxetine Metabolism

Paroxetine as a Probe Inhibitor in Clinical DDI Trials

ATOMOXETINE

Atomoxetine is a selective norepinephrine reuptake inhibitor used in the treatment of attention deficit hyperactivity disorder (ADHD) in children, adolescents and adults [105]. Atomoxetine is a frequently

prescribed drug with more than 1 million total prescriptions in 2020 in the United States alone [77]. Contrary to most first-line ADHD medications, such as methylphenidate and amphetamine, atomoxetine shows only little stimulation of the central nervous system and is therefore considered to be less prone to abuse and is generally well tolerated [106, 107]. Atomoxetine is primarily metabolized via 4-hydroxylation to its active metabolite 4-hydroxyatomoxetine [108]. This pathway is predominately mediated by CYP2D6 with minor contributions from CYP1A2, CYP2B6, CYP2C19 and CYP subfamily 2E1 (CYP2E1) [109]. Alternatively, atomoxetine is demethylated to N-desmethylatomoxetine by CYP2C19, CYP2B6, CYP1A2, CYP3A4 and CYP2C9 [109]. Both metabolites are subsequently metabolized by UGTs to their respective glucuronide conjugates which are then excreted via the kidneys [105]. Overall, CYP2D6 activity is the major determinant of atomoxetine exposure. However, exposure to its active metabolite 4-hydroxyatomoxetine may be polygenically determined and significantly affected by both *CYP2D6* and *CYP2C19* DDGIs [108, 110]. The FDA recommends the use of atomoxetine in clinical DDI trials as a sensitive substrate of CYP2D6 [58, 59].

Atomoxetine Metabolism

Atomoxetine as a Probe Substrate in Clinical DDI Trials

PGx Information in Atomoxetine Drug Labels

Drug labels approved by FDA, HCSC, the Japanese Pharmaceuticals and Medical Device Agency (PMDA) and Swissmedic contain actionable PGx information on atomoxetine [111]. Specifically, the drug label for STRATTERA® recommends reducing atomoxetine doses in poor metabolizers of CYP2D6 and patients that are also administered strong inhibitors of CYP2D6, such as quinidine and paroxetine [112].

RISPERIDONE

Risperidone is an atypic antipsychotic used in the treatment of schizophrenia and bipolar disorder [113]. Its mechanism of action is based on the antagonism of dopamine D2 and serotonin 5-HT2A receptors by both the parent compound and its main metabolite 9-hydroxyrisperidone [113, 114]. Risperidone ranks 138th among the most frequently prescribed drugs in the United States with more than 4 million total prescriptions in 2020 [77]. It is primarily metabolized via CYP2D6, CYP3A4 and CYP3A5 to its active metabolite 9-hydroxyrisperidone [115]. This metabolite shows comparable efficacy and safety to risperidone and, due to its longer half-life, is marketed as a standalone drug under the name paliperidone [116]. Both risperidone and 9-hydroxyrisperidone AUC are significantly affected by CYP2D6 activity after oral administration of risperidone. Here, an 8-fold increase in risperidone AUC was observed in CYP2D6 poor metabolizers, whereas 9-hydroxyrisperidone AUC was reduced by 70% compared to normal metabolizers [117]. Typically, the sum of risperidone and 9-hydroxyrisperidone (total active moiety) is considered to be the most relevant pharmacokinetic parameter to assess the clinical efficacy of risperidone. Consequently, as the AUC of the

Risperidone Metabolism

total active moiety differs only slightly between CYP2D6 phenotypes, the overall effect of *CYP2D6* polymorphisms on the pharmacodynamics of risperidone are considered negligible [117]. This is reflected in drug labels for risperidone by FDA, HCSC and Swissmedic, all noting substantial difference in risperidone and 9-hydroxyrisperidone concentrations but negligible differences in combined concentrations between different metabolizer phenotypes [118].

PGx Information in Risperidone Drug Labels

(*E*)-CLOMIPHENE

Clomiphene is a selective estrogen receptor modulator (SERM) used in the treatment of infertility caused by polycystic ovary syndrome (PCOS) [119]. It is administered as a racemic mixture of *(E)*- and *(Z)*-clomiphene, with *(E)*-clomiphene with its metabolites *(E)*-4-hydroxyclomiphene and *(E)*-4-hydroxy-N-desethylclomiphene being the active compounds [120]. The mechanism of action is based on the antagonism of estrogen receptors in the arcuate nucleus of the hypothalamus, which results in increased secretion of gonadotropin-releasing hormone (GnRH) and subsequently increased secretion of luteinizing hormone (LH) and follicle-stimulating hormone (FSH) [121]. Clomiphene enantiomers are metabolized by a variety of CYP enzymes. Here, the formation of active metabolites *(E)*-4-hydroxyclomiphene and *(E)*-4-hydroxy-N-desethylclomiphene has been observed to be predominantly mediated by CYP2D6 and CYP3A4 [120]. Consequently, CYP2D6 activity has been suggested to be predominately responsible for interpatient differences in both the PK and PD of clomiphene [120].

(E)-Clomiphene Metabolism

(*E*)-clomiphene is not recommended for clinical DDI trials, likely due to the availability of more affordable, safe and suitable alternatives [58, 59]. To date, no FDA- or EMA-approved drug labels contain PGx information for clomiphene [122].

QUINIDINE

Quinidine is a class I antiarrhythmic drug used in the treatment of atrial fibrillation and ventricular arrhythmias and its mechanism of action is based on blockage of voltage-gated sodium channels [123]. Due to its narrow therapeutic index and the availability of safer and more effective drugs, the use of quinidine has been declining for several decades [124]. Quinidine is primarily metabolized via CYP3A4-mediated 3-hydroxylation to 3-hydroxyquinidine [125]. Alternatively, quinidine undergoes N-oxidation to quinidine-N-oxide via various CYP enzymes with the largest contribution from CYP3A4 [125]. Although quinidine shows high affinity towards the active site of CYP2D6 and displays many structural characteristics commonly found in CYP2D6 substrates, it is not a substrate of CYP2D6 [126]. Instead, quinidine is considered a potent inhibitor of CYP2D6 and also P-glycoprotein (P-gp) [126, 127]. Moreover, quinidine metabolites have

Quinidine as a Probe Inhibitor in Clinical DDI Trials

been shown to contribute to both the pharmacodynamics of quinidine as well as its inhibitory potential towards CYP2D6 [128, 129]. Consequently, the FDA recommends quinidine as a probe substrate for P-gp in *in vitro* DDI studies, as well as a probe inhibitor of P-gp and CYP2D6 in both *in vitro* and *in vivo* DDI studies [58, 59].

PGx Information in Quinidine Drug Labels

Although quinidine is not a substrate of CYP2D6, PGx information is contained in various drugs containing quinidine such as NUEDEXTA® (dextromethorphan/quinidine, see dextromethorphan) [95, 130]. Additionally, the FDA-approved label for quinidine gluconate products notes that caution should be exercised when prescribing quinidine together with drugs metabolized by CYP2D6 [131].

1.3 PHYSIOLOGICALLY BASED PHARMACOKINETIC MODELING

1.3.1 *Concept*

PBPK modeling is a mathematic approach to quantitatively characterize the PK of compounds [132]. Compared to data-driven, empirical model approaches, PBPK modeling represents a more mechanistic technique, integrating anatomical and physiological parameters of the organism (system-dependent parameters) as well as biochemical and physicochemical information on the compound (drug-dependent parameters) [20]. An organism is typically represented as a set of compartments, reflecting important organs and tissues of the body. Here, ordinary differential equations (ODEs) describe mass transfer based on blood flow to and from a given compartment [133]. Drug-dependent parameters are necessary to describe important absorption, distribution, metabolism and excretion (ADME) processes, for instance, to calculate organ permeabilities and partition coefficients or model processes such as enzymatic metabolism, transport, binding, and excretion. Finally, information on the study design including dose, dosing regimen, formulation, route of administration, and food intake, is incorporated into the model. While the concept of PBPK modeling has first been described in 1937, the application of this technique in drug development has only gained momentum in the last decades [134] as PBPK models are highly complex and require substantial computational resources [132]. Today, a wide range of both commercial and non-commercial software solutions are available, providing flexible and modular PBPK modeling frameworks [135].

PBPK model input parameters

History of PBPK modeling and PBPK modeling frameworks

1.3.2 *Applications of PBPK Modeling*

PBPK modeling has been applied in a wide range of areas throughout model-informed drug discovery and development (MID3) as well as in clinical practice. Due to their flexibility and modularity, PBPK models can be used to address research questions in the area of DDIs,

Special Populations

DGI, PD, formulation design and scaling to special populations. These special populations include pediatric, newborn, pregnant, obese or geriatric patient populations as well as patients with organ impairment such as CKD or liver diseases. Regulatory authorities including the FDA and EMA have recognized the enormous potential of PBPK modeling and regularly publish guidance documents on the use of PBPK modeling in drug development [136, 137]. Over recent years, PBPK modeling has increasingly been applied to investigate DGI scenarios [20]. Here, PBPK models have been successfully used to integrate findings from *in vitro* experiments and *in vivo* studies to predict the effect of DGIs on the PK and PD of drugs. These PBPK DGI models can subsequently be applied to answer different research questions such as the investigation of complex DDGI or drug-drug-gene-disease interactions (DDGDIs), to perform virtual trials, develop dose recommendations or answer other "what-if" questions [20]. Finally, PBPK modeling has successfully been applied to investigate and characterize IPV in drug pharmacokinetics, a domain that has been traditionally dominated by classic PK modeling strategies such as population pharmacokinetic (PopPK) modeling [138, 139].

Drug-Gene and Drug-Drug-(Gene) Interaction Modeling

Overall, PBPK modeling provides a valuable tool to support not only the decision-making process in MID3 [140] but also to establish a more personalized approach to drug therapy [9, 141].

2 OBJECTIVES

The objectives of this thesis were (i) to develop and evaluate whole-body PBPK models for important CYP2D6 substrates and inhibitors, (ii) to implement the CYP2D6 activity score-dependent metabolism of the different substrates in the respective models to describe and predict the impact of CYP2D6 activity scores on the PK of the substrates, and (iii) to use the final PBPK models for different DGI and DDGI model applications.

2.1 PROJECT I: PBPK MODELING OF METOPROLOL

The objectives of project I were (i) to develop a whole-body PBPK model of (*R*)- and (*S*)-metoprolol as well as the metabolite α-hydroxymetoprolol (ii) to describe the impact of CYP2D6 activity scores on the PK of metoprolol and (iii) to apply the final PBPK DGI model to generate dose adaptations for metoprolol and compare these adaptations to the current DPWG guideline.

2.2 PROJECT II: PBPK MODELING OF DEXTROMETHORPHAN

The objectives of project II were (i) to develop a parent-metabolite-metabolite PBPK model of dextromethorphan and its metabolites dextrorphan and dextrorphan *O*-glucuronide, (ii) to implement the CYP2D6 activity score-dependent metabolism of dextromethorphan to describe CYP2D6 DGIs and (iii) to investigate the observed IIV in the CYP2D6-mediated metabolism of dextromethorphan for individual subjects sharing the same CYP2D6 activity score.

2.3 PROJECT III: PBPK MODELING OF PAROXETINE, ATOMOXETINE AND RISPERIDONE

The objectives of project III were (i) to develop new whole-body PBPK models of paroxetine and atomoxetine, (ii) implement the scale of CYP2D6 activity score-dependent metabolism of metoprolol and dextromethorphan (projects I and II) into the new models of paroxetine and atomoxetine, as well as an established PBPK model of risperidone [142] and (iii) to apply the final PBPK DGI models to simulate steady-state exposure of paroxetine, atomoxetine and risperidone in different DGI scenarios.

2.4 PROJECT IV: PBPK MODELING OF (*E*)-CLOMIPHENE

The objectives of project IV were (i) to develop a whole-body parent-metabolite model of *(E)*-clomiphene, *(Z)*-clomiphene and its metabolite *(E)*-4-hydroxyclomiphene, *(E)*-N-desethylclomiphene and *(E)*-4-hydroxydesethylclomiphene, (ii) to investigate the effect of CYP2D6 DGIs on the pharmacokinetics of clomiphene and its metabolites and (iii) to predict the effect of CYP2D6 and CYP3A4 DDGIs in scenarios involving CYP2D6 inhibitor paroxetine and CYP3A4 inhibitor clarithromycin on the pharmacokinetics of clomiphene and its metabolites.

2.5 PROJECT V: PBPK MODELING OF QUINIDINE

The objectives of project V were (i) to develop a comprehensive PBPK parent-metabolite model of quinidine and its major metabolite 3-hydroxyquinidine, (ii) to investigate complex CYP3A4 and P-gp DDIs of the victim drug quinidine within a comprehensive interaction network incorporating perpetrator drugs carbamazepine, cimetidine, fluvoxamine, itraconazole, omeprazole, rifampicin and verapamil, and (iii) to investigate P-gp DDIs and CYP2D6 DDGIs with quinidine acting as a perpetrator including victim drugs digoxin (P-gp substrate), dextromethorphan, mexiletine, metoprolol (CYP2D6 substrates) and paroxetine (CYP2D6 substrate and inhibitor of CYP2D6 and CYP3A4).

3 METHODS

3.1 SOFTWARE

PBPK models were developed in PK-Sim® and MoBi® (Open Systems Pharmacology Suite 9 (projects I, II and IV), 10 (project III) and 11 (project V) www.open-systems-pharmacology.org). Clinical study data were digitized with GetData Graph Digitizer® 2.26.0.20 (S. Fedorov, http://www.getdata-graph-digitizer.com) (projects I–IV) or Engauge Digitizer 10.12 (M. Mitchell, https://markummitchell.github.io/engauge-digitizer) (project V) from the published literature according to best practices [143]. Sensitivity analyses and model parameter optimizations (Monte Carlo algorithm) were performed within PK-Sim®. Calculation of pharmacokinetic parameters, model performance metrics and the generation plots were achieved using Python 3.7.4 (project I), 3.9.1 (project II) or 3.10.4 (project III), Python Software Foundation, Wilmington, DE, USA or the R programming language 3.6.3 (project IV) or 4.2.1 (project V), The R Foundation for Statistical Computing, Vienna, Austria. Regression analyses were performed using ordinary least squares (OLS) regression utilizing the *statsmodels* package 0.12.2 (project II) or 0.13.2 (project III), https://www.statsmodels.org/stable in Python [144].

3.2 PHYSIOLOGICALLY BASED PHARMACOKINETIC MODELING

The PBPK models developed in project I (metoprolol), project II (dextromethorphan), project III (paroxetine and atomoxetine), project IV ((*E*)-clomiphene) and project V (quinidine) were built according to the workflow described below. For risperidone (project III) PBPK modeling, a previously published PBPK model [142] was used and extended by the DGI modeling approach described in Section 3.2.7.

3.2.1 *PBPK Modeling Workflow*

The PBPK modeling workflow for projects I–V included (i) the collection of clinical data, (ii) PBPK base model building and (iii) PBPK base model evaluation. Different approaches were used to (iv) develop DGI models for projects I–IV (see Section 3.2.7). After (v) DGI model evaluation (projects I–IV), (vi) the developed PBPK models were used for different model applications (projects I–V). Figure 3.1 shows the PBPK DGI modeling workflow for projects I–IV.

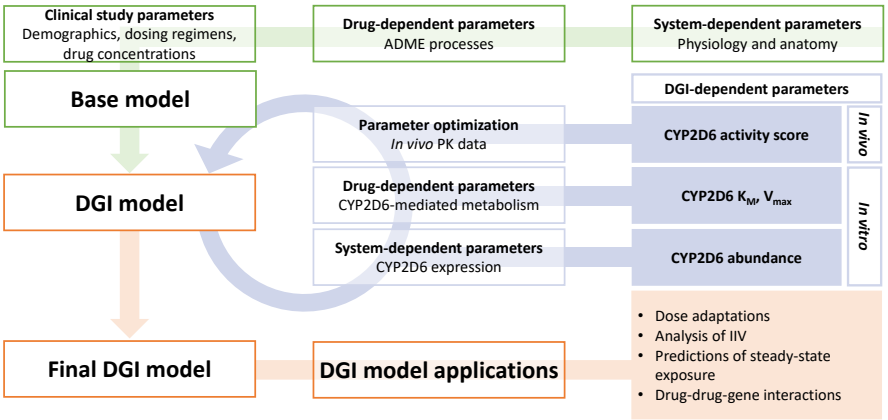

Figure 3.1: **CYP2D6 DGI modeling workflow.** The base model is developed with system-dependent, drug-dependent, and clinical study parameters (green path). Model refinement and implementation of DGI-relevant input parameters is achieved in a learn-and-confirm cycle (blue path). DGI-dependent parameter values can be identified and measured in different systems and used to describe the activity score dependent metabolism of CYP2D6 substrates. The final DGI models can be used for applications such as the investigation of DGI effects or dose adaptations (orange path). ADME: absorption, distribution, metabolism and excretion, DGI: drug-gene interaction, IIV: interindividual variability, K_M: Michaelis-Menten constant, V_{max}: maximum reaction velocity. Figure adapted from Türk et al. [20].

3.2.2 *Clinical Study Data*

Clinical data including individual and aggregated plasma concentration-time profiles were collected from the published literature. Different routes of administration (intravenous (iv) and oral), dosing regimen (single dose (sd) and multiple dose (md)) as well as different formulations (immediate release and extended release) were considered. Demographic data on study populations or individual participants (sex, age, weight and height) were extracted for all modeled studies. Additionally, data on CYP2D6 activity (phenotype, genotype or activity score) were collected where available.

3.2.3 *Dataset Assignment*

Collected clinical data were split into a training dataset (model development) and a test dataset (model evaluation). Studies for the training dataset were predominately selected to cover: (i) different routes of administration or different formulations, (ii) a wide dose range or different dosing regimen and (iii) comparisons of the effect of different CYP2D6 activity levels on the PK of the respective drug.

3.2.4 *PBPK Base Model Building*

Physicochemical properties were collected from the published literature alongside information on important ADME processes. Subsequently, PBPK base models were built following a sequential approach using individual simulations based on typical individuals (mean or median) for the respective study population. First, appropriate quantity structure-activity relationship (QSAR) methods for the estimation of partition coefficients and cellular permeabilities were selected based on the smallest residual error by fitting simulations after iv administration of the respective compound to their observed data. Second, simulations of administrations of oral solutions were optimized against their observed data to inform intestinal permeability. Simulations of poor metabolizers were fitted to their observed data to inform metabolic parameters for the CYP2D6-independent pathways of the substrate's metabolism. Finally, parameters for CYP2D6-mediated metabolism were estimated by fitting simulations of extensive metabolizers to their observed data. Here, the term *extensive metabolizer* was used to group individuals and populations that were either phenotyped using traditional phenotyping methods or not phenotyped.

3.2.5 *PBPK Base Model Evaluation*

A combination of graphical and statistical methods was used to evaluate the PBPK base model performance. Predicted plasma concentration-time profiles (arithmetic mean $\pm$ standard deviation (SD)) were plotted alongside their observed for graphical comparison. For this, virtual populations of 100 (project I) or 1000 (projects II–V) individuals were created based on reported demographic data of the respective study population. Variability in population demographics (age, weight, height, organ weight, blood flow rates and tissue composition) was accounted for by sampling the respective parameters according to the implemented algorithm in PK-Sim®. Additionally, variability on relevant transporter and enzyme expression was implemented according to the PK-Sim® ontogeny database [145].

Goodness-of-fit plots were generated by plotting the predicted arithmetic mean of population predicted plasma concentrations against the respective observed data. Similarly, predicted compared to observed AUC from the time of the first concentration measurement to the time of the last concentration measurement (AUC_{last}) and maximum plasma concentration (C_{max}) values were plotted in goodness-of-fit plots. Statistical methods to assess model performance included the calculation of the mean relative deviation (MRD) of predicted plasma concentrations and the geometric mean fold error (GMFE) of predicted

AUC_{last} and C_{max} values for all simulations according to equations 3.1 and 3.2, respectively.

$$MRD = 10^x; x = \sqrt{\frac{\sum_{i=1}^{k}(\log_{10}\hat{c}_i - \log_{10}c_i)^2}{k}} \tag{3.1}$$

where $\hat{c}_i$ = i-th predicted plasma concentration and c_i = i-th observed plasma concentration, k = number of observations.

$$GMFE = 10^x; x = \frac{\sum_{i=1}^{m}\left|\log_{10}\left(\frac{\hat{\rho}_i}{\rho_i}\right)\right|}{m} \tag{3.2}$$

where $\hat{\rho}_i$ = predicted AUC_{last} or C_{max} of study i, ρ_i = observed AUC_{last} or C_{max} of study i, m = total number of studies.

3.2.6 *Local Sensitivity Analysis*

Local sensitivity analyses were performed to quantify the impact of individual model parameters on the the predicted AUC from 0 to 24 hours (AUC_{0-24h}) of the respective compound. Here, simulations of a single oral standard dose were used to perform sensitivity analyses using a relative perturbation of 1000% (variation range = 10, maximum number of steps = 9). Generally, parameters were included if they (i) had been optimized, (ii) were associated with optimized parameters or (iii) might have a strong impact due to calculation and QSAR methods used. Sensitivity to a parameter was calculated according to equation 3.3.

$$S = \frac{\Delta AUC_{0-24h}}{\Delta p} \times \frac{p}{AUC_{0-24h}} \tag{3.3}$$

where S = sensitivity of the AUC_{0-24h} to the examined model parameter, ΔAUC_{0-24h} = relative change of the AUC_{0-24h} to the respective parameter, Δp = relative variation of the parameter, p = parameter value and AUC_{0-24h} = simulated AUC_{0-24h} of the respective compound.

Parameters with associated sensitivity values >0.5 were considered sensitive, reflecting a >50% change in the AUC_{0-24h} of the respective compound when the parameter was varied by 100%.

3.2.7 *DGI Model Building*

CYP2D6-mediated metabolic pathways were modeled using Michaelis-Menten kinetics according to equation 3.4.

$$v = \frac{v_{max} \times [S]}{K_M + [S]} = \frac{k_{cat} \times [E] \times [S]}{K_M + [S]} \tag{3.4}$$

where v = reaction velocity, v_{max} = maximum reaction velocity, [S] = substrate concentration, K_M = Michaelis-Menten constant, k_{cat} = catalytic rate constant, [E] = enzyme concentration.

CYP2D6 Michaelis-Menten constant (K_M) values were kept constant over the whole range of modeled CYP2D6 activity. In projects I–II, CYP2D6 activity was described by optimizing catalytic rate constant (k_{cat}) values for all modeled activity scores, separately. For project III, CYP2D6 k_{cat} values were optimized for populations with an activity score of 2. Subsequently, catalytic rate constant relative to activity score 2 ($k_{cat,\,rel}$) values obtained from optimizations for project I–II were then analyzed using OLS regression with a polynomial of degree 2 and no intercept. Finally, the resulting regression equation was used to calculate relative k_{cat} values for the remaining activity scores. Generally, CYP2D6 poor metabolizers (activity score = 0) were assumed to have no (0%) CYP2D6 activity, whereas normal metabolizers with an activity score of 2 were assumed to correspond to 100% CYP2D6 activity. For projects I–III, $k_{cat,\,rel}$ values were then calculated according to equation 3.5.

$$k_{cat,rel,AS=i} = \frac{k_{cat,AS=i}}{k_{cat,AS=2}} \times 100\% \tag{3.5}$$

where $k_{cat,rel,AS=i}$ = relative k_{cat} for population with the investigated activity score i, $k_{cat,AS=i}$ = k_{cat} for population with the investigated activity score i, $k_{cat,AS=2}$ = k_{cat} for populations with an activity score of 2.

For project IV, CYP2D6 k_{cat} values for the different activity scores were extrapolated from *in vitro* data on CYP2D6 activity score-dependent formation rates of the respective metabolites according to equation 3.6.

$$k_{cat,AS=i} = k_{cat,AS=2} \times IVSF_i \tag{3.6}$$

where $k_{cat,AS=i}$ = k_{cat} for population with the investigated activity score i, $k_{cat,AS=2}$ = k_{cat} for population with activity score of two, $IVSF_i$ = in vitro scaling factor (IVSF) for population with the investigated activity score i.

3.2.8 *DD(G)I Model Network Building*

The performance of (*E*)-clomiphene (project IV) and quinidine (project V) models to predict various DDGI scenarios was assessed by linking the respective models to other published PBPK models. The (*E*)-clomiphene victim model was linked to the models of the strong CYP2D6 inhibitor paroxetine (developed in project III) and the strong CYP3A4 inhibitor clarithromycin [58, 146]. The quinidine model was assessed as a victim drug for CYP3A4 and P-gp-mediated interactions and linked to perpetrator PBPK models of carbamazepine [147],

cimetidine [148], fluvoxamine [149], itraconazole [146], omeprazole [150], rifampicin [146] and verapamil [151]. Additionally, quinidine model performance as a perpetrator drug inhibiting CYP2D6 and P-gp was assessed linking the quinidine model to models of dextromethorphan (developed in project II), digoxin [146], metoprolol (developed in project I), mexiletine [150] and paroxetine (developed in project III).

3.2.9 *Effect Model Evaluation*

To evaluate the effects of DGIs (projects I–IV), DDIs and DDGIs (projects IV–V), predicted plasma concentration-time profiles were plotted against their corresponding observed data for populations with variant CYP2D6 activity scores and/or drug co-administration (effect) and compared to profiles of populations with normal CYP2D6 activity (corresponding to an activity score of 2 or extensive metabolizer phenotype) and/or administrations of the victim drug alone (reference). Here, reference CYP2D6 activity was defined as an activity score of 2 or an extensive metabolizer phenotype for DGI, DDI and DDGI studies where only CYP2D6 phenotypes were reported. Moreover, predicted effect PK ratios (AUC_{last} and C_{max} ratios) were calculated for DGI, DDI and DDGI scenarios according to equation 3.7 and GMFE values were calculated for PK ratios according to equation 3.2.

$$\text{Effect PK ratio} = \frac{PK_{Effect}}{PK_{Reference}} \tag{3.7}$$

where Effect PK ratio = PK ratio (C_{max} or AUC_{last} ratio) for the investigated effect (variant activity and/or drug co-administration), PK_{Effect} = PK value of the population with the investigated effect and $PK_{Reference}$ = PK value of the respective reference (normal CYP2D6 activity and/or victim drug alone) population.

4 RESULTS

4.1 PROJECT I: PHYSIOLOGICALLY BASED PHARMACOKINETIC MODELING OF METOPROLOL ENANTIOMERS AND α-HYDROXYMETOPROLOL TO DESCRIBE CYP2D6 DRUG-GENE INTERACTIONS

Publication

The following original research article has been published in the peer-reviewed journal *Pharmaceutics*:

Rüdesheim, S.; Wojtyniak, J.-G.; Selzer, D.; Hanke, N.; Mahfoud, F.; Schwab, M.; Lehr, T. Physiologically Based Pharmacokinetic Modeling of Metoprolol Enantiomers and α-Hydroxymetoprolol to Describe CYP2D6 Drug-Gene Interactions. *Pharmaceutics* **2020**, *12*, 1200, DOI: 10.3390/pharmaceutics12121200.

Supplementary Material

The supplementary material to this publication can be accessed via this link.

Copyright

Author Contributions

Author contributions according to CRediT [6]:

Simeon Rüdesheim	Conceptualization, Investigation, Writing–Original Draft, Writing–Review & Editing
Jan-Georg Wojtyniak	Investigation, Writing–Review & Editing
Dominik Selzer	Conceptualization, Writing–Original Draft, Writing–Review & Editing
Nina Hanke	Conceptualization, Writing–Original Draft, Writing–Review & Editing
Felix Mahfoud	Writing–Review & Editing
Matthias Schwab	Funding Acquisition, Writing–Review & Editing
Thorsten Lehr	Conceptualization, Funding Acquisition, Investigation, Writing–Original Draft, Writing–Review & Editing

pharmaceutics

MDPI

Article

Physiologically Based Pharmacokinetic Modeling of Metoprolol Enantiomers and α-Hydroxymetoprolol to Describe CYP2D6 Drug-Gene Interactions

Simeon Rüdesheim [1,2], Jan-Georg Wojtyniak [1,2], Dominik Selzer [1], Nina Hanke [1], Felix Mahfoud [3,4], Matthias Schwab [2,5,6] and Thorsten Lehr [1,*]

1 Clinical Pharmacy, Saarland University, 66123 Saarbrücken, Germany; simeon.ruedesheim@uni-saarland.de (S.R.); jangeorg.wojtyniak@uni-saarland.de (J.-G.W.); dominik.selzer@uni-saarland.de (D.S.); n.hanke@mx.uni-saarland.de (N.H.)
2 Dr. Margarete Fischer-Bosch—Institute of Clinical Pharmacology, 70376 Stuttgart, Germany; matthias.schwab@ikp-stuttgart.de
3 Department of Internal Medicine III, Cardiology, Angiology, Intensive Care Medicine, Saarland University Medical Center and Saarland University Faculty of Medicine, 66421 Homburg, Germany; felix.mahfoud@uks.eu
4 Institute for Medical Engineering and Science, Massachusetts Institute of Technology, Cambridge, MA 02139, USA
5 Departments of Clinical Pharmacology, Pharmacy and Biochemistry, University of Tübingen, 72076 Tübingen, Germany
6 Cluster of Excellence iFIT (EXC2180) "Image-Guided and Functionally Instructed Tumor Therapies", University of Tübingen, 72076 Tübingen, Germany
* Correspondence: thorsten.lehr@mx.uni-saarland.de; Tel.: +49-681-302-70255

Received: 10 November 2020; Accepted: 5 December 2020; Published: 11 December 2020

check for updates

Abstract: The beta-blocker metoprolol (the sixth most commonly prescribed drug in the USA in 2017) is subject to considerable drug–gene interaction (DGI) effects caused by genetic variations of the *CYP2D6* gene. CYP2D6 poor metabolizers (5.7% of US population) show approximately five-fold higher metoprolol exposure compared to CYP2D6 normal metabolizers. This study aimed to develop a whole-body physiologically based pharmacokinetic (PBPK) model to predict CYP2D6 DGIs with metoprolol. The metoprolol (*R*)- and (*S*)-enantiomers as well as the active metabolite α-hydroxymetoprolol were implemented as model compounds, employing data of 48 different clinical studies (dosing range 5–200 mg). To mechanistically describe the effect of CYP2D6 polymorphisms, two separate metabolic CYP2D6 pathways (α-hydroxylation and *O*-demethylation) were incorporated for both metoprolol enantiomers. The good model performance is demonstrated in predicted plasma concentration–time profiles compared to observed data, goodness-of-fit plots, and low geometric mean fold errors of the predicted AUC_{last} (1.27) and C_{max} values (1.23) over all studies. For DGI predictions, 18 out of 18 DGI AUC_{last} ratios and 18 out of 18 DGI C_{max} ratios were within two-fold of the observed ratios. The newly developed and carefully validated model was applied to calculate dose recommendations for CYP2D6 polymorphic patients and will be freely available in the Open Systems Pharmacology repository.

Keywords: physiologically based pharmacokinetic (PBPK) modeling; metoprolol; metoprolol enantiomers; α-hydroxymetoprolol; drug-gene interactions (DGIs); cytochrome P450 2D6 (CYP2D6); dose adaptation; model-informed precision dosing

1. Introduction

Metoprolol is one of the most frequently administered beta-blockers in the U.S. with well over 50 million total prescriptions per year [1]. It is used in the treatment of hypertension, coronary artery disease, heart failure, and arterial fibrillation [2]. Metoprolol is listed by the U.S. Food and Drug Administration (FDA) as a moderately sensitive substrate for clinical drug-drug interaction (DDI) studies as it is predominantly metabolized by cytochrome P450 2D6 (CYP2D6) [3].

CYP2D6 is an important drug metabolizing enzyme which is estimated to contribute to the metabolism of 15–25% of all clinically used drugs [4,5]. The gene encoding CYP2D6 is subject to different genetic variations, ranging from null alleles to several-fold amplification [5], resulting in considerable phenotypical interindividual differences in CYP2D6-dependent drug metabolism [6]. The main purpose of the CYP2D6 activity score (AS) is to translate a patients' *CYP2D6* genotype to the corresponding phenotype [7]. For this, *CYP2D6* alleles are assigned a value indicating no (0), decreased (0.25 or 0.5), normal function (1), or a copy number variation of a normal function allele (2). However, as this assignment is based on semiquantitative observations, an activity score of 0.5 does not necessarily imply a reduction of enzymatic activity by 50% [6,8]. Nevertheless, the activity score has been shown to correlate well with metoprolol oral clearance in vivo [9]. Yet, considerable interindividual variability in metoprolol plasma concentrations, caused by genetic components independent of the *CYP2D6* genotype, such as the rs5758550 SNP, has been observed [9,10].

Metoprolol is a BCS Class I drug, characterized by high permeability and high solubility. After its rapid absorption, metoprolol undergoes extensive first-pass metabolism, reducing its bioavailability to 40% in CYP2D6 normal metabolizers (NMs), whereas bioavailability approaches 100% in poor metabolizers (PMs) [11]. Only 12% of metoprolol are bound to plasma proteins, primarily albumin [12]. *O*-demethylation, α-hydroxylation, and *N*-dealkylation by CYP2D6 and, to lesser extents, CYP2B6, CYP2C9, and CYP3A4, are described as the pathways of metoprolol metabolism [13,14]. Of the major metabolites, α-hydroxymetoprolol is of particular clinical interest, as it is pharmacologically active, exhibiting 10% of the β_1-blocking activity of metoprolol [15], and it is almost exclusively formed via CYP2D6 [16]. Therefore, α-hydroxymetoprolol/metoprolol urinary metabolic ratios are employed for CYP2D6 phenotyping [17]. Overall, CYP2D6 is estimated to be responsible for 80% of metoprolol metabolism in normal metabolizers [14]. Depending on the CYP2D6 phenotype, only 1.5–12% of orally administered metoprolol are excreted unchanged in urine [18].

Metoprolol is a chiral molecule, marketed as a racemic mixture of *(R)*- and *(S)*-metoprolol, even though its enantiomers differ in their pharmacodynamic and pharmacokinetic properties. The (*S*)-enantiomer has been shown to be 33-fold more potent in blocking β_1-adrenoceptors in rats than the (*R*)-enantiomer [19]. Moreover, in ultrarapid metabolizers (UMs) and normal metabolizers, but not in poor metabolizers, the (*S*)-metoprolol area under the plasma concentration–time curve (AUC) is significantly higher than the AUC of *(R)*-metoprolol, showing the enantiopreference of CYP2D6 towards the (*R*)-enantiomer [18,20]. The distribution of *CYP2D6* genotypes varies substantially between ethnicities. For instance, 5.7% of the US and 0.9% of Middle Eastern or Oceanian populations were found to be poor metabolizers (AS = 0), whereas the prevalence of ultrarapid metabolizers (AS > 2) was 2.2% in the US and 11.2% in Middle Eastern or Oceanian populations [21,22]. Interestingly, the reduced-function *CYP2D6*10* allele occurs more often in East Asian populations than the *CYP2D6*1* allele (42% vs. 34%), which results in an overall decreased CYP2D6 activity compared to other populations [23].

Previously published metoprolol PBPK models were either based on traditional CYP2D6 phenotypes [24,25] or did not take CYP2D6 DGIs into consideration [26,27]. Moreover, none of the previously published metoprolol PBPK models incorporated the metoprolol (*R*)- and (*S*)-enantiomers to describe the enantioselective metabolism via CYP2D6.

This study aimed to develop and qualify a novel, whole-body physiologically based pharmacokinetic (PBPK) model of metoprolol to describe the effects of the different *CYP2D6* genotypes and the resulting activity scores on the pharmacokinetics of metoprolol. The resulting drug–gene interaction (DGI) PBPK model includes (*R*)- and *(S)*-metoprolol with their specific CYP2D6

activity score-dependent metabolism, as well as the metabolite α-hydroxymetoprolol. In addition, the established model was applied to generate metoprolol dose adaptations for patients with different CYP2D6 activity scores and these adaptations were compared to a current guideline [28]. The model was developed as a whole-body PBPK model to allow future model applications such as DDI modeling, model scaling to special populations or PBPK-PD modeling. The final PBPK model will be publicly available in the Open Systems Pharmacology (OSP) repository (www.open-systems-pharmacology.org) [29] as a clinical research tool, and the Supplementary Materials to this article provide a detailed and transparent evaluation of the model performance to be used as a reference manual and evaluation report.

2. Materials and Methods

2.1. Software

PBPK modeling, model parameter optimization (Monte Carlo algorithm), and local sensitivity analysis were performed using PK-Sim® and MoBi® (Open Systems Pharmacology Suite 9.1). Published clinical study data were digitized with GetData Graph Digitizer 2.26.0.20 (© S. Fedorov) according to best practices [30]. Pharmacokinetic parameters (area under the plasma concentration-time curve from the time of the first concentration measurement to the time of the last concentration measurement (AUC_{last}) and maximum plasma concentration (C_{max})) and model performance metrics (mean relative deviation (MRD), geometric mean fold error (GMFE), DGI AUC_{last}, and C_{max} ratios) were calculated using Python (version 3.7.4, Python Software Foundation, Wilmington, DE, USA) in Visual Studio Code (version 1.49.1, Microsoft Corporation, Redmond, WA, USA). Plots were also generated using Python in Visual Studio Code.

2.2. PBPK Model Building

The PBPK model building was initiated with an extensive literature search to gather information on metoprolol absorption, distribution, metabolism, and excretion (ADME) processes, to obtain physicochemical data and to collect clinical studies of the intravenous and oral administration of metoprolol, in single- and multiple-dose regimens, performed in healthy individuals. Subsequently, plasma concentration-time profiles from the published clinical studies were digitized and split into a training dataset, for model building, and a test dataset, for model evaluation. Studies for model training were selected to include different routes of administration (intravenous and oral), a wide range of administered doses, single- and multiple-dose regimens, as well as stratification for *CYP2D6* genotype or activity score. The training dataset was used for estimation of model input parameters which could not be obtained from literature.

The metoprolol PBPK model was built in a stepwise approach. First, appropriate quantitative structure-activity relationship (QSAR) methods to estimate the cellular permeabilities and partition coefficients (e.g., Rodgers & Rowland, Berezhkovskiy) were selected, by fitting simulations of intravenous metoprolol administration to their observed data. Subsequently, studies of orally administered metoprolol in poor metabolizers were used to optimize parameters independent of CYP2D6 metabolism. A single study in which metoprolol was administered as an oral solution was used to optimize the intestinal permeability for both metoprolol enantiomers [31]. Finally, *(R)*- and *(S)*-enantiomer CYP2D6 catalytic rate constant (k_{cat}) values were optimized for studies of the training dataset where the volunteers were either normal metabolizers or not phenotyped. Racemic metoprolol plasma concentration–time profiles were modeled by the administration of racemic doses of metoprolol (50% (*R*)- and 50% (*S*)-metoprolol and the use of a customized "observer" within PK-Sim®, which adds up the simulated (*R*)- and (*S*)-metoprolol plasma concentrations to directly display the racemic metoprolol plasma concentration–time profiles. Figure 1 provides an overview of metoprolol metabolic pathways.

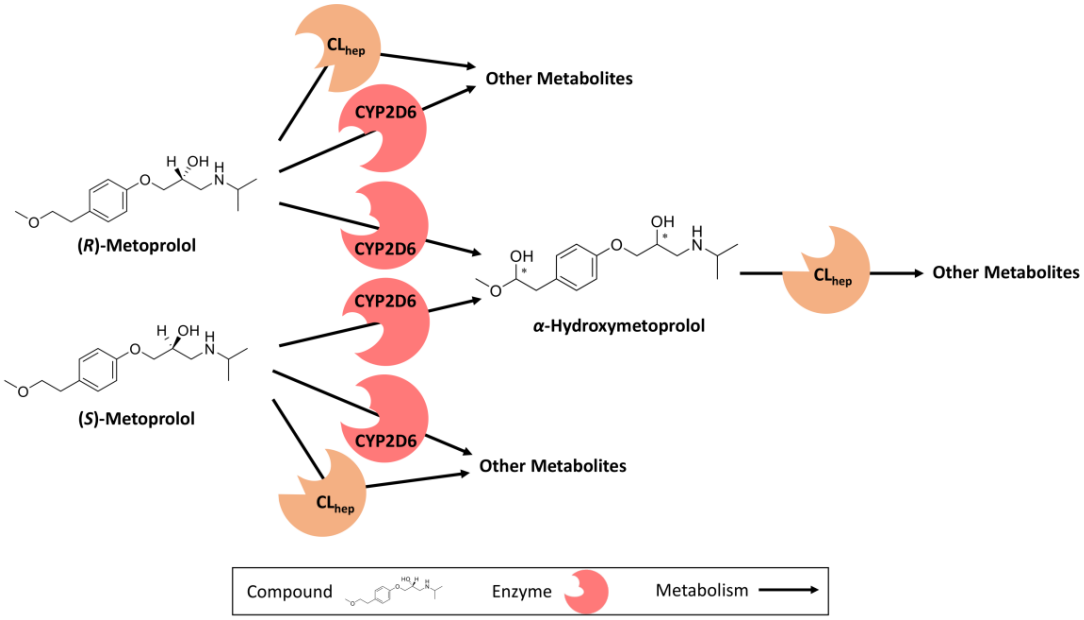

Figure 1. Implemented metoprolol metabolic pathways. (*R*)- and (*S*)-metoprolol are both metabolized via two different CYP2D6-dependent metabolic pathways: α-hydroxylation and *O*-demethylation, as well as by an unspecific hepatic clearance process. The four α-hydroxymetoprolol diastereomers (stereocenters are marked with asterisks) were modeled as one single compound due to lacking published clinical data. CL_{hep}: hepatic clearance, CYP2D6: cytochrome P450 2D6.

Supplementary Table S2.2.1 contains information concerning all studies included in the training and test datasets. Supplementary Table S4.0.1 provides system-dependent parameters with technical details on the implementation of CYP2D6.

2.3. DGI Modeling

The metoprolol clearance processes via CYP2D6 were implemented using Michaelis–Menten kinetics according to Equation (1) [32]:

$$v = \frac{v_{max} \cdot S}{K_m + S} = \frac{k_{cat} \cdot E \cdot S}{K_m + S} \quad (1)$$

where v = reaction velocity, v_{max} = maximum reaction velocity, S = free substrate concentration, K_m = Michaelis-Menten constant, k_{cat} = catalytic rate constant, and E = enzyme concentration.

CYP2D6 Michaelis–Menten constant (K_m) values were kept constant over the whole range of modeled activity scores. CYP2D6 k_{cat} values were optimized for each activity score separately. CYP2D6 poor metabolizers (AS = 0) were assumed to show no CYP2D6 activity (0%), whereas populations with two wildtype alleles (AS = 2) were used as reference (100%) to calculate relative k_{cat} values according to Equation (2).

$$k_{cat,\ rel,\ AS=i} = \frac{k_{cat,\ AS=i}}{k_{cat,\ AS=2}} \times 100\% \quad (2)$$

where $k_{cat,\ rel,\ AS=i} = k_{cat}$ for the investigated activity score relative to AS = 2, $k_{cat,\ AS=i} = k_{cat}$ for the investigated activity score, and $k_{cat,\ AS=2} = k_{cat}$ for AS = 2.

The assignment of activity scores was carried out according to [33] as described in Table 1.

Table 1. CYP2D6 activity score assignment according to [33].

Activity Score	Projected Phenotype	Examples of Relevant *CYP2D6* Genotypes
0	PM	**3/*3, *3/*4, *4/*4, *5/*6*
0.25	IM	**4/*10, *5/*10*
0.5		**4/*41, *5/*17, *10/*10*
0.75		**17/*10, *41/*10*
1		**1/*4, *2/*5, *17/*17, *17/*41*
1.25	NM	**1/*10, *2/*10, *35/*10*
1.5		**1/*41, *2/*17, *35/*41*
2		**1/*1, *1/*2, *2/*35*
2.25		**1x2/*17, *35x2/*41*
>2.25	UM	**1/*1x3, *1/*35x2, *2x2/*9*

CYP2D6: Cytochrome P450 2D6, IM: intermediate metabolizer, NM: normal metabolizer, PM: poor metabolizer, UM: ultrarapid metabolizer.

2.4. PBPK Model Evaluation

The performance of the metoprolol PBPK model regarding the prediction of racemic metoprolol, its enantiomers and α-hydroxymetoprolol was evaluated using graphical and statistical methods. First, predicted plasma concentration-time profiles were compared graphically with the profiles measured in the respective clinical studies by plotting model population predictions (arithmetic mean ± SD) together with observed data points. For this purpose, virtual populations of 100 individuals were created based on the population characteristics stated in the respective publication. System-dependent parameters, such as age, weight, height, organ weights, blood flow rates, tissue composition, etc., were varied by the implemented algorithm in PK-Sim. A comprehensive description of virtual populations is given in Supplementary Section S1.1.3. Second, the plasma concentration values of all studies predicted using the arithmetic mean of the population were plotted against their corresponding observed values in goodness-of-fit plots.

In addition, model performance was evaluated by a comparison of predicted to observed AUC values and C_{max} values. All AUC values (predicted as well as observed) were calculated from the time of the first concentration measurement to the time of the last concentration measurement (AUC_{last}).

As quantitative measures of the model performance, the MRD of all predicted plasma concentrations (Equation (3)) and the GMFE of all predicted AUC_{last} and C_{max} values (Equation (4)) were calculated.

$$\mathrm{MRD} = 10^{x};\ x = \sqrt{\frac{\sum_{i=1}^{k} \left(\log_{10}\hat{c}_i - \log_{10}c_i\right)^2}{k}} \tag{3}$$

where $\hat{c}_i$ = predicted plasma concentration that corresponds to the *i*-th observed concentration, c_i = *i*-the observed plasma concentration, and k = number of observed values.

$$\mathrm{GMFE} = 10^{x};\ x = \frac{\sum_{i=1}^{m}\left|\log_{10}\left(\frac{\hat{\rho}_i}{\rho_i}\right)\right|}{m} \tag{4}$$

where $\hat{\rho}_i$ = predicted AUC_{last} or C_{max} value of study i, ρ_i = corresponding observed AUC_{last} or C_{max} value of study i, and m = number of studies.

A detailed description of the local sensitivity analysis is provided in Supplementary Section S1.2.2.

2.5. DGI Modeling Evaluation

The DGI modeling performance was assessed by a comparison of predicted versus observed plasma concentration–time profiles of racemic metoprolol, its enantiomers, and α-hydroxymetoprolol.

Furthermore, predicted DGI AUC_{last} ratios (Equation (5)) and DGI C_{max} ratios (Equation (6)) were evaluated to assess, if the impact of the observed DGIs was well described by the model.

$$\text{DGI } AUC_{last} \text{ ratio } = \frac{AUC_{last,\ DGI}}{AUC_{last,\ reference}} \tag{5}$$

where $AUC_{last,\ DGI}$ = AUC_{last} of variant activity score or phenotype, while $AUC_{last,\ reference}$ = AUC_{last} of AS = 2 or normal metabolizer phenotype.

$$\text{DGI } C_{max} \text{ ratio } = \frac{C_{max,\ DGI}}{C_{max,\ reference}} \tag{6}$$

where $C_{max,\ DGI}$ = C_{max} of variant activity score or phenotype, $C_{max,\ reference}$ = C_{max} of AS = 2 or normal metabolizer phenotype. As a quantitative measure of the prediction accuracy, GMFE values of the predicted DGI AUC_{last} ratios and DGI C_{max} ratios were calculated according to Equation (4).

3. Results

3.1. Metoprolol PBPK Model Development and Evaluation

A total of 48 clinical studies concerning the intravenous or oral administration of metoprolol were used in the model development process, with doses ranging from 5 to 200 mg metoprolol in single or multiple dose regimens. Of the 48 studies, nine included measurements of the metabolite α-hydroxymetoprolol and 16 studies included measurements of the metoprolol enantiomers.

Metoprolol enantiomers were modeled as stand-alone compounds, to allow for the implementation of enantioselective CYP2D6 metabolism. The four α-hydroxymetoprolol diastereomers were modeled as one single compound, due to a lack of enantiomeric differentiation in the published clinical data.

For both metoprolol enantiomers, enantioselective metabolism via CYP2D6, an unspecific hepatic clearance process, as well as passive glomerular filtration were implemented. Each of the metoprolol enantiomers can be metabolized via CYP2D6 to produce either α-hydroxymetoprolol or to generate other metabolites such as *O*-demethylmetoprolol which were not included as separately modeled compounds. The metabolite α-hydroxymetoprolol is eliminated via an unspecific hepatic clearance process. Figure 1 depicts a schematic overview of the implemented metabolic pathways. The drug-dependent model input parameters of the metoprolol enantiomers are presented in Table 2. The drug-dependent parameters of the α-hydroxymetoprolol model are provided in Supplementary Table S2.4.3.

Overall, the PBPK model accurately described and predicted the plasma concentration–time profiles of metoprolol and α-hydroxymetoprolol after intravenous and oral administration, as illustrated in Figure 2. This figure presents population predictions of selected clinical studies from the test and training datasets. Plots documenting the model performance for all 48 clinical studies included in this analysis are provided in Supplementary Sections S2.5 and S3.2. All simulated plasma profiles are in good agreement with the observed metoprolol racemate, (*R*)-, and (*S*)-metoprolol as well as α-hydroxymetoprolol plasma concentrations.

Table 2. (*R*)- and (*S*)-metoprolol drug-dependent model parameters.

Parameter	Unit	(*R*)-Metoprolol				(*S*)-Metoprolol				Description
		Value	Source	Literature	Reference	Value	Source	Literature	Reference	
MW	g/mol	267.36	Lit.	267.36	[34]	267.36	Lit.	267.36	[34]	Molecular weight
pK_a (base)	-	9.7	Lit.	9.70	[34]	9.7	Lit.	9.70	[34]	Acid dissociation constant
Solubility tart. (pH 7.4)	g/mL	1.00	Lit.	1.00	[35]	1.00	Lit.	1.00	[35]	Solubility
Solubility succ. (pH 5.5)	g/mL	0.16	Lit.	0.16	[36]	0.16	Lit.	0.16	[36]	Solubility
logP	-	1.77	Lit.	1.77	[37]	1.77	Lit.	1.77	[37]	Lipophilicity
f_u	%	88	Lit.	88	[38]	88	Lit.	88	[38]	Fraction unbound
CYP2D6 $K_m \rightarrow \alpha$HM	µmol/L	10.08	Lit.	10.08 ‡	[39]	10.75	Lit.	10.75 ‡	[39]	Michaelis-Menten constant
CYP2D6 $k_{cat} \rightarrow \alpha$HM	1/min	6.02	Optim. †	7.50	[39]	6.55	Optim. †	8.27	[39]	Catalytic rate constant
CYP2D6 $K_m \rightarrow$ ODM	µmol/L	8.82	Lit.	8.82 ‡	[39]	12.43	Lit.	12.43 ‡	[39]	Michaelis-Menten constant
CYP2D6 $k_{cat} \rightarrow$ ODM	1/min	9.87	Optim. †	12.30	[39]	8.21	Optim. †	10.37	[39]	Catalytic rate constant
$CL_{hep., unsp.}$	1/min	0.08	Optim.	-	-	0.09	Optim.	-	-	Unspecific hepatic clearance
GFR fraction	-	1.00	Asm.	-	-	1.00	Asm.	-	-	Filtered drug in the urine
EHC continuous fraction	-	1.00	Asm.	-	-	1.00	Asm.	-	-	Bile fraction cont. released
Intestinal permeability	cm/min	4.14×10^{-5}	Optim.	1.12×10^{-5}	Calc. [40]	4.14×10^{-5}	Optim.	1.12×10^{-5}	Calc. [40]	Transcellular intestinal perm.
Cellular permeability	cm/min	4.64×10^{-3}	Calc.	PK-Sim	[32]	4.64×10^{-3}	Calc.	PK-Sim	[32]	Perm. into the cellular space
Partition coefficients	-	Diverse	Calc.	R&R	[41,42]	Diverse	Calc.	R&R	[41,42]	Cell to plasma partitioning
NR Weibull time parameter	min	12.31	Optim.	-	[43,44]	12.31	Optim.	-	[43,44]	Dissolution time (50%)
NR Weibull shape parameter	-	0.72	Optim.	-	[43,44]	0.72	Optim.	-	[43,44]	Dissolution profile shape
CR Weibull time parameter	min	331.92	Optim.	-	[45]	331.92	Optim.	-	[45]	Dissolution time (50%)
CR Weibull shape parameter	-	1.53	Optim.	-	[45]	1.53	Optim.	-	[45]	Dissolution profile shape

-: not available, †: CYP2D6 k_{cat} values were optimized in a fixed ratio ($k_{cat} \rightarrow \alpha$HM:$k_{cat} \rightarrow$ ODM) equivalent to the ratio of reported k_{cat} values [39], ‡: in vitro values corrected for binding in the assay, using estimated fraction unbound to microsomal protein ($f_{u, mic, estimated}$ = 84%) [46], αHM: α-hydroxymetoprolol, asm.: assumed, calc.: calculated, cont.: continuously, CR: controlled release, CYP2D6: cytochrome P450 2D6, EHC: enterohepatic circulation, GFR: glomerular filtration rate, hep.: hepatic, lit.: literature, NR: normal release, ODM: *O*-demethylmetoprolol, optim.: optimized, perm. permeability, PK-Sim: PK-Sim standard calculation method, R&R: Rodgers and Rowland calculation method, succ.: metoprolol succinate, tart.: metoprolol tartrate, unsp.: unspecific.

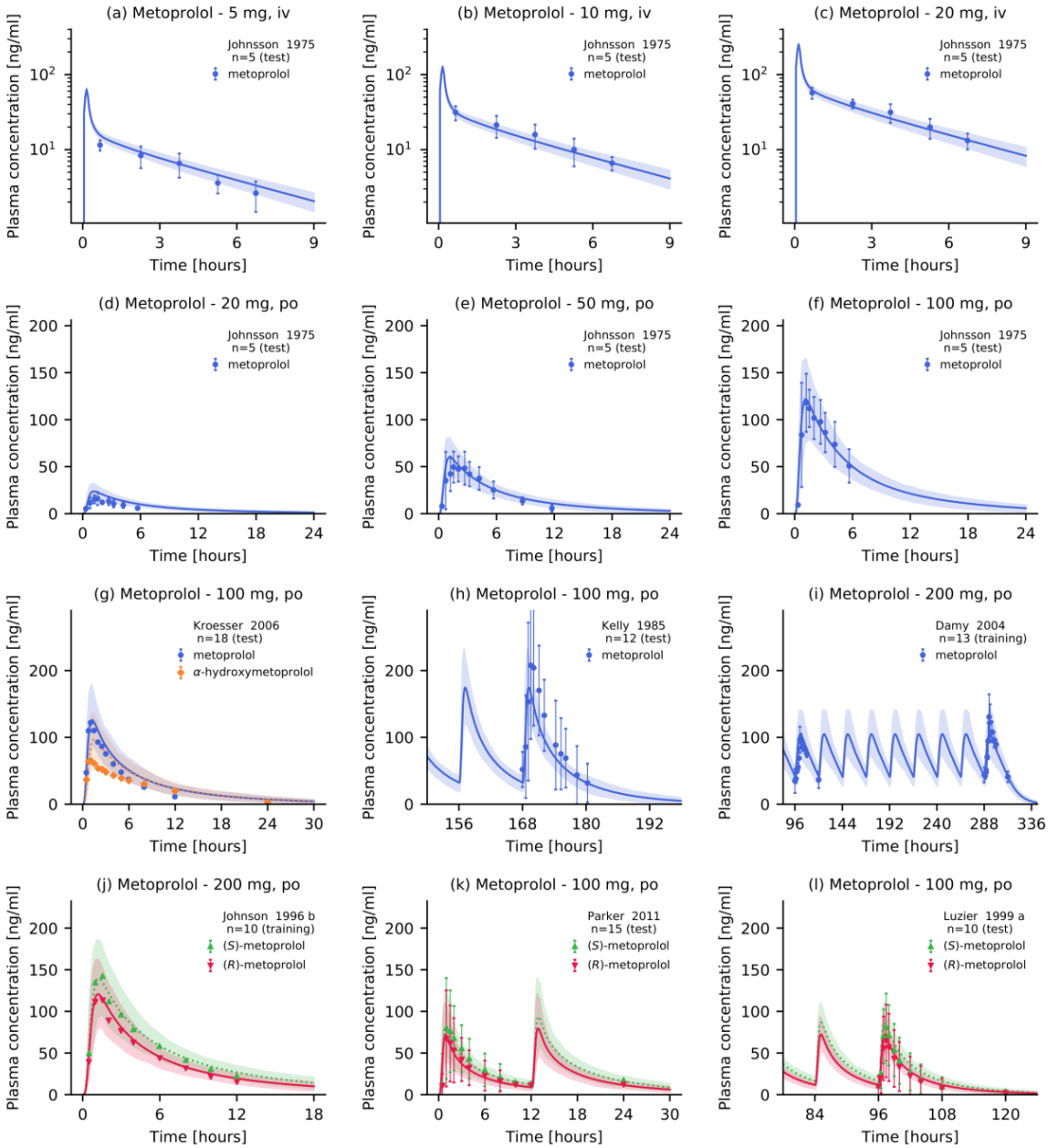

Figure 2. Metoprolol plasma concentrations. Model predictions of metoprolol and its metabolite α-hydroxymetoprolol plasma concentration-time profiles of selected (**a**–**c**) intravenous and (**d**–**l**) oral studies of the training and test datasets, compared to observed data [43–45,47–50]. Population predictions (n = 100) are shown as lines with ribbons (arithmetic mean ± standard deviation (SD)), symbols represent the corresponding observed data ± SD. Detailed information on all clinical studies is listed in Supplementary Table S2.2.1. iv: intravenous, po: oral.

Goodness-of-fit plots showing plasma concentrations, AUC_{last} and C_{max} values, respectively, are presented in Figure 3. Predicted plasma concentrations were predominantly (88.3%) within two-fold of the corresponding observed concentrations. Furthermore, a total of 72 out of 75 of the predicted AUC_{last} values (several studies included measurements of multiple analytes) and 64 out of 66 of the predicted C_{max} values were within the two-fold acceptance criterion. The metoprolol model GMFE values were 1.27 (range 1.01–2.94) for the predicted AUC_{last} values, and 1.23 (range 1.00–2.97) for the predicted C_{max} values. The MRD values and predicted to observed AUC_{last} and C_{max} ratios for all 48 clinical studies and all measured analytes are provided in Supplementary Tables S2.6.4–S2.6.7.

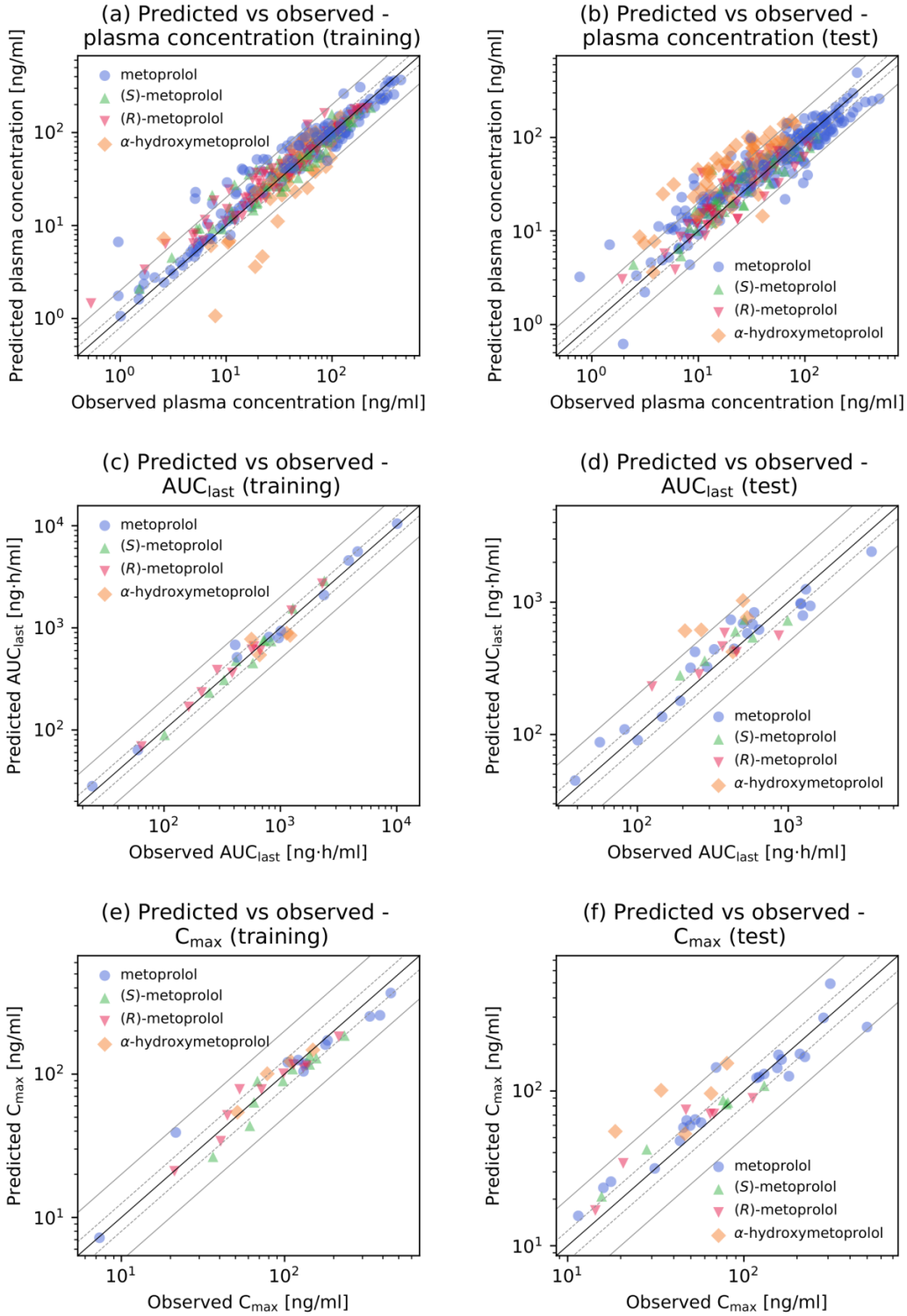

Figure 3. Goodness-of-fit plots of the final metoprolol model. Predicted versus observed (**a**,**b**) plasma concentrations, (**c**,**d**) AUC_{last} values and (**e**,**f**) C_{max} values for the training (left column) and test (right column) datasets. The solid black line indicates the line of identity, solid grey lines show two-fold deviation, dashed grey lines indicate 1.25-fold deviation. Detailed information on all clinical studies is listed in Supplementary Table S2.2.1. AUC_{last}: area under the plasma concentration-time curve from the time of the first concentration measurement to the time of the last concentration measurement, C_{max}: maximum plasma concentration, vs: versus.

The local sensitivity analysis of a simulation of 100 mg metoprolol tartrate administered orally (standard dose) revealed that the model predictions were most sensitive to the values of (*R*)- and (*S*)-metoprolol fraction unbound (f_u), which were gathered from literature and used unmodified as model input parameters. Setting a sensitivity threshold of 0.5 (100% parameter value change = 50% change of predicted AUC), the only other parameter value that the model predictions were sensitive to is the CYP2D6 (*R*)-metoprolol → *O*-demethylmetoprolol catalytic rate constant (optimized). A comprehensive visual and quantitative presentation of the sensitivity analysis results can be found in Supplementary Section S2.6.7.

3.2. Metoprolol CYP2D6 DGI Model Development and Evaluation

The model training dataset included 11 plasma concentration-time profiles from studies that reported the CYP2D6 activity scores of their study subjects, ranging from 0 (poor metabolizer) to 3 (ultrarapid metabolizer). These studies were utilized to optimize $k_{cat,\ rel}$ values for the different CYP2D6 activity scores. The identified values for both CYP2D6 pathways and both metoprolol enantiomers are given in Table 3.

Table 3. Optimized $k_{cat,\ rel}$ values for the different modeled CYP2D6 activity scores.

Activity Score	(*R*)-Metoprolol		(*S*)-Metoprolol		$k_{cat,\ rel}$
	k_{cat} → αHM	k_{cat} → ODM	k_{cat} → αHM	k_{cat} → ODM	
0	0.00 1/min	0.00 1/min	0.00 1/min	0.00 1/min	0%
0.5	1.65 1/min	2.70 1/min	1.82 1/min	2.27 1/min	19%
1.25	5.73 1/min	9.40 1/min	6.30 1/min	7.89 1/min	64%
1.5	6.38 1/min	10.48 1/min	7.03 1/min	8.81 1/min	72%
2	10.17 1/min	16.69 1/min	11.19 1/min	14.02 1/min	100%
3	19.03 1/min	31.22 1/min	20.93 1/min	26.23 1/min	213%

αHM: α-hydroxymetoprolol, k_{cat}: catalytic rate constant, $k_{cat,\ rel}$: catalytic rate constant relative to activity score = 2, ODM: *O*-demethylmetoprolol.

Of all 48 analyzed clinical profiles, 15 metoprolol plasma concentration–time profiles belong to studies that stratified their subjects by CYP2D6 activity score or phenotype. These studies either provided the activity score for the investigated population (three studies), the CYP2D6 phenotype (two studies), or comprehensive information on the *CYP2D6* genotype of all individuals (10 studies). To simulate the latter studies, mean activity scores were calculated according to current recommendations [33]. The good performance of the final metoprolol DGI model is demonstrated in Figure 4, showing predicted metoprolol plasma concentration-time profiles of populations with different CYP2D6 activity scores, compared with their corresponding observed data. Plots documenting the model performance for all 15 metoprolol DGI profiles found in the literature are provided in Supplementary Section S3.2.

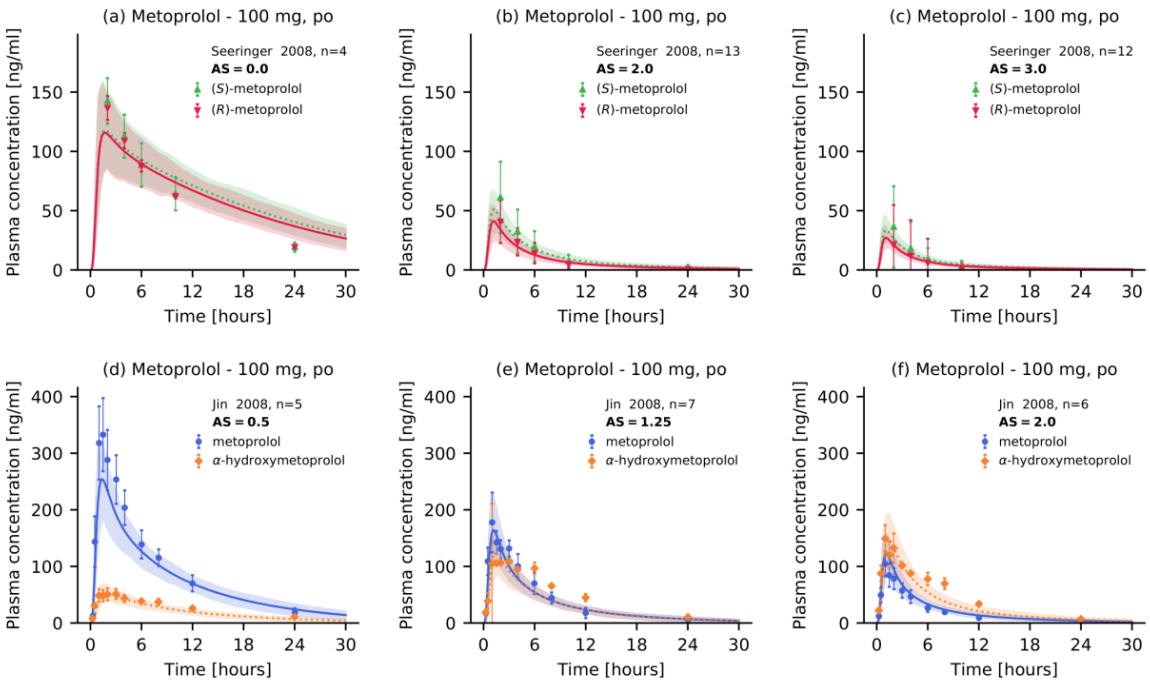

Figure 4. Metoprolol plasma concentrations of the modeled CYP2D6 drug-gene interaction. Model predictions of (**a**–**c**) (R)-metoprolol and (S)-metoprolol as well as (**d**–**f**) metoprolol and α hydroxymetoprolol plasma concentration-time profiles of selected metoprolol CYP2D6 DGI studies, compared to observed data [18,51]. Population predictions (n = 100) are shown as lines with ribbons (arithmetic mean ± standard deviation (SD)), symbols represent the corresponding observed data ± SD. Detailed information on all clinical studies is listed in Supplementary Table S2.2.1. AS: activity score, po: oral.

Predicted DGI AUC_{last} and C_{max} ratios were in very good agreement with the observed DGI ratios, demonstrating that the impact of the different CYP2D6 activity scores on the pharmacokinetics of racemic metoprolol, (*R*)-, and (*S*)-metoprolol and the metabolite α-hydroxymetoprolol was well described by the model. Specifically, 18 out of 18 AUC_{last} and 17 out of 18 C_{max} ratios were within the prediction success limits suggested by Guest et al. adopted for DGI evaluations [52], as visualized in Figure 5. Predicted DGI AUC_{last} ratios show an overall GMFE of 1.21 (range 1.00–1.69), while predicted DGI C_{max} ratios showed an overall GMFE of 1.21 (range 1.00–1.56). The predicted and observed ratios and corresponding predicted to observed DGI AUC_{last} and C_{max} ratios for all studies are provided in Supplementary Table S3.3.2.

3.3. Metoprolol Dose Adaptation for CYP2D6 DGIs

The developed metoprolol CYP2D6 DGI model was applied to calculate dose adaptations for individuals with different CYP2D6 activity scores. Simulated doses for "variant" activity scores were adapted in a stepwise approach until the AUC during steady-state (AUC_{ss}) matched the AUC_{ss} (±10%) of a 100 mg twice daily metoprolol regimen in AS = 2 (wildtype) subjects. Predictions of plasma concentration-time profiles for individuals with different activity scores, all administered with 100 mg of metoprolol tartrate twice daily, are shown in Figure 6a. Simulations for different activity scores after dose adaptation are shown in Figure 6b. The resulting model-based dose adaptations compared to the Dutch Pharmacogenetics Working Group (DPWG) guideline recommendations for metoprolol [28] are shown in Figure 6c. The corresponding AUC_{ss} values before (Figure 6d) and after (Figure 6e) dose adaptation are visualized in the lower panel.

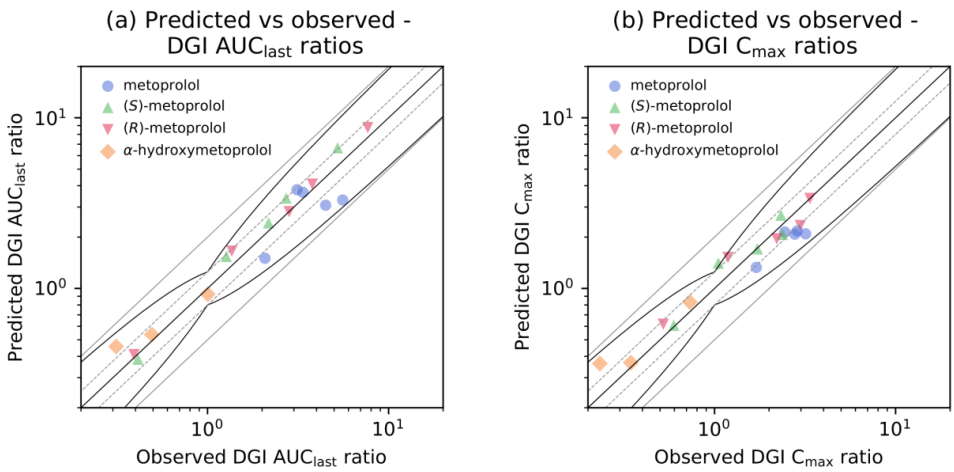

Figure 5. Predicted versus observed metoprolol DGI ratios. Comparison of predicted versus observed (**a**) DGI AUC_{last} ratios and (**b**) DGI C_{max} ratios for all analyzed metoprolol CYP2D6 DGI studies. The straight black line indicates the line of identity, curved black lines show prediction success limits proposed by Guest et al. including 1.25-fold variability [52]. Solid grey lines indicate two-fold deviation, dashed grey lines show 1.25-fold deviation. Detailed information on all clinical studies as well as the plotted values are listed in Tables S2.2.1 and S3.3.2 of the Supplementary Materials. AUC_{last}: area under the plasma concentration-time curve from the time of the first concentration measurement to the time of the last concentration measurement, C_{max}: maximum plasma concentration, DGI: drug-gene interaction, vs: versus.

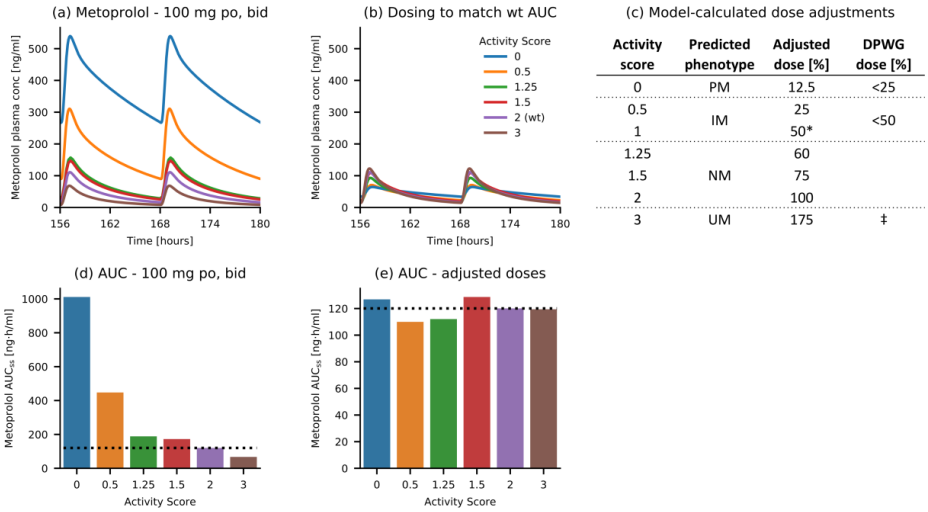

Activity score	Predicted phenotype	Adjusted dose [%]	DPWG dose [%]
0	PM	12.5	<25
0.5	IM	25	<50
1		50*	
1.25	NM	60	
1.5		75	
2		100	
3	UM	175	‡

Figure 6. Model-based CYP2D6 DGI dose recommendations. (**a**) Simulations of metoprolol exposure in individuals with different CYP2D6 activity scores, all administered with 100 mg metoprolol twice daily. (**b**) Simulations of metoprolol exposure in individuals with different CYP2D6 activity scores, administered with the model-based dose recommendations. Doses were adjusted to match the $AUC_{168–180\,h}$ of 100 mg metoprolol twice daily in AS = 2 (wt) individuals. (**c**) Model-based dose adjustments, compared to the DPWG guideline recommendations for metoprolol [28]. (**d**) Metoprolol $AUC_{168–180\,h}$ values for administration of 100 mg twice daily to individuals with different CYP2D6 activity scores. (**e**) Metoprolol AUC_{ss} values for administration of the model-based dose recommendations to individuals with different CYP2D6 activity scores. The dotted horizontal line marks the wt AUC_{ss}. *: value interpolated due to a lack of clinical studies with AS = 1, ‡: dose titration or change of medication recommended, AS: activity score, AUC_{ss}: area under the plasma concentration-time curve during steady state (168–180 h), bid: twice daily, DPWG: Dutch Pharmacogenetics Working Group, IM: intermediate metabolizer, NM: normal metabolizer, PM: poor metabolizer, po: oral, UM: ultrarapid metabolizer, wt: wild type.

4. Discussion

In this study, a whole-body PBPK model of metoprolol, including separate representations of its (*R*)- and (*S*)-enantiomers and the metabolite α-hydroxymetoprolol, was built and carefully evaluated to dynamically predict drug plasma concentrations over a wide dosing range (5–200 mg). Moreover, the model was extended to describe the impact of different CYP2D6 activity scores on the pharmacokinetics of racemic metoprolol, (*R*)-metoprolol, (*S*)-metoprolol, and α-hydroxymetoprolol.

Previously published metoprolol PBPK models were mostly developed for different applications. Indeed, two models investigated the effects of pregnancy [24,27] and one model analyzed the effects of investigational formulations [26]. A fourth published minimal PBPK-PD model of metoprolol was built to describe the impact of CYP2D6 DGIs on metoprolol plasma concentration profiles and heart rate. The DGI was implemented for three "traditional" phenotypes (poor, normal and ultrarapid metabolizers). This model, however, did not further differentiate the CYP2D6 activity between AS = 0 and AS = 2 [25]. Our model is the first to integrate current knowledge on CYP2D6 activity to accurately predict the impact of CYP2D6 DGIs over a wide range of activity scores. Moreover, this model is the first PBPK model of metoprolol to include metoprolol enantiomers (and enantiospecific CYP2D6 metabolism), as well as the active metabolite α-hydroxymetoprolol.

The limitations of the presented model are related to the incompleteness of published knowledge and data. Our model focused on CYP2D6 activity scores as opposed to CYP2D6 genotypes. Grouping genotypes by activity scores was necessary, due to the limited amount of data available on the enzyme kinetics of the >100 different CYP2D6 isoforms [53]. Consequently, the model is not able to further differentiate between different genotypes within the same activity score group (e.g., between **1/*1*, **1/*2*, and **2/*2*, which all belong to the AS = 2 group) [7]. The primary aim of this model, namely the characterization, description, and prediction of metoprolol exposure in individuals with *CYP2D6* polymorphisms to enable model-informed precision dosing, was met [54]. As more data (in vitro and clinical) regarding the CYP2D6 activity of the different individual genotypes emerge, the model can be easily extended for an even finer graduation of the CYP2D6 activity, to differentiate between genotypes within the same activity score group.

In addition, although the different CYP2D6 metabolic reactions (O-demethylation and α-hydroxylation of both (*R*)-metoprolol and (*S*)-metoprolol) were successfully implemented using K_m values from in vitro literature [39], these K_m values were assumed to be the same across all CYP2D6 activity scores. Using metoprolol as the substrate, only three genotype-specific in vitro K_m values (**1*, **2* and **17* isoforms), could be obtained from literature (metoprolol α-hydroxylation and *O*-demethylation), showing a slightly higher K_m for the **17* allele (AS = 0.5) [8]. Other studies reported no clear trend of K_m values using a wide range of CYP2D6 substrates to investigate the enzyme kinetics of the reduced-function alleles **10* and **17* in comparison to the wildtype **1* allele [55]. Hence, due to an insufficient amount of data, the same K_m values were used in the model across all activity scores. The final optimized $k_{cat,\,rel}$ values increased with increasing activity scores, reflecting an apparent correlation of metoprolol oral clearance with the CYP2D6 activity score [9]. Plasma concentration–time profiles and DGI AUC_{last} and C_{max} ratios of all analyzed clinical studies were well described by the final model.

The enzymes CYP2B6, CYP2C9 and CYP3A4 have also been found to metabolize metoprolol in vitro [14]. However, the fractions metabolized by these CYP enzymes in vivo, or which of those enzymes is the second most relevant enzyme for metoprolol metabolism besides CYP2D6, is not known (clinical DDI studies with fluconazole, ketoconazole or other strong CYP3A4 inhibitors could not be found in the literature). In two of the previously published metoprolol PBPK models, a CYP3A4-dependent clearance process was implemented [24,25]. Yet, the formation of O-demethylmetoprolol and α-hydroxymetoprolol in human liver microsomes were less impacted by inhibition of CYP3A4 than by inhibition of CYP2C9 or CYP2B6 [14]. However, as CYP2D6 is estimated to account for >70% of metoprolol oral clearance [43], the impact of variations in CYP2B6, CYP2C9 or CYP3A4 enzymatic activity on metoprolol PK was considered negligible. Moreover,

model input parameters such as CYP2B6, CYP2C9, or CYP3A4 K_m and k_{cat}, that would be necessary for a mechanistic implementation of the respective metabolic pathways, are not available in the literature. Consequently, the authors decided to incorporate an unspecific hepatic clearance process in addition to the CYP2D6-dependent pathways.

The final metoprolol PBPK model was applied to generate dose adaptations for populations with different CYP2D6 activity scores. While it is generally acknowledged that metoprolol exposure is mainly determined by the CYP2D6 activity score [56,57], there is no consensus in the literature on whether increased metoprolol plasma concentrations in poor and intermediate metabolizers result in a higher incidence of adverse drug reactions [58–61].

The model-based dose recommendations calculated for CYP2D6 DGIs were well in line with the recommendations provided by the DPWG [28], except for the poor metabolizers, where this analysis suggests even lower doses than the Dutch guidance document. Adapting a patients' metoprolol dose based on the CYP2D6 activity score will decrease the occurrence of adverse drug reactions or therapy failure [56,59] and consequently help to provide more safe and efficient personalized dosing regimens. Future possible applications of the newly developed PBPK model include the prediction of CYP2D6 DDI effects on metoprolol pharmacokinetics or scaling of the metoprolol model to special populations such as pediatric patients, geriatric patients, or patients with renal or hepatic impairment.

5. Conclusions

A whole-body parent-metabolite PBPK model of metoprolol and its enantiomers was developed to predict racemic metoprolol, (*R*)-metoprolol, (*S*)-metoprolol, and α-hydroxymetoprolol plasma concentration–time profiles. The model focused on CYP2D6 activity score-dependent metabolism and has been utilized to calculate dose adaptations in populations with various CYP2D6 activities and genotypes. The Supplementary Materials of this manuscript provide an in-depth documentation and evaluation of the final model and the PBPK model file will be made publicly available in the OSP repository. The model can be applied to generate dose adaption for patients with different CYP2D6 activity scores, to complement and refine the recommendations by existing guidelines and facilitate personalized medicine. Due to the mechanistic implementation of the human physiology and important pharmacokinetic pathways, the model allows for knowledge-based scaling to special populations and can serve as the basis for future investigations of CYP2D6 DDI scenarios.

Supplementary Materials: The following are available online at http://www.mdpi.com/1999-4923/12/12/1200/s1, Table S2.2.1: Metoprolol study table, Table S2.3.2: (*R*)-and(*S*)-metoprolol drug-dependent parameters, Table S2.4.3: α-hydroxymetoprolol drug-dependent parameters, Figure S2.5.1: Metoprolol plasma concentrations. Model predictions of metoprolol and its metabolite α-hydroxymetoprolol plasma concentration-time profiles of intravenous studies of the training and test datasets, compared to observed data (semilogarithmic representation), Figure S2.5.2: Metoprolol plasma concentrations. Model predictions of metoprolol and its metabolite α-hydroxymetoprolol plasma concentration-time profiles of oral studies of the training and test datasets, compared to observed data (semilogarithmic representation), Figure S2.5.3: Metoprolol plasma concentrations, Figure S2.5.4: Metoprolol enantiomers plasma concentrations. Model predictions of (*R*)-metoprolol and (*S*)-metoprolol plasma concentration-time profiles of oral studies of the trainingand test datasets, compared to observed data (semilogarithmic representation), Figure S2.5.5: Metoprolol plasma concentrations, Figure S2.5.6: Metoprolol plasma concentrations, Figure S2.5.7: Metoprolol plasma concentrations, Figure S2.5.8: Metoprolol enantiomers plasma concentrations, Figure S2.6.9: Plasma concentrations goodness-of-fit plots of the final metoprolol model, Figure S2.6.10: Plasmaconcentrationsgoodness-of-fitplotsofthefinalmetoprololmodel, Table S2.6.4: Mean relative deviation of plasma concentration predictions (metoprolol, αhydroxymetoprolol), Table S2.6.5: Mean relative deviation of plasma concentration predictions ((*R*)-metoprolol, (*S*)-metoprolol), Figure S2.6.11: AUC_{last} values goodness-of-fit plots for the final metoprolol model, Figure S2.6.12: AUC_{last} goodness-of-fit plots for the final metoprolol model, Figure S2.6.13: C_{max} values goodness-of-fit plots for the final metoprolol model, Figure S2.6.14: AUC_{last} goodness-of-fit plots for the final metoprolol model, Table S2.6.6: Predicted and observed AUC_{last} and C_{max} values (metoprolol, α-hydroxymetoprolol), Table S2.6.7: Predictedandobserved AUC_{last} and C_{max} values ((*R*)-metoprolol,(*S*)-metoprolol), Figure S2.6.15: Sensitivity analysis of the (*R*)-metoprolol (upper panel) and (*S*)-metoprolol (lower panel) model, Table S3.1.1: $k_{cat,\ rel}$ values for the different CYP2D6 activity scores, Figure S3.2.1: Metoprolol plasma concentrations of the modeled CYP2D6 drug-gene interaction, Figure S3.2.2: Metoprolol plasma concentrations of the modeled CYP2D6 drug-gene interaction, Figure S3.2.3: Metoprolol plasma concentrations of the modeled CYP2D6 drug-gene interaction, Figure S3.2.4: Metoprolol plasma concentrations of the modeled CYP2D6 drug-gene interaction,

Figure S3.2.5: Metoprolol plasma concentrations of the modeled CYP2D6 drug-gene interaction, Figure S3.2.6: Metoprolol plasma concentrations of the modeled CYP2D6 drug-gene interaction., Figure S3.2.7: Metoprolol plasma concentrations of the modeled CYP2D6 drug-gene interaction, Figure S3.2.8: Metoprolol plasma concentrations of the modeled CYP2D6 drug-gene interaction, Figure S3.2.9: Metoprolol plasma concentrations of the modeled CYP2D6 drug-gene interaction, Figure S3.2.10: Metoprolol plasma concentrations of the modeled CYP2D6 drug-gene interaction, Figure S3.2.11: Metoprolol plasma concentrations of the modeled CYP2D6 drug-gene interaction, Figure S3.2.12: Metoprolol plasma concentrations of the modeled CYP2D6 drug-gene interaction, Figure S3.3.13: Predicted versus observed metoprolol DGI ratios. Comparison of predicted versus observed AUC_{last} ratios (a) and C_{max} ratios (b) for metoprolol CYP2D6 DGI-studies, Table S3.3.2: Geometric mean fold error of predicted metoprolol DGI AUC_{last} andC_{max} ratios, Table S4.0.1: System-dependent parameters.

Author Contributions: Conceptualization, S.R., N.H., D.S., and T.L.; funding acquisition, M.S. and T.L.; investigation, S.R., J.-G.W., and T.L.; visualization, S.R.; writing—original draft, S.R., D.S., N.H., and T.L.; writing—review and editing, S.R., J.-G.W., D.S., N.H., F.M., M.S., and T.L. All authors have read and agreed to the published version of the manuscript.

Funding: F.M. is supported by Deutsche Gesellschaft für Kardiologie (DGK), and Deutsche Forschungsgemeinschaft (SFB TRR219). M.S. was supported by the Robert Bosch Stiftung (Stuttgart, Germany), the European Commission Horizon 2020 UPGx grant 668353, a grant from the German Federal Ministry of Education and Research (BMBF 031L0188D), and the Deutsche Forschungsgemeinschaft (DFG, German Research Foundation) under Germany's Excellence Strategy—EXC 2180—390900677. T.L. was supported by the German Federal Ministry of Education and Research (BMBF, Horizon 2020 INSPIRATION grant 643271), under the frame of ERACoSysMed. The APC was funded by the German Research Foundation (DFG) and Saarland University within the funding program "Open Access Publishing".

Conflicts of Interest: J.-G.W. is an employee of Boehringer Ingelheim Pharma GmbH & Co. KG. F.M. received scientific support and speaker honoraria from Bayer, Boehringer Ingelheim, Medtronic and ReCor Medical. S.R., D.S., N.H., M.S. and T.L. declare that they have no conflict of interest. The funders had no role in the design of the study; in the collection, analyses, or interpretation of data; in the writing of the manuscript, or in the decision to publish the results.

References

1. ClinCalc LLC. ClinCalc DrugStats Database. Available online: https://clincalc.com/Drugstats/ (accessed on 10 September 2020).
2. Novartis Pharmaceuticals Corporation Lopressor®Tablet and Injection—Prescribing Information. Available online: https://www.accessdata.fda.gov/drugsatfda_docs/label/2008/017963s062,018704s021lbl.pdf (accessed on 10 September 2020).
3. U.S. Food and Drug Administration Drug Development and Drug Interactions: Table of Substrates, Inhibitors and Inducers. FDA. Available online: https://www.fda.gov/drugs/drug-interactions-labeling/drug-development-and-drug-interactions-table-substrates-inhibitors-and-inducers (accessed on 10 September 2020).
4. Michaels, S.; Wang, M.Z. The Revised Human Liver Cytochrome P450 "Pie": Absolute Protein Quantification of CYP4F and CYP3A Enzymes Using Targeted Quantitative Proteomics. *Drug Metab. Dispos.* **2014**, *42*, 1241–1251. [CrossRef] [PubMed]
5. Zanger, U.M.; Schwab, M. Cytochrome P450 enzymes in drug metabolism: Regulation of gene expression, enzyme activities, and impact of genetic variation. *Pharmacol. Ther.* **2013**, *138*, 103–141. [CrossRef] [PubMed]
6. Gaedigk, A.; Dinh, J.C.; Jeong, H.; Prasad, B.; Leeder, J.S. Ten years' experience with the CYP2D6 activity score: A perspective on future investigations to improve clinical predictions for precision therapeutics. *J. Pers. Med.* **2018**, *8*, 15. [CrossRef] [PubMed]
7. Gaedigk, A.; Simon, S.D.; Pearce, R.E.; Bradford, L.D.; Kennedy, M.J.; Leeder, J.S. The CYP2D6 activity score: Translating genotype information into a qualitative measure of phenotype. *Clin. Pharmacol. Ther.* **2008**, *83*, 234–242. [CrossRef]
8. Bapiro, T.E.; Hasler, J.A.; Ridderström, M.; Masimirembwa, C.M. The molecular and enzyme kinetic basis for the diminished activity of the cytochrome P450 2D6.17 (CYP2D6.17) variant: Potential implications for CYP2D6 phenotyping studies and the clinical use of CYP2D6 substrate drugs in some African populations. *Biochem. Pharmacol.* **2002**, *64*, 1387–1398. [CrossRef]
9. Thomas, C.D.; Mosley, S.A.; Kim, S.; Lingineni, K.; El Rouby, N.; Langaee, T.Y.; Gong, Y.; Wang, D.; Schmidt, S.O.; Binkley, P.F.; et al. Examination of Metoprolol Pharmacokinetics and Pharmacodynamics Across CYP2D6 Genotype-Derived Activity Scores. *CPT Pharmacometrics Syst. Pharmacol.* **2020**. [CrossRef]

10. Matthaei, J.; Brockmöller, J.; Tzvetkov, M.; Sehrt, D.; Sachse-Seeboth, C.; Hjelmborg, J.; Möller, S.; Halekoh, U.; Hofmann, U.; Schwab, M.; et al. Heritability of metoprolol and torsemide pharmacokinetics. *Clin. Pharmacol. Ther.* **2015**, *98*, 611–621. [CrossRef]
11. Kirchheiner, J.; Heesch, C.; Bauer, S.; Meisel, C.; Seringer, A.; Goldammer, M.; Tzvetkov, M.; Meineke, I.; Roots, I.; Brockmöller, J. Impact of the ultrarapid metabolizer genotype of cytochrome P450 2D6 on metoprolol pharmacokinetics and pharmacodynamics. *Clin. Pharmacol. Ther.* **2004**, *76*, 302–312. [CrossRef]
12. Plosker, G.L.; Clissold, S.P. Controlled Release Metoprolol Formulations. *Drugs* **1992**, *43*, 382–414. [CrossRef]
13. Regårdh, C.G.; Johnsson, G. Clinical Pharmacokinetics of Metoprolol. *Clin. Pharmacokinet.* **1980**, *5*, 557–569. [CrossRef]
14. Berger, B.; Bachmann, F.; Duthaler, U.; Krähenbühl, S.; Haschke, M. Cytochrome P450 enzymes involved in metoprolol metabolism and use of metoprolol as a CYP2D6 phenotyping probe drug. *Front. Pharmacol.* **2018**, *9*, 1–11. [CrossRef] [PubMed]
15. Cerqueira, P.M.; Cesarino, E.J.; Mateus, F.H.; Mere, Y.; Santos, S.R.; Lanchote, V.L. Enantioselectivity in the steady-state pharmacokinetics of metoprolol in hypertensive patients. *Chirality* **1999**, *11*, 591–597. [CrossRef]
16. Lennard, M.S.; Tucker, G.T.; Silas, J.H.; Woods, H.F. Debrisoquine polymorphism and the metabolism and action of metoprolol, timolol, propranolol and atenolol. *Xenobiotica* **1986**, *16*, 435–447. [CrossRef] [PubMed]
17. Bozkurt, A.; Başçi, N.B.; Işimer, A.; Sayal, A.; Kayaalp, S.O. Metabolic ratios of four probes of CYP2D6 in Turkish subjects: A cross-over study. *Eur. J. Drug Metab. Pharmacokinet.* **1996**, *21*, 309–314. [CrossRef] [PubMed]
18. Seeringer, A.; Brockmöller, J.; Bauer, S.; Kirchheiner, J. Enantiospecific pharmacokinetics of metoprolol in CYP2D6 ultra-rapid metabolizers and correlation with exercise-induced heart rate. *Eur. J. Clin. Pharmacol.* **2008**, *64*, 883–888. [CrossRef] [PubMed]
19. Nathanson, J.A. Stereospecificity of beta adrenergic antagonists: R-enantiomers show increased selectivity for beta-2 receptors in ciliary process. *J. Pharmacol. Exp. Ther.* **1988**, *245*, 94–101.
20. Blake, C.M.; Kharasch, E.D.; Schwab, M.; Nagele, P. A Meta-Analysis of CYP2D6 Metabolizer Phenotype and Metoprolol Pharmacokinetics. *Clin. Pharmacol. Ther.* **2013**, *94*, 394–399. [CrossRef]
21. Gaedigk, A.; Sangkuhl, K.; Whirl-Carrillo, M.; Klein, T.; Leeder, J.S. Prediction of CYP2D6 phenotype from genotype across world populations. *Genet. Med.* **2017**, *19*, 69–76. [CrossRef]
22. Del Tredici, A.L.; Malhotra, A.; Dedek, M.; Espin, F.; Roach, D.; Zhu, G.-d.; Voland, J.; Moreno, T.A. Frequency of CYP2D6 alleles including structural variants in the United States. *Front. Pharmacol.* **2018**, *9*, 305. [CrossRef]
23. Gaedigk, A. Complexities of CYP2D6 gene analysis and interpretation. *Int. Rev. Psychiatry* **2013**, *25*, 534–553. [CrossRef]
24. Ke, A.B.; Nallani, S.C.; Zhao, P.; Rostami-Hodjegan, A.; Isoherranen, N.; Unadkat, J.D. A Physiologically Based Pharmacokinetic Model to Predict Disposition of CYP2D6 and CYP1A2 Metabolized Drugs in Pregnant Women. *Drug Metab. Dispos.* **2013**, *41*, 801–813. [CrossRef] [PubMed]
25. Chetty, M.; Rose, R.H.; Abduljalil, K.; Patel, N.; Lu, G.; Cain, T.; Jamei, M.; Rostami-Hodjegan, A. Applications of linking PBPK and PD models to predict the impact of genotypic variability, formulation differences, differences in target binding capacity and target site drug concentrations on drug responses and variability. *Front. Pharmacol.* **2014**, *5*, 1–29. [CrossRef] [PubMed]
26. Kim, S.; Sharma, V.D.; Lingineni, K.; Farhan, N.; Fang, L.; Zhao, L.; Brown, J.D.; Cristofoletti, R.; Vozmediano, V.; Ait-Oudhia, S.; et al. Evaluating the Clinical Impact of Formulation Variability: A Metoprolol Extended-Release Case Study. *J. Clin. Pharmacol.* **2019**, *59*, 1266–1274. [CrossRef] [PubMed]
27. Dallmann, A.; Ince, I.; Coboeken, K.; Eissing, T.; Hempel, G. A Physiologically Based Pharmacokinetic Model for Pregnant Women to Predict the Pharmacokinetics of Drugs Metabolized Via Several Enzymatic Pathways. *Clin. Pharmacokinet.* **2018**, *57*, 749–768. [CrossRef] [PubMed]
28. The Royal Dutch Pharmacists Association—Pharmacogenetics Working Group (DPWG) Annotation of DPWG Guideline for Metoprolol and CYP2D6. Available online: https://www.pharmgkb.org/guidelineAnnotation/PA166104995 (accessed on 22 September 2020).
29. Lippert, J.; Burghaus, R.; Edginton, A.; Frechen, S.; Karlsson, M.; Kovar, A.; Lehr, T.; Milligan, P.; Nock, V.; Ramusovic, S.; et al. Open Systems Pharmacology Community—An Open Access, Open Source, Open Science Approach to Modeling and Simulation in Pharmaceutical Sciences. *CPT Pharmacometrics Syst. Pharmacol.* **2019**, *8*, 878–882. [CrossRef]

30. Wojtyniak, J.G.; Britz, H.; Selzer, D.; Schwab, M.; Lehr, T. Data Digitizing: Accurate and Precise Data Extraction for Quantitative Systems Pharmacology and Physiologically-Based Pharmacokinetic Modeling. *CPT Pharmacometrics Syst. Pharmacol.* **2020**, *9*, 322–331. [CrossRef]
31. Regårdh, C.G.; Borg, K.O.; Johansson, R.; Johnsson, G.; Palmer, L. Pharmacokinetic studies on the selective beta1-receptor antagonist metoprolol in man. *J. Pharmacokinet. Biopharm.* **1974**, *2*, 347–364. [CrossRef]
32. Open Systems Pharmacology Suite Community Open Systems Pharmacology Suite Manual, Version 7.4. Available online: https://github.com/Open-Systems-Pharmacology/OSPSuite.Documentation/blob/master/OpenSystemsPharmacologySuite.pdf (accessed on 12 October 2020).
33. Caudle, K.E.; Sangkuhl, K.; Whirl-Carrillo, M.; Swen, J.J.; Haidar, C.E.; Klein, T.E.; Gammal, R.S.; Relling, M.V.; Scott, S.A.; Hertz, D.L.; et al. Standardizing CYP 2D6 Genotype to Phenotype Translation: Consensus Recommendations from the Clinical Pharmacogenetics Implementation Consortium and Dutch Pharmacogenetics Working Group. *Clin. Transl. Sci.* **2020**, *13*, 116–124. [CrossRef]
34. Kim, S.; Chen, J.; Cheng, T.; Gindulyte, A.; He, J.; He, S.; Li, Q.; Shoemaker, B.A.; Thiessen, P.A.; Yu, B.; et al. PubChem 2019 update: Improved access to chemical data. *Nucleic Acids Res.* **2019**, *47*, D1102–D1109. [CrossRef]
35. Avdeef, A.; Berger, C.M. pH-metric solubility.: 3. Dissolution titration template method for solubility determination. *Eur. J. Pharm. Sci.* **2001**, *14*, 281–291. [CrossRef]
36. Boldhane, S.; Kuchekar, B. Development and optimization of metoprolol succinate gastroretentive drug delivery system. *Acta Pharm.* **2010**, *60*, 415–425. [CrossRef] [PubMed]
37. Zhao, Y.; Jona, J.; Chow, D.T.; Rong, H.; Semin, D.; Xia, X.; Zanon, R.; Spancake, C.; Maliski, E. High-throughput logP measurement using parallel liquid chromatography/ultraviolet/mass spectrometry and sample-pooling. *Rapid Commun. Mass Spectrom.* **2002**, *16*, 1548–1555. [CrossRef] [PubMed]
38. Mateus, A.; Matsson, P.; Artursson, P. A High-Throughput Cell-Based Method to Predict the Unbound Drug Fraction in the Brain. *J. Med. Chem.* **2014**, *57*, 3005–3010. [CrossRef] [PubMed]
39. Mautz, D.S.; Nelson, W.L.; Shen, D.D. Regioselective and stereoselective oxidation of metoprolol and bufuralol catalyzed by microsomes containing cDNA-expressed human P4502D6. *Drug Metab. Dispos.* **1995**, *23*, 513–517.
40. Thelen, K.; Coboeken, K.; Willmann, S.; Burghaus, R.; Dressman, J.B.; Lippert, J. Evolution of a detailed physiological model to simulate the gastrointestinal transit and absorption process in humans, Part 1: Oral solutions. *J. Pharm. Sci.* **2011**, *100*, 5324–5345. [CrossRef]
41. Rodgers, T.; Leahy, D.; Rowland, M. Physiologically based pharmacokinetic modeling 1: Predicting the tissue distribution of moderate-to-strong bases. *J. Pharm. Sci.* **2005**, *94*, 1259–1276. [CrossRef]
42. Rodgers, T.; Rowland, M. Physiologically based pharmacokinetic modeling 2: Predicting the tissue distribution of acids, very weak bases, neutrals and zwitterions. *J. Pharm. Sci.* **2006**, *95*, 1238–1257. [CrossRef]
43. Johnson, J.A.; Burlew, B.S. Metoprolol metabolism via cytochrome P4502D6 in ethnic populations. *Drug Metab. Dispos.* **1996**, *24*, 350–355.
44. Kelly, J.G.; Salem, S.A.; Kinney, C.D.; Shanks, R.G.; McDevitt, D.G. Effects of ranitidine on the disposition of metoprolol. *Br. J. Clin. Pharmacol.* **1985**, *19*, 219–224. [CrossRef]
45. Damy, T.; Pousset, F.; Caplain, H.; Hulot, J.-S.S.; Lechat, P. Pharmacokinetic and pharmacodynamic interactions between metoprolol and dronedarone in extensive and poor CYP2D6 metabolizers healthy subjects. *Fundam. Clin. Pharmacol.* **2004**, *18*, 113–123. [CrossRef]
46. Austin, R.P.; Barton, P.; Cockroft, S.L.; Wenlock, M.C.; Riley, R.J. The influence of nonspecific microsomal binding on apparent intrinsic clearance, and its prediction from physicochemical properties. *Drug Metab. Dispos.* **2002**, *30*, 1497–1503. [CrossRef] [PubMed]
47. Johnsson, G.; Regärdh, C.-G.; Sölvell, L. Combined pharmacokinetic and pharmacodynamic studies in man of the adrenergic β1-receptor antagonist metoprolol. *Acta Pharmacol. Toxicol. (Copenh).* **1975**, *36*, 31–44. [CrossRef] [PubMed]
48. Krösser, S.; Neugebauer, R.; Dolgos, H.; Fluck, M.; Rost, K.-L.; Kovar, A. Investigation of sarizotan's impact on the pharmacokinetics of probe drugs for major cytochrome P450 isoenzymes: A combined cocktail trial. *Eur. J. Clin. Pharmacol.* **2006**, *62*, 277–284. [CrossRef] [PubMed]
49. Parker, R.B.; Soberman, J.E. Effects of paroxetine on the pharmacokinetics and pharmacodynamics of immediate-release and extended-release metoprolol. *Pharmacotherapy* **2011**, *31*, 630–641. [CrossRef]

50. Luzier, A.B.; Killian, A.; Wilton, J.H.; Wilson, M.F.; Forrest, A.; Kazierad, D.J. Gender-related effects on metoprolol pharmacokinetics and pharmacodynamics in healthy volunteers. *Clin. Pharmacol. Ther.* **1999**, *66*, 594–601. [CrossRef]
51. Jin, S.K.; Chung, H.J.; Chung, M.W.; Kim, J.-I.; Kang, J.-H.; Woo, S.W.; Bang, S.; Lee, S.H.; Lee, H.J.; Roh, J. Influence of CYP2D6*10 on the pharmacokinetics of metoprolol in healthy Korean volunteers. *J. Clin. Pharm. Ther.* **2008**, *33*, 567–573. [CrossRef]
52. Guest, E.J.; Aarons, L.; Houston, J.B.; Rostami-Hodjegan, A.; Galetin, A. Critique of the Two-Fold Measure of Prediction Success for Ratios: Application for the Assessment of Drug-Drug Interactions. *Drug Metab. Dispos.* **2011**, *39*, 170–173. [CrossRef]
53. Pharmacogene Variation Consortium (PharmVar) CYP2D6 gene. Available online: https://www.pharmvar.org/gene/CYP2D6 (accessed on 7 October 2020). (Gaedigk et al. 2018, CPT 103:399; Gaedigk et al. 2019, CPT 105:29).
54. Gonzalez, D.; Rao, G.G.; Bailey, S.C.; Brouwer, K.L.R.; Cao, Y.; Crona, D.J.; Kashuba, A.D.M.; Lee, C.R.; Morbitzer, K.; Patterson, J.H.; et al. Precision Dosing: Public Health Need, Proposed Framework, and Anticipated Impact. *Clin. Transl. Sci.* **2017**, *10*, 443–454. [CrossRef]
55. Shen, H.; He, M.M.; Liu, H.; Wrighton, S.A.; Wang, L.; Guo, B.; Li, C. Comparative metabolic capabilities and inhibitory profiles of CYP2D6.1, CYP2D6.10, and CYP2D6.17. *Drug Metab. Dispos.* **2007**, *35*, 1292–1300. [CrossRef]
56. Goryachkina, K.; Burbello, A.; Boldueva, S.; Babak, S.; Bergman, U.; Bertilsson, L. CYP2D6 is a major determinant of metoprolol disposition and effects in hospitalized Russian patients treated for acute myocardial infarction. *Eur. J. Clin. Pharmacol.* **2008**, *64*, 1163–1173. [CrossRef]
57. Rau, T.; Heide, R.; Bergmann, K.; Wuttke, H.; Werner, U.; Feifel, N.; Eschenhagen, T. Effect of the CYP2D6 genotype on metoprolol metabolism persists during long-term treatment. *Pharmacogenetics* **2002**, *12*, 465–472. [CrossRef] [PubMed]
58. Hamadeh, I.S.; Langaee, T.Y.; Dwivedi, R.; Garcia, S.; Burkley, B.M.; Skaar, T.C.; Chapman, A.B.; Gums, J.G.; Turner, S.T.; Gong, Y.; et al. Impact of CYP2D6 polymorphisms on clinical efficacy and tolerability of metoprolol tartrate. *Clin. Pharmacol. Ther.* **2014**, *96*, 175–181. [CrossRef] [PubMed]
59. Bijl, M.J.; Visser, L.E.; Van Schaik, R.H.N.; Kors, J.A.; Witteman, J.C.M.; Hofman, A.; Vulto, A.G.; Van Gelder, T.; Stricker, B.H.C. Genetic variation in the CYP2D6 gene is associated with a lower heart rate and blood pressure in β-blocker users. *Clin. Pharmacol. Ther.* **2009**, *85*, 45–50. [CrossRef] [PubMed]
60. Yuan, H.; Huang, Z.; Yang, G.; Lv, H.; Sang, H.; Yao, Y. Effects of Polymorphism of the β 1 Adrenoreceptor and CYP2D6 on the Therapeutic Effects of Metoprolol. *J. Int. Med. Res.* **2008**, *36*, 1354–1362. [CrossRef]
61. Fux, R.; Mörike, K.; Pröhmer, A.M.T.T.; Delabar, U.; Schwab, M.; Schaeffeler, E.; Lorenz, G.; Gleiter, C.H.; Eichelbaum, M.; Kivistö, K.T. Impact of CYP2D6 genotype on adverse effects during treatment with metoprolol: A prospective clinical study. *Clin. Pharmacol. Ther.* **2005**, *78*, 378–387. [CrossRef]

4.2 PROJECT II: PHYSIOLOGICALLY-BASED PHARMACOKINETIC MODELING OF DEXTROMETHORPHAN TO INVESTIGATE INTERINDIVIDUAL VARIABILITY WITHIN CYP2D6 ACTIVITY SCORE GROUPS

Publication

The following original research article has been published in the peer-reviewed journal *CPT: Pharmacometrics & Systems Pharmacology*:

Rüdesheim, S.; Selzer, D.; Fuhr, U.; Schwab, M.; Lehr, T. Physiologically-based pharmacokinetic modeling of dextromethorphan to investigate interindividual variability within CYP2D6 activity score groups. *CPT: pharmacometrics & systems pharmacology* **2022**, *11*, 494–511, DOI: 10.1002/psp4.12776.

Supplementary Material

The supplementary material to this publication can be accessed via this link.

Copyright

Author Contributions

Author contributions according to CRediT [6]:

Simeon Rüdesheim	Conceptualization, Investigation, Visualization, Writing–Original Draft, Writing–Review & Editing
Dominik Selzer	Conceptualization, Writing–Original Draft, Writing–Review & Editing
Uwe Fuhr	Writing–Original Draft, Writing–Review & Editing
Matthias Schwab	Writing–Original Draft, Writing–Review & Editing
Thorsten Lehr	Conceptualization, Writing–Original Draft, Writing–Review & Editing

Received: 21 October 2021 | Revised: 1 February 2022 | Accepted: 9 February 2022

DOI: 10.1002/psp4.12776

ARTICLE

Physiologically-based pharmacokinetic modeling of dextromethorphan to investigate interindividual variability within CYP2D6 activity score groups

Simeon Rüdesheim[1,2] | Dominik Selzer[1] | Uwe Fuhr[3] | Matthias Schwab[2,4,5] | Thorsten Lehr[1]

[1]Clinical Pharmacy, Saarland University, Saarbrücken, Germany

[2]Dr. Margarete Fischer-Bosch-Institute of Clinical Pharmacology, University of Tübingen, Stuttgart, Germany

[3]Department I of Pharmacology, Center for Pharmacology, Faculty of Medicine and University Hospital Cologne, University of Cologne, Cologne, Germany

[4]Departments of Clinical Pharmacology, Pharmacy and Biochemistry, University of Tübingen, Tübingen, Germany

[5]Cluster of Excellence iFIT (EXC2180) "Image-guided and Functionally Instructed Tumor Therapies", University of Tübingen, Tübingen, Germany

Correspondence
Thorsten Lehr, Clinical Pharmacy, Saarland University, Campus C2 2, 66123 Saarbrücken, Germany.
Email: thorsten.lehr@mx.uni-saarland.de

Funding information
M.S. was supported by the Robert Bosch Stiftung (Stuttgart, Germany), the European Commission Horizon 2020 UPGx grant 668353, a grant from the German Federal Ministry of Education and Research (BMBF 031L0188D), and the Deutsche Forschungsgemeinschaft (DFG, German Research Foundation) under Germany's Excellence Strategy—EXC 2180—390900677. T.L. was supported by the German Federal

Abstract

This study provides a whole-body physiologically-based pharmacokinetic (PBPK) model of dextromethorphan and its metabolites dextrorphan and dextrorphan *O*-glucuronide for predicting the effects of cytochrome P450 2D6 (CYP2D6) drug-gene interactions (DGIs) on dextromethorphan pharmacokinetics (PK). Moreover, the effect of interindividual variability (IIV) within CYP2D6 activity score groups on the PK of dextromethorphan and its metabolites was investigated. A parent-metabolite-metabolite PBPK model of dextromethorphan, dextrorphan, and dextrorphan *O*-glucuronide was developed in PK-Sim and MoBi. Drug-dependent parameters were obtained from the literature or optimized. Plasma concentration-time profiles of all three analytes were gathered from published studies and used for model development and model evaluation. The model was evaluated comparing simulated plasma concentration-time profiles, area under the concentration-time curve from the time of the first measurement to the time of the last measurement (AUC_{last}) and maximum concentration (C_{max}) values to observed study data. The final PBPK model accurately describes 28 population plasma concentration-time profiles and plasma concentration-time profiles of 72 individuals from four cocktail studies. Moreover, the model predicts CYP2D6 DGI scenarios with six of seven DGI AUC_{last} and seven of seven DGI C_{max} ratios within the acceptance criteria. The high IIV in plasma concentrations was analyzed by characterizing the distribution of individually optimized CYP2D6 k_{cat} values stratified by activity score group. Population simulations with sampling from the resulting distributions with calculated log-normal dispersion and mean parameters could explain a large extent of the observed IIV. The model is publicly available alongside comprehensive documentation of model building and model evaluation.

Ministry of Education and Research (BMBF, Horizon 2020 INSPIRATION grant 643271), under the frame of ERACoSysMed

Study Highlights

WHAT IS THE CURRENT KNOWLEDGE ON THE TOPIC?

Dextromethorphan is a substrate of cytochrome P450 2D6 (CYP2D6) and is consequently subject to considerable drug-gene interaction (DGI) effects. High interindividual variability (IIV) in dextromethorphan plasma concentrations is apparent, even within activity score groups.

WHAT QUESTION DID THIS STUDY ADDRESS?

The objective of this study was to develop a physiologically-based pharmacokinetic (PBPK) model that can describe and predict the effect of CYP2D6 DGIs on the pharmacokinetics (PK) of dextromethorphan and its metabolites dextrorphan and dextrorphan *O*-glucuronide.

WHAT DOES THIS STUDY ADD TO OUR KNOWLEDGE?

This study presents a PBPK model of dextromethorphan and its major metabolites that integrates current knowledge on relevant PK processes and DGIs. The model can accurately describe and predict the impact of CYP2D6 DGIs on the PK of the modeled analytes and was applied to explain a large extent of observed IIV in dextromethorphan plasma concentrations.

HOW MIGHT THIS CHANGE DRUG DISCOVERY, DEVELOPMENT, AND/OR THERAPEUTICS?

The developed PBPK model serves as a prototype for the development of PBPK models for other CYP2D6 substrates. Modeling provides valuable insights regarding the extent of observed overall IIV in plasma concentrations of CYP2D6 substrates as well as the observed IIV within activity score groups.

INTRODUCTION

Dextromethorphan is a widely used over-the-counter cough suppressant and a common ingredient of cold medicines marketed toward children and adults.[1] The mechanisms of action of dextromethorphan and its major metabolite dextrorphan are multifarious and include antagonism of σ1- and *N*-methyl-D-aspartate (NMDA) receptors as well as inhibition of serotonin reuptake transporters (SERTs) and norepinephrine reuptake transporters (NERTs).[2] Dextrorphan has a higher affinity to NMDA receptors than dextromethorphan and is considered to be mainly responsible for the psychoactive and euphoric effects when dextromethorphan is ingested in supratherapeutic doses as a recreational drug.[3]

Dextromethorphan is typically administered as its hydrobromide salt, which is considered a Biopharmaceutics Drug Disposition Classification System (BDDCS) class I drug with high solubility and permeability.[4] After oral administration, dextromethorphan is rapidly absorbed. Next, dextromethorphan undergoes an extensive first-pass metabolism, predominately mediated by CYP2D6, reducing the bioavailability to 1%–2% in CYP2D6 extensive metabolizers (EMs) and 80% in CYP2D6 poor metabolizers (PMs).[5] Unbound dextromethorphan accounts for 35% of the total drug plasma concentration.[2] Dextromethorphan-*O*-demethylation via CYP2D6 leads to the formation of the major active metabolite dextrorphan. Dextrorphan subsequently undergoes rapid glucuronidation via uridine diphosphate-glucuronosyltransferases 2B (UGT2Bs), namely UGT2B15, or *N*-demethylation via CYP3A4.[6] Alternatively, dextromethorphan is *N*-demethylated by CYP3A4, which was found to be the main pathway of dextromethorphan metabolism in CYP2D6 PMs.[2] Depending on the CYP2D6 phenotype, up to 50% of orally administered dextromethorphan is excreted unchanged in urine.[5,7] Because the *CYP2D6* gene is prone to genetic alterations, dextromethorphan pharmacokinetics (PK) is subject to considerable drug-gene interaction (DGI) effects. For instance, the dextromethorphan area under the plasma concentration-time curve (AUC) in CYP2D6 PMs was reported to be 26-fold higher than that of CYP2D6 EMs.[8] Hence, the US Food and Drug Administration (FDA) lists dextromethorphan as a sensitive substrate of CYP2D6 and recommends its usage in clinical drug-drug interaction studies and dextromethorphan *O*-demethylation as an in vitro marker reaction for CYP2D6 metabolism.[9] Furthermore, the dextromethorphan/dextrorphan metabolic ratio is frequently used to determine the CYP2D6 phenotype in vivo.[10,11] Hence, dextromethorphan is frequently included in different phenotyping cocktails.[12,13]

To date, more than 140 alleles of the *CYP2D6* gene are known, some of which have only been discovered in recent years.[14] With well over 10,000 potential *CYP2D6* diplotypes, investigating the effect of every genotype on a drug's PK is an unfeasible task for clinical researchers.[15] Consequently, an activity score system is in place to facilitate the process of translating the *CYP2D6* diplotype into a patient's phenotype.[15,16] This process has since been harmonized between pharmacogenomics laboratories and between clinical guidelines of the Dutch Pharmacogenomics Working Group (DPWG) and the Clinical Pharmacogenetics Implementation Consortium (CPIC).[17] Here, a patients' activity score is defined as the sum of activity values assigned to the patients' alleles with values encoding for no (0), decreased (0.25–0.5), or normal function (1), or a copy number variation of a normal function allele (>2).[15] The activity score system is an eminently useful concept for grouping study subjects based on their genotypes. However, a large interindividual variability (IIV) in the PK of CYP2D6 substrates in subjects with an identical activity score remains largely unexplained and requires further research.[16]

The objectives of this study were (1) to develop and evaluate a physiologically-based pharmacokinetic (PBPK) parent-metabolite DGI model of dextromethorphan, dextrorphan, and dextrorphan *O*-glucuronide, (2) to describe the effects of different CYP2D6 activity scores on the PK of dextromethorphan by implementing specific CYP2D6 activity score-dependent metabolic processes, and (3) to apply the developed model to explain the observed IIV in individual subjects sharing the same CYP2D6 activity score. The final PBPK model will be publicly available in the Open Systems Pharmacology (OSP) repository (www.open-systems-pharmacology.org)[18] as a clinical research tool. Moreover, the Supplementary document (Supplementary S1) to this article provides an in-depth evaluation of the model performance and can be used as a model reference manual.

METHODS

Software

The dextromethorphan PBPK model was developed using PK-Sim and MoBi (Open Systems Pharmacology Suite 9.1, www.open-systems-pharmacology.org). Model parameter optimizations via Monte Carlo algorithm and local sensitivity analyses were conducted in PK-Sim. Published clinical study data were digitized according to the recommended practice[19] using GetData Graph Digitizer 2.26.0.20 (© S. Fedorov). PK parameters, model performance metrics, and plots were calculated and generated using Python (version 3.9.1; Python Software Foundation, Wilmington, DE). Regression analyses were performed using ordinary least squares utilizing the *statsmodels* package (version 0.12.2) in Python.[20]

Clinical study data

Published clinical studies were obtained from the literature, including aggregated plasma concentration-time profiles after intravenous and oral administrations in single and multiple dose regimens of dextromethorphan alone or various phenotyping cocktails. It was assumed that there were no relevant mutual interactions between the cocktail compounds affecting dextromethorphan PK.[12,21] The composition of phenotyping cocktails used in the respective studies is provided in Section S1.1 of Supplementary S1. All collected dextromethorphan plasma concentration-time profiles were split into a training dataset, for model building and a test dataset, for model evaluation. Studies for model training were selected to include different routes of administration (intravenous and oral), a wide range of administered doses as well as data covering all investigated *CYP2D6* genotypes or activity scores. The training dataset was used for estimation of model input parameters which could not be obtained from the literature. Studies were complemented by individual dextromethorphan, dextrorphan, and total dextrorphan (dextrorphan and dextrorphan *O*-glucuronide) plasma profiles from 72 study participants. The respective data was reported in a PhD thesis by Frank in 2009 as a compilation of four clinical cocktail studies (studies A–E).[22] Study B was excluded from the dataset due to inconsistencies between the reported individual genotypes and the corresponding plasma concentrations of dextromethorphan, which may be explained by the limited set of genetic *CYP2D6* variants assessed (see Section S6.1 of Supplementary S1 for a detailed analysis). Sections S2.2, S4.2, and S6.3 of Supplementary S1 provide comprehensive information on population and individual demographics (sex, age, weight, and height), analyzed compounds, CYP2D6 activity (CYP2D6 phenotype, genotype, and activity score, if available), drug dosing regimens and the assignment to the respective test and training datasets for all modeled studies and individual profiles.

PBPK base model building

The dextromethorphan PBPK model building process started with an extensive literature search to obtain physicochemical data on dextromethorphan, dextrorphan, and dextrorphan *O*-glucuronide as well as information on absorption, distribution, metabolism, and excretion. The

dextromethorphan PBPK model was developed using individual simulations based on typical mean individuals for the respective study populations (see Section S1.3 of Supplementary S1). First, a combination of quantitative structure-activity relationship methods implemented in PK-Sim was selected for the estimation of cellular permeabilities and organ/plasma partition coefficients. Here, the selection of the optimal combination was based on the minimum residual error for parameter estimations fitting intravenous dextromethorphan administration simulations to their respective observed data. Subsequently, studies of orally administered dextromethorphan in PMs were used to optimize model parameters independent of CYP2D6 metabolism, as the CYP2D6 activity of poor metabolizers was assumed to be 0% due to the lack of expression of functional CYP2D6 protein in carriers of two CYP2D6 loss-of-function alleles (e.g., *CYP2D6*3*, **4*, and **6*).[10] Finally, CYP2D6 catalytic rate constant (k_{cat}) values were optimized for EMs by fitting to EM plasma concentration-time profiles of the training dataset. Here, the historical term "extensive metabolizer" was used to describe populations which were either not phenotyped or phenotyped via classical phenotyping methods, such as measurements of metabolic ratios or screening for *CYP2D6* null alleles. Genotyped populations possessing activity scores ranging from 1.25–2.25 were considered "normal metabolizers."[17]

Overall, the minimal number of processes necessary to mechanistically describe the PK of dextromethorphan, dextrorphan, and dextrorphan *O*-glucuronide were implemented to limit the number of unknown parameter values to be optimized. Total dextrorphan was calculated as the sum of simulated dextrorphan and dextrorphan *O*-glucuronide. System-dependent parameters and details on the implementation of CYP2D6, CYP3A4, and UGT2B15 are presented in Section S7 of Supplementary S1.

PBPK model evaluation

Performance of the PBPK model regarding the prediction of dextromethorphan and its metabolites dextrorphan and dextrorphan *O*-glucuronide was evaluated using graphical and statistical methods.

First, simulated population plasma concentrations (arithmetic mean ± SD) were compared graphically to observed data of the respective clinical studies. For this, virtual populations of 1000 individuals were created using the mode of reported sex and ethnicity as well as mean values for age, weight, and height from each study protocol. Sections S1.3 and S1.4 of Supplementary S1 provide a comprehensive description of virtual individuals and virtual populations.

Second, the arithmetic mean of population simulations or individual predictions for all plasma concentration-time profiles were plotted against their corresponding observed values in goodness-of-fit plots.

Third, predicted and observed AUC values and maximum plasma concentration (C_{max}) values were graphically compared. Here, all AUC values (predicted as well as observed) were calculated from the time of the first measurement to the time of the last measurement (AUC_{last}).

Finally, as quantitative measures of the model performance, the mean relative deviation (MRD) of all predicted plasma concentrations (Equation 1) and the geometric mean fold error (GMFE) of all predicted AUC_{last} and C_{max} values (Equation 2) were calculated.

$$\mathrm{MRD} = 10^{x};\ x = \sqrt{\frac{\sum_{i=1}^{k} (\log_{10}\hat{c}_i - \log_{10}c_i)^2}{k}} \tag{1}$$

where $\hat{c}_i$ = predicted plasma concentration that corresponds to the i-th observed concentration, c_i = i-th observed plasma concentration, k = number of observed values.

$$\mathrm{GMFE} = 10^{x};\ x = \frac{\sum_{i=1}^{m} \left|\log_{10}\left(\frac{\hat{\rho}_i}{\rho_i}\right)\right|}{m} \tag{2}$$

where $\hat{p}_i$ = predicted AUC_{last} or C_{max} value of study p_i = corresponding observed AUC_{last} or C_{max} value of study i, m = total number of studies.

Local sensitivity of the $AUC_{0-24\,h}$ of dextromethorphan, dextrorphan, and dextrorphan *O*-glucuronide to single parameter changes was analyzed for a simulation of 30 mg orally administered dextromethorphan hydrobromide as a single dose (standard dose). Parameters were included if they have been optimized (k_{cat} values and dextromethorphan intestinal permeability), if they are associated with optimized parameters (K_M values) or if they might have a strong impact due to calculation methods used (lipophilicity, fraction unbound, and pK_a values). A detailed description is provided in Section S1.6 of Supplementary S1 and a list of all parameters included in the sensitivity analysis is given in Section S3.6 of Supplementary S1.

DGI model building

The principal pathway of dextromethorphan metabolism is the CYP2D6-mediated *O*-demethylation, leading to the formation of dextrorphan. This pathway was implemented using Michaelis-Menten kinetics according to Equation 3[23]:

$$V = \frac{V_{max} \cdot S}{K_M + S} = \frac{k_{cat} \cdot E \cdot S}{K_M + S} \tag{3}$$

where v = reaction velocity at substrate concentration S, V_{max} = maximum reaction velocity, K_M = Michaelis-Menten constant, k_{cat} = catalytic rate constant, and E = enzyme concentration.

For DGI modeling, the CYP2D6 Michaelis-Menten constant (K_M) values for the dextromethorphan *O*-demethylation were kept constant over the whole range of modeled activity scores.[24] CYP2D6 k_{cat} values were optimized separately for each activity score. CYP2D6 PMs (activity score = 0) were assumed to show no CYP2D6 activity (0%), whereas populations with two wildtype alleles (activity score = 2) were assumed to possess normal CYP2D6 activity (100%). Activity scores were assigned according to Caudle et al.[17]

DGI model evaluation

Modeled DGIs were evaluated by comparison of predicted versus observed plasma concentration-time profiles of dextromethorphan and its metabolites. Plasma concentration-time profiles for populations displaying variant phenotypes were compared to those of the EM phenotype, whereas plasma concentration-time profiles for populations with a variant activity score were compared to profiles of a population with normal activity (activity score = 2) in studies reporting activity scores or genotypes. Similarly, predicted DGI AUC_{last} ratios (Equation 4) and DGI C_{max} ratios (Equation 5) were evaluated for study populations with different CYP2D6 activity scores or phenotypes.

$$\text{DGI AUC}_{\text{last}}\text{ ratio} = \frac{\text{AUC}_{\text{last, DGI}}}{\text{AUC}_{\text{last, reference}}} \tag{4}$$

Here, $AUC_{last,\ DGI}$ = AUC_{last} of variant activity score or phenotype, $AUC_{last,\ reference}$ = AUC_{last} of activity score = 2 or EM phenotype.

$$\text{DGI C}_{\text{max}}\text{ ratio} = \frac{\text{C}_{\text{max, DGI}}}{\text{C}_{\text{max, reference}}} \tag{5}$$

with $C_{max,\ DGI}$ = C_{max} of variant activity score or phenotype, $C_{max,\ reference}$ = C_{max} of activity score = 2 or EM phenotype.

Additionally, GMFE values of the predicted DGI AUC_{last} ratios and DGI C_{max} ratios were calculated according to Equation 2 as a quantitative measure of prediction accuracy.

Assessment of interindividual variability within activity score groups

To assess the impact of IIV on the PK of dextromethorphan, CYP2D6 k_{cat} values were optimized separately, using their respective observed data, for all individual plasma concentration-time profiles of the four cocktail studies. Activity scores for all genotyped subjects were calculated according to Caudle et al.[17] Subjects with the same activity scores were grouped and geometric means and standard deviations were calculated from the optimized individual CYP2D6 k_{cat} values. Subsequently, these values were graphically compared to the population k_{cat} values, obtained in the model building process. Finally, an ordinary least squares regression analysis was applied between individual optimized k_{cat} and their population k_{cat} counterpart for the respective activity score.

RESULTS

PBPK base model building

The dextromethorphan PBPK model was developed using a total of 28 clinical studies where dextromethorphan was administered as an intravenous infusion (one study), orally in single (26 studies), or multiple doses (one study), alone (17 studies) or as part of a phenotyping cocktail (11 studies). Doses ranged between 5 and 80 mg of administered dextromethorphan. Table 1 provides an overview of demographics and CYP2D6 activity for all modeled studies.

For dextromethorphan, the PBPK model implements metabolism via CYP2D6 (leading to the formation of dextrorphan) and CYP3A4 as well as excretion via passive glomerular filtration. To emulate the effect of lysosomal trapping in the gastrointestinal mucosa,[25,26] a binding process was included in the model that is comprehensively described in Section S1.5 of Supplementary S1.

The primary metabolite dextrorphan is metabolized via CYP3A4 and UGT2B15. The latter serves as a surrogate pathway in the model for the glucuronidation via multiple UGT2B enzymes, as UGT2B15 was reported to have the largest contribution of all involved UGTs.[6] Dextrorphan *O*-glucuronide is renally eliminated via passive glomerular filtration and active secretion to the urine. Other dextromethorphan metabolites, such as 3-methoxymorphinan or 3-hydroxymorphinan, were not included as model compounds due to the limited number of published plasma concentration-time profiles for these analytes.

An overview of the implemented model compounds and pathways is provided in Figure 1. For dextromethorphan, dextrorphan, and dextrorphan *O*-glucuronide, the drug-dependent model input parameters are provided in Section S2.1 of Supplementary S1.

PBPK base model evaluation

Overall, the PBPK model accurately predicted dextromethorphan, dextrorphan, and dextrorphan O-glucuronide plasma

TABLE 1 Summary of demographic parameters and CYP2D6 activity for all modeled studies

	Dataset I: Base model building and evaluation	Dataset II: DGI model building and evaluation	Dataset III: Studies reporting individual data				
			A	B	C	D	E
Number of studies	15	13					
Number of individuals	309	120	16	12	16	12	28
Demographics							
Females, %	27	37	0	0	0	0	25
Age, years	31 (19–74)	26 (18–55)	29 (23–42)	36 (24–49)	29 (21–43)	32 (18–48)	40 (25–60)
Weight, kg	74 (49–110)	69 (60–79)	78 (65–101)	80 (60–103)	80 (66–99)	72 (60–82)	72 (49–106)
Height, cm	*	*	182 (171–195)	181 (165–198)	182 (173–194)	180 (171–190)	174 (156–190)
CYP2D6 activity							
Phenotype[a]							
PM	1	2	1	1	–	–	1
IM	–	3	7	5	2	4	13
EM	14	2	–	–	4	1	–
NM	–	6	4	6	9	7	13
UM	–	–	2	–	1	–	1
Activity score[a]							
0	–	–	1	1	–	–	1
0.25	–	2	1	–	–	–	–
0.5	–	2	–	1	1	–	–
1	–	1	7	3	1	4	13
1.25	–	2	–	–	–	–	–
1.5	–	–	1	1	4	2	–
2	–	4	4	5	4	5	13
3	–	–	2	–	1	–	1
Dextromethorphan observed AUC_{last}, ng·h/ml							
Phenotype							
PM	981.2	756.7 (547.7)					
EM	39.2 (30.1)	40.4 (25.8)					

TABLE 1 (Continued)

	Dataset I: Base model building and evaluation	Dataset II: DGI model building and evaluation	Dataset III: Studies reporting individual data				
			A	B	C	D	E
Activity score							
0			162.4	3.1			97.6
0.25			146.3				
0.5		73.5 (5.8)		3.9 (2.5)	63.7		
1		63.54	5.7 (1.5)	8.2 (5.2)	5.1	14.6 (15.3)	36.4 (57.4)
1.25		22.0 (1.1)					
1.5			17.3	5.9	3.5 (2.3)	16.4 (16.2)	
2		10.2 (3.7)	0.6 (0.5)	49.3 (53.6)	0.5 (0.2)	4.3 (5.2)	8.7 (7.0)
3			0.4 (0.2)				2.3

Note: AUC_{last} values are given as arithmetic mean (SD), demographic parameters are given as mean (range). *Insufficient data available to calculate mean values; –, not available, [a]given as mode of every study for datasets I and II, or number of individuals with the respective activity score for dataset III.

Abbreviations: AUC_{last}, area under the plasma concentration-time curve from the time of the first concentration measurement to the time of the last concentration measurement; DGI, drug-gene interaction.

concentrations after intravenous and oral administration with a selection of predicted compared to observed plasma concentration time-profiles presented in Figure 2. The simulations of all 28 modeled population studies are shown in sections S3.1 and S5.1 of Supplementary S1.

Goodness-of-fit plots comparing predicted and observed plasma concentrations, AUC_{last} and C_{max} values are presented in Figure 3. Overall, 70.6% of predicted plasma concentrations were within the two-fold range of the corresponding observed concentrations. Furthermore, 35 of 42 of the predicted AUC_{last} values (several studies included measurements of multiple analytes) and 35 of 41 of the predicted C_{max} values were within two-fold range with model GMFE values of 1.53 (range 1.01–3.45) for predicted AUC_{last} and 1.46 (range 1.01–2.97) for predicted C_{max} values. MRD values of predicted plasma concentrations as well as AUC_{last} and C_{max} ratios for all 28 clinical studies and all measured analytes are provided in sections S3.3, S3.5, S5.3, and S5.5 of Supplementary S1.

A simulation of 30 mg dextromethorphan hydrobromide administered orally (standard dose) was used for local sensitivity analysis. Parameters with associated sensitivity values greater than 0.5 (100% parameter value perturbation resulting in a greater than 50% change of predicted AUC) were considered sensitive. Sensitive parameters were, in order of highest to lowest impact, f_u (literature value), CYP2D6 k_{cat} (optimized value), lipophilicity (literature value), CYP2D6 K_M (literature value), and intestinal permeability (optimized value). A quantitative and visual representation of the local sensitivity analysis is provided in Section S3.6 of Supplementary S1.

DGI model building

The DGI model training dataset consisted of four studies that reported CYP2D6 activity scores or genotypes of their respective study populations. To complement these studies, 24 individual plasma concentration-time profiles were included. The assignment of studies and individual profiles to the respective datasets is listed in sections S4.2 and S6.3 of Supplementary S1.

Overall, activity scores in the DGI model training dataset ranged from 0 (PM) to 3 (ultrarapid metabolizer) and covered a total of eight activity scores. This dataset was used to optimize population k_{cat} values for the activity scores of the respective studies or individual profiles (see Section S4.1 of Supplementary S1).

DGI model evaluation

The DGI model was evaluated using a total of 13 clinical population studies, which stratified their subjects by

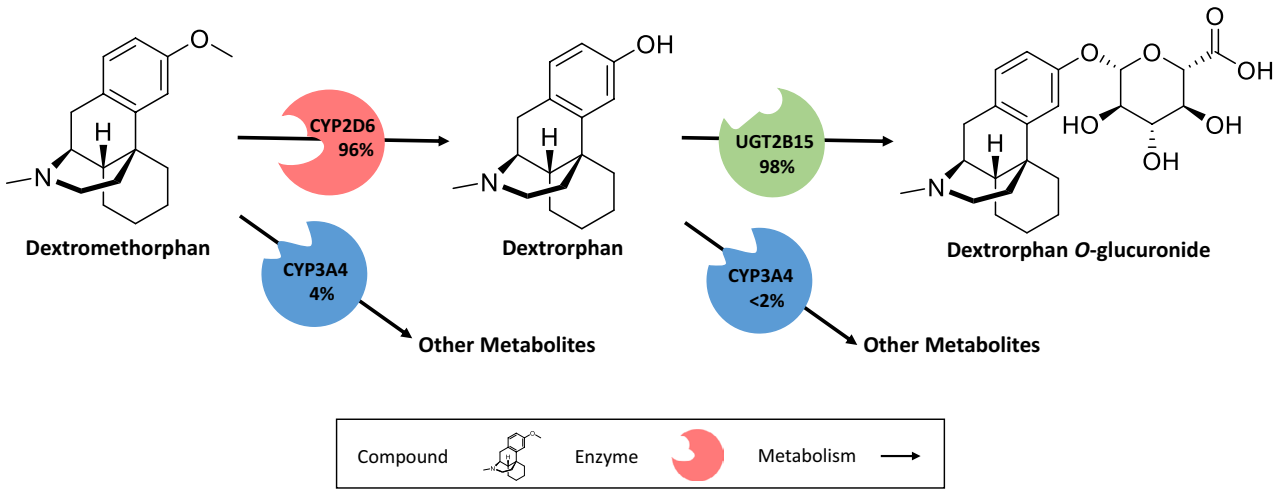

FIGURE 1 Implemented dextromethorphan metabolic pathways. Dextromethorphan is *O*-demethylated by CYP2D6 and *N*-demethylated by CYP3A4. The metabolite dextrorphan is further metabolized via CYP3A4 (*N*-demethylation) and UGT2B15 (*O*-glucuronidation). Dextrorphan *O*-glucuronide is excreted in the urine. Percentages shown refer to the fraction metabolized by the respective enzyme, calculated for extensive metabolizers of CYP2D6. CYP2D6: cytochrome P450 2D6, CYP3A4: cytochrome P450 3A4, UGT2B15: Uridine 5′-diphospho-glucuronosyltransferase 2B15

CYP2D6 activity score or phenotype. These studies either provided the CYP2D6 phenotype (4 studies) or comprehensive information on the *CYP2D6* genotype of individuals (9 studies). Simulations were performed using the corresponding k_{cat} values with respect to activity score (Section S4.1 of Supplementary S1) or phenotype (Section S2.1 of Supplementary S1).

The good performance of the final dextromethorphan DGI model is demonstrated in Figure 4a–e depicting predicted dextromethorphan plasma concentration-time profiles of populations with different activity scores compared to their respective observed data. Plots documenting the model performance of all 15 DGI studies are provided in Section S5.1 of Supplementary S1.

Predicted DGI AUC_{last} and C_{max} ratios were in good agreement with observed DGI ratios, demonstrating that the effect of different CYP2D6 activity scores on the PK of dextromethorphan and dextrorphan was well-described by the model. Specifically, six of seven AUC_{last} and six of six C_{max} ratios were within the prediction success limits suggested by Guest et al. adopted for DGI evaluations,[27] as visualized in Figure 4f,g. The predicted DGI AUC_{last} ratios showed an overall GMFE of 1.45 (range 1.04–2.84) and the overall GMFE of predicted DGI C_{max} ratios was calculated as 1.21 (range 1.02–1.40). Predicted to observed DGI AUC_{last} and C_{max} ratios for all studies are provided in Section S5.5 of Supplementary S1. Predictions of dextromethorphan, dextrorphan, and dextrorphan *O*-glucuronide exposure in individuals with different activity scores after a single oral dose of 30 mg dextromethorphan hydrobromide and a comparison of the corresponding AUC values are given in Figure 5.

Interindividual variability within activity score groups

The individual profiles from four cocktail studies were used to assess the extent of IIV within activity score groups. For 66 of the 72 study subjects, the *CYP2D6* genotype was provided. Six subjects were not genotyped and consequently excluded from this analysis.

The distribution of activity scores from the dataset is listed in Section S6.2 of Supplementary S1. Plasma concentration-time profiles of dextromethorphan, dextrorphan, and total dextrorphan were simulated using the population k_{cat} values given in Section S4.1 of Supplementary S1. Additionally, the profiles were simulated using individually optimized k_{cat} values and the geometric mean with geometric standard deviation of the individual k_{cat} values were calculated for all activity score groups with n greater than 2 (see Section S6.2 of Supplementary S1).

A representative selection of predictions using individual and model CYP2D6 k_{cat} values is visualized in Figure 6. Furthermore, Section S6.4 of Supplementary S1 includes plots with model and individual predictions for all 66 genotyped individuals alongside model predictions for the six non-genotyped individuals. The latter were simulated using the population k_{cat} value for EMs (see Section S2.1 of Supplementary S1).

The predictive performance using model k_{cat} was compared to using the individual optimized k_{cat} values by calculating the GMFE for all individual plasma concentration-time profiles (see Sections S6.7, S6.8, and S8 of Supplementary S1). Generally, model performance improved for simulations of dextromethorphan and

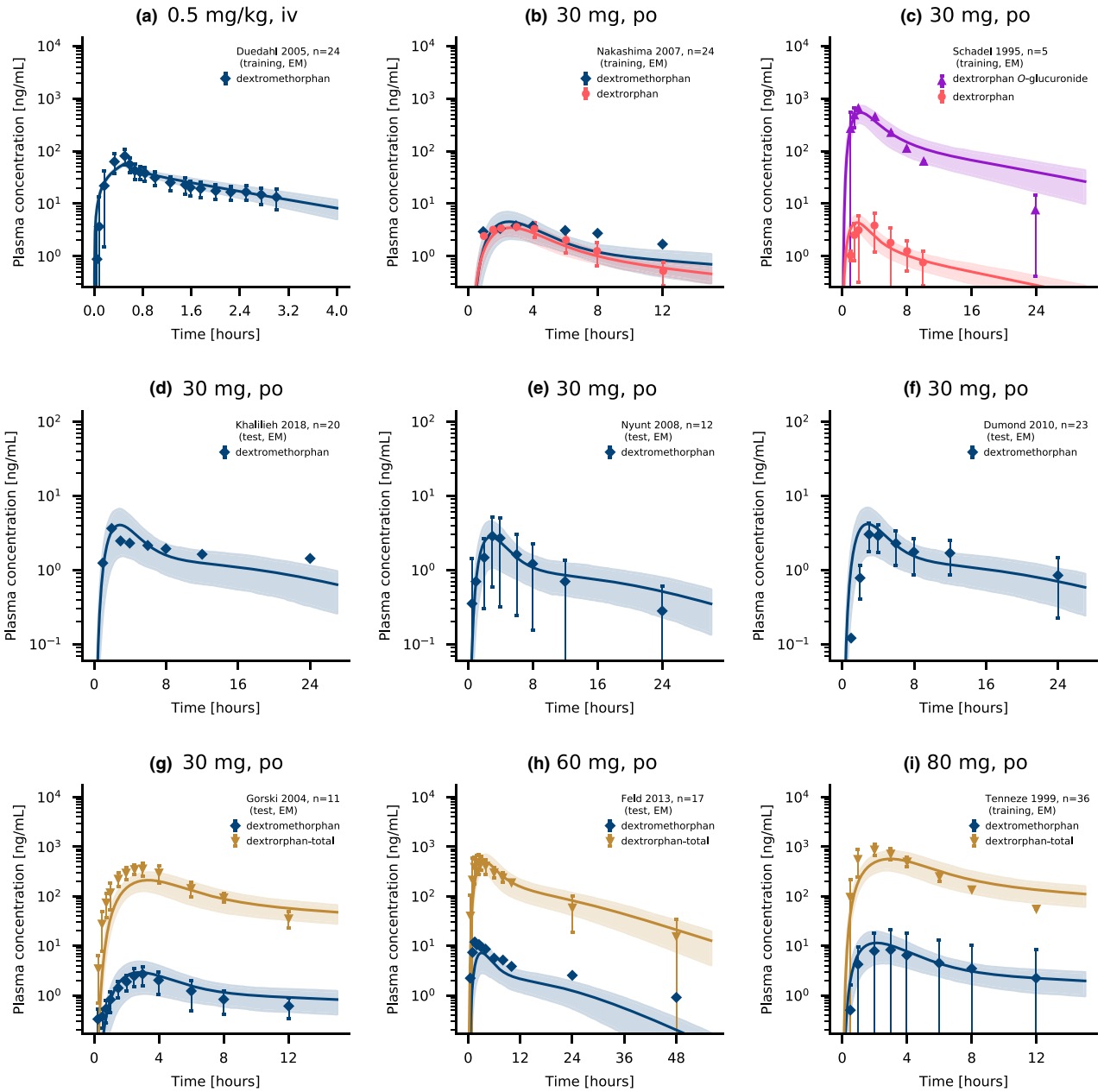

FIGURE 2 Dextromethorphan and dextrorphan plasma concentrations. Model predictions of dextromethorphan and its metabolites dextrorphan and dextrorphan *O*-glucuronide as well as total dextrorphan (dextrorphan + dextrorphan *O*-glucuronide) plasma concentration-time profiles of selected intravenous (a) and oral studies (b–i) from the training and test datasets, compared to observed data.[7,8,45–51] Population predictions (n = 1000) are shown as lines with ribbons (arithmetic mean ± SD), symbols present the corresponding observed data ±SD. Detailed information on all clinical studies is listed in sections S2.2 and S4.2 of Supplementary S1. iv, intravenous; po, oral

dextrorphan plasma concentration-time profiles using the individually optimized k_{cat} when compared to simulations, where population k_{cat} values were used across all activity scores and analyzed studies. However, total dextrorphan AUC_{last} and C_{max} values were markedly underpredicted for studies D and E (GMFEs of 3.93 and 3.28 for study D and 2.81 and 2.69 for study E) compared to studies A and C (GMFEs of 1.30 and 1.44 for study A and 1.20 and 1.24 for study C). Predicted to observed AUC_{last} and C_{max} ratios for all individual simulations using the model k_{cat} and the individual optimized k_{cat} are listed in Section S6.7 of Supplementary S1. Section S6.8 of Supplementary S1 gives a detailed breakdown of AUC_{last} and C_{max} ratios grouped by study and activity score.

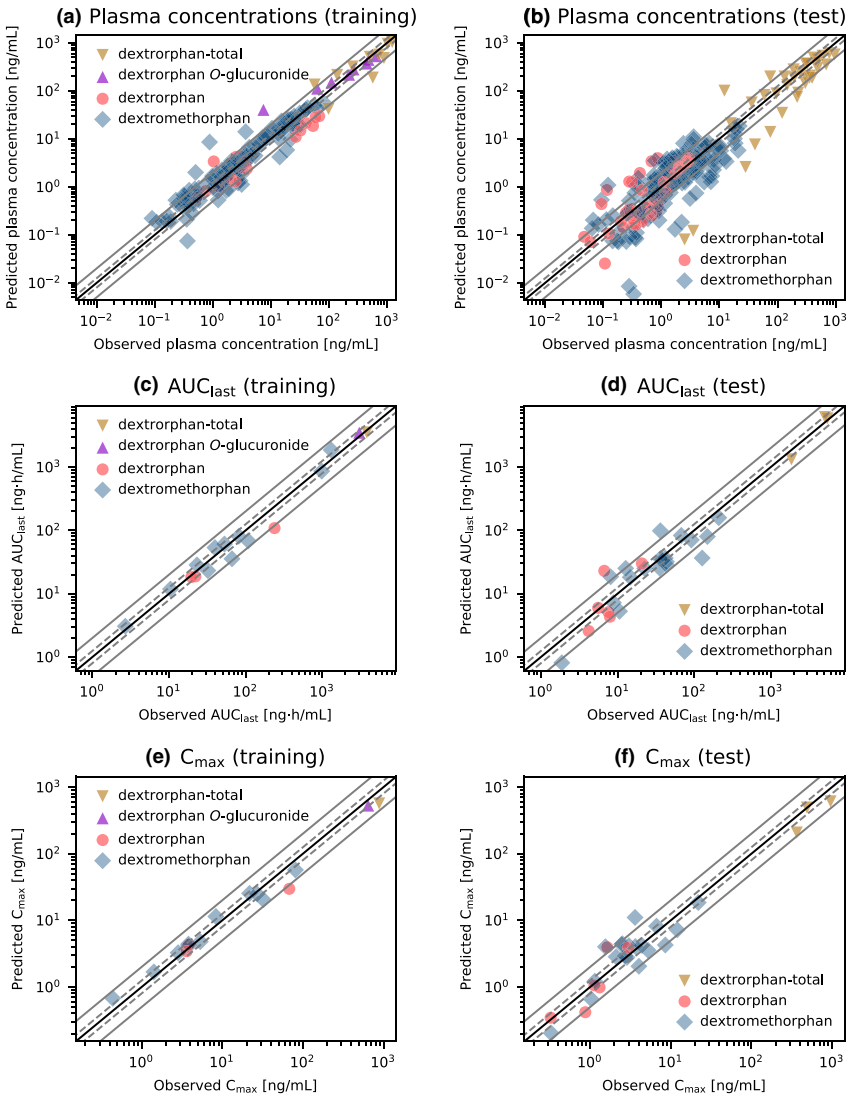

FIGURE 3 Goodness-of fit plots for the final dextromethorphan model. Predicted versus observed plasma concentrations (a, b), AUC_{last} values (c, d) and C_{max} values (e, f) for the training (left column) and test (right column) datasets. The solid black line indicates the line of identity, solid gray lines show two-fold deviation, dashed gray lines indicate 1.25-fold deviation. Detailed information on all clinical studies is listed in sections S2.2 and S4.2 of Supplementary S1. AUC_{last}, area under the plasma concentration-time curve from the time of the first concentration measurement to the time of the last concentration measurement; C_{max}, maximum plasma concentration, dextrorphan-total: sum of dextrorphan and dextrorphan *O*-glucuronide concentrations

Moreover, the optimized individual k_{cat} values for the different activity score groups were plotted against their activity score to visualize the distribution of individual k_{cat} values in the respective activity score groups (see Figure 7a). A regression analysis of model k_{cat} values compared to the geometric mean of optimized individual k_{cat} values revealed a high correlation ($R^2 = 0.9988$). Consequently, the individual profiles were sufficiently well-described with the model k_{cat} values. The results of the regression analysis are illustrated in Figure 7b.

Finally, population simulations were performed with sampling from a log-normal distribution with mean and dispersion parameters calculated from the samples of optimized individual k_{cat} values (see Section S6.2 of Supplementary S1) to analyze the simulated coverage of IIV observed in dextromethorphan plasma concentrations from the study populations.

Subsequently, predictions were compared graphically in population simulations with no variability of the CYP2D6 population k_{cat}. As expected, model predictions including the k_{cat} variability improved describing the large extent of IIV within an activity score group compared to predictions with no variability on the CYP2D6 k_{cat} (see Figure 7c–f).

DISCUSSION

In this study, a whole-body PBPK model of dextromethorphan and its metabolites dextrorphan and dextrorphan *O*-glucuronide was developed and evaluated to predict drug plasma concentrations over a wide dosing range (5–80 mg). A CYP2D6 activity score-dependent metabolism of dextromethorphan was implemented to describe the effect of CYP2D6 DGIs on the PK of the modeled compounds. Moreover, the model was applied to investigate the IIV of dextromethorphan PK within different activity score groups.

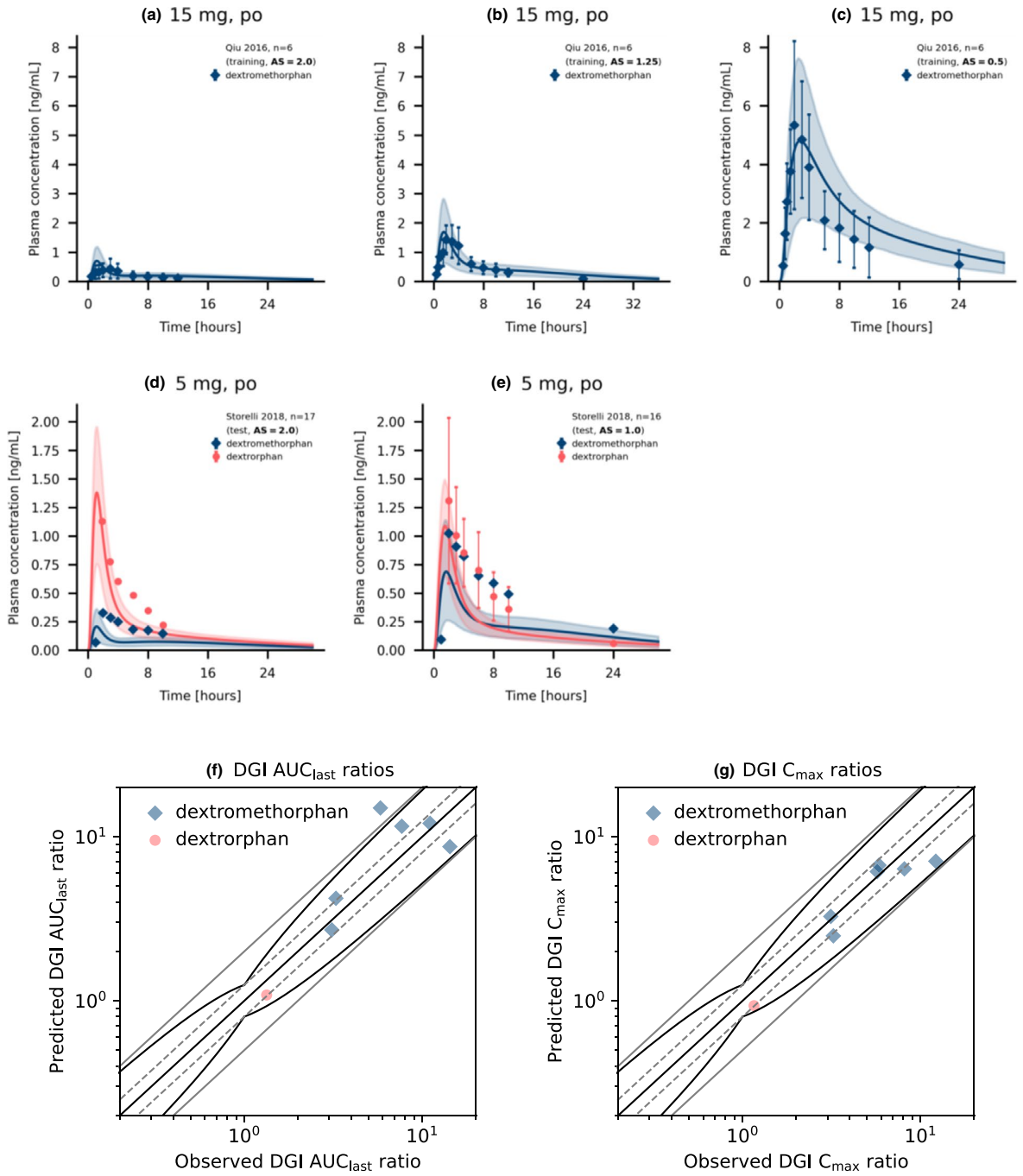

FIGURE 4 Simulated dextromethorphan and dextrorphan plasma concentrations and DGI ratios for different CYP2D6 activity scores. Upper panel: Dextromethorphan (a–c) as well as Dextromethorphan and dextrorphan (d, e) plasma concentration-time profiles of selected dextromethorphan CYP2D6 DGI studies, compared to observed data.[52,53] Population predictions ($n = 1000$) are shown as lines with ribbons (arithmetic mean ± SD), symbols present the corresponding observed data ±SD. Lower panel: comparison of predicted versus observed DGI AUC_{last} ratios (f) and DGI C_{max} ratios (g) for all analyzed dextromethorphan CYP2D6 DGI studies. The straight black line indicates the line of identity, curved black lines show prediction success limits proposed by Guest et al. including 1.25-fold variability.[27] Solid gray lines indicate two-fold deviation, dashed gray lines show 1.25-fold deviation. Detailed information on all DGI studies as well as the plotted values are given in section S4.1 and S5.4 of Supplementary S1, respectively. AS, activity score; AUC, area under the plasma concentration-time curve; AUC_{last}, AUC from the time of the first concentration measurement to the time of the last concentration measurement; C_{max}, maximum plasma concentration; DGI, drug-gene interaction; po, oral

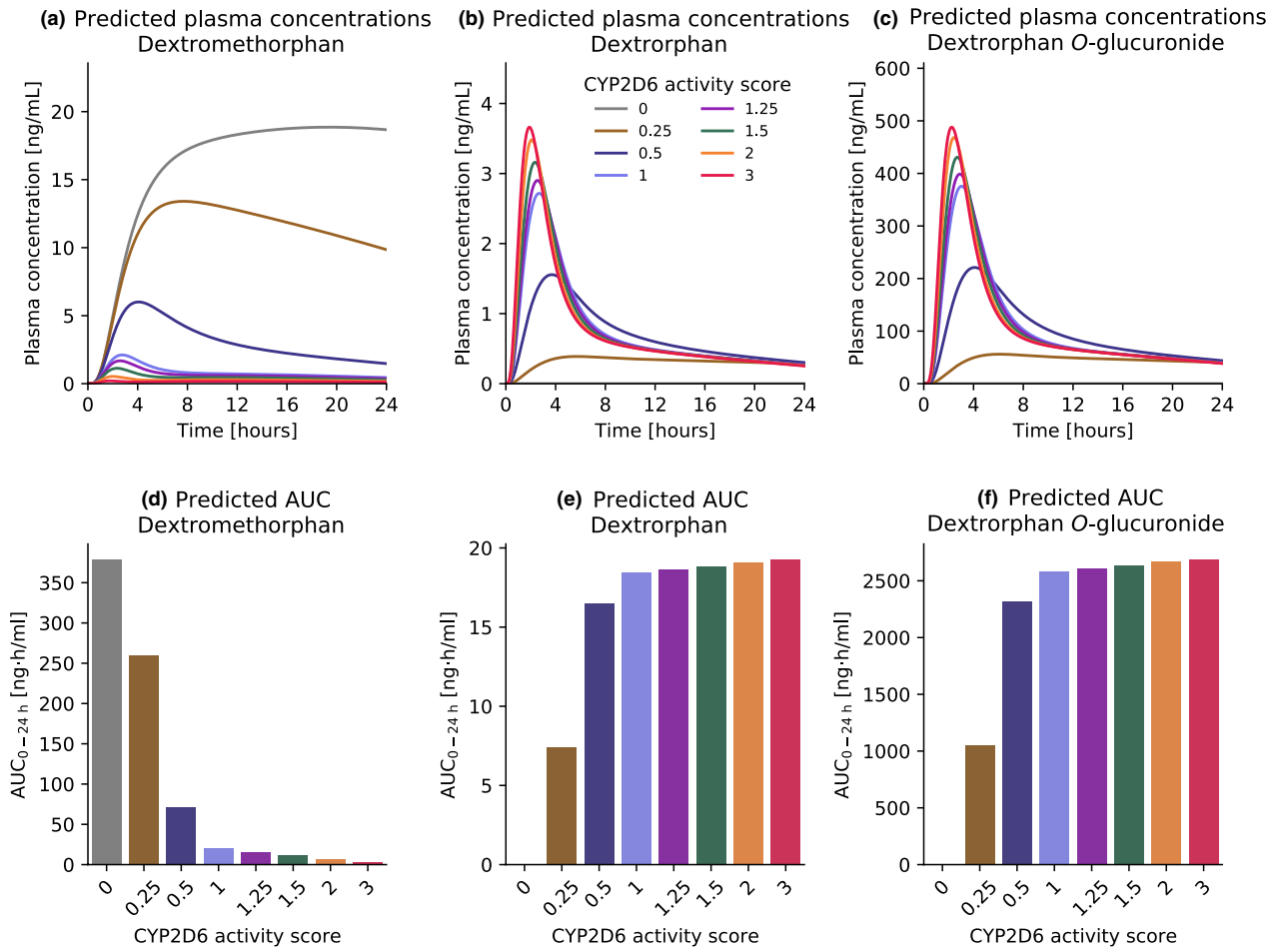

FIGURE 5 Predicted dextromethorphan, dextrorphan and dextrorphan *O*-glucuronide exposure in individuals with different activity scores. Simulations were performed for a single oral dose of 30 mg dextromethorphan hydrobromide in healthy male individuals. Top row: dextromethorphan (a), dextrorphan (b) and dextrorphan *O*-glucuronide (c) plasma concentrations. Bottom row: Dextromethorphan (d), dextrorphan (e) and dextrorphan *O*-glucuronide (f) $AUC_{0-24\,h}$ values for different activity scores. AUC, area under the plasma concentration-time curve

Three previously published PBPK models of dextromethorphan were found in the literature that focused on different aspects of PBPK modeling, specifically cross-species modeling,[28] investigation of pregnancy effects,[29] and the impact of formulations (and, by extension, lysosomal trapping)[26] on dextromethorphan pharmacokinetics. Two studies included either dextrorphan[29] or dextrorphan and dextrorphan *O*-glucuronide[26] as model compounds. These studies also included "traditional" phenotypes (EMs and PMs) in the model and did not further differentiate between CYP2D6 activity scores. Consequently, our model is the first whole-body parent-metabolite-metabolite PBPK model of dextromethorphan, aiming to investigate the effect of CYP2D6 activity scores on dextromethorphan PK, with a total of eight different activity scores implemented.

In our model, the dextromethorphan CYP2D6 DGIs were described without explicitly modeling distinct *CYP2D6* genotypes. Although a wide variety of relevant genotype-specific in vitro parameters, such as K_M and V_{max} are available in the literature,[30–32] implementing all possible genotypes using a genotype-specific approach would be infeasible due to the large (and still growing) amount of known CYP2D6 alleles.[33] Thus, a CYP2D6 activity

FIGURE 6 Dextromethorphan and dextrorphan plasma concentrations for individuals of several activity score groups. Selected dextromethorphan, dextrorphan, and total dextrorphan (dextrorphan + dextrorphan *O*-glucuronide) plasma concentration-time profiles compared to observed data reported by Frank 2009.[22] Predictions are shown as lines. Solid lines represent model predictions, dotted lines represent individual predictions. Symbols present the corresponding observed data. Detailed information on all individual profiles is listed in Sections S6.1, S6.2, and S6.3 of Supplementary S1. AS, activity score; po, oral

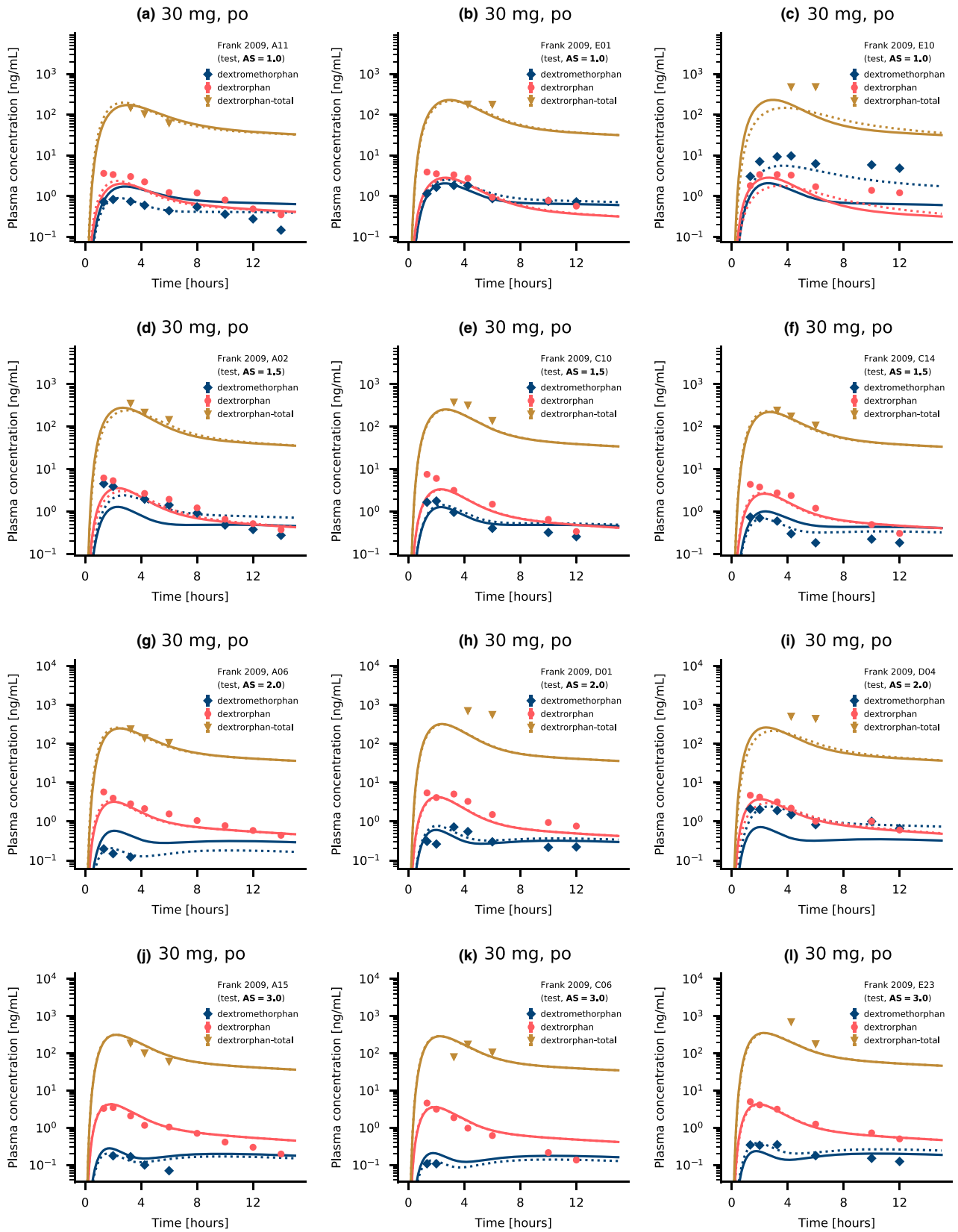
(a) 30 mg, po
Frank 2009, A11
(test, AS = 1.0)
(b) 30 mg, po
Frank 2009, E01
(test, AS = 1.0)
(c) 30 mg, po
Frank 2009, E10
(test, AS = 1.0)
(d) 30 mg, po
Frank 2009, A02
(test, AS = 1.5)
(e) 30 mg, po
Frank 2009, C10
(test, AS = 1.5)
(f) 30 mg, po
Frank 2009, C14
(test, AS = 1.5)
(g) 30 mg, po
Frank 2009, A06
(test, AS = 2.0)
(h) 30 mg, po
Frank 2009, D01
(test, AS = 2.0)
(i) 30 mg, po
Frank 2009, D04
(test, AS = 2.0)
(j) 30 mg, po
Frank 2009, A15
(test, AS = 3.0)
(k) 30 mg, po
Frank 2009, C06
(test, AS = 3.0)
(l) 30 mg, po
Frank 2009, E23
(test, AS = 3.0)
dextromethorphan
dextrorphan
dextrorphan-total
Plasma concentration [ng/mL]
Time [hours]

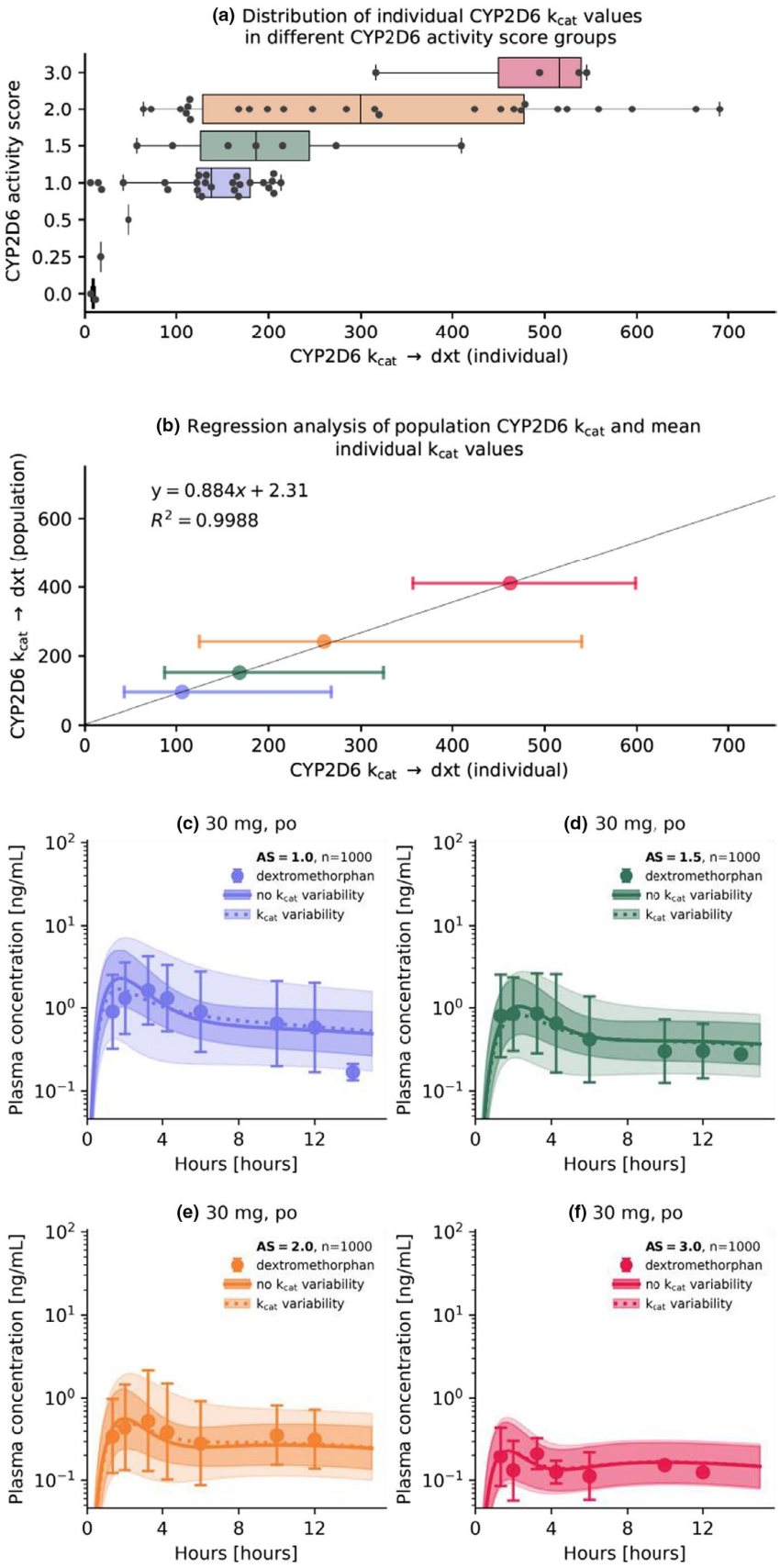

FIGURE 7 Analysis of optimized individual CYP2D6 k_{cat} values for the different activity scores and population simulations for different activity score groups. (a) Box- and scatterplots for optimized individual k_{cat} values in the respective activity score groups. Boxes represent interquartile ranges, lines within boxes represent median values. (b) Comparison of model k_{cat} and optimized geometric mean k_{cat} values and regression analysis. Colored circles represent the geometric mean k_{cat} value for an activity score group compared to the population k_{cat} value. Error bars represent the geometric standard deviation. Simulations were performed with the population k_{cat} values using a standard administration protocol (a single dose of 30 mg dextromethorphan hydrobromide) for populations with an CYP2D6 activity score of 1 (c), 1.5 (d), 2 (e), and 3 (f) with no variability and variability (calculated geometric standard deviation) on the CYP2D6 population k_{cat}. Population predictions ($n = 1000$) are represented as lines with ribbons (geometric mean with geometric standard deviation), symbols represent the corresponding observed data (geometric mean with geometric standard deviation) for the population reported by Frank 2009.[22] AS, activity score; CYP2D6, cytochrome p450 2D6; dxt, dextrorphan; k_{cat}, catalytic rate constant; R^2, coefficient of determination

score-specific approach was developed. As a result, this PBPK model cannot further differentiate between different genotypes within the same activity score group, for instance, *CYP2D6*1/*1* and *CYP2D6*2/*2*. However, the model could be readily extended to include a genotype-specific CYP2D6 metabolism in the future.

Moreover, CYP2D6 metabolism for different activity scores was implemented with a fixed K_M literature value[6] for all covered activity scores. However, in vitro data shows that K_M may vary between different genotypes and activity scores.[31,32,34] Nonetheless, a study investigating the effect of activity scores on the CYP2D6-dependent metabolism of dextromethorphan in vitro found no significant correlation between activity score and CYP2D6 K_M.[30] Most studies reported a reduction of CYP2D6-dependent clearance (CL_{int} and V_{max}/K_M) when comparing reduced function alleles (**10* and **17*) to the wildtype **1* allele.[30–32] Additionally, analyses of CYP2D6 content in HLMs showed a high positive correlation between CYP2D6 abundances and activity score, albeit substantial IIV in CYP2D6 content within activity score groups and even in groups sharing the same *CYP2D6* diplotype has been observed.[16] These trends in CYP2D6 content in HLMs and CYP2D6 CL_{int} are reflected in the final dextromethorphan PBPK model with higher CYP2D6 activity scores inferring higher population k_{cat} values (see Section S4.1 of Supplementary S1). A similar modeling approach was also utilized for previously developed PBPK models of CYP2D6 substrates.[24] The CYP2D6 k_{cat} value for populations grouped as EMs was observed to be lower than for genotyped normal metabolizers with activity scores ranging from 1.25–2.25 (compare sections S2.1 and S4.1 of Supplementary S1). Typically, study subjects in the literature were either phenotyped via measurements of urinary metabolic ratio, often using arbitrary cutoff points for poor metabolizers,[15] or via screening for null alleles.[35] Thus, there is only a limited intersection between the broad EM phenotype category and the genetically determined NMs.[36] Overall, the presented model was able to accurately describe DGI AUC_{last} and C_{max} ratios as well as the plasma concentration-time profiles of all analyzed clinical studies.

The final dextromethorphan PBPK model was applied to investigate the effect of IIV on the PK of dextromethorphan with a total of 72 individual plasma concentration-time profiles of dextromethorphan, dextrorphan, and total dextrorphan. A substantial variability was observed within activity scores 1–3 (geometric standard deviation range of 1.29–2.52). For activity scores less than 1, the number of individual profiles per score (less than 5) was insufficient to make meaningful assessments of the IIV. The large extent of IIV in the PK of CYP2D6 substrates within activity score groups or even within subjects possessing the same *CYP2D6* genotype, is a well-documented phenomenon.[16] A twin study on the heritability of metoprolol PK, concluded that genetic components independent of the *CYP2D6* gene may be responsible for the IIV in CYP2D6 activity.[37] Indeed, the rs5758550 single-nucleotide polymorphism (SNP) was identified as an enhancer SNP and may, in the future, even lead to a reclassification of activity scores based on *CYP2D6* and rs5758550 genotype.[38] Currently published literature lacks clinical in vivo studies describing the effect of the rs5758550 genotype on the PK of dextromethorphan. Other genetic factors, such as regulation of CYP2D6 expression via transcription factors or miRNA, are also likely to contribute to IIV and intraindividual variability.[16] Additionally, genetic and non-genetic variability in enzymes other than CYP2D6 are expected to contribute to the IIV in dextromethorphan PK, specifically for CYP2D6 PMs, as the fraction metabolized by CYP2D6 decreases for dextromethorphan from greater than 95% for EMs[5] to 0% for PMs of CYP2D6,[10] consequently increasing the fraction of dextromethorphan metabolized by CYP3A4. Additionally, IIV can be observed in plasma concentrations of dextrorphan and dextrorphan *O*-glucuronide, possibly caused by variability in CYP3A4 and UGT enzymes. As genotypic data for CYP3A and UGT was unavailable for study subjects, the analysis of IIV was performed for dextromethorphan plasma concentrations purely in the context of CYP2D6 activity score groups. However, as new data emerges, the presented PBPK model can mechanistically be adapted to describe these genotypic effects of *CYP2D6* and other pharmacogenes affecting the PK of dextromethorphan and its metabolites. A large extent of IIV in plasma concentrations and CYP2D6 activity was observed and quantified in this study. To reflect this in the model, the distributions of CYP2D6 k_{cat} values for activity scores 1, 1.5, 2, and 3 were characterized from k_{cat} optimizations in 72 individuals to improve population predictions, as demonstrated in Figure 7c–f, and may be used in future PBPK models of CYP2D6 substrates.

To supplement the limited number of studies in which dextromethorphan was administered alone (14 studies), studies in which dextromethorphan was administered as part of a phenotyping cocktail (11 studies and the studies compiled by Frank et al.[22]) were included in the model dataset. All modeled cocktail studies administered either the "Cologne" cocktail,[21,39] the "Cooperstown 5+1"[12] cocktail, or minor variations thereof (see Section 1.1 of Supplementary S1). No relevant mutual interactions have been observed for these cocktails, although sample sizes for these assessments were often small.[21] Additionally, assessments of these interactions are generally concerned with the effect of the cocktail on primary pathways of the cocktail compounds (i.e., dextromethorphan *O*-demethylation).[40] Here, additional in vitro experiments

are needed to evaluate possible effects of phenotyping cocktails on other model pathways, such as dextrorphan *O*-glucuronidation. Overall, plasma concentration-time profiles were well-predicted for all population studies regardless of whether dextromethorphan was administered alone or as part of a phenotyping cocktail (see Sections S3.1–S3.5 and Sections S5.1–S5.5).

Overall, model predictions were considered adequate for all population studies regardless of whether the study was a cocktail study or not (see Sections S3.2–S3.5 and S5.2–5.7 of Supplementary S1). For studies reporting individual plasma concentration-time profiles, the model performed comparably well across all activity scores. However, a large interstudy variability was observed for dextromethorphan and total dextrorphan AUC_{last} and C_{max} values (see Section S6.8 of Supplementary S1). For instance, studies D and E reported up to four-fold higher AUC_{last} and C_{max} values for total dextrorphan compared with studies A and C. As these studies were comparable in study design, cocktail composition, and sample analysis, as well as dextromethorphan and dextrorphan plasma concentrations, this apparent discrepancy was attributed to relatively small study cohorts and the large extent of IIV in CYP2D6 activity (see Figure 7a,b) described in the published literature.[16]

Finally, the developed and evaluated PBPK model of dextromethorphan is a useful tool for clinicians to investigate the effect of CYP2D6 DGIs and the associated IIV on the PK of dextromethorphan and its metabolites. The mechanistical model can be extended to be used in other PBPK modeling scenarios, such as the prediction of drug-drug interaction and DGI effects[41] and scaling to special populations, such as pediatrics,[42] geriatrics,[43] or patients with renal or hepatic impairment.[44] Moreover, the modeling approach presented in this study can serve as a blueprint to develop PBPK models of other CYP2D6 substrates.

ACKNOWLEDGEMENTS

Open Access funding enabled and organized by Projekt DEAL.

CONFLICT OF INTEREST

The authors declared no competing interests for this work.

AUTHOR CONTRIBUTIONS

S.R., D.S., U.F., M.S., and T.L. wrote the manuscript. T.L., D.S., and S.R. designed the research. S.R. performed the research. S.R., D.S., and T.L. analyzed the data.

REFERENCES

1. Guenin E, Armogida M, Riff D. Pharmacokinetic profile of dextromethorphan hydrobromide in a syrup formulation in children and adolescents. *Clin Drug Investig*. 2014;34:609-616.
2. Taylor CP, Traynelis SF, Siffert J, Pope LE, Matsumoto RR. Pharmacology of dextromethorphan: Relevance to dextromethorphan/quinidine (Nuedexta®) clinical use. *Pharmacol Ther*. 2016;164:170-182.
3. Zawertailo LA, Kaplan HL, Busto UE, Tyndale RF, Sellers EM. Psychotropic effects of dextromethorphan are altered by the CYP2D6 polymorphism. *J Clin Psychopharmacol*. 1998;18:332-337.
4. Benet LZ, Broccatelli F, Oprea TI. BDDCS applied to over 900 drugs. *AAPS J*. 2011;13:519-547.
5. Capon DA, Bochner F, Kerry N, Mikus G, Danz C, Somogyi AA. The influence of CYP2D6 polymorphism and quinidine on the disposition and antitussive effect of dextromethorphan in humans. *Clin Pharmacol Ther*. 1996;60:295-307.
6. Lutz JD, Isoherranen N. Prediction of relative in vivo metabolite exposure from in vitro data using two model drugs: dextromethorphan and omeprazole. *Drug Metab Dispos*. 2012;40:159-168.
7. Schadel M, Wu D, Otton SV, Kalow W, Sellers EM. Pharmacokinetics of dextromethorphan and metabolites in humans. *J Clin Psychopharmacol*. 1995;15:263-269.
8. Gorski JC, Huang S-M, Pinto A, et al. The effect of echinacea (Echinacea purpurea root) on cytochrome P450 activity in vivo. *Clin Pharmacol Ther*. 2004;75:89-100.
9. FDA. FDA Drug Development and Drug Interactions: Table of Substrates, Inhibitors and Inducers. https://www.fda.gov/drugs/drug-interactions-labeling/drug-development-and-drug-interactions-table-substrates-inhibitors-and-inducers#table2-1.
10. Zanger UM, Raimundo S, Eichelbaum M. Cytochrome P450 2D6: overview and update on pharmacology, genetics, biochemistry. *Naunyn Schmiedebergs Arch Pharmacol*. 2004;369:23-37.
11. Cicali EJ, Smith DM, Duong BQ, Kovar LG, Cavallari LH, Johnson JA. A scoping review of the evidence behind cytochrome P450 2D6 isoenzyme inhibitor classifications. *Clin Pharmacol Ther*. 2020;108:116-125.
12. Chainuvati S, Nafziger AN, Steven Leeder J, et al. Combined phenotypic assessment of cytochrome P450 1A2, 2C9, 2C19, 2D6, and 3A, N-acetyltransferase-2, and xanthine oxidase activities with the 'Cooperstown 5+1 cocktail'. *Clin Pharmacol Ther*. 2003;74:437-447.
13. Ryu JY, Song IS, Sunwoo YE, et al. Development of the 'Inje cocktail' for high-throughput evaluation of five human cytochrome P450 isoforms in vivo. *Clin Pharmacol Ther*. 2007;82:531-540.
14. Pharmacogene Variation Consortium (PharmVar) CYP2D6 gene. *Gaedigk al. 2018, CPT 103399; Gaedigk al. 2019, CPT 10529* at https://www.pharmvar.org/gene/CYP2D6, (Gaedigk et al 2018, CPT 103:399; Gaedigk et al 2019, CPT 105:29).
15. Gaedigk A, Simon SD, Pearce RE, Bradford LD, Kennedy MJ, Leeder JS. The CYP2D6 activity score: translating genotype information into a qualitative measure of phenotype. *Clin Pharmacol Ther*. 2008;83:234-242.
16. Gaedigk A, Dinh JC, Jeong H, Prasad B, Ten Leeder JS. years' experience with the CYP2D6 activity score: a perspective on future investigations to improve clinical predictions for precision therapeutics. *J Pers Med*. 2018;8:1-15.
17. Caudle KE, Sangkuhl K, Whirl-Carrillo M, et al. Standardizing CYP 2D6 genotype to phenotype translation: consensus recommendations from the clinical pharmacogenetics

implementation consortium and Dutch pharmacogenetics working group. *Clin Transl Sci*. 2020;13:116-124.
18. Lippert J, Burghaus R, Edginton A, et al. Open systems pharmacology community—an open access, open source, open science approach to modeling and simulation in pharmaceutical sciences. *CPT Pharmacometrics Syst Pharmacol*. 2019;8:878-882.
19. Wojtyniak JG, Britz H, Selzer D, Schwab M, Lehr T. Data digitizing: accurate and precise data extraction for quantitative systems pharmacology and physiologically-based pharmacokinetic modeling. *CPT Pharmacometrics Syst Pharmacol*. 2020;9:322-331.
20. Seabold S, Perktold J. Statsmodels: econometric and statistical modeling with Python. *Proc 9th Python Sci Conf*. 2010:92-96. https://conference.scipy.org/proceedings/scipy2010/seabold.html
21. Fuhr U, Jetter A, Kirchheiner J. Appropriate phenotyping procedures for drug metabolizing enzymes and transporters in humans and their simultaneous use in the 'cocktail' approach. *Clin Pharmacol Ther*. 2007;81:270-283.
22. Frank D. Bewertung von pharmakokinetischen Parametern zur Phänotypisierung des menschlichen Cytochrom P450 Enzyms CYP2D6 mittels Dextromethorphan. (2009). https://bonndoc.ulb.uni-bonn.de/xmlui/bitstream/handle/20.500.11811/4056/1707.pdf?sequence=1&isAllowed=y
23. Open Systems Pharmacology Suite Community Open Systems Pharmacology Suite Manual, Version 7.4. (2018). https://github.com/Open-Systems-Pharmacology/OSPSuite.Documentation/blob/master/OpenSystemsPharmacologySuite.pdf
24. Rüdesheim S, Wojtyniak J-G, Selzer D, et al. Physiologically based pharmacokinetic modeling of metoprolol enantiomers and α-hydroxymetoprolol to describe CYP2D6 drug-gene interactions. *Pharmaceutics*. 2020;12:1200.
25. Kazmi F, Hensley T, Pope C, et al. Lysosomal sequestration (trapping) of lipophilic amine (cationic amphiphilic) drugs in immortalized human hepatocytes (Fa2N-4 cells). *Drug Metab Dispos*. 2013;41:897-905.
26. Bolger MB, Macwan JS, Sarfraz M, Almukainzi M, Löbenberg R. The irrelevance of in vitro dissolution in setting product specifications for drugs like dextromethorphan that are subject to lysosomal trapping. *J Pharm Sci*. 2019;108:268-278.
27. Guest EJ, Aarons L, Houston JB, Rostami-Hodjegan A, Galetin A. Critique of the two-fold measure of prediction success for ratios: application for the assessment of drug-drug interactions. *Drug Metab Dispos*. 2011;39:170-173.
28. Thiel C, Schneckener S, Krauss M, et al. A systematic evaluation of the use of physiologically based pharmacokinetic modeling for cross-species extrapolation. *J Pharm Sci*. 2015;104:191-206.
29. Ke AB, Nallani SC, Zhao P, Rostami-Hodjegan A, Isoherranen N, Unadkat JD. A physiologically based pharmacokinetic model to predict disposition of CYP2D6 and CYP1A2 metabolized drugs in pregnant women. *Drug Metab Dispos*. 2013;41:801-813.
30. Storelli F, Desmeules J, Daali Y. Genotype-sensitive reversible and time-dependent CYP2D6 inhibition in human liver microsomes. *Basic Clin Pharmacol Toxicol*. 2019;124:170-180.
31. Marcucci KA, Pearce RE, Crespi C, Steimel DT, Steven Leeder J, Gaedigk A. Characterization of cytochrome P450 2D6.1 (CYP2D6.1), CYP2D6.2, and CYP2D6.17 activities toward model CYP2D6 substrates dextromethorphan, bufuralol, and debrisoquine. *Drug Metab Dispos*. 2002;30:595-601.
32. Shen H, He MM, Liu H, et al. Comparative metabolic capabilities and inhibitory profiles of CYP2D6.1, CYP2D6.10, and CYP2D6.17. *Drug Metab Dispos*. 2007;35:1292-1300.
33. Nofziger C, Turner AJ, Sangkuhlet K, et al. PharmVar GeneFocus: CYP2D6. *Clin Pharmacol Ther*. 2020;107:154-170.
34. Bapiro TE, Hasler JA, Ridderström M, Masimirembwa CM. The molecular and enzyme kinetic basis for the diminished activity of the cytochrome P450 2D6.17 (CYP2D6.17) variant: Potential implications for CYP2D6 phenotyping studies and the clinical use of CYP2D6 substrate drugs in some African populations. *Biochem Pharmacol*. 2002;64:1387-1398.
35. Heim M, Meyer U. Genotyping of poor metabolisers of debrisoquine by allele-specific PCR amplification. *Lancet*. 1990;336:529-532.
36. Lu S, Nand RA, Yang JS, Chen G, Gross AS. Pharmacokinetics of CYP2C9, CYP2C19, and CYP2D6 substrates in healthy Chinese and European subjects. *Eur J Clin Pharmacol*. 2018;74:285-296.
37. Matthaei J, Brockmöller J, Tzvetkov MV, et al. Heritability of metoprolol and torsemide pharmacokinetics. *Clin Pharmacol Ther*. 2015;98:611-621.
38. Thomas CD, Mosley SA, Kim S, et al. Examination of metoprolol pharmacokinetics and pharmacodynamics across CYP2D6 genotype-derived activity scores. *CPT Pharmacometrics Syst Pharmacol*. 2020;9:678-685.
39. Gazzaz M, Kinzig M, Schaeffeler E, et al. Drinking ethanol has few acute effects on CYP2C9, CYP2C19, NAT2, and P-glycoprotein activities but somewhat inhibits CYP1A2, CYP2D6, and intestinal CYP3A: so what? *Clin Pharmacol Ther*. 2018;104:1249-1259.
40. Frank D, Jaehde U, Fuhr U. Evaluation of probe drugs and pharmacokinetic metrics for CYP2D6 phenotyping. *Eur J Clin Pharmacol*. 2007;63:321-333.
41. Türk D, Hanke N, Lehr T. A physiologically-based pharmacokinetic model of trimethoprim for MATE1, OCT1, OCT2, and CYP2C8 drug–drug–gene interaction predictions. *Pharmaceutics*. 2020;12:1074.
42. Edginton AN, Schmitt W, Willmann S. Development and evaluation of a generic physiologically based pharmacokinetic model for children. *Clin Pharmacokinet*. 2006;45:1013-1034.
43. Schlender J-F, Meyer M, Thelen K, et al. Development of a whole-body physiologically based pharmacokinetic approach to assess the pharmacokinetics of drugs in elderly individuals. *Clin Pharmacokinet*. 2016;55:1573-1589.
44. Hanke N, Türk D, Selzer D, et al. A comprehensive whole-body physiologically based pharmacokinetic drug–drug–gene interaction model of metformin and cimetidine in healthy adults and renally impaired individuals. *Clin Pharmacokinet*. 2020;59:1419-1431.
45. Duedahl TH, Dirks J, Petersen KB, et al. Intravenous dextromethorphan to human volunteers: relationship between pharmacokinetics and anti-hyperalgesic effect. *Pain*. 2005;113:360-368.
46. Nakashima D, Takama H, Ogasawara Y, et al. Effect of cinacalcet hydrochloride, a new calcimimetic agent, on the pharmacokinetics of dextromethorphan. in vitro and clinical studies. *J Clin Pharmacol*. 2007;47:1311-1319.
47. Khalilieh S, Hussain A, Montgomery D, et al. Effect of tildrakizumab (MK-3222), a high affinity, selective anti-IL23p19 monoclonal antibody, on cytochrome P450 metabolism in

subjects with moderate to severe psoriasis. *Br J Clin Pharmacol*. 2018;84:2292-2302.

48. Nyunt MM, Becker S, MacFarland RT, et al. Pharmacokinetic effect of AMD070, an Oral CXCR4 antagonist, on CYP3A4 and CYP2D6 substrates midazolam and dextromethorphan in healthy volunteers. *JAIDS J Acquir Immune Defic Syndr*. 2008;47:559-565.
49. Dumond JB, Vourvahis M, Rezk NL, et al. A phenotype-genotype approach to predicting CYP450 and P-glycoprotein drug interactions with the mixed inhibitor/inducer tipranavir/ritonavir. *Clin Pharmacol Ther*. 2010;87:735-742.
50. Feld R, Woo MM, Leighl N, et al. A clinical investigation of inhibitory effect of panobinostat on CYP2D6 substrate in patients with advanced cancer. *Cancer Chemother Pharmacol*. 2013;72:747-755.
51. Tennezé L, Verstuyft C, Becquemont L, Poirier JM, Wilkinson GR, Funck-Brentano C. Assessment of CYP2D6 and CYP2C19 activity in vivo in humans: a cocktail study with dextromethorphan and chloroguanide alone and in combination. *Clin Pharmacol Ther*. 1999;66:582-588.
52. Qiu F, Liu S, Miao P, et al. Effects of the Chinese herbal formula "Zuojin Pill" on the pharmacokinetics of dextromethorphan in healthy Chinese volunteers with CYP2D6*10 genotype. *Eur J Clin Pharmacol*. 2016;72:689-695.
53. Storelli F, Matthey A, Lenglet S, et al. Impact of CYP2D6 functional allelic variations on phenoconversion and drug-drug interactions. *Clin Pharmacol Ther*. 2018;104:148-157.

SUPPORTING INFORMATION

Additional supporting information may be found in the online version of the article at the publisher's website.

How to cite this article: Rüdesheim S, Selzer D, Fuhr U, Schwab M, Lehr T. Physiologically-based pharmacokinetic modeling of dextromethorphan to investigate interindividual variability within CYP2D6 activity score groups. *CPT Pharmacometrics Syst Pharmacol*. 2022;00:1-18. doi:10.1002/psp4.12776

4.3 PROJECT III: PHYSIOLOGICALLY BASED PHARMACOKINETIC MODELING TO DESCRIBE THE CYP2D6 ACTIVITY SCORE-DEPENDENT METABOLISM OF PAROXETINE, ATOMOXETINE AND RISPERIDONE

Publication

The following original research article has been published in the peer-reviewed journal *Pharmaceutics*:

Rüdesheim, S.; Selzer, D.; Mürdter, T.; Igel, S.; Kerb, R.; Schwab, M.; Lehr, T. Physiologically Based Pharmacokinetic Modeling to Describe the CYP2D6 Activity Score-Dependent Metabolism of Paroxetine, Atomoxetine and Risperidone. *Pharmaceutics* **2022**, *2022*, 1734, DOI: 10.3390/pharmaceutics14081734.

Supplementary Material

The supplementary material to this publication can be accessed via this link.

Copyright

Author Contributions

Author contributions according to CRediT [6]:

Simeon Rüdesheim	Conceptualization, Investigation, Visualization, Writing–Original Draft, Writing–Review & Editing
Dominik Selzer	Conceptualization, Writing–Original Draft, Writing–Review & Editing
Thomas Mürdter	Writing–Original Draft, Writing–Review & Editing
Svitlana Igel	Writing–Original Draft, Writing–Review & Editing
Reinhold Kerb	Conceptualization, Writing–Original Draft, Writing–Review & Editing
Matthias Schwab	Conceptualization, Writing–Original Draft, Writing–Review & Editing, Funding Acquisition
Thorsten Lehr	Conceptualization, Writing–Original Draft, Writing–Review & Editing, Funding Acquisition

pharmaceutics

MDPI

Article

Physiologically Based Pharmacokinetic Modeling to Describe the CYP2D6 Activity Score-Dependent Metabolism of Paroxetine, Atomoxetine and Risperidone

Simeon Rüdesheim [1,2], Dominik Selzer [1], Thomas Mürdter [2], Svitlana Igel [2], Reinhold Kerb [2], Matthias Schwab [2,3,4] and Thorsten Lehr [1,*]

1 Department of Clinical Pharmacy, Saarland University, 66123 Saarbrücken, Germany
2 Dr. Margarete Fischer-Bosch-Institute of Clinical Pharmacology, 70376 Stuttgart, Germany
3 Departments of Clinical Pharmacology, Pharmacy and Biochemistry, University of Tübingen, 72076 Tübingen, Germany
4 Cluster of Excellence iFIT (EXC2180) "Image-Guided and Functionally Instructed Tumor Therapies", University of Tübingen, 72076 Tübingen, Germany
* Correspondence: thorsten.lehr@mx.uni-saarland.de; Tel.: +49-681-302-70255

Abstract: The cytochrome P450 2D6 (*CYP2D6*) genotype is the single most important determinant of CYP2D6 activity as well as interindividual and interpopulation variability in CYP2D6 activity. Here, the CYP2D6 activity score provides an established tool to categorize the large number of CYP2D6 alleles by activity and facilitates the process of genotype-to-phenotype translation. Compared to the broad traditional phenotype categories, the CYP2D6 activity score additionally serves as a superior scale of CYP2D6 activity due to its finer graduation. Physiologically based pharmacokinetic (PBPK) models have been successfully used to describe and predict the activity score-dependent metabolism of CYP2D6 substrates. This study aimed to describe CYP2D6 drug–gene interactions (DGIs) of important CYP2D6 substrates paroxetine, atomoxetine and risperidone by developing a substrate-independent approach to model their activity score-dependent metabolism. The models were developed in PK-Sim®, using a total of 57 plasma concentration–time profiles, and showed good performance, especially in DGI scenarios where 10/12, 5/5 and 7/7 of DGI AUC_{last} ratios and 9/12, 5/5 and 7/7 of DGI C_{max} ratios were within the prediction success limits. Finally, the models were used to predict their compound's exposure for different CYP2D6 activity scores during steady state. Here, predicted DGI AUC_{ss} ratios were 3.4, 13.6 and 2.0 (poor metabolizers; activity score = 0) and 0.2, 0.5 and 0.95 (ultrarapid metabolizers; activity score = 3) for paroxetine, atomoxetine and risperidone active moiety (risperidone + 9-hydroxyrisperidone), respectively.

Keywords: physiologically based pharmacokinetic (PBPK) modeling; paroxetine; atomoxetine; risperidone; cytochrome P450 2D6 (CYP2D6)

Citation: Rüdesheim, S.; Selzer, D.; Mürdter, T.; Igel, S.; Kerb, R.; Schwab, M.; Lehr, T. Physiologically Based Pharmacokinetic Modeling to Describe the CYP2D6 Activity Score-Dependent Metabolism of Paroxetine, Atomoxetine and Risperidone. *Pharmaceutics* **2022**, *14*, 1734. https://doi.org/10.3390/pharmaceutics14081734

Academic Editor: Im-Sook Song

Received: 11 July 2022
Accepted: 17 August 2022
Published: 18 August 2022

1. Introduction

Differences in CYP2D6 activity have been described as early as the 1970s [1,2] and have since been a major focus of clinical research, as CYP2D6 is involved in the metabolism of approximately 20% of clinically relevant drugs [3]. Polymorphic expression of the *CYP2D6* gene has been identified as the single most important determinant of CYP2D6 activity leading to a substantial interindividual and interpopulation variability observed in the pharmacokinetics of CYP2D6 substrates [4]. For instance, homozygous carriers of loss-of-function alleles (genetic poor metabolizers) show no detectable CYP2D6 activity [3] and are consequently unable to biotransform drugs via CYP2D6 [4]. In contrast, individuals carrying multiple copies of a normal function allele (genetic ultrarapid metabolizers) generally display increased CYP2D6 activity compared to homozygous carriers of

wildtype alleles (genetic normal metabolizers) [5] and show accelerated biotransformation of CYP2D6 substrates. Both poor and ultrarapid metabolizers are at an increased risk for experiencing dose-dependent adverse drug effects or a lack of response, depending on the CYP2D6 substrate [4].

To address this issue, pharmacogenetic testing for variants in *CYP2D6* has become an important cornerstone for personalized drug therapy [6] with the overall aim to improve efficacy and patient safety while simultaneously reducing costs of drug therapy, for example, due to hospitalizations caused by adverse drug reactions (ADRs) [7]. Here, the CYP2D6 activity score system serves as an indispensable tool to translate genotype data into phenotypes. Moreover, the activity score system can provide more fine-grained estimations of CYP2D6-dependent drug clearance [8], and, by extension, serves as an important basis for the development of actionable clinical guidelines [9]. Its main benefit is the aggregation of the >10,000 possible *CYP2D6* [10–13] genotypes into a manageable scoring system by assigning a numeric value ranging from 0 to 1 to *CYP2D6* alleles based on their in vitro and in vivo CYP2D6 activity [8]. Based on their genetic makeup, an individual's activity score can subsequently be translated into one of the following metabolizer phenotypes: poor (AS = 0), intermediate (0 < AS ≤ 1), normal (1 < AS ≤ 2.25) or ultrarapid metabolizer (AS > 2.25) [5]. Importantly, these phenotype categories are not identical to the "traditional" phenotype definitions, determined using phenotyping methods (e.g., calculating urinary metabolic ratios or screening for null alleles [8,14,15]). Consequently, the "traditional" extensive metabolizer and the normal metabolizer categories only display a limited intersection in terms of CYP2D6 activity [16].

While the activity score system's main purpose is the facilitation of genotype-to-phenotype translation, it has been suggested to provide an even finer graduated scale of CYP2D6 activity, allowing to infer a percentage of CYP2D6 activity (relative to activity score = 2) compared to the broad categories of traditional phenotypes [5]. Findings obtained from previously published physiologically based pharmacokinetic (PBPK) models of important CYP2D6 substrates dextromethorphan and metoprolol demonstrated a possibility to translate the CYP2D6 activity score into an apparent CYP2D6 clearance, reflected in increasing CYP2D6 catalytic rate constant (k_{cat}) values with increasing activity scores [15,17]. Here, drug–gene interaction (DGI) PBPK models provide a practical approach to mechanistically implement the activity score-dependent metabolism of CYP2D6 substrates [18].

The objective of this study was to implement the activity score-dependent metabolism in PBPK models of various important CYP2D6 substrates. For this, new models were developed for the selective serotonin reuptake inhibitor (SSRI) and CYP2D6 inhibitor paroxetine and the norepinephrine reuptake inhibitor (NRI) atomoxetine. The continuous scale of activity score-dependent metabolism derived from PBPK models of CYP2D6 substrates dextromethorphan and metoprolol was additionally implemented in these new PBPK models as well as an established PBPK model of the atypical antipsychotic risperidone, originally based on traditional phenotype categories.

2. Materials and Methods

2.1. Workflow

The overall workflow for this study included (I) the collection of clinical study data, (II) PBPK base model building (paroxetine, atomoxetine) and (III) PBPK base model evaluation (paroxetine, atomoxetine. Published PBPK DGI models (metoprolol, dextromethorphan) were used to (IV) derive the scale of their CYP2D6 activity score-dependent metabolism and implement it during the (V) DGI model building process (paroxetine, atomoxetine, and risperidone). After (VI) DGI model evaluation (paroxetine, atomoxetine, and risperidone), the models were applied to (VII) simulate steady-state exposure in different DGI scenarios (paroxetine, atomoxetine, and risperidone). Figure 1 schematically depicts the workflow for this study.

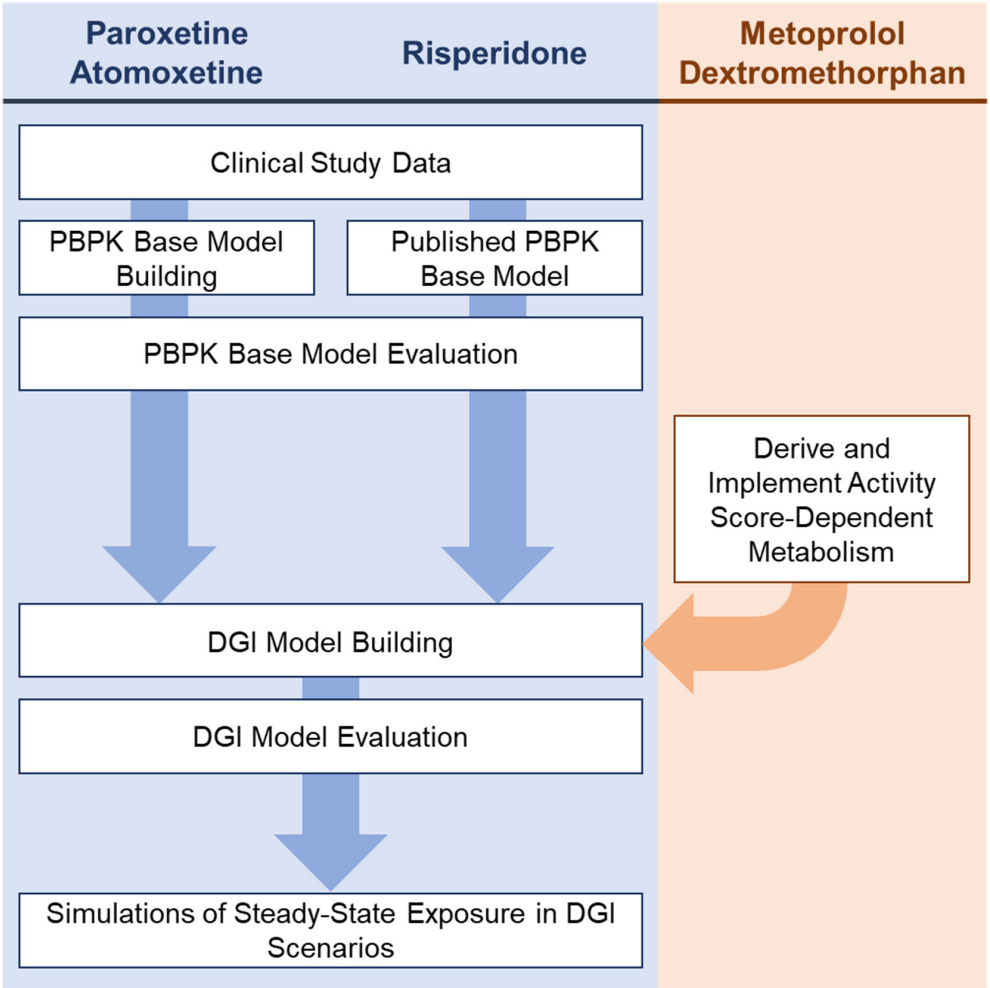

Figure 1. Workflow of the literature search of clinical study data, PBPK base model building, PBPK base model evaluation, DGI model building, DGI model evaluation and DGI model application processes for the modeled compounds.

2.2. Software

PBPK models were developed in PK-Sim® (Open Systems Pharmacology Suite 10, www.open-systems-pharmacology.org, 2021). Clinical study data from the literature were digitized with GetData Graph Digitizer 2.26.0.20 (© S. Fedorov, http://www.getdata-graph-digitizer.com/index.php, 2013) according to best practices [19]. Sensitivity analyses and model parameter optimizations (Monte Carlo algorithm) were performed within PK-Sim®. Pharmacokinetic parameters, model performance metrics and plots were calculated and generated using Python (version 3.10.4, Python Software Foundation, Wilmington, DE, USA, 2022). Regression analyses were performed using ordinary least squares (OLS) regression utilizing the *statsmodels* package (version 0.13.2, https://github.com/statsmodels/statsmodels, 2021) [20].

2.3. Clinical Study Data

An extensive literature search was conducted to gather individual and aggregated plasma concentration–time profiles after intravenous and oral administrations in single and multiple-dose regimes of paroxetine, atomoxetine, and risperidone. Additionally, population or individual demographics (sex, age, weight, and height) alongside CYP2D6 activity (phenotype, genotype, or activity score) were extracted from the respective

studies. The collected plasma concentration–time profiles were split into a training dataset for model development, and a test dataset for model performance evaluation. Studies for model training were selected to include sufficient data covering different routes of administration (intravenous and oral), formulations (oral solution or solid dosage forms), a wide range of doses as well different *CYP2D6* genotypes, activity scores or phenotypes.

2.4. PBPK Base Model Building

The paroxetine and atomoxetine PBPK base models were developed using a sequential approach. First, appropriate quantitative structure–activity relationship (QSAR) methods to estimate partition coefficients and cellular permeabilities were selected by the smallest residual error for fitting simulations of intravenous administrations (paroxetine) or all studies of the training dataset (atomoxetine) to their observed data. Second, simulations of administrations of oral solutions were optimized against the respective clinical data to estimate intestinal permeability. Third, parameters for CYP2D6-independent metabolism were informed by fitting simulations of single and multiple-dose oral administrations in poor metabolizers of CYP2D6 to their respective observed data. Finally, parameters for CYP2D6-mediated metabolism were optimized for studies of the training dataset where the volunteers were extensive metabolizers. Here, the term "extensive metabolizers" was used to group populations that were either phenotyped via traditional phenotyping methods or populations, which were not phenotyped.

For the risperidone base model, a published PBPK model by Kneller et al. [21] was used.

2.5. PBPK Base Model Evaluation

The performance of the presented models was evaluated using graphical and statistical methods. First, predicted plasma concentration–time profiles were compared graphically with measured data from the respective clinical studies by plotting model population predictions (arithmetic mean ± SD) together with observed data points. For this purpose, virtual populations of 1000 individuals were created based on the population characteristics reported in the respective publication. System-dependent parameters, such as age, body weight, height, organ weights, blood flow rates, and tissue composition, were varied by the implemented algorithm in PK-Sim®. Second, the plasma concentration values of all studies using the predicted arithmetic mean of the population were plotted against the corresponding observed values in goodness-of-fit plots. In addition, model performance was evaluated by a comparison of predicted to observed area under the concentration–time curve (AUC) and maximum plasma concentration (C_{max}) values. All AUC values (predicted as well as observed) were calculated from the time of the first concentration measurement to the time of the last concentration measurement (AUC_{last}).

Finally, as quantitative measures of the model performance, the mean relative deviation (MRD) of all predicted plasma concentrations (Equation (1)) and the geometric mean fold error (GMFE) of all predicted AUC_{last} and C_{max} values (Equation (2)) were calculated.

$$\mathrm{MRD} = 10^{x}; \quad x = \sqrt{\frac{\sum_{i=1}^{k} (\log_{10}\hat{c}_i - \log_{10}c_i)^2}{k}} \tag{1}$$

where $\hat{c}_i$ = predicted plasma concentration that corresponds to the i-th observed concentration, c_i = i-th observed plasma concentration, and k = number of observed values.

$$\mathrm{GMFE} = 10^{x}; \quad x = \frac{\sum_{i=1}^{m} \left|\log_{10}\left(\frac{\hat{p}_i}{p_i}\right)\right|}{m} \tag{2}$$

where $\hat{p}_i$ = predicted AUC_{last} or C_{max} value of study, p_i = corresponding observed AUC_{last} or C_{max} value of study, i, and m = total number of studies.

2.6. Local Sensitivity Analysis

Local sensitivity of the $AUC_{0–24\ h}$ of paroxetine, atomoxetine, risperidone or 9-hydroxyrisperidone to single parameter changes was analyzed for simulations of single orally administered standard doses of paroxetine, atomoxetine, and risperidone, respectively. Parameters were included in the analysis if they have been optimized (intestinal permeabilities and k_{cat} values), if they are associated with optimized parameters (K_M values) or if they might have a strong impact due to calculation and QSAR methods used (lipophilicities, pK_a values and fractions unbound (f_u)). A detailed description of the model sensitivity analysis is provided in Section S1.4 of Supplementary Materials S1. Overviews of all varied parameters for the respective compounds are provided in Sections S2.2.3, S3.2.3 and S4.2.3 of Supplementary Materials S1.

2.7. DGI Model Building

CYP2D6-dependent clearance processes were modeled using Michaelis–Menten kinetics according to Equation (3):

$$v = \frac{V_{max} \cdot S}{K_M + S} = \frac{k_{cat} \cdot E \cdot S}{K_M + S} \quad (3)$$

where v = reaction velocity at substrate concentration S, V_{max} = maximum reaction velocity, K_M = Michaelis–Menten constant, k_{cat} = catalytic rate constant, and E = enzyme concentration.

The CYP2D6 DGI models for paroxetine, atomoxetine, and risperidone were developed based on two previously published models for the CYP2D6 substrates metoprolol [17] and dextromethorphan [15]. Relative k_{cat} values, defined as the ratio of k_{cat} values for populations with a variant activity score and the k_{cat} for populations with an activity score of 2 (corresponding to 100% of CYP2D6 activity), were calculated according to Equation (4):

$$k_{cat,\ rel,\ AS=i} = \frac{k_{cat,\ AS\ =\ i}}{k_{cat,\ AS\ =\ 2}} \times 100\% \quad (4)$$

where $k_{cat,\ rel,\ AS\ =\ i}$ = k_{cat} for the investigated activity score relative to AS = 2 and $k_{cat,\ AS\ =\ i}$ = k_{cat} for activity score i.

Activity scores were assigned according to the current consensus [5]. CYP2D6 $k_{cat,\ rel}$ values used to describe the activity score-dependent metabolism of metoprolol [17] and dextromethorphan [15] in their respective DGI PBPK models, were analyzed using OLS regression (polynomial of degree 2, no intercept). For the paroxetine, atomoxetine and risperidone models, CYP2D6 k_{cat} values were optimized for studies, which reported plasma concentration–time profiles of populations with two wildtype alleles (AS = 2) and were set to 0 for poor metabolizers of CYP2D6 (AS = 0) as they were assumed to show no CYP2D6 activity [3]. Subsequently, k_{cat} values for all other modeled activity scores were calculated using the polynomial equation obtained from the OLS regression of metoprolol and dextromethorphan k_{cat} values. Here, CYP2D6 K_M values as well as CYP2D6 reference concentrations were kept constant over the whole range of modeled activity scores.

2.8. DGI Model Evaluation

To evaluate the performance of the presented DGI models, as well as the implemented scale of CYP2D6 activity score-dependent metabolism derived from the published metoprolol and dextromethorphan PBPK DGI models, predicted plasma concentration–time profiles were plotted alongside their respective observed data. Plasma concentration–time profiles for populations with variant activity scores were compared to profiles of a population with normal activity (AS = 2) in studies reporting activity scores or genotypes, whereas plasma concentration–time profiles for variant phenotypes were compared to those of the extensive metabolizer phenotype, where only CYP2D6 phenotypes were reported. Furthermore, predicted DGI PK ratios (AUC_{last} and C_{max} ratios) (Equation

(5)) were evaluated for study populations with variant CYP2D6 activity scores or phenotypes alongside GMFE values (Equation (2)) for the predicted PK ratios.

$$\text{DGI PK ratio} = \frac{PK_{DGI}}{PK_{reference}} \quad (5)$$

where PK_{DGI} = AUC_{last} or C_{max} of either a variant activity score or a variant phenotype; $PK_{reference}$ = AUC_{last} or C_{max} of either AS = 2 or the extensive metabolizer phenotype, respectively.

Additionally, steady-state exposures (AUC_{ss}) of model compounds were predicted for different CYP2D6 activity scores. Here, simulations were performed for individuals with different activity scores after multiple oral doses of 40 mg paroxetine, 40 mg atomoxetine, or 2 mg risperidone.

3. Results

3.1. PBPK Base Model Building

A total of 57 plasma concentration–time profiles obtained from 29 published clinical trials were used for the development and the evaluation of the paroxetine, atomoxetine, and risperidone PBPK models and are summarized in Table 1. Clinical study tables providing comprehensive information such as individual and population demographics (sex, age, weight, and height) and CYP2D6 activity (phenotype, genotype, or activity score) as well as the assignment of the study to the respective dataset are presented in Sections S2.1.2, S3.1.2 and S4.1.2 of Supplementary Materials S1 for paroxetine, atomoxetine, and risperidone, respectively.

For the paroxetine PBPK model, a total of 33 plasma concentration–time profiles where paroxetine was administered as an intravenous infusion (four profiles) or orally in single (16 profiles) or multiple (13 profiles) doses were used to develop the paroxetine PBPK model. Here, administered doses ranged from 10 to 70 mg of paroxetine. The paroxetine PBPK model incorporates CYP2D6- and CYP3A4-dependent metabolism of paroxetine [22] as well as irreversible inhibition of CYP2D6 and CYP3A4 [23]. Additionally, an unspecific hepatic clearance process and renal elimination via passive glomerular filtration were included. A schematic overview of implemented paroxetine metabolic pathways is provided in Figure 2a. Drug-dependent model parameters for paroxetine are presented in Section S2.1.1 of Supplementary Materials S1.

The atomoxetine PBPK model was developed using 12 plasma concentration–time profiles after oral administrations of atomoxetine in single (nine profiles) and multiple-dose administrations (three profiles) with doses of administered atomoxetine ranging between 20 and 50 mg. The atomoxetine PBPK model includes metabolism via CYP2D6 and CYP2C19 [24] as well as a passive glomerular filtration process. Figure 2b depicts the pathways implemented in the atomoxetine model. Atomoxetine drug-dependent model parameters are presented in Section S3.1.1 of Supplementary Materials S1.

An overview of risperidone model pathways as published by Kneller et al. [21] is provided in Figure 2c. Risperidone and 9-hydroxyrisperidone drug-dependent parameters are listed in Section S4.1.1 of Supplementary Materials S1.

Table 1. Summary of clinical studies used for model development and evaluation.

Study	Dose [mg]	*n*	Females [%]	Age [Years]	Weight [kg]	CYP2D6 Status	References
Paroxetine							
Belle et al., 2002	20, p.o. (tab)	22	23	38 (20–49)		-EM	[25]
Calvo et al., 2004	20, p.o. (tab)	25	64	26		64-	[26]
Chen et al., 2015	25, p.o. (cr)	24	42	26 (18–45)		610.5, 1.0, 1.5, 2	[27]
Lund et al., 1982	23—28, i.v. (inf.); 45, p.o. (sol)	4	0	(24–28)	(66–88)	-	[28]
Massaroti et al., 2005	20, p.o. (tab)	28	0	28 (18–42)	72 (57–87)	-	[29]
McClelland et al., 1984	70, p.o. (tab)	28	0	31 (22–44)		--	[30]
Mürdter et al., 2016	40, p.o. (tab)	16	100	26 (21–43)	61 (48–74)	0, 0.5, 0.75, 1, 2, 3	[31–33]
Schoedel et al., 2012	20, p.o. (tab)	14	14	34 (19–55)		75-	[34]
Segura et al., 2005	20, p.o. (tab)	7	0	23		65EM	[35]
Sindrup et al., 1992	40, p.o. (tab)	17	0	25 (20–39)	77 (65–95)	EM, PM	[36]
van der Lee et al., 2007	20, p.o. (tab)	26	69	44 (18–64)	69 (51–89)	EM	[37]
Yasui-Furukori et al., 2006	20, p.o. (tab)	12	25	25 (20–35)	58 (46–75)	1.25	[38]
Yasui-Furukori et al., 2007	20, p.o. (tab)	13	23	24 (21–35)	57 (45–67)	EM	[39]
Yoon et al., 2000	40, p.o. (tab)	16	13	22		640, 0.5, 1.25, 2	[40]
Atomoxetine							
Belle et al., 2002	20, p.o. (tab)	22	23	38 (20–49)		-EM	[25]
Byeon et al., 2015	40, p.o. (tab)	62	0	23		660, 1.25, 2	[41]
Cui et al., 2007	40-80, p.o. (tab)	16	33	(20–29)	(53–72)	1	[42]
Kim et al., 2018	20, p.o. (tab)	19	0	(19–25)	(49–73)	0.5, 2	[43]
Nakano et al., 2016	50, p.o. (tab, sol)	42	0	23 (20–37)	62 (52–76)	EM	[44]
Sauer et al., 2003	20, p.o. (tab)	7	0	41 (19–54)		-EM, PM	[45]
Todor et al., 2016	40, p.o. (tab)	30	0	(18–55)		-EM, PM	[46]
Risperidone							
Bondolfi et al., 2001	2, p.o. (tab)	11	27	43 (18–63)		-EM, PM	[47]
Darwish et al., 2015	2, p.o. (tab)	36	33	32		79-	[48]
Kim et al., 2008	1, p.o. (tab)	10	0	(23–38)	(65–80)	1.25	[49]
Markowitz et al., 2002	1, p.o. (tab)	11	21	28 (22–42)		--	[50]
Mahatthanatrakul 2007	4, p.o. (tab)	10	0	31	(55–76)	-	[51]
Mahatthanatrakul 2012	2, p.o. (tab)	10	0	33 (23–44)	64 (55–76)	-	[52]
Nakagami et al., 2005	1, p.o. (tab)	12	0	24 (20–28)	65 (53–86)	1	[53]
Novalbos et al., 2010	1, p.o. (tab)	71	51	23 (19–34)	66 (43–106)	0, 1, 2, 3	[21,54]

Demographic parameters are given as the mean (range). CYP2D6 status is reported as the mode of the study population phenotype or activity score or the different phenotypes and activity scores reported for the respective study sub-populations. -: not given, cr: controlled release tablet, EM: extensive metabolizer, inf: infusion, i.v. intravenous, PM: poor metabolizer, p.o.: oral, sol: oral solution, and tab: tablet.

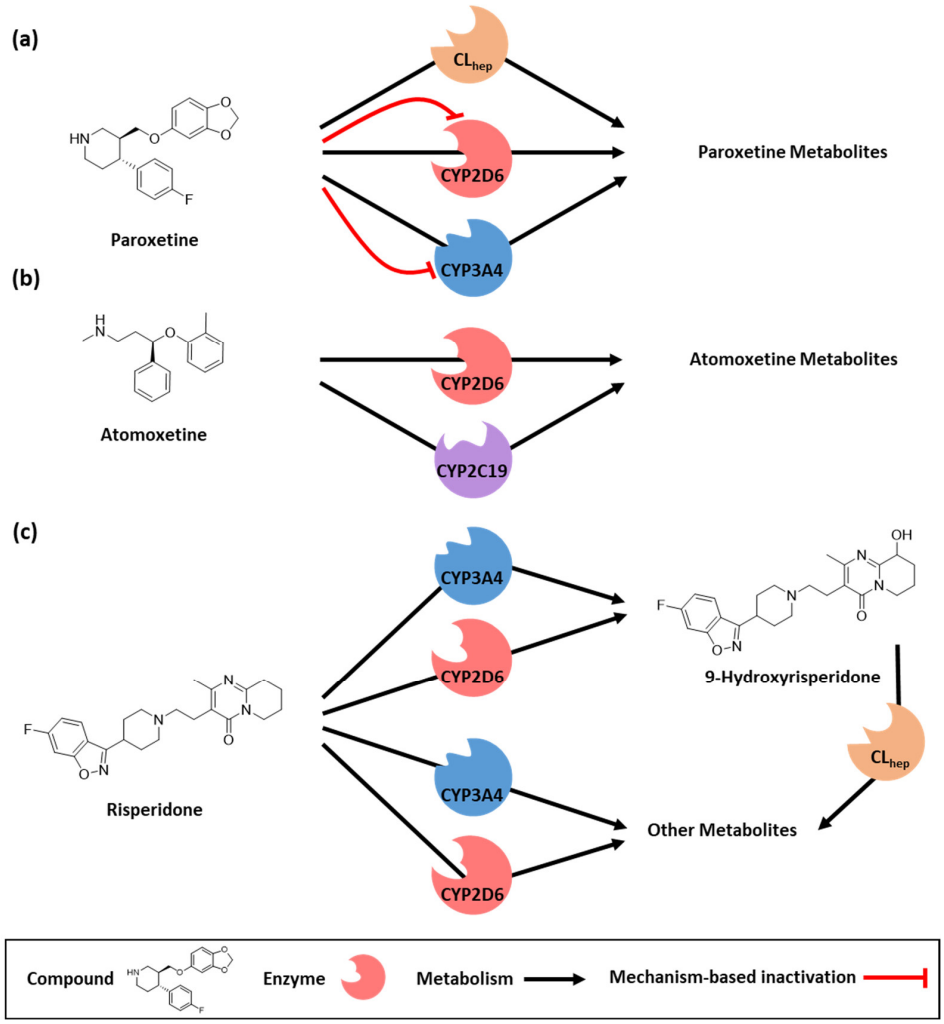

Figure 2. Implemented metabolic pathways for the modeled compounds. (**a**) Paroxetine is metabolized via CYP2D6, CYP3A4, and an unspecific clearance process [22]. Moreover, paroxetine is a mechanism-based inhibitor of CYP2D6 and CYP3A4 resulting in an irreversible auto-inhibition of paroxetine metabolism [23,55]. Paroxetine metabolites were not included as model compounds. (**b**) Atomoxetine is metabolized via CYP2D6 and CYP2C19 [24]. Atomoxetine metabolites were not included as model compounds. (**c**) Risperidone is metabolized to its active metabolite 9-hydroxyrisperidone via CYP2D6 and CYP3A4 [56]. Moreover, other metabolites are formed via CYP2D6- and CYP3A4-mediated metabolism [56]. 9-Hydroxyrisperidone is metabolized via an unspecific hepatic clearance process. Other risperidone metabolites were not included in the model. CL_{hep}: unspecific hepatic clearance, and CYP: cytochrome P450.

3.2. PBPK Base Model Evaluation

The three presented models could accurately predict the plasma concentrations for their respective model compounds. A representative selection of plots displaying predicted compared to observed plasma concentration–time profiles for paroxetine (a–f), atomoxetine (g–i) and risperidone and its metabolite 9-hydroxrisperidone (j–l) is shown in Figure 3.

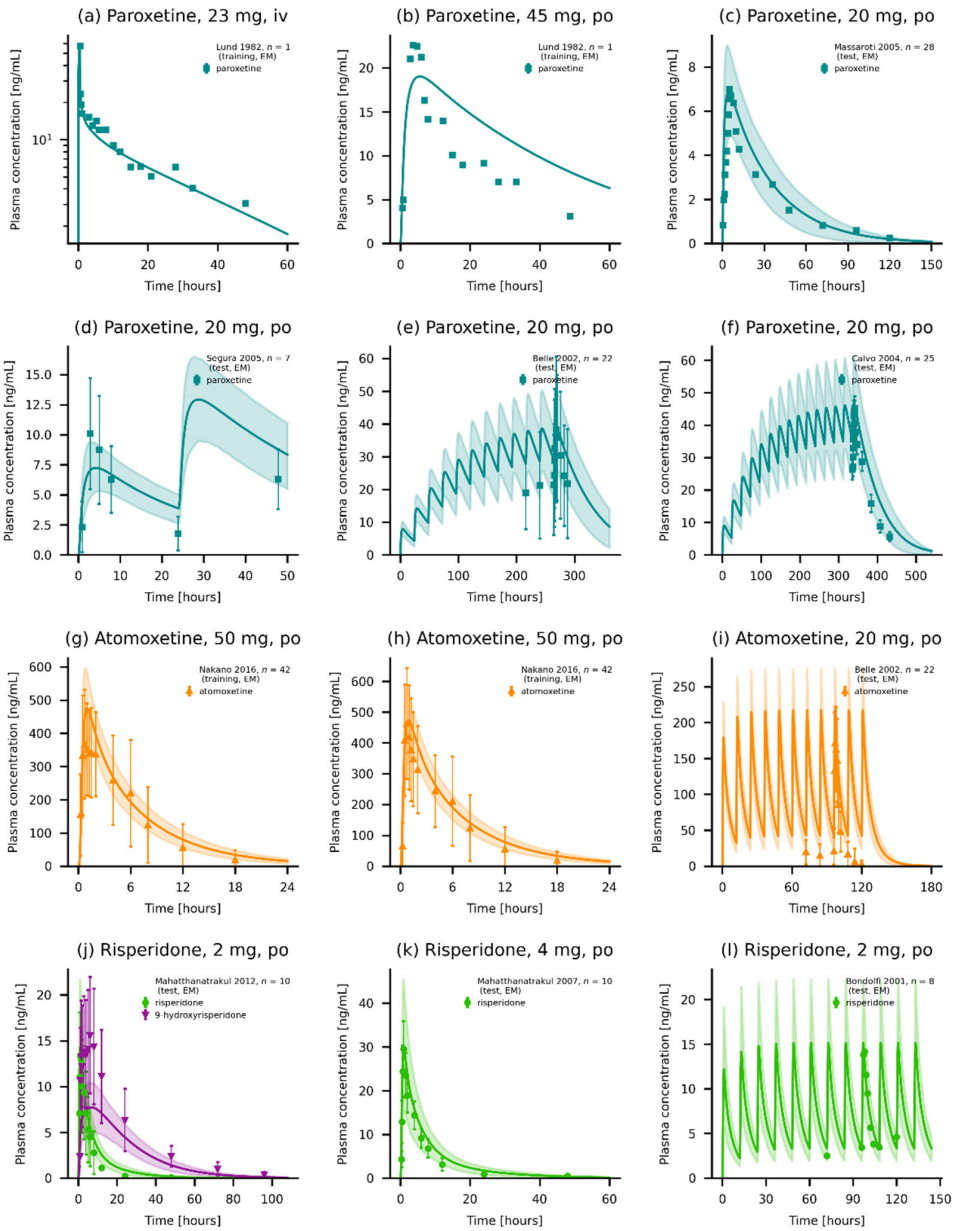

Figure 3. Plasma concentrations of the modeled compounds. (**a**–**f**) Model predictions of paroxetine of selected (**a**–**c**) single-dose administrations of (**a**) an intravenous infusion, (**b**) an oral solution, and (**c**) a normal release tablet. (**d**–**f**) Multiple-dose administrations of paroxetine as normal release tablets [25,26,28,29,35]. (**g**–**i**) Model predictions of atomoxetine as (**g**,**h**) single-dose administrations of (**g**) an oral solution, (**h**) a capsule and (**i**) multiple-dose administration of atomoxetine [25,44]. (**j**–**l**) Model predictions of risperidone and 9-hydroxyrisperidone (if available) of (**j**,**k**) single-dose administrations and (**l**) a multiple-dose administration of risperidone [47,51,52]. Individual predictions are shown as lines. Population predictions (n = 1000) are shown as lines with ribbons (arithmetic mean ± standard deviation (SD)), and symbols present the corresponding observed data ± SD (if available). Detailed information on all clinical studies is listed in Sections S2.1.2 [27,30,33,34,36–40], S3.1.2 [41–43,45,57] and S4.1.2 [48,49,53,54] of the Supplementary Materials S1. iv: intravenous, and po: oral.

Additionally, plots displaying predicted compared to observed plasma concentration–time profiles of the three compounds alongside their respective GMFEs for AUC_{last} and C_{max} values as well as MRD of predicted and observed plasma concentrations are

given in Sections S2.2.1, S3.2.1, and S4.2.1 of Supplementary Materials S1. Furthermore, goodness-of-fit plots showing predicted compared to observed plasma concentrations, AUC_{last} and C_{max} values are presented in Sections S2.2.2, S3.2.2, and S4.2.2 of Supplementary Materials S1. Overall, 82.7%, 88.9% and 89.2% of predicted plasma concentrations were within two-fold of their corresponding observed value for paroxetine, atomoxetine, and risperidone, respectively. Mean (and range) model GMFEs for paroxetine, atomoxetine and risperidone were 1.51 (1.06–3.02), 1.20 (1.00–1.88) and 1.21 (1.00–1.83) for AUC_{last} values, and 1.41 (1.01–3.64), 1.18 (1.02–1.34) and 1.21 (1.01–2.02) for C_{max} values.

3.3. Local Sensitivity Analysis

Local sensitivity analyses were performed using simulations after oral administrations of the respective standard doses for paroxetine (20 mg), atomoxetine (40 mg) and risperidone (2 mg). Parameters with associated sensitivity values >0.5 (100% parameter value perturbation resulting in a >50% change of predicted AUC) were considered sensitive. Here, lipophilicity (literature value) and f_u (literature value) were sensitive parameters for the paroxetine model. Lipophilicity (optimized value), f_u (literature value), CYP2D6 k_{cat} (optimized) and CYP2D6 K_M (literature value) were sensitive parameters for the atomoxetine model. Lipophilicity (literature value), f_u (literature value) and intestinal permeability (optimized value) were sensitive parameters for the risperidone model. A quantitative and visual representation of the local sensitivity analysis is provided in Sections S2.2.3, S3.2.3 and S4.2.3 of Supplementary Materials S1.

3.4. DGI Model Building

An OLS regression of CYP2D6 $k_{cat,\ rel}$ values was performed for the published metoprolol and dextromethorphan models to derive a substrate-independent scale of activity score-dependent metabolism for the newly developed models of paroxetine, atomoxetine, and risperidone. The results of the OLS regression are displayed in Figure 4.

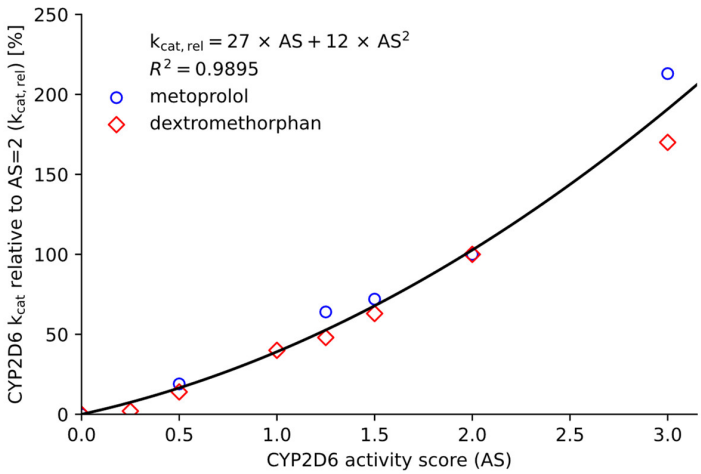

Figure 4. OLS regression of CYP2D6 $k_{cat,\ rel}$ values for the published DGI models of metoprolol and dextromethorphan [15,17]. The solid line represents the regression curve (degree = 2, intercept = 0), and symbols represent $k_{cat,\ rel}$ values for the different activity scores. AS: activity score, $k_{cat,\ rel}$: k_{cat} relative to AS = 2, and R^2: coefficient of determination.

Input values and results of the regression analysis as well as CYP2D6 model k_{cat} values for the modeled activity scores (calculated using the Equation given in Figure 4) are shown in Table 2. Here, paroxetine, atomoxetine, and risperidone CYP2D6 model k_{cat} values were calculated by multiplying interpolated $k_{cat, rel}$ values with the optimized baseline k_{cat} value (activity score 2).

Table 2. OLS regression input values and interpolated $k_{cat, rel}$ values alongside model CYP2D6 k_{cat} values for paroxetine, atomoxetine, and risperidone for different CYP2D6 activity scores.

CYP2D6 Activity Score	CYP2D6 $k_{cat, rel}$ [%]			CYP2D6 k_{cat} [1/min] [a]			
	MET	DEX	INTRPL	PAR	ATO	RIS_{9HR}	RIS_{other}
0	0	0	0	0.00	0.00	0	0.00
0.25	-	2	8	0.30	7.63	0.23	0.14
0.5	19	14	17	0.66	16.79	0.52	0.31
0.75	-	-	27	1.08	27.48	0.84	0.51
1	-	40	39	1.56	39.70	1.22	0.74
1.25	64	48	53	2.11	53.44	1.64	1.00
1.5	72	63	68	2.71	68.70	2.11	1.29
2	100	100	102	4.09 [b]	103.82 [b]	3.19 [b]	1.94 [b]
3	213	170	189	7.58	192.37	5.91	3.60

-: not available, [a]: values calculated as the product of the relative k_{cat} value and the optimized k_{cat} for populations with an activity score of 2, [b]: optimized value, ATO: atomoxetine, DEX: dextromethorphan, INTRPL: interpolated values using the polynomial equation of the OLS regression, $k_{cat, rel}$: k_{cat} relative to AS = 2, MET: metoprolol, PAR: paroxetine, RIS_{9HR}: risperidone → 9-hydroxyrisperidone, and RIS_{other}: risperidone → other metabolites.

3.5. DGI Model Evaluation

The newly developed DGI models were evaluated using clinical studies, which stratified their subjects by CYP2D6 activity score or phenotype. These studies either provided the activity score for the investigated population, the CYP2D6 phenotype, or *CYP2D6* genotypes of all study participants. Simulations were performed using the corresponding k_{cat} values with respect to activity score (Table 2) or phenotype (Sections S2.1.1, S3.1.1 and S4.1.1 of Supplementary Materials S1). DGI model performance is presented in Figure 5, depicting representative predicted compared to observed plasma concentration–time profiles of populations with different activity scores for paroxetine (a–f), atomoxetine (g–i) and risperidone (j–l). Plots depicting the model performance of all DGI studies are presented in Sections S2.3.1, S3.3.1 and S4.3.1 of Supplementary Materials S1.

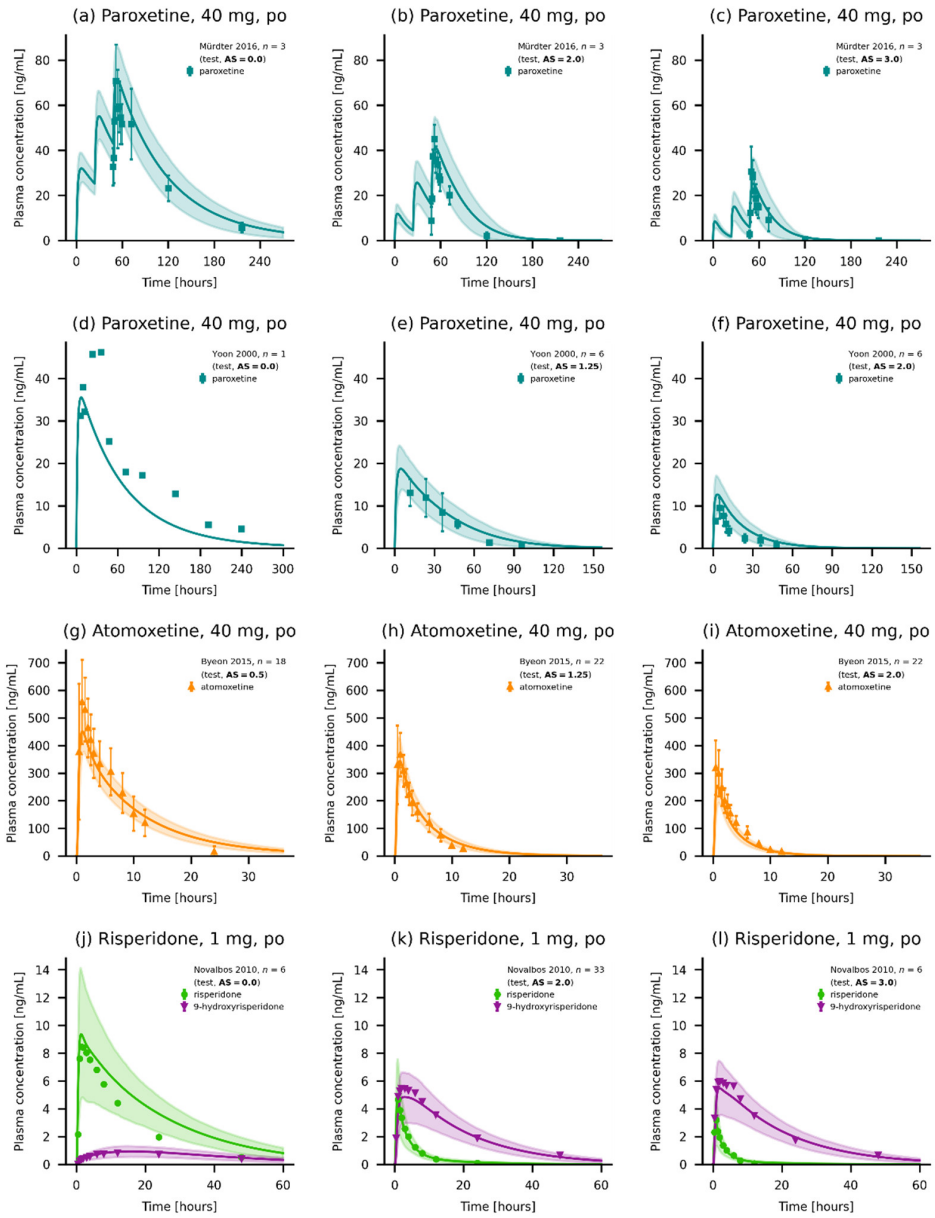

Figure 5. Simulated plasma concentrations of the modeled compounds for different CYP2D6 activity scores. (**a**–**f**) Paroxetine [33,40], (**g**–**i**) atomoxetine [41] and (**j**–**l**) risperidone [54] plasma concentration–time profiles of selected CYP2D6 DGI studies, compared to their observed data [33,40,41,54]. Individual predictions are shown as lines. Population predictions ($n = 1000$) are shown as lines with ribbons (arithmetic mean ± standard deviation (SD)), and symbols represent the corresponding observed data ± SD (if available).

Overall, predicted DGI AUC_{last} and C_{max} ratios were in good agreement with observed DGI ratios, highlighting the good performance of the DGI models predicting the activity score-dependent metabolism of paroxetine, atomoxetine, and risperidone, with 22/24 DGI AUC_{last} and 22/24 C_{max} ratios within the prediction success limits proposed by Guest et al. [58] as depicted in Figure 6. The predicted DGI AUC_{last} ratios showed mean GMFEs of 1.37, 1.25 and 1.11 whereas the overall GMFEs of predicted DGI C_{max} ratios were 1.33, 1.28 and 1.16 for paroxetine, atomoxetine, and risperidone, respectively. Predicted to observed DGI AUC_{last} and C_{max} ratios for all studies are presented in Sections S2.3.3, S3.3.3, and S4.3.3 of Supplementary Materials S1.

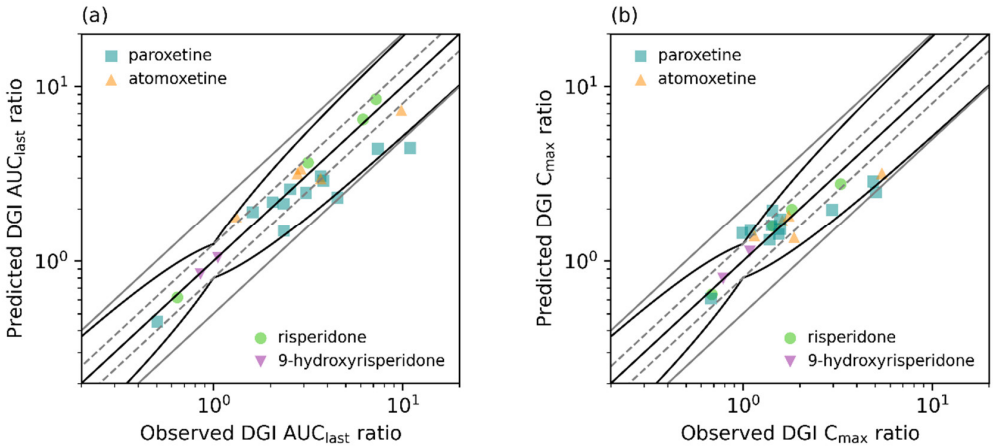

Figure 6. Comparison plot of predicted versus observed (**a**) DGI AUC_{last} ratios and (**b**) DGI C_{max} ratios for all analyzed CYP2D6 DGI studies. The straight black line indicates the line of identity, curved black lines show prediction success limits proposed by Guest et al., including 1.25-fold variability [58]. Solid gray lines indicate two-fold deviation, dashed gray lines show 1.25-fold deviation. AUC_{last}: area under the plasma concentration–time curve from the time of the first concentration measurement to the time of the last concentration measurement, C_{max}: maximum plasma concentration, and DGI: drug–gene interaction.

Simulations of steady-state plasma concentration–time profiles and AUC_{ss} values in individuals with different activity scores after multiple oral doses of 20 mg paroxetine, 40 mg atomoxetine or 2 mg risperidone and a comparison of the corresponding AUC_{ss} values are given in Figure 7. Predicted DGI AUC_{ss} ratios were 3.4, 13.6 and 2.0 for poor metabolizers (activity score 0) compared to normal metabolizers (activity score 2) for paroxetine, atomoxetine and risperidone active moiety (risperidone + 9-hydroxyrisperidone), respectively. Conversely, predicted DGI AUC_{ss} ratios were 0.2, 0.5 and 0.95 for ultrarapid metabolizers (activity score 3).

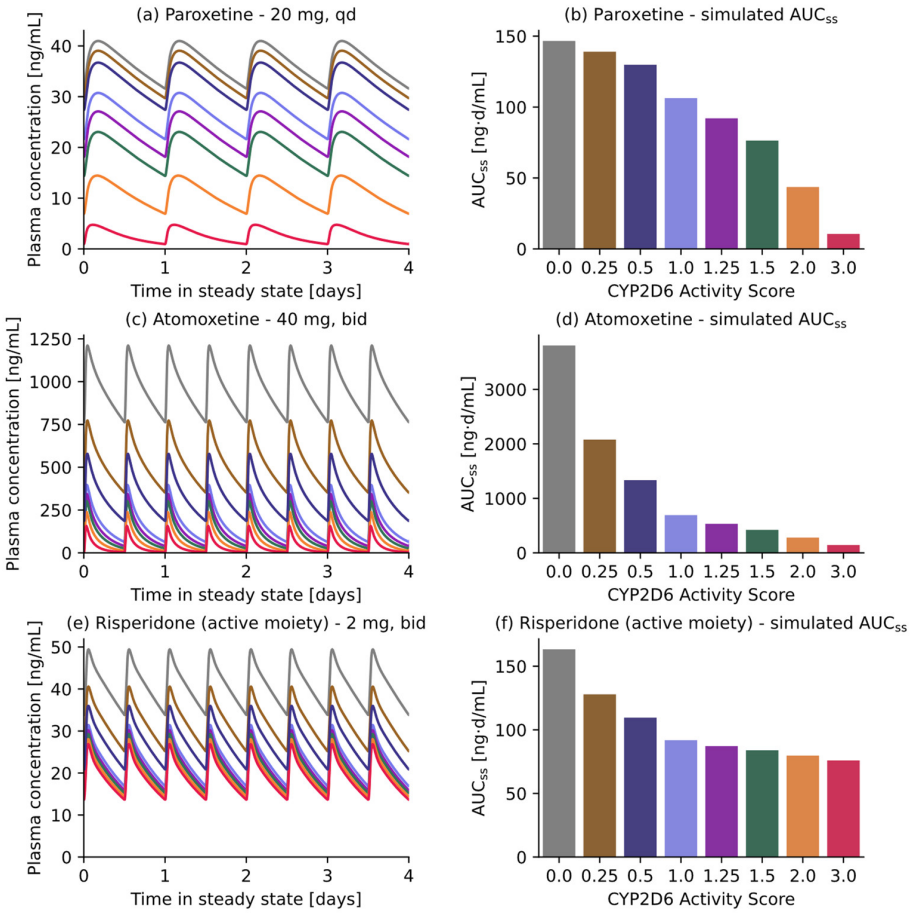

Figure 7. Model-based CYP2D6 DGI predictions. **Left panel**: simulations of drug exposure in individuals with different CYP2D6 activity scores after multiple oral doses of 40 mg paroxetine once daily (**a**), 40 mg atomoxetine twice daily (**c**) or 2 mg risperidone twice daily (**e**). **Right panel:** comparison of the corresponding AUC_{ss} values for the different activity scores for paroxetine (**b**), atomoxetine (**d**) and risperidone active moiety ((**f**) risperidone and 9-hydroxyrisperidone concentrations). AUC_{ss}: area under the plasma concentration–time curve during steady state (calculated for days 24–28), bid: twice daily, and qd: once daily.

4. Discussion

In this study, whole-body PBPK models of paroxetine, atomoxetine, and risperidone, including its active metabolite 9-hydroxyrisperidone, are presented. A total of 57 studies were used for model building and evaluation. CYP2D6 DGIs were modeled by implementing CYP2D6 activity score-dependent metabolism of the respective compounds for activity scores ranging from 0 to 3. Parameters for the CYP2D6 activity score-dependent metabolism for the presented models were derived from previously published models [15,17] via interpolation and represent a substrate-independent approach of modeling CYP2D6 DGIs. All three models showed good performance as highlighted in the model evaluation sections.

Previously published PBPK models of paroxetine, atomoxetine and risperidone typically implemented CYP2D6 DGIs by adjusting model parameters such as CL_{int}, K_M or k_{cat} values based on traditional CYP2D6 phenotypes (extensive and poor metabolizer) [59,60] or specific *CYP2D6* genotypes such as *CYP2D6*1/*1* and *CYP2D6*10/*10* [43], whereas the presented model can accurately describe both traditional phenotypes as well as CYP2D6 activity scores, allowing the models to predict compound plasma concentrations for all relevant genotypes to provide a finer graduation of CYP2D6 activity [17].

The CYP2D6 activity score-dependent metabolism was modeled by adjusting CYP2D6 k_{cat} values based on the activity score of the respective individual or population. Hence, the k_{cat} value serves as a surrogate parameter, reflecting changes in both in vivo reference concentration [61] and in vitro V_{max} [62] that typically occur due to polymorphisms in the *CYP2D6* gene. Here, K_M and CYP2D6 reference concentrations were fixed over the whole range of modeled activity scores and phenotypes [18]. Model CYP2D6 k_{cat} values for extensive metabolizers were consistently lower compared to normal metabolizers (activity scores 1.25–2, see Table 2 and Sections S2.1.1, S3.1.1 and S4.1.1 of Supplementary Materials S1 for paroxetine, atomox

etine and risperidone, respectively). Specifically, the CYP2D6 k_{cat} values for extensive metabolizers were 35%, 30% and 36% lower compared to activity score 1.25 for paroxetine, atomoxetine and risperidone, respectively. This is caused by the limited intersection between the aforementioned activities, mainly due to the often arbitrary definition of the extensive metabolizer phenotype [16].

While the presented approach of modeling CYP2D6 DGIs based on the activity score categories was a necessary simplification, it also represents one of the limitations of the presented study and, by extension, the activity score system itself. As suggested by van der Lee et al., CYP2D6 DGIs may be more accurately described using a continuous scale approach, reflecting the effect of *CYP2D6* allelic variants on the pharmacokinetics of CYP2D6 substrates in vivo and in vitro compared to the activity score system [9]. Additionally, certain *CYP2D6* alleles have been described to display substrate-specific effects in vitro and in vivo. For instance, the *CYP2D6*17* allele, classified as a reduced function (activity score 0.5) allele, shows increased activity in risperidone metabolism when compared to the wildtype **1* allele [63]. These effects are not considered in the classification of alleles using the activity score system [61]. Regardless, current clinical guidelines by the Dutch Pharmacogenetics Working Group (DPWG), the Clinical Pharmacogenetics Implementation Consortium (CPIC) and other major institutions in this field, are based on the activity score system [5]. Moreover, a allele-specific modeling approach would drastically increase model complexity and would require an extensive amount of in vitro and in vitro model input data [18]. Hence, the approach presented in this study was deemed a more practical choice in the context of PBPK modeling.

The presented paroxetine model includes metabolism via CYP2D6 and CYP3A4 and an unspecific hepatic clearance pathway as a surrogate pathway for metabolism via other CYP enzymes that were reported to metabolize paroxetine in vitro [22]. Here, additional experimental in vitro data such as K_M and V_{max} values were available for paroxetine metabolism via CYP1A2, CYP2C19 and CYP3A5. However, these enzymes were described to have a smaller effect on paroxetine kinetics compared to CYP2D6 and CYP3A4 [22]. Furthermore, CYP3A4 was implemented to describe the effect of auto-inhibition via CYP3A4 on the pharmacokinetics of paroxetine [23,55], especially in poor metabolizers of CYP2D6. No metabolite of paroxetine was implemented in the model due to a lack of reported metabolite plasma concentrations in the published literature, presumably due to the chemical and metabolic instability of major metabolite paroxetine-catechol [22,35]. Furthermore, paroxetine has been suggested as a substrate of P-glycoprotein (P-gp) in the published literature [39,64]. However, while a moderate affinity of paroxetine to P-gp was observed in in vitro experiments [65], genetic polymorphisms in the *ABCB1* gene were described to have no significant on paroxetine plasma concentrations in vivo [66]. Hence, the authors did not implement active transport via P-gp in the model. Regardless, the model was able to describe paroxetine plasma concentrations for all doses (20–70 mg) in published clinical studies.

CYP2D6 has been described to be mainly responsible for atomoxetine metabolism, as atomoxetine AUC was found to be increased by 400% in poor metabolizers of CYP2D6 compared to extensive metabolizers [45]. In the presented PBPK model, atomoxetine metabolism was described by implementing CYP2D6 and CYP2C19. Although 4-hydroxyatomoxetine has been reported to be primarily formed via CYP2D6, only a total of four

plasma concentration–time profiles of 4-hydroxyatomoxetine were reported in the published literature [41,67]. Thus, the metabolite was not explicitly modeled. However, as more clinical studies reporting 4-hydroxyatomoxetine plasma concentrations become available, the presented PBPK model of atomoxetine can be extended to cover the formation of 4-hydroxyatomoxetine.

While CYP1A2, CYP2B6, CYP2C9 and CYP3A4 were also described to contribute to the metabolism of atomoxetine in vitro, their relative contribution to atomoxetine depletion was found to be far smaller compared to CYP2C19 [24]. Hence, CYP2C19 serves as a surrogate pathway for multiple CYP enzymes in the presented model. While CYP2C19 is also polymorphically expressed, and CYP2C19 DGIs in CYP2C19 have been described in the literature [68], they were considered negligible, as CYP2D6 accounts for approximately 90% of atomoxetine oral clearance in normal metabolizers of CYP2D6 [45] and the CYP2C19 k_{cat} value was below the sensitivity threshold for atomoxetine model parameters (see Section S3.2.3 of Supplementary Materials S1).

To describe the activity score-dependent metabolism of risperidone, an established parent-metabolite model was used [21] and adapted. The model includes metabolism via CYP2D6 and CYP3A4 for risperidone as well as active transport via P-gp for both risperidone and its active metabolite 9-hydroxyrisperidone [69].

Simulations of steady-state plasma concentrations for the modeled compounds revealed that, although $k_{cat,\ rel}$ values implemented in the respective DGI models for the different activity scores were the same, AUC_{ss} values behaved differently between the three compounds. For instance, AUC_{ss} DGI ratios for CYP2D6 poor metabolizers (activity score 0) were 3.4, 13.6 and 2.0, whereas AUC_{ss} DGI ratios for ultrarapid metabolizers (activity score 3) were 0.2, 0.5 and 0.95 for paroxetine, atomoxetine and risperidone, respectively. Here, different model-specific factors might influence predicted AUC_{ss} DGI ratios. For risperidone, the total active moiety was considered (risperidone + 9-hydroxyrisperidone). Here, a decrease in the risperidone AUC with increasing activity scores typically infers an increase in 9-hydroxyrisperidone AUC, partially compensating the effect of CYP2D6 DGIs on the AUC of the total active moiety, and the overall pharmacodynamic effect of risperidone, as 9-hydroxyrisperidone has similar activity compared to risperidone [70]. Conversely, the paroxetine model includes auto-inhibition via mechanism-based inhibition of CYP2D6 and CYP3A4, reducing the differences between DGI AUC_{ss} values for the different modeled activity scores.

5. Conclusions

This study presents whole-body PBPK models of paroxetine, atomoxetine, and risperidone. The models implement CYP2D6 activity score-dependent metabolism informed from previously published PBPK models of CYP2D6 substrates and have been successfully used to predict the plasma concentrations of their model compounds both in non-DGI and DGI scenarios with various CYP2D6 activity scores. The final PBPK model files will be made publicly available in the Clinical Pharmacy Saarland University GitHub model repository (http://models.clinicalpharmacy.me/). Due to the mechanistic implementation of human physiology and important pharmacokinetic pathways, the models allow for knowledge-based scaling to special populations and can serve as the basis for future investigations of CYP2D6 drug-drug–gene interaction (DDGI) scenarios.

Supplementary Materials: The following supporting information can be downloaded at: www.mdpi.com/article/10.3390/pharmaceutics14081734/s1, Supplementary Materials. Section 1: Methods (Addendum); Section 2: Paroxetine; Section 3: Atomoxetine; Section 4: Risperidone; Section 5: Abbreviations. References [71–90] are cited in the Supplementary Materials.

Author Contributions: Conceptualization, S.R., D.S., R.K., M.S. and T.L.; investigation, S.R.; writing—original draft preparation, S.R., D.S., T.M., S.I., R.K., M.S. and T.L.; writing—review and editing, S.R., D.S., T.M., S.I., R.K., M.S. and T.L.; visualization, S.R.; funding acquisition, M.S. and T.L. All authors have read and agreed to the published version of the manuscript.

Funding: T.M.: S.I. and R.K., were supported by the Robert Bosch Stiftung (Stuttgart, Germany). M.S. was supported by the Robert Bosch Stiftung (Stuttgart, Germany), the European Commission Horizon 2020 UPGx grant 668353, a grant from the German Federal Ministry of Education and Research (BMBF 031L0188D), and the Deutsche Forschungsgemeinschaft (DFG, German Research Foundation) under Germany's Excellence Strategy—EXC 2180—390900677. T.L. was supported by the German Federal Ministry of Education and Research (BMBF, Horizon 2020 INSPIRATION grant 643271), under the frame of ERACoSysMed.

Institutional Review Board Statement: Not applicable.

Informed Consent Statement: Not applicable.

Data Availability Statement: All modeling files, including the clinical study data utilized, can be found at http://models.clinicalpharmacy.me/.

Conflicts of Interest: The authors declare no conflict of interest.

References

1. Eichelbaum, M.; Spannbrucker, N.; Steincke, B.; Dengler, H.J. Defective N-oxidation of sparteine in man: A new pharmacogenetic defect. *Eur. J. Clin. Pharmacol.* **1979**, *16*, 183–187. https://doi.org/10.1007/BF00562059.
2. Mahgoub, A.; Idle, J.R.; Dring, L.G.; Lancaster, R.; Smith, R.L. Polymorphic hydroxylation of Debrisoquine in man. *Lancet* **1977**, *2*, 584–586. https://doi.org/10.1016/s0140-6736(77)91430-1.
3. Zanger, U.M.; Raimundo, S.; Eichelbaum, M. Cytochrome P450 2D6: Overview and update on pharmacology, genetics, biochemistry. *Naunyn. Schmiedebergs. Arch. Pharmacol.* **2004**, *369*, 23–37. https://doi.org/10.1007/s00210-003-0832-2.
4. Gaedigk, A.; Sangkuhl, K.; Whirl-Carrillo, M.; Klein, T.; Leeder, J.S. Prediction of CYP2D6 phenotype from genotype across world populations. *Genet. Med.* **2017**, *19*, 69–76. https://doi.org/10.1038/gim.2016.80.
5. Caudle, K.E.; Sangkuhl, K.; Whirl-Carrillo, M.; Swen, J.J.; Haidar, C.E.; Klein, T.E.; Gammal, R.S.; Relling, M.V.; Scott, S.A.; Hertz, D.L.; et al. Standardizing CYP 2D6 Genotype to Phenotype Translation: Consensus Recommendations from the Clinical Pharmacogenetics Implementation Consortium and Dutch Pharmacogenetics Working Group. *Clin. Transl. Sci.* **2020**, *13*, 116–124. https://doi.org/10.1111/cts.12692.
6. Verbelen, M.; Weale, M.E.; Lewis, C.M. Cost-effectiveness of pharmacogenetic-guided treatment: Are we there yet? *Pharm. J.* **2017**, *17*, 395–402. https://doi.org/10.1038/tpj.2017.21.
7. Haycox, A.; Pirmohamed, M.; McLeod, C.; Houten, R.; Richards, S. Through a Glass Darkly: Economics and Personalised Medicine. *Pharmacoeconomics* **2014**, *32*, 1055–1061. https://doi.org/10.1007/s40273-014-0190-6.
8. Gaedigk, A.; Simon, S.; Pearce, R.; Bradford, L.; Kennedy, M.; Leeder, J. The CYP2D6 Activity Score: Translating Genotype Information into a Qualitative Measure of Phenotype. *Clin. Pharmacol. Ther.* **2008**, *83*, 234–242. https://doi.org/10.1038/sj.clpt.6100406.
9. van der Lee, M.; Allard, W.G.; Vossen, R.H.A.M.; Baak-Pablo, R.F.; Menafra, R.; Deiman, B.A.L.M.; Deenen, M.J.; Neven, P.; Johansson, I.; Gastaldello, S.; et al. Toward predicting CYP2D6-mediated variable drug response from CYP2D6 gene sequencing data. *Sci. Transl. Med.* **2021**, *13*. https://doi.org/10.1126/scitranslmed.abf3637.
10. Pharmacogene Variation Consortium (PharmVar) CYP2D6 Gene. Available online: https://www.pharmvar.org/gene/CYP2D6 (accessed on 13 May 2022).
11. Nofziger, C.; Turner, A.J.; Sangkuhl, K.; Whirl-Carrillo, M.; Agúndez, J.A.G.; Black, J.L.; Dunnenberger, H.M.; Ruano, G.; Kennedy, M.A.; Phillips, M.S.; et al. PharmVar GeneFocus: CYP2D6. *Clin. Pharmacol. Ther.* **2020**, *107*, 154–170. https://doi.org/10.1002/cpt.1643.
12. Gaedigk, A.; Sangkuhl, K.; Whirl-Carrillo, M.; Twist, G.P.; Klein, T.E.; Miller, N.A. The Evolution of PharmVar. *Clin. Pharmacol. Ther.* **2019**, *105*, 29–32. https://doi.org/10.1002/cpt.1275.
13. Gaedigk, A.; Ingelman-Sundberg, M.; Miller, N.A.; Leeder, J.S.; Whirl-Carrillo, M.; Klein, T.E. The Pharmacogene Variation (PharmVar) Consortium: Incorporation of the Human Cytochrome P450 (CYP) Allele Nomenclature Database. *Clin. Pharmacol. Ther.* **2018**, *103*, 399–401. https://doi.org/10.1002/cpt.910.
14. Heim, M.; Meyer, U. Genotyping of poor metabolisers of debrisoquine by allele-specific PCR amplification. *Lancet* **1990**, *336*, 529–532. https://doi.org/10.1016/0140-6736(90)92086-W.
15. Rüdesheim, S.; Selzer, D.; Fuhr, U.; Schwab, M.; Lehr, T. Physiologically-based pharmacokinetic modeling of dextromethorphan to investigate interindividual variability within CYP2D6 activity score groups. *CPT Pharmacomet. Syst. Pharmacol.* **2022**, *11*, 494–511. https://doi.org/10.1002/psp4.12776.
16. Lu, S.; Nand, R.A.; Yang, J.S.; Chen, G.; Gross, A.S. Pharmacokinetics of CYP2C9, CYP2C19, and CYP2D6 substrates in healthy Chinese and European subjects. *Eur. J. Clin. Pharmacol.* **2018**, *74*, 285–296. https://doi.org/10.1007/s00228-017-2375-3.
17. Rüdesheim, S.; Wojtyniak, J.-G.; Selzer, D.; Hanke, N.; Mahfoud, F.; Schwab, M.; Lehr, T. Physiologically Based Pharmacokinetic Modeling of Metoprolol Enantiomers and α-Hydroxymetoprolol to Describe CYP2D6 Drug-Gene Interactions. *Pharmaceutics* **2020**, *12*, 1200. https://doi.org/10.3390/pharmaceutics12121200.

18. Türk, D.; Fuhr, L.M.; Marok, F.Z.; Rüdesheim, S.; Kühn, A.; Selzer, D.; Schwab, M.; Lehr, T. Novel models for the prediction of drug–gene interactions. *Expert Opin. Drug Metab. Toxicol.* **2021**, *17*, 1293–1310. https://doi.org/10.1080/17425255.2021.1998455.
19. Wojtyniak, J.G.; Britz, H.; Selzer, D.; Schwab, M.; Lehr, T. Data Digitizing: Accurate and Precise Data Extraction for Quantitative Systems Pharmacology and Physiologically-Based Pharmacokinetic Modeling. *CPT Pharmacomet. Syst. Pharmacol.* **2020**, *9*, 322–331. https://doi.org/10.1002/psp4.12511.
20. Seabold, S.; Perktold, J. Statsmodels: Econometric and Statistical Modeling with Python. In Proceedings of the 9th Python in Science Conference, Austin, TX, USA, 28 June–3 July 2010; pp. 92–96. https://doi.org/10.25080/Majora-92bf1922-011.
21. Kneller, L.A.; Abad-Santos, F.; Hempel, G. Physiologically Based Pharmacokinetic Modelling to Describe the Pharmacokinetics of Risperidone and 9-Hydroxyrisperidone According to Cytochrome P450 2D6 Phenotypes. *Clin. Pharmacokinet.* **2020**, *59*, 51–65. https://doi.org/10.1007/s40262-019-00793-x.
22. Jornil, J.; Jensen, K.G.; Larsen, F.; Linnet, K. Identification of Cytochrome P450 Isoforms Involved in the Metabolism of Paroxetine and Estimation of Their Importance for Human Paroxetine Metabolism Using a Population-Based Simulator. *Drug Metab. Dispos.* **2010**, *38*, 376–385. https://doi.org/10.1124/dmd.109.030551.
23. Obach, R.S.; Walsky, R.L.; Venkatakrishnan, K. Mechanism-Based Inactivation of Human Cytochrome P450 Enzymes and the Prediction of Drug-Drug Interactions. *Drug Metab. Dispos.* **2007**, *35*, 246–255. https://doi.org/10.1124/dmd.106.012633.
24. Ring, B.J.; Gillespie, J.S.; Eckstein, J.A.; Wrighton, S.A. Identification of the Human Cytochromes P450 Responsible for Atomoxetine Metabolism. *Drug Metab. Dispos.* **2002**, *30*, 319–323. https://doi.org/10.1124/dmd.30.3.319.
25. Belle, D.J.; Ernest, C.S.; Sauer, J.-M.; Smith, B.P.; Thomasson, H.R.; Witcher, J.W. Effect of Potent CYP2D6 Inhibition by Paroxetine on Atomoxetine Pharmacokinetics. *J. Clin. Pharmacol.* **2002**, *42*, 1219–1227. https://doi.org/10.1177/009127002762491307.
26. Calvo, G.; García-Gea, C.; Luque, A.; Morte, A.; Dal-Ré, R.; Barbanoj, M. Lack of pharmacologic interaction between paroxetine and alprazolam at steady state in healthy volunteers. *J. Clin. Psychopharmacol.* **2004**, *24*, 268–276. https://doi.org/10.1097/01.jcp.0000125689.05091.c6.
27. Chen, R.; Wang, H.; Shi, J.; Shen, K.; Hu, P. Cytochrome P450 2D6 genotype affects the pharmacokinetics of controlled-release paroxetine in healthy Chinese subjects: Comparison of traditional phenotype and activity score systems. *Eur. J. Clin. Pharmacol.* **2015**, *71*, 835–841. https://doi.org/10.1007/s00228-015-1855-6.
28. Lund, J.; Thayssen, P.; Mengel, H.; Pedersen, O.L.; Kristensen, C.B.; Gram, L.F. Paroxetine: Pharmacokinetics and Cardiovascular Effects after Oral and Intravenous Single Doses in Man. *Acta Pharmacol. Toxicol.* **2009**, *51*, 351–357. https://doi.org/10.1111/j.1600-0773.1982.tb01036.x.
29. Massaroti, P.; Cassiano, N.M.; Duarte, L.F.; Campos, D.R.; Marchioretto, M.A.M.; Bernasconi, G.; Calafatti, S.; Barros, F.A.P.; Meurer, E.C.; Pedrazzoli, J. Validation of a selective method for determination of paroxetine in human plasma by LC-MS/MS. *J. Pharm. Pharm. Sci.* **2005**, *8*, 340–347.
30. McClelland, G.R.; Raptopoulos, P. EEG and blood level of the potential antidepressant paroxetine after a single oral dose to normal volunteers. *Psychopharmacology* **1984**, *83*, 327–329. https://doi.org/10.1007/BF00428539.
31. Mürdter, T.; Lehr, T.; Igel, S.; Kröner, P.; Ganchev, B.; Schaeffeler, E.; Böhmer, G.; Sonnenberg, M.; Brauch, H.; Kerb, R.; et al. Abstracts of the 82(nd) Annual Meeting of the German Society for Experimental and Clinical Pharmacology and Toxicology (DGPT) and the 18(th) Annual Meeting of the Network Clinical Pharmacology Germany (VKliPha) in cooperation with the Arbeitsgemeinschaft für Angewandte Humanpharmakologie e.V. (AGAH). *Naunyn-Schmiedeberg's Arch. Pharmacol.* **2016**, *389* S1, 1–104. https://doi.org/10.1007/s00210-016-1213-y.
32. Influence of Pharmacogenetic Factors, Paroxetine and Clarithromycin on Pharmacokinetics of Clomiphene—EudraCT 2009-014531-20. Available online: https://clinicaltrials.gov/ct2/show/NCT01289756 (accessed on 14 June 2022).
33. Ganchev, B. *Charakterisierung der Metabolischen Bioaktivierung des Clomifens unter Besonderer Berücksichtigung Genetischer Polymorphismen*, University of Tübingen: Tübingen, Germany, 2014.
34. Schoedel, K.A.; Pope, L.E.; Sellers, E.M. Randomized Open-Label Drug-Drug Interaction Trial of Dextromethorphan/Quinidine and Paroxetine in Healthy Volunteers. *Clin. Drug Investig.* **2012**, *32*, 157–169. https://doi.org/10.2165/11599870-000000000-00000.
35. Segura, M.; Farré, M.; Pichini, S.; Peiró, A.M.; Roset, P.N.; Ramírez, A.; Ortuño, J.; Pacifici, R.; Zuccaro, P.; Segura, J.; et al. Contribution of cytochrome P450 2D6 to 3,4-methylenedioxymethamphetamine disposition in humans: Use of paroxetine as a metabolic inhibitor probe. *Clin. Pharmacokinet.* **2005**, *44*, 649–660. https://doi.org/10.2165/00003088-200544060-00006.
36. Sindrup, S.H.; Brøsen, K.; Gram, L.F.; Hallas, J.; Skjelbo, E.; Allen, A.; Allen, G.D.; Cooper, S.M.; Mellows, G.; Tasker, T.C.G.G.; et al. The relationship between paroxetine and the sparteine oxidation polymorphism. *Clin. Pharmacol. Ther.* **1992**, *51*, 278–287. https://doi.org/10.1038/clpt.1992.23.
37. van der Lee, M.J.; Blenke, A.A.M.; Rongen, G.A.; Verwey-van Wissen, C.P.W.G.M.; Koopmans, P.P.; Pharo, C.; Burger, D.M. Interaction Study of the Combined Use of Paroxetine and Fosamprenavir-Ritonavir in Healthy Subjects. *Antimicrob. Agents Chemother.* **2007**, *51*, 4098–4104. https://doi.org/10.1128/AAC.01243-06.
38. Yasui-Furukori, N.; Saito, M.; Inoue, Y.; Niioka, T.; Sato, Y.; Tsuchimine, S.; Kaneko, S. Terbinafine increases the plasma concentration of paroxetine after a single oral administration of paroxetine in healthy subjects. *Eur. J. Clin. Pharmacol.* **2006**, *63*, 51–56. https://doi.org/10.1007/s00228-006-0217-9.
39. Yasui-Furukori, N.; Saito, M.; Niioka, T.; Inoue, Y.; Sato, Y.; Kaneko, S. Effect of Itraconazole on Pharmacokinetics of Paroxetine: The Role of Gut Transporters. *Ther. Drug Monit.* **2007**, *29*, 45–48. https://doi.org/10.1097/FTD.0b013e31802bb20d.

40. Yoon, Y.R.; Cha, I.J.; Shon, J.H.; Kim, K.A.; Cha, Y.N.; Jang, I.J.; Park, C.W.; Shin, S.G.; Flockhart, D.A.; Shin, J.G. Relationship of paroxetine disposition to metoprolol metabolic ratio and CYP2D6*10 genotype of Korean subjects. *Clin. Pharmacol. Ther.* **2000**, *67*, 567–576. https://doi.org/10.1067/mcp.2000.106128.
41. Byeon, J.Y.; Kim, Y.H.; Na, H.S.; Jang, J.H.; Kim, S.H.; Lee, Y.J.; Bae, J.W.; Kim, I.S.; Jang, C.G.; Chung, M.W.; et al. Effects of the CYP2 ∗ allele on the pharmacokinetics of atomoxetine and its metabolites. *Arch. Pharm. Res.* **2015**, *38*, 2083–2091. https://doi.org/10.1007/s12272-015-0646-z.
42. Cui, Y.M.; Teng, C.H.; Pan, A.X.; Yuen, E.; Yeo, K.P.; Zhou, Y.; Zhao, X.; Long, A.J.; Bangs, M.E.; Wise, S.D. Atomoxetine pharmacokinetics in healthy Chinese subjects and effect of the CYP2D6*10 allele. *Br. J. Clin. Pharmacol.* **2007**, *64*, 445–449. https://doi.org/10.1111/j.1365-2125.2007.02912.x.
43. Kim, S.H.; Byeon, J.Y.; Kim, Y.H.; Lee, C.M.; Lee, Y.J.; Jang, C.G.; Lee, S.Y. Physiologically based pharmacokinetic modelling of atomoxetine with regard to CYP2D6 genotypes. *Sci. Rep.* **2018**, *8*, 12405. https://doi.org/10.1038/s41598-018-30841-8.
44. Nakano, M.; Witcher, J.; Satoi, Y.; Goto, T. Pharmacokinetic Profile and Palatability of Atomoxetine Oral Solution in Healthy Japanese Male Adults. *Clin. Drug Investig.* **2016**, *36*, 903–911. https://doi.org/10.1007/s40261-016-0430-y.
45. Sauer, J.-M.; Ponsler, G.D.; Mattiuz, E.L.; Long, A.J.; Witcher, J.W.; Thomasson, H.R.; Desante, K.A. Disposition and Metabolic Fate of Atomoxetine Hydrochloride: The Role of CYP2D6 in Human Disposition and Metabolism. *Drug Metab. Dispos.* **2003**, *31*, 98–107. https://doi.org/10.1124/dmd.31.1.98.
46. Todor, I.; Popa, A.; Neag, M.; Muntean, D.; Bocsan, C.; Buzoianu, A.; Vlase, L.; Gheldiu, A.-M.; Briciu, C. Evaluation of the Potential Pharmacokinetic Interaction between Atomoxetine and Fluvoxamine in Healthy Volunteers. *Pharmacology* **2017**, *99*, 84–88. https://doi.org/10.1159/000452223.
47. Bondolfi, G.; Eap, C.; Bertschy, G.; Zullino, D.; Vermeulen, A.; Baumann, P. The Effect of Fluoxetine on the Pharmacokinetics and Safety of Risperidone in Psychotic Patients. *Pharmacopsychiatry* **2002**, *35*, 50–56. https://doi.org/10.1055/s-2002-25026.
48. Darwish, M.; Bond, M.; Yang, R.; Hellriegel, E.T.; Robertson, P. Evaluation of Potential Pharmacokinetic Drug-Drug Interaction Between Armodafinil and Risperidone in Healthy Adults. *Clin. Drug Investig.* **2015**, *35*, 725–733. https://doi.org/10.1007/s40261-015-0330-6.
49. Kim, K.-A.; Park, P.-W.; Liu, K.-H.; Kim, K.-B.; Lee, H.-J.; Shin, J.-G.; Park, J.-Y. Effect of Rifampin, an Inducer of CYP3A and P-glycoprotein, on the Pharmacokinetics of Risperidone. *J. Clin. Pharmacol.* **2008**, *48*, 66–72. https://doi.org/10.1177/0091270007309888.
50. Markowitz, J.S.; DeVane, C.L.; Liston, H.L.; Boulton, D.W.; Risch, S.C. The effects of probenecid on the disposition of risperidone and olanzapine in healthy volunteers. *Clin. Pharmacol. Ther.* **2002**, *71*, 30–38. https://doi.org/10.1067/mcp.2002.119815.
51. Mahatthanatrakul, W.; Nontaput, T.; Ridtitid, W.; Wongnawa, M.; Sunbhanich, M. Rifampin, a cytochrome P450 3A inducer, decreases plasma concentrations of antipsychotic risperidone in healthy volunteers. *J. Clin. Pharm. Ther.* **2007**, *32*, 161–167. https://doi.org/10.1111/j.1365-2710.2007.00811.x.
52. Mahatthanatrakul, W.; Sriwiriyajan, S.; Ridtitid, W.; Boonleang, J.; Wongnawa, M.; Rujimamahasan, N.; Pipatrattanaseree, W. Effect of cytochrome P450 3A4 inhibitor ketoconazole on risperidone pharmacokinetics in healthy volunteers. *J. Clin. Pharm. Ther.* **2012**, *37*, 221–225. https://doi.org/10.1111/j.1365-2710.2011.01271.x.
53. Nakagami, T.; Yasui-Furukori, N.; Saito, M.; Tateishi, T.; Kaneo, S. Effect of verapamil on pharmacokinetics and pharmacodynamics of risperidone: In vivo evidence of involvement of P-glycoprotein in risperidone disposition. *Clin. Pharmacol. Ther.* **2005**, *78*, 43–51. https://doi.org/10.1016/j.clpt.2005.03.009.
54. Novalbos, J.; López-Rodríguez, R.; Román, M.; Gallego-Sandín, S.; Ochoa, D.; Abad-Santos, F. Effects of CYP2D6 Genotype on the Pharmacokinetics, Pharmacodynamics, and Safety of Risperidone in Healthy Volunteers. *J. Clin. Psychopharmacol.* **2010**, *30*, 504–511. https://doi.org/10.1097/JCP.0b013e3181ee84c7.
55. Bertelsen, K.M.; Venkatakrishnan, K.; von Moltke, L.L.; Obach, R.S.; Greenblatt, D.J. Apparent Mechanism-based Inhibition of Human CYP2D6 in Vitro by Paroxetine: Comparison with Fluoxetine and Quinidine. *Drug Metab. Dispos.* **2003**, *31*, 289–293. https://doi.org/10.1124/dmd.31.3.289.
56. Okubo, M.; Morita, S.; Murayama, N.; Akimoto, Y.; Goto, A.; Yamazaki, H. Individual differences in in vitro and in vivo metabolic clearances of antipsychotic risperidone from Japanese subjects genotyped for cytochrome P450 2D6 and 3A5. *Hum. Psychopharmacol. Clin. Exp.* **2016**, *31*, 93–102. https://doi.org/10.1002/hup.2516.
57. Todor, I.; Popa, A.; Neag, M.; Muntean, D.; Bocsan, C.; Buzoianu, A.; Vlase, L.; Gheldiu, A.-M.; Briciu, C. Evaluation of a Potential Metabolism-Mediated Drug-Drug Interaction Between Atomoxetine and Bupropion in Healthy Volunteers. *J. Pharm. Pharm. Sci.* **2016**, *19*, 198–207. https://doi.org/10.18433/J3H03R.
58. Guest, E.J.; Aarons, L.; Houston, J.B.; Rostami-Hodjegan, A.; Galetin, A. Critique of the Two-Fold Measure of Prediction Success for Ratios: Application for the Assessment of Drug-Drug Interactions. *Drug Metab. Dispos.* **2011**, *39*, 170–173. https://doi.org/10.1124/dmd.110.036103.
59. Xu, M.; Zheng, L.; Zeng, J.; Xu, W.; Jiang, X.; Wang, L. Physiologically based pharmacokinetic modeling of tramadol to inform dose adjustment and drug-drug interactions according to CYP2D6 phenotypes. *Pharmacotherapy* **2021**, *41*, 277–290. https://doi.org/10.1002/phar.2494.
60. Ke, A.B.; Nallani, S.C.; Zhao, P.; Rostami-Hodjegan, A.; Isoherranen, N.; Unadkat, J.D. A physiologically based pharmacokinetic model to predict disposition of CYP2D6 and CYP1A2 metabolized drugs in pregnant women. *Drug Metab. Dispos.* **2013**, *41*, 801–813. https://doi.org/10.1124/dmd.112.050161.

61. Gaedigk, A.; Dinh, J.; Jeong, H.; Prasad, B.; Leeder, J. Ten Years' Experience with the CYP2D6 Activity Score: A Perspective on Future Investigations to Improve Clinical Predictions for Precision Therapeutics. *J. Pers. Med.* **2018**, *8*, 15. https://doi.org/10.3390/jpm8020015.
62. Shen, H.; He, M.M.; Liu, H.; Wrighton, S.A.; Wang, L.; Guo, B.; Li, C. Comparative metabolic capabilities and inhibitory profiles of CYP2D6.1, CYP2D6.10, and CYP2D6.17. *Drug Metab. Dispos.* **2007**, *35*, 1292–1300. https://doi.org/10.1124/dmd.107.015354.
63. Cai, W.-M.; Nikoloff, D.M.; Pan, R.-M.; de Leon, J.; Fanti, P.; Fairchild, M.; Koch, W.H.; Wedlund, P.J. CYP2D6 genetic variation in healthy adults and psychiatric African-American subjects: Implications for clinical practice and genetic testing. *Pharm. J.* **2006**, *6*, 343–350. https://doi.org/10.1038/sj.tpj.6500378.
64. Uhr, M.; Grauer, M.T.; Holsboer, F. Differential enhancement of antidepressant penetration into the brain in mice with abcb1ab (mdr1ab) P-Glycoprotein gene disruption. *Biol. Psychiatry* **2003**, *54*, 840–846. https://doi.org/10.1016/S0006-3223(03)00074-X.
65. Feng, B.; Mills, J.B.; Davidson, R.E.; Mireles, R.J.; Janiszewski, J.S.; Troutman, M.D.; De Morais, S.M. In vitro P-glycoprotein assays to predict the in vivo interactions of P-glycoprotein with drugs in the central nervous system. *Drug Metab. Dispos.* **2008**, *36*, 268–275. https://doi.org/10.1124/dmd.107.017434.
66. Gex-Fabry, M.; Eap, C.B.; Oneda, B.; Gervasoni, N.; Aubry, J.M.; Bondolfi, G.; Bertschy, G. CYP2D6 and ABCB1 Genetic variability: Influence on paroxetine plasma level and therapeutic response. *Ther. Drug Monit.* **2008**, *30*, 474–482. https://doi.org/10.1097/FTD.0b013e31817d6f5d.
67. Sauer, J.-M.; Long, A.J.; Ring, B.; Gillespie, J.S.; Sanburn, N.P.; DeSante, K.A.; Petullo, D.; VandenBranden, M.R.; Jensen, C.B.; Wrighton, S.A.; et al. Atomoxetine hydrochloride: Clinical drug-drug interaction prediction and outcome. *J. Pharmacol. Exp. Ther.* **2004**, *308*, 410–418. https://doi.org/10.1124/jpet.103.058727.
68. Choi, C.I.; Bae, J.W.; Lee, Y.J.; Lee, H.I.; Jang, C.G.; Lee, S.Y. Effects of CYP2C19 genetic polymorphisms on atomoxetine pharmacokinetics. *J. Clin. Psychopharmacol.* **2014**, *34*, 139–142. https://doi.org/10.1097/JCP.0b013e3182a608a2.
69. Ejsing, T.B.; Pedersen, A.D.; Linnet, K. P-glycoprotein interaction with risperidone and 9-OH-risperidone studied in vitro, in knock-out mice and in drug-drug interaction experiments. *Hum. Psychopharmacol. Clin. Exp.* **2005**, *20*, 493–500. https://doi.org/10.1002/hup.720.
70. Nasrallah, H.A. Atypical antipsychotic-induced metabolic side effects: Insights from receptor-binding profiles. *Mol. Psychiatry* **2008**, *13*, 27–35. https://doi.org/10.1038/sj.mp.4002066.
71. Agrawal, N. Determination of Paroxetine in Pharmaceutical Preparations Using HPLC with Electrochemical Detection. *Open Anal. Chem. J.* **2013**, *7*, 1–5. https://doi.org/10.2174/1874065001307010001.
72. Austin, R.P.; Barton, P.; Cockroft, S.L.; Wenlock, M.C.; Riley, R.J. The influence of nonspecific microsomal binding on apparent intrinsic clearance, and its prediction from physicochemical properties. *Drug Metab. Dispos.* **2002**, *30*, 1497–1503. https://doi.org/10.1124/dmd.30.12.1497.
73. Berezhkovskiy, L.M. Volume of distribution at steady state for a linear pharmacokinetic system with peripheral elimination. *J. Pharm. Sci.* **2004**, *93*, 1628–1640. https://doi.org/10.1002/jps.20073.
74. Hanke, N.; Frechen, S.; Moj, D.; Britz, H.; Eissing, T.; Wendl, T.; Lehr, T. PBPK Models for CYP3A4 and P-gp DDI Prediction: A Modeling Network of Rifampicin, Itraconazole, Clarithromycin, Midazolam, Alfentanil, and Digoxin. *CPT Pharmacomet. Syst. Pharmacol.* **2018**, *7*, 647–659. https://doi.org/10.1002/psp4.12343.
75. Greenblatt, D.J.; von Moltke, L.L.; Harmatz, J.S.; Chen, G.; Weemhoff, J.L.; Jen, C.; Kelley, C.J.; LeDuc, B.W.; Zinny, M.A. Time course of recovery of cytochrome p450 3A function after single doses of grapefruit juice. *Clin. Pharmacol. Ther.* **2003**, *74*, 121–9. https://doi.org/10.1016/S0009-9236(03)00118-8.
76. Kawai, R.; Lemaire, M.; Steimer, J.L.; Bruelisauer, A.; Niederberger, W.; Rowland, M. Physiologically based pharmacokinetic study on a cyclosporin derivative, SDZ IMM 125. *J. Pharmacokinet. Biopharm.* **1994**, *22*, 327–65.
77. Kaye, C.M.; Haddock, R.E.; Langley, P.F.; Mellows, G.; Tasker, T.C.G.; Zussman, B.D.; Greb, W.H. A review of the metabolism and pharmacokinetics of paroxetine in man. *Acta Psychiatr. Scand.* **1989**, *80*, 60–75. https://doi.org/10.1111/j.1600-0447.1989.tb07176.x.
78. Khatavkar, U.N.; Jayaram Kumar, K.; Shimpi, S.L. Novel approaches for development of oral controlled release compositions of galantamine hydrobromide and paroxetine hydrochloride hemihydrate: A review. *Int. J. Appl. Pharm.* **2016**, *8*, 1–6.
79. Khatavkar, U.N.; Shimpi, S.L.; Jayaram Kumar, K.; Deo, K.D. Development and comparative evaluation of in vitro, in vivo properties of novel controlled release compositions of paroxetine hydrochloride hemihydrate as against Geomatrix™ platform technology. *Drug Dev. Ind. Pharm.* **2013**, *39*, 1175–1186. https://doi.org/10.3109/03639045.2012.682222.
80. National Center for Health Statistics Hyattsville, M. 20782 Third National Health and Nutrition Examination Survey, NHANES III (1988–1994) Available online: https://wwwn.cdc.gov/nchs/nhanes/nhanes3/default.aspx (accessed on 26 November 2020).
81. Zhong, H.; Mashinson, V.; Woolman, T.; Zha, M. Understanding the Molecular Properties and Metabolism of Top Prescribed Drugs. *Curr. Top. Med. Chem.* **2013**, *13*, 1290–1307. https://doi.org/10.2174/1568026613139990034.
82. Yu, G.; Li, G.-F.; Markowitz, J.S. Atomoxetine: A Review of Its Pharmacokinetics and Pharmacogenomics Relative to Drug Disposition. *J. Child Adolesc. Psychopharmacol.* **2016**, *26*, 314–326. https://doi.org/10.1089/cap.2015.0137.
83. Venkatakrishnan, K.; Obach, R.S. In vitro-in vivo extrapolation of CYP2D6 inactivation by paroxetine: prediction of nonstationary pharmacokinetics and drug interaction magnitude. *Drug Metab. Dispos.* **2005**, *33*, 845–52. https://doi.org/10.1124/dmd.105.004077.

84. Valentin, J. Basic anatomical and physiological data for use in radiological protection: reference values. A report of age- and gender-related differences in the anatomical and physiological characteristics of reference individuals. ICRP Publication 89. *Ann. ICRP* **2002**, *32*, 5–265.
85. Swain, M. chemicalize.org. *J. Chem. Inf. Model.* **2012**, *52*, 613–615. https://doi.org/10.1021/ci300046g.
86. Tanaka, G.; Kawamura, H. *Division of Radioecology*; National Institute of Radiological Sciences: Hitachinaka, Japan, 1996; p. NIRS-M-115.
87. Rowland Yeo, K.; Walsky, R.L.; Jamei, M.; Rostami-Hodjegan, A.; Tucker, G.T. Prediction of time-dependent CYP3A4 drug-drug interactions by physiologically based pharmacokinetic modelling: impact of inactivation parameters and enzyme turnover. *Eur. J. Pharm. Sci.* **2011**, *43*, 160–73. https://doi.org/10.1016/j.ejps.2011.04.008.
88. Rodrigues, A.D. Integrated cytochrome P450 reaction phenotyping. Attempting to bridge the gap between cDNA-expressed cytochromes P450 and native human liver microsomes. *Biochem. Pharmacol.* **1999**, *57*, 465–480. https://doi.org/10.1016/S0006-2952(98)00268-8.
89. Open Systems Pharmacology Suite Community PK-Sim® Ontogeny Database Documentation, Version 7.3. Available online: https://github.com/Open-Systems-Pharmacology/OSPSuite.Documentation/blob/master/PK-SimOntogenyDatabaseVersion7.3.pdf (accessed on 4 April 2022).
90. Nishimura, M.; Naito, S. Tissue-specific mRNA Expression Profiles of Human ATP-binding Cassette and Solute Carrier Transporter Superfamilies. *Drug Metab. Pharmacokinet.* **2005**, *20*, 452–477. https://doi.org/10.2133/dmpk.20.452.

4.4 PROJECT IV: PREDICTION OF DRUG–DRUG–GENE INTERACTION SCENARIOS OF (*E*)-CLOMIPHENE AND ITS METABOLITES USING PHYSIOLOGICALLY BASED PHARMACOKINETIC MODELING

Publication

The following original research article has been published in the peer-reviewed journal *Pharmaceutics*:

Kovar, C.; Kovar, L.; Rüdesheim, S.; Selzer, D.; Ganchev, B.; Kröner, P.; Igel, S.; Kerb, R.; Schaeffeler, E.; Mürdter, T. E.; Schwab, M.; Lehr, T. Prediction of Drug–Drug–Gene Interaction Scenarios of (*E*)-Clomiphene and Its Metabolites Using Physiologically Based Pharmacokinetic Modeling. *Pharmaceutics* **2022**, *14*, 2604, DOI: 10.3390/pharmaceutics14122604.

Supplementary Material

The supplementary material to this publication can be accessed via this link.

Copyright

Author Contributions

Author contributions according to CRediT [6]:

Christina Kovar	Conceptualization, Data curation, Formal analysis, Investigation, Methodology, Software, Validation, Visualization, Writing–Original Draft, Writing–Review & Editing
Lukas Kovar	Conceptualization, Investigation, Methodology, Validation, Visualization, Writing–Review & Editing
Simeon Rüdesheim	Formal analysis, Methodology, Writing–Review & Editing
Dominik Selzer	Formal analysis, Methodology, Software, Validation, Writing–Review & Editing
Boian Ganchev	Investigation, Methodology, Writing–Review & Editing
Patrick Kröner	Investigation, Methodology, Writing–Review & Editing
Svitlana Igel	Investigation, Writing–Review & Editing
Reinhold Kerb	Investigation, Conceptualization, Writing–Review & Editing
Elke Schaeffeler	Investigation, Methodology, Writing–Review & Editing
Thomas Mürdter	Investigation, Conceptualization, Methodology, Project administration, Supervision, Writing–Review & Editing
Matthias Schwab	Conceptualization, Funding acquisition, Project administration, Resources, Supervision, Writing–Review & Editing, Funding Acquisition
Thorsten Lehr	Conceptualization, Funding acquisition, Project administration, Resources, Supervision, Writing–Original Draft, Writing–Review & Editing, Funding Acquisition

pharmaceutics

MDPI

Article

Prediction of Drug–Drug–Gene Interaction Scenarios of (*E*)-Clomiphene and Its Metabolites Using Physiologically Based Pharmacokinetic Modeling

Christina Kovar [1,2], Lukas Kovar [1], Simeon Rüdesheim [1,2], Dominik Selzer [1], Boian Ganchev [2], Patrick Kröner [2], Svitlana Igel [2], Reinhold Kerb [2], Elke Schaeffeler [2], Thomas E. Mürdter [2], Matthias Schwab [2,3] and Thorsten Lehr [1,*]

1 Clinical Pharmacy, Saarland University, 66123 Saarbrücken, Germany
2 Dr. Margarete Fischer-Bosch Institute of Clinical Pharmacology, University of Tübingen, 70376 Stuttgart, Germany
3 Departments of Clinical Pharmacology, Pharmacy and Biochemistry, University of Tübingen, 72076 Tübingen, Germany
* Correspondence: thorsten.lehr@mx.uni-saarland.de; Tel.: +49-681-302-70255

Abstract: Clomiphene, a selective estrogen receptor modulator (SERM), has been used for the treatment of anovulation for more than 50 years. However, since (*E*)-clomiphene ((*E*)-Clom) and its metabolites are eliminated primarily via Cytochrome P450 (CYP) 2D6 and CYP3A4, exposure can be affected by CYP2D6 polymorphisms and concomitant use with CYP inhibitors. Thus, clomiphene therapy may be susceptible to drug–gene interactions (DGIs), drug–drug interactions (DDIs) and drug–drug–gene interactions (DDGIs). Physiologically based pharmacokinetic (PBPK) modeling is a tool to quantify such DGI and DD(G)I scenarios. This study aimed to develop a whole-body PBPK model of (*E*)-Clom including three important metabolites to describe and predict DGI and DD(G)I effects. Model performance was evaluated both graphically and by calculating quantitative measures. Here, 90% of predicted C_{max} and 80% of AUC_{last} values were within two-fold of the corresponding observed value for DGIs and DD(G)Is with clarithromycin and paroxetine. The model also revealed quantitative contributions of different CYP enzymes to the involved metabolic pathways of (*E*)-Clom and its metabolites. The developed PBPK model can be employed to assess the exposure of (*E*)-Clom and its active metabolites in as-yet unexplored DD(G)I scenarios in future studies.

Keywords: clomiphene; pharmacokinetics; cytochrome P450 2D6 (CYP2D6) polymorphisms; drug–drug interactions (DDIs); drug–drug–gene interactions (DDGIs); drug–gene interactions (DGIs); (*E*)-clomiphene; physiologically based pharmacokinetic (PBPK) modeling

check for updates

Citation: Kovar, C.; Kovar, L.; Rüdesheim, S.; Selzer, D.; Ganchev, B.; Kröner, P.; Igel, S.; Kerb, R.; Schaeffeler, E.; Mürdter, T.E.; et al. Prediction of Drug–Drug–Gene Interaction Scenarios of (*E*)-Clomiphene and Its Metabolites Using Physiologically Based Pharmacokinetic Modeling. *Pharmaceutics* **2022**, *14*, 2604. https://doi.org/10.3390/pharmaceutics14122604

Academic Editors: Yoon-Jee Chae and Kyeong-Ryoon Lee

Received: 24 October 2022
Accepted: 22 November 2022
Published: 25 November 2022

1. Introduction

Ovulation disorders resulting in infertility can be caused by polycystic ovary syndrome (PCOS), which shows a prevalence of 4–20% in women of reproductive age worldwide [1,2]. Clomiphene has been used for the treatment of infertility in women with PCOS since the late 1960s and is administered orally as a racemic mixture of (*E*)- and (*Z*)-clomiphene ((*E*)-Clom and (*Z*)-Clom) [1,3]. As a selective estrogen receptor modulator (SERM), clomiphene—particularly (*E*)-Clom and its metabolites—inhibits the estrogen receptor at the hypothalamic arcuate nucleus [4–6]. Here, a rise in gonadotropin-releasing hormone levels leads to an increase in follicle-stimulating and luteinizing hormones, which in turn, induces ovulation [7]. In addition, antimicrobial activity of SERMs against different strains of bacteria has been shown in recent work [8,9].

During clomiphene therapy, 8–54% of women do not respond, while variability in response is affected by various factors such as hyperandrogenemia and obesity [10–12]. Additionally, research efforts have identified the importance of the highly polymorphic cytochrome

P450 (CYP) 2D6 enzyme in the bioactivation of (*E*)-Clom [6,13]. Here, the two metabolites (*E*)-4-hydroxyclomiphene ((*E*)-4-OH-Clom) and (*E*)-4-hydroxy-N-desethylclomiphene ((*E*)-4-OH-DE-Clom) were identified to exhibit the highest inhibitory affinity towards the estrogen receptor with half-maximal inhibitory concentrations of 2.2 and 0.9 nM, respectively [7]. In contrast, the parent drug (*E*)-Clom as well as (*Z*)-Clom and its metabolites showed lower inhibitory effects in in vitro assays [5,6]. Thus, (*E*)-4-OH-Clom and (*E*)-4-OH-DE-Clom are assumed to be key components in the bioactivation process of clomiphene with their pharmacokinetics (PK) strongly depending on CYP2D6 activity [5].

As a result, treatment with clomiphene can be subject to drug–gene interactions (DGIs) which has been confirmed in a study with healthy female volunteers [5]. Here, CYP2D6 poor metabolizers (PM) showed approximately ten-fold lower maximum plasma concentrations (C_{max}) of (*E*)-4-OH-Clom and (*E*)-4-OH-DE-Clom compared with normal metabolizers (NM) [5]. Furthermore, the in vitro formation rates for both (*E*)-4-OH-Clom and (*E*)-4-OH-DE-Clom increased with CYP2D6 activity [5]. The impact of CYP2D6 polymorphisms has also been observed in a recent clinical trial, where all CYP2D6 intermediate metabolizers (IM) responded to clomiphene therapy, while 30% of NM were non-responders [14]. However, this non-classical gene–dose effect points to a more complex metabolic scheme.

As the biotransformation of its active metabolites does not only depend on CYP2D6, but also on CYP3A4 metabolism, among others, systemic exposure of (*E*)-Clom and its metabolites can be altered by drug–drug interactions (DDIs) with CYP2D6 inhibitors and additionally with CYP3A4 inhibitors/inducers [15,16]. This dependency of (*E*)-Clom PK and bioactivation on CYP2D6 and CYP3A4 leads to a complex network of possible DGI, DDI and drug–drug–gene interaction (DDGI) scenarios that can cause a high variability in the longitudinal trajectory of plasma concentrations for (*E*)-Clom and its metabolites. The fact, that not only the formation, but also the elimination, of the active metabolites depends on CYP2D6 and CYP3A4 activity, adds to the complexity of the PK. Here, physiologically based pharmacokinetic (PBPK) modeling can integrate available in vitro and in vivo information on these processes to quantify and investigate DGI, DDI and DDGI scenarios.

Thus, this study aimed to develop a whole-body parent–metabolite PBPK model of (*E*)-Clom and its metabolites (*E*)-4-OH-Clom, (*E*)-N-desethylclomiphene ((*E*)-DE-Clom) and (*E*)-4-OH-DE-Clom to support the investigation of CYP2D6 DGI effects on the PK and bioactivation of (*E*)-Clom. In addition, the model was applied to predict various DD(G)I scenarios with the CYP2D6 inhibitor paroxetine and the CYP3A4 inhibitor clarithromycin and to gain insights into the PK regarding the contribution of different metabolic pathways to the elimination of (*E*)-Clom and its metabolites. The supplementary document to this article serves as a model reference and includes a detailed evaluation of the model performance. In addition, the model files will be made publicly available (http://models.clinicalpharmacy.me/).

2. Materials and Methods

2.1. Clinical Study Data

Clinical data from a recently performed pharmacokinetic panel study (EudraCT-Nr.: 2009-014531-20, ClinicalTrails.gov: NCT01289756) were used for PBPK model development [6]. The study protocol, patient information sheet and consent form were approved by the Ethics Committee of the University of Tübingen and the German Federal Institute for Drugs and Medical Devices (BfArM). All study participants had signed an informed consent form.

The study was conducted in 20 healthy, Caucasian, premenopausal female volunteers that were genotyped for CYP2D6 polymorphisms and subsequently assigned to predicted phenotypes according to the respective CYP2D6 activity score (AS) as depicted in Table 1 [17,18]. All subjects received 100 mg clomiphene citrate (two 50 mg tablets Ratiopharm GmbH, Ulm, Germany, with 62:38 (*E*)-Clom:(*Z*)-Clom) as a single dose after an overnight fast and without any concomitant medication. After a wash-out phase of at least three weeks, clomiphene was administered concomitantly with the strong CYP3A4

inhibitor clarithromycin [19]. Here, the participants received 500 mg clarithromycin twice daily for four days. On day 5, a single dose of clomiphene citrate was administered together with 500 mg clarithromycin. Finally, in the third period, all subjects received clomiphene citrate together with the strong CYP2D6 inhibitor paroxetine [19]. Here, 40 mg paroxetine was administered once daily for two days. On day 3, participants received a single dose of clomiphene citrate concomitantly with 40 mg paroxetine (Figure 1).

Table 1. Overview of clinical data integrated from the pharmacokinetic panel study.

	AS = 0	AS = 0.5	AS = 0.75	AS = 1	AS = 2	AS = 3
n	6 #	4	1 +	2	3	3
CYP2D6 phenotypes	PM	IM	IM	IM	NM	UM
CYP2D6 genotypes	**4/*4* **4/*5* **4/*6*	**4/*41* **4/*9*	**9/*10*	**1/*4*	**1/*1*	**1/*1 × 3*
Demographics						
Age [years]	25.2 (22–29)	24.3 (21–30)	22.0 (-)	25.5 (23–28)	32.3 (26–43)	25.7 (22–28)
Weight [kg]	62.3 (50.0–70.0)	59.3 (55.5–64.0)	63.0 (-)	68.8 (63.5–74.0)	56.5 (48.0–63.5)	61.7 (54.0–73.0)
Height [cm]	1.70 (1.53–1.75)	1.68 (1.59–1.72)	1.66 (-)	1.71 (1.68–1.73)	1.63 (1.60–1.67)	1.65 (1.57–1.75)
BMI [kg/m^2]	21.6 (20.6–22.9)	21.1 (20.3–22.0)	22.9 (-)	23.6 (22.5–24.7)	21.3 (18.8–24.2)	22.6 (20.3–23.8)

number of study participants decreased during the DDGI setting due to drop-outs (*n* = 5 for clarithromycin, *n* = 4 for paroxetine); + one study participant classified as AS = 0.75 was excluded from the analysis (see Section S1.1 of the supplementary document); demographic parameters are presented as mean (range); AS, CYP2D6 activity score; BMI, body mass index; IM, intermediate metabolizers; *n*, number of subjects; NM, normal metabolizers; PM, poor metabolizers; UM, ultrarapid metabolizers.

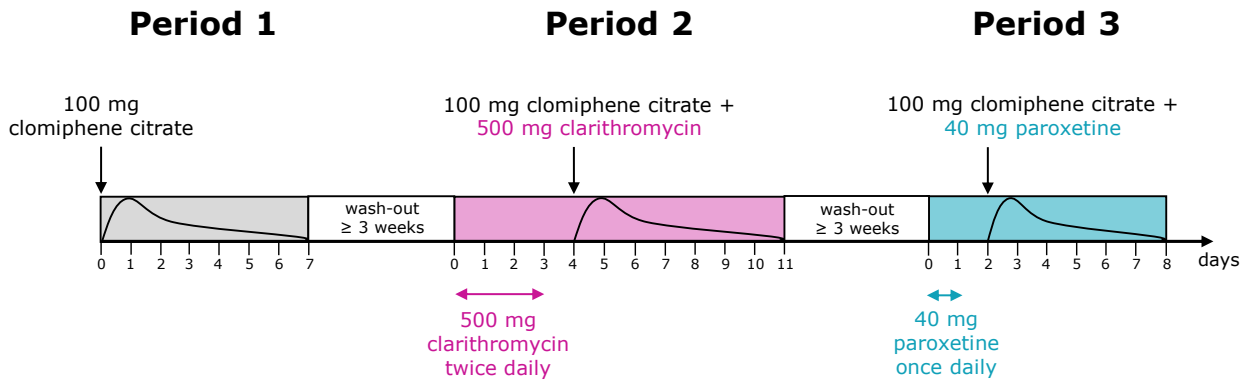

Figure 1. Drug administration schedule in the pharmacokinetic panel study. In period I, clomiphene citrate alone; in period II, combined with clarithromycin; and in period III, combined with paroxetine was administered.

Both plasma concentration–time profiles as well as renal excretion data of (*E*)-Clom and its metabolites (*E*)-4-OH-Clom, (*E*)-DE-Clom and (*E*)-4-OH-DE-Clom were obtained by validated liquid chromatography–tandem mass spectrometry (LC-MS/MS) methods [13,20]. The demographic and clinical characteristics of the study population are shown in Table 1.

Additionally, (*E*)-Clom plasma concentration–time profiles from two single-dose [21,22] and two multiple-dose [23,24] studies were identified in a literature search and plasma profiles were digitized for further model evaluation. In these clinical trials, *CYP2D6* genotypes of study participants were not reported. Additional information including study populations and the corresponding administration protocols are listed in Table S2 of the supplementary document.

2.2. Software

PBPK modeling and simulation was performed in PK-Sim® and MoBi® (version 9.1 part of the Open Systems Pharmacology (OSP) Suite, http://www.open-systems-pharmacology.org) [25]. Published clinical data of (*E*)-Clom were digitized with GetData Graph Digitizer version 2.26.0.20 (S. Fedorov) according to Wojtyniak and coworkers [26]. PK parameter calculations, model performance evaluations and graphics were accomplished with the R programming language version 3.6.3 (R Foundation for Statistical Computing, Vienna, Austria) [27]. Model parameter estimation via Monte-Carlo optimization as well as local sensitivity analysis were performed within PK-Sim®.

2.3. PBPK Model Development

For PBPK model building, information on physicochemical properties, as well as absorption, distribution, metabolism and excretion (ADME) processes of all investigated compounds, were gathered from the literature. Clinical data were split into a training and a test dataset. The training dataset for model development comprised mean plasma and renal excretion profiles of (*E*)-Clom and its metabolites from NM and PM study populations (n = 8 plasma concentration–time profiles and n = 8 renal excretion profiles). This dataset was selected to inform catalytic rate constant (k_{cat}) parameters associated with CYP2D6-dependent and -independent metabolic pathways, respectively. Plasma concentration–time profiles and renal excretion data of IM and ultrarapid metabolizers (UM) in the DGI setting, data from all phenotypes in the DD(G)I setting as well as digitized clinical study data from the published literature were utilized as the test dataset for PBPK model evaluation (n = 70 plasma concentration–time profiles and n = 64 renal excretion profiles).

Metabolic pathways of (*E*)-Clom and its metabolites comprising hydroxylation, N-de-ethylation and glucuronidation, among others, were implemented via CYP enzymes (CYP2D6, CYP3A4 and CYP2B6) and unspecific hepatic clearance mechanisms (Figure 2). In summary, (*E*)-Clom is primarily metabolized via CYP2D6 to the active metabolite (*E*)-4-OH-Clom as well as to (*Z*)-3-hydroxyclomiphene (implemented as an undefined metabolite) [6]. An additional biotransformation process via CYP2B6 to (*E*)-4-OH-Clom was implemented to cover the fraction of CYP2D6-independent metabolism observed in the PM population and in CYP2D6 DD(G)I scenarios [5,6]. Biotransformation of (*E*)-Clom to (*E*)-DE-Clom was implemented mainly through CYP3A4 with CYP2D6 playing only a minor role in this metabolic pathway [5,28].

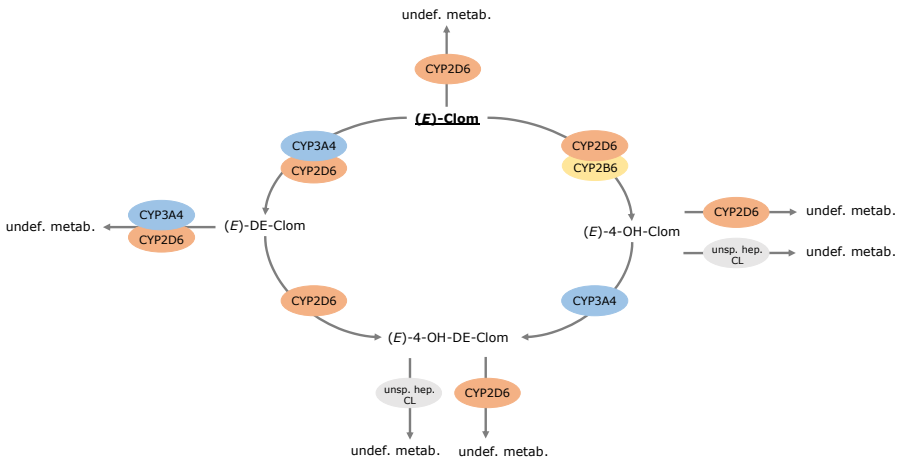

Figure 2. Overview of implemented metabolic processes in the (*E*)-Clom PBPK model. CYP, cytochrome P450; (*E*)-4-OH-Clom, (*E*)-4-hydroxyclomiphene; (*E*)-4-OH-DE-Clom, (*E*)-4-hydroxy-N-desethylclomiphene; (*E*)-Clom, (*E*)-clomiphene; (*E*)-DE-Clom, (*E*)-N-desethylclomiphene; undef. metab., undefined metabolite; unsp. hep. CL, unspecific hepatic clearance.

(*E*)-4-OH-Clom is metabolized via CYP2D6 to (*Z*)-3,4-dihydroxyclomiphene (implemented as an undefined metabolite), via an unspecific hepatic clearance mechanism and via CYP3A4 to the second active metabolite (*E*)-4-OH-DE-Clom [5,6,28]. (*E*)-4-OH-DE-Clom is also formed via CYP2D6 metabolism of (*E*)-DE-Clom, which in turn, represents the main route of elimination of (*E*)-DE-Clom [5,28]. Furthermore, (*E*)-DE-Clom is metabolized to minor extents through CYP2D6 and CYP3A4 to (*E*)-N,N-didesethylclomiphene (implemented as an undefined metabolite) [5,28]. The metabolism of (*E*)-4-OH-DE-Clom has not been extensively investigated, yet. According to work by Kröner [6], (*E*)-4-OH-DE-Clom is presumably metabolized through a CYP-mediated pathway to (*Z*)-3,4-dihydroxydesethylclomiphene. Additionally, glucuronidation, sulfation and potentially further unexplored pathways play a role in (*E*)-4-OH-DE-Clom biotransformation [6] and were grouped under an unspecific hepatic clearance process in the PBPK model (Figure 2).

Renal excretion through glomerular filtration was implemented and potential reabsorption or secretion processes were informed via renal excretion data. Model parameters that could not be informed from experimental reports during model development were optimized by fitting the model to the observed data of the training dataset. Moreover, a fraction of (*E*)-Clom metabolized via CYP3A4 was calculated (see Section S1.5 of the supplementary document) and used to inform k_{cat} model parameters associated with (*E*)-Clom metabolism. For detailed information on PBPK model building, see Section S1 of the supplementary document.

2.4. DGI and DD(G)I Modeling

Using the training dataset, k_{cat} values for CYP2D6-mediated pathways were estimated for the NM population, while CYP2D6 k_{cat} values for the PM population were set to zero. To predict DGIs and plasma concentration–time profiles in the IM and UM populations, IM and UM k_{cat} values for CYP2D6-dependent pathways were extrapolated from the estimated NM-k_{cat} value (Equation (1)):

$$k_{cat,\ AS=i} = k_{cat,\ AS=2} \cdot IVSF_i \quad (1)$$

Here, $k_{cat,\ AS=i}$ represents the catalytic rate constant for CYP2D6 AS = i, $k_{cat,\ AS=2}$ is the catalytic rate constant for the NM population and $IVSF_i$ is the corresponding in vitro scaling factor (IVSF). IVSFs were obtained using in vitro information on CYP2D6 AS-specific formation rates regarding the metabolism of (*E*)-Clom and its three metabolites (see Table S8 of the supplementary document) [5]. For predictions of plasma concentrations from clinical trials that did not report CYP2D6 phenotypes, CYP2D6 k_{cat} parameters were fitted to the respective plasma concentration–time profiles for each study.

In the DD(G)I setting, study participants in the pharmacokinetic panel study received clomiphene citrate together with the CYP3A4 inhibitor clarithromycin or the CYP2D6 inhibitor paroxetine that additionally acts as a weak inhibitor of CYP3A4 [19,29]. Predictions for DD(G)I scenarios of (*E*)-Clom and the investigated metabolites were performed for all CYP2D6 AS by coupling the developed parent–metabolite PBPK model with previously published PBPK models of the perpetrator drugs clarithromycin [16] and paroxetine [30]. Inhibition mechanisms of CYP3A4 and CYP2D6 were implemented as described in the OSP Suite manual [31]. Interaction parameters were used as published in the respective perpetrator PBPK models [16].

2.5. PBPK DGI and DD(G)I Model Evaluation

The performance of the parent–metabolite PBPK model was evaluated, applying several graphical and quantitative methods. The predicted plasma concentration–time profiles of (*E*)-Clom, (*E*)-4-OH-Clom, (*E*)-DE-Clom and (*E*)-4-OH-DE-Clom were graphically compared with their respective observed plasma profiles for all investigated CYP2D6 AS populations. Additionally, goodness-of-fit plots were used to compare predicted and observed areas under the plasma concentration–time curves from the first to the last time point of measurements (AUC_{last}), C_{max} values and plasma concentrations of all model

compounds for the DGI and DD(G)I scenarios. As quantitative measures, the mean relative deviation (MRD) of predicted plasma concentrations and the geometric mean fold error (GMFE) of predicted AUC_{last} and C_{max} were calculated according to Equations (2) and (3), respectively:

$$\text{MRD} = 10^{x} \text{ with } x = \sqrt{\frac{1}{n} \sum_{i=1}^{n} \left(\log_{10} \hat{c}_i - \log_{10} c_i\right)^2} \quad (2)$$

Here, $\hat{c}_i$ represents the i-th predicted plasma concentration, c_i is the corresponding observed plasma concentration and n equals the number of observed values.

$$\text{GMFE} = 10^{x} \text{ with } x = \frac{1}{n} \sum_{i=1}^{n} \left| \log_{10} \left(\frac{\hat{a}_i}{a_i} \right) \right| \quad (3)$$

Here, $\hat{a}_i$ represents the i-th predicted AUC_{last} and C_{max} value, respectively, a_i is the corresponding observed value and n equals the number of predicted plasma profiles.

For the evaluation of DGI and DD(G)I effects, the predicted AUC_{last} and C_{max} effect ratios were calculated according to Equations (4) and (5) and compared with the corresponding observed values. Here, model performance was assessed using the prediction acceptance limits proposed by Guest et al. with 1.25-fold variability [32].

$$AUC_{\text{last, AS=i}} \text{ ratio} = \frac{AUC_{\text{last, effect, AS=i}}}{AUC_{\text{last, control}}} \quad (4)$$

$$C_{\text{max, AS=i}} \text{ ratio} = \frac{C_{\text{max, effect, AS=i}}}{C_{\text{max, control}}} \quad (5)$$

For the calculation of DGI ratios, $AUC_{\text{last, effect, AS=i}}$ and $C_{\text{max, effect, AS=i}}$ represent the AUC_{last} and C_{max} for CYP2D6 AS = i, while $AUC_{\text{last, control}}$ and $C_{\text{max, control}}$ are the AUC_{last} and C_{max} values for the NM (AS = 2) population. For the calculation of DD(G)I ratios, $AUC_{\text{last, effect, AS=i}}$ and $C_{\text{max, effect, AS=i}}$ represent the AUC_{last} and C_{max} for the CYP2D6 AS = i in the DD(G)I scenario with clarithromycin or paroxetine, while $AUC_{\text{last, control}}$ and $C_{\text{max, control}}$ are the AUC_{last} and C_{max} values for the CYP2D6 AS = i without the concomitant use of perpetrator drugs.

Moreover, a local sensitivity analysis was performed using PK-Sim®. A detailed description of the analysis and results is provided in Section S4.4 of the supplementary document.

3. Results

3.1. PBPK Model Building and Evaluation

The developed whole-body parent–metabolite PBPK model successfully described plasma concentration–time profiles and renal excretion profiles in NM and PM populations. In addition, DGI effects in IM and UM populations as well as DD(G)I scenarios with clarithromycin and paroxetine in various phenotypes could be successfully predicted. With that, the PBPK model of (*E*)-Clom and the three metabolites (*E*)-4-OH-Clom, (*E*)-DE-Clom and (*E*)-4-OH-DE-Clom was able to capture the complexity of the parent–metabolite network and was used to characterize the contribution of various elimination pathways.

For model building and evaluation, plasma concentration–time and renal excretion–time profiles of various CYP2D6 AS from a pharmacokinetic panel study as well as from four published clinical studies with a dose range from 6.25 mg to 62 mg of orally administered (*E*)-Clom citrate were included. In total, 22 plasma concentration–time profiles for (*E*)-Clom, 16 plasma profiles each for (*E*)-4-OH-Clom, (*E*)-DE-Clom and (*E*)-4-OH-DE-Clom as well as 64 renal excretion profiles were available. With the observed increase in exposure for NM during concomitant clarithromycin administration, a fraction metabolized (f_m) of (*E*)-Clom via CYP3A4 of approximately 13% could be estimated (cf., Section S1.5 of the supplementary document) and subsequently integrated into the model building process to inform the contribution of the CYP3A4-dependent pathway. The drug-dependent model input parameters of (*E*)-Clom, (E)-4-OH-Clom, (*E*)-DE-Clom and (*E*)-4-OH-DE-Clom are provided in Tables S4–S7 of the supplementary document.

3.2. DGI Modeling and Evaluation

The final PBPK model precisely captured mean plasma concentration–time profiles of the NM (AS = 2) population for (*E*)-Clom and all three integrated metabolites (see Figure 3, third column). All predicted AUC_{last} and C_{max} values were in good agreement with the observed values: GMFEs for AUC_{last} and C_{max} in the NM population were 1.11 and 1.13, respectively. The overall MRD value for predicted plasma concentrations was 1.37.

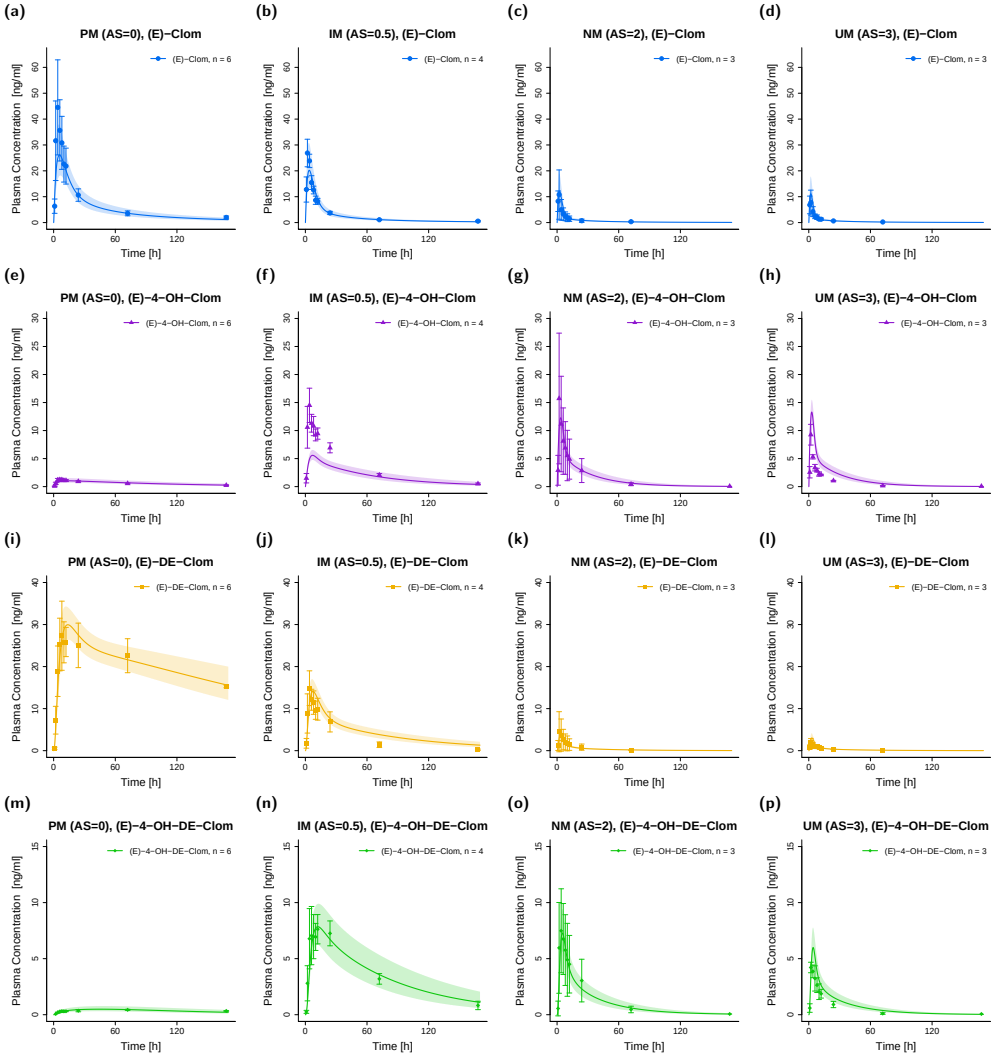

Figure 3. Predicted and observed plasma concentration–time profiles of (*E*)-Clom (**a**–**d**), (*E*)-4-OH-Clom (**e**–**h**), (*E*)-DE-Clom (**i**–**l**) and (*E*)-4-OH-DE-Clom (**m**–**p**) in PM (first column), IM (only AS = 0.5 shown; second column), NM (third column) and UM (last column) for DGI scenarios. Solid lines depict predicted geometric mean concentration–time profiles in the PM, IM (AS = 0.5), NM and UM populations. Colored ribbons show the corresponding geometric standard deviation of the population simulations (n = 1000). Mean observed data are shown as symbols with the corresponding standard deviation. Linear and semilogarithmic predicted and observed plasma concentration–time profiles of all studies and AS are shown in Section S4.1 of the supplementary document. AS, CYP2D6 activity score; DGI, drug–gene interaction; (*E*)-4-OH-Clom, (*E*)-4-hydroxyclomiphene; (*E*)-4-OH-DE-Clom, (*E*)-4-hydroxy-N-desethylclomiphene; (*E*)-Clom, (*E*)-clomiphene; (*E*)-DE-Clom, (*E*)-N-desethylclomiphene; IM, intermediate metabolizers; n, number of subjects; NM, normal metabolizers, PM, poor metabolizers; UM, ultrarapid metabolizers.

For DGI model predictions, CYP2D6 k_{cat} values were extrapolated from NM to IM (AS = 0.5, AS = 0.75 and AS = 1) and UM populations. The extrapolation of k_{cat} parameters based on in vitro scaling factors led to successful predictions of plasma profiles in IM and UM phenotypes. Plasma profiles in PM volunteers that were part of the training dataset were also well captured in model simulations (Figure 3).

Since (*E*)-Clom is primarily metabolized via CYP2D6 (predicted f_m = 86%), the PM population showed the highest AUC_{last} for the parent compound (*E*)-Clom (AUC_{PM} > AUC_{IM} > AUC_{NM} > AUC_{UM}), but the lowest AUC_{last} for the two most active metabolites (*E*)-4-OH-Clom and (*E*)-4-OH-DE-Clom. However, since (*E*)-4-OH-Clom and (*E*)-4-OH-DE-Clom were not only formed but also degraded via CYP2D6, their highest AUC_{last} could not be found in UM, but in IM with AS = 0.5 ($AUC_{IM\ (AS = 0.5)}$ > AUC_{NM} > AUC_{UM} > AUC_{PM}). A detailed listing of all predicted and observed AUC_{last} and C_{max} values for all phenotypes in the DGI study setting is depicted in Table S11 of the supplementary document.

Goodness-of-fit plots for all modeled compounds showing predicted compared with observed plasma concentrations, AUC_{last} and C_{max} values in the DGI study setting are depicted in Figure 4. Here, 90% of C_{max}, 80% of AUC_{last} and 78% of the predicted concentrations were within the two-fold acceptance criterion. GMFEs for the predicted C_{max} and AUC_{last} values were 1.41 and 1.43, respectively, and the overall MRD value for predicted plasma concentrations was 1.95.

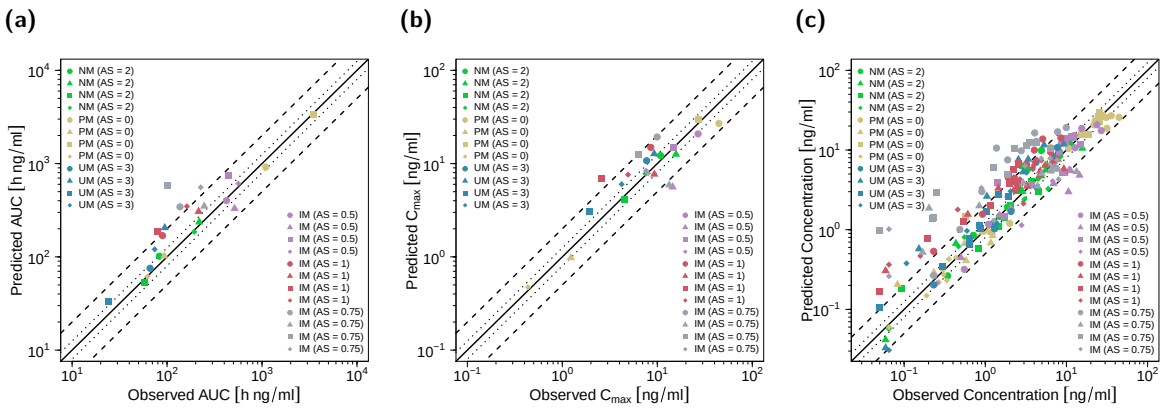

Figure 4. Predicted versus observed AUC_{last} (**a**), C_{max} (**b**) and plasma concentrations (**c**) of (*E*)-Clom (circles), (*E*)-4-OH-Clom (triangles), (*E*)-DE-Clom (squares) and (*E*)-4-OH-DE-Clom (diamonds) in PM, IM, NM and UM (DGI scenarios). The black solid lines mark the lines of identity. Black dotted lines indicate 1.25-fold; black dashed lines indicate two-fold deviation. Goodness-of-fit plots of digitized studies are depicted in Figure S8 of the supplementary document. AS, CYP2D6 activity score; DGI, drug–gene interaction; (*E*)-4-OH-Clom, (*E*)-4-hydroxyclomiphene; (*E*)-4-OH-DE-Clom, (*E*)-4-hydroxy-N-desethylclomiphene; (*E*)-Clom, (*E*)-clomiphene; (*E*)-DE-Clom, (*E*)-N-desethylclomiphene; IM, intermediate metabolizers; NM, normal metabolizers; PM, poor metabolizers; UM, ultrarapid metabolizers.

The predicted impact of CYP2D6 polymorphisms on the PK of (*E*)-Clom and its three metabolites (DGI effect ratios) is shown in Figure 5 and is highly consistent with observed effects. GMFEs for the predicted C_{max} and AUC_{last} ratios in the DGI setting were 1.46 and 1.65, respectively. Predicted and observed renal excretion profiles are visualized in Section S4.1 of the supplementary document. Moreover, complementary prediction results of concentration–time profiles for the remaining AS and included published clinical studies are shown in Sections S4.1.3 and S4.1.7, respectively, of the supplementary document.

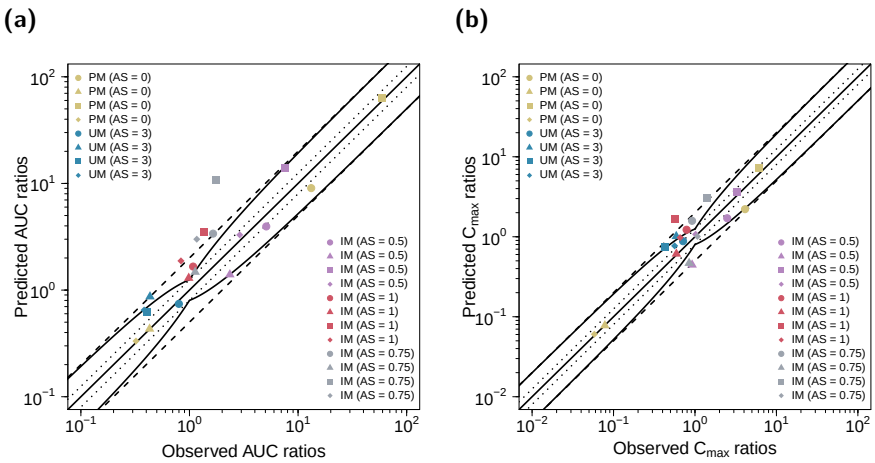

Figure 5. Predicted versus observed DGI (**a**) AUC_{last} and (**b**) C_{max} ratios of (*E*)-Clom (circles), (*E*)-4-OH-Clom (triangles), (*E*)-DE-Clom (squares) and (*E*)-4-OH-DE-Clom (diamonds). The straight black lines mark the lines of identity; the curved solid black lines show the limits of the predictive measure proposed by Guest et al. with 1.25-fold variability [32]. Black dotted lines indicate 1.25-fold; black dashed lines indicate two-fold deviation. AS, CYP2D6 activity score; (*E*)-4-OH-Clom, (*E*)-4-hydroxyclomiphene; (*E*)-4-OH-DE-Clom, (*E*)-4-hydroxy-N-desethylclomiphene; (*E*)-Clom, (*E*)-clomiphene; (*E*)-DE-Clom, (*E*)-N-desethylclomiphene; IM, intermediate metabolizers; NM, normal metabolizers; PM, poor metabolizers; UM, ultrarapid metabolizers.

3.3. DD(G)I Modeling and Evaluation

In total, 40 plasma concentration–time profiles and 40 renal excretion profiles of (*E*)-Clom and its metabolites were used for the investigation of DD(G)I scenarios with clarithromycin (mechanism-based inhibitor of CYP3A4) and paroxetine (mechanism-based inhibitor of CYP3A4 and CYP2D6) for various CYP2D6 AS (AS = 0, AS = 0.5, AS = 1, AS = 2 and AS = 3). Here, the impact of clarithromycin- and paroxetine-induced DD(G)I effects on plasma concentration–time profiles, AUC_{last} and C_{max} values of (*E*)-Clom and its metabolites was assessed. For this, published PBPK model parameters for clarithromycin [16] and paroxetine [30] were used including the respective competitive inhibition (K_i) and the maximum inactivation rate (k_{inact}) constants. Plasma and renal excretion profiles were predicted, compared with observed profiles and served for evaluations of DD(G)I model performance. DD(G)I model prediction performance is visually demonstrated in the concentration–time profiles (Figure 6) and the corresponding goodness-of-fit plots (Figure 7). GMFEs for the predicted AUC_{last} and C_{max} values were 1.30 and 1.40, respectively, and the overall MRD value for predicted plasma concentrations was 1.83.

Since the metabolism of (*E*)-Clom is predominantly mediated via CYP2D6, the AUC_{last} of (*E*)-Clom substantially increased with concomitant administration of the CYP2D6 inhibitor paroxetine (2.5–12-fold) for all phenotypes, except PM, which possess no CYP2D6 activity. Furthermore, due to inhibition of CYP2D6, C_{max} of the metabolite (*E*)-4-OH-Clom decreased in all phenotypes except for PM. However, as (*E*)-4-OH-Clom is not only formed but also degraded via CYP2D6, a substantial decrease in AUC_{last} during paroxetine DD(G)I was only predicted for the IM population in concordance with observed values. The minor involvement of CYP3A4 in the metabolism of (*E*)-Clom and (*E*)-4-OH-Clom is supported by the slight increase in the respective AUC_{last} during CYP3A4 inhibition in all phenotypes.

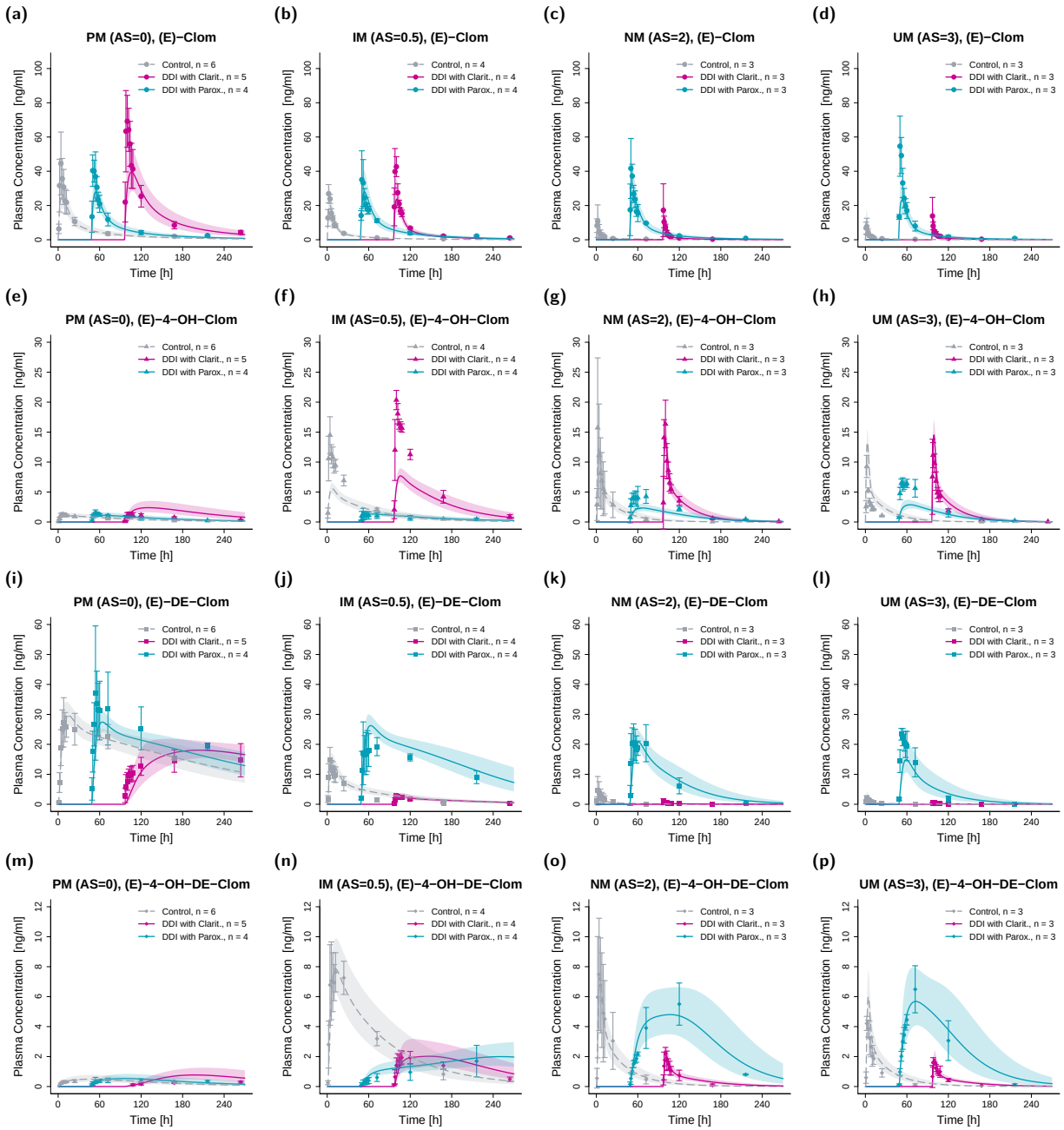

Figure 6. Predicted and observed plasma concentration–time profiles of (*E*)-Clom (**a**–**d**), (*E*)-4-OH-Clom (**e**–**h**), (*E*)-DE-Clom (**i**–**l**) and (*E*)-4-OH-DE-Clom (**m**–**p**) for DD(G)I scenarios in PM (first column), IM (only AS = 0.5 shown; second column), NM (third column) and UM (last column). Grey dashed lines depict the predicted geometric mean concentration–time profiles in absence of clarithromycin and paroxetine (control); turquoise solid lines represent the predicted geometric mean profiles in the presence of paroxetine; and pink solid lines represent the predicted geometric mean profiles in the presence of clarithromycin (DD(G)I). Colored ribbons show the corresponding geometric standard deviation of the population simulations ($n = 1000$). Mean observed data are shown as symbols with the corresponding standard deviation. Linear and semilogarithmic predicted and observed plasma concentration–time profiles of all AS are shown in Section S4.2 of the supplementary document. For better visibility, DD(G)I scenarios were plotted with a time offset with t = 0 at the first dose of the perpetrator drug. AS, CYP2D6 activity score; Clarit., Clarithromycin; DD(G)I, drug–drug

and drug–drug–gene interactions; (*E*)-4-OH-Clom, (*E*)-4-hydroxyclomiphene; (*E*)-4-OH-DE-Clom, (*E*)-4-hydroxy-N-desethylclomiphene; (*E*)-Clom, (*E*)-clomiphene; (*E*)-DE-Clom, (*E*)-N-desethylclomiphene; IM, intermediate metabolizers; *n*, number of subjects; NM, normal metabolizers; Parox., Paroxetine; PM, poor metabolizers; UM, ultrarapid metabolizers.

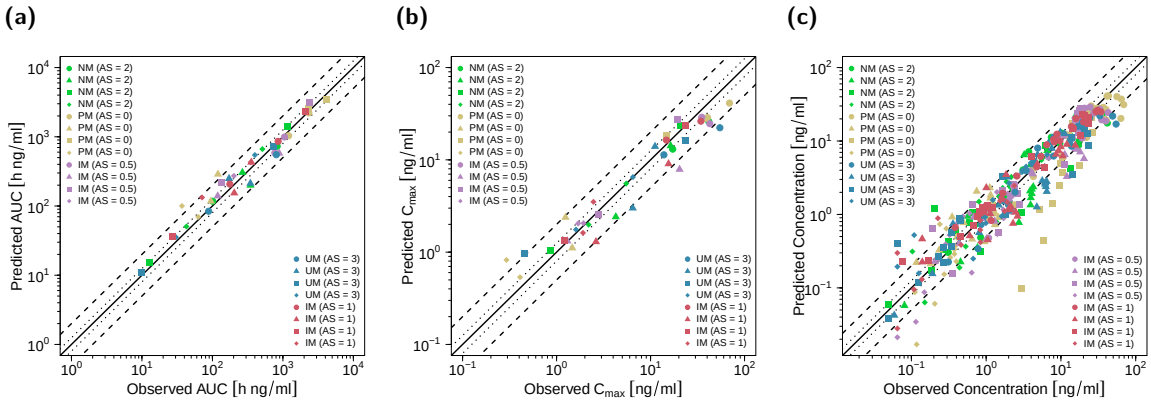

Figure 7. Predicted versus observed AUC_{last} (**a**), C_{max} (**b**) and plasma concentrations (**c**) of (*E*)-Clom (circles), (*E*)-4-OH-Clom (triangles), (*E*)-DE-Clom (squares) and (*E*)-4-OH-DE-Clom (diamonds) for DD(G)I scenarios with clarithromycin and paroxetine, respectively. The black solid lines mark the lines of identity. Black dotted lines indicate 1.25-fold; black dashed lines indicate two-fold deviation. AS, CYP2D6 activity score; DD(G)I, drug–drug and drug–drug–gene interactions; (*E*)-4-OH-Clom, (*E*)-4-hydroxyclomiphene; (*E*)-4-OH-DE-Clom, (*E*)-4-hydroxy-N-desethylclomiphene; (*E*)-Clom, (*E*)-clomiphene; (*E*)-DE-Clom, (*E*)-N-desethylclomiphene; IM, intermediate metabolizers; NM, normal metabolizers, PM, poor metabolizers; UM, ultrarapid metabolizers.

The AUC_{last} of (*E*)-DE-Clom is substantially reduced in all phenotypes by values between ~70% and 80% (NM and IM) and ~34% (PM) during concomitant clarithromycin administration, demonstrating that CYP3A4 is likely the major enzyme in the formation of (*E*)-DE-Clom. During CYP3A4 inhibition, AUC_{last} and C_{max} values, as well as the corresponding DDGI effects for (*E*)-4-OH-Clom and (*E*)-4-OH-DE-Clom in PM, were overpredicted by ~2.5-fold.

Predicted and observed AUC_{last} and C_{max} ratios of (*E*)-Clom, (*E*)-4-OH-Clom, (*E*)-DE-Clom and (*E*)-4-OH-DE-Clom for the DD(G)I setting are shown in Figure 8. GMFEs for the predicted C_{max} and AUC_{last} ratios in the DD(G)I setting were 1.50 and 1.40, respectively. All predicted and observed values for AUC_{last} and C_{max}, DD(G)I effect ratios as well as calculated MRDs and GMFEs are listed in Section S4.3 of the supplementary document.

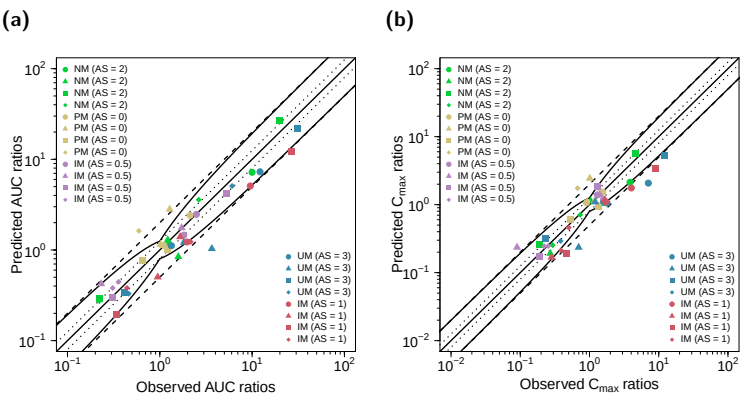

Figure 8. Predicted versus observed DD(G)I AUC_{last} (**a**) and C_{max} (**b**) ratios of (*E*)-Clom (circles), (*E*)-4-OH-Clom (triangles), (*E*)-DE-Clom (squares) and (*E*)-4-OH-DE-Clom (diamonds). The straight

black lines mark the lines of identity; the curved black lines show the limits of the predictive measure proposed by Guest et al. with 1.25-fold variability [32]. Black dotted lines indicate 1.25-fold; black dashed lines indicate two-fold deviation. AS, CYP2D6 activity score; DD(G)I, drug–drug and drug–drug–gene interactions; (*E*)-4-OH-Clom, (*E*)-4-hydroxyclomiphene; (*E*)-4-OH-DE-Clom, (*E*)-4-hydroxy-N-desethylclomiphene; (*E*)-Clom, (*E*)-clomiphene; (*E*)-DE-Clom, (*E*)-N-desethylclomiphene; IM, intermediate metabolizers; NM, normal metabolizers, PM, poor metabolizers; UM, ultrarapid metabolizers.

3.4. Contribution of Metabolic Pathways to (E)-Clom and Metabolite Disposition

In the PBPK model simulations, (*E*)-Clom is fully absorbed from the gastrointestinal tract (fraction absorbed = 1.0); however, it undergoes a substantial first-pass metabolism leading to a bioavailability of approximately 9% in UM, 11% in NM, 30% in IM (AS = 0.5) and 49% in PM. (*E*)-Clom is metabolized via three pathways to (*E*)-4-OH-Clom, (*E*)-DE-Clom and (Z)-3-hydroxyclomiphene with model-calculated f_m for NM of 41%, 17% and 42%, respectively (Figure 9).

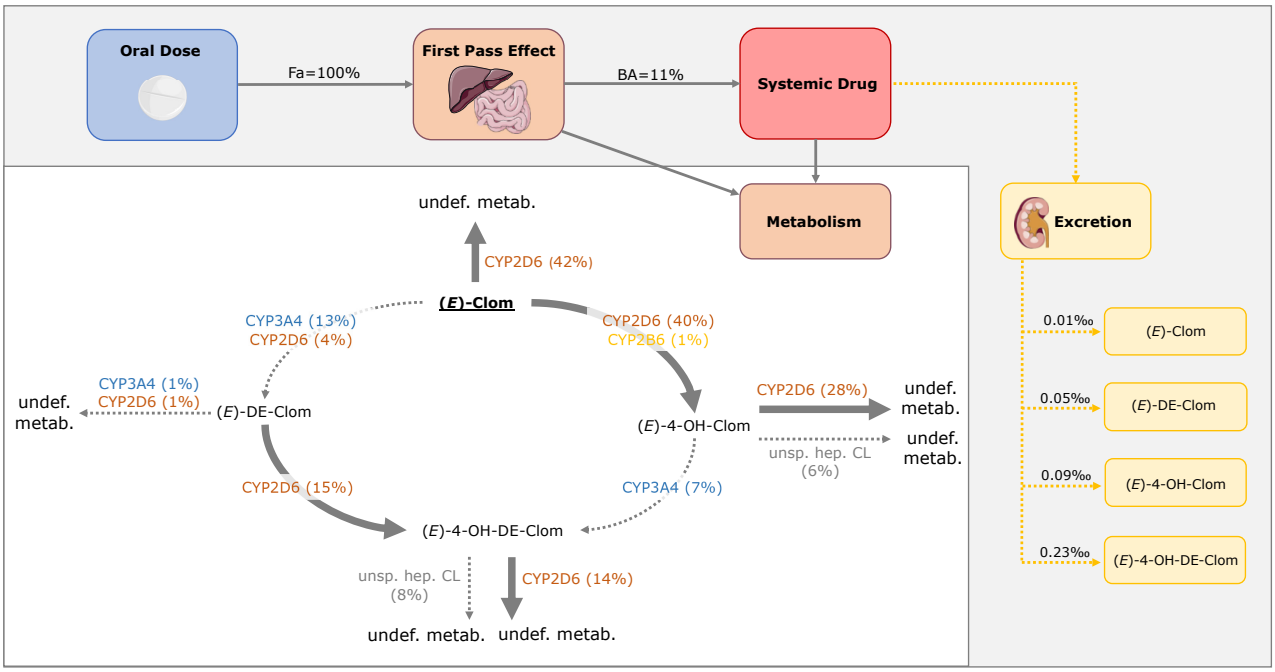

Figure 9. Mass balance diagram after oral administration of 62 mg (*E*)-Clom citrate in CYP2D6 normal metabolizers (AS = 2) including fraction absorbed, bioavailability and fractions of dose excreted in urine for (*E*)-Clom and the three implemented metabolites. Drawings by Servier, licensed under CC BY 3.0 [33]. BA, bioavailability; CL, clearance; CYP, cytochrome P450; (*E*)-4-OH-Clom, (*E*)-4-hydroxyclomiphene; (*E*)-4-OH-DE-Clom, (*E*)-4-hydroxy-N-desethylclomiphene; (*E*)-Clom, (*E*)-clomiphene; (*E*)-DE-Clom, (*E*)-N-desethylclomiphene; Fa, fraction absorbed; undef. metab., undefined metabolite; unsp. hep. CL, unspecific hepatic clearance.

The metabolism of the active metabolite (*E*)-4-OH-Clom in NM is mediated primarily via CYP2D6 (69%) and, to a minor extent, via an unspecific hepatic clearance (15%). Only 17% of (*E*)-4-OH-Clom is degraded to the second active metabolite (*E*)-4-OH-DE-Clom via CYP3A4. In addition, (*E*)-4-OH-DE-Clom is formed of (*E*)-DE-Clom via CYP2D6 (90% of (*E*)-DE-Clom elimination), while 10% of (*E*)-DE-Clom is metabolized via CYP2D6 and CYP3A4 to (*E*)-N,N-didesethylclomiphene. The renal excretion of (*E*)-Clom and its three metabolites can be considered negligible (0.01–0.23‰). Calculated contributions for all

implemented metabolic pathways and fractions of dose excreted in urine of (*E*)-Clom and its metabolites in PBPK model simulations for NM as well as fractions of dose excreted in urine are illustrated in Figure 9.

4. Discussion

Since the approval of clomiphene for the treatment of anovulation in women by the U.S. Food and Drug Administration (FDA) in the late 1960s, several efforts have been made to explain the inter-individual variability in clomiphene PK and drug response [13,14,34–36]. While early studies identified obesity, hyperandrogenemia and high levels of serum anti-Müllerian hormone as predictors for non-response [34,35,37–39], polymorphisms of CYP2D6 were additionally identified to alter drug disposition and response [5,14,36]. This study presents the first (*E*)-Clom PBPK model that investigates and characterizes the impact of CYP2D6 polymorphisms and the concomitant use of CYP3A4 and CYP2D6 inhibitors on the PK of (*E*)-Clom and its three important metabolites (*E*)-4-OH-Clom, (*E*)-DE-Clom and (*E*)-4-OH-DE-Clom.

For this, a whole-body parent–metabolite PBPK model of (*E*)-Clom has been successfully built and evaluated, predicting plasma concentration–time profiles for various CYP2D6 AS in DGI and DD(G)I scenarios. The predicted DGI and DD(G)I effects on the PK of (*E*)-Clom and its active metabolites were in good agreement with the effects observed in a pharmacokinetic panel study. Despite the complex nature of the disposition of (*E*)-Clom and its metabolites, the PBPK model could capture and quantify the contribution of the different metabolic pathways. The developed model described and predicted plasma profiles of the training and test dataset for the DGI setting with GMFEs of 1.43 and 1.41 for predictions of AUC_{last} and C_{max}, respectively. GMFEs in the DD(G)I settings with clarithromycin and paroxetine were 1.30 and 1.40 for predictions of AUC_{last} and C_{max}, respectively, highlighting the good descriptive and predictive model performance.

DGI predictions for IM and UM populations were based on in vitro–in vivo extrapolation of CYP2D6 activity. Here, the application of AS-specific k_{cat} values based on estimated in vivo NM-k_{cat} and published in vitro information on differences in metabolic activity between CYP2D6 AS led to successful predictions of observed plasma concentrations and DGI effect ratios. The predicted DGI effects of CYP2D6 polymorphisms on the AUC of the four modeled compounds ranged from a ~60-fold increase ((*E*)-DE-Clom in PM vs. NM) to a ~70% decrease ((*E*)-4-OH-DE-Clom in PM vs. NM).

The observed DGI AUC_{last} effect ratio for (*E*)-Clom in IM (AS = 1) was ~1 representing "no effect", while the model predicted effect ratio was about 1.7, suggesting a ~70% increase in AUC from NM to IM (AS = 1), which seems reasonable due to the strong CYP2D6 involvement in (*E*)-Clom degradation. The corresponding predicted effect on (*E*)-4-OH-DE-Clom exposure (~1.9) was also higher than the effect observed (~0.8). Similarly, DGI AUC_{last} effect ratios for IM (AS = 0.75) were higher than the corresponding effect ratios observed for (*E*)-Clom and its metabolites. Several genetic and non-genetic factors in addition to the *CYP2D6* genotype have previously been described to affect CYP2D6 activity in vivo, resulting in substantial interindividual variability in the PK of CYP2D6 substrates [5,40,41]. Here, the pharmacokinetic panel study might lack the required power to reliably predict the low observed mean effect ratios for IM (AS =1 and AS = 0.75) individuals (n = 2 and n =1, respectively). Thus, additional studies with an increased number of CYP2D6 genotyped individuals would be helpful to further evaluate these prediction scenarios.

The underprediction of (*E*)-4-OH-Clom AUC_{last} DGI effects in IM (AS = 0.5) and UM populations based on the in vitro–in vivo extrapolation of CYP2D6 activity could hint towards a stronger involvement of CYP2D6 in the metabolism of (*E*)-4-OH-Clom or indicate lower CYP2D6 k_{cat} values in IM and higher values in UM than was extrapolated from in vitro. Moreover, the relative importance of other enzymes for pathways mediated by CYP2D6 increases for lower CYP2D6 AS. Consequently, the impact of variability in activity for alternative pathways (e.g., due to polymorphisms in *CYP2B6*) increases [41,42]. Notably, only a small number of participants (n = 3) in the pharmacokinetic panel study

were assigned to the IM (AS = 0.5) group and were genotyped for *CYP2D6* only. Hence, as a result of the underprediction (IM (AS = 0.5)) and overprediction (UM) of (*E*)-4-OH-Clom exposure, respectively, DD(G)I model predictions for this metabolite should be interpreted carefully in these populations.

Since (*E*)-Clom is primarily metabolized via CYP2D6 (f_m of ~86% according to model simulations) PM showed the highest exposure for the parent compound ($AUC_{last,\ (E)\text{-Clom}}$ order: PM > IM > NM > UM). Additionally, as (*E*)-4-OH-DE-Clom is primarily formed via CYP2D6-dependent pathways, PM showed the lowest AUC_{last} for the active metabolite. However, the complex metabolic network with additional involvement of other CYP enzymes and contribution of multiple CYP2D6-dependent pathways resulted in a different order for (*E*)-4-OH-DE-Clom AUC values compared with (*E*)-Clom. Here, the AUC_{last} of (*E*)-4-OH-DE-Clom was highest in IM (AS = 0.5), while it was lowest for PM and second-lowest for UM, proposing a contribution of CYP2D6 not only in the formation but also in the degradation of (*E*)-4-OH-DE-Clom. This is supported by model simulations, where the integration of a CYP2D6 metabolic route for (*E*)-4-OH-Clom and (*E*)-4-OH-DE-Clom degradation [6,28] was crucial for successful predictions of the respective plasma profiles. The involvement of CYP2D6 in the degradation of the active metabolites might also explain findings from a study by Ji et al., where all nine study participants with IM phenotype responded to clomiphene therapy, whereas 30% of NM were non-responders [14].

For the investigated clarithromycin DD(G)I scenario, (*E*)-Clom exposure increased by only ~15% for NM compared with the control scenario without CYP3A4 inhibition. In contrast, for PM, (*E*)-Clom exposure increased ~2.4-fold, which was successfully predicted by the PBPK model. The increase in (*E*)-Clom AUC_{last}, however, also led to a model-predicted increase in (*E*)-4-OH-Clom AUC_{last} (~2.8-fold) and consequently to an increase in (*E*)-4-OH-DE-Clom AUC_{last} (~1.6-fold) for PM. This elevation was not observed in the available clinical data (effect ratio ~1.3-fold and ~0.6-fold, respectively). These differences between observation and prediction might be attributed to a saturated CYP2B6 metabolism from (*E*)-Clom to (*E*)-4-OH-Clom in vivo that was not reflected in the PBPK model or to non-implemented alternative metabolic pathways that are active in scenarios of low CYP3A4 and CYP2D6 activity.

The underprediction of paroxetine DDGI effects on (*E*)-4-OH-Clom AUC_{last} in the IM (AS = 0.5) and UM population supports the aforementioned hint towards lower CYP2D6 k_{cat} values in IM and higher values in UM or a stronger involvement of CYP2D6 in the metabolism of (*E*)-4-OH-Clom than was extrapolated from in vitro.

Many different CYP enzymes are involved in the metabolic pathways of (*E*)-Clom and its metabolites [5,28]; therefore, the implementation of biotransformation generally focused on main CYP enzymes. However, of note, the implementation of CYP2D6 as an additional enzyme, complementing CYP3A4 in the formation of (*E*)-DE-Clom [43], led to a substantial improvement in the prediction of clarithromycin DD(G)I scenarios, preventing an underprediction of AUC_{last} values for (*E*)-DE-Clom. Here, CYP2D6 was incorporated with a ~20% contribution to the formation of the desethyl metabolite [43].

In contrast, the initial assumption of a CYP3A4-mediated desethylation of (*E*)-4-OH-DE-Clom (as for (*E*)-4-OH-Clom, cf. Figure 9) was rejected, since this implemented process led to a consistent overprediction of (*E*)-4-OH-DE-Clom AUC_{last} in the clarithromycin DD(G)I scenarios for all phenotypes. Instead, the metabolic pathway was replaced by an unspecific hepatic clearance process representing glucuronidation, sulfation and potential other metabolic processes of (*E*)-4-OH-DE-Clom as suggested by Kröner [6].

PBPK modeling was also leveraged to gain insights into the PK of (*E*)-Clom and to investigate contributions of the different metabolic pathways for (*E*)-Clom and its metabolites. According to model simulations in NM, about 22% of the administered (*E*)-Clom dose is eventually metabolized to the metabolite with the highest target affinity ((*E*)-4-OH-DE-Clom [28]), mainly via the (*E*)-DE-Clom-pathway (~69%) and ~31% via the (*E*)-4-OH-Clom pathway. This is of note, as only ~17% of (*E*)-Clom is initially metabolized to (*E*)-DE-Clom, while ~41% is metabolized to (*E*)-4-OH-Clom. However, ~90% of (*E*)-DE-Clom metabolism

results in (*E*)-4-OH-DE-Clom formation (vs. only ~17% of (*E*)-4-OH-Clom metabolism), eventually representing the main pathway of (*E*)-4-OH-DE-Clom formation according to model simulations.

Clomiphene is typically administered as a racemic mixture of (*E*)- and (*Z*)-Clom (62:38) [22]. Both isomers show highly distinct pharmacokinetic characteristics and also differ in affinity to the target receptor [22,28]. In contrast to (*Z*)-Clom, (*E*)-Clom undergoes an extensive first-pass metabolism resulting in a lower bioavailability [44]. The model predicted bioavailability for (*E*)-Clom in NM was ~11%, which is in congruence with the low bioavailability of ~6.3% for the (*E*)-isomer calculated from the reported $AUC_{0\text{-}24h}$ after oral [21] and intravenous application of 50 mg clomiphene citrate [45]. While the calculated value from the literature is based on an intravenous study with a small number of study participants (n = 2) [45], a low bioavailability can be supported with the developed PBPK model. The model calculated bioavailabilities in PM, IM (AS = 0.5, AS = 0.75, AS = 1) and UM were 49%, 30%, 27%, 18% and 9%, respectively.

In the pharmacokinetic panel study, renal excretion of the parent compound (*E*)-Clom and the three modeled metabolites was quantified and showed negligible overall contribution to the respective compound elimination. The PBPK model was able to quantify this small contribution of renal excretion for the four investigated compounds. The respective simulated fractions of dose excreted in urine for NM were calculated to be 0.01‰, 0.09‰, 0.05‰ and 0.23‰, for (*E*)-Clom, (*E*)-4-OH-Clom, (*E*)-DE-Clom and (*E*)-4-OH-DE-Clom, respectively. This is in concordance with recent studies, where unchanged (*E*)-Clom and unconjugated metabolites could only be detected in small amounts, or not at all in urine samples [46,47].

The pharmacokinetic panel study was conducted in a cross-over design [28]. One limitation of this work is the small number of participants in the panel study (n = 20), with only one to six individuals per AS group available for model development. Additionally, from the PM group, one participant dropped out of the clinical trial during the clarithromycin DDGI scenario and two participants during the paroxetine DDGI scenario. In the case of the IM (AS = 0.75) group, no data for the DDGI scenarios were available due to drop-out.

When additional pharmacokinetic data become available, the PBPK model can be further evaluated according to the "learn–confirm–refine" principle [48,49] to be used for further model applications. Moreover, the presented parent–metabolite PBPK model of (*E*)-Clom provides a basis for future investigations of different covariates (e.g., body mass index), individual CYP2D6 genotypes and the concomitant use of additional perpetrator drugs influencing the PK of (*E*)-Clom and its metabolites. The evaluated model can be leveraged to simulate plasma concentration–time profiles and investigate the exposure of (*E*)-Clom and its active metabolites in as-yet unexplored DD(G)I scenarios with the concomitant administration of moderate and weak CYP enzyme inhibitors as well as CYP enzyme inducers (e.g., carbamazepine [15]). Here, future clinical investigations of DD(G)I scenarios with concomitant use of (*E*)-Clom and CYP enzyme inducers are required for evaluation of such model predictions with clinically observed data. For the translation of exposure differences into dose recommendations, studies quantifying the efficacy- and safety-related contributions of (*E*)-Clom and its metabolites would be of high interest.

5. Conclusions

A whole-body parent–metabolite PBPK model of (*E*)-Clom including the metabolites (*E*)-4-OH-Clom, (*E*)-DE-Clom and (*E*)-4-OH-DE-Clom was successfully developed. The model predicted plasma concentration–time profiles of (*E*)-Clom and its metabolites for CYP2D6 DGI, as well as CYP2D6 and CYP3A4 DDI and DDGI scenarios in six different CYP2D6 AS groups. For this, an in vitro–in vivo extrapolation approach to obtain CYP2D6 k_{cat} values for different AS was successfully integrated to predict plasma profiles for IM (AS = 0.5, AS = 0.75, AS = 1) and UM populations. Furthermore, the model was applied to investigate the contribution of metabolic pathways to the elimination of (*E*)-Clom and its metabolites. The developed PBPK model will be made publicly available (http:

//models.clinicalpharmacy.me/) and can be further leveraged to investigate the PK of (*E*)-Clom and its metabolites for various DD(G)I scenarios.

Supplementary Materials: The following supporting information can be downloaded at: https://www.mdpi.com/article/10.3390/pharmaceutics14122604/s1, Figure S1: Predicted and observed plasma concentration-time profiles (linear scale) of (*E*)-Clom (a–f), (*E*)-4-OH-Clom (g–l), (*E*)-DE-Clom (m–r) and (*E*)-4-OH-DE-Clom (s–x) for DGI scenarios; Figure S2: Predicted and observed plasma concentration-time profiles (semilogarithmic scale) of (*E*)-Clom (a–f), (*E*)-4-OH-Clom (g–l), (*E*)-DE-Clom (m–r) and (*E*)-4-OH-DE-Clom (s–x) for DGI scenarios; Figure S3: Predicted versus observed AUClast (a), Cmax (b) and plasma concentrations (c) of (E)-Clom (circles), (*E*)-4-OH-Clom (triangles), (*E*)-DE-Clom (squares) and (*E*)-4-OH-DE-Clom (diamonds) in PM, IM, NM and UM (DGI scenarios); Figure S4: Predicted versus observed DGI AUClast (a) and Cmax (b) ratios of (*E*)-Clom (circles), (*E*)-4-OH-Clom (tri-angles), (*E*)-DE-Clom (squares) and (*E*)-4-OH-DE-Clom (diamonds) in PM, IM and UM; Figure S5: Predicted and observed renal excretion profiles (linear scale) of (*E*)-Clom (a–f), (*E*)-4-OH-Clom (g–l), (*E*)-DE-Clom (m–r) and (*E*)-4-OH-DE-Clom (s–x) for DGI scenarios; Figure S6: Predicted and observed plasma concentration-time profiles (linear scale) of digitized studies from literature after single (a,b) and multiple (c–f) dosing; Figure S7: Predicted and observed plasma concentration-time profiles (semilogarithmic scale) of digitized studies from literature after single (a,b) and multiple (c–f) dosing; Figure S8: Predicted versus observed (a) AUClast, (b) Cmax and (c) plasma concentrations of (*E*)-Clom; Figure S9: Predicted and observed plasma concentration-time profiles (linear scale) of (E)-Clom (a–e), (*E*)-4-OH-Clom (f–j), (*E*)-DE-Clom (k–o) and (*E*)-4-OH-DE-Clom (p–t) for DD(G)I scenarios in PM, IM, NM and UM; Figure S10: Predicted and observed plasma concentration-time profiles (semilogarithmic scale) of (*E*)-Clom (a–e), (*E*)-4-OH-Clom (f–j), (*E*)-DE-Clom (k–o) and (*E*)-4-OH-DE-Clom (p–t) for DD(G)I scenar-ios in PM, IM, NM and UM; Figure S11: Predicted versus observed AUClast (a), Cmax (b) and plasma concentrations (c) of (*E*)-Clom (circles), (*E*)-4-OH-Clom (triangles), (*E*)-DE-Clom (squares) and (*E*)-4-OH-DE-Clom (diamonds) for DD(G)I scenarios with clarithromycin and paroxetine, respectively in PM, IM, NM and UM; Figure S12: Predicted versus observed DD(G)I AUClast (a) and Cmax (b) ratios of (*E*)-Clom (circles), (*E*)-4-OH-Clom (triangles), (*E*)-DE-Clom (squares) and (*E*)-4-OH-DE-Clom (diamonds) in PM, IM, NM and UM; Figure S13: Predicted and observed renal excretion profiles (linear scale) of (*E*)-Clom (a–e), (*E*)-4-OH-Clom (f–j), (*E*)-DE-Clom (k–o) and (*E*)-4-OH-DE-Clom (p–t) for DD(G)I scenarios in PM, IM, NM and UM; Figure S14: Sensitivity analysis of the PBPK model for (*E*)-Clom, (*E*)-4-OH-Clom, (*E*)-DE-Clom and (*E*)-4-OH-DE-Clom; Figure S15: Molecular structures of (*E*)-Clom (a) and its metabolites (*E*)-DE-Clom (b), (*E*)-4-OH-Clom (c) and (*E*)-4-OH-DE-Clom (d); Table S1: Optimized CYP2D6 kcat values for each study; Table S2: Overview of clinical study data from literature used for model evaluation; Table S3: System-dependent parameters and expression of relevant enzymes; Table S4: Drug-dependent parameters for (*E*)-clomiphene; Table S5: Drug-dependent parameters for (*E*)-N-desethylclomiphene; Table S6: Drug-dependent parameters for (*E*)-4-hydroxyclomiphene; Table S7: Drug-dependent parameters for (*E*)-4-hydroxy-N-desethyl-clomiphene; Table S8: Employed in vitro scaling factors (IVSFs) for individual CYP2D6 activity scores; Table S9: Mean relative deviation (MRD) values of DGI plasma concentration predictions; Table S10: Mean relative deviation (MRD) values of DD(G)I plasma concentration predictions; Table S11: Geometric Mean Fold Error (GMFE) of AUClast and Cmax DGI Predictions; Table S12: Geometric Mean Fold Error (GMFE) of DGI AUC_{last} and C_{max} ratio; Table S13: Geometric Mean Fold Error (GMFE) of AUC_{last} and C_{max} DD(G)I Predictions; Table S14: Geometric Mean Fold Error (GMFE) of DD(G)I AUC_{last} and C_{max} ratios. References [50–80] are cited in the Supplementary Materials.

Author Contributions: Conceptualization, C.K., L.K., R.K., T.E.M., M.S. and T.L.; Data curation, C.K.; Formal analysis, C.K., S.R. and D.S.; Funding acquisition, M.S. and T.L.; Investigation, C.K., L.K., B.G., P.K., S.I., R.K., E.S. and T.E.M.; Methodology, C.K., L.K., S.R., D.S., B.G., P.K., E.S. and T.E.M.; Project administration, T.E.M., M.S. and T.L.; Resources, M.S. and T.L.; Software, C.K. and D.S.; Supervision, T.E.M., M.S. and T.L.; Validation, C.K., L.K., D.S., T.E.M., M.S. and T.L.; Visualization, C.K. and L.K.; Writing—original draft, C.K. and T.L.; Writing—review and editing, C.K., L.K., S.R., D.S., B.G., P.K., S.I., R.K., E.S., T.E.M., M.S. and T.L. All authors have read and agreed to the published version of the manuscript.

Funding: This research was funded by the Robert Bosch Stiftung, Stuttgart, Germany, the European Commission Horizon 2020 UPGx grant 668353 and the German Federal Ministry of Education and Research (BMBF) grant 031L0188D "GUIDE-IBD".

Institutional Review Board Statement: The pharmacokinetic panel study (EudraCT-Nr.: 2009-014531-20, ClinicalTrails.gov: NCT01289756) was conducted in accordance with the Declaration of Helsinki, and approved by the Ethics Committee of the University of Tübingen (408/2009AMG1) and the German Federal Institute for Drugs and Medical Devices (BfArM: 4035694).

Informed Consent Statement: Informed consent was obtained from all subjects involved in the study.

Data Availability Statement: The developed PBPK model will be made publicly available (http://models.clinicalpharmacy.me/).

Conflicts of Interest: The authors declare no conflict of interest.

References

1. Legro, R.S.; Barnhart, H.X.; Schlaff, W.D.; Carr, B.R.; Diamond, M.P.; Carson, S.A.; Steinkampf, M.P.; Coutifaris, C.; McGovern, P.G.; Cataldo, N.A.; et al. Clomiphene, metformin, or both for infertility in the polycystic ovary syndrome. *N. Engl. J. Med.* **2007**, *356*, 551–566. [CrossRef] [PubMed]
2. Deswal, R.; Narwal, V.; Dang, A.; Pundir, C.S. The prevalence of polycystic ovary syndrome: A brief systematic review. *J. Hum. Reprod. Sci.* **2022**, *13*, 261–271. [CrossRef]
3. Jungheim, E.S.; Odibo, A.O. Fertility treatment in women with polycystic ovary syndrome: A decision analysis of different oral ovulation induction agents. *Fertil. Steril.* **2010**, *94*, 2659–2664. [CrossRef] [PubMed]
4. European Medicines Agency (2018) Assessment Report EnCyzix. Available online: https://www.ema.europa.eu/en/documents/assessment-report/encyzix-epar-public-assessment-report_en.pdf (accessed on 12 August 2021).
5. Mürdter, T.E.; Kerb, R.; Turpeinen, M.; Schroth, W.; Ganchev, B.; Böhmer, G.M.; Igel, S.; Schaeffeler, E.; Zanger, U.; Brauch, H.; et al. Genetic polymorphism of cytochrome p450 2D6 determines oestrogen receptor activity of the major infertility drug clomiphene via its active metabolites. *Hum. Mol. Genet.* **2012**, *21*, 1145–1154. [CrossRef] [PubMed]
6. Kröner, P. Hydroxylierte Metaboliten des Clomifens: In vitro und in vivo Untersuchungen zur Bildung, Aktivität und Konjugation. Ph.D. Thesis, Eberhard-Karls-University Tübingen, Tübingen, Germany, 2018.
7. Dickey, R.P.; Holtkamp, D.E. Development, pharmacology and clinical experience with clomiphene citrate. *Hum. Reprod. Update* **1996**, *2*, 483–506. [CrossRef]
8. Garg, A.; Singh, B.; Sharma, R.; Singh, A.; Kumar, A. Selective Estrogen Receptor Modulators (SERMs): Mechanistic insights against microbial infections. *Curr. Mol. Med.* **2019**, *20*, 102–115. [CrossRef]
9. Garg, A.; Singh, A.; Kumar, A. Selective estrogen receptor modulators against Gram-positive and Gram-negative bacteria: An experimental study. *Future Microbiol.* **2021**, *16*, 987–1001. [CrossRef]
10. Homburg, R. Clomiphene citrate–end of an era? A mini-review. *Hum. Reprod.* **2005**, *20*, 2043–2051. [CrossRef]
11. Rostami-Hodjegan, A.; Lennard, M.S.; Tucker, G.T.; Ledger, W.L. Monitoring plasma concentrations to individualize treatment with clomiphene citrate. *Fertil. Steril.* **2004**, *81*, 1187–1193. [CrossRef]
12. Saha, L.; Kaur, S.; Saha, P.K. Pharmacotherapy of polycystic ovary syndrome—An update. *Fundam. Clin. Pharmacol.* **2012**, *26*, 54–62. [CrossRef]
13. Kröner, P.; Heinkele, G.; Kerb, R.; Igel, S.; Schwab, M.; Mürdter, T.E. Stereoselective quantification of phase 1 and 2 metabolites of clomiphene in human plasma and urine. *Talanta* **2021**, *221*, 121658. [CrossRef]
14. Ji, M.; Kim, K.-R.; Lee, W.; Choe, W.; Chun, S.; Min, W.-K. Genetic polymorphism of CYP2D6 and clomiphene concentrations in infertile patients with ovulatory dysfunction treated with clomiphene citrate. *J. Korean Med. Sci.* **2016**, *31*, 310–314. [CrossRef] [PubMed]
15. Fuhr, L.M.; Marok, F.Z.; Hanke, N.; Selzer, D.; Lehr, T. Pharmacokinetics of the CYP3A4 and CYP2B6 inducer carbamazepine and its drug-drug interaction potential: A physiologically based pharmacokinetic modeling approach. *Pharmaceutics* **2021**, *13*, 270. [CrossRef] [PubMed]
16. Hanke, N.; Frechen, S.; Moj, D.; Britz, H.; Eissing, T.; Wendl, T.; Lehr, T. PBPK models for CYP3A4 and P-gp DDI prediction: A modeling network of rifampicin, itraconazole, clarithromycin, midazolam, alfentanil, and digoxin. *CPT Pharmacomet. Syst. Pharmacol.* **2018**, *7*, 647–659. [CrossRef] [PubMed]
17. Schroth, W.; Winter, S.; Mürdter, T.; Schaeffeler, E.; Eccles, D.; Eccles, B.; Chowbay, B.; Khor, C.C.; Tfayli, A.; Zgheib, N.K.; et al. Improved prediction of endoxifen metabolism by CYP2D6 genotype in breast cancer patients treated with tamoxifen. *Front. Pharmacol.* **2017**, *8*, 582. [CrossRef]
18. Caudle, K.E.; Sangkuhl, K.; Whirl-Carrillo, M.; Swen, J.J.; Haidar, C.E.; Klein, T.E.; Gammal, R.S.; Relling, M.V.; Scott, S.A.; Hertz, D.L.; et al. Standardizing CYP2D6 genotype to phenotype translation: Consensus recommendations from the clinical pharmacogenetics implementation consortium and dutch pharmacogenetics working group. *Clin. Transl. Sci.* **2020**, *13*, 116–124. [CrossRef]

19. FDA Drug Development and Drug Interactions. Table of Substrates, Inhibitors and Inducers. Available online: https://www.fda.gov/drugs/drug-interactions-labeling/drug-development-and-drug-interactions-table-substrates-inhibitors-and-inducers (accessed on 13 January 2022).
20. Ganchev, B.; Heinkele, G.; Kerb, R.; Schwab, M.; Mürdter, T.E. Quantification of clomiphene metabolite isomers in human plasma by rapid-resolution liquid chromatography-electrospray ionization-tandem mass spectrometry. *Anal. Bioanal. Chem.* **2011**, *400*, 3429–3441. [CrossRef] [PubMed]
21. Mikkelson, T.J.; Kroboth, P.D.; Cameron, W.J.; Dittert, L.W.; Chungi, V.; Manberg, P.J. Single-dose pharmacokinetics of clomiphene citrate in normal volunteers **Supported by a grant from Serono Laboratories, Inc., Randolph, Massachusetts. *Fertil. Steril.* **1986**, *46*, 392–396. [CrossRef]
22. Ratiopharm GmbH Clomifen-ratiopharm®50 mg Tabletten (Study 1991). Available online: https://www.ratiopharm.de/produkte/details/praeparate/praeparatedaten/detail/pzn-3884844.html (accessed on 23 November 2021).
23. Wiehle, R.; Cunningham, G.R.; Pitteloud, N.; Wike, J.; Hsu, K.; Fontenot, G.K.; Rosner, M.; Dwyer, A.; Podolski, J. Testosterone restoration by enclomiphene citrate in men with secondary hypogonadism: Pharmacodynamics and pharmacokinetics. *BJU Int.* **2013**, *112*, 1188–1200. [CrossRef]
24. Miller, G.D.; Moore, C.; Nair, V.; Hill, B.; Willick, S.E.; Rogol, A.D.; Eichner, D. Hypothalamic-pituitary-testicular axis effects and urinary detection following clomiphene administration in males. *J. Clin. Endocrinol. Metab.* **2019**, *104*, 906–914. [CrossRef]
25. Lippert, J.; Burghaus, R.; Edginton, A.; Frechen, S.; Karlsson, M.; Kovar, A.; Lehr, T.; Milligan, P.; Nock, V.; Ramusovic, S.; et al. Open systems pharmacology community-an open access, open source, open science approach to modeling and simulation in pharmaceutical sciences. *CPT Pharmacomet. Syst. Pharmacol.* **2019**, *8*, 878–882. [CrossRef]
26. Wojtyniak, J.-G.; Britz, H.; Selzer, D.; Schwab, M.; Lehr, T. Data digitizing: Accurate and precise data extraction for quantitative systems pharmacology and physiologically-based pharmacokinetic modeling. *CPT Pharmacomet. Syst. Pharmacol.* **2020**, *9*, 322–331. [CrossRef] [PubMed]
27. R Core Team. *R: A Language and Environment for Statistical Computing*; R Foundation for Statistical Computing: Vienna, Austria, 2021.
28. Ganchev, B. Charakterisierung der Metabolischen Bioaktivierung des Clomifens unter Besonderer Berücksichtigung Genetischer Polymorphismen. Ph.D. Thesis, Eberhard Karls University Tübingen, Tübingen, Germany, 2014.
29. Obach, R.S.; Walsky, R.L.; Venkatakrishnan, K. Mechanism-based inactivation of human cytochrome p450 enzymes and the prediction of drug-drug interactions. *Drug Metab. Dispos.* **2007**, *35*, 246–255. [CrossRef] [PubMed]
30. Rüdesheim, S.; Selzer, D.; Mürdter, T.; Igel, S.; Kerb, R.; Schwab, M.; Lehr, T. Physiologically based pharmacokinetic modeling to describe the CYP2D6 activity score-dependent metabolism of paroxetine, atomoxetine and risperidone. *Pharmaceutics* **2022**, *14*, 1734. [CrossRef] [PubMed]
31. Open Systems Pharmacology Suite Community. Open Systems Pharmacology Suite Manual. Available online: https://raw.githubusercontent.com/Open-Systems-Pharmacology/OSPSuite.Documentation/master/OpenSystemsPharmacologySuite.pdf (accessed on 23 November 2021).
32. Guest, E.J.; Aarons, L.; Houston, J.B.; Rostami-Hodjegan, A.; Galetin, A. Critique of the two-fold measure of prediction success for ratios: Application for the assessment of drug-drug interactions. *Drug Metab. Dispos.* **2011**, *39*, 170–173. [CrossRef]
33. Les Laboratoires Servier Servier Medical Art. Available online: https://smart.servier.com/ (accessed on 12 August 2021).
34. Kousta, E.; White, D.M.; Franks, S. Modern use of clomiphene citrate in induction of ovulation. *Hum. Reprod. Update* **1997**, *3*, 359–365. [CrossRef]
35. Imani, B.; Eijkemans, M.J.C.; Te Velde, E.R.; Habbema, J.D.F.; Fauser, B.C.J.M. Predictors of patients remaining anovulatory during clomiphene citrate induction of ovulation in normogonadotropic oligoamenorrheic infertility. *J. Clin. Endocrinol. Metab.* **1998**, *83*, 2361–2365. [CrossRef]
36. Kim, M.-J.; Byeon, J.-Y.; Kim, Y.-H.; Kim, S.-H.; Lee, C.-M.; Jung, E.H.; Chae, W.K.; Lee, Y.J.; Jang, C.-G.; Lee, S.-Y.; et al. Effect of the CYP2D6*10 allele on the pharmacokinetics of clomiphene and its active metabolites. *Arch. Pharm. Res.* **2018**, *41*, 347–353. [CrossRef]
37. Ellakwa, H.E.; Sanad, Z.F.; Hamza, H.A.; Emara, M.A.; Elsayed, M.A. Predictors of patient responses to ovulation induction with clomiphene citrate in patients with polycystic ovary syndrome experiencing infertility. *Int. J. Gynaecol. Obstet.* **2016**, *133*, 59–63. [CrossRef]
38. Mahran, A.; Abdelmeged, A.; El-Adawy, A.R.; Eissa, M.K.; Shaw, R.W.; Amer, S.A. The predictive value of circulating anti-Müllerian hormone in women with polycystic ovarian syndrome receiving clomiphene citrate: A prospective observational study. *J. Clin. Endocrinol. Metab.* **2013**, *98*, 4170–4175. [CrossRef]
39. Amer, S.A.; Mahran, A.; Abdelmaged, A.; El-Adawy, A.R.; Eissa, M.K.; Shaw, R.W. The influence of circulating anti-Müllerian hormone on ovarian responsiveness to ovulation induction with gonadotrophins in women with polycystic ovarian syndrome: A pilot study. *Reprod. Biol. Endocrinol.* **2013**, *11*, 115. [CrossRef]
40. Ghobadi, C.; Gregory, A.; Crewe, H.K.; Rostami-Hodjegan, A.; Lennard, M.S. CYP2D6 is primarily responsible for the metabolism of clomiphene. *Drug Metab. Pharmacokinet.* **2008**, *23*, 101–105. [CrossRef] [PubMed]
41. Rüdesheim, S.; Selzer, D.; Fuhr, U.; Schwab, M.; Lehr, T. Physiologically-based pharmacokinetic modeling of dextromethorphan to investigate interindividual variability within CYP2D6 activity score groups. *CPT Pharmacomet. Syst. Pharmacol.* **2022**, *11*, 494–511. [CrossRef]

42. Gaedigk, A.; Dinh, J.C.; Jeong, H.; Prasad, B.; Leeder, J.S. Ten years' experience with the CYP2D6 activity score: A perspective on future investigations to improve clinical predictions for precision therapeutics. *J. Pers. Med.* **2018**, *8*, 15. [CrossRef] [PubMed]
43. Mazzarino, M.; Biava, M.; de la Torre, X.; Fiacco, I.; Botrè, F. Characterization of the biotransformation pathways of clomiphene, tamoxifen and toremifene as assessed by LC-MS/(MS) following in vitro and excretion studies. *Anal. Bioanal. Chem.* **2013**, *405*, 5467–5487. [CrossRef] [PubMed]
44. Hill, S.; Arutchelvam, V.; Quinton, R. Enclomiphene, an estrogen receptor antagonist for the treatment of testosterone deficiency in men. *IDrugs* **2009**, *12*, 109–119.
45. Szutu, M.; Morgan, D.J.; McLeish, M.; Phillipou, G.; Blackman, G.L.; Cox, L.W.; Dollman, W. Pharmacokinetics of intravenous clomiphene isomers. *Br. J. Clin. Pharmacol.* **1989**, *27*, 639–640. [CrossRef]
46. Mazzarino, M.; Fiacco, I.; de la Torre, X.; Botrè, F. A mass spectrometric approach for the study of the metabolism of clomiphene, tamoxifen and toremifene by liquid chromatography time-of-flight spectroscopy. *Eur. J. Mass Spectrom.* **2008**, *14*, 171–180. [CrossRef]
47. Lu, J.; He, G.; Wang, X.; Xu, Y.; Wu, Y.; Dong, Y.; He, Z.; Liu, X.; Bo, T.; Ouyang, G. Mass spectrometric identification and characterization of new clomiphene metabolites in human urine by liquid chromatography-quadrupole time-of-flight tandem mass spectrometry. *J. Chromatogr. A* **2012**, *1243*, 23–32. [CrossRef]
48. Sheiner, L.B. Learning versus confirming in clinical drug development. *Clin. Pharmacol. Ther.* **1997**, *61*, 275–291. [CrossRef]
49. Jones, H.; Rowland-Yeo, K. Basic concepts in physiologically based pharmacokinetic modeling in drug discovery and development. *CPT Pharmacomet. Syst. Pharmacol.* **2013**, *2*, 63. [CrossRef] [PubMed]
50. Van der Lee, M.; Allard, W.G.; Vossen, R.H.A.M.; Baak-Pablo, R.F.; Menafra, R.; Deiman, B.A.L.M.; Deenen, M.J.; Neven, P.; Johansson, I.; Gastaldello, S.; et al. Toward predicting CYP2D6-mediated variable drug response from CYP2D6 gene sequencing data. *Sci. Transl. Med.* **2021**, *13*, eabf3637. [CrossRef] [PubMed]
51. Valentin, J. Basic anatomical and physiological data for use in radiological protection: Reference values. A report of age- and gender-related differences in the anatomical and physiological characteristics of reference individuals. ICRP Publication 89. *Ann. ICRP.* **2002**, *32*, 5–265.
52. Open Systems Pharmacology Suite Community. PK-Sim®Ontogeny Database Documentation, Version 7.3. Available online: https://github.com/Open-Systems-Pharmacology/OSPSuite.Documentation/blob/master/PK-Sim%20Ontogeny%20Database%20Version%207.3.pdf (accessed on 25 March 2020).
53. National Center for Health Statistics Hyattsville. 20782 Third National Health and Nutrition Examination Survey, NHANES III (1988–1994). Available online: https://wwwn.cdc.gov/nchs/nhanes/nhanes3/default.aspx (accessed on 25 March 2020).
54. Willmann, S.; Höhn, K.; Edginton, A.; Sevestre, M.; Solodenko, J.; Weiss, W.; Lippert, J.; Schmitt, W. Development of a physiology-based whole-body population model for assessing the influence of individual variability on the pharmacokinetics of drugs. *J. Pharmacokinet. Pharmacodyn.* **2007**, *34*, 401–431. [CrossRef]
55. Rodrigues, A.D. Integrated cytochrome P450 reaction phenotyping. Attempting to bridge the gap between cDNA-expressed cytochromes P450 and native human liver microsomes. *Biochem. Pharmacol.* **1999**, *57*, 465–480. [CrossRef]
56. Nishimura, M.; Naito, S. Tissue-specific mRNA Expression Profiles of Human ATP-binding Cassette and Solute Carrier Transporter Superfamilies. *Drug Metab. Pharmacokinet.* **2005**, *20*, 452–477. [CrossRef]
57. Rowland Yeo, K.; Walsky, R.L.; Jamei, M.; Rostami-Hodjegan, A.; Tucker, G.T. Prediction of time-dependent CYP3A4 drug-drug interactions by physiologically based pharmacokinetic modelling: Impact of inactivation parameters and enzyme turnover. *Eur. J. Pharm. Sci.* **2011**, *43*, 160–173. [CrossRef]
58. Greenblatt, D.J.; von Moltke, L.L.; Harmatz, J.S.; Chen, G.; Weemhoff, J.L.; Jen, C.; Kelley, C.J.; LeDuc, B.W.; Zinny, M.A. Time course of recovery of cytochrome p450 3A function after single doses of grapefruit juice. *Clin. Pharmacol. Ther.* **2003**, *74*, 121–129. [CrossRef]
59. Tsamandouras, N.; Rostami-Hodjegan, A.; Aarons, L. Combining the 'bottom up' and 'top down' approaches in pharmacokinetic modelling: Fitting PBPK models to observed clinical data. *Br. J. Clin. Pharmacol.* **2015**, *79*, 48–55. [CrossRef]
60. Austin, R.P.; Barton, P.; Cockroft, S.L.; Wenlock, M.C.; Riley, R.J. The influence of nonspecific microsomal binding on apparent intrinsic clearance, and its prediction from physicochemical properties. *Drug Metab. Dispos.* **2002**, *30*, 1497–1503. [CrossRef]
61. Obach, R.S. Nonspecific binding to microsomes: Impact on scale-up of in vitro intrinsic clearance to hepatic clearance as assessed through examination of warfarin, imipramine, and propranolol. *Drug Metab. Dispos. Biol. Fate Chem.* **1997**, *25*, 1359–1369. [PubMed]
62. Watanabe, R.; Esaki, T.; Kawashima, H.; Natsume-Kitatani, Y.; Nagao, C.; Ohashi, R.; Mizuguchi, K. Predicting Fraction Unbound in Human Plasma from Chemical Structure: Improved Accuracy in the Low Value Ranges. *Mol. Pharm.* **2018**, *15*, 5302–5311. [CrossRef] [PubMed]
63. Siramshetty, V.B.; Grishagin, I.; Nguyễn, Đ.T.; Peryea, T.; Skovpen, Y.; Stroganov, O.; Katzel, D.; Sheils, T.; Jadhav, A.; Mathé, E.A.; et al. NCATS Inxight Drugs: A comprehensive and curated portal for translational research. *Nucleic Acids Res.* **2022**, *50*, D1307–D1316. [CrossRef] [PubMed]
64. Developed by ChemAxon (2009), Chemicalize Was Used for Prediction of (E)-Clomiphene Properties. Available online: https://chemicalize.com/ (accessed on 9 August 2021).
65. Das, P.; Prajapati, M.; Maity, A. Study of equilibrium solubility of Clomiphene Citrate as model compound by Saturation orbital shake flask method. *J. Pharm. Adv. Res.* **2020**, *3*, 843–847.

66. Smith, D.A.; Dalvie, D. Why do metabolites circulate? *Xenobiotica* **2012**, *42*, 107–126. [CrossRef] [PubMed]
67. Wishart, D.S.; Knox, C.; Guo, A.C.; Shrivastava, S.; Hassanali, M.; Stothard, P.; Chang, Z.; Woolsey, J. DrugBank: A comprehe sive resource for in silico drug discovery and exploration. *Nucleic Acids Res.* **2006**, *34*, D668–D672. [CrossRef]
68. Güngör, S.; Delgado-Charro, M.B.; Masini-Etévé, V.; Potts, R.O.; Guy, R.H. Transdermal flux predictions for selected selective oestrogen receptor modulators (SERMs): Comparison with experimental results. *J. Control. Release Off. J. Control. Release Soc.* **2013**, *172*, 601–606. [CrossRef]
69. Schmitt, W. General approach for the calculation of tissue to plasma partition coefficients. *Toxicol. Vitr. Int. J. Publ. Assoc. BIBRA* **2008**, *22*, 457–467. [CrossRef]
70. Kawai, R.; Lemaire, M.; Steimer, J.L.; Bruelisauer, A.; Niederberger, W.; Rowland, M. Physiologically based pharmacokinetic study on a cyclosporin derivative, SDZ IMM 125. *J. Pharmacokinet. Biopharm.* **1994**, *22*, 327–365. [CrossRef] [PubMed]
71. Developed by ChemAxon (2009), Chemicalize Was Used for Prediction of (E)-N-Desethylclomiphene Properties. Available online: https://chemicalize.com/ (accessed on 9 August 2021).
72. Kim, S.; Chen, J.; Cheng, T.; Gindulyte, A.; He, J.; He, S.; Li, Q.; Shoemaker, B.A.; Thiessen, P.A.; Yu, B.; et al. PubChem in 2021: New data content and improved web interfaces. *Nucleic Acids Res.* **2021**, *49*, D1388–D1395. [CrossRef]
73. Rodgers, T.; Leahy, D.; Rowland, M. Physiologically based pharmacokinetic modeling 1: Predicting the tissue distribution of moderate-to-strong bases. *J. Pharm. Sci.* **2005**, *94*, 1259–1276. [CrossRef] [PubMed]
74. Rodgers, T.; Rowland, M. Physiologically based pharmacokinetic modelling 2: Predicting the tissue distribution of acids, very weak bases, neutrals and zwitterions. *J. Pharm. Sci.* **2006**, *95*, 1238–1257. [CrossRef] [PubMed]
75. Developed by ChemAxon (2009), Chemicalize Was Used for Prediction of (E)-4-Hydroxyclomiphene Properties. Available online: https://chemicalize.com/ (accessed on 9 August 2021).
76. Berezhkovskiy, L.M. Volume of distribution at steady state for a linear pharmacokinetic system with peripheral elimination. *J. Pharm. Sci.* **2004**, *93*, 1628–1640. [CrossRef]
77. Developed by ChemAxon (2009), Chemicalize Was Used for Prediction of (E)-4-Hydroxy-N-desethylclomiphene Properties. Available online: https://chemicalize.com/ (accessed on 9 August 2021).
78. T'jollyn, H.; Snoeys, J.; Vermeulen, A.; Michelet, R.; Cuyckens, F.; Mannens, G.; Van Peer, A.; Annaert, P.; Allegaert, K.; Van Bocxlaer, J.; et al. Physiologically Based Pharmacokinetic Predictions of Tramadol Exposure Throughout Pediatric Life: An Analysis of the Different Clearance Contributors with Emphasis on CYP2D6 Maturation. *AAPS J.* **2015**, *17*, 1376–1387. [CrossRef]
79. United States Pharmacopeial Convention. United States Pharmacopeia and National Formulary (USP 29-NF 24). 2006, p. 553. Available online: http://www.pharmacopeia.cn/v29240/usp29nf24s0_m18490.html (accessed on 24 August 2021).
80. Beal, S.L. Ways to fit a PK model with some data below the quantification limit. *J. Pharmacokinet. Pharmacodyn.* **2001**, *28*, 481–504. [CrossRef]

4.5 PROJECT V: PHYSIOLOGICALLY BASED PHARMACOKINETIC MODELING OF QUINIDINE TO ESTABLISH A CYP3A4, P-GP AND CYP2D6 DRUG-DRUG-GENE INTERACTION NETWORK

Publication

The following original research article has been published in the peer-reviewed journal *CPT: Pharmacometrics & Systems Pharmacology*:

Feick, D.; Rüdesheim, S.; Marok, F. Z.; Selzer, D.; Loer, H. L. H.; Teutonico, D.; Frechen, S.; van der Lee, M.; Moes, D. J. A. R.; Swen, J. J.; Schwab, M.; Lehr, T. Physiologically-based pharmacokinetic modeling of quinidine to establish a CYP3A4, P-gp, and CYP2D6 drug-drug-gene interaction network. *CPT: pharmacometrics & systems pharmacology* **2023**, 1–14, DOI: 10.1002/psp4.12981.

Supplementary Material

The supplementary material to this publication can be accessed via this link.

Copyright

Author Contributions

Author contributions according to CRediT [6]:

Denise Feick	Conceptualization, Formal analysis, Investigation, Visualization, Writing–Original Draft, Writing–Review & Editing
Simeon Rüdesheim	Conceptualization, Formal analysis, Investigation, Visualization, Writing–Original Draft, Writing–Review & Editing
Fatima Zahra Marok	Formal analysis, Visualization, Writing–Original Draft, Writing–Review & Editing
Dominik Selzer	Conceptualization, Formal analysis, Visualization, Writing–Original Draft, Writing–Review & Editing
Helena Leonie Hanae Loer	Writing–Original Draft, Writing–Review & Editing
Donato Teutonico	Writing–Review & Editing
Sebastian Frechen	Writing–Review & Editing
Maaike van der Lee	Writing–Review & Editing
Dirk Jan A. R. Moes	Writing–Review & Editing
Jesse J. Swen	Writing–Review & Editing
Matthias Schwab	Writing–Review & Editing, Funding Acquisition
Thorsten Lehr	Conceptualization, Writing–Original Draft, Writing–Review & Editing, Funding Acquisition

Received: 12 December 2022 | Revised: 31 March 2023 | Accepted: 13 April 2023

DOI: 10.1002/psp4.12981

ARTICLE

Physiologically-based pharmacokinetic modeling of quinidine to establish a CYP3A4, P-gp, and CYP2D6 drug–drug–gene interaction network

Denise Feick[1] | **Simeon Rüdesheim**[1,2] | **Fatima Zahra Marok**[1] | **Dominik Selzer**[1] | **Helena Leonie Hanae Loer**[1] | **Donato Teutonico**[3] | **Sebastian Frechen**[4] | **Maaike van der Lee**[5] | **Dirk Jan A. R. Moes**[5] | **Jesse J. Swen**[5] | **Matthias Schwab**[2,6,7] | **Thorsten Lehr**[1]

[1]Clinical Pharmacy, Saarland University, Saarbrücken, Germany

[2]Dr. Margarete Fischer-Bosch-Institute of Clinical Pharmacology, Stuttgart, Germany

[3]Translational Medicine & Early Development, Sanofi-Aventis R&D, Chilly-Mazarin, France

[4]Bayer AG, Pharmaceuticals, Research & Development, Systems Pharmacology & Medicine, Leverkusen, Germany

[5]Department of Clinical Pharmacy & Toxicology, Leiden University Medical Center, Leiden, The Netherlands

[6]Departments of Clinical Pharmacology, Pharmacy and Biochemistry, University of Tübingen, Tübingen, Germany

[7]Cluster of Excellence iFIT (EXC2180) "Image-guided and Functionally Instructed Tumor Therapies", University of Tübingen, Tübingen, Germany

Correspondence
Thorsten Lehr, Clinical Pharmacy, Saarland University, Campus C5 3, 66123 Saarbrücken, Germany.
Email: thorsten.lehr@mx.uni-saarland.de

Abstract

The antiarrhythmic agent quinidine is a potent inhibitor of cytochrome P450 (CYP) 2D6 and P-glycoprotein (P-gp) and is therefore recommended for use in clinical drug–drug interaction (DDI) studies. However, as quinidine is also a substrate of CYP3A4 and P-gp, it is susceptible to DDIs involving these proteins. Physiologically-based pharmacokinetic (PBPK) modeling can help to mechanistically assess the absorption, distribution, metabolism, and excretion processes of a drug and has proven its usefulness in predicting even complex interaction scenarios. The objectives of the presented work were to develop a PBPK model of quinidine and to integrate the model into a comprehensive drug–drug(–gene) interaction (DD(G)I) network with a diverse set of CYP3A4 and P-gp perpetrators as well as CYP2D6 and P-gp victims. The quinidine parent-metabolite model including 3-hydroxyquinidine was developed using pharmacokinetic profiles from clinical studies after intravenous and oral administration covering a broad dosing range (0.1–600 mg). The model covers efflux transport via P-gp and metabolic transformation to either 3-hydroxyquinidine or unspecified metabolites via CYP3A4. The 3-hydroxyquinidine model includes further metabolism by CYP3A4 as well as an unspecific hepatic clearance. Model performance was assessed graphically and quantitatively with greater than 90% of predicted pharmacokinetic parameters within two-fold of corresponding observed values. The model was successfully used to simulate various DD(G)I scenarios with greater than 90% of predicted DD(G)I pharmacokinetic parameter ratios within two-fold prediction success limits. The presented network will be provided to the research community and can be extended to include further perpetrators, victims, and targets, to support investigations of DD(G)Is.

Study Highlights

WHAT IS THE CURRENT KNOWLEDGE ON THE TOPIC?

Quinidine is an inhibitor of cytochrome P450 (CYP) 2D6 and P-gp as well as a substrate of CYP3A4 and P-gp. It is recommended for use in clinical drug–drug interaction studies.

WHAT QUESTION DID THIS STUDY ADDRESS?

Quinidine pharmacokinetics were extensively studied applying physiologically-based pharmacokinetic (PBPK) modeling. Furthermore, its interaction potential was assessed within a comprehensive CYP2D6-CYP3A4-P-gp drug–drug–gene interaction (DDGI) network, involving quinidine as both perpetrator and victim drug.

WHAT DOES THIS STUDY ADD TO OUR KNOWLEDGE?

The in vivo interaction potential of quinidine could be accurately modeled, emphasizing the potential of the PBPK approach to investigate even complex DDGI scenarios.

HOW MIGHT THIS CHANGE DRUG DISCOVERY, DEVELOPMENT AND/OR THERAPEUTICS?

This work highlights the evaluation of PBPK models in the context of a complex interaction network. The quinidine model can assist in future investigations on CYP2D6-CYP3A4-P-gp DDGIs during model-informed drug development.

INTRODUCTION

Cytochrome P450 (CYP) 2D6 is thought to be involved in the metabolism of about 20–25% of drugs and exhibits a highly polymorphic expression.[1] Consequently, CYP2D6 drug–gene interactions (DGIs) adversely affecting drug pharmacology frequently occur in clinical practice. Additionally, the concomitant administration of drugs can also modulate CYP2D6 metabolism, potentially resulting in drug–drug–gene interactions (DDGIs) which may further increase the risk of adverse drug reactions (ADRs).[2] Here, drug-induced CYP2D6 phenoconversion (i.e., the conversion from normal to poor metabolizer phenotypes due to the co-administration of strong inhibitors), has been described in the literature with varying magnitudes of interaction effects in different CYP2D6 phenotypes.[3]

Quinidine is a class 1A anti-arrhythmic drug and acts by blocking voltage-gated sodium channels. Due to its high risk for side effects and interaction potential as well as the availability of more advantageous anti-arrhythmic treatment options, the clinical relevance of quinidine has been in decline with steadily decreasing prescription rates over the last decades.[4] However, as a strong CYP2D6 inhibitor and inhibitor of P-glycoprotein (P-gp), quinidine is still used in clinical drug–drug interaction (DDI) studies, as recommended by the US Food and Drug Administration (FDA).[5] Here, the investigation of these interactions can provide valuable insights into the involved absorption, distribution, metabolism, and excretion (ADME) processes of concomitantly administered CYP2D6 and P-gp substrates.

Quinidine exhibits extensive hepatic and intestinal first-pass metabolism.[6] For this, CYP3A4 was found to be the most important enzyme in vitro and researchers have proposed to utilize quinidine 3-hydroxylation as a specific in vitro marker reaction for CYP3A4 activity.[7] Furthermore, quinidine has been identified as a substrate of P-gp in vitro,[5] making it susceptible to DDIs involving CYP3A4 and P-gp. Quinidine displays nonlinear pharmacokinetics that can be attributed to a saturation of intestinal CYP3A4 and P-gp.[8] Although quinidine shares structural similarities with many CYP2D6 substrates, the contribution of CYP2D6 to the metabolism of quinidine is negligible.[7] However, due to its high affinity to the metabolic site of CYP2D6, quinidine is a potent competitive inhibitor of CYP2D6.[9] Its metabolites have been found to contribute to the inhibition of CYP2D6.[10]

Several DDGI studies have been published investigating the effect of CYP2D6 polymorphisms and quinidine administration on victim drug pharmacokinetics (e.g., metoprolol[11]), resulting in considerable increases in drug exposure. Here, innovative tools are required to investigate DDGIs, as performing dedicated clinical trials routinely in drug development is infeasible due to combinatorical complexities and can put study subjects at a considerable risk of experiencing ADRs.[2] For this, physiologically-based pharmacokinetic (PBPK) modeling is a powerful

mechanistic approach to model the pharmacokinetics of a drug, taking an individual's physiological and genetic profile into account.[2] Thoroughly built and evaluated PBPK models can be valuable to describe the underlying ADME processes and investigate even complex DD(G)I scenarios.[2] Furthermore, these models can assist in generating and testing hypotheses regarding, for instance, (patho-) physiological changes affecting ADME processes where in vitro and in vivo data are incomplete or inconclusive.[12] Mechanistic DGI models have shown their usefulness in describing and predicting the effect of polymorphisms on drug pharmacokinetics (e.g., for the CYP2D6 substrates metoprolol and dextromethorphan), demonstrating how PBPK models can assist in understanding the underlying ADME-related processes and explain observed interindividual variability.[13,14] PBPK DD(G)I networks can have enormous potential in this area, as evaluated models can support simulating untested DD(G)I scenarios and support model-informed drug discovery and development.[15]

Due to the importance of quinidine as DDI probe drug for CYP2D6 and P-gp inhibition as well as CYP3A4 and P-gp substrate, the main objectives of this work were (i) to develop a comprehensive PBPK model of quinidine and its major metabolite 3-hydroxyquinidine and (ii) to predict complex quinidine DD(G)Is within a comprehensive PBPK interaction network involving CYP3A4, CYP2D6, and P-gp.

METHODS

Software

The development of the quinidine PBPK model, parameter optimizations, and sensitivity analysis, as well as simulation of different DD(G)I scenarios were performed with PK-Sim (version 11, Open Systems Pharmacology Suite, www.open-systems-pharmacology.org). Published plasma concentration-time profiles were digitized with Engauge Digitizer 10.12 (M. Mitchell, https://markummitchell.github.io/engauge-digitizer). Model evaluations (i.e., graph generation and calculation of pharmacokinetic parameters as well as statistics) were accomplished using the R programming language version 4.2.1 (The R Foundation for Statistical Computing, Vienna, Austria) and Rstudio 2022.07.0 (Rstudio).

Quinidine PBPK model building

PBPK model building was initialized by collecting physicochemical and ADME-related parameters of quinidine and 3-hydroxyquinidine from the literature. Additionally, studies reporting quinidine and 3-hydroxyquinidine plasma concentrations alongside subject information and administration protocols were collected. Studies were preferably included if performed in healthy volunteers and if concentration-time profiles were reported alongside unambiguous dosing and regimen information. Gathered concentration-time profiles were split into a model training (model development) and a test dataset (model evaluation). The model training dataset was assembled to (i) maximize the cardinality of the test dataset and to cover (ii) intravenous and oral administration, (iii) the whole dosing range of published studies, and (iv) single and multiple dose administration while preferring information-dense as well as (v) additional measurements of 3-hydroxyquinidine profiles. Virtual individuals ("mean individuals") were created based on the mean and mode of the reported study demographics if available. By selecting ethnicities according to the study cohorts from the PK-Sim database, varying organ volumes and perfusion rates were taken into account. Relevant enzymes and transporters were implemented according to literature reports and the PK-Sim expression database (see Tables S1–S3). Parameter optimizations were performed to identify suitable quantitative structure–activity relationship methods to calculate cellular permeabilities and partition coefficients. Furthermore, model parameter values that could not be informed from literature reports (e.g., quinidine intestinal permeability as well as relevant catalytic and transport rate constants) were optimized by fitting model simulations against all studies of the training dataset applying Monte Carlo optimization minimizing the least-squares objective function.[16]

Quinidine PBPK model evaluation

Model performance was evaluated graphically by comparison of population simulation predictions and observed quinidine and 3-hydroxyquinidine plasma concentration-time profiles. For this, virtual populations of 1000 individuals were generated, based on the study demographics listed in the respective publications, such as ethnic background as well as age and weight range. Additional variability regarding the expression of metabolizing enzymes and transporters was implemented according to the PK-Sim ontogeny database (see Table S1).

Furthermore, predicted plasma concentrations for mean individuals, area under the plasma concentration-time curve calculated between the first and last concentration measurement (AUC_{last}) and maximum plasma concentration (C_{max}) values were compared to their respective observed values in goodness-of-fit plots by

assessing the proportion of predictions within two-fold of observed concentration, AUC_{last} and C_{max} data. As quantitative measures to evaluate the model performance, mean relative deviations (MRDs) for all predicted concentration-time profiles and geometric mean fold errors (GMFEs) for all predicted AUC_{last}, C_{max}, apparent volume of distribution (V_d) and half-life values were calculated as previously described.[13,17] Predictions with MRDs and GMFEs less than two were considered successful.

To assess the influence of single parameter changes on model-simulated AUC, a local sensitivity analysis was performed using a parameter perturbation of 1000%. Parameters were considered sensitive if their sensitivity value was equal or greater than 0.5. More details on the conducted local sensitivity analysis are provided in Supplement S1 (Section S2.10).

DD(G)I modeling network building

To assess the performance of the newly developed quinidine model to predict various DD(G)I scenarios, the model was linked to previously published PBPK models of carbamazepine,[18] cimetidine,[12] fluvoxamine,[19] itraconazole,[20] R-/S-omeprazole,[21] rifampicin,[20] and R-/S-verapamil[22] (here, quinidine is acting as CYP3A4 and P-gp victim drug) as well as to models of dextromethorphan,[14] digoxin,[20] metoprolol,[13] mexiletine,[21] and paroxetine[23] (here, quinidine is acting as an inhibitor of CYP2D6 and P-gp). Moreover, CYP2D6 DDGI scenarios with dextromethorphan, metoprolol, and mexiletine were modeled by adjusting CYP2D6 activity related to the phenotype (normal and poor metabolizers) according to previous modeling work.[13,14,21] For all simulated interactions, the quinidine inhibitory constant (K_i) values were kept constant over the whole range of CYP2D6 activity.

DD(G)I modeling network evaluation

DD(G)I model performances were evaluated by comparing victim drug population predictions with observed plasma concentrations alone and during perpetrator co-administration. Furthermore, predicted compared to observed DD(G)I pharmacokinetic parameter ratios (ratios between AUC_{last} or C_{max} during the DD(G)I and of the victim drug alone) were plotted in goodness-of-fit plots. Here, limits for the assessment of DD(G)I ratios were applied according to Guest et al.[24] including 20% variability. Additionally, GMFEs of DD(G)I AUC_{last} and C_{max} ratios were calculated.

RESULTS

Quinidine PBPK model

A comprehensive quinidine-3-hydroxyquinidine parent-metabolite whole-body PBPK model was built and evaluated using data from 22 clinical studies reporting a total of 43 plasma concentration-time profiles for quinidine. Additionally, two profiles of unbound quinidine and eight plasma concentration-time profiles of 3-hydroxyquinidine were included in the model datasets. In these studies, plasma concentration-time profiles were reported after single intravenous administration of 260.3–520.6 mg quinidine gluconate (corresponding to 162.2–324.4 mg quinidine base) and single or multiple oral administrations of 0.1–600 mg quinidine sulfate (corresponding to 0.08–497.2 mg quinidine base). The training dataset included 10 profiles of quinidine in plasma, two profiles of quinidine in urine, and five profiles of 3-hydroxyquinidine in plasma. Information about all utilized studies, including the demographics and implemented ethnicities of study subjects, is provided in Tables S4, S13, and S14. Efflux transport of quinidine via P-gp was incorporated and metabolism via CYP3A4 (saturable Michaelis–Menten kinetics) was implemented for the building of 3-hydroxyquinidine and other unspecific metabolites. The 3-hydroxyquinidine metabolism was modeled via CYP3A4 and an unspecific hepatic clearance process as a surrogate for further unspecified enzymes (both first-order kinetics). Renal excretion of both compounds was modeled as passive glomerular filtration. Additionally, active tubular secretion via P-gp transport was incorporated in the model for quinidine. For oral formulations (quinidine sulfate immediate release), a Weibull dissolution was incorporated. All relevant quinidine and 3-hydroxyquinidine drug-dependent parameters are listed in Table S5, information about the expression and localization of relevant proteins is provided in Tables S1–S3.

A selection of population predictions of quinidine and 3-hydroxyquinidine compared to their respective observed data after intravenous and oral administration is shown in Figure 1a–f. Semilogarithmic and linear plots of all modeled studies are shown in Figures S1–S14. The good descriptive and predictive model performance is displayed in goodness-of-fit plots (Figures 1g–i, S15, S16), where 94%, 100%, and 100% of quinidine training dataset, 90%, 97%, and 91% of quinidine test dataset, 79%, 100%, and 80% of 3-hydroxyquinidine training dataset and 89%, 100%, and 100% of 3-hydroxyquinidine test dataset predicted plasma concentrations, AUC_{last} and C_{max} values were within two-fold of the corresponding observed values, respectively. Moreover, nine of 10 quinidine training dataset, 30 of 33 quinidine test dataset, five of five 3-hydroxyquinidine

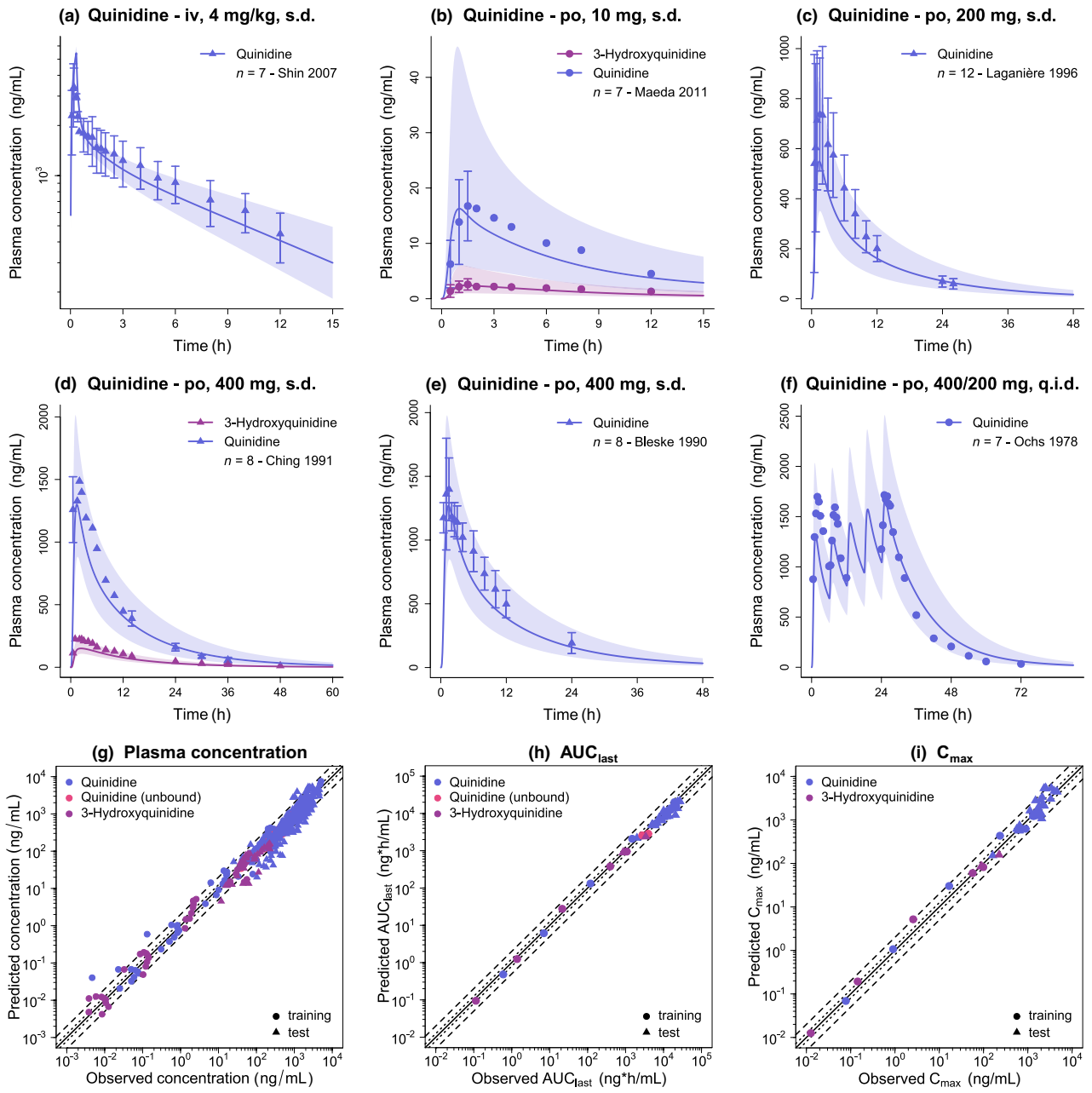

FIGURE 1 Quinidine physiologically-based pharmacokinetic modeling performance evaluation. (a–f) Predicted compared to observed plasma concentration-time profiles of quinidine and 3-hydroxyquinidine after (a) intravenous and (b–f) oral administration. Population geometric means are shown as lines, geometric standard deviations are shown as shaded areas, and observed data are shown as dots (training dataset) and triangles (test dataset) (±standard deviation, if reported).[8,25–29] (g–i) Goodness-of-fit plots comparing predicted and observed (g) plasma concentrations, (h) area under the plasma concentration-time curve calculated between first and last concentration measurement (AUC_{last}) and (i) maximum plasma concentration (C_{max}) values. The solid line represents the line of identity, whereas 1.25-fold and two-fold prediction limits are shown as dotted and dashed lines, respectively. Doses indicate (a) quinidine gluconate and (b–f) quinidine sulfate administration. Respective doses of quinidine base were calculated and incorporated in simulations. iv, intravenous; *n*, number of study participants; po, oral, q.i.d., four times daily; s.d., single dose.

training dataset, and three of three 3-hydroxyquinidine test dataset predicted plasma concentration profile MRDs were less than two. For quinidine, 10 of 10 (training dataset) and 32 of 33 (test dataset) AUC_{last} GMFEs, and eight of eight (training dataset) and 30 of 33 (test dataset) C_{max} GMFEs were below two. For 3-hydroxyquinidine, five of five (training dataset) and three of three (test dataset) AUC_{last} GMFEs, and four of five (training dataset) and

three of three (test dataset) C_{max} GMFEs values were within the two-fold threshold. For quinidine, all predicted V_d and half-life values are within twofold of observed values. The calculated MRD and GMFE values for all studies are listed and summarized in Tables S6–S9.

A local sensitivity analysis using a multiple dose simulation of 200 mg quinidine sulfate (protocol according to Ochs et al.[25]) revealed that the quinidine model is sensitive to the quinidine fraction unbound in plasma and lipophilicity (both implemented as fixed literature values). The 3-hydroxyquinidine model is sensitive to 3-hydroxyquinidine fraction unbound, the Michaelis–Menten (both fixed values from the literature) and catalytic-rate constants (optimized) describing the CYP3A4-dependent metabolism of quinidine to 3-hydroxyquinidine and the optimized unspecific hepatic clearance process. Parameters evaluated during sensitivity analysis are provided in Table S10, results of the local sensitivity analyses are visualized in Figures S17 and S18.

DD(G)I modeling network

The quinidine model was evaluated within a comprehensive CYP2D6-CYP3A4-P-gp DD(G)I network (Figure 2). Information about published perpetrator and victim models' relevant interaction constants and model parameters are provided in Tables S11 and S12. A total of nine quinidine and four 3-hydroxyquinidine profiles obtained from eight DDI studies were utilized to assess the quinidine-3-hydroxyquinidine model performance in DDI scenarios affected by CYP3A4 and P-gp perpetrator drugs. Here, one study described the carbamazepine-quinidine DDI, two studies the cimetidine-quinidine DDI, and one study each the fluvoxamine-quinidine, itraconazole-quinidine, and omeprazole-quinidine DDIs, one study the rifampicin-quinidine DDI, and one study the verapamil-quinidine DDI. Interaction parameters for the various modes of interaction (see Figure 2) were gathered from literature reports, if not already defined in the respective model files. To inform the relative contributions of CYP3A4 and P-gp to quinidine metabolism and transport during quinidine model building, data from the carbamazepine-quinidine DDI (i.e., the extent of 3-hydroxyquinidine formed) was included in the training dataset. Data from the remaining DDIs were used for the evaluation of model predictive performance.

Moreover, eight studies were utilized to model DD(G)I scenarios where quinidine and 3-hydroxyquinidine act as inhibitors of CYP2D6 and P-gp. One study was available to assess the effect of CYP2D6 inhibition via quinidine and 3-hydroxyquinidine for the quinidine-metoprolol interaction and one study on the effect of the quinidine-paroxetine-dextromethorphan interactions. Additionally, several DDGI studies in subpopulations with different CYP2D6 activities were available for the victim drugs dextromethorphan (two studies), metoprolol (one study), and mexiletine (one study). Finally, two studies reported data on the quinidine-digoxin DDI (P-gp inhibition). Multiple studies included plasma concentration-time profiles of multiple compounds, including parent victim drugs, respective enantiomers, and metabolites. For competitive inhibition of CYP2D6, K_i values of 0.017 μmol/L (quinidine[30]) and 2.30 μmol/L (3-hydroxyquinidine[10]) were incorporated from the literature as well as a K_i value of 0.10 μmol/L to describe competitive inhibition of P-gp by quinidine.[31] Information about all utilized studies covering perpetrator and victim drug regimens and subject demographics are provided in Tables S13 and S14.

Population predictions of victim plasma concentration-time profiles alone or with perpetrator co-administration compared to observed data demonstrated a good DD(G)I model performance (Figures 3 and 4). Semilogarithmic and linear plots of all studies are shown in Figures S19–S28.

Graphical comparisons of predicted and observed DD(G)I AUC_{last} and C_{max} ratios of all investigated DD(G)Is are shown in Figures 5, S29, and S30, revealing adequate model performance of quinidine either as a victim or perpetrator drug. For quinidine as CYP3A4 and P-gp victim, 12 of 13 and 12 of 13 of DDI AUC_{last} and C_{max} ratios were within two-fold of observed values and 12 of 13 and 11 of 13 within the prediction success limits proposed by Guest et al.[24] with mean GMFEs of 1.29 and 1.34, respectively. Overall, DD(G)Is with quinidine as a perpetrator of CYP2D6 and P-gp and the victim drugs dextromethorphan, digoxin, metoprolol, mexiletine, and paroxetine were accurately predicted with 15 of 17 DD(G)I AUC_{last} ratios and 13 of 15 DD(G)I C_{max} ratios within two-fold of the corresponding observed ratios. All AUC_{last} and C_{max} ratios grouped by the respective victim drugs and their metabolites are listed in Tables S15 and S16.

DISCUSSION

In this study, we present a newly developed whole-body parent-metabolite PBPK model of quinidine and its major metabolite 3-hydroxyquinidine. The good predictive performance simulating quinidine and 3-hydroxyquinidine plasma concentration-time profiles was evaluated by established graphical and quantitative measures. The model was further evaluated by simulating various modes of interactions in a comprehensive DD(G)I network. Here, the final model could be successfully linked with a diverse set of previously published CYP3A4 and P-gp perpetrator

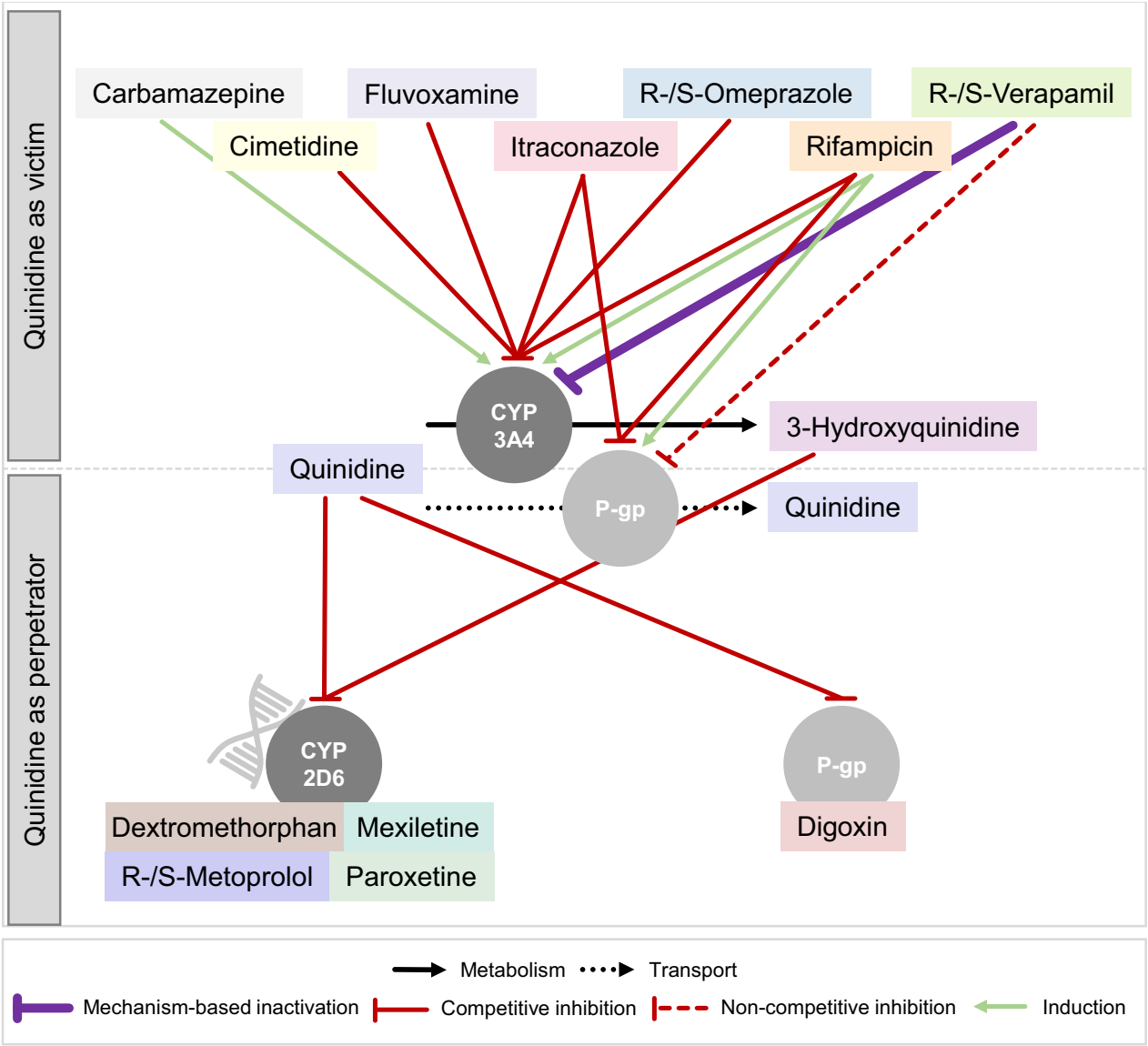

FIGURE 2 Quinidine drug–drug(–gene) interaction (DD(G)I) modeling network. (Upper panel) With quinidine acting as cytochrome P450 (CYP) 3A4 and P-glycoprotein (P-gp) victim drug, interactions with carbamazepine, cimetidine, fluvoxamine, itraconazole, R-/S-omeprazole, rifampicin, and R-/S-verapamil were modeled, taking different modes of interaction into account. (Lower panel) With quinidine acting as CYP2D6 and P-gp perpetrator drug, interactions were modeled with dextromethorphan, mexiletine, R-/S-metoprolol, and paroxetine in subjects with varying CYP2D6 activity (depending on data availability) and with digoxin (P-gp substrate).

models (quinidine acting as victim) as well as CYP2D6 and P-gp victim models (quinidine acting as perpetrator) to predict various DD(G)I scenarios.

Quinidine ADME processes include efflux via P-gp[5] (e.g., located at the intestinal barrier and, therefore, affecting oral bioavailability). Furthermore, quinidine is described as a substrate of CYP3A4 in vitro[7] and this enzyme can be attributed to the extensive first-pass metabolism of quinidine.[6] The reported quinidine average oral bioavailability of 70%[6] is in good agreement with our model simulations of oral bioavailabilities ranging from 37% (0.1 mg single dose) to 79% (600 mg single dose) and is in line with the proposed P-gp saturation as one cause for its nonlinear pharmacokinetics.[8] Total fractions of dose metabolized via CYP3A4 vary between very low (17%) and high doses (65%) of quinidine. This might be a result of varying fraction absorbed due to P-gp activity at the intestinal barrier and therefore a different impact of first-pass metabolism in the intestinal mucosa and in the liver. Another site of the body where P-gp contributes to quinidine pharmacokinetics is in tubule cells, where P-gp is responsible for the active tubular secretion of quinidine.

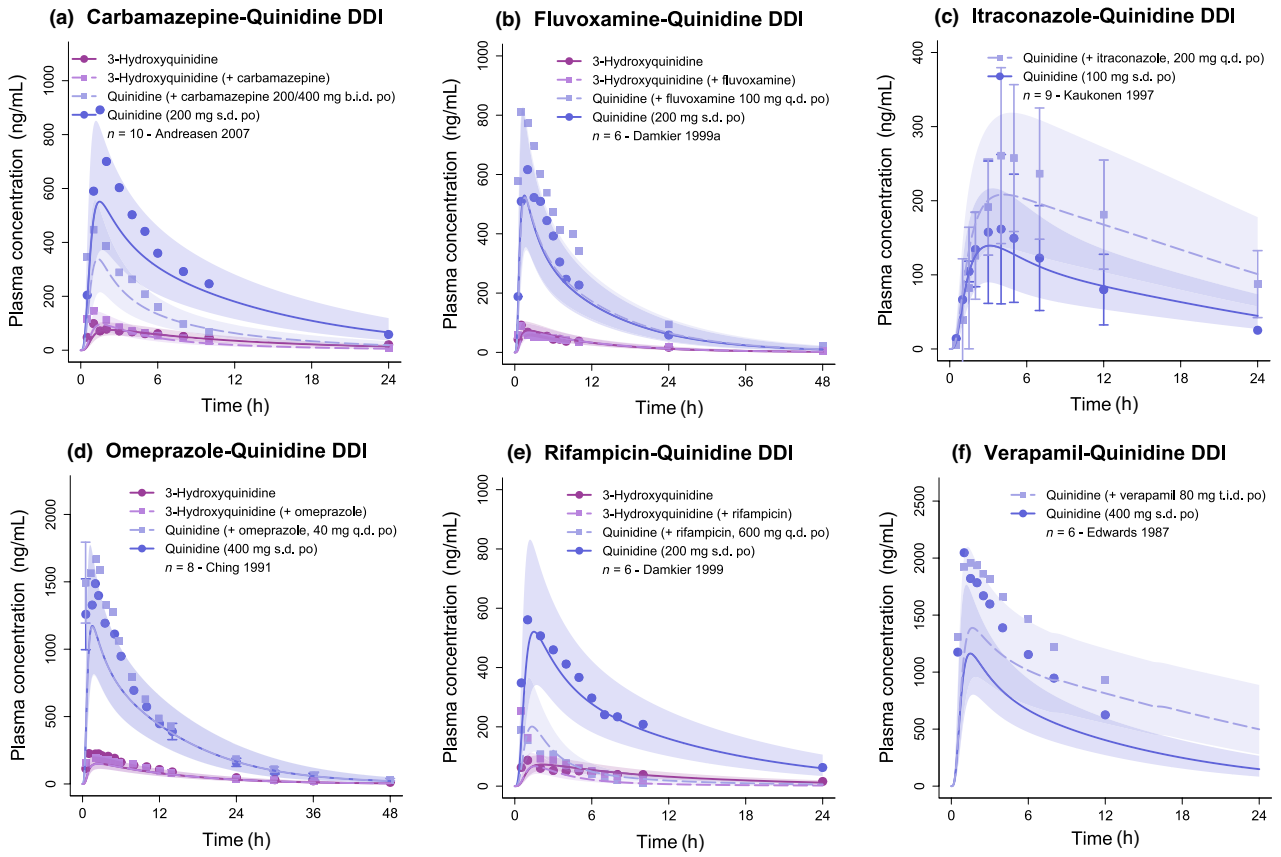

FIGURE 3 Modeled drug–drug interactions (DDIs) involving quinidine as cytochrome P450 (CYP) 3A4 and P-glycoprotein (P-gp) victim. (a–f) Predicted compared to observed plasma concentration-time profiles of quinidine and 3-hydroxyquinidine alone and after pretreatment with and/or concomitant administration of (a) carbamazepine, (b) fluvoxamine, (c) itraconazole, (d) R-/S-omeprazole, (e) rifampicin, and (f) R-/S-verapamil (low verapamil dose regimen). Population geometric means are shown as lines (solid: quinidine and 3-hydroxyquinidinde alone, dashed: quinidine and 3-hydroxyquinidinde during DDI), geometric standard deviations are shown as shaded areas and observed data are shown as dots (control) and squares (DDI) (±standard deviation, if reported).[26,32–36] Quinidine doses indicate quinidine sulfate administration. Respective doses of quinidine base were calculated and incorporated in simulations. b.i.d., twice daily; *n*, number of study participants; po, oral; q.d., once daily; s.d., single dose; t.i.d, three times daily.

Profiles of the amount of quinidine excreted in urine over time have been included in parameter optimizations to inform this process. However, urinary excretion of quinidine has been described to be pH dependent,[32] which might explain challenging the description and prediction of urine data.

Metabolism via CYP3A4 shows the largest contribution in vitro compared to other CYP enzymes.[7] However, in vivo metabolism via CYP3A4 was not easily assessable from literature reports, because competitive inhibitors of CYP3A4 in clinical DDI studies showed only a small effect on quinidine plasma concentrations.[26,33] Therefore, plasma concentration-time profiles of quinidine and 3-hydroxyquinidine during interaction with carbamazepine, a CYP3A4 inducer, were consulted to serve as a surrogate for lacking in vitro and in vivo data to estimate the relative contribution of CYP3A4 to quinidine metabolism. This approach has been successfully applied before, to estimate the previously unknown contribution of CYP3A4 and tubular secretion (also mediated via P-gp) in a PBPK model of trimethoprim.[17] Here, a DDI study with rifampicin, a CYP3A4 and P-gp competitive inhibitor and inducer, was included in the training dataset during the model building process, leading to a favorable description of trimethoprim concentrations in plasma and fractions excreted in urine.[17]

The co-administration of quinidine and various perpetrator and victim drugs covering different modes of interaction on several targets has been investigated in this work. To cover relevant interaction mechanisms and targets, the main metabolite of quinidine, 3-hydroxyquinidine, was included, (i) to adequately assess the impact of CYP3A4 perpetrator drugs and (ii) to incorporate its interaction potential, as inhibition of CYP2D6 has also been reported for the metabolite.[10]

Cimetidine is classified as a weak clinical inhibitor of CYP3A4 by the FDA.[5] In the model, inhibition of CYP3A4

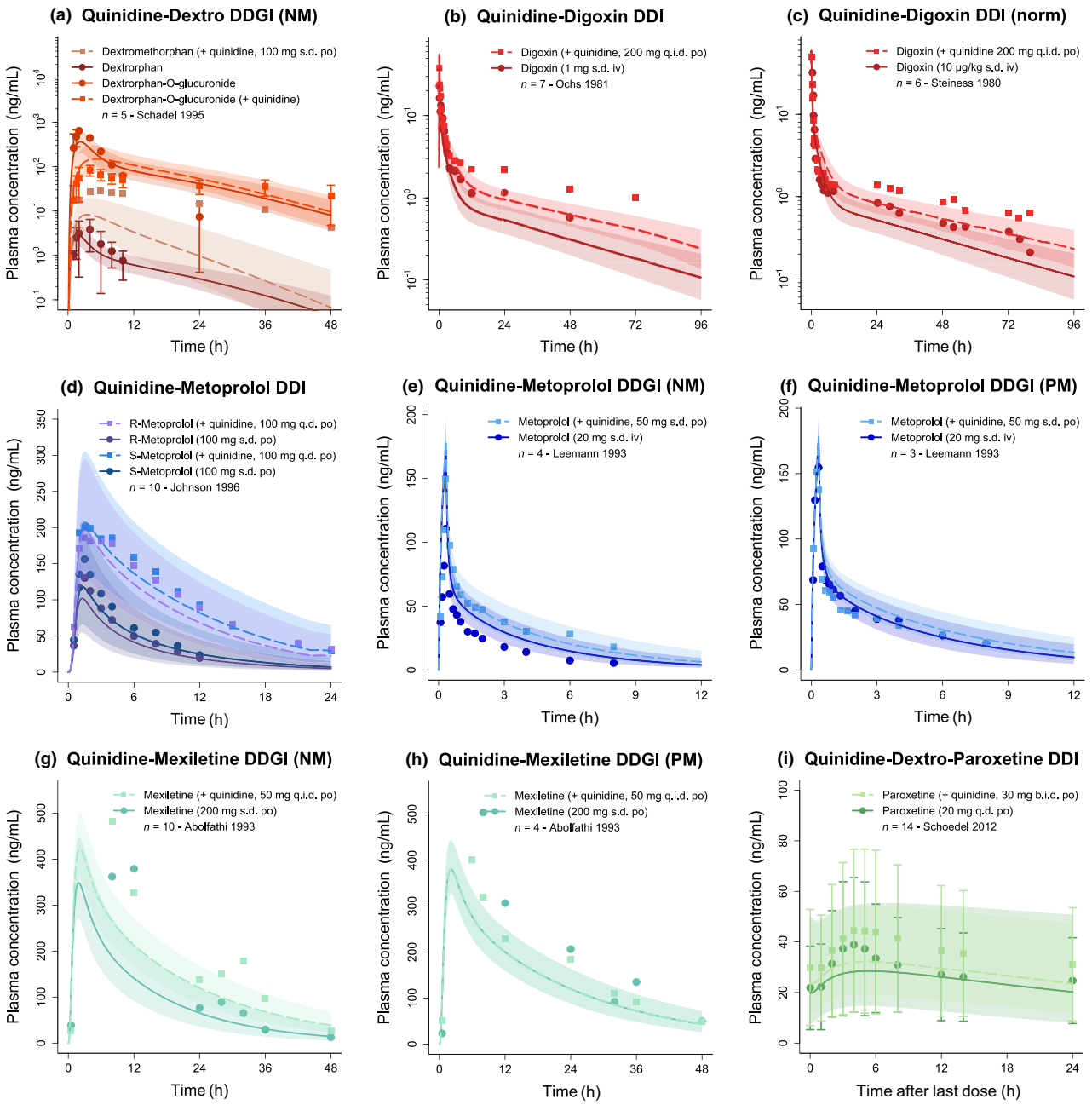

FIGURE 4 Modeled drug–drug(–gene) interactions (DD(G)Is) involving quinidine as cytochrome P450 (CYP) 2D6 and P-glycoprotein (P-gp) perpetrator. (a–i) Predicted compared to observed plasma concentration-time profiles of (a) dextromethorphan (+ metabolites) in CYP2D6 normal metabolizers (NMs), (b, c) digoxin, (d) R-/S-metoprolol, (e, f) racemic metoprolol (low quinidine dose regimen), (g, h) mexiletine, and (i) paroxetine (in combination with dextromethorphan) alone and after pretreatment with and/or concomitant administration of quinidine. Population geometric means are shown as lines (solid: victim alone, dashed: victim during drug-drug interaction [DDI]), geometric standard deviations are shown as shaded areas and observed data are shown as dots (control) and squares (DDI) (± standard deviation, if reported).[11,37–42] Quinidine doses indicate quinidine sulfate administration. Respective doses of quinidine base were calculated and incorporated in simulations. b.i.d., twice daily; iv, intravenous; *n*, number of study participants; norm, dose-normalized; PM, CYP2D6 poor metabolizer; po, oral; q.d., once daily; q.i.d., four times daily; s.d., single dose.

by cimetidine is incorporated, and the model has been evaluated in DDI predictions with the CYP3A4 index substrate midazolam.[5,12] Linking the cimetidine model to the newly developed quinidine model, no interaction effect could be observed via simulation. However, as a small interaction effect could be observed in clinical studies,[43,44]

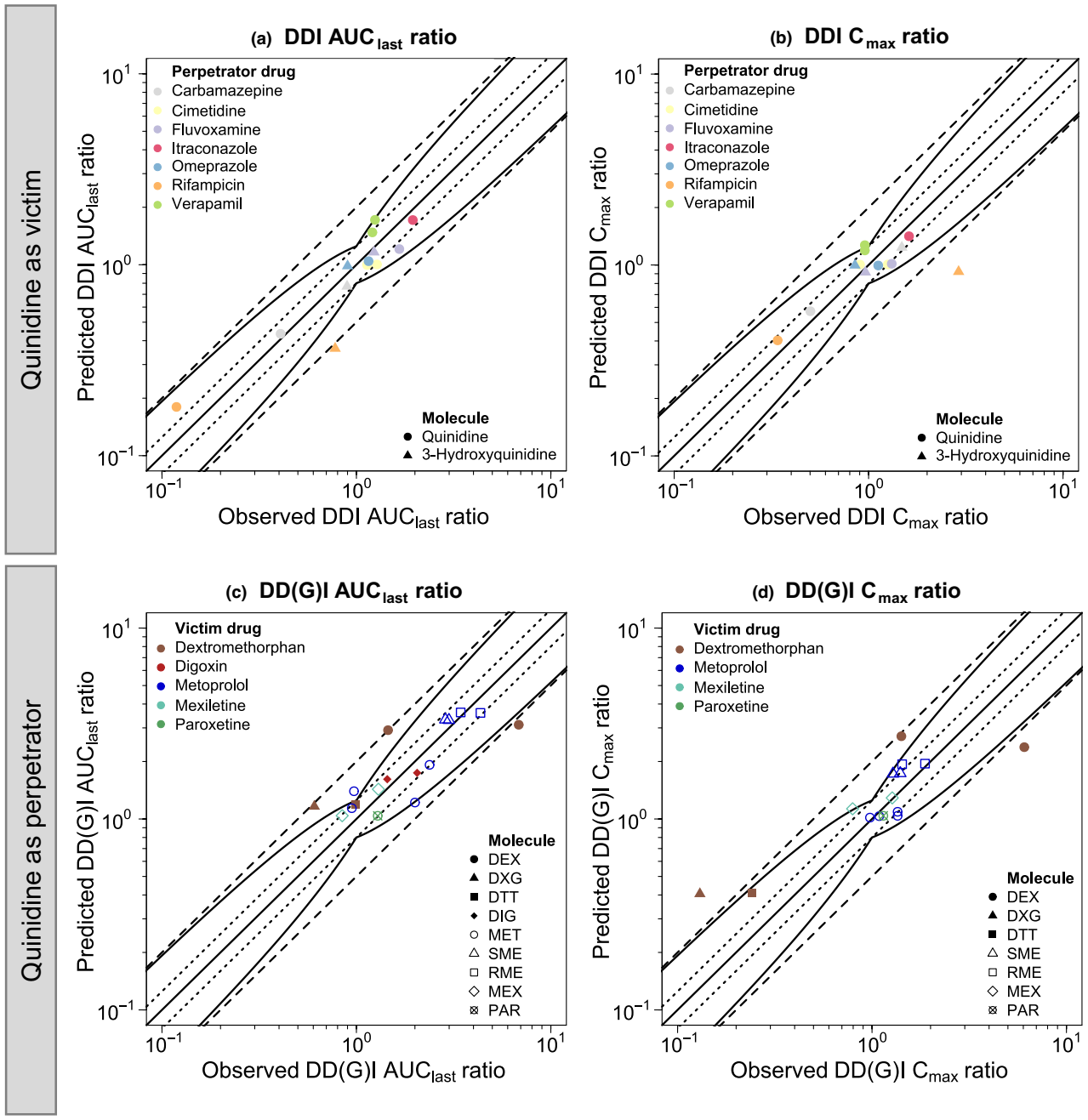

FIGURE 5 Quinidine drug–drug(–gene) interaction (DD(G)I) model performance evaluation. (a, b) For quinidine acting as a cytochrome P450 (CYP) 3A4 and P-glycoprotein (P-gp) victim, predicted drug–drug interaction (DDI) (a) area under the plasma concentration-time curve calculated between the first and last concentration measurement (AUC_{last}) and (b) maximum plasma concentration (C_{max}) ratios of quinidine and 3-hydroxyquinidine are plotted against their respective observed values after pretreatment with and/or concomitant administration of carbamazepine, cimetidine, fluvoxamine, itraconazole, R-/S-omeprazole, rifampicin, and R-/S-verapamil.[26,32–36,43,44] (c, d) For quinidine acting as a CYP2D6 and P-gp perpetrator, predicted DD(G)I (c) AUC_{last} and (d) C_{max} ratios of dextromethorphan (DEX), dextrorphan-O-glucuronide (DXG), total dextrorphan (DTT), digoxin (DIG), metoprolol (MET), S-metoprolol (SME), and R-metoprolol (RME), mexiletine (MEX) and paroxetine (PAR) are plotted against their respective observed values after pretreatment with and/or concomitant administration of quinidine.[11,37–42,45] The solid line represents the line of identity, whereas 1.25-fold and two-fold prediction limits are shown as dotted and dashed lines, respectively. Prediction success limits proposed by Guest et al.[24] are shown as curved lines (including 20% variability).

this effect might be attributed to interaction processes which could not be attributed to incorporated processes. For instance, cimetidine is a known inhibitor of several other proteins (e.g., transporters and other metabolic enzymes),[12] and further transport mechanisms have been discussed for quinidine but not incorporated due to limited information.

Quinidine has been described as P-gp substrate and inhibitior,[5] and mutual interactions with other drugs that can also be classified as P-gp substrate and inhibitor or inducer are plausible. This was considered for the modeled interaction between quinidine and verapamil by incorporating interaction parameters for both quinidine and verapamil. However, in the analyzed verapamil-quinidine interaction study by Edwards et al.,[34] only quinidine plasma concentrations were reported with no profiles of verapamil. Therefore, the effect of quinidine on verapamil pharmacokinetics could not be evaluated.

Regarding the rifampicin-quinidine DDI, which involves induction and inhibition of CYP3A4 (metabolism of quinidine and 3-hydroxyquinidine) and P-gp (transport of quinidine), plasma concentration-time profiles, DDI AUC_{last} and C_{max} ratios are well-predicted for the parent drug quinidine. However, for the metabolite, AUC_{last} and C_{max} are underpredicted during the DDI. This might be attributed to CYP3A4 involved in the formation as well as the metabolism of 3-hydroxyquinidine with an unknown extent of contribution for the latter process. In addition, other enzymes that might be involved in the metabolism could be the subject of induction by rifampicin. Additionally, P-gp may play a role in the active transport of 3-hydroxyquinidine. This could account for the underestimation of 3-hydroxyquinidine levels in urine, although this process was not included in the model due to insufficient data. Conducting in vitro studies to determine the extent of inducible CYP enzymes involved in 3-hydroxyquinidine metabolism, as well as the potential contribution of P-gp, may enhance our understanding of DDI mechanisms. This information could then be incorporated into the model as it becomes available.

The investigated DDIs with CYP2D6 victim drugs could be satisfactorily predicted with the model. For the modeled DDGIs with dextromethorphan (two studies)[37,45] and metoprolol (one study)[11] as victim drugs, CYP2D6-dependent metabolism was estimated from the control studies without an interaction partner to cover the extensive unexplained interindividual variability in CYP2D6 activity (Table S14). Subsequently, these adjustments were carried over to the DDI simulations. These studies solely provided CYP2D6 phenotypes, however, applying a finer-scaled activity score-based system to classify polymorphic CYP2D6 activity has been shown to lead to accurate DGI modeling results.[13,14,23] Here, no quinidine DDGI studies reporting CYP2D6 genotypes or activity scores could be obtained from published literature. Hence, the quinidine DDGI model performance of such scenarios remained unassessed, but the model could be extended in the future as far as such studies come available. For mexiletine, plasma-concentration-time profiles are slightly underpredicted, especially in CYP2D6 normal metabolizers. However, the profiles reported in the study by Abolfathi et al.[38] show representative profiles rather than mean profiles. Additionally, the variability in CYP2D6 activity and also other metabolic processes, such as CYP1A2-mediated metabolism, might contribute to interindividual variability of mexiletine pharmacokinetics. Of note, the model has a tendency to underpredict mexiletine clearance in normal metabolizers, as mentioned by the authors of the model publication,[21] likely resulting in a slight misprediction of mexiletine in both control and DDI scenarios. Nonetheless, DDI AUC_{last} and C_{max} ratios were within the prediction success limits proposed by Guest et al.,[24] indicating good performance of the quinidine model in CYP2D6 DDI scenarios.

Several PBPK model analyses have been published for quinidine. These focused on DDI predictions with quinidine as either a perpetrator drug with, for example, tramadol,[46] nifedipine and metoprolol[47] or as a victim drug, in DDI scenarios with rifampicin[48] or itraconazole and verapamil.[49] Furthermore, one article presented a PBPK/pharmacodynamic model of quinidine to investigate its effect on the length of QT-interval.[50] In contrast to previous work, our whole-body PBPK model covers the formation of the main quinidine metabolite, 3-hydroxyquinidine (mainly via CYP3A4) for correct interaction predictions considering CYP3A4 and CYP2D6 as well as the mechanistic implementation of ADME processes for both compounds (e.g., quinidine transport via P-gp). Furthermore, several DD(G)I scenarios could be successfully described and predicted within a comprehensive interaction network, evaluating quinidine as a perpetrator (CYP2D6 and P-gp) and as a victim drug (CYP3A4 and P-gp). Moreover, the presented quinidine PBPK model was developed using a variety of quinidine and 3-hydroxyquinidine concentration-time profiles covering two routes of administration (intravenous and oral administration), a large dosing range (0.1–600 mg) and both single and multiple administrations. The presented quinidine model focuses on quinidine sulfate formulations for oral administration, but implementation of further formulations (e.g., extended-release), could be performed with the model once required data (e.g., in vitro dissolution profiles), become available.

To conclude, this work presents a comprehensive quinidine whole-body PBPK model that describes and predicts quinidine and 3-hydroxyquinidine

pharmacokinetics administered alone or in combination with CYP3A4 and P-gp inhibitors or inducers. Moreover, the model has demonstrated its predictive performance in interaction scenarios with a diverse set of CYP2D6 and P-gp victim drugs—also in subjects with altered CYP2D6 activity due to genetic polymorphisms. The presented network can be extended in the future by integrating more interaction studies on further perpetrator and victim drugs. The PBPK model files are provided to the modeling community (http://models.clinicalpharmacy.me/) to assist model-informed drug development through further investigations on DD(G)Is involving quinidine.

AUTHOR CONTRIBUTIONS

All authors wrote the manuscript. D.F., S.R., D.S., and T.L. designed the research. D.F. and S.R. performed the research. D.F., S.R., F.Z.M., and D.S. analyzed the data.

FUNDING INFORMATION

This work is part of the Horizon 2020 INSPIRATION (Qualified Open Systems Pharmacology Modeling Network of Drug–Drug–Gene-Interactions) project. The INSPIRATION project (FKZ 031L0241) is supported by the German Federal Ministry of Education and Research under the framework of ERACoSysMed. M.S. was supported in parts by the Robert Bosch Stiftung Stuttgart, Germany, and the Deutsche Forschungsgemeinschaft (DFG) under Germany's Excellence Strategy-EXC 2180-390900677.

CONFLICT OF INTEREST STATEMENT

D.T. is an employee of Sanofi. D.T. uses Open Systems Pharmacology software, tools, or models in his professional role. D.T. and T.L. are members of the Open Systems Pharmacology Management Team. S.F. uses Open Systems Pharmacology software, tools, or models in his professional role. S.F. is a member of the Open Systems Pharmacology Sounding Board. All other authors declared no competing interest for this work.

ORCID

Simeon Rüdesheim https://orcid.org/0000-0002-5741-2511
Matthias Schwab https://orcid.org/0000-0002-9984-075X
Thorsten Lehr https://orcid.org/0000-0002-8372-1465

REFERENCES

1. Ingelman-Sundberg M. Genetic polymorphisms of cytochrome P450 2D6 (CYP2D6): clinical consequences, evolutionary aspects and functional diversity. *Pharmacogenomics J*. 2005;5:6-13.
2. Türk D, Fuhr LM, Marok FZ, et al. Novel models for the prediction of drug-gene interactions. *Expert Opin Drug Metab Toxicol*. 2021;17:1293-1310.
3. Storelli F, Matthey A, Lenglet S, Thomas A, Desmeules J, Daali Y. Impact of CYP2D6 functional allelic variations on phenoconversion and drug–drug interactions. *Clin Pharmacol Ther*. 2018;104:148-157.
4. Vitali Serdoz L, Rittger H, Furlanello F, Bastian D. Quinidine–a legacy within the modern era of antiarrhythmic therapy. *Pharmacol Res*. 2019;144:257-263.
5. U.S. Food and Drug Administration. Drug development and drug interactions: table of substrates, inhibitors and inducers. 2022 https://www.fda.gov/drugs/drug-interactions-labeling/drug-development-and-drug-interactions-table-substrates-inhibitors-and-inducers
6. Guentert TW, Holford NHG, Coafes PE, Upton RA, Riegelman S. Quinidine pharmacokinetics in man: choice of a disposition model and absolute bioavailability studies. *J Pharmacokinet Biopharm*. 1979;7:315-330.
7. Nielsen TL, Rasmussen BB, Flinois JP, Beaune P, Brosen K. In vitro metabolism of quinidine: the (3S)-3-hydroxylation of quinidine is a specific marker reaction for cytochrome P-4503A4 activity in human liver microsomes. *J Pharmacol Exp Ther*. 1999;289:31-37.
8. Maeda K, Takano J, Ikeda Y, et al. Nonlinear pharmacokinetics of Oral quinidine and verapamil in healthy subjects: a clinical microdosing study. *Clin Pharmacol Ther*. 2011;90:263-270.
9. McLaughlin LA, Paine MJI, Kemp CA, et al. Why is quinidine an inhibitor of cytochrome P450 2D6? The role of key active-site residues in quinidine binding. *J Biol Chem*. 2005;280:38617-38624.
10. Ching MS, Blake CL, Ghabrial H, et al. Potent inhibition of yeast-expressed CYP2D6 by dihydroquinidine, quinidine, and its metabolites. *Biochem Pharmacol*. 1995;50:833-837.
11. Leemann TD, Devi KP, Dayer P. Similar effect of oxidation deficiency (debrisoquine polymorphism) and quinidine on the apparent volume of distribution of (+/−)-metoprolol. *Eur J Clin Pharmacol*. 1993;45:65-71.
12. Hanke N, Türk D, Selzer D, et al. A comprehensive whole-body physiologically based pharmacokinetic drug-drug-gene interaction model of metformin and cimetidine in healthy adults and Renally impaired individuals. *Clin Pharmacokinet*. 2020;59:1419-1431.
13. Rüdesheim S, Wojtyniak JG, Selzer D, et al. Physiologically based pharmacokinetic modeling of metoprolol enantiomers and α-hydroxymetoprolol to describe CYP2D6 drug-gene interactions. *Pharmaceutics*. 2020;12:1200.
14. Rüdesheim S, Selzer D, Fuhr U, Schwab M, Lehr T. Physiologically-based pharmacokinetic modeling of dextromethorphan to investigate interindividual variability within CYP2D6 activity score groups. *CPT Pharmacometrics Syst Pharmacol*. 2022;11:494-511.
15. Wendl T, Frechen S, Gerisch M, Heinig R, Eissing T. Physiologically-based pharmacokinetic modeling to predict CYP3A4-mediated drug-drug interactions of finerenone. *CPT Pharmacometrics Syst Pharmacol*. 2022;11:199-211.
16. Woodruff TJ, Bois FY. Optimization issues in physiological toxicokinetic modeling: a case study with benzene. *Toxicol Lett*. 1993;69:181-196.

17. Türk D, Hanke N, Lehr T. A physiologically-based pharmacokinetic model of trimethoprim for MATE1, OCT1, OCT2, and CYP2C8 drug-drug-gene interaction predictions. *Pharmaceutics*. 2020;12:1074.
18. Fuhr LM, Marok FZ, Hanke N, Selzer D, Lehr T. Pharmacokinetics of the CYP3A4 and CYP2B6 inducer carbamazepine and its drug–drug interaction potential: a physiologically based pharmacokinetic modeling approach. *Pharmaceutics*. 2021;13:270.
19. Britz H, Hanke N, Volz AK, et al. Physiologically-based pharmacokinetic models for CYP1A2 drug-drug interaction prediction: a modeling network of fluvoxamine, theophylline, caffeine, rifampicin, and midazolam. *CPT Pharmacometrics Syst Pharmacol*. 2019;8:296-307.
20. Hanke N, Frechen S, Moj D, et al. PBPK models for CYP3A4 and P-gp DDI prediction: a modeling network of rifampicin, itraconazole, clarithromycin, midazolam, alfentanil, and digoxin. *CPT Pharmacometrics Syst Pharmacol*. 2018;7:647-659.
21. Kanacher T, Lindauer A, Mezzalana E, et al. A physiologically-based pharmacokinetic (PBPK) model network for the prediction of CYP1A2 and CYP2C19 drug-drug-gene interactions with fluvoxamine, omeprazole, S-mephenytoin, moclobemide, tizanidine, mexiletine, ethinylestradiol, and caffeine. *Pharmaceutics*. 2020;12:1-15.
22. Hanke N, Türk D, Selzer D, et al. A mechanistic, enantioselective, physiologically based pharmacokinetic model of verapamil and Norverapamil, built and evaluated for drug–drug interaction studies. *Pharmaceutics*. 2020;12:556.
23. Rüdesheim S, Selzer D, Mürdter T, et al. Physiologically based pharmacokinetic modeling to describe the CYP2D6 activity score-dependent metabolism of paroxetine, atomoxetine and risperidone. *Pharmaceutics*. 2022;14:1734.
24. Guest EJ, Aarons L, Houston JB, Rostami-Hodjegan A, Galetin A. Critique of the two-fold measure of prediction success for ratios: application for the assessment of drug-drug interactions. *Drug Metab Dispos*. 2011;39:170-173.
25. Ochs HR, Greenblatt DJ, Woo E, Franke K, Pfeifer HJ, Smith TW. Single and multiple dose pharmacokinetics of oral quinidine sulfate and gluconate. *Am J Cardiol*. 1978;41:770-777.
26. Ching MS, Elliott SL, Stead CK, et al. Quinidine single dose pharmacokinetics and pharmacodynamics are unaltered by omeprazole. *Aliment Pharmacol Ther*. 1991;5:523-531.
27. Shin J-G, Kang WK, Shon JH, et al. Possible interethnic differences in quinidine-induced QT prolongation between healthy Caucasian and Korean subjects. *Br J Clin Pharmacol*. 2007;63:206-215.
28. Laganière S, Davies RF, Carignan G, et al. Pharmacokinetic and pharmacodynamic interactions between diltiazem and quinidine. *Clin Pharmacol Ther*. 1996;60:255-264.
29. Bleske BE, Carver PL, Annesley TM, Bleske JRM, Morady F. The effect of ciprofloxacin on the pharmacokinetic and ECG parameters of quinidine. *J Clin Pharmacol*. 1990;30:911-915.
30. Moghadamnia AA, Rostami-Hodjegan A, Abdul-Manap R, Wright CE, Morice AH, Tucker GT. Physiologically based modelling of inhibition of metabolism and assessment of the relative potency of drug and metabolite: dextromethorphan vs. dextrorphan using quinidine inhibition. *Br J Clin Pharmacol*. 2003;56:57-67.
31. Lumen AA, Acharya P, Polli JW, Ayrton A, Ellens H, Bentz J. If the KI is defined by the free energy of binding to P-glycoprotein, which kinetic parameters define the IC50 for the Madin-Darby canine kidney II cell line overexpressing human multidrug resistance 1 confluent cell monolayer? *Drug Metab Dispos*. 2010;38:260-269.
32. Kaukonen KM, Olkkola KT, Neuvonen PJ. Itraconazole increases plasma concentrations of quinidine. *Clin Pharmacol Ther*. 1997;62:510-517.
33. Damkier P, Hansen LL, Brøsen K. Effect of fluvoxamine on the pharmacokinetics of quinidine. *Eur J Clin Pharmacol*. 1999;55:451-456.
34. Edwards DJ, Lavoie R, Beckman H, Blevins R, Rubenfire M. The effect of coadministration of verapamil on the pharmacokinetics and metabolism of quinidine. *Clin Pharmacol Ther*. 1987;41:68-73.
35. Andreasen A-H, Brøsen K, Damkier P. A comparative pharmacokinetic study in healthy volunteers of the effect of carbamazepine and oxcarbazepine on cyp3a4. *Epilepsia*. 2007;48:490-496.
36. Damkier P, Hansen LL, Brøsen K. Rifampicin treatment greatly increases the apparent oral clearance of quinidine. *Pharmacol Toxicol*. 1999;85:257-262.
37. Schoedel KA, Pope LE, Sellers EM. Randomized open-label drug-drug interaction trial of dextromethorphan/quinidine and paroxetine in healthy volunteers. *Clin Drug Investig*. 2012;32:157-169.
38. Abolfathi Z, Fiset C, Gilbert M, Moerike K, Bélanger PM, Turgeon J. Role of polymorphic debrisoquin 4-hydroxylase activity in the stereoselective disposition of mexiletine in humans. *J Pharmacol Exp Ther*. 1993;266:1196-1201.
39. Schadel M, Wu D, Otton SV, Kalow W, Sellers EM. Pharmacokinetics of dextromethorphan and metabolites in humans: influence of the CYP2D6 phenotype and quinidine inhibition. *J Clin Psychopharmacol*. 1995;15:263-269.
40. Ochs HR, Bodem G, Greenblatt DJ. Impairment of digoxin clearance by coadministration of quinidine. *J Clin Pharmacol*. 1981;21:396-400.
41. Steiness E, Waldorff S, Hansen PB, Egebald H, Buch J, Egeblad H. Reduction of digoxin-induced inotropism during quinidine administration. *Clin Pharmacol Ther*. 1980;27:791-795.
42. Johnson JA, Burlew BS. Metoprolol metabolism via cytochrome P4502D6 in ethnic populations. *Drug Metab Dispos*. 1996;24:350-355.
43. Kolb KW, Garnett WR, Small RE, Vetrovec GW, Kline BJ, Fox T. Effect of cimetidine on quinidine clearance. *Ther Drug Monit*. 1984;6:306-312.
44. Hardy BG, Schentag JJ. Lack of effect of cimetidine on the metabolism of quinidine: effect on renal clearance. *Int J Clin Pharmacol Ther Toxicol*. 1983;26:388-391.
45. Capon DA, Bochner F, Kerry N, Mikus G, Danz C, Somogyi AA. The influence of CYP2D6 polymorphism and quinidine on the disposition and antitussive effect of dextromethorphan in humans. *Clin Pharmacol Ther*. 1996;60:295-307.
46. Long T, Cristofoletti R, Cicali B, et al. Physiologically based pharmacokinetic modeling to assess the impact of CYP2D6-mediated drug-drug interactions on tramadol and O-desmethyltramadol exposures via allosteric and competitive inhibition. *J Clin Pharmacol*. 2022;62:76-86.
47. Marsousi N, Desmeules JA, Rudaz S, Daali Y. Prediction of drug-drug interactions using physiologically-based pharmacokinetic models of CYP450 modulators included in Simcyp software. *Biopharm Drug Dispos*. 2018;39:3-17.

48. Asaumi R, Nunoya K, Yamaura Y, Taskar KS, Sugiyama Y. Robust physiologically based pharmacokinetic model of rifampicin for predicting drug–drug interactions via P-glycoprotein induction and inhibition in the intestine, liver, and kidney. *CPT Pharmacometrics Syst Pharmacol*. 2022;11:919-933.
49. Yamazaki S, Evers R, De Zwart L. Physiologically-based pharmacokinetic modeling to evaluate in vitro-to-in vivo extrapolation for intestinal P-glycoprotein inhibition. *CPT Pharmacometrics Syst Pharmacol*. 2022;11:55-67.
50. Chetty M, Rose RH, Abduljalil K, et al. Applications of linking PBPK and PD models to predict the impact of genotypic variability, formulation differences, differences in target binding capacity and target site drug concentrations on drug responses and variability. *Front Pharmacol*. 2014;5:258.

SUPPORTING INFORMATION

Additional supporting information can be found online in the Supporting Information section at the end of this article.

How to cite this article: Feick D, Rüdesheim S, Marok FZ, et al. Physiologically-based pharmacokinetic modeling of quinidine to establish a CYP3A4, P-gp, and CYP2D6 drug–drug–gene interaction network. *CPT Pharmacometrics Syst Pharmacol*. 2023;00:1-14. doi:10.1002/psp4.12981

5 DISCUSSION AND FUTURE DIRECTIONS

This thesis outlines comprehensive approaches for the development of whole-body PBPK models to describe and predict the PK of various drugs in CYP2D6 DGI and DDGI scenarios. New PBPK models have been carefully developed and evaluated for the important CYP2D6 substrates metoprolol, dextromethorphan, paroxetine, atomoxetine, risperidone and *(E)*-clomiphene as well as for the strong CYP2D6 inhibitor quinidine. Subsequently, these models were employed in different applications, including: (i) developing metoprolol dose adaptations based on the CYP2D6 activity score, (ii) investigating the observed IIV in the CYP2D6-mediated metabolism of dextromethorphan for individual subjects sharing the same CYP2D6 activity score, (iii) simulating steady-state exposure of paroxetine, atomoxetine and risperidone in various DGI scenarios and (iv) predicting various DDGI scenarios involving the CYP2D6 and CYP3A4 substrate (*E*)-clomiphene as well as the CYP3A4 and P-gp substrate and CYP2D6 and P-gp inhibitor quinidine.

Furthermore, this thesis presents a blueprint for the development of PBPK models for CYP2D6 substrates and a novel approach to describing the CYP2D6 activity score-dependent metabolism in these models, based on established PBPK DGI models of CYP2D6 substrates. The models and applications presented demonstrate the vast potential of PBPK modeling when incorporating the CYP2D6 activity score system to model CYP2D6 substrates and complex DGI and DDGI scenarios.

5.1 CYP2D6 DRUG-GENE INTERACTIONS AND THE CYP2D6 ACTIVITY SCORE

CYP2D6 is arguably one of the most important pharmacogenes, as the CYP2D6 enzyme is involved in the metabolism of 15–25% of clinically used drugs. Simultaneously, its activity is highly susceptible to genetic variants in the *CYP2D6* gene [24]. With more than 140 *CYP2D6* alleles having been identified to date [32] and the resulting combinatorial complexity of CYP2D6 genotypes, CYP2D6 genotype-to-phenotype translation represents a challenging task [43]. Here, the CYP2D6 activity score system aims to provide an easy-to-use approach to translate *CYP2D6* genotype information into a semiquantitative measure of CYP2D6 phenotype [43]. As such, the activity score system has proven its raison d'être as it has since been adopted by major institutions and working groups concerned with the investigation of

Genotype-to-Phenotype Translation

PGx [45]. Moreover, the activity score system has been adapted for genotype-to-phenotype translations of other pharmacogenes such as the *dihydropyrimidine dehydrogenase (DPYD)* [152] and *CYP2C9* [153] genes, underlining the general usefulness of this approach. However, while phenotype categories inferred from genotype data are widely used in PGx guidelines and clinical practice, they may not grasp the full complexity of the relationship between CYP2D6 genotypes and phenotypes. This is highlighted by extensive inter-category variability in CYP2D6 activity and substantial overlap between the phenotype categories [42]. For instance, twin studies in monozygotic and dizygotic twins revealed that phenotypes inferred from the CYP2D6 activity score system were only able to predict 39% of the variability in metoprolol AUC even though 91% of variability could be attributed to genetic factors with only 9% of variability attributable to environmental factors [154]. While genetic factors outside of the *CYP2D6* gene [47] and rare, uncategorized variants of the *CYP2D6* gene [155, 156] may contribute to this variability, the categorization into phenotype categories and the resulting loss of information may explain a substantial proportion of this large variability [157, 158].

Variability in CYP2D6 Activity Within Phenotype Categories

Continuous Scales of CYP2D6 Activity

The activity score system has itself been suggested to provide a more fine-grained estimate of CYP2D6 activity compared to the more broad traditional phenotype categories. For instance, Caudle et al. proposed a *percent activity system* assigning a percentage of CYP2D6 activity based on an individuals CYP2D6 activity score [45]. Here, an activity score of zero corresponds to 0% CYP2D6 activity, an activity score of two (corresponding to the wild-type *1/*1 genotype) corresponds to 100% CYP2D6 activity whereas, for instance, an activity score of one could correspond to 40%–60% CYP2D6 activity [45]. Other studies have also expanded on the concept of the activity score system to assign activity values to CYP2D6 alleles instead of the fixed categories to better reflect differences in CYP2D6 activity between individual alleles within the same activity score category (i.e., 0, 0.25, 0.5, 1) and provide a continuous scale of CYP2D6 activity. Here, van der Lee et al. demonstrated for a cohort of 561 European patients treated with tamoxifen, that while the established CYP2D6 activity score system outperformed traditional phenotype categories in predicting endoxifen/desmethyltamoxifen metabolic ratios (R^2 = 0.66 vs. 0.54), the adjusted continuous activity scale presented by the authors was an even better predictor of endoxifen/desmethyltamoxifen metabolic ratios (R^2 = 0.79), and was able to explain 79% of IIV in endoxifen/desmethyltamoxifen metabolic ratios [158]. Similarly, other studies have suggested moving away from fixed activity score categories to allele-specific activity values to better reflect differences between alleles within the same activity score category [159–161].

The Future of the CYP2D6 Activity Score System

Hence, the activity score system itself is not only a useful tool for genotype-to-phenotype translation and may in itself be an accurate

predictor of CYP2D6 activity. The system may be further improved upon in the future by moving from phenotype or activity score categories to a the continuous scale of CYP2D6 activity and even include additional effects such as co-medication, other genetic and non-genetic factors as well as mixed effects observed for certain allele-substrate combinations [42, 46, 158].

5.2 CYP2D6 DRUG-GENE INTERACTION MODELING

DGI models provide useful tools to investigate the impact of genetic variants on the PK of drugs [20]. Most published CYP2D6 DGI models are developed based on traditional CYP2D6 phenotype categories [162–170]. This is likely due to the fact, that especially mechanistic implementations of CYP2D6 DGIs, i.e., adapting CYP2D6 substrate affinity (K_M) and activity (maximum reaction velocity (V_{max}) and/or enzyme abundance) based on genotype data, would require an extensive amount of experimental data to be collected and analyzed [20]. Consequently, CYP2D6 DGI models based on mechanistic implementations of genotype effects can typically only describe a small number of specific *CYP2D6* genotypes (e.g., *1/*1 and *10/*10) [171–173]. Here, DGI models based on the activity score system may provide a useful alternative, as they provide a more fine-grained estimate of CYP2D6 activity compared to the more broad traditional phenotype categories without requiring an extensive amount of experimental data [1, 174]. So far, the use of the activity score system in DGI modeling has been limited to a handful of studies in recent years [159, 175–177].

The CYP2D6 Activity Score System in DGI Modeling

The models of metoprolol and dextromethorphan presented in this thesis (projects I and II) highlight the potential of an activity score-dependent approach to assess CYP2D6 DGI effects in PBPK models, supplementing incomplete or missing experimental *in vitro* data by estimating CYP2D6 activity for various activity scores based on *in vivo* data [1, 2]. In accordance with the concept of continuous scales of CYP2D6 activity [45], metoprolol and dextromethorphan CYP2D6 k_{cat} values obtained from parameter optimizations revealed generally increasing CYP2D6 activity with increasing activity score and only slight differences in $k_{cat,\ rel}$ for the modeled activity score categories between the two drugs. For instance, estimated $k_{cat,\ rel}$ were 19% and 14% activity compared to the wild-type (activity score = 2) activity for activity score 0.5, 64% and 48% for activity score 1.25 and 72% and 63% for activity score 1.5 for metoprolol and dextromethorphan, respectively [3]. As a consequence, project III features a substrate-independent approach to model CYP2D6 DGI effects in PBPK models with the help of the activity score system by applying a continuous scale of CYP2D6 activity derived from the metoprolol and dextromethorphan CYP2D6 DGI models [3]. Here, model CYP2D6 k_{cat} values for paroxetine, atomoxetine and risperidone for variant activity scores were

Continuous and Substrate-Independent CYP2D6 Activity

calculated based on OLS regression analyses of CYP2D6 $k_{cat, rel}$ values for metoprolol and dextromethorphan and the CYP2D6 k_{cat} value for the wild-type (activity score of two) [3]. Overall, good model performance was achieved in various CYP2D6 DGI scenarios, highlighting the usefulness of the presented approach approximating CYP2D6 k_{cat} value estimates based on the generated empirical equation for the whole range of modeled activity scores.

Semi-Mechanistic Implementation of CYP2D6 Activity in PBPK Models

Alternatively, the CYP2D6 activity score-dependent metabolism parameters of a specific substrate may be informed by scaling CYP2D6 activity from *in vitro* data as highlighted in project IV. Here, IVSFs were scaled from optimized k_{cat} values for the wild-type (activity score = 2) to the activity score of interest individually for each of the four CYP2D6-dependent pathways of the (*E*)-clomiphene parent-metabolite model [4]. These IVSFs were informed from parameters obtained from *in vitro* experiments on the respective pathways [120].

Applications of DGI Models

DGI models can be applied in a variety of scenarios, ranging from the investigation of DGI effects, such as predicting drug exposure in relevant tissues, designing virtual clinical trials to investigate complex DDGI scenarios. Moreover, DGI models can be used to generate dose recommendations for patients with specific genetic variants [20]. Project I showcased this approach by calculating optimal doses for populations with specific CYP2D6 activity scores based on the developed metoprolol CYP2D6 DGI model. Interestingly, model dose recommendations were in good agreement with the dose recommendations provided by the DPWG for phenotype categories. For instance, the DPWG guideline recommends <25% and <50% of the normal dose for poor metabolizers and intermediate metabolizers, whereas the model calculated doses were 12.5% and 25–50% of the normal dose, respectively [1, 178]. Patients may benefit from model-derived dose adaptations based on CYP2D6 activity scores, as the activity score provides a more fine-grained estimate of CYP2D6 activity compared to the traditional phenotype categories [48]. Finally, the metoprolol PBPK model may be extended to incorporate the impact of other genetic variants, namely in the *ADRB1* and *ADRB2* genes, as variants in these pharmacogenes have been shown to significantly impact the PD of metoprolol [87, 88].

Metoprolol Dose Recommendations

5.3 PBPK DDGI MODELING IN MID3

Over the past two decades, PBPK modeling has moved from being predominately used in academic research to also being an established tool in the context of MID3 and is now widely used in the pharmaceutical industry and regulatory agencies [179]. With the introduction of the Prescription Drug User Fee Act Reauthorization (PDUFA) VI in 2018, MID3 has been codified as a routine part of the drug development process, with the FDA requiring the use of PK modeling for

many new drug application (NDA) submissions [180] and the EMA and other regulatory agencies following suit [181]. This is reflected in NDA submissions to the FDA, where in 2008, only one NDA submission included PBPK modeling, whereas this number increased to 27 in 2017 [182] and 293 between 2018–2021 [183]. The main application of PBPK models in MID3 is the prediction of DDI scenarios, making up for approximately 60% of PBPK modeling applications in NDAs between 2018–2019, followed by pediatric scaling (9%), modeling of drug absorption and food effects (9%), hepatic and renal impairment (8%), PGx (3%) and others (11%) [184]. Here, prospective DDI assessment presents a particularly useful application of PBPK models, where the impact of DDI scenarios on the PK of a drug can be extrapolated to untested DDI scenarios, consequently reducing the need for costly clinical trials [185, 186]. For instance, the FDA has recently waived the need for clinical trials assessing the impact of various CYP3A4 inhibitors on the PK of the CYP3A4 substrate finerenone, based on PBPK model simulations [187]. The underlying concept of DDI modeling in MID3 is based on the idea of DDI networks, where the impact of a drug on the PK of other drugs and vice versa is investigated in a network of PBPK models, enabled by the modular nature of PBPK models developed within the same framework [146, 149, 150, 188]. While DDI modeling is a well-established field in the realm of PBPK modeling and one of the most common applications of PBPK models, especially in the context of MID3 [134], real-world interactions between drugs are often more complex than the isolated interaction between two drugs in a controlled clinical trial setting [22]. Instead, they typically occur in fragile populations such as the elderly, often taking five or more drugs and possessing genetic variants in important pharmacogenes. Due to their mechanistic nature, PBPK DGI models are well suited for the investigation of such complex DDGI scenarios and modeling results can be scaled to such fragile populations [20]. Although PBPK DDGI networks have been developed for a variety of drugs and pharmacogenes [22, 188] and for even more complex DDGDI scenarios [148], their application in the context of MID3 is still in its infancy as compared to the application of PBPK models in the context of DDI assessment.

PBPK in Regulatory Submissions

DDI Modeling in NDA Submissions and DDI Networks

DDGI as Clinical Reality

Project IV of this thesis features a comprehensive PBPK DDGI model of (*E*)-clomiphene and its metabolites, investigating the simultaneous impact of CYP2D6 genetic variants and co-administration of the CYP2D6 inhibitor paroxetine and the CYP3A4 inhibitor clarithromycin on the PK of (*E*)-clomiphene and its metabolites [4]. Similarly, project V showcases a complex DDGI network developed around the CYP3A4 and P-gp substrate as well as CYP2D6 and P-gp inhibitor, quinidine [5]. This network incorporated a total of 13 drugs, either acting as CYP3A4 or P-gp perpetrator drugs or as substrates of P-gp and CYP2D6, including also DDGI scenarios where study participants possessed a

DDGI Networks

variant phenotype. Among other previously published models, the network also incorporated three PBPK models developed in projects I–III of this thesis, namely metoprolol, dextromethorphan and paroxetine. This aspect underlines the modular nature of thoroughly developed PBPK models, as they can be seamlessly integrated into complex DDGI networks. Moreover, the networks presented in projects IV and V may serve as an extension of the existing DDI networks [146, 149, 150, 188] and the openly accessible PBPK model library on GitHub, and may be used to investigate the impact of DDGI scenarios on the PK of drugs in the context of MID3 in the future.

5.4 PBPK MODELING IN PRECISION DOSING

While the idea of using computational approaches to individualize dosing has been around for several decades [189], the field has been gaining momentum in recent years. This is highlighted by the former US President Barack Obama calling for personalized medicine initiatives in his 2015 State of the Union address [190]. Increasing scientific efforts as well as steadily increasing computational power have enabled the idea of applying PK models to optimize treatment based on individual patient characteristics to improve treatment outcomes – a concept termed model-informed precision dosing (MIPD) [191]. MIPD is typically applied for the optimization of drug dosing regimens, especially for drugs with a narrow therapeutic window, and/or highly variable PK. Here, dose optimizations are often performed for an individual patient based on model covariates, i.e., patient characteristics, such as weight, sex or genetic make-up as well as a defined PK or PD target, in a probabilistic approach. Additionally, Bayesian forecasting can be integrated to update PK and PD model predictions after feeding in observed data (typically measurements of drug concentrations or PD markers) and subsequent identification of an individual parameter estimate from the posterior distribution [72], a concept also used in therapeutic drug monitoring (TDM) [192].

Model-Informed Precision Dosing

These MIPD approaches are typically based on PopPK models, due to the computationally demanding nature of PBPK model frameworks. However, PBPK models hold enormous potential in this field, due to the ability of modern PBPK modeling frameworks to seamlessly link multiple compound models to describe complex DDI and DDGI scenarios. Additionally, whole-body PBPK models typically allow for a more detailed representation of the individual in the model, so-called *virtual twins*, mechanistically reflecting interpatient differences based on patient characteristics as opposed to mostly empirical relationships established in PopPK models [193, 194].

Virtual Twins

Similarly, project II of this thesis showcased an approach, where virtual twins were created for 72 study participants of four different studies, where phenotyping cocktails containing dextromethorphan

were administered. Subsequently, individual PK parameter estimates for the highly variable CYP2D6 k_{cat} value were identified based on the individual dextromethorphan plasma concentrations. Resulting distributions of the CYP2D6 k_{cat} values highlighted the extensive IIV in CYP2D6 activity, even within activity score groups [2]. The presented modeling approach can serve as a blueprint for generating posterior distributions of highly variable PK parameters based on individual patient data and stratified by the patients' activity score, which can then be used to optimize dosing regimens for individual patients in MIPD or TDM applications.

Implementation of MIPD in Clinical Practice

While clinicians, regulators and pharmaceutical companies have recognized the need for MIPD, the implementation of such approaches in clinical practice is still in its infancy [192]. Clinical decision support systems (CDSS) are important tools to communicate the results and recommendations of MIPD approaches to prescribers. As stand-alone CDSS applications would require the prescriber to input all relevant patient characteristics manually, CDSS should ideally be directly integrated into electronic health records (EHRs) and electronic prescribing systems [191, 192]. Here, CDSS require careful evaluation prior to their clinical application in regards to their performance and safety, as they typically fall under medical device regulation [20, 192]. Finally, clinical evidence on the clinical benefits of MIPD approaches needs to be generated to support acceptance by prescribers – a task requiring interdisciplinary efforts between academic researchers, pharmaceutical companies, health care providers and regulators [192].

Clinical Decision Support Systems

6 CONCLUSION

CYP2D6 is a major drug-metabolizing enzyme in the human body and its activity is influenced by many factors, such as CYP2D6 DGIs and DDIs. Both personalized medicine and pharmaceutical drug development and discovery processes are increasingly dependent on PK modeling, as many complex interaction scenarios are impossible to assess in dedicated clinical trials. These scenarios include DDGIs, which can adversely affect the efficacy and safety of pharmacotherapy and are therefore of great interest to clinicians and researchers. The PBPK DGI models presented in this thesis have been developed to support the investigation of DDGIs and to predict the effect of DGIs on CYP2D6 activity. Here, the activity score has been observed to be a suitable measure to quantify the effect of DGIs on CYP2D6 activity and the resulting DGI models have been used (i) to generate dose recommendations for patients with different CYP2D6 activity scores, (ii) to analyze the extent and impact of IIV on CYP2D6 activity, (iii) to develop an empirical scale of CYP2D6 activity transferable to other CYP2D6 substrates, and (iv) to investigate the impact of CYP2D6 DDGIs on CYP2D6 activity. As such, the presented models may serve as promising tools to support investigations of DDIs and DDGIs during MID3 or to generate dose recommendations in the context of MIPD.

BIBLIOGRAPHY

1. Rüdesheim, S.; Wojtyniak, J.-G.; Selzer, D.; Hanke, N.; Mahfoud, F.; Schwab, M.; Lehr, T. Physiologically Based Pharmacokinetic Modeling of Metoprolol Enantiomers and α-Hydroxymetoprolol to Describe CYP2D6 Drug-Gene Interactions. *Pharmaceutics* **2020**, *12*, 1200, DOI: 10.3390/pharmaceutics12121200.
2. Rüdesheim, S.; Selzer, D.; Fuhr, U.; Schwab, M.; Lehr, T. Physiologically-based pharmacokinetic modeling of dextromethorphan to investigate interindividual variability within CYP2D6 activity score groups. *CPT: pharmacometrics & systems pharmacology* **2022**, *11*, 494–511, DOI: 10.1002/psp4.12776.
3. Rüdesheim, S.; Selzer, D.; Mürdter, T.; Igel, S.; Kerb, R.; Schwab, M.; Lehr, T. Physiologically Based Pharmacokinetic Modeling to Describe the CYP2D6 Activity Score-Dependent Metabolism of Paroxetine, Atomoxetine and Risperidone. *Pharmaceutics* **2022**, *2022*, 1734, DOI: 10.3390/pharmaceutics14081734.
4. Kovar, C.; Kovar, L.; Rüdesheim, S.; Selzer, D.; Ganchev, B.; Kröner, P.; Igel, S.; Kerb, R.; Schaeffeler, E.; Mürdter, T. E.; Schwab, M.; Lehr, T. Prediction of Drug–Drug–Gene Interaction Scenarios of (*E*)-Clomiphene and Its Metabolites Using Physiologically Based Pharmacokinetic Modeling. *Pharmaceutics* **2022**, *14*, 2604, DOI: 10.3390/pharmaceutics14122604.
5. Feick, D.; Rüdesheim, S.; Marok, F. Z.; Selzer, D.; Loer, H. L. H.; Teutonico, D.; Frechen, S.; van der Lee, M.; Moes, D. J. A. R.; Swen, J. J.; Schwab, M.; Lehr, T. Physiologically-based pharmacokinetic modeling of quinidine to establish a CYP3A4, P-gp, and CYP2D6 drug-drug-gene interaction network. *CPT: pharmacometrics & systems pharmacology* **2023**, 1–14, DOI: 10.1002/psp4.12981.
6. Brand, A.; Allen, L.; Altman, M.; Hlava, M.; Scott, J. Beyond authorship: attribution, contribution, collaboration, and credit. *Learned Publishing* **2015**, *28*, 151–155, DOI: 10.1087/20150211.
7. Les Laboratoires Servier. Servier Medical ART (SMART), https://smart.servier.com/ (accessed 10/03/2022).
8. Gonzalez, D.; Rao, G. G.; Bailey, S. C.; Brouwer, K. L.; Cao, Y.; Crona, D. J.; Kashuba, A. D.; Lee, C. R.; Morbitzer, K.; Patterson, J. H.; Wiltshire, T.; Easter, J.; Savage, S. W.; Powell, J. R. Precision Dosing: Public Health Need, Proposed Framework, and Anticipated Impact. *Clinical and Translational Science* **2017**, *10*, 443–454, DOI: 10.1111/cts.12490.

9. Marsousi, N.; Desmeules, J. A.; Rudaz, S.; Daali, Y. Usefulness of PBPK modeling in incorporation of clinical conditions in personalized medicine. *Journal of pharmaceutical sciences* **2017**, *106*, 2380–2391, DOI: 10.1016/j.xphs.2017.04.035.

10. Haycox, A.; Pirmohamed, M.; McLeod, C.; Houten, R.; Richards, S. Through a Glass Darkly: Economics and Personalised Medicine. *PharmacoEconomics* **2014**, *32*, 1055–1061, DOI: 10.1007/s40273-014-0190-6.

11. Lazarou, J.; Pomeranz, B. H.; Corey, P. N. Incidence of Adverse Drug Reactions in Hospitalized Patients. *JAMA* **1998**, *279*, 1200, DOI: 10.1001/jama.279.15.1200.

12. Miller, I.; Ashton-Chess, J.; Spolders, H.; Fert, V.; Ferrara, J.; Kroll, W.; Askaa, J.; Larcier, P.; Terry, P. F.; Bruinvels, A.; Huriez, A. Market access challenges in the EU for high medical value diagnostic tests. *Personalized Medicine* **2011**, *8*, 137–148, DOI: 10.2217/pme.11.2.

13. Formica, D.; Sultana, J.; Cutroneo, P.; Lucchesi, S.; Angelica, R.; Crisafulli, S.; Ingrasciotta, Y.; Salvo, F.; Spina, E.; Trifirò, G. The economic burden of preventable adverse drug reactions: a systematic review of observational studies. *Expert Opinion on Drug Safety* **2018**, *17*, 681–695, DOI: 10.1080/14740338.2018.1491547.

14. Kalow, W.; Tang, B. K.; Endrenyi, L. Hypothesis: comparisons of inter- and intra-individual variations can substitute for twin studies in drug research. *Pharmacogenetics* **1998**, *8*, 283–9, DOI: 10.1097/00008571-199808000-00001.

15. Collins, S. L.; Carr, D. F.; Pirmohamed, M. Advances in the Pharmacogenomics of Adverse Drug Reactions. *Drug Safety* **2016**, *39*, 15–27, DOI: 10.1007/s40264-015-0367-8.

16. Nebert, D. W. Pharmacogenetics and pharmacogenomics: why is this relevant to the clinical geneticist? *Clinical Genetics* **1999**, *56*, 247–258, DOI: 10.1034/j.1399-0004.1999.560401.x.

17. Swen, J.; Wilting, I.; de Goede, A.; Grandia, L.; Mulder, H.; Touw, D.; de Boer, A.; Conemans, J.; Egberts, T.; Klungel, O.; Koopmans, R.; van der Weide, J.; Wilffert, B.; Guchelaar, H.-J.; Deneer, V. Pharmacogenetics: From Bench to Byte. *Clinical Pharmacology & Therapeutics* **2008**, *83*, 781–787, DOI: 10.1038/sj.clpt.6100507.

18. Whirl-Carrillo, M.; Huddart, R.; Gong, L.; Sangkuhl, K.; Thorn, C. F.; Whaley, R.; Klein, T. E. An Evidence-Based Framework for Evaluating Pharmacogenomics Knowledge for Personalized Medicine. *Clinical Pharmacology & Therapeutics* **2021**, *110*, 563–572, DOI: 10.1002/cpt.2350.

19. Barbarino, J. M.; Whirl-Carrillo, M.; Altman, R. B.; Klein, T. E. PharmGKB: A worldwide resource for pharmacogenomic information. *WIREs Systems Biology and Medicine* **2018**, *10*, DOI: 10.1002/wsbm.1417.

20. Türk, D.; Fuhr, L. M.; Marok, F. Z.; Rüdesheim, S.; Kühn, A.; Selzer, D.; Schwab, M.; Lehr, T. Novel models for the prediction of drug–gene interactions. *Expert Opinion on Drug Metabolism & Toxicology* **2021**, *17*, 1293–1310, DOI: 10.1080/17425255.2021.1998455.

21. Emami Riedmaier, A.; Burt, H.; Abduljalil, K.; Neuhoff, S. More Power to OATP1B1: An Evaluation of Sample Size in Pharmacogenetic Studies Using a Rosuvastatin PBPK Model for Intestinal, Hepatic, and Renal Transporter-Mediated Clearances. *Journal of clinical pharmacology* **2016**, *56 Suppl 7*, S132–42, DOI: 10.1002/jcph.669.

22. Wojtyniak, J.-G.; Selzer, D.; Schwab, M.; Lehr, T. Physiologically Based Precision Dosing Approach for Drug-Drug-Gene Interactions: A Simvastatin Network Analysis. *Clinical Pharmacology & Therapeutics* **2021**, *109*, 201–211, DOI: 10.1002/cpt.2111.

23. Zanger, U. M.; Schwab, M. Cytochrome P450 enzymes in drug metabolism: Regulation of gene expression, enzyme activities, and impact of genetic variation. *Pharmacology & Therapeutics* **2013**, *138*, 103–141, DOI: 6.

24. Zanger, U. M.; Raimundo, S.; Eichelbaum, M. Cytochrome P450 2D6: overview and update on pharmacology, genetics, biochemistry. *Naunyn-Schmiedeberg's Archives of Pharmacology* **2004**, *369*, 23–37, DOI: 10.1007/s00210-003-0832-2.

25. Coutts, R. T. Polymorphism in the metabolism of drugs, including antidepressant drugs: comments on phenotyping. *Journal of psychiatry & neuroscience : JPN* **1994**, *19*, 30–44.

26. Islam, S. A.; Wolf, C. R.; Lennard, M. S.; Sternberg, M. J. A three-dimensional molecular template for substrates of human cytochrome P450 involved in debrisoquine 4-hydroxylation. *Carcinogenesis* **1991**, *12*, 2211–2219, DOI: 10.1093/carcin/12.12.2211.

27. Frank, D.; Jaehde, U.; Fuhr, U. Evaluation of probe drugs and pharmacokinetic metrics for CYP2D6 phenotyping. *European Journal of Clinical Pharmacology* **2007**, *63*, 321–333, DOI: 10.1007/s00228-006-0250-8.

28. Mahgoub, A.; Idle, J. R.; Dring, L. G.; Lancaster, R.; Smith, R. L. Polymorphic hydroxylation of Debrisoquine in man. *Lancet (London, England)* **1977**, *2*, 584–6, DOI: 10.1016/s0140-6736(77)91430-1.

29. Eichelbaum, M.; Spannbrucker, N.; Steincke, B.; Dengler, H. J. Defective N-oxidation of sparteine in man: A new pharmacogenetic defect. *European Journal of Clinical Pharmacology* **1979**, *16*, 183–187, DOI: 10.1007/BF00562059.

30. Silas, J. H.; Lennard, M. S.; Tucker, G. T.; Smith, A. J.; Malcolm, S. L.; Marten, T. R. Why hypertensive patients vary in their response to oral debrisoquine. *British medical journal* **1977**, *1*, 422–5, DOI: 10.1136/bmj.1.6058.422.

31. Eichelbaum, M.; Baur, M.; Dengler, H.; Osikowska-Evers, B.; Tieves, G.; Zekorn, C.; Rittner, C. Chromosomal assignment of human cytochrome P-450 (debrisoquine/sparteine type) to chromosome 22. *British Journal of Clinical Pharmacology* **1987**, *23*, 455–458, DOI: 10.1111/j.1365-2125.1987.tb03075.x.

32. Nofziger, C.; Turner, A. J.; Sangkuhl, K.; Whirl-Carrillo, M.; Agúndez, J. A.; Black, J. L.; Dunnenberger, H. M.; Ruano, G.; Kennedy, M. A.; Phillips, M. S.; Hachad, H.; Klein, T. E.; Gaedigk, A. PharmVar GeneFocus: CYP2D6. *Clinical Pharmacology and Therapeutics* **2020**, *107*, 154–170, DOI: 10.1002/cpt.1643.

33. Gaedigk, A. Complexities of CYP2D6 gene analysis and interpretation. *International Review of Psychiatry* **2013**, *25*, 534–553, DOI: 10.3109/09540261.2013.825581.

34. Johansson, I.; Ingelman-Sundberg, M. CNVs of human genes and their implication in pharmacogenetics. *Cytogenetic and genome research* **2008**, *123*, 195–204, DOI: 10.1159/000184709.

35. Gaedigk, A.; Blum, M.; Gaedigk, R.; Eichelbaum, M.; Meyer, U. A. Deletion of the entire cytochrome P450 CYP2D6 gene as a cause of impaired drug metabolism in poor metabolizers of the debrisoquine/sparteine polymorphism. *American journal of human genetics* **1991**, *48*, 943–50.

36. Gaedigk, A.; Sangkuhl, K.; Whirl-Carrillo, M.; Klein, T.; Leeder, J. S. Prediction of CYP2D6 phenotype from genotype across world populations. *Genetics in Medicine* **2017**, *19*, 69–76, DOI: 10.1038/gim.2016.80.

37. Koopmans, A. B.; Braakman, M. H.; Vinkers, D. J.; Hoek, H. W.; van Harten, P. N. Meta-analysis of probability estimates of worldwide variation of CYP2D6 and CYP2C19. *Translational Psychiatry* **2021**, *11*, 141, DOI: 10.1038/s41398-020-01129-1.

38. Fuhr, U.; Jetter, A.; Kirchheiner, J. Appropriate phenotyping procedures for drug metabolizing enzymes and transporters in humans and their simultaneous use in the "cocktail" approach. *Clinical Pharmacology and Therapeutics* **2007**, *81*, 270–283, DOI: 10.1038/sj.clpt.6100050.

39. Meyer, U. A.; Zanger, U. M. Molecular mechanisms of genetic polymorphisms of drug metabolism. *Annual review of pharmacology and toxicology* **1997**, *37*, 269–96, DOI: 10.1146/annurev.pharmtox.37.1.269.

40. Caudle, K. E.; Dunnenberger, H. M.; Freimuth, R. R.; Peterson, J. F.; Burlison, J. D.; Whirl-Carrillo, M.; Scott, S. A.; Rehm, H. L.; Williams, M. S.; Klein, T. E.; Relling, M. V.; Hoffman, J. M. Standardizing terms for clinical pharmacogenetic test results: Consensus terms from the Clinical Pharmacogenetics Implementation Consortium (CPIC). *Genetics in Medicine* **2017**, *19*, 215–223, DOI: 10.1038/gim.2016.87.

41. Verbelen, M.; Weale, M. E.; Lewis, C. M. Cost-effectiveness of pharmacogenetic-guided treatment: are we there yet? *The Pharmacogenomics Journal* **2017**, *17*, 395–402, DOI: 10.1038/tpj.2017.21.

42. Gaedigk, A.; Dinh, J. C.; Jeong, H.; Prasad, B.; Leeder, J. S. Ten Years' Experience with the CYP2D6 Activity Score: A Perspective on Future Investigations to Improve Clinical Predictions for Precision Therapeutics. *Journal of Personalized Medicine* **2018**, *8*, 15, DOI: 10.3390/jpm8020015.

43. Gaedigk, A.; Simon, S.; Pearce, R.; Bradford, L.; Kennedy, M.; Leeder, J. The CYP2D6 Activity Score: Translating Genotype Information into a Qualitative Measure of Phenotype. *Clinical Pharmacology & Therapeutics* **2008**, *83*, 234–242, DOI: 10.1038/sj.clpt.6100406.

44. Steimer, W.; Zöpf, K.; von Amelunxen, S.; Pfeiffer, H.; Bachofer, J.; Popp, J.; Messner, B.; Kissling, W.; Leucht, S. Allele-Specific Change of Concentration and Functional Gene Dose for the Prediction of Steady-State Serum Concentrations of Amitriptyline and Nortriptyline in CYP2C19 and CYP2D6 Extensive and Intermediate Metabolizers. *Clinical Chemistry* **2004**, *50*, 1623–1633, DOI: 10.1373/clinchem.2003.030825.

45. Caudle, K. E.; Sangkuhl, K.; Whirl-Carrillo, M.; Swen, J. J.; Haidar, C. E.; Klein, T. E.; Gammal, R. S.; Relling, M. V.; Scott, S. A.; Hertz, D. L.; Guchelaar, H.-J.; Gaedigk, A. Standardizing CYP2D6 Genotype to Phenotype Translation: Consensus Recommendations from the Clinical Pharmacogenetics Implementation Consortium and Dutch Pharmacogenetics Working Group. *Clinical and translational science* **2020**, *13*, 116–124, DOI: 10.1111/cts.12692.

46. Shen, H.; He, M. M.; Liu, H.; Wrighton, S. A.; Wang, L.; Guo, B.; Li, C. Comparative metabolic capabilities and inhibitory profiles of CYP2D6.1, CYP2D6.10, and CYP2D6.17. *Drug Metabolism and Disposition* **2007**, *35*, 1292–1300, DOI: 10.1124/dmd.107.015354.

47. Yang, X.; Zhang, B.; Molony, C.; Chudin, E.; Hao, K.; Zhu, J.; Gaedigk, A.; Suver, C.; Zhong, H.; Leeder, J. S.; Guengerich, F. P.; Strom, S. C.; Schuetz, E.; Rushmore, T. H.; Ulrich, R. G.; Slatter, J. G.; Schadt, E. E.; Kasarskis, A.; Lum, P. Y. Systematic genetic and genomic analysis of cytochrome P450 enzyme activities in human liver. *Genome Research* **2010**, *20*, 1020–1036, DOI: 10.1101/gr.103341.109.

48. Thomas, C. D.; Mosley, S. A.; Kim, S.; Lingineni, K.; El Rouby, N.; Langaee, T. Y.; Gong, Y.; Wang, D.; Schmidt, S. O.; Binkley, P. F.; Estores, D. S.; Feng, K.; Kim, H.; Kinjo, M.; Li, Z.; Fang, L.; Chapman, A. B.; Cooper-DeHoff, R. M.; Gums, J. G.; Hamadeh, I. S.; Zhao, L.; Schmidt, S.; Frye, R. F.; Johnson, J. A.; Cavallari, L. H. Examination of Metoprolol Pharmacokinetics and Pharmacodynamics Across CYP2D6 Genotype-Derived Activity Scores. *CPT: Pharmacometrics and Systems Pharmacology* **2020**, *9*, 678–685, DOI: 10.1002/psp4.12563.

49. Wang, D.; Papp, A. C.; Sun, X. Functional characterization of CYP2D6 enhancer polymorphisms. *Human Molecular Genetics* **2015**, *24*, 1556–1562, DOI: 10.1093/hmg/ddu566.

50. Ray, B.; Ozcagli, E.; Sadee, W.; Wang, D. CYP2D6 haplotypes with enhancer single-nucleotide polymorphism rs5758550 and rs16947 (*2 allele). *Pharmacogenetics and Genomics* **2019**, *29*, 39–47, DOI: 10.1097/FPC.0000000000000363.

51. Dinh, J. C.; Boone, E. C.; Staggs, V. S.; Pearce, R. E.; Wang, W. Y.; Gaedigk, R.; Leeder, J. S.; Gaedigk, A. The Impact of the CYP2D6 "Enhancer" Single Nucleotide Polymorphism on CYP2D6 Activity. *Clinical Pharmacology & Therapeutics* **2022**, *111*, 646–654, DOI: 10.1002/cpt.2469.

52. Ke, A. B.; Nallani, S. C.; Zhao, P.; Rostami-Hodjegan, A.; Isoherranen, N.; Unadkat, J. D. A physiologically based pharmacokinetic model to predict disposition of CYP2D6 and CYP1A2 metabolized drugs in pregnant women. *Drug Metabolism and Disposition* **2013**, *41*, 801–813, DOI: 10.1124/dmd.112.050161.

53. Wadelius, M.; Darj, E.; Frenne, G.; Rane, A. Induction of CYP2D6 in pregnancy. *Clinical Pharmacology & Therapeutics* **1997**, *62*, 400–407, DOI: 10.1016/S0009-9236(97)90118-1.

54. Högstedt, S.; Lindberg, B.; Peng, D. R.; Regårdh, C.-G. G.; Rane, A. Pregnancy-induced increase in metoprolol metabolism. *Clinical Pharmacology and Therapeutics* **1985**, *37*, 688–692, DOI: 10.1038/clpt.1985.114.

55. Pan, X.; Ning, M.; Jeong, H. Transcriptional Regulation of CYP2D6 Expression. *Drug Metabolism and Disposition* **2017**, *45*, 42–48, DOI: 10.1124/dmd.116.072249.

56. Manikandan, P.; Nagini, S. Cytochrome P450 Structure, Function and Clinical Significance: A Review. *Current Drug Targets* **2018**, *19*, 38–54, DOI: 10.2174/1389450118666170125144557.

57. Deodhar, M.; Al Rihani, S. B.; Arwood, M. J.; Darakjian, L.; Dow, P.; Turgeon, J.; Michaud, V. Mechanisms of CYP450 Inhibition: Understanding Drug-Drug Interactions Due to Mechanism-Based Inhibition in Clinical Practice. *Pharmaceutics* **2020**, *12*, 846, DOI: 10.3390/pharmaceutics12090846.

58. FDA Drug Development and Drug Interactions: Table of Substrates, Inhibitors and Inducers | FDA, https://www.fda.gov/drugs/drug-interactions-labeling/drug-development-and-drug-interactions-table-substrates-inhibitors-and-inducers%7B%5C#%7Dtable2-1 (accessed 06/11/2022).

59. FDA For Healthcare Professionals | FDA's Examples of Drugs that Interact with CYP Enzymes and Transporter Systems | FDA, https://www.fda.gov/drugs/drug-interactions-labeling/healthcare-professionals-fdas-examples-drugs-interact-cyp-enzymes-and-transporter-systems (accessed 06/08/2023).

60. Sager, J. E.; Tripathy, S.; Price, L. S. L.; Nath, A.; Chang, J.; Stephenson-Famy, A.; Isoherranen, N. In vitro to in vivo extrapolation of the complex drug-drug interaction of bupropion and its metabolites with CYP2D6; simultaneous reversible inhibition and CYP2D6 downregulation. *Biochemical pharmacology* **2017**, *123*, 85–96, DOI: 10.1016/j.bcp.2016.11.007.

61. Sager, J. E.; Tripathy, S.; Price, L. S.; Nath, A.; Chang, J.; Stephenson-Famy, A.; Isoherranen, N. Corrigendum to "In vitro to in vivo extrapolation of the complex drug-drug interaction of bupropion and its metabolites with CYP2D6; simultaneous reversible inhibition and CYP2D6 downregulation" [Biochem. Pharmacol. 123(2017)85–96] (Biochemical Pharmacolo. *Biochemical Pharmacology* **2021**, *183*, 114306, DOI: 10.1016/j.bcp.2020.114306.

62. Schadel, M.; Wu, D.; Otton, S. V.; Kalow, W.; Sellers, E. M. Pharmacokinetics of Dextromethorphan and Metabolites in Humans. *Journal of Clinical Psychopharmacology* **1995**, *15*, 263–269, DOI: 10.1097/00004714-199508000-00005.

63. Capon, D. A.; Bochner, F.; Kerry, N.; Mikus, G.; Danz, C.; Somogyi, A. A. The influence of CYP2D6 polymorphism and quinidine on the disposition and antitussive effect of dextromethorphan in humans. *Clinical Pharmacology and Therapeutics* **1996**, *60*, 295–307, DOI: 10.1016/S0009-9236(96)90056-9.

64. Storelli, F.; Matthey, A.; Lenglet, S.; Thomas, A.; Desmeules, J.; Daali, Y. Impact of CYP2D6 Functional Allelic Variations on Phenoconversion and Drug-Drug Interactions. *Clinical Pharmacology & Therapeutics* **2018**, *104*, 148–157, DOI: 10.1002/cpt.889.

65. Bahar, M. A.; Kamp, J.; Borgsteede, S. D.; Hak, E.; Wilffert, B. The impact of CYP2D6 mediated drug–drug interaction: a systematic review on a combination of metoprolol and paroxetine/fluoxetine. *British Journal of Clinical Pharmacology*, DOI: 10.1111/bcp.13741.

66. Moltke, L. L.; Greenblatt, D. J.; Grassi, J. M.; Granda, B. W.; Venkatakrishnan, K.; Schmider, J.; Harmatz, J. S.; Shader, R. I. Multiple Human Cytochromes Contribute to Biotransformation of Dextromethorphan In-vitro: Role of CYP2C9, CYP2C19, CYP2D6, and CYP3A. *Journal of Pharmacy and Pharmacology* **1998**, *50*, 997–1004, DOI: 10.1111/j.2042-7158.1998.tb06914.x.

67. Cacabelos, R.; Cacabelos, N.; Carril, J. C. The role of pharmacogenomics in adverse drug reactions. *Expert Review of Clinical Pharmacology* **2019**, *12*, 407–442, DOI: 10.1080/17512433.2019.1597706.

68. Cerqueira, P. M.; Coelho, E. B.; Geleilete, T. J. M.; Goldman, G. H.; Lanchote, V. L. Influence of Chronic Renal Failure on Stereoselective Metoprolol Metabolism in Hypertensive Patients. *The Journal of Clinical Pharmacology* **2005**, *45*, 1422–1433, DOI: 10.1177/0091270005281816.

69. Labbé, L.; Sirois, C.; Pilote, S.; Arseneault, M.; Robitaille, N. M.; Turgeon, J.; Hamelin, B. A. Effect of gender, sex hormones, time variables and physiological urinary pH on apparent CYP2D6 activity as assessed by metabolic ratios of marker substrates. *Pharmacogenetics* **2000**, *10*, 425–438, DOI: 10.1097/00008571-200007000-00006.

70. Stipp, M. C.; Acco, A. Involvement of cytochrome P450 enzymes in inflammation and cancer: a review. *Cancer Chemotherapy and Pharmacology* **2021**, *87*, 295–309, DOI: 10.1007/s00280-020-04181-2.

71. Shah, R. R.; Smith, R. L. Inflammation-induced phenoconversion of polymorphic drug metabolizing enzymes: hypothesis with implications for personalized medicine. *Drug metabolism and disposition: the biological fate of chemicals* **2015**, *43*, 400–10, DOI: 10.1124/dmd.114.061093.

72. Sheiner, L. B.; Beal, S.; Rosenberg, B.; Marathe, V. V. Forecasting individual pharmacokinetics. *Clinical Pharmacology & Therapeutics* **1979**, *26*, 294–305, DOI: 10.1002/cpt1979263294.

73. Jaber, M. M.; Brundage, R. C. Investigating the contribution of residual unexplained variability components on bias and imprecision of parameter estimates in population pharmacokinetic mixed-effects modeling. *Journal of Pharmacokinetics and Pharmacodynamics* **2023**, *50*, DOI: 10.1007/s10928-022-09837-5.

74. CYP2D6 - Drug Label Annotations - PharmGKB, https://www.pharmgkb.org/gene/PA128/labelAnnotation (accessed 11/06/2022).

75. Taylor, C.; Crosby, I.; Yip, V.; Maguire, P.; Pirmohamed, M.; Turner, R. M. A Review of the Important Role of CYP2D6 in Pharmacogenomics. *Genes* **2020**, *11*, 1295, DOI: 10.3390/genes11111295.

76. Novartis Pharmaceuticals Corporation Lopressor® tablet and injection - Prescribing information, https://www.accessdata.fda.gov/drugsatfda%7B%5C_%7Ddocs/label/2008/017963s062,018704s021lbl.pdf (accessed 09/10/2020).

77. ClinCalc DrugStats Database, https://clincalc.com/DrugStats/ (accessed 11/06/2022).

78. Seeringer, A.; Brockmöller, J.; Bauer, S.; Kirchheiner, J. Enantiospecific pharmacokinetics of metoprolol in CYP2D6 ultrarapid metabolizers and correlation with exercise-induced heart rate. *European journal of clinical pharmacology* **2008**, *64*, 883–8, DOI: 10.1007/s00228-008-0504-8.

79. Hilas, O.; Ezzo, D. Nebivolol (bystolic), a novel Beta blocker for hypertension. *P & T : a peer-reviewed journal for formulary management* **2009**, *34*, 188–92.

80. Yoshimoto, K.; Echizen, H.; Chiba, K.; Tani, M.; Ishizaki, T. Identification of human CYP isoforms involved in the metabolism of propranolol enantiomers-N-desisopropylation is mediated mainly by CYP1A2. *British Journal of Clinical Pharmacology* **1995**, *39*, 421–431, DOI: 10.1111/j.1365-2125.1995.tb04472.x.

81. Minder, E. I.; Meier, P. J.; Müller, H. K.; Minder, C.; Meyer, U. A. Bufuralol metabolism in human liver: a sensitive probe for the debrisoquine-type polymorphism of drug oxidation. *European journal of clinical investigation* **1984**, *14*, 184–9, DOI: 10.1111/j.1365-2362.1984.tb01121.x.

82. Hemeryck, A.; De Vriendt, C. A.; Belpaire, F. M. Metoprolol-paroxetine interaction in human liver microsomes: stereoselective aspects and prediction of the in vivo interaction. *Drug metabolism and disposition: the biological fate of chemicals* **2001**, *29*, 656–63.

83. Berger, B.; Bachmann, F.; Duthaler, U.; Krähenbühl, S.; Haschke, M. Cytochrome P450 enzymes involved in metoprolol metabolism and use of metoprolol as a CYP2D6 phenotyping probe drug. *Frontiers in Pharmacology* **2018**, *9*, 1–11, DOI: 10.3389/fphar.2018.00774.

84. Krösser, S.; Neugebauer, R.; Dolgos, H.; Fluck, M.; Rost, K.-L.; Kovar, A. Investigation of sarizotan's impact on the pharmacokinetics of probe drugs for major cytochrome P450 isoenzymes: a combined cocktail trial. *European Journal of Clinical Pharmacology* **2006**, *62*, 277–284, DOI: 10.1007/s00228-006-0101-7.

85. Metoprolol - Drug Label Annotations - PharmGKB, https://www.pharmgkb.org/chemical/PA450480/labelAnnotation (accessed 06/04/2023).

86. TOPROL-XL Labeling-Package Insert - Drugs@FDA, https://www.accessdata.fda.gov/drugsatfda%7B%5C_%7Ddocs/label/2023/019962s050s052lbl.pdf (accessed 06/04/2023).

87. Shahin, M. H.; Rouby, N. E.; Conrado, D. J.; Gonzalez, D.; Gong, Y.; Lobmeyer, M. T.; Beitelshees, A. L.; Boerwinkle, E.; Gums, J. G.; Chapman, A.; Turner, S. T.; Pepine, C. J.; Cooper-Dehoff, R. M.; Johnson, J. A. β 2-Adrenergic Receptor Gene Affects the Heart Rate Response of β-Blockers: Evidence From 3 Clinical Studies. *Pharmacogenomics The Journal of Clinical Pharmacology*, *2019*, 1462–1470, DOI: 10.1002/jcph.1443.

88. Cotarlan, V.; Brofferio, A.; Gerhard, G. S.; Chu, X.; Shirani, J. Impact of β(1)- and β(2)-adrenergic receptor gene single nucleotide polymorphisms on heart rate response to metoprolol prior to coronary computed tomographic angiography. *The American journal of cardiology* **2013**, *111*, 661–6, DOI: 10.1016/j.amjcard.2012.11.015.

89. Silva, A. R.; Dinis-Oliveira, R. J. Pharmacokinetics and pharmacodynamics of dextromethorphan: clinical and forensic aspects. *Drug Metabolism Reviews* **2020**, *52*, 258–282, DOI: 10.1080/03602532.2020.1758712.

90. Taylor, C. P.; Traynelis, S. F.; Siffert, J.; Pope, L. E.; Matsumoto, R. R. Pharmacology of dextromethorphan: Relevance to dextromethorphan/quinidine (Nuedexta®) clinical use. *Pharmacology & therapeutics* **2016**, *164*, 170–82, DOI: 10.1016/j.pharmthera.2016.04.010.

91. Majeed, A.; Xiong, J.; Teopiz, K. M.; Ng, J.; Ho, R.; Rosenblat, J. D.; Phan, L.; Cao, B.; McIntyre, R. S. Efficacy of dextromethorphan for the treatment of depression: a systematic review of preclinical and clinical trials. *Expert Opinion on Emerging Drugs* **2021**, *26*, 63–74, DOI: 10.1080/14728214.2021.1898588.

92. Jasinski, D. R. Abuse potential of morphine/dextromethorphan combinations. *Journal of pain and symptom management* **2000**, *19*, S26–30, DOI: 10.1016/s0885-3924(99)00127-x.

93. Lutz, J. D.; Isoherranen, N. Prediction of Relative In Vivo Metabolite Exposure from In Vitro Data Using Two Model Drugs: Dextromethorphan and Omeprazole. *Drug Metabolism and Disposition* **2012**, *40*, 159–168, DOI: 10.1124/dmd.111.042200.

94. Dextromethorphan - Drug Label Annotations - PharmGKB, https://www.pharmgkb.org/chemical/PA449273/labelAnnotation (accessed 06/04/2023).

95. NUEDEXA Labeling-Package Insert - Drugs@FDA, https://www.accessdata.fda.gov/drugsatfda%7B%5C_%7Ddocs/label/2010/021879s000lbl.pdf (accessed 06/04/2023).

96. AUVELITY Labeling-Package Insert - Drugs@FDA, https://www.accessdata.fda.gov/drugsatfda%7B%5C_%7Ddocs/label/2022/215430Orig1s000Correctedlbl.pdf (accessed 06/04/2023).

97. Kaye, C. M.; Haddock, R. E.; Langley, P. F.; Mellows, G.; Tasker, T. C. G.; Zussman, B. D.; Greb, W. H. A review of the metabolism and pharmacokinetics of paroxetine in man. *Acta Psychiatrica Scandinavica* **1989**, *80*, 60–75, DOI: 10.1111/j.1600-0447.1989.tb07176.x.

98. Maurer, H. H.; Bickeboeller-Friedrich, J.; Kraemer, T. Gas chromatographic-mass spectrometric procedures for determination of the catechol-O-methyltransferase (COMT) activity and for detection of unstable catecholic metabolites in human and rat liver preparations after COMT catalyzed in statu nascendi derivat. *Journal of Chromatography B: Biomedical Sciences and Applications* **2000**, *739*, 325–335, DOI: 10.1016/S0378-4347(00)00025-6.

99. Jornil, J.; Jensen, K. G.; Larsen, F.; Linnet, K. Identification of Cytochrome P450 Isoforms Involved in the Metabolism of Paroxetine and Estimation of Their Importance for Human Paroxetine Metabolism Using a Population-Based Simulator. *Drug Metabolism and Disposition* **2010**, *38*, 376–385, DOI: 10.1124/dmd.109.030551.

100. Wu, D.; Otton, S.; Inaba, T.; Kalow, W.; Sellers, E. M. Interactions of amphetamine analogs with human liver CYP2D6. *Biochemical Pharmacology* **1997**, *53*, 1605–1612, DOI: 10.1016/S0006-2952(97)00014-2.

101. Bertelsen, K. M.; Venkatakrishnan, K.; von Moltke, L. L.; Obach, R. S.; Greenblatt, D. J. Apparent Mechanism-based Inhibition of Human CYP2D6 in Vitro by Paroxetine: Comparison with

Fluoxetine and Quinidine. *Drug Metabolism and Disposition* **2003**, *31*, 289–293, DOI: 10.1124/dmd.31.3.289.

102. Hemeryck, A.; Lefebvre, R. A.; De Vriendt, C.; Belpaire, F. M. Paroxetine affects metoprolol pharmacokinetics and pharmacodynamics in healthy volunteers. *Clinical pharmacology and therapeutics* **2000**, *67*, 283–91, DOI: 10.1067/mcp.2000.104788.

103. Paroxetine - Drug Label Annotations - PharmGKB, https://www.pharmgkb.org/labelAnnotation/PA166104864 (accessed 06/08/2023).

104. PEXEVA Labeling-Package Insert - Drugs@FDA, https://www.accessdata.fda.gov/drugsatfda%7B%5C_%7Ddocs/label/2002/21299lbl.pdf (accessed 06/08/2023).

105. Sauer, J.-M.; Ponsler, G. D.; Mattiuz, E. L.; Long, A. J.; Witcher, J. W.; Thomasson, H. R.; Desante, K. A. Disposition and Metabolic Fate of Atomoxetine Hydrochloride: The Role of CYP2D6 in Human Disposition and Metabolism. *Drug Metabolism and Disposition* **2003**, *31*, 98–107, DOI: 10.1124/dmd.31.1.98.

106. Hennissen, L.; Bakker, M. J.; Banaschewski, T.; Carucci, S.; Coghill, D.; Danckaerts, M.; Dittmann, R. W.; Hollis, C.; Kovshoff, H.; McCarthy, S.; Nagy, P.; Sonuga-Barke, E.; Wong, I. C. K.; Zuddas, A.; Rosenthal, E.; Buitelaar, J. K. Cardiovascular Effects of Stimulant and Non-Stimulant Medication for Children and Adolescents with ADHD: A Systematic Review and Meta-Analysis of Trials of Methylphenidate, Amphetamines and Atomoxetine. *CNS Drugs* **2017**, *31*, 199–215, DOI: 10.1007/s40263-017-0410-7.

107. Ruppert, K.; Geffert, C.; Clement, H.-W.; Bachmann, C.; Haberhausen, M.; Schulz, E.; Fleischhaker, C.; Biscaldi-Schäfer, M. Therapeutic drug monitoring of atomoxetine in children and adolescents with attention-deficit/ hyperactivity disorder: a naturalistic study. *Journal of Neural Transmission* **2022**, *129*, 945–959, DOI: 10.1007/s00702-022-02483-8.

108. Yu, G.; Li, G.-F.; Markowitz, J. S. Atomoxetine: A Review of Its Pharmacokinetics and Pharmacogenomics Relative to Drug Disposition. *Journal of Child and Adolescent Psychopharmacology* **2016**, *26*, 314–326, DOI: 10.1089/cap.2015.0137.

109. Ring, B. J.; Gillespie, J. S.; Eckstein, J. A.; Wrighton, S. A. Identification of the Human Cytochromes P450 Responsible for Atomoxetine Metabolism. *Drug Metabolism and Disposition* **2002**, *30*, 319–323, DOI: 10.1124/dmd.30.3.319.

110. Choi, C.-I.; Bae, J.-W.; Lee, Y.-J.; Lee, H.-I.; Jang, C.-G.; Lee, S.-Y. Effects of CYP2C19 genetic polymorphisms on atomoxetine pharmacokinetics. *Journal of clinical psychopharmacology* **2014**, *34*, 139–42, DOI: 10.1097/JCP.0b013e3182a608a2.

111. Atomoxetine - Drug Label Annotations - PharmGKB, https://www.pharmgkb.org/chemical/PA134688071/labelAnnotation (accessed 06/08/2023).

112. STRATTERA Labeling-Package Insert - Drugs@FDA, https://www.accessdata.fda.gov/drugsatfda%7B%5C_%7Ddocs/label/2002/21411%7B%5C_%7Dstrattera%7B%5C_%7Dlbl.pdf (accessed 06/08/2023).

113. Gupta, S.; Black, D.; Smith, D. Risperidone: Review of Its Pharmacology and Therapeutic Use in Schizophrenia. *Annals of Clinical Psychiatry* **1994**, *6*, 173–180, DOI: 10.3109/10401239409149000.

114. Nasrallah, H. A. Atypical antipsychotic-induced metabolic side effects: insights from receptor-binding profiles. *Molecular Psychiatry* **2008**, *13*, 27–35, DOI: 10.1038/sj.mp.4002066.

115. Fang, J.; Bourin, M.; Baker, G. B. Metabolism of risperidone to 9-hydroxyrisperidone by human cytochromes P450 2D6 and 3A4. *Naunyn-Schmiedeberg's archives of pharmacology* **1999**, *359*, 147–51, DOI: 10.1007/pl00005334.

116. Nussbaum, A. M.; Stroup, T. S. Paliperidone palmitate for schizophrenia. *The Cochrane database of systematic reviews* **2012**, *38*, CD008296, DOI: 10.1002/14651858.CD008296.pub2.

117. Novalbos, J.; López-Rodríguez, R.; Román, M.; Gallego-Sandín, S.; Ochoa, D.; Abad-Santos, F. Effects of CYP2D6 Genotype on the Pharmacokinetics, Pharmacodynamics, and Safety of Risperidone in Healthy Volunteers. *Journal of Clinical Psychopharmacology* **2010**, *30*, 504–511, DOI: 10.1097/JCP.0b013e3181ee84c7.

118. Risperidone - Drug Label Annotations - PharmGKB, https://www.pharmgkb.org/chemical/PA451257/labelAnnotation (accessed 06/08/2023).

119. Legro, R. S.; Barnhart, H. X.; Schlaff, W. D.; Carr, B. R.; Diamond, M. P.; Carson, S. A.; Steinkampf, M. P.; Coutifaris, C.; McGovern, P. G.; Cataldo, N. A.; Gosman, G. G.; Nestler, J. E.; Giudice, L. C.; Leppert, P. C.; Myers, E. R. Clomiphene, Metformin, or Both for Infertility in the Polycystic Ovary Syndrome. *New England Journal of Medicine* **2007**, *356*, 551–566, DOI: 10.1056/NEJMoa063971.

120. Mürdter, T. E.; Kerb, R.; Turpeinen, M.; Schroth, W.; Ganchev, B.; Böhmer, G. M.; Igel, S.; Schaeffeler, E.; Zanger, U.; Brauch, H.; Schwab, M. Genetic polymorphism of cytochrome P450 2D6 determines oestrogen receptor activity of the major infertility drug clomiphene via its active metabolites. *Human Molecular Genetics* **2012**, *21*, 1145–1154, DOI: 10.1093/hmg/ddr543.

121. Dickey, R. P.; Holtkamp, D. E. Development, pharmacology and clinical experience with clomiphene citrate. *Human Reproduction Update* **1996**, *2*, 483–506, DOI: 10.1093/humupd/2.6.483.

122. Clomifene - Drug Label Annotations - PharmGKB, https://www.pharmgkb.org/chemical/PA449046/labelAnnotation (accessed 06/08/2023).

123. Vaughan Williams, E. M. A classification of antiarrhythmic actions reassessed after a decade of new drugs. *Journal of clinical pharmacology* **1984**, *24*, 129–47, DOI: 10.1002/j.1552-4604.1984.tb01822.x.

124. Vitali Serdoz, L.; Rittger, H.; Furlanello, F.; Bastian, D. Quinidine—A legacy within the modern era of antiarrhythmic therapy. *Pharmacological Research* **2019**, *144*, 257–263, DOI: 10.1016/j.phrs.2019.04.028.

125. Nielsen, T. L.; Rasmussen, B. B.; Flinois, J. P.; Beaune, P.; Brosen, K. In vitro metabolism of quinidine: the (3S)-3-hydroxylation of quinidine is a specific marker reaction for cytochrome P-4503A4 activity in human liver microsomes. *The Journal of pharmacology and experimental therapeutics* **1999**, *289*, 31–7.

126. McLaughlin, L. A.; Paine, M. J.; Kemp, C. A.; Maréchal, J. D.; Flanagan, J. U.; Ward, C. J.; Sutcliffe, M. J.; Roberts, G. C.; Wolf, C. R. Why is quinidine an inhibitor of cytochrome P450 2D6? The role of key active-site residues in quinidine binding. *Journal of Biological Chemistry*, *280*, 38617–38624, DOI: 10.1074/jbc.M505974200.

127. Lumen, A. A.; Acharya, P.; Polli, J. W.; Ayrton, A.; Ellens, H.; Bentz, J. If the K I Is Defined by the Free Energy of Binding to P-Glycoprotein, Which Kinetic Parameters Define the IC 50 for the Madin-Darby Canine Kidney II Cell Line Overexpressing Human Multidrug Resistance 1 Confluent Cell Monolayer? *Drug Metabolism and Disposition* **2010**, *38*, 260–269, DOI: 10.1124/dmd.109.029843.

128. Ching, M. S.; Blake, C. L.; Ghabrial, H.; Ellis, S.; Lennard, M. S.; Tucker, G. T.; Smallwood, R. A. Potent inhibition of yeast-expressed CYP2D6 by dihydroquinidine, quinidine, and its metabolites. *Biochemical Pharmacology* **1995**, *50*, 833–837, DOI: 10.1016/0006-2952(95)00207-G.

129. Ochs, H. R.; Greenblatt, D. J.; Woo, E. Clinical pharmacokinetics of quinidine. *Clinical pharmacokinetics* **1980**, *5*, 150–68, DOI: 10.2165/00003088-198005020-00003.

130. Quinidine - Drug Label Annotations - PharmGKB, https://www.pharmgkb.org/chemical/PA451209/labelAnnotation (accessed 06/08/2023).

131. QUINIDINE GLUCONATE Labeling-Package Insert - Drugs@FDA, https://www.accessdata.fda.gov/scripts/cder/daf/index.cfm?event=overview.process%7B%5C&%7DvarApplNo=089338 (accessed 06/08/2023).

132. Marchenko, O. V., *Quantitative Methods in Pharmaceutical Research and Development*; Marchenko, O. V., Katenka, N. V., Eds.; Springer International Publishing: Cham, 2020, DOI: 10.1007/978-3-030-48555-9.

133. README - Open Systems Pharmacology, https://docs.open-systems-pharmacology.org/ (accessed 12/15/2022).

134. El-Khateeb, E.; Burkhill, S.; Murby, S.; Amirat, H.; Rostami-Hodjegan, A.; Ahmad, A. Physiological-based pharmacokinetic modeling trends in pharmaceutical drug development over the last 20-years; in-depth analysis of applications, organizations, and platforms. *Biopharmaceutics & Drug Disposition* **2021**, *42*, 107–117, DOI: 10.1002/bdd.2257.

135. Frechen, S.; Rostami-Hodjegan, A. Quality Assurance of PBPK Modeling Platforms and Guidance on Building, Evaluating, Verifying and Applying PBPK Models Prudently under the Umbrella of Qualification: Why, When, What, How and By Whom? *Pharmaceutical Research* **2022**, *39*, 1733–1748, DOI: 10.1007/s11095-022-03250-w.

136. U.S. Food and Drug Administration. Physiologically Based Pharmacokinetic Analyses — Format and Content Guidance for Industry, 2018, https://www.fda.gov/regulatory-information/search-fda-guidance-documents/physiologically-based-pharmacokinetic-analyses-format-and-content-guidance-industry (accessed 12/15/2022).

137. European Medicines Agency. Guideline on the reporting of physiologically based pharmacokinetic (PBPK) modelling and simulation, 2018, https://www.ema.europa.eu/en/documents/scientific-guideline/guideline-reporting-physiologically-based-pharmacokinetic-pbpk-modelling-simulation%7B%5C_%7Den.pdf (accessed 12/15/2022).

138. Huisinga, W.; Solms, A.; Fronton, L.; Pilari, S. Modeling Interindividual Variability in Physiologically Based Pharmacokinetics and Its Link to Mechanistic Covariate Modeling. *CPT:*

Pharmacometrics & Systems Pharmacology **2012**, *1*, 4, DOI: 10.1038/psp.2012.3.

139. Krauss, M.; Tappe, K.; Schuppert, A.; Kuepfer, L.; Goerlitz, L. Bayesian Population Physiologically-Based Pharmacokinetic (PBPK) Approach for a Physiologically Realistic Characterization of Interindividual Variability in Clinically Relevant Populations. *PloS one* **2015**, *10*, e0139423, DOI: 10.1371/journal.pone.0139423.

140. Loer, H. L. H.; Feick, D.; Rüdesheim, S.; Selzer, D.; Schwab, M.; Teutonico, D.; Frechen, S.; van der Lee, M.; Moes, D. J. A. R.; Swen, J. J.; Lehr, T. Physiologically based pharmacokinetic modeling of tacrolimus for food-drug and CYP3A drug-drug-gene interaction predictions. *CPT: pharmacometrics & systems pharmacology* **2023**, *00*, 1–15, DOI: 10.1002/psp4.12946.

141. Marshall, S.; Burghaus, R.; Cosson, V.; Cheung, S.; Chenel, M.; DellaPasqua, O.; Frey, N.; Hamrén, B.; Harnisch, L.; Ivanow, F.; Kerbusch, T.; Lippert, J.; Milligan, P.; Rohou, S.; Staab, A.; Steimer, J.; Tornøe, C.; Visser, S. Good Practices in Model-Informed Drug Discovery and Development: Practice, Application, and Documentation. *CPT: Pharmacometrics & Systems Pharmacology* **2016**, *5*, 93–122, DOI: 10.1002/psp4.12049.

142. Kneller, L. A.; Abad-Santos, F.; Hempel, G. Physiologically Based Pharmacokinetic Modelling to Describe the Pharmacokinetics of Risperidone and 9-Hydroxyrisperidone According to Cytochrome P450 2D6 Phenotypes. *Clinical Pharmacokinetics* **2020**, *59*, 51–65, DOI: 10.1007/s40262-019-00793-x.

143. Wojtyniak, J. G.; Britz, H.; Selzer, D.; Schwab, M.; Lehr, T. Data Digitizing: Accurate and Precise Data Extraction for Quantitative Systems Pharmacology and Physiologically-Based Pharmacokinetic Modeling. *CPT: Pharmacometrics and Systems Pharmacology* **2020**, *9*, 322–331, DOI: 10.1002/psp4.12511.

144. Seabold, S.; Perktold, J. In *Proc. of the 9th Python in Science Conf*, 2010, pp 92–96, DOI: 10.25080/Majora-92bf1922-011.

145. Open Systems Pharmacology Suite Community PK-Sim® Ontogeny Database Documentation, Version 7.3. **2018**.

146. Hanke, N.; Frechen, S.; Moj, D.; Britz, H.; Eissing, T.; Wendl, T.; Lehr, T. PBPK Models for CYP3A4 and P-gp DDI Prediction: A Modeling Network of Rifampicin, Itraconazole, Clarithromycin, Midazolam, Alfentanil, and Digoxin. *CPT: Pharmacometrics and Systems Pharmacology* **2018**, *7*, 647–659, DOI: 10.1002/psp4.12343.

147. Fuhr, L. M.; Marok, F. Z.; Hanke, N.; Selzer, D.; Lehr, T. Pharmacokinetics of the CYP3A4 and CYP2B6 Inducer Carbamazepine and Its Drug–Drug Interaction Potential: A Physiologically Based Pharmacokinetic Modeling Approach. *Pharmaceutics* **2021**, *13*, 270, DOI: 10.3390/pharmaceutics13020270.

148. Hanke, N.; Türk, D.; Selzer, D.; Ishiguro, N.; Ebner, T.; Wiebe, S.; Müller, F.; Stopfer, P.; Nock, V.; Lehr, T. A Comprehensive Whole-Body Physiologically Based Pharmacokinetic Drug–Drug–Gene Interaction Model of Metformin and Cimetidine in Healthy Adults and Renally Impaired Individuals. *Clinical Pharmacokinetics* **2020**, *59*, 1419–1431, DOI: 10.1007/s40262-020-00896-w.

149. Britz, H.; Hanke, N.; Volz, A. K.; Spigset, O.; Schwab, M.; Eissing, T.; Wendl, T.; Frechen, S.; Lehr, T. Physiologically-Based Pharmacokinetic Models for CYP1A2 Drug–Drug Interaction Prediction: A Modeling Network of Fluvoxamine, Theophylline, Caffeine, Rifampicin, and Midazolam. *CPT: Pharmacometrics and Systems Pharmacology* **2019**, *8*, 296–307, DOI: 10.1002/psp4.12397.

150. Kanacher, T.; Lindauer, A.; Mezzalana, E.; Michon, I.; Veau, C.; Mantilla, J. D. G.; Nock, V.; Fleury, A. A Physiologically-Based Pharmacokinetic (PBPK) Model Network for the Prediction of CYP1A2 and CYP2C19 Drug–Drug–Gene Interactions with Fluvoxamine, Omeprazole, S-mephenytoin, Moclobemide, Tizanidine, Mexiletine, Ethinylestradiol, and Caffeine. *Pharmaceutics* **2020**, *12*, 1191, DOI: 10.3390/pharmaceutics12121191.

151. Hanke, N.; Türk, D.; Selzer, D.; Wiebe, S.; Fernandez, É.; Stopfer, P.; Nock, V.; Lehr, T. A mechanistic, enantioselective, physiologically based pharmacokinetic model of verapamil and norverapamil, built and evaluated for drug–drug interaction studies. *Pharmaceutics* **2020**, *12*, 1–19, DOI: 10.3390/pharmaceutics12060556.

152. Henricks, L. M.; Lunenburg, C. A.; Meulendijks, D.; Gelderblom, H.; Cats, A.; Swen, J. J.; Schellens, J. H.; Guchelaar, H.-J. Translating DPYD genotype into DPD phenotype: using the DPYD gene activity score. *Pharmacogenomics* **2015**, *16*, 1275–1284, DOI: 10.2217/pgs.15.70.

153. Karnes, J. H.; Rettie, A. E.; Somogyi, A. A.; Huddart, R.; Fohner, A. E.; Formea, C. M.; Ta Michael Lee, M.; Llerena, A.; Whirl-Carrillo, M.; Klein, T. E.; Phillips, E. J.; Mintzer, S.; Gaedigk, A.; Caudle, K. E.; Callaghan, J. T. Clinical Pharmacogenetics Implementation Consortium (CPIC) Guideline for CYP2C9 and HLA-B Genotypes and Phenytoin Dosing: 2020 Update. *Clinical Pharmacology & Therapeutics* **2021**, *109*, 302–309, DOI: 10.1002/cpt.2008.

154. Matthaei, J.; Brockmeoller, J.; Tzvetkov, M. V. M.; Sehrt, D.; Sachse-Seeboth, C.; Hjelmborg, J. B. J. B.; Moller, S.; Halekoh, U.; Hofmann, U.; Schwab, M.; Kerb, R.; Brockmöller, J.; Tzvetkov, M. V. M.; Sehrt, D.; Sachse-Seeboth, C.; Hjelmborg, J. B. J. B.; Möller, S.; Halekoh, U.; Hofmann, U.; Schwab, M.; Kerb, R. Heritability of Metoprolol and Torsemide Pharmacokinetics. *Clinical Pharmacology and Therapeutics* **2015**, *98*, 611–621, DOI: 10.1002/cpt.258.

155. Kozyra, M.; Ingelman-Sundberg, M.; Lauschke, V. M. Rare genetic variants in cellular transporters, metabolic enzymes, and nuclear receptors can be important determinants of interindividual differences in drug response. *Genetics in medicine : official journal of the American College of Medical Genetics* **2017**, *19*, 20–29, DOI: 10.1038/gim.2016.33.

156. Ingelman-Sundberg, M.; Mkrtchian, S.; Zhou, Y.; Lauschke, V. M. Integrating rare genetic variants into pharmacogenetic drug response predictions. *Human Genomics* **2018**, *12*, 26, DOI: 10.1186/s40246-018-0157-3.

157. Hertz, D. L.; Snavely, A. C.; McLeod, H. L.; Walko, C. M.; Ibrahim, J. G.; Anderson, S.; Weck, K. E.; Magrinat, G.; Olajide, O.; Moore, S.; Raab, R.; Carrizosa, D. R.; Corso, S.; Schwartz, G.; Peppercorn, J. M.; Evans, J. P.; Jones, D. R.; Desta, Z.; Flockhart, D. A.; Carey, L. A.; Irvin, W. J. In vivo assessment of the metabolic activity of CYP2D6 diplotypes and alleles. *British Journal of Clinical Pharmacology* **2015**, *80*, 1122–1130, DOI: 10.1111/bcp.12665.

158. Van der Lee, M.; Allard, W. G.; Vossen, R. H. A. M.; Baak-Pablo, R. F.; Menafra, R.; Deiman, B. A. L. M.; Deenen, M. J.; Neven, P.; Johansson, I.; Gastaldello, S.; Ingelman-Sundberg, M.; Guchelaar, H.-J.; Swen, J. J.; Anvar, S. Y. Toward predicting CYP2D6-mediated variable drug response from CYP2D6 gene sequencing data. *Science translational medicine* **2021**, *13*, DOI: 10.1126/scitranslmed.abf3637.

159. Frederiksen, T.; Areberg, J.; Schmidt, E.; Bjerregaard Stage, T.; Brøsen, K. Quantification of In Vivo Metabolic Activity of CYP2D6 Genotypes and Alleles Through Population Pharmacokinetic Analysis of Vortioxetine. *Clinical Pharmacology and Therapeutics* **2021**, *109*, 150–159, DOI: 10.1002/cpt.1972.

160. Abduljalil, K.; Frank, D.; Gaedigk, A.; Klaassen, T.; Tomalik-Scharte, D.; Jetter, A.; Jaehde, U.; Kirchheiner, J.; Fuhr, U. Assessment of activity levels for CYP2D6*1, CYP2D6*2, and CYP2D6*41 genes by population pharmacokinetics of dextromethorphan. *Clinical Pharmacology and Therapeutics* **2010**, *88*, 643–651, DOI: 10.1038/clpt.2010.137.

161. Haslemo, T.; Eliasson, E.; Jukić, M. M.; Ingelman-Sundberg, M.; Molden, E. Significantly lower CYP2D6 metabolism measured as the O/N -desmethylvenlafaxine metabolic ratio in carriers of CYP2D6*41 versus CYP2D6*9 or CYP2D6*10 : a study on therapeutic drug monitoring data from 1003 genotyped Scandinavian patients. *British Journal of Clinical Pharmacology* **2019**, *85*, 194–201, DOI: 10.1111/bcp.13788.

162. Huang, W.; Nakano, M.; Sager, J.; Ragueneau-Majlessi, I.; Isoherranen, N. Physiologically Based Pharmacokinetic Model of the CYP2D6 Probe Atomoxetine: Extrapolation to Special Populations and Drug-Drug Interactions. *Drug metabolism and disposition: the biological fate of chemicals* **2017**, *45*, 1156–1165, DOI: 10.1124/dmd.117.076455.

163. Xu, M.; Zheng, L.; Zeng, J.; Xu, W.; Jiang, X.; Wang, L. Physiologically based pharmacokinetic modeling of tramadol to inform dose adjustment and drug-drug interactions according to CYP2D6 phenotypes. *Pharmacotherapy: The Journal of Human Pharmacology and Drug Therapy* **2021**, *41*, 277–290, DOI: 10.1002/phar.2494.

164. Jeong, H.-C.; Bae, S. H.; Bae, J.-W.; Lee, S.; Kim, A.; Jang, Y.; Shin, K.-H. Evaluation of the Effect of CYP2D6 Genotypes on Tramadol and O-Desmethyltramadol Pharmacokinetic Profiles in a Korean Population Using Physiologically-Based Pharmacokinetic Modeling. *Pharmaceutics* **2019**, *11*, DOI: 10.3390/pharmaceutics11110618.

165. Li, J.; Kim, S.; Sha, X.; Wiegand, R.; Wu, J.; LoRusso, P. Complex Disease–, Gene–, and Drug–Drug Interactions: Impacts of Renal Function, CYP2D6 Phenotype, and OCT2 Activity on Veliparib Pharmacokinetics. *Clinical Cancer Research* **2014**, *20*, 3931–3944, DOI: 10.1158/1078-0432.CCR-14-0791.

166. Almurjan, A.; Macfarlane, H.; Badhan, R. K. S. Precision dosing-based optimisation of paroxetine during pregnancy for poor and ultrarapid CYP2D6 metabolisers: a virtual clinical trial pharmacokinetics study. *Journal of Pharmacy and Pharmacology* **2020**, *72*, 1049–1060, DOI: 10.1111/jphp.13281.

167. Badaoui, S.; Hopkins, A. M.; Rodrigues, A. D.; Miners, J. O.; Sorich, M. J.; Rowland, A. Application of Model Informed Precision Dosing to Address the Impact of Pregnancy Stage and CYP2D6 Phenotype on Foetal Morphine Exposure. *The AAPS journal* **2021**, *23*, 15, DOI: 10.1208/s12248-020-00541-1.

168. Dickschen, K.; Willmann, S.; Thelen, K.; Lippert, J.; Hempel, G.; Eissing, T. Physiologically Based Pharmacokinetic Modeling of Tamoxifen and its Metabolites in Women of Different CYP2D6 Phenotypes Provides New Insight into the Tamoxifen Mass

Balance. *Frontiers in pharmacology* **2012**, *3*, 92, DOI: 10.3389/fphar.2012.00092.

169. Gueorguieva, I.; Jackson, K.; Wrighton, S. A.; Sinha, V. P.; Chien, J. Y. Desipramine, substrate for CYP2D6 activity: population pharmacokinetic model and design elements of drug-drug interaction trials. *British Journal of Clinical Pharmacology* **2010**, *70*, 523–536, DOI: 10.1111/j.1365-2125.2010.03731.x.

170. Yang, J.; Jamei, M.; Heydari, A.; Yeo, K. R.; de la Torre, R.; Farré, M.; Tucker, G. T.; Rostami-Hodjegan, A. Implications of mechanism-based inhibition of CYP2D6 for the pharmacokinetics and toxicity of MDMA. *Journal of Psychopharmacology* **2006**, *20*, 842–849, DOI: 10.1177/0269881106065907.

171. Kim, S.-H. H.; Byeon, J.-Y. Y.; Kim, Y.-H. H.; Lee, C.-M. M.; Lee, Y. J.; Jang, C.-G. G.; Lee, S.-Y. Y. Physiologically based pharmacokinetic modelling of atomoxetine with regard to CYP2D6 genotypes. *Scientific Reports* **2018**, *8*, 12405, DOI: 10.1038/s41598-018-30841-8.

172. Yoo, H.-D.; Cho, H.-Y.; Lee, S.-N.; Yoon, H.; Lee, Y.-B. Population pharmacokinetic analysis of risperidone and 9-hydroxyrisperidone with genetic polymorphisms of CYP2D6 and ABCB1. *Journal of Pharmacokinetics and Pharmacodynamics* **2012**, *39*, 329–341, DOI: 10.1007/s10928-012-9253-5.

173. Lee, J.; Yoo, H.-D.; Bae, J.-W.; Lee, S.; Shin, K.-H. Population pharmacokinetic analysis of tramadol and O-desmethyltramadol with genetic polymorphism of CYP2D6. *Drug Design, Development and Therapy* **2019**, *Volume 13*, 1751–1761, DOI: 10.2147/DDDT.S199574.

174. Lu, S.; Nand, R. A.; Yang, J. S.; Chen, G.; Gross, A. S. Pharmacokinetics of CYP2C9, CYP2C19, and CYP2D6 substrates in healthy Chinese and European subjects. *European Journal of Clinical Pharmacology* **2018**, *74*, 285–296, DOI: 10.1007/s00228-017-2375-3.

175. Nakamura, T.; Toshimoto, K.; Lee, W.; Imamura, C. K.; Tanigawara, Y.; Sugiyama, Y. Application of PBPK Modeling and Virtual Clinical Study Approaches to Predict the Outcomes of CYP2D6 Genotype-Guided Dosing of Tamoxifen. *CPT: pharmacometrics & systems pharmacology* **2018**, *7*, 474–482, DOI: 10.1002/psp4.12307.

176. Notsu, Y.; Shimizu, M.; Sasaki, T.; Nakano, A.; Ota, M.; Yoshida, S.; Yamazaki, H. Simple pharmacokinetic models accounting for drug monitoring results of atomoxetine and its 4-hydroxylated metabolites in Japanese pediatric patients genotyped for cytochrome P450 2D6. *Drug Metabolism and Pharmacokinetics* **2020**, *35*, 191–200, DOI: 10.1016/j.dmpk.2019.08.005.

177. Storelli, F.; Desmeules, J.; Daali, Y. Physiologically-Based Pharmacokinetic Modeling for the Prediction of CYP2D6-Mediated Gene–Drug–Drug Interactions. *CPT: Pharmacometrics & Systems Pharmacology* **2019**, psp4.12411, DOI: 10.1002/psp4.12411.

178. The Royal Dutch Pharmacists Association - Pharmacogenetics Working Group (DPWG) - Annotation of DPWG Guideline for Metoprolol and CYP2D6. https://www.pharmgkb.org/guidelineAnnotation/PA166104995 (accessed 01/15/2023).

179. Polak, S.; Tylutki, Z.; Holbrook, M.; Wiśniowska, B. Better prediction of the local concentration–effect relationship: the role of physiologically based pharmacokinetics and quantitative systems pharmacology and toxicology in the evolution of model-informed drug discovery and development. *Drug Discovery Today* **2019**, *24*, 1344–1354, DOI: 10.1016/j.drudis.2019.05.016.

180. Lesko, L. J. Perspective on model-informed drug development. *CPT: Pharmacometrics & Systems Pharmacology* **2021**, *10*, 1127–1129, DOI: 10.1002/psp4.12699.

181. Marshall, S.; Madabushi, R.; Manolis, E.; Krudys, K.; Staab, A.; Dykstra, K.; Visser, S. A. Model-Informed Drug Discovery and Development: Current Industry Good Practice and Regulatory Expectations and Future Perspectives. *CPT: Pharmacometrics & Systems Pharmacology* **2019**, *8*, 87–96, DOI: 10.1002/psp4.12372.

182. Grimstein, M.; Yang, Y.; Zhang, X.; Grillo, J.; Huang, S.-M.; Zineh, I.; Wang, Y. Physiologically Based Pharmacokinetic Modeling in Regulatory Science: An Update From the U.S. Food and Drug Administration's Office of Clinical Pharmacology. *Journal of pharmaceutical sciences* **2019**, *108*, 21–25, DOI: 10.1016/j.xphs.2018.10.033.

183. Chu, X.; Prasad, B.; Neuhoff, S.; Yoshida, K.; Leeder, J. S.; Mukherjee, D.; Taskar, K.; Varma, M. V. S.; Zhang, X.; Yang, X.; Galetin, A. Clinical Implications of Altered Drug Transporter Abundance/Function and PBPK Modeling in Specific Populations: An ITC Perspective. *Clinical pharmacology and therapeutics* **2022**, *112*, 501–526, DOI: 10.1002/cpt.2643.

184. Zhang, X.; Yang, Y.; Grimstein, M.; Fan, J.; Grillo, J. A.; Huang, S.-M.; Zhu, H.; Wang, Y. Application of PBPK Modeling and Simulation for Regulatory Decision Making and Its Impact on US Prescribing Information: An Update on the 2018-2019 Submissions to the US FDA's Office of Clinical Pharmacology. *The Journal of Clinical Pharmacology* **2020**, *60*, 60, DOI: 10.1002/jcph.1767.

185. Kilford, P. J.; Chen, K.-F.; Crewe, K.; Gardner, I.; Hatley, O.; Ke, A. B.; Neuhoff, S.; Zhang, M.; Rowland Yeo, K. Prediction of CYP-mediated DDIs involving inhibition: Approaches to

address the requirements for system qualification of the Simcyp Simulator. *CPT: Pharmacometrics & Systems Pharmacology* **2022**, *11*, 822–832, DOI: 10.1002/psp4.12794.

186. Frechen, S.; Solodenko, J.; Wendl, T.; Dallmann, A.; Ince, I.; Lehr, T.; Lippert, J.; Burghaus, R. A generic framework for the physiologically-based pharmacokinetic platform qualification of PK-Sim and its application to predicting cytochrome P450 3A4–mediated drug–drug interactions. *CPT: Pharmacometrics & Systems Pharmacology* **2021**, *10*, 633–644, DOI: 10.1002/psp4.12636.

187. Wendl, T.; Frechen, S.; Gerisch, M.; Heinig, R.; Eissing, T. Physiologically-based pharmacokinetic modeling to predict CYP3A4-mediated drug-drug interactions of finerenone. *CPT: Pharmacometrics & Systems Pharmacology* **2022**, *11*, 199–211, DOI: 10.1002/psp4.12746.

188. Türk, D.; Hanke, N.; Wolf, S.; Frechen, S.; Eissing, T.; Wendl, T.; Schwab, M.; Lehr, T. Physiologically Based Pharmacokinetic Models for Prediction of Complex CYP2C8 and OATP1B1 (SLCO1B1) Drug–Drug–Gene Interactions: A Modeling Network of Gemfibrozil, Repaglinide, Pioglitazone, Rifampicin, Clarithromycin and Itraconazole. *Clinical Pharmacokinetics* **2019**, *58*, 1595–1607, DOI: 10.1007/s40262-019-00777-x.

189. Sheiner, L. B. Computer-aided long-term anticoagulation therapy. *Computers and biomedical research, an international journal* **1969**, *2*, 507–18, DOI: 10.1016/0010-4809(69)90030-5.

190. Terry, S. F. Obama's Precision Medicine Initiative. *Genetic Testing and Molecular Biomarkers* **2015**, *19*, 113–114, DOI: 10.1089/gtmb.2015.1563.

191. Darwich, A. S.; Ogungbenro, K.; Vinks, A. A.; Powell, J. R.; Reny, J.-L.; Marsousi, N.; Daali, Y.; Fairman, D.; Cook, J.; Lesko, L. J.; McCune, J. S.; Knibbe, C. A. J.; de Wildt, S. N.; Leeder, J. S.; Neely, M.; Zuppa, A. F.; Vicini, P.; Aarons, L.; Johnson, T. N.; Boiani, J.; Rostami-Hodjegan, A. Why Has Model-Informed Precision Dosing Not Yet Become Common Clinical Reality? Lessons From the Past and a Roadmap for the Future. *Clinical Pharmacology & Therapeutics* **2017**, *101*, 646–656, DOI: 10.1002/cpt.659.

192. Darwich, A. S.; Polasek, T. M.; Aronson, J. K.; Ogungbenro, K.; Wright, D. F. B.; Achour, B.; Reny, J.-L.; Daali, Y.; Eiermann, B.; Cook, J.; Lesko, L.; McLachlan, A. J.; Rostami-Hodjegan, A. Model-Informed Precision Dosing: Background, Requirements, Validation, Implementation, and Forward Trajectory of Individualizing Drug Therapy. *Annual review of pharmacology and toxicology* **2021**, *61*, 225–245, DOI: 10.1146/annurev-pharmtox-033020-113257.

193. Fendt, R.; Hofmann, U.; Schneider, A. R. P.; Schaeffeler, E.; Burghaus, R.; Yilmaz, A.; Blank, L. M.; Kerb, R.; Lippert, J.; Schlender, J.-F.; Schwab, M.; Kuepfer, L. Data-driven personalization of a physiologically based pharmacokinetic model for caffeine: A systematic assessment. *CPT: Pharmacometrics & Systems Pharmacology* **2021**, *10*, 782–793, DOI: 10.1002/psp4.12646.

194. Polasek, T. M.; Rostami-Hodjegan, A. Virtual Twins: Understanding the Data Required for Model-Informed Precision Dosing. *Clinical Pharmacology & Therapeutics* **2020**, *107*, 742–745, DOI: 10.1002/cpt.1778.

APPENDIX A

A.1 PUBLICATIONS

A.1.1 *Original Research Articles*

1. Rüdesheim, S.; Wojtyniak, J.-G.; Selzer, D.; Hanke, N.; Mahfoud, F.; Schwab, M.; Lehr, T. Physiologically Based Pharmacokinetic Modeling of Metoprolol Enantiomers and α-Hydroxymetoprolol to Describe CYP2D6 Drug-Gene Interactions. *Pharmaceutics* **2020**, *12*, 1200, DOI: 10.3390/pharmaceutics12121200

2. Rüdesheim, S.; Selzer, D.; Fuhr, U.; Schwab, M.; Lehr, T. Physiologically-based pharmacokinetic modeling of dextromethorphan to investigate interindividual variability within CYP2D6 activity score groups. *CPT: pharmacometrics & systems pharmacology* **2022**, *11*, 494–511, DOI: 10.1002/psp4.12776

3. Rüdesheim, S.; Selzer, D.; Mürdter, T.; Igel, S.; Kerb, R.; Schwab, M.; Lehr, T. Physiologically Based Pharmacokinetic Modeling to Describe the CYP2D6 Activity Score-Dependent Metabolism of Paroxetine, Atomoxetine and Risperidone. *Pharmaceutics* **2022**, *2022*, 1734, DOI: 10.3390/pharmaceutics14081734

4. Kovar, C.; Kovar, L.; Rüdesheim, S.; Selzer, D.; Ganchev, B.; Kröner, P.; Igel, S.; Kerb, R.; Schaeffeler, E.; Mürdter, T. E.; Schwab, M.; Lehr, T. Prediction of Drug–Drug–Gene Interaction Scenarios of (*E*)-Clomiphene and Its Metabolites Using Physiologically Based Pharmacokinetic Modeling. *Pharmaceutics* **2022**, *14*, 2604, DOI: 10.3390/pharmaceutics14122604

5. Loer, H. L. H.; Feick, D.; Rüdesheim, S.; Selzer, D.; Schwab, M.; Teutonico, D.; Frechen, S.; van der Lee, M.; Moes, D. J. A. R.; Swen, J. J.; Lehr, T. Physiologically based pharmacokinetic modeling of tacrolimus for food-drug and CYP3A drug-drug-gene interaction predictions. *CPT: pharmacometrics & systems pharmacology* **2023**, *00*, 1–15, DOI: 10.1002/psp4.12946

6. Feick, D.; Rüdesheim, S.; Marok, F. Z.; Selzer, D.; Loer, H. L. H.; Teutonico, D.; Frechen, S.; van der Lee, M.; Moes, D. J. A. R.; Swen, J. J.; Schwab, M.; Lehr, T. Physiologically-based pharmacokinetic modeling of quinidine to establish a CYP3A4, P-gp, and CYP2D6 drug-drug-gene interaction network. *CPT: pharmacometrics & systems pharmacology* **2023**, 1–14, DOI: 10.1002/psp4.12981

A.1.2 *Review Articles*

1. Türk, D.; Fuhr, L. M.; Marok, F. Z.; Rüdesheim, S.; Kühn, A.; Selzer, D.; Schwab, M.; Lehr, T. Novel models for the prediction of drug–gene interactions. *Expert Opinion on Drug Metabolism & Toxicology* **2021**, *17*, 1293–1310, DOI: 10.1080/17425255.2021.1998455

B

APPENDIX B: SUPPLEMENTARY MATERIALS

Contents:

1. Supplementary Materials Project I: PBPK Modeling of Metoprolol

   Rüdesheim, S.; Wojtyniak, J.-G.; Selzer, D.; Hanke, N.; Mahfoud, F.; Schwab, M.; Lehr, T. Physiologically Based Pharmacokinetic Modeling of Metoprolol Enantiomers and α-Hydroxymetoprolol to Describe CYP2D6 Drug-Gene Interactions. *Pharmaceutics* **2020**, *12*, 1200, DOI: 10.3390/pharmaceutics12121200

2. Supplementary Materials Project II: PBPK Modeling of Dextromethorphan

   Rüdesheim, S.; Selzer, D.; Fuhr, U.; Schwab, M.; Lehr, T. Physiologically-based pharmacokinetic modeling of dextromethorphan to investigate interindividual variability within CYP2D6 activity score groups. *CPT: pharmacometrics & systems pharmacology* **2022**, *11*, 494–511, DOI: 10.1002/psp4.12776

3. Supplementary Materials Project III: PBPK Modeling of Paroxetine, Atomoxetine and Risperidone

   Rüdesheim, S.; Selzer, D.; Mürdter, T.; Igel, S.; Kerb, R.; Schwab, M.; Lehr, T. Physiologically Based Pharmacokinetic Modeling to Describe the CYP2D6 Activity Score-Dependent Metabolism of Paroxetine, Atomoxetine and Risperidone. *Pharmaceutics* **2022**, *2022*, 1734, DOI: 10.3390/pharmaceutics14081734

4. Supplementary Materials Project IV: PBPK Modeling of (*E*)-Clomiphene

   Kovar, C.; Kovar, L.; Rüdesheim, S.; Selzer, D.; Ganchev, B.; Kröner, P.; Igel, S.; Kerb, R.; Schaeffeler, E.; Mürdter, T. E.; Schwab, M.; Lehr, T. Prediction of Drug–Drug–Gene Interaction Scenarios of (*E*)-Clomiphene and Its Metabolites Using Physiologically Based Pharmacokinetic Modeling. *Pharmaceutics* **2022**, *14*, 2604, DOI: 10.3390/pharmaceutics14122604

5. Supplementary Materials Project V: PBPK Modeling of Quinidine

   Feick, D.; Rüdesheim, S.; Marok, F. Z.; Selzer, D.; Loer, H. L. H.; Teutonico, D.; Frechen, S.; van der Lee, M.; Moes, D. J. A. R.; Swen, J. J.; Schwab, M.; Lehr, T. Physiologically-based pharmacokinetic modeling of quinidine to establish a CYP3A4, P-gp, and CYP2D6 drug-drug-gene interaction network. *CPT: pharmacometrics & systems pharmacology* **2023**, 1–14, DOI: 10.1002/psp4.12981

B.1 PROJECT I: SUPPLEMENTARY MATERIALS

pharmaceutics

MDPI

Supplementary Materials

Physiologically Based Pharmacokinetic Modeling of Metoprolol Enantiomers and α-Hydroxymetoprolol to Describe CYP2D6 Drug-Gene Interactions

Simeon Rüdesheim[1,2], Jan-Georg Wojtyniak[1,2], Dominik Selzer[1], Nina Hanke[1], Felix Mahfoud[3,4], Matthias Schwab[2,5,6], Thorsten Lehr[1], ∗

1 Clinical Pharmacy, Saarland University, 66123 Saarbrücken, Germany; simeon.ruedesheim@uni-saarland.de (S.R.); jangeorg.wojtyniak@uni-saarland.de (J.-G.W.); dominik.selzer@uni-saarland.de (D.S.); n.hanke@mx.uni-saarland.de (N.H.)
2 Dr. Margarete Fischer-Bosch-Institute of Clinical Pharmacology, 70376 Stuttgart, Germany; matthias.schwab@ikp-stuttgart.de
3 Department of Internal Medicine III, Cardiology, Angiology, Intensive Care Medicine, Saarland University Medical Center and Saarland University Faculty of Medicine, 66421 Homburg/Saar, Germany; felix.mahfoud@uks.eu
4 Institute for Medical Engineering and Science, Massachusetts Institute of Technology, 02139 Cambridge, MA, USA
5 Departments of Clinical Pharmacology, Pharmacy and Biochemistry, University Tübingen, 72076 Tübingen, Germany
6 Cluster of Excellence iFIT (EXC2180) "Image-Guided and Functionally Instructed Tumor Therapies", University of Tübingen, 72076 Tübingen, Germany
∗ Correspondence: thorsten.lehr@mx.uni-saarland.de; Tel.: +49-681-302-70255

Received: 10 November 2020; Accepted: 5 December 2020; Published: 11 December 2020

Funding: F.M. is supported by Deutsche Gesellschaft für Kardiologie (DGK), and Deutsche Forschungsgemeinschaft (SFB TRR219). M.S. was supported by by the Robert Bosch Stiftung (Stuttgart, Germany), the European Commission Horizon 2020 UPGx grant 668353, a grant from the German Federal Ministry of Education and Research (BMBF 031L0188D), and the Deutsche Forschungsgemeinschaft (DFG, German Research Foundation) under Germany's Excellence Strategy-EXC 2180—390900677. T.L. was supported by the German Federal Ministry of Education and Research (BMBF, Horizon 2020 INSPIRATION grant 643271), under the frame of ERACoSysMed The APC was funded by the German Research Foundation (DFG) and Saarland University within the funding program "Open Access Publishing".

Conflict of Interest: J.-G.W. is an employee of Boehringer Ingelheim Pharma GmbH & Co. KG. F.M. received scientific support and speaker honoraria from Bayer, Boehringer Ingelheim, Medtronic and ReCor Medical. S.R., N.H., D.S., M.S. and T.L. declare that they have no conflict of interest. The funders had no role in the design of the study; in the collection, analyses, or interpretation of data; in the writing of the manuscript, or in the decision to publish the results.

Pharmaceutics **2020**, *12*, 1200; doi.org/10.3390/pharmaceutics12121200

Contents

Pharmaceutics **2020**, *12*, 1200; doi.org/10.3390/pharmaceutics12121200

S1 Physiologically based pharmacokinetic (PBPK) modeling

S1.1 PBPK model building

S1.1.1 PBPK model building

Physiologically based pharmacokinetic (PBPK) modeling and model parameter optimization (Monte Carlo algorithm) were performed using PK-Sim® and MoBi® (Open Systems Pharmacology Suite 9.1). Published clinical study data were digitized with GetData Graph Digitizer 2.26.0.20 (©S. Fedorov) according to best practices [56]. For calculation of pharmacokinetic parameters and model performance metrics as well as generation of figures Python (version 3.7.4, Python Software Foundation, Wilmington, DE, USA) and Visual Studio Code (version 1.49.1, Microsoft Corporation, Redmond, WA, USA) were used. PBPK model building was initiated with an extensive literature search to gather information on metoprolol absorption, distribution, metabolism and excretion (ADME) processes, to obtain physicochemical data and to collect clinical studies of intravenous and oral administration of metoprolol, in single- and multiple-dose regimens, performed in healthy individuals. Subsequently, plasma concentration-time profiles from the published clinical studies were digitized and split into a training dataset, for model building and a test dataset, for model evaluation (see Table S2.2.1 for information on all studies). Studies for model training were selected to include different routes of administration (intravenous and oral), a wide range of administered doses, single- and multiple-dose regimens as well as stratification for *cytochrome P450 2D6 (CYP2D6)* genotype or activity score. The training dataset was used for estimation of model input parameters which could not be obtained from literature. The final model parameters for metoprolol enantiomers and α-hydroxymetoprolol are provided in Tables S2.3.2 and S2.4.3, respectively. The metoprolol enantiomer PBPK model was built in a stepwise approach; first, appropriate quantitative structure-activity relationship (QSAR) methods to estimate the cellular permeabilities and partition coefficients were selected by minimizing the residual sum of squares of simulations of intravenous metoprolol administration and their observed data. Subsequently, studies of orally administered metoprolol in poor metabolizers (PMs) were used to optimize parameters independent of CYP2D6 metabolism. Finally, *(R)*- and *(S)*-enantiomer CYP2D6 catalytic rate constant (k_{cat}) values were optimized for studies of the training dataset where the volunteers were either normal metabolizers (NMs) or not phenotyped.

Pharmaceutics **2020**, *12*, 1200; doi.org/10.3390/pharmaceutics12121200

S1.1.2 Metoprolol formulations

The weibull function was implemented according to Equations S1 and S2 [28] to describe the dissolution process for different solid metoprolol formulations.

$$m = 1 - \exp\left(\frac{-(t - T_{lag})^{\beta}}{\alpha}\right) \tag{S1}$$

$$\alpha = (T_d)^{\beta} \tag{S2}$$

where m = fraction of dissolved drug at time t, T_{lag} = lag time before the onset of dissolution, α = scale parameter, β = shape parameter, T_d = time needed to dissolve 63% of the formulation.

The final Weibull shape parameters and Weibull time parameters (50% dissolved) for all solid formulations used in the metoprolol PBPK-model are given in Table S2.3.2.

S1.1.3 Virtual individuals

The PBPK model was built based on data from healthy individuals, using the reported sex, ethnicity and mean values for age, weight and height from each study protocol. If no demographic information was provided, the following default values were substituted: male, European, 30 years of age, 73 kg body weight and 176 cm body height (characteristics from the PK-Sim® population database ([35, 49, 52]). CYP2D6 was implemented in accordance with literature, using the PK-Sim® expression database to define their relative expression in the different organs of the body [38]. Details on the implementation of CYP2D6 are summarized in Section S4.

S1.1.4 Virtual populations

For population simulations, virtual populations of 100 individuals were created based on the population characteristics stated in the respective publication. If no information was provided in the publication, populations based on european male individuals aged 20–50 years were assumed. Metrics were generated (depending on ethnicity) from one of the following databases; American: Third National Health and Nutrition Examination Survey (NHANES) [35] database, Asian: Tanaka model [49], European: International Commission on Radiological Protection (ICRP) database [52]. In the generated virtual populations, system-dependent parameters such as weight, height, organ volumes, blood flow rates, tissue compositions, etc. were varied by the implemented algorithm in PK-Sim® within the limits of the databases listed above [35, 49, 52]. Since study populations were grouped by their CYP2D6 activity score or phenotype, no variability in CYP2D6 reference concentrations was assumed for population simulations. Reference concentrations of implemented proteins as well as their relative expression are provided in Section S4.

Pharmaceutics **2020**, *12*, 1200; doi.org/10.3390/pharmaceutics12121200

S1.2 PBPK model evaluation

S1.2.1 PBPK model evaluation

Model evaluation was carried out with different methods based on the clinical data of the test dataset. The population predicted plasma concentration-time profiles were compared to the data observed in the clinical studies. Furthermore, predicted plasma concentration values of all studies were compared to the observed plasma concentrations in goodness-of-fit plots. In addition, the model performance was evaluated by comparison of predicted to observed area under the plasma concentration-time curve (AUC) from the time of the first concentration measurement to the last time point of concentration measurement (AUC_{last}) and peak plasma concentration (C_{max}) values. As quantitative performance measures, a mean relative deviation (MRD) of the predicted plasma concentrations for all observed and the corresponding predicted plasma concentrations as well as geometric mean fold errors (GMFEs) of the AUC_{last} and C_{max} values were calculated according to Equation S3 and Equation S4, respectively.

$$\mathrm{MRD} = 10^x;\ x = \sqrt{\frac{\sum_{i=1}^{k}(\log_{10}\hat{c}_i - \log_{10} c_i)^2}{k}} \tag{S3}$$

where $\hat{c}_i$ = ith predicted plasma concentration, c_i = ith observed plasma concentration and k = number of observed values.

$$\mathrm{GMFE} = 10^x;\ x = \frac{\sum_{i=1}^{m}\left|\log_{10}\left(\frac{\hat{\rho}_i}{\rho_i}\right)\right|}{m} \tag{S4}$$

where $\hat{\rho}_i$ = ith predicted plasma AUC_{last} or C_{max} value, ρ_i = ith observed plasma AUC_{last} or C_{max} value and m = number of studies.

S1.2.2 PBPK model sensitivity analysis

Sensitivity of the final models to single parameter changes (local sensitivity analysis) was calculated as relative change of the $AUC_{0–24}$. Sensitivity analysis was carried out using a relative perturbation of 1000% (variation range 10.0, maximum number of 9 steps). Parameters were included into the analysis if they have been optimized, if they are associated with optimized parameters or if they might have a strong impact due to calculation methods used in the model. Sensitivity to a parameter was calculated as the ratio of the relative change of the simulated $AUC_{0–24\,h}$ to the relative variation of the parameter according to Equation S5:

$$S = \frac{\Delta AUC_{0-24\ h}}{\Delta p} \times \frac{p}{AUC_{0-24\ h}} \tag{S5}$$

where S = sensitivity of the AUC to the examined model parameter, $\Delta AUC_{0-24\ h}$ = change of the $AUC_{0–24\,h}$, $AUC_{0-24\ h}$ = simulated $AUC_{0–24\,h}$ with the original parameter value, Δp = change of the examined parameter value, p = original parameter value.

Pharmaceutics **2020**, *12*, 1200; doi.org/10.3390/pharmaceutics12121200

A sensitivity of +1.0 signifies that a 10% increase of the examined parameter value causes a 10% increase of the simulated $AUC_{0–24\,h}$. The results of the sensitivity analysis are provided in Section S2.6.7

S1.3 CYP2D6 DGI Modeling

S1.3.1 Implementation of CYP2D6 DGI

The model training dataset included 11 plasma concentration-time profiles from studies that reported the CYP2D6 activity scores of their study subjects, ranging from 0 (PM) to 3 (ultrarapid metabolizer (UM)). These studies were utilized to optimize catalytic rate constant relative to CYP2D6 activity score (AS)=2 ($k_{cat,\,rel}$) values for the different CYP2D6 activity scores. CYP2D6 poor metabolizers (AS=0) were assumed to show no CYP2D6 activity (0%), whereas populations with two wildtype alleles (AS=2) were used as reference (100%) to calculate relative k_{cat} values according to Equation S6:

$$k_{cat,\,rel,\,AS=i} = \frac{k_{cat,\,AS=i}}{k_{cat,\,AS=2}} \cdot 100\% \tag{S6}$$

where $k_{cat,\,rel}$ = k_{cat} relative to AS=2 for the investigated AS, $k_{cat,\,AS=i}$ = k_{cat} for the investigated AS and $k_{cat,\,AS=2}$ = k_{cat} for AS = 2.

The identified values for both CYP2D6 pathways and both metoprolol enantiomers are listed in Table S3.1.1. CYP2D6 Michaelis-Menten constant (K_m) values were kept constant over the whole range of modeled activity scores. Since study populations were grouped by their CYP2D6 activity score or phenotype, no variability in CYP2D6 reference concentrations was implemented for population simulations (see Section S4 for details on the implementation of CYP2D6).

S1.3.2 DGI Model Evaluation

The drug-gene interaction (DGI) modeling performance was assessed by comparison of predicted versus observed plasma concentration-time profiles of racemic metoprolol, its enantiomers and α-hydroxymetoprolol (see Chapter S3). Furthermore, predicted DGI AUC_{last} ratios (Equation S7) and DGI C_{max} ratios (Equation S8) were evaluated.

$$DGI\ AUC_{last}\ ratio = \frac{AUC_{last,\,DGI}}{AUC_{last,\,reference}} \tag{S7}$$

where $AUC_{last,\,DGI}$ = AUC_{last} of variant activity score or phenotype, $AUC_{last,\,reference}$ = AUC_{last} of AS=2 or normal metabolizer phenotype.

$$DGI\ C_{max}\ ratio = \frac{C_{max,\,DGI}}{C_{max,\,reference}} \tag{S8}$$

Pharmaceutics **2020**, *12*, 1200; doi.org/10.3390/pharmaceutics12121200

where $C_{max,\ DGI}$ = C_{max} of variant activity score or phenotype, $C_{max,\ reference}$ = C_{max} of AS=2 or normal metabolizer phenotype. As a quantitative measure of the prediction accuracy, GMFE values of the predicted DGI AUC_{last} ratios and DGI C_{max} ratios were calculated according to Equation S4 and are given in Table S3.3.2.

Pharmaceutics **2020**, *12*, 1200; doi.org/10.3390/pharmaceutics12121200

S2 PBPK modeling of metoprolol

S2.1 Metoprolol model development

Metoprolol is the most frequently administered beta-blocker in the U.S. with well over 50 million total prescriptions per year [10]. It is used in the treatment of hypertension, angina pectoris, heart failure, arterial fibrillation as well as acute myocardial infarction [36]. Metoprolol is listed by the U. S. Food and Drug Administration (FDA) as a moderately sensitive substrate for clinical drug-drug interaction (DDI) studies as it is predominantly metabolized by CYP2D6 [51]. Metoprolol is a Biopharmaceutics Classification System (BCS) Class I drug, characterized by high permeability and high solubility. After its rapid absorption, metoprolol undergoes extensive first-pass metabolism, reducing its bioavailability (BA) to 40% in CYP2D6 NMs, whereas BA approaches 100% in PMs [25]. Only 12% of metoprolol are bound to plasma proteins, primarily albumin [40]. *O*-demethylation, α-hydroxylation and *N*-dealkylation by CYP2D6 and, to lesser extents CYP2B6, CYP2C9, CYP3A4 are described as the pathways of metoprolol metabolism [5, 42]. Of the major metabolites, α-hydroxymetoprolol is of particular clinical interest, as it is pharmacologically active, exhibiting 10% of the β_1-blocking activity of metoprolol [8], and it is almost exclusively formed via CYP2D6 [29]. Therefore, α-hydroxymetoprolol/metoprolol urinary metabolic ratios are employed for CYP2D6 phenotyping [7]. Overall, CYP2D6 is estimated to be responsible for 80% of metoprolol metabolism in normal metabolizers [5]. Depending on the CYP2D6 phenotype, only 1.5–12% of orally administered metoprolol are excreted unchanged in urine [46]. Metoprolol is a chiral molecule, marketed as racemic mixture of (*R*)- and (*S*)-metoprolol, even though its enantiomers differ in their pharmacodynamic and pharmacokinetic properties. The (*S*)-enantiomer has been shown to be 33-fold more potent in blocking β_1-adrenoceptors in rats than the (*R*)-enantiomer [34]. Moreover, in UMs and NMs but not in PMs, the (*S*)-metoprolol AUC is significantly higher than the AUC of (*R*)-metoprolol, showing the enantiopreference of CYP2D6 towards the (*R*)-enantiomer [46].

A total of 48 clinical studies of intravenous or oral administration of metoprolol were used in the model development process, with doses ranging from 5–200 mg metoprolol in single or multiple dose regimens. Of the 48 studies, nine included measurements of the metabolite α-hydroxymetoprolol and 16 studies included measurements of the metoprolol enantiomers. Details on all studies used for PBPK modeling are given in Table S2.2.1. The four α-hydroxymetoprolol diastereomers were modeled as one single compound, due to a lack of enantiomeric differentiation in the published clinical data. For both metoprolol enantiomers, enantioselective metabolism via CYP2D6, an unspecific hepatic clearance (CL) process as well as passive glomerular filtration were implemented. Each of the metoprolol enantiomers can be metabolized via CYP2D6 to either produce α-hydroxymetoprolol or to generate other metabolites such as *O*-

Pharmaceutics **2020**, *12*, 1200; doi.org/10.3390/pharmaceutics12121200

demethylmetoprolol which were not included as separately modeled compounds. The metabolite α-hydroxymetoprolol is eliminated via an unspecific hepatic CL process. The drug-dependent model input parameters of the metoprolol enantiomers are presented in Table S2.3.2; the drug-dependent parameters of the α-hydroxymetoprolol model are given in S2.4.3.

The performance of the metoprolol model is demonstrated in semilogarithmic (Section S2.5.1) and linear plots (Section S2.5.2) of population simulations compared to observed plasma concentration-time profiles of all clinical studies. Furthermore, goodness-of-fit plots comparing all predicted to their corresponding observed plasma concentrations of metoprolol enantiomers, racemic metoprolol and α-hydroxymetoprolol (Figures S2.6.9 and S2.6.10) as well as MRD values for each study (see Tables S2.6.4 and S2.6.5) are presented. Moreover, correlation plots of predicted versus observed AUC_{last} (Figures S2.6.11 and S2.6.12) and C_{max} (Figures S2.6.13 and S2.6.14) values are shown, including calculated model GMFE values (Tables S2.6.6 and S2.6.7). Finally, a sensitivity analysis of a simulation of a single oral dose of 100 mg metoprolol tartrate, administered as a tablet in the fasted state was performed. The results of the sensitivity analysis are given in Section S2.6.7.

Pharmaceutics **2020**, *12*, 1200; doi:10.3390/pharmaceutics12121200

S2.2 Clinical studies

Table S2.2.1: Metoprolol study table

Route	Dose [mg]	n	Females [%]	Age [years]	Weight [kg]	Metabolite measured	Enantiomers measured	CYP2D6 activity	Dataset	Reference
iv (inf, 150 min, sd)	88.7	6	17	(23–29)	-	yes	no	-	test	Godbillon et al. 1985 [12]
iv (inf, 10 min, sd)	50	12	0	(19–26)	(60–98)	no	no	-	training	Kelly et al. 1985 [23]
iv (inf, 10 min, sd)	20	5	0	(23–28)	(62–70)	no	no	-	test	Johnsson et al. 1975 [22]
iv (inf, 10 min, sd)	15	5	0	(23–28)	(62–70)	no	no	-	test	Johnsson et al. 1975 [22]
iv (inf, 10 min, sd)	10	5	0	(23–28)	(62–70)	no	no	-	test	Johnsson et al. 1975 [22]
iv (inf, 5 min, sd)	10	6	0	(23–28)	-	no	no	-	test	Regårdh et al. 1980 [42]
iv (inf, 10 min, sd)	5	5	0	(23–28)	(62–70)	no	no	-	training	Regårdh et al. 1974 [41]
iv (inf, 10 min, sd)	5	5	0	(23–28)	(62–70)	no	no	-	test	Johnsson et al. 1975 [22]
po (tab, CR, daily)	200	15	27	(21–45)	-	no	no	-	training	Damy et al. 2004 [11]
po (tab, sd)	200	10	0	29 (24–40)	85	no	yes	p-NM	training	Johnson et al. 1996 a [20]
po (tab, sd)	200	10	0	29 (24–36)	82	no	yes	p-NM	training	Johnson et al. 1996 b [20]
po (tab, CR, sd)	200	15	27	(21–45)	-	no	yes	AS=1.5*	test	Parker et al. 2011 [39]
po (tab, sd)	100	4	0	-	-	yes	no	AS=2.0*	test	Bae et al. 2014 [3]
po (tab, sd)	100	3	0	-	-	yes	no	AS=0.5*	test	Bae et al. 2014 [3]
po (-, sd)	100	12	0	28 (21–35)	71 (62–82)	no	no	-	test	Bennett et al. 1982 [4]
po (tab, sd)	100	12	50	(22–34)	-	no	no	-	test	Chellingsworth et al. 1988 [9]
po (tab, bid)	100	12	0	(23–32)	-	no	no	-	test	Chellingsworth et al. 1988 [9]
po (tab, sd)	100	10	0	26 (20–36)	73 (59–96)	no	no	p-NM	test	Hamelin et al. 2000 [14]
po (tab, sd)	100	6	0	26 (20–36)	73 (59–96)	no	no	p-PM	test	Hamelin et al. 2000 [14]
po (tab, sd)	100	8	0	(20–29)	-	no	yes	g-NM	test	Hemeryck et al. 2000 [15]
po (tab, sd)	100	7	43	52 (29–68)	-	no	no	-	test	Houtzagers et al. 1982 [16]
po (tab, sd)	100	15	0	(19–23)	-	no	no	-	test	Jack et al. 1982 [18]

*: AS calculated from genotype provided in publication, AS: CYP2D6 activity score, bid: twice daily, CR: controlled release, g-: genotyped, inf: infusion, iv: intravenous, NM: normal metabolizer, p-: phenotyped, PM: poor metabolizer, po: oral, sd: single dose, sol: oral solution, tab: tablet
Values are given as arithmetic means, the range of values are given in parentheses

Pharmaceutics **2020**, *12*, 1200; doi.org/10.3390/pharmaceutics12121200

Table S2.2.1: Metoprolol study table *(continued)*

Route	Dose [mg]	n	Females [%]	Age [years]	Weight [kg]	Metabolite measured	Enantiomers measured	CYP2D6 activity	Dataset	Reference
po (tab, sd)	100	5	0	(23–28)	(62–70)	no	no	-	test	Johnsson et al. 1975 [22]
po (tab, sd)	100	16	0	25	65	no	yes	AS=2*	training	Huang et al. 1999 [17]
po (tab, sd)	100	12	0	24	65	no	yes	AS=1.25*	training	Huang et al. 1999 [17]
po (tab, sd)	100	12	0	24	63	no	yes	AS=0.5*	training	Huang et al. 1999 [17]
po (tab, sd)	100	6	22	23	67	yes	no	AS=2*	training	Jin et al. 2008 [19]
po (tab, sd)	100	7	22	23	67	yes	no	AS=1.25*	training	Jin et al. 2008 [19]
po (tab, sd)	100	15	22	23	67	yes	no	AS=0.5*	training	Jin et al. 2008 [19]
po (-, sd)	100	12	0	(19–26)	(60–98)	no	no	-	training	Kelly et al. 1985 [23]
po (-, bid)	100	12	0	(19–26)	(60–98)	no	no	-	training	Kelly et al. 1985 [23]
po (tab, sd)	100	18	0	29 (18–39)	79 (62–100)	yes	no	g-NM	test	Krösser et al. 2006 [27]
po (-, sd)	100	12	0	33 (19–55)	-	yes	no	g-NM	test	Krauwinkel et al. 2013 [28]
po (tab, bid)	100	10	0	26 (20–36)	84 (66–97)	no	yes	p-NM	test	Luzier et al. 1999 a [30]
po (tab, bid)	100	10	100	25 (21–35)	62 (54–77)	no	yes	p-NM	test	Luzier et al. 1999 b [30]
po (tab, bid)	100	15	27	(21–45)	-	no	yes	AS=1.5*	test	Parker et al. 2011 [39]
po (tab, CR, sd)	100	15	27	(21–45)	-	no	yes	AS=1.5*	test	Parker et al. 2011 [39]
po (tab, sd)	100	12	8	28 (25–37)	76 (70–80)	no	yes	AS=3	training	Seeringer et al. 2008 [25,26]
po (tab, sd)	100	13	0	28 (23–34)	77 (69–81)	no	yes	AS=2	training	Seeringer et al. 2008 [25,26]
po (tab, sd)	100	4	0	38 (29–40)	90 (77–101)	no	yes	AS=0	training	Seeringer et al. 2008 [25,26]
po (tab, sd)	100	16	100	27 (18–40)	60 (49–100)	no	yes	AS=1.5*	training	Sharma et al. 2005 [47]
po (-, sd)	100	4	100	27 (18–40)	60 (49–100)	no	yes	AS=0	training	Sharma et al. 2005 [47]
po (tab, sd)	50	5	0	(23–28)	(62–70)	no	no	-	test	Johnsson et al. 1975 [22]
po (-, sd)	50	10	0	28 (18–45)	82 (63–94)	no	no	-	test	Stout et al. 2011 [48]
po (tab, CR, sd)	50	10	0	28 (18–45)	82 (63–94)	no	no	-	test	Stout et al. 2011 [48]
po (tab, sd)	50	12	0	31	78	yes	no	AS=1.5*	test	Werner et al. 2003 [54]
po (tab, sd)	20	5	0	(23–28)	(62–70)	no	no	-	test	Johnsson et al. 1975 [22]
po (sol, sd)	5	5	0	(23–28)	(62–70)	no	no	-	training	Regårdh et al. 1974 [41]

*: AS calculated from genotype provided in publication, AS: CYP2D6 activity score, bid: twice daily, CR: controlled release, g-: genotyped, inf: infusion, iv: intravenous, NM: normal metabolizer, p-: phenotyped, PM: poor metabolizer, po: oral, sd: single dose, sol: oral solution, tab: tablet
Values are given as arithmetic means, the range of values are given in parentheses

Pharmaceutics **2020**, *12*, 1200; doi.org/10.3390/pharmaceutics12121200

S2.3 Drug-dependent parameters: (*R*)- and (*S*)-metoprolol

Table S2.3.2: (*R*)- and (*S*)-metoprolol drug-dependent parameters

		(*R*)-Metoprolol				(*S*)-Metoprolol				
Parameter	Unit	Value	Source	Literature	Reference	Value	Source	Literature	Reference	Description
MW	g/mol	267.36	Lit.	267.36	[24]	267.36	Lit.	267.36	[24]	Molecular weight
pKa (base)	-	9.70	Lit.	9.70	[24]	9.70	Lit.	9.70	[24]	Acid dissociation constant
Solubility tart. (pH 7.4)	g/ml	1.00	Lit.	1.00	[2]	1.00	Lit.	1.00	[2]	Solubility
Solubility succ. (pH 5.5)	g/ml	0.16	Lit.	0.16	[6]	0.16	Lit.	0.16	[6]	Solubility
logP	-	1.77	Lit.	1.77	[57]	1.77	Lit.	1.77	[57]	Lipophilicity
f_u	%	88	Lit.	88	[32]	88	Lit.	88	[32]	Fraction unbound
CYP2D6 $K_m \rightarrow \alpha$HM	µmol/l	10.08	Lit.	10.08‡	[33]	10.75	Lit.	10.75‡	[33]	Michaelis-Menten constant
CYP2D6 $k_{cat}{}^{NM} \rightarrow \alpha$HM	1/min	6.02	Optim.†	7.50	[33]	6.55	Optim.†	8.27	[33]	Catalytic rate constant
CYP2D6 $k_{cat}{}^{AS=2} \rightarrow \alpha$HM	1/min	10.17	Optim.†	-	-	11.19	Optim.†	-	-	Catalytic rate constant
CYP2D6 $K_m \rightarrow$ ODM	µmol/l	8.82	Lit.	8.82‡	[33]	12.43	Lit.	12.43‡	[33]	Michaelis-Menten constant
CYP2D6 $k_{cat}{}^{NM} \rightarrow$ ODM	1/min	9.87	Optim.†	12.30	[33]	8.21	Optim.†	10.37	[33]	Catalytic rate constant
CYP2D6 $k_{cat}{}^{AS=2} \rightarrow$ ODM	1/min	16.69	Optim.†	-	-	14.02	Optim.†	-	-	Catalytic rate constant
$CL_{hep,\ unsp.}$	1/min	0.08	Optim.	-	-	0.09	Optim.	-	-	Unspecific hepatic clearance
GFR fraction	-	1.00	Asm.	-	-	1.00	Asm.	-	-	Filtered drug in the urine
EHC continuous fraction	-	1.00	Asm.	-	-	1.00	Asm.	-	-	Bile fraction cont. released
NR Weibull time parameter	min	12.31	Optim.	-	[20, 23]	12.31	Optim.	-	[20, 23]	Dissolution profile time
NR Weibull shape parameter	-	0.72	Optim.	-	[20, 23]	0.72	Optim.	-	[20, 23]	Dissolution profile shape
CR Weibull time parameter	min	331.92	Optim.	-	[11]	331.92	Optim.	-	[11]	Dissolution profile time
CR Weibull shape parameter	-	1.53	Optim.	-	[11]	1.53	Optim.	-	[11]	Dissolution profile shape
Partition coefficients	-	Diverse	Calc.	R&R	[43, 44]	Diverse	Calc.	R&R	[43, 44]	Cell to plasma partitioning
Cellular permeability	cm/min	4.64E-03	Calc.	PK-Sim	[37]	4.64E-03	Calc.	PK-Sim	[37]	Perm. into cellular space
Intestinal permeability	cm/min	4.14E-05	Optim.	1.12E-05	Calc. [50]	4.14E-05	Optim.	1.12E-05	Calc. [50]	Transcellular intestinal perm.

-: not available, †: all CYP2D6 k_{cat} values were optimized in a fixed ratio ($k_{cat} \rightarrow \alpha$HM:$k_{cat} \rightarrow$ ODM) equivalent to the ratio of reported v_{max} values [33].
‡: in vitro values corrected for binding in the assay using estimated fraction unbound to microsomal protein ($fu_{mic,\ estimated}$ = 84%) [1], αHM: α-hydroxylation,
asm.: assumed, CR: controlled release release tablet, calc.: calculated, cont.: continously, CYP2D6: cytochrome P450 2D6, EHC: enterohepatic circulation, lit.: literature,
GFR: glomerular filtration rate, NR: normal release tablet, NM: normal metabolizer, ODM: *O*-demethylation, optim.: optimized, PK-Sim: PK-Sim calculation method,
R&R: Rodgers and Rowland calculation method, succ.: metoprolol succinate, tart.: metoprolol tartrate, unsp.: unspecific

Pharmaceutics ***2020***, *12*, 1200; doi.org/10.3390/pharmaceutics12121200

S2.4 Drug-dependent parameters: α-hydroxymetoprolol

Table S2.4.3: α-hydroxymetoprolol drug-dependent parameters

Parameter	Unit	Value	Source	Literature	Reference	Description
MW	g/mol	283.36	Lit.	283.36	[24]	Molecular weight
pKa (strongest basic)	-	9.67	Lit.	9.67	[55]	Acid dissociation constant
pKa (strongest acidic)	-	13.55	Lit.	13.55	[55]	Acid dissociation constant
Solubility	g/ml	1.43	Lit.	1.43	[55]	Solubility
logP	-	0.87	Optim.	0.84	[55]	Lipophilicity
f_u	%	63	Calc.	63	[53]	Fraction unbound
$CL_{hep,\ unsp.}$	1/min	0.34	Optim.	-	-	Unspecific hepatic clearance
GFR fraction	-	1.00	Asm.	-	-	Filtered drug in the urine
EHC continuous fraction	-	1.00	Asm.	-	-	Bile fraction cont. released
Partition coefficients	-	Diverse	Calc.	R&R	[43, 44]	Cell to plasma partitioning
Cellular permeability	cm/min	4.08E-04	Calc.	PK-Sim	[37]	Perm. into the cellular space
Intestinal permeability	cm/min	1.08E-06	Calc.	1.08E-06	Calc. [50]	Transcellular intestinal perm.

-: not available, calc.: calculated, cont.: continuously, EHC: enterohepatic circulation, intest.: intestinal,
GFR: glomerular filtration rate, perm.: permeability, PK-Sim: PK-Sim calculation method,
R&R: Rodgers and Rowland calculation method, unsp.: unspecific

Pharmaceutics ***2020***, *12*, 1200; doi.org/10.3390/pharmaceutics12121200

S2.5 Plasma profiles

S2.5.1 Semilogarithmic plots

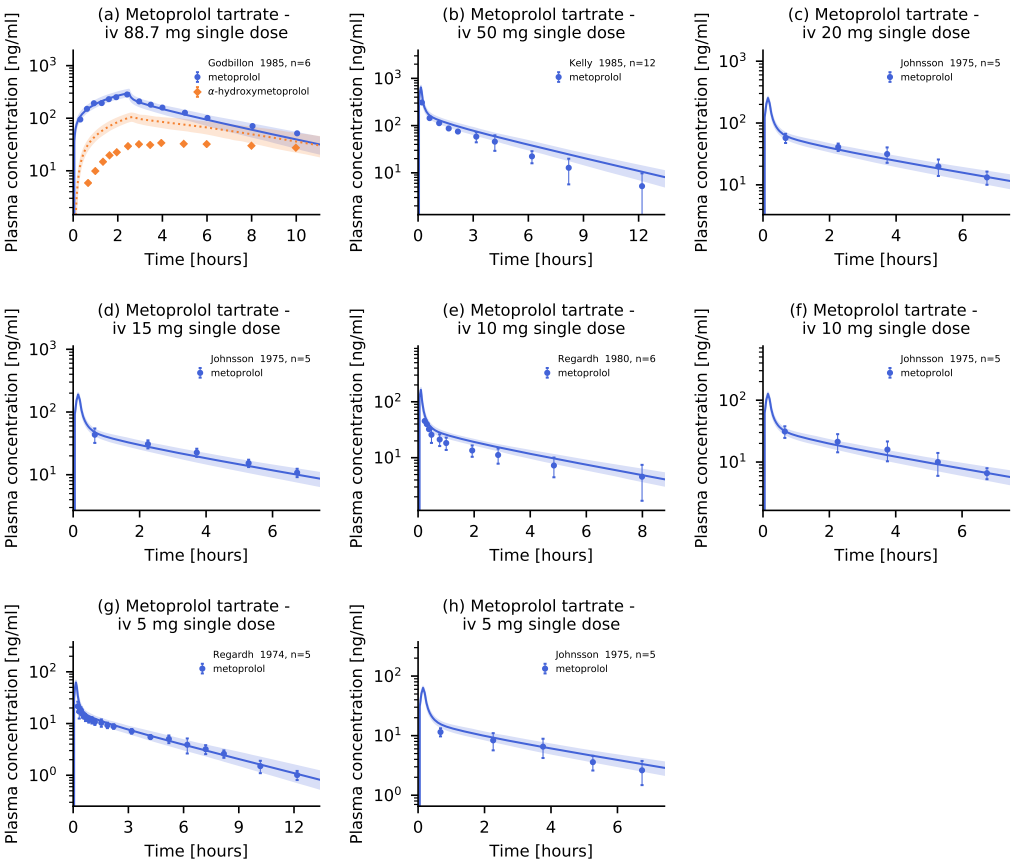

Figure S2.5.1: Metoprolol plasma concentrations. Model predictions of metoprolol and its metabolite α-hydroxymetoprolol plasma concentration-time profiles of intravenous studies of the training and test datasets, compared to observed data (semilogarithmic representation). Population predictions (n=100) are shown as lines with ribbons (arithmetic mean $\pm$ standard deviation (SD)), symbols represent the corresponding observed data $\pm$ SD. iv: intravenous

Pharmaceutics ***2020***, *12*, 1200; doi.org/10.3390/pharmaceutics12121200

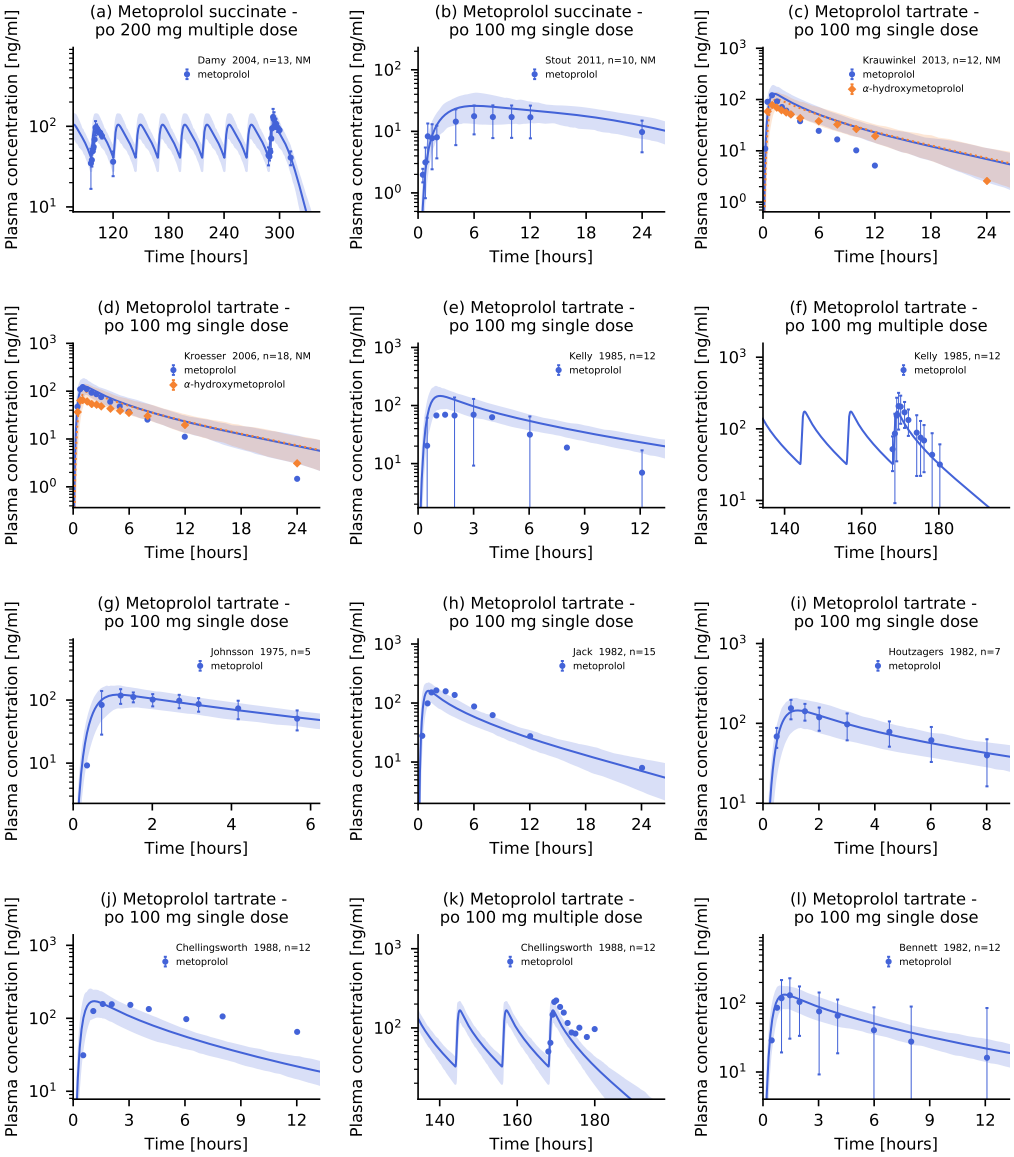

Figure S2.5.2: Metoprolol plasma concentrations. Model predictions of metoprolol and its metabolite α-hydroxymetoprolol plasma concentration-time profiles of oral studies of the training and test datasets, compared to observed data (semilogarithmic representation). Population predictions (n=100) are shown as lines with ribbons (arithmetic mean $\pm$ standard deviation (SD)), symbols represent the corresponding observed data $\pm$ SD. NM: normal metabolizer, po: oral

Pharmaceutics ***2020***, *12*, 1200; doi.org/10.3390/pharmaceutics12121200

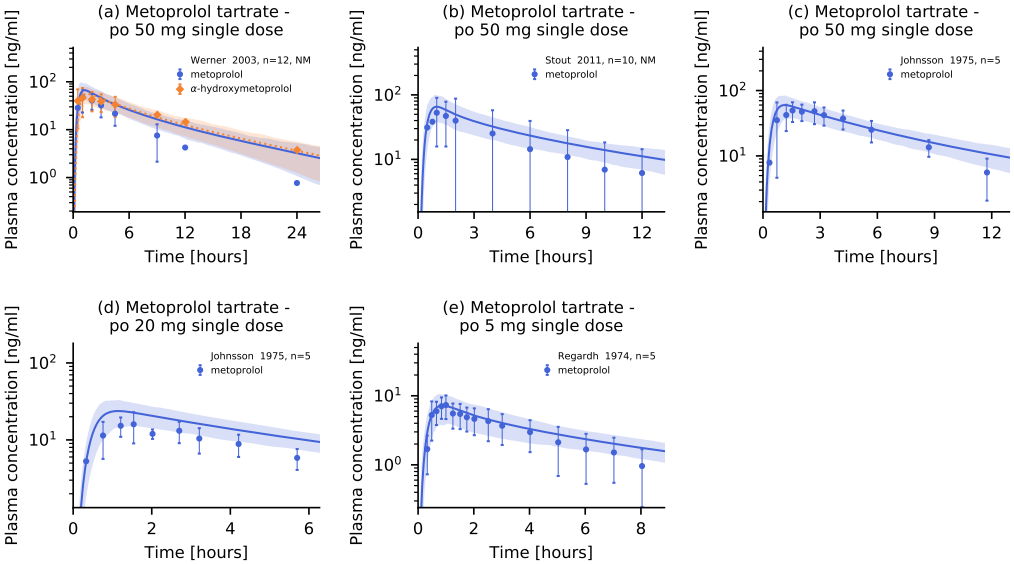

Figure S2.5.3: Metoprolol plasma concentrations. Model predictions of metoprolol and its metabolite α-hydroxymetoprolol plasma concentration-time profiles of oral studies of the training and test datasets, compared to observed data (semilogarithmic representation). Population predictions (n=100) are shown as lines with ribbons (arithmetic mean $\pm$ standard deviation (SD)), symbols represent the corresponding observed data $\pm$ SD. NM: normal metabolizer, po: oral

Pharmaceutics ***2020***, *12*, 1200; doi.org/10.3390/pharmaceutics12121200

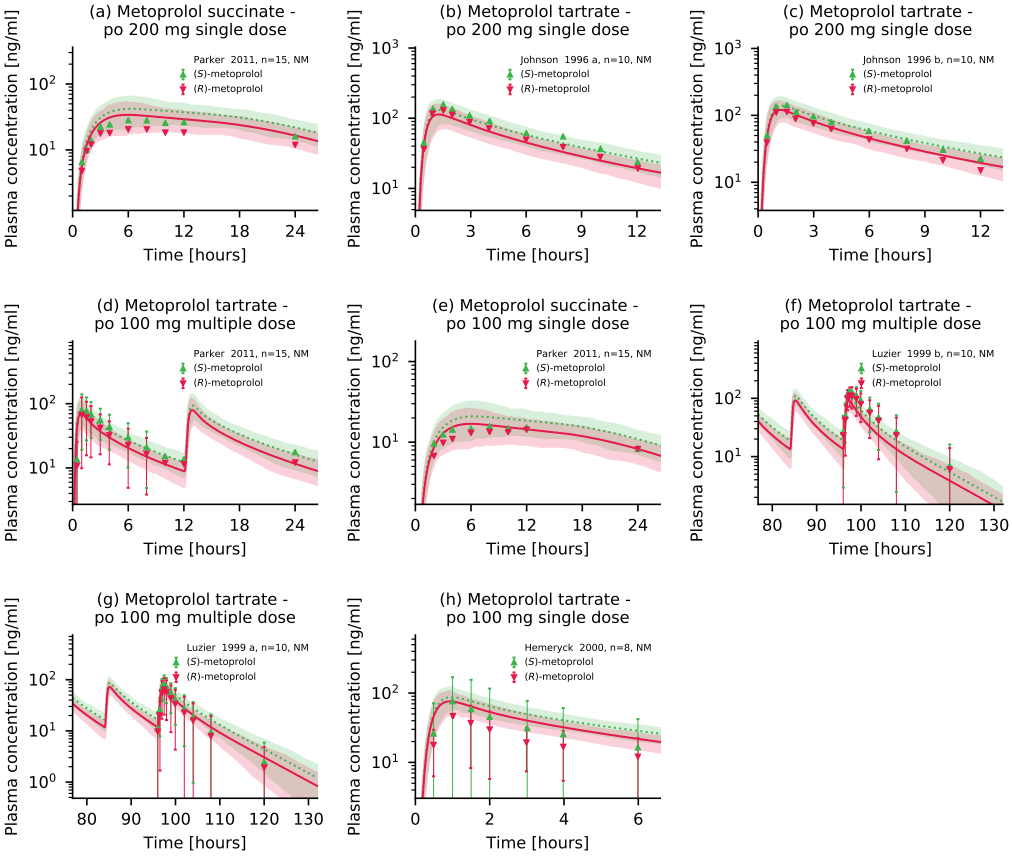

Figure S2.5.4: Metoprolol enantiomers plasma concentrations. Model predictions of *(R)*-metoprolol and *(S)*-metoprolol plasma concentration-time profiles of oral studies of the training and test datasets, compared to observed data (semilogarithmic representation). Population predictions (n=100) are shown as lines with ribbons (arithmetic mean ± standard deviation (SD)), symbols represent the corresponding observed data ± SD. NM: normal metabolizer, po: oral

Pharmaceutics **2020**, *12*, 1200; doi.org/10.3390/pharmaceutics12121200

S2.5.2 Linear plots

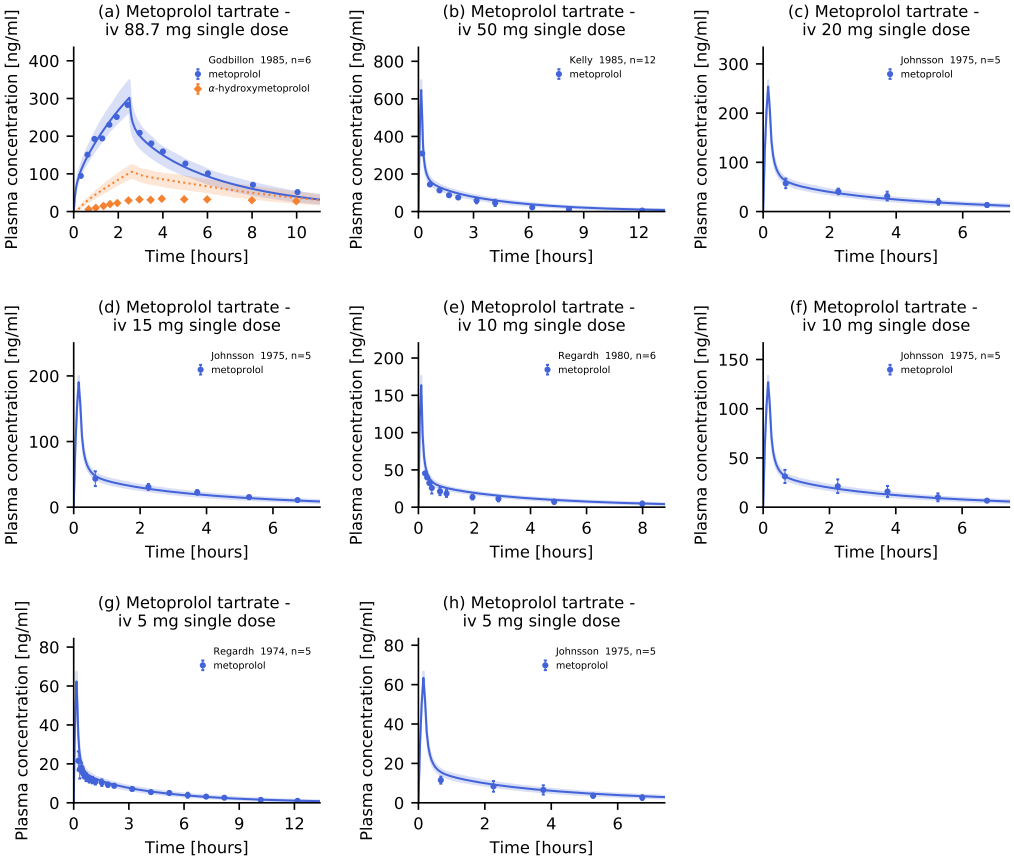

Figure S2.5.5: Metoprolol plasma concentrations. Model predictions of metoprolol and its metabolite α-hydroxymetoprolol plasma concentration-time profiles of intravenous studies of the training and test datasets, compared to observed data (linear representation). Population predictions (n=100) are shown as lines with ribbons (arithmetic mean $\pm$ standard deviation (SD)), symbols represent the corresponding observed data $\pm$ SD. iv: intravenous

Pharmaceutics **2020**, *12*, 1200; doi.org/10.3390/pharmaceutics12121200

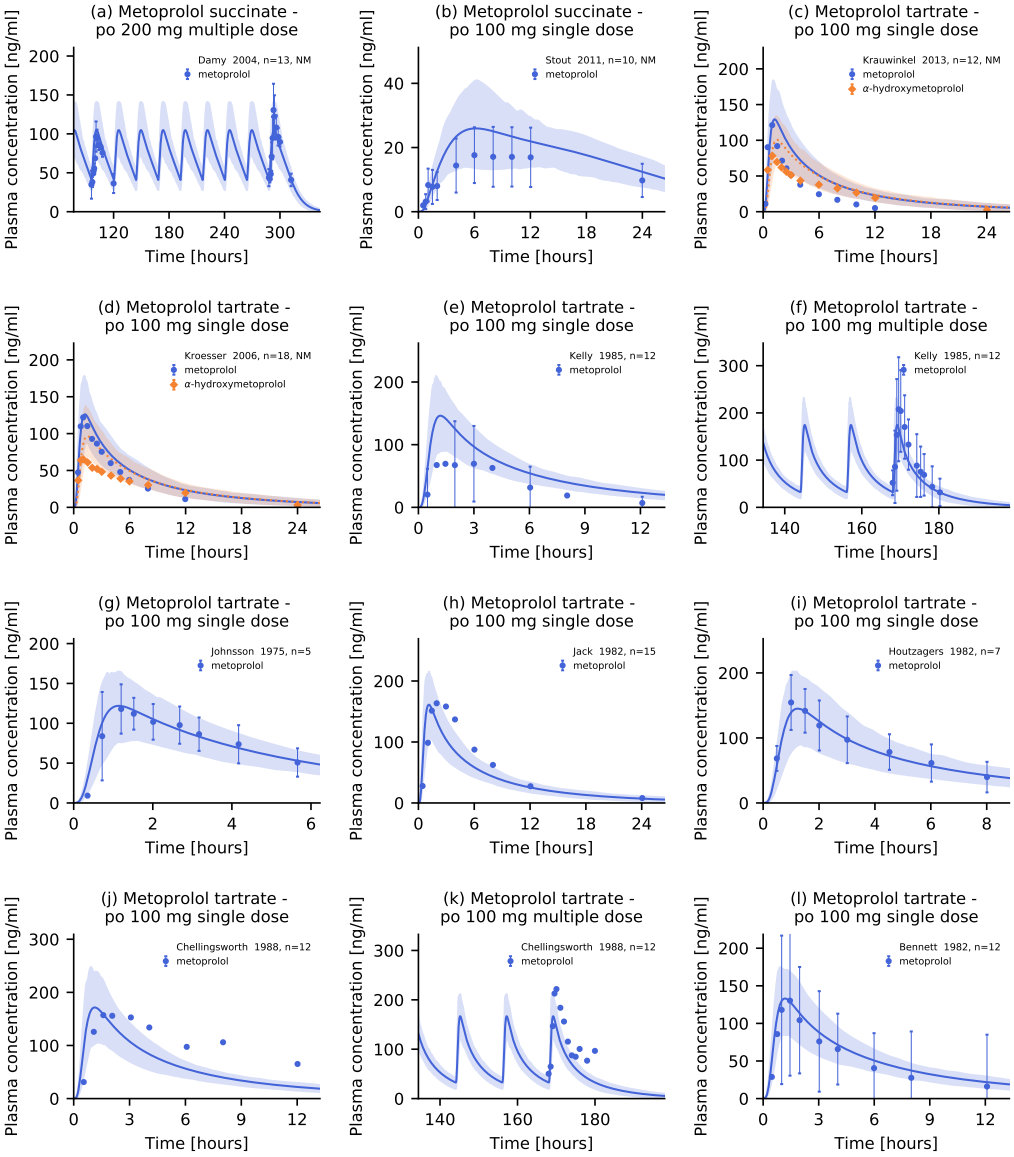

Figure S2.5.6: Metoprolol plasma concentrations. Model predictions of metoprolol and its metabolite α-hydroxymetoprolol plasma concentration-time profiles of oral studies of the training and test datasets, compared to observed data (linear representation). Population predictions (n=100) are shown as lines with ribbons (arithmetic mean $\pm$ standard deviation (SD)), symbols represent the corresponding observed data $\pm$ SD. NM: normal metabolizer, po: oral

Pharmaceutics ***2020***, *12*, 1200; doi.org/10.3390/pharmaceutics12121200

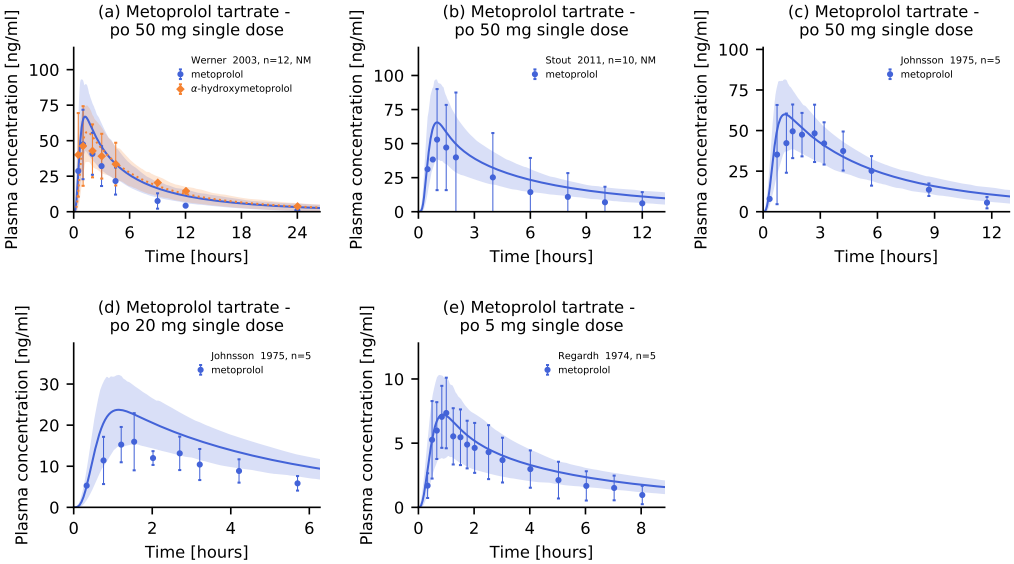

Figure S2.5.7: Metoprolol plasma concentrations. Model predictions of metoprolol and its metabolite α-hydroxymetoprolol plasma concentration-time profiles of oral studies of the training and test datasets, compared to observed data (linear representation). Population predictions (n=100) are shown as lines with ribbons (arithmetic mean $\pm$ standard deviation (SD)), symbols represent the corresponding observed data $\pm$ SD. NM: normal metabolizer, po: oral

Pharmaceutics ***2020***, *12*, 1200; doi.org/10.3390/pharmaceutics12121200

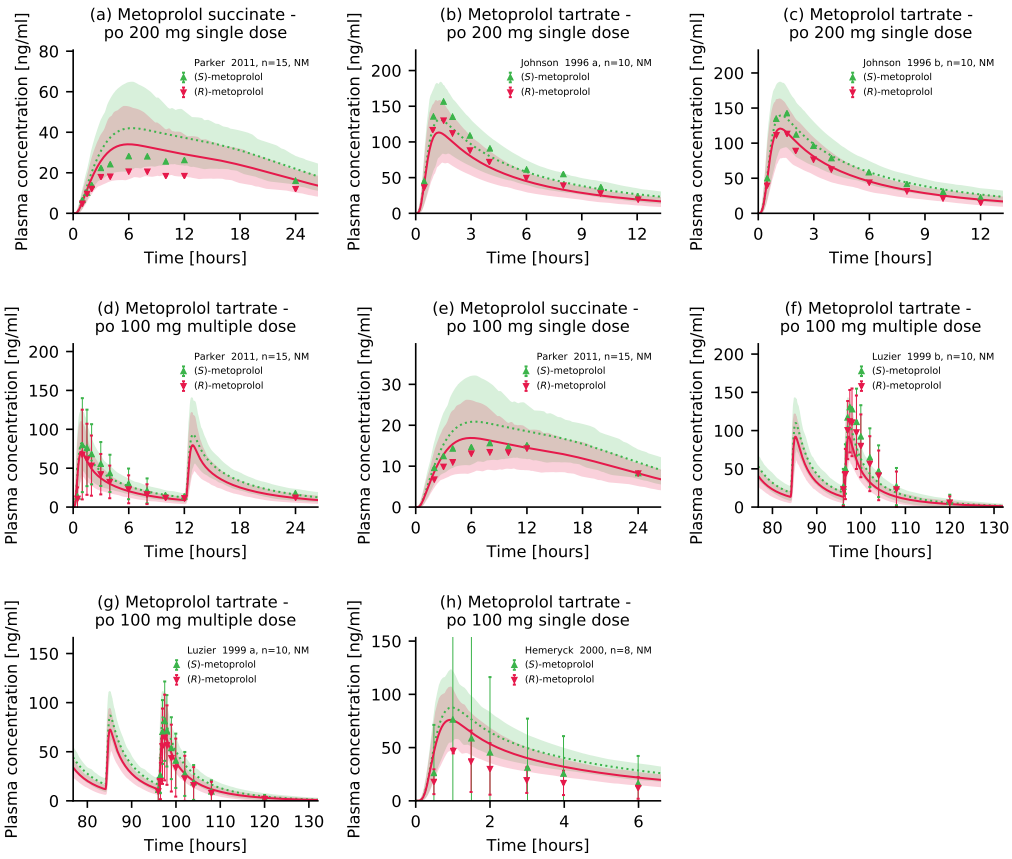

Figure S2.5.8: Metoprolol enantiomers plasma concentrations. Model predictions of *(R)*-metoprolol and *(S)*-metoprolol plasma concentration-time profiles of oral studies of the training and test datasets, compared to observed data (linear representation). Population predictions (n=100) are shown as lines with ribbons (arithmetic mean ± standard deviation (SD)), symbols represent the corresponding observed data ± SD. NM: normal metabolizer, po: oral

Pharmaceutics ***2020***, *12*, 1200; doi.org/10.3390/pharmaceutics12121200

S2.6 Model evaluation

S2.6.1 Plasma concentrations goodness-of-fit plots

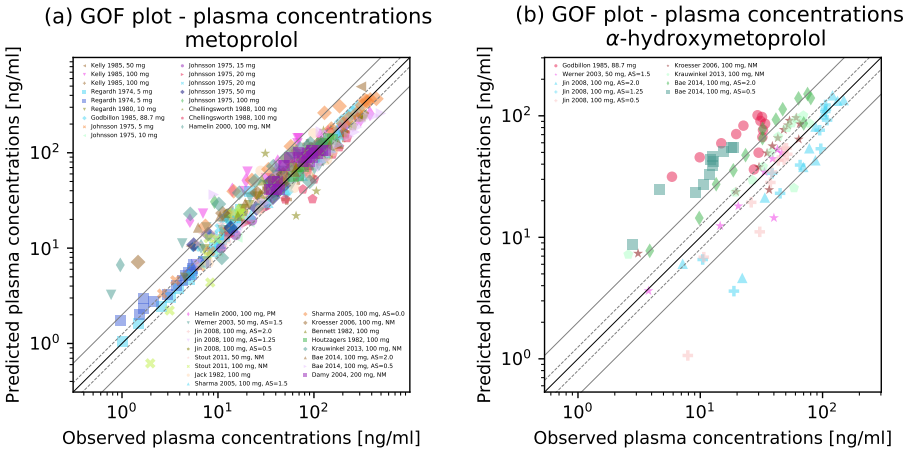

Figure S2.6.9: Plasma concentrations goodness-of-fit plots of the final metoprolol model. Predicted versus observed plasma concentrations for (a) metoprolol and (b) α-hydroxymetoprolol for all studies. The solid black line indicates the line of identity, solid grey lines show 2-fold deviation, dashed grey lines indicate 1.25-fold deviation. AS: CYP2D6 activity score, gof: goodness-of-fit, NM: normal metabolizer, PM: poor metabolizer, vs: versus

Pharmaceutics ***2020***, *12*, 1200; doi.org/10.3390/pharmaceutics12121200

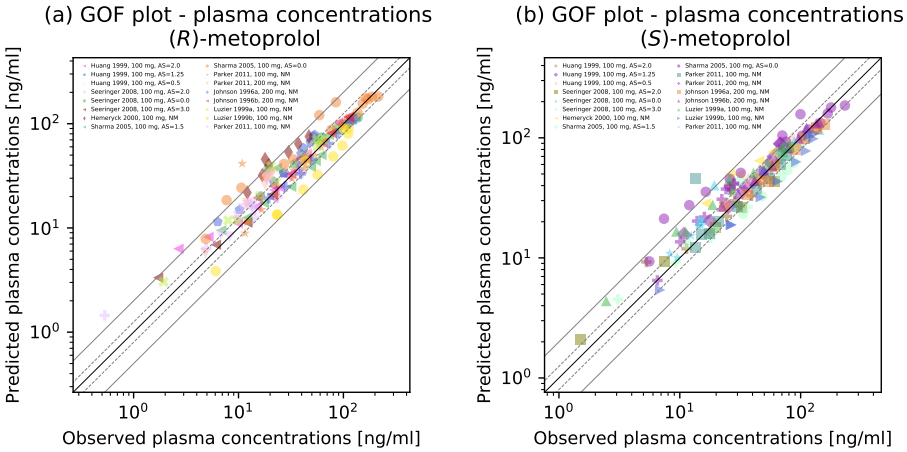

Figure S2.6.10: Plasma concentrations goodness-of-fit plots of the final metoprolol model. Predicted versus observed plasma concentrations for (a) *(R)*-metoprolol and (b) *(S)*-metoprolol for all studies. The solid black line indicates the line of identity, solid grey lines show 2-fold deviation, dashed grey lines indicate 1.25-fold deviation. AS: CYP2D6 activity score, gof: goodness-of-fit, NM: normal metabolizer, vs: versus

Pharmaceutics **2020**, *12*, 1200; doi.org/10.3390/pharmaceutics12121200

S2.6.2 Mean relative deviation of plasma concentration predictions (metoprolol, α-hydroxymetoprolol)

Table S2.6.4: Mean relative deviation of plasma concentration predictions (metoprolol, α-hydroxymetoprolol)

Dosing	Molecule	CYP2D6 status	MRD	Reference
iv, inf, 88.7 mg	α-hydroxymetoprolol	-	3.12	Godbillon et al. 1985 [12]
po, tab, 100 mg	α-hydroxymetoprolol	AS=2.0	1.99	Bae et al. 2014 [3]
po, tab, 100 mg	α-hydroxymetoprolol	AS=0.5	3.25	Bae et al. 2014 [3]
po, tab, 100 mg	α-hydroxymetoprolol	AS=2.0	1.79	Jin et al. 2008 [19]
po, tab, 100 mg	α-hydroxymetoprolol	AS=1.25	1.85	Jin et al. 2008 [19]
po, tab, 100 mg	α-hydroxymetoprolol	AS=0.5	2.02	Jin et al. 2008 [19]
po, -, 100 mg	α-hydroxymetoprolol	NM	1.62	Krauwinkel et al. 2013 [26]
po, tab, 100 mg	α-hydroxymetoprolol	NM	1.54	Kroesser et al. 2006 [27]
po, tab, 50 mg	α-hydroxymetoprolol	AS=1.5	1.46	Werner et al. 2003 [54]
iv, inf, 88.7 mg	metoprolol	-	1.11	Godbillon et al. 1985 [12]
iv, inf, 50 mg	metoprolol	-	1.51	Kelly et al. 1985 [23]
iv, inf, 20 mg	metoprolol	-	1.11	Johnsson et al. 1975 [22]
iv, inf, 15 mg	metoprolol	-	1.11	Johnsson et al. 1975 [22]
iv, inf, 10 mg	metoprolol	-	1.13	Johnsson et al. 1975 [22]
iv, inf, 10 mg	metoprolol	-	1.31	Regardh et al. 1980 [42]
iv, inf, 5 mg	metoprolol	-	1.23	Johnsson et al. 1975 [22]
iv, inf, 5 mg	metoprolol	-	1.20	Regardh et al. 1974 [41]
po, CR, tab, 200 mg, daily	metoprolol	NM	1.25	Damy et al. 2004 [11]
po, tab, 100 mg	metoprolol	AS=2.0	1.53	Bae et al. 2014 [3]
po, tab, 100 mg	metoprolol	AS=0.5	1.77	Bae et al. 2014 [3]
po, -, 100 mg	metoprolol	-	1.29	Bennett et al. 1982 [4]
po, tab, 100 mg	metoprolol	-	1.67	Chellingsworth et al. 1988 [9]
po, tab, 100 mg, bid	metoprolol	-	1.99	Chellingsworth et al. 1988 [9]
po, tab, 100 mg	metoprolol	NM	1.95	Hamelin et al. 2000 [14]
po, tab, 100 mg	metoprolol	PM	1.90	Hamelin et al. 2000 [14]
po, tab, 100 mg	metoprolol	-	1.09	Houtzagers et al. 1982 [16]
po, tab, 100 mg	metoprolol	-	1.51	Jack et al. 1982 [18]
po, tab, 100 mg	metoprolol	AS=2.0	1.24	Jin et al. 2008 [19]
po, tab, 100 mg	metoprolol	AS=1.25	1.24	Jin et al. 2008 [19]
po, tab, 100 mg	metoprolol	AS=0.5	1.34	Jin et al. 2008 [19]
po, tab, 100 mg	metoprolol	-	1.50	Johnsson et al. 1975 [22]
po, -, 100 mg, bid	metoprolol	-	1.33	Kelly et al. 1985 [23]
po, -, 100 mg	metoprolol	-	2.13	Kelly et al. 1985 [23]
po, -, 100 mg	metoprolol	NM	2.06	Krauwinkel et al. 2013 [26]
po, tab, 100 mg	metoprolol	NM	1.68	Kroesser et al. 2006 [27]
po, -, 100 mg	metoprolol	AS=1.5	1.26	Sharma et al. 2005 [47]
po, -, 100 mg	metoprolol	AS=0.0	1.67	Sharma et al. 2005 [47]
po, CR, tab, 100 mg	metoprolol	NM	1.66	Stout et al. 2011 [48]

-: not available, AS: CYP2D6 activity score, bid: twice daily, CR: controlled release, inf: infusion, iv: intravenous NM: normal metabolizer, PM: poor metabolizer, po: oral,sol: oral solution, tab: tablet

Pharmaceutics **2020**, *12*, 1200; doi.org/10.3390/pharmaceutics12121200

Table S2.6.4: Mean relative deviation of plasma concentration predictions (metoprolol, α-hydroxymetoprolol)

Dosing	Molecule	CYP2D6 status	MRD	Reference
po, tab, 50 mg	metoprolol	-	1.37	Johnsson et al. 1975 [22]
po, tab, 50 mg	metoprolol	NM	1.52	Stout et al. 2011 [48]
po, tab, 50 mg	metoprolol	AS=1.5	2.06	Werner et al. 2003 [54]
po, tab, 20 mg	metoprolol	-	1.55	Johnsson et al. 1975 [22]
po, sol, 5 mg	metoprolol	-	1.29	Regardh et al. 1974 [41]
MRD			1.61 (1.09–3.25) 37/43 with MRD $\leq$ 2	

-: not available, AS: CYP2D6 activity score, bid: twice daily, CR: controlled release, inf: infusion, iv: intravenous NM: normal metabolizer, PM: poor metabolizer, po: oral,sol: oral solution, tab: tablet

Pharmaceutics **2020**, *12*, 1200; doi.org/10.3390/pharmaceutics12121200

S2.6.3 Mean relative deviation of plasma concentration predictions ((*R*)-metoprolol, (*S*)-metoprolol)

Table S2.6.5: Mean relative deviation of plasma concentration predictions ((*R*)-metoprolol, (*S*)-metoprolol)

Dosing	Molecule	CYP2D6 status	MRD	Reference
po, tab, 200 mg	(*R*)-metoprolol	NM	1.13	Johnson et al. 1996 a [20]
po, tab, 200 mg	(*R*)-metoprolol	NM	1.13	Johnson et al. 1996 b [21]
po, CR, tab, 200 mg	(*R*)-metoprolol	NM	1.50	Parker et al. 2011 [39]
po, tab, 100 mg	(*R*)-metoprolol	NM	1.93	Hemeryck et al. 2000 [15]
po, tab, 100 mg	(*R*)-metoprolol	AS=2.0	1.34	Huang et al. 1999 [17]
po, tab, 100 mg	(*R*)-metoprolol	AS=1.25	1.39	Huang et al. 1999 [17]
po, tab, 100 mg	(*R*)-metoprolol	AS=0.5	1.24	Huang et al. 1999 [17]
po, tab, 100 mg, bid	(*R*)-metoprolol	NM	1.36	Luzier et al. 1999 a [30]
po, tab, 100 mg, bid	(*R*)-metoprolol	NM	1.55	Luzier et al. 1999 b [31]
po, tab, 100 mg, bid	(*R*)-metoprolol	NM	1.52	Parker et al. 2011 [39]
po, CR, tab, 100 mg	(*R*)-metoprolol	NM	1.24	Parker et al. 2011 [39]
po, tab, 100 mg	(*R*)-metoprolol	AS=3.0	1.41	Seeringer et al. 2008 [46]
po, tab, 100 mg	(*R*)-metoprolol	AS=2.0	1.62	Seeringer et al. 2008 [46]
po, tab, 100 mg	(*R*)-metoprolol	AS=0.0	1.37	Seeringer et al. 2008 [46]
po, -, 100 mg	(*R*)-metoprolol	AS=1.5	1.28	Sharma et al. 2005 [47]
po, -, 100 mg	(*R*)-metoprolol	AS=0.0	1.55	Sharma et al. 2005 [47]
po, tab, 200 mg	(*S*)-metoprolol	NM	1.14	Johnson et al. 1996 a [20]
po, tab, 200 mg	(*S*)-metoprolol	NM	1.09	Johnson et al. 1996 b [21]
po, CR, tab, 200 mg	(*S*)-metoprolol	NM	1.42	Parker et al. 2011 [39]
po, tab, 100 mg	(*S*)-metoprolol	NM	1.56	Hemeryck et al. 2000 [15]
po, tab, 100 mg	(*S*)-metoprolol	AS=2.0	1.20	Huang et al. 1999 [17]
po, tab, 100 mg	(*S*)-metoprolol	AS=1.25	1.20	Huang et al. 1999 [17]
po, tab, 100 mg	(*S*)-metoprolol	AS=0.5	1.17	Huang et al. 1999 [17]
po, tab, 100 mg, bid	(*S*)-metoprolol	NM	1.35	Luzier et al. 1999 a [30]
po, tab, 100 mg, bid	(*S*)-metoprolol	NM	1.44	Luzier et al. 1999 b [31]
po, tab, 100 mg, bid	(*S*)-metoprolol	NM	1.46	Parker et al. 2011 [39]
po, CR, tab, 100 mg	(*S*)-metoprolol	NM	1.29	Parker et al. 2011 [39]
po, tab, 100 mg	(*S*)-metoprolol	AS=3.0	1.31	Seeringer et al. 2008 [46]
po, tab, 100 mg	(*S*)-metoprolol	AS=2.0	1.29	Seeringer et al. 2008 [46]
po, tab, 100 mg	(*S*)-metoprolol	AS=0.0	1.43	Seeringer et al. 2008 [46]
po, -, 100 mg	(*S*)-metoprolol	AS=1.5	1.31	Sharma et al. 2005 [47]
po, -, 100 mg	(*S*)-metoprolol	AS=0.0	1.64	Sharma et al. 2005 [47]
MRD			1.37 (1.09–1.93) 32/32 with MRD $\leq$ 2	
Overall MRD (all four compounds)			1.51 (1.09–3.25) 69/75 with MRD $\leq$ 2	

-: not available, AS: CYP2D6 activity score, bid: twice daily, CR: controlled release, po: oral, tab: tablet.

Pharmaceutics ***2020***, *12*, 1200; doi.org/10.3390/pharmaceutics12121200

S2.6.4 AUC_{last} and C_{max} values goodness-of-fit plots

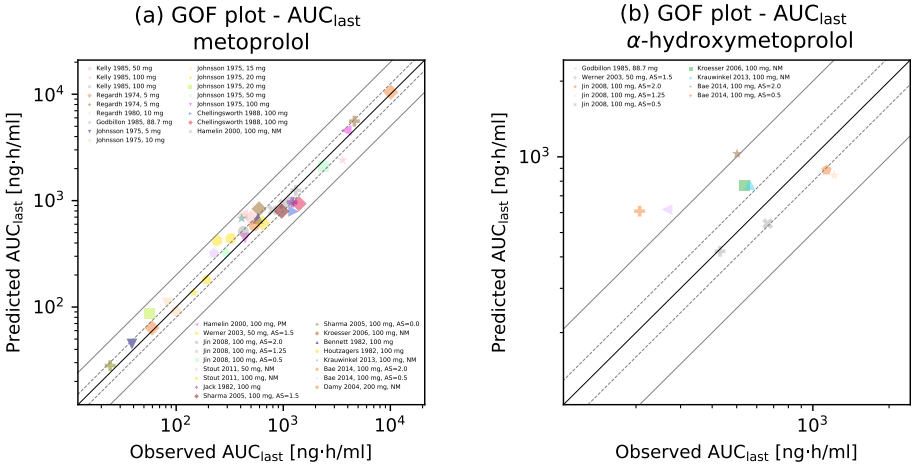

Figure S2.6.11: AUC_{last} values goodness-of-fit plots for the final metoprolol model. Predicted versus observed AUC_{last} values for racemic (a) metoprolol and (b) α-hydroxymetoprolol for all studies. The solid black line marks the line of identity, the dotted grey lines mark the 0.8- to 1.25-fold range, the dashed black lines indicate the 0.5- to 2-fold range. AS: CYP2D6 activity score, gof: goodness-of-fit, NM: normal metabolizer, PM: poor metabolizer, vs: versus

Pharmaceutics **2020**, *12*, 1200; doi.org/10.3390/pharmaceutics12121200

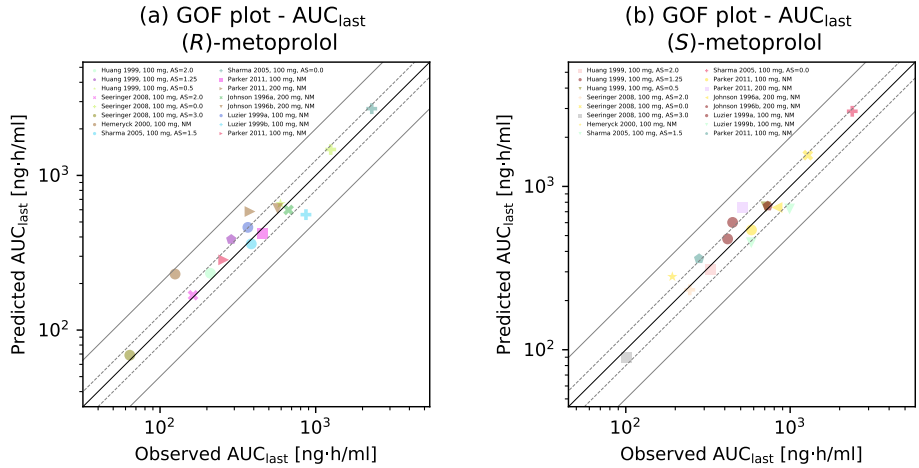

Figure S2.6.12: AUC$_{last}$ goodness-of-fit plots for the final metoprolol model. Predicted versus observed AUC$_{last}$ values for (a) (*S*)-metoprolol and (b) (*R*)-metoprolol for all studies. The solid black line marks the line of identity, the dotted grey lines mark the 0.8- to 1.25-fold range, the dashed black lines indicate the 0.5- to 2-fold range. AS: CYP2D6 activity score, gof: goodness-of-fit, NM: normal metabolizer, vs: versus

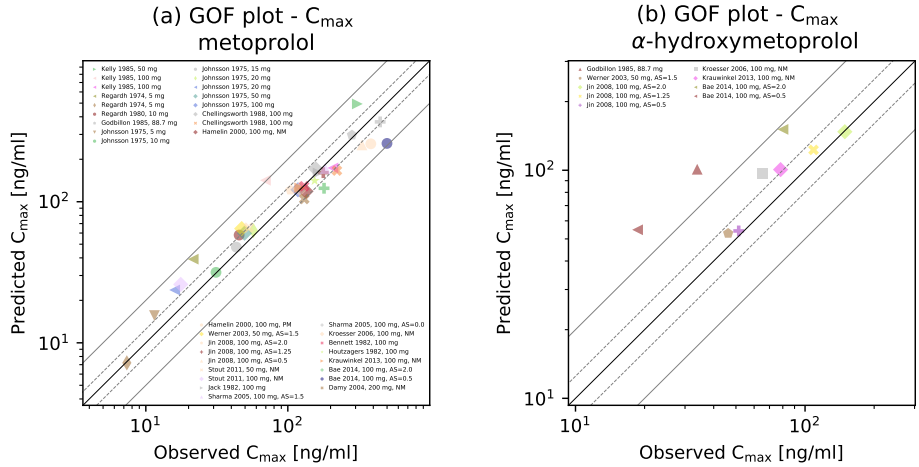

Figure S2.6.13: C$_{max}$ values goodness-of-fit plots for the final metoprolol model. Predicted versus observed C$_{max}$ values for racemic (a) metoprolol and (b) α-hydroxymetoprolol for all studies. The solid black line marks the line of identity, the dotted grey lines mark the 0.8- to 1.25-fold range, the dashed black lines indicate the 0.5- to 2-fold range. AS: CYP2D6 activity score, gof: goodness-of-fit, NM: normal metabolizer, PM: poor metabolizer, vs: versus

Pharmaceutics ***2020***, *12*, 1200; doi.org/10.3390/pharmaceutics12121200

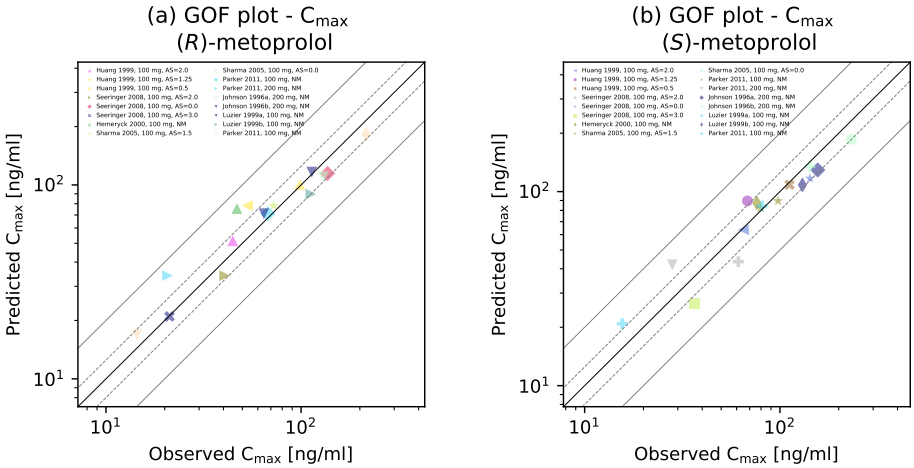

Figure S2.6.14: AUC_{last} goodness-of-fit plots for the final metoprolol model. Predicted versus observed AUC_{last} values for (a) (*S*)-metoprolol and (b) (*R*)-metoprolol for all studies. The solid black line marks the line of identity, the dotted grey lines mark the 0.8- to 1.25-fold range, the dashed black lines indicate the 0.5- to 2-fold range. AS: CYP2D6 activity score, gof: goodness-of-fit, NM: normal metabolizer, vs: versus

Pharmaceutics **2020**, *12*, 1200; doi.org/10.3390/pharmaceutics12121200

S2.6.5 Geometric mean fold error of predicted AUC_{last} and C_{max} values (metoprolol, α-hydroxymetoprolol)

Table S2.6.6: Predicted and observed AUC_{last} and C_{max} values (metoprolol, α-hydroxymetoprolol)

Dosing	Molecule	CYP2D6 status	AUC_{last} Pred [h·ng/ml]	AUC_{last} Obs [h·ng/ml]	AUC_{last} Pred/Obs	C_{max} Pred [ng/ml]	C_{max} Obs [ng/ml]	C_{max} Pred/Obs	Reference
iv, inf, 88.7 mg	α-hydroxymetoprolol	-	617.20	265.13	2.33	-	-	-	Godbillon et al. 1985 [12]
po, tab, 100 mg	α-hydroxymetoprolol	AS=2.0	1028.84	501.89	2.05	152.15	80.13	1.90	Bae et al. 2014 [3]
po, tab, 100 mg	α-hydroxymetoprolol	AS=0.5	607.99	206.78	2.94	55.34	18.64	2.97	Bae et al. 2014 [3]
po, tab, 100 mg	α-hydroxymetoprolol	AS=2.0	886.17	1131.93	0.78	148.83	149.04	1.00	Jin et al. 2008 [19]
po, tab, 100 mg	α-hydroxymetoprolol	AS=1.25	843.16	1212.70	0.70	123.06	108.88	1.13	Jin et al. 2008 [19]
po, tab, 100 mg	α-hydroxymetoprolol	AS=0.5	542.62	662.97	0.82	54.84	51.41	1.07	Jin et al. 2008 [19]
po, -, 100 mg	α-hydroxymetoprolol	NM	775.17	564.03	1.37	100.67	78.25	1.29	Krauwinkel et al. 2013 [26]
po, tab, 100 mg	α-hydroxymetoprolol	NM	765.96	534.92	1.43	96.50	65.12	1.48	Kroesser et al. 2006 [27]
po, tab, 50 mg	α-hydroxymetoprolol	AS=1.5	421.10	429.62	0.98	56.25	46.25	1.22	Werner et al. 2003 [54]
iv, inf, 88.7 mg	metoprolol	-	1251.70	1310.03	0.96	-	-	-	Godbillon et al. 1985 [12]
iv, inf, 50 mg	metoprolol	-	692.12	501.71	1.38	-	-	-	Kelly et al. 1985 [23]
iv, inf, 20 mg	metoprolol	-	179.84	192.31	0.94	-	-	-	Johnsson et al. 1975 [22]
iv, inf, 15 mg	metoprolol	-	136.42	145.74	0.94	-	-	-	Johnsson et al. 1975 [22]
iv, inf, 10 mg	metoprolol	-	90.64	100.45	0.90	-	-	-	Johnsson et al. 1975 [22]
iv, inf, 10 mg	metoprolol	-	109.25	82.28	1.33	-	-	-	Regardh et al. 1980 [42]
iv, inf, 5 mg	metoprolol	-	44.91	38.63	1.16	-	-	-	Johnsson et al. 1975 [22]
iv, inf, 5 mg	metoprolol	-	63.61	59.56	1.07	-	-	-	Regardh et al. 1974 [41]
po, CR, tab, 200 mg, daily	metoprolol	NM	10470.95	10087.41	1.04	104.92	130.54	0.80	Damy et al. 2004 [11]
po, tab, 100 mg	metoprolol	AS=2.0	580.39	535.59	1.08	126.63	179.95	0.70	Bae et al. 2014 [3]
po, tab, 100 mg	metoprolol	AS=0.5	2410.05	3570.91	0.67	259.49	499.36	0.52	Bae et al. 2014 [3]
po, -, 100 mg	metoprolol	-	682.28	580.40	1.18	133.15	130.30	1.02	Bennett et al. 1982 [4]
po, tab, 100 mg bid	metoprolol	-	936.86	1401.85	0.67	166.91	221.75	0.75	Chellingsworth et al. 1988 [9]
po, tab, 100 mg	metoprolol	-	792.38	1250.28	0.63	171.58	157.08	1.09	Chellingsworth et al. 1988 [9]
po, tab, 100 mg	metoprolol	NM	812.74	798.21	1.02	132.33	134.26	0.99	Hamelin et al. 2000 [14]
po, tab, 100 mg	metoprolol	PM	4569.86	3861.13	1.18	266.39	384.09	0.69	Hamelin et al. 2000 [14]
po, tab, 100 mg	metoprolol	-	620.28	640.42	0.97	145.05	154.54	0.94	Houtzagers et al. 1982 [16]
po, tab, 100 mg	metoprolol	-	968.18	1213.24	0.80	161.20	163.49	0.99	Jack et al. 1982 [18]
po, tab, 100 mg	metoprolol	AS=2.0	514.07	423.56	1.21	122.15	104.49	1.17	Jin et al. 2008 [19]
po, tab, 100 mg	metoprolol	AS=1.25	934.51	1009.15	0.93	164.11	177.83	0.92	Jin et al. 2008 [19]
po, tab, 100 mg	metoprolol	AS=0.5	2095.14	2367.57	0.88	254.16	332.72	0.76	Jin et al. 2008 [19]
po, tab, 100 mg	metoprolol	-	444.47	437.96	1.01	121.90	117.92	1.03	Johnsson et al. 1975 [22]
po, -, 100 mg bid	metoprolol	-	980.20	1208.41	0.81	174.50	207.73	0.84	Kelly et al. 1985 [23]
po, -, 100 mg	metoprolol	-	737.05	416.18	1.77	146.25	69.54	2.10	Kelly et al. 1985 [23]
po, -, 100 mg	metoprolol	NM	681.74	408.75	1.67	129.35	121.20	1.07	Krauwinkel et al. 2013 [26]
po, tab, 100 mg	metoprolol	NM	835.96	594.21	1.41	126.23	121.97	1.03	Kroesser et al. 2006 [27]
po, -, 100 mg	metoprolol	AS=1.5	795.72	965.96	0.82	177.69	183.30	0.97	Sharma et al. 2005 [47]
po, -, 100 mg	metoprolol	AS=0.0	5585.63	4612.83	1.21	368.73	447.28	0.82	Sharma et al. 2005 [47]
po, CR, tab, 100 mg	metoprolol	NM	439.65	323.13	1.36	25.96	17.62	1.47	Stout et al. 2011 [48]
po, tab, 50 mg	metoprolol	-	323.70	289.99	1.12	59.99	49.54	1.21	Johnsson et al. 1975 [22]
po, tab, 50 mg	metoprolol	NM	319.14	225.06	1.42	65.57	52.93	1.24	Stout et al. 2011 [48]
po, tab, 50 mg	metoprolol	AS=1.5	421.32	240.97	1.75	66.95	47.34	1.41	Werner et al. 2003 [54]
po, tab, 20 mg	metoprolol	-	87.44	56.33	1.55	23.74	15.96	1.49	Johnsson et al. 1975 [22]
po, sol, 5 mg	metoprolol	-	28.19	24.18	1.17	7.23	7.35	0.98	Regardh et al. 1974 [41]
Overall GMFE					1.31 (1.01–2.94)			1.27 (1.00–2.97)	

-: not available, AUC_{last}: AUC from the time of the first concentration measurement to the last time point of concentration measurement, bid: twice daily, CR: controlled release, GMFE: geometric mean fold error, inf: infusion, iv: intravenous, po: oral, Pred: predicted, Obs: observed, sol: oral solution, tab: tablet

Pharmaceutics **2020**, *12*, 1200; doi.org/10.3390/pharmaceutics12121200

Table S2.6.6: Predicted and observed AUC_{last} and C_{max} values (metoprolol, α-hydroxymetoprolol) *(continued)*

Dosing	Molecule	CYP2D6 status	AUC_{last}			C_{max}			Reference
			Pred [h·ng/ml]	Obs [h·ng/ml]	Pred/Obs	Pred [ng/ml]	Obs [ng/ml]	Pred/Obs	
					40/43 with GMFE ≤ 2			32/34 with GMFE ≤ 2	

-: not available, AUC_{last}: AUC from the time of the first concentration measurement to the last time point of concentration measurement, bid: twice daily, CR: controlled release, GMFE: geometric mean fold error, inf: infusion, iv: intravenous, po: oral, Pred: predicted, Obs: observed, sol: oral solution, tab: tablet

Pharmaceutics **2020**, *12*, 1200; doi.org/10.3390/pharmaceutics12121200

S2.6.6 Geometric mean fold error of predicted AUC_{last} and C_{max} values ((*R*)-metoprolol, (*S*)-metoprolol)

Table S2.6.7: Predicted and observed AUC_{last} and C_{max} values ((*R*)-metoprolol, (*S*)-metoprolol)

Dosing	Molecule	CYP2D6 status	AUC_{last} Pred [h·ng/ml]	AUC_{last} Obs [h·ng/ml]	AUC_{last} Pred/Obs	C_{max} Pred [ng/ml]	C_{max} Obs [ng/ml]	C_{max} Pred/Obs	Reference
po, tab, 200 mg	(*R*)-metoprolol	NM	598.16	669.28	0.89	113.26	130.14	0.87	Johnson et al. 1996 a [20]
po, tab, 200 mg	(*R*)-metoprolol	NM	610.43	569.08	1.07	120.72	113.42	1.06	Johnson et al. 1996 b [21]
po, CR, tab, 200 mg	(*R*)-metoprolol	NM	584.15	378.38	1.54	34.06	20.67	1.65	Parker et al. 2011 [39]
po, tab, 100 mg	(*R*)-metoprolol	NM	230.19	124.91	1.84	76.01	46.90	1.62	Hemeryck et al. 2000 [15]
po, tab, 100 mg	(*R*)-metoprolol	AS=2.0	232.98	210.57	1.11	52.48	44.64	1.18	Huang et al. 1999 [17]
po, tab, 100 mg	(*R*)-metoprolol	AS=1.25	385.55	286.63	1.35	79.93	53.02	1.51	Huang et al. 1999 [17]
po, tab, 100 mg	(*R*)-metoprolol	AS=0.5	656.06	593.93	1.10	101.14	98.46	1.03	Huang et al. 1999 [17]
po, tab, 100 mg, bid	(*R*)-metoprolol	NM	461.34	366.57	1.26	72.56	64.46	1.13	Luzier et al. 1999 a [30]
po, tab, 100 mg, bid	(*R*)-metoprolol	NM	557.74	865.88	0.64	92.11	112.25	0.82	Luzier et al. 1999 b [31]
po, tab, 100 mg, bid	(*R*)-metoprolol	NM	418.97	453.99	0.92	79.58	67.56	1.18	Parker et al. 2011 [39]
po, CR, tab, 100 mg	(*R*)-metoprolol	NM	284.50	256.35	1.11	16.90	14.36	1.18	Parker et al. 2011 [39]
po, tab, 100 mg	(*R*)-metoprolol	AS=3.0	68.78	63.90	1.08	27.15	21.16	1.28	Seeringer et al. 2008 [46]
po, tab, 100 mg	(*R*)-metoprolol	AS=2.0	167.96	162.85	1.03	41.22	40.60	1.02	Seeringer et al. 2008 [46]
po, tab, 100 mg	(*R*)-metoprolol	AS=0.0	1471.47	1248.95	1.18	115.72	136.60	0.85	Seeringer et al. 2008 [46]
po, -, 100 mg	(*R*)-metoprolol	AS=1.5	360.85	385.76	0.94	82.29	72.24	1.14	Sharma et al. 2005 [47]
po, -, 100 mg	(*R*)-metoprolol	AS=0.0	2701.57	2291.56	1.18	182.75	215.01	0.85	Sharma et al. 2005 [47]
po, tab, 200 mg	(*S*)-metoprolol	NM	742.75	832.00	0.89	131.15	156.19	0.84	Johnson et al. 1996 a [20]
po, tab, 200 mg	(*S*)-metoprolol	NM	758.90	730.46	1.04	139.53	142.40	0.98	Johnson et al. 1996 b [21]
po, CR, tab, 200 mg	(*S*)-metoprolol	NM	739.36	512.79	1.44	42.03	28.11	1.50	Parker et al. 2011 [39]
po, tab, 100 mg	(*S*)-metoprolol	NM	280.28	191.91	1.46	87.63	76.15	1.15	Hemeryck et al. 2000 [15]
po, tab, 100 mg	(*S*)-metoprolol	AS=2.0	309.70	328.25	0.94	65.03	64.97	1.00	Huang et al. 1999 [17]
po, tab, 100 mg	(*S*)-metoprolol	AS=1.25	476.96	416.56	1.14	92.01	68.17	1.35	Huang et al. 1999 [17]
po, tab, 100 mg	(*S*)-metoprolol	AS=0.5	749.80	712.83	1.05	108.67	111.98	0.97	Huang et al. 1999 [17]
po, tab, 100 mg, bid	(*S*)-metoprolol	NM	602.11	446.50	1.35	86.88	81.12	1.07	Luzier et al. 1999 a[30]
po, tab, 100 mg, bid	(*S*)-metoprolol	NM	727.77	991.69	0.73	109.92	130.35	0.84	Luzier et al. 1999 b[31]
po, tab, 100 mg, bid	(*S*)-metoprolol	NM	541.62	581.77	1.29	93.65	79.62	1.34	Parker et al. 2011 [39]
po, CR, tab, 100 mg	(*S*)-metoprolol	NM	360.97	279.26	0.93	20.88	15.58	1.18	Parker et al. 2011 [39]
po, tab, 100 mg	(*S*)-metoprolol	AS=3.0	89.57	101.02	0.89	33.56	36.43	0.92	Seeringer et al. 2008 [46]
po, tab, 100 mg	(*S*)-metoprolol	AS=2.0	232.74	245.02	0.95	51.27	61.24	0.84	Seeringer et al. 2008 [46]
po, tab, 100 mg	(*S*)-metoprolol	AS=0.0	1552.77	1280.16	1.21	117.90	142.52	0.83	Seeringer et al. 2008 [46]
po, -, 100 mg	(*S*)-metoprolol	AS=1.5	452.28	580.03	0.78	95.42	97.80	0.98	Sharma et al. 2005 [47]
po, -, 100 mg	(*S*)-metoprolol	AS=0.0	2885.08	2387.00	1.21	186.00	232.43	0.80	Sharma et al. 2005 [47]
GMFE					1.21 (1.03–1.84) 32/32 with GMFE $\leq$ 2			1.19 (1.00–1.65) 32/32 with GMFE $\leq$ 2	
Overall GMFE (all four compounds)					1.27 (1.01–2.94) 72/75 with GMFE $\leq$ 2			1.23 (1.00–2.97) 64/66 with GMFE $\leq$ 2	

-: not available, AS: CYP2D6 activity score, AUC_{last}: AUC from the time of the first concentration measurement to the last time point of concentration measurement, bid: twice daily, CR: controlled release, GMFE: geometric mean fold error, NM: normal metabolizer, po: oral, Pred: predicted, Obs: observed, tab: tablet.

Pharmaceutics **2020**, *12*, 1200; doi.org/10.3390/pharmaceutics12121200

S2.6.7 Sensitivity analysis

Sensitivity of the final metoprolol model to single parameters (local sensitivity analysis) was calculated as the relative change of the $AUC_{0–24\,h}$ of a 100 mg single dose of metoprolol tartrate administered as tablet in the fasted state. Sensitivity analysis was carried out using a relative parameter perturbation of 1000% (variation range 10.0, maximum number of 9 steps). Parameters were included into the analysis if they were optimized (CYP2D6 k_{cat}, unspecific clearance, weibull shape and dissolution time (50% dissolved), intestinal permeability), if they were associated with optimized parameters (CYP2D6 K_m) or if they might have had a strong impact due to calculation methods used in the model (solubility, lipophilicity, fraction unbound).

Pharmaceutics ***2020***, *12*, 1200; doi.org/10.3390/pharmaceutics12121200

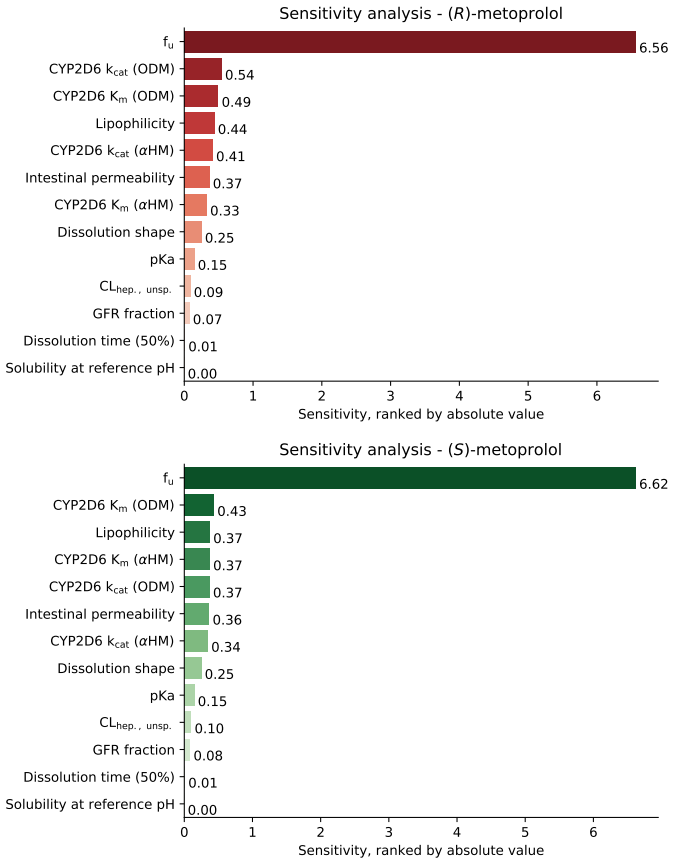

Figure S2.6.15: Sensitivity analysis of the (*R*)-metoprolol (upper panel) and (*S*)-metoprolol (lower panel) model. A sensitivity of +1.0 signifies that a 10% increase of the examined parameter value causes a 10% increase of the simulated $AUC_{0–24\,h}$. αHM: α-hydroxymetoprolol, CYP2D6: cytochrome P450 2D6, f_u: fraction unbound, GFR: glomerular filtration rate, k_{cat}: catalytic rate constant, K_m: Michaelis-Menten constant, ODM: *O*-desmethylmetoprolol.

Pharmaceutics ***2020***, *12*, 1200; doi.org/10.3390/pharmaceutics12121200

S3 Metoprolol CYP2D6 DGI model

S3.1 Metoprolol k_{cat} values for the modeled activity scores

Table S3.1.1: $k_{cat,\ rel}$ values for the different CYP2D6 activity scores

	(*R*)-metoprolol		(*S*)-metoprolol		
Activity score	$k_{cat} \rightarrow \alpha$HM	$k_{cat} \rightarrow$ ODM	$k_{cat} \rightarrow \alpha$HM	$k_{cat} \rightarrow$ ODM	$k_{cat,\ rel}$
0	0.00 1/min	0.00 1/min	0.00 1/min	0.00 1/min	0%
0.5	1.65 1/min	2.70 1/min	1.82 1/min	2.27 1/min	19%
1.25	5.73 1/min	9.40 1/min	6.30 1/min	7.89 1/min	64%
1.5	6.38 1/min	10.48 1/min	7.03 1/min	8.81 1/min	72%
2	10.17 1/min	16.69 1/min	11.19 1/min	14.02 1/min	100%
3	19.03 1/min	31.22 1/min	20.93 1/min	26.23 1/min	213%

αHM: α-hydroxylation, k_{cat}: catalytic rate constant, $k_{cat,\ rel}$: k_{cat} relative to AS=2, ODM: *O*-demethylation

Pharmaceutics ***2020***, *12*, 1200; doi.org/10.3390/pharmaceutics12121200

S3.2 Plasma profiles

S3.2.1 Semilogarithmic plots

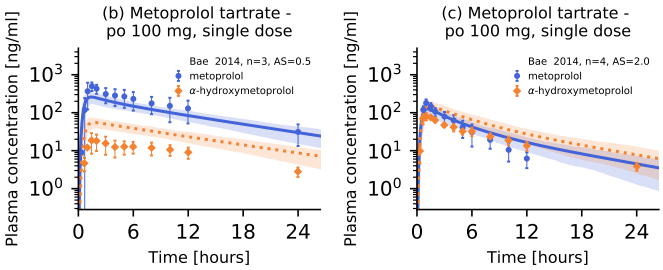

Figure S3.2.1: Metoprolol plasma concentrations of the modeled CYP2D6 drug-gene interaction. Model predictions of metoprolol and α-hydroxymetoprolol plasma concentration-time profiles of the CYP2D6 DGI study, compared to observed data [3] (semilogarithmic representation). Population predictions (n=100) are shown as lines with ribbons (arithmetic mean $\pm$ standard deviation (SD)), symbols represent the corresponding observed data $\pm$ SD. AS: activity score, oral (po): oral

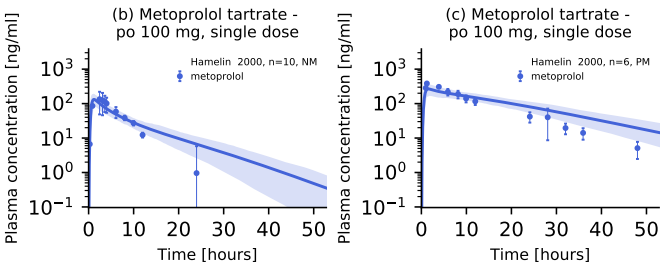

Figure S3.2.2: Metoprolol plasma concentrations of the modeled CYP2D6 drug-gene interaction. Model predictions of metoprolol plasma concentration-time profiles of the CYP2D6 DGI study, compared to observed data [14] (semilogarithmic representation). Population predictions (n=100) are shown as lines with ribbons (arithmetic mean $\pm$ standard deviation (SD)), symbols represent the corresponding observed data $\pm$ SD. NM: normal metabolizer, PM: poor metabolizer, po: oral

Pharmaceutics **2020**, *12*, 1200; doi.org/10.3390/pharmaceutics12121200

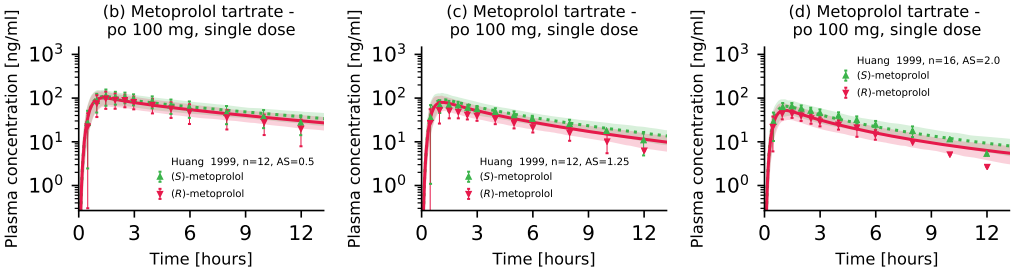

Figure S3.2.3: Metoprolol plasma concentrations of the modeled CYP2D6 drug-gene interaction. Model predictions of (*S*)-metoprolol and (*R*)-metoprolol plasma concentration-time profiles of the CYP2D6 DGI study, compared to observed data [17] (semilogarithmic representation). Population predictions (n=100) are shown as lines with ribbons (arithmetic mean ± standard deviation (SD)), symbols represent the corresponding observed data ± SD. AS: activity score, po: oral

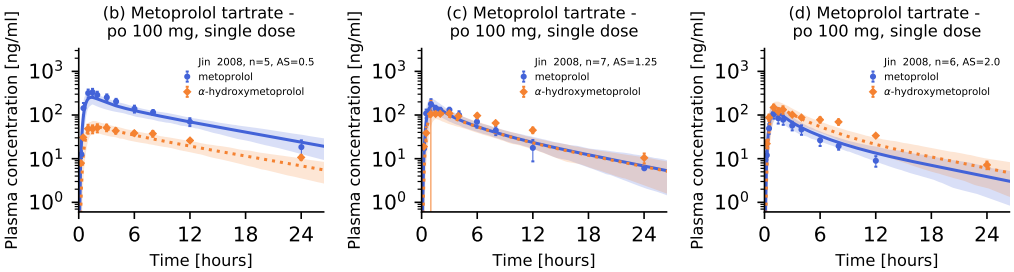

Figure S3.2.4: Metoprolol plasma concentrations of the modeled CYP2D6 drug-gene interaction. Model predictions of metoprolol and α-hydroxymetoprolol plasma concentration-time profiles of the CYP2D6 DGI study, compared to observed data [19] (semilogarithmic representation). Population predictions (n=100) are shown as lines with ribbons (arithmetic mean ± standard deviation (SD)), symbols represent the corresponding observed data ± SD. AS: activity score, po: oral

Pharmaceutics **2020**, *12*, 1200; doi.org/10.3390/pharmaceutics12121200

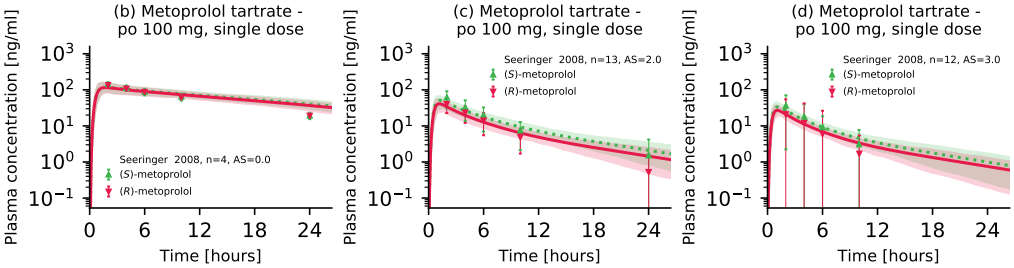

Figure S3.2.5: Metoprolol plasma concentrations of the modeled CYP2D6 drug-gene interaction. Model predictions of (*S*)-metoprolol and (*R*)-metoprolol plasma concentration-time profiles of the CYP2D6 DGI study, compared to observed data [46] (semilogarithmic representation). Population predictions (n=100) are shown as lines with ribbons (arithmetic mean ± standard deviation (SD)), symbols represent the corresponding observed data ± SD. AS: activity score, po: oral

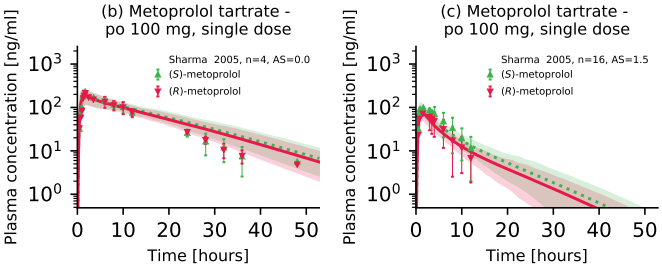

Figure S3.2.6: Metoprolol plasma concentrations of the modeled CYP2D6 drug-gene interaction. Model predictions of metoprolol, (*S*)-metoprolol and (*R*)-metoprolol plasma concentration-time profiles of the CYP2D6 DGI study, compared to observed data [47] (semilogarithmic representation). Population predictions (n=100) are shown as lines with ribbons (arithmetic mean ± standard deviation (SD)), symbols represent the corresponding observed data ± SD. AS: activity score, po: oral

Pharmaceutics ***2020***, *12*, 1200; doi.org/10.3390/pharmaceutics12121200

S3.2.2 Linear plots

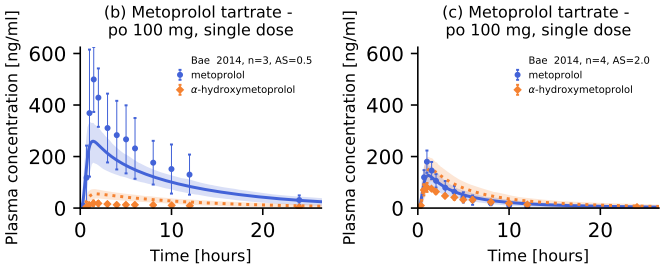

Figure S3.2.7: Metoprolol plasma concentrations of the modeled CYP2D6 drug-gene interaction. Model predictions of metoprolol and α-hydroxymetoprolol plasma concentration-time profiles of the CYP2D6 DGI study, compared to observed data [3] (linear representation). Population predictions (n=100) are shown as lines with ribbons (arithmetic mean $\pm$ standard deviation (SD)), symbols represent the corresponding observed data $\pm$ SD. AS: activity score, po: oral

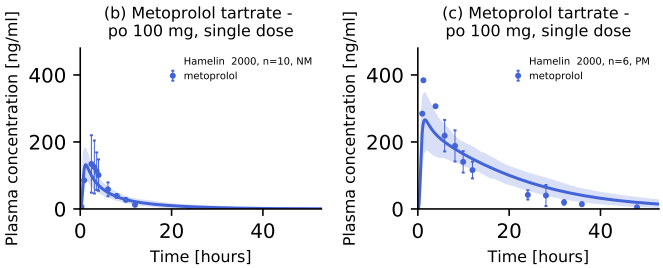

Figure S3.2.8: Metoprolol plasma concentrations of the modeled CYP2D6 drug-gene interaction. Model predictions of metoprolol plasma concentration-time profiles of the CYP2D6 DGI study, compared to observed data [14] (linear representation). Population predictions (n=100) are shown as lines with ribbons (arithmetic mean $\pm$ standard deviation (SD)), symbols represent the corresponding observed data $\pm$ SD. NM: normal metabolizer, PM: poor metabolizer, po: oral

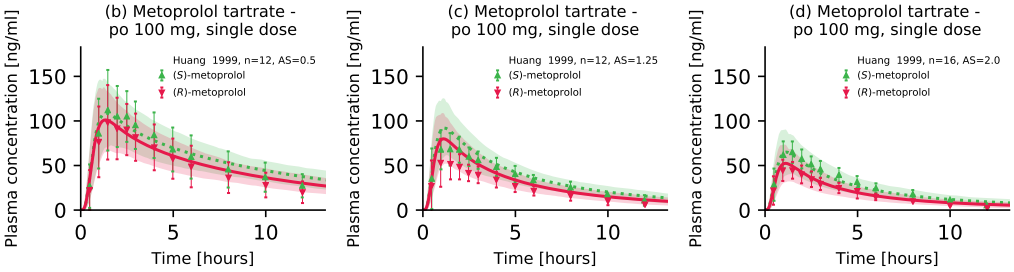

Figure S3.2.9: Metoprolol plasma concentrations of the modeled CYP2D6 drug-gene interaction. Model predictions of (*S*)-metoprolol and (*R*)-metoprolol plasma concentration-time profiles of the CYP2D6 DGI study, compared to observed data [17] (linear representation). Population predictions (n=100) are shown as lines with ribbons (arithmetic mean ± standard deviation (SD)), symbols represent the corresponding observed data ± SD. AS: activity score, po: oral

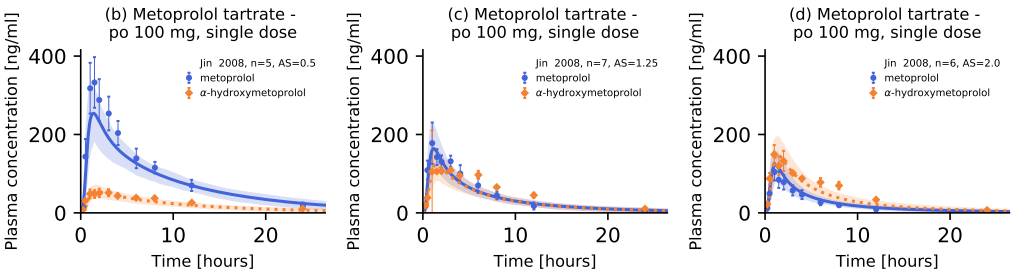

Figure S3.2.10: Metoprolol plasma concentrations of the modeled CYP2D6 drug-gene interaction. Model predictions of metoprolol and α-hydroxymetoprolol plasma concentration-time profiles of the CYP2D6 DGI study, compared to observed data [19] (linear representation). Population predictions (n=100) are shown as lines with ribbons (arithmetic mean ± standard deviation (SD)), symbols represent the corresponding observed data ± SD. AS: activity score, po: oral

Pharmaceutics **2020**, *12*, 1200; doi.org/10.3390/pharmaceutics12121200

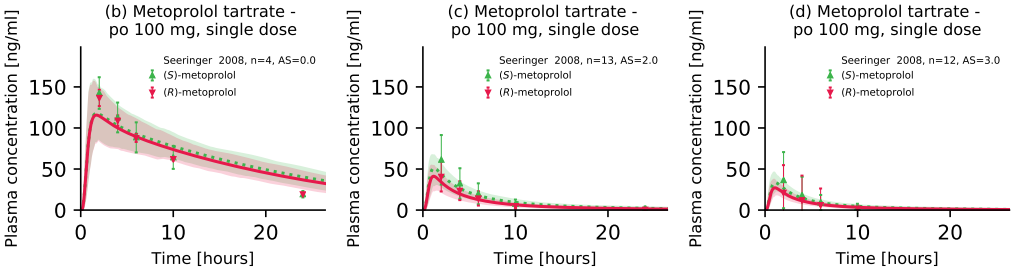

Figure S3.2.11: Metoprolol plasma concentrations of the modeled CYP2D6 drug-gene interaction. Model predictions of (*S*)-metoprolol and (*R*)-metoprolol plasma concentration-time profiles of the CYP2D6 DGI study, compared to observed data [46] (linear representation). Population predictions (n=100) are shown as lines with ribbons (arithmetic mean ± standard deviation (SD)), symbols represent the corresponding observed data ± SD. AS: activity score, po: oral

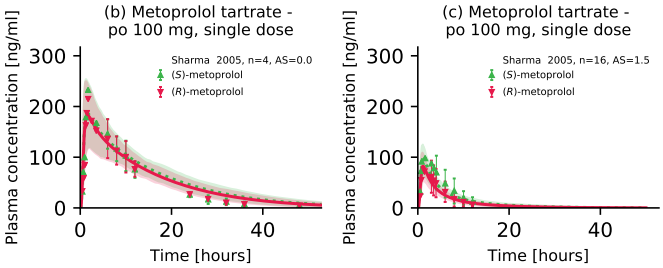

Figure S3.2.12: Metoprolol plasma concentrations of the modeled CYP2D6 drug-gene interaction. Model predictions of metoprolol, (*S*)-metoprolol and (*R*)-metoprolol plasma concentration-time profiles of the CYP2D6 DGI study, compared to observed data [47] (linear representation). Population predictions (n=100) are shown as lines with ribbons (arithmetic mean ± standard deviation (SD)), symbols represent the corresponding observed data ± SD. AS: activity score, po: oral

Pharmaceutics **2020**, *12*, 1200; doi.org/10.3390/pharmaceutics12121200

S3.3 Model evaluation

S3.3.1 Metoprolol CYP2D6 DGI AUC_{last} and C_{max} ratio plots

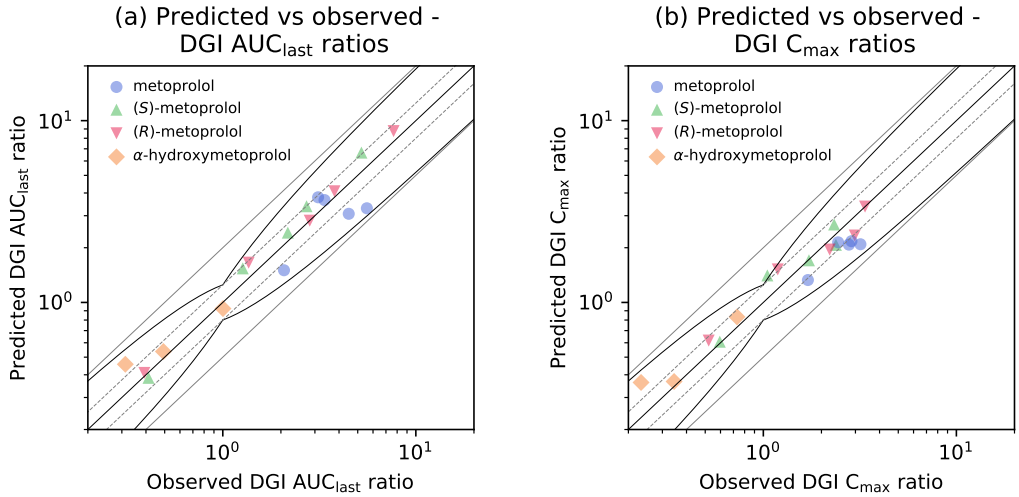

Figure S3.3.13: Predicted versus observed metoprolol DGI ratios. Comparison of predicted versus observed AUC_{last} ratios (a) and C_{max} ratios (b) for metoprolol CYP2D6 DGI-studies. The straight black line indicates the line of identity, curved black lines show prediction success limits proposed by Guest et al. including 1.25-fold variability [13]. Solid light grey lines indicate 2-fold deviation, dashed light grey lines show 1.25-fold deviation. AUC_{last}: AUC from the time of the first concentration measurement to the last time point of concentration measurement, C_{max}: peak plasma concentration, DGI: drug-gene interaction

Pharmaceutics **2020**, *12*, 1200; doi.org/10.3390/pharmaceutics12121200

S3.3.2 Geometric mean fold error of predicted metoprolol DGI AUC_{last} and C_{max} ratios

Table S3.3.2: Geometric mean fold error of predicted metoprolol DGI AUC_{last} and C_{max} ratios

Molecule	Dosing	Activity score	*CYP2D6* Genotype	CYP2D6 Phenotype	DGI AUC_{last} ratio			DGI C_{max} ratio			Reference
					Pred	Obs	Pred/Obs	Pred	Obs	Pred/Obs	
α-hydroxymetoprolol	100 mg, tab, sd	0.5	**10/*10*	IM	0.46	0.31	1.46	0.36	0.23	1.56	Bae et al. 2014 [3]
α-hydroxymetoprolol	100 mg, tab, sd	1.25	**1/*10*	NM	0.93	1.00	0.92	0.83	0.73	1.14	Jin et al. 2008 [19]
α-hydroxymetoprolol	100 mg, tab, sd	0.5	**10/*10*	IM	0.54	0.49	1.09	0.37	0.34	1.06	Jin et al. 2008 [19]
metoprolol	100 mg, tab, sd	0.5	**10/*10*	IM	3.30	5.58	1.69	2.08	2.77	0.75	Bae et al. 2014 [3]
metoprolol	100 mg, tab, sd	-	-	PM	3.66	3.36	1.09	2.17	2.86	0.76	Hamelin et al. 2000 [14]
metoprolol	100 mg, tab, sd	1.25	**1/*10*	NM	1.50	2.08	0.72	1.33	1.70	0.78	Jin et al. 2008 [19]
metoprolol	100 mg, tab, sd	0.5	**10/*10*	IM	3.07	4.49	0.68	2.09	3.18	0.66	Jin et al. 2008 [19]
metoprolol	100 mg, -, sd	0	†	PM	3.79	3.12	1.22	2.14	2.44	0.88	Sharma et al. 2005 [40]
(*R*)-metoprolol	100 mg, tab, sd	1.25	**1/*10*	NM	1.65	1.36	1.22	1.52	1.19	1.28	Huang et al. 1999 [15]
(*R*)-metoprolol	100 mg, tab, sd	0.5	**10/*10*	IM	2.82	2.82	1.00	1.95	2.21	0.89	Huang et al. 1999 [15]
(*R*)-metoprolol	100 mg, tab, sd	3	†	UM	0.41	0.39	1.04	0.62	0.52	1.18	Seeringer et al. 2008 [46]
(*R*)-metoprolol	100 mg, tab, sd	0	†	PM	8.76	7.67	1.14	3.37	3.36	1.00	Seeringer et al. 2008 [46]
(*R*)-metoprolol	100 mg, -, sd	0	†	PM	4.09	3.79	1.08	2.33	2.98	0.78	Sharma et al. 2005 [40]
(*S*)-metoprolol	100 mg, tab, sd	1.25	**1/*10*	NM	1.54	1.27	1.21	1.41	1.05	1.34	Huang et al. 1999 [15]
(*S*)-metoprolol	100 mg, tab, sd	0.5	**10/*10*	IM	2.42	2.17	1.11	1.71	1.72	0.99	Huang et al. 1999 [15]
(*S*)-metoprolol	100 mg, tab, sd	3	†	UM	0.38	0.41	0.93	0.61	0.59	1.02	Seeringer et al. 2008 [46]
(*S*)-metoprolol	100 mg, tab, sd	0	†	PM	6.67	5.22	1.28	2.68	2.33	1.15	Seeringer et al. 2008 [46]
(*S*)-metoprolol	100 mg, -, sd	0	†	PM	3.38	2.72	1.25	2.07	2.38	0.87	Sharma et al. 2005 [40]
Overall GMFE							1.21 (1.00–1.69) 18/18 with GMFE ≤ 2			1.21 (1.00–1.56) 18/18 with GMFE ≤ 2	
Ratios within the limits of *Guest et al.* [13] (including 1.25-fold deviation)							18/18			17/18	

-: not available, †: mixed genotype (given in publication), AUC_{last}: AUC from the time of the first concentration measurement to the last time point of concentration measurement, C_{max}: peak plasma concentration, CYP2D6: cytochrome P450 2D6, IM: intermediate metabolizer, NM: normal metabolizer, Obs: observed, PM: poor metabolizer, Pred: predicted, sd: single dose, tab: tablet, UM: ultrarapid metabolizer

Pharmaceutics ***2020***, *12*, 1200; doi.org/10.3390/pharmaceutics12121200

S4 System-dependent parameters

Details on the implementation of CYP2D6 are summarized in Table S4.0.1.

Table S4.0.1: System-dependent parameters

Enyzme	Reference concentration		Localization	Half-life	
	Mean[a]	Relative expression[b]		Liver [h]	Intestine [h]
CYP2D6	0.40 [45]	RT-PCR [38]	intracellular	51 [38]	23 [38]
EHC fraction: Fraction of biliary secreted compound directly entering the duodenum = 1					

[a]: µmol protein/l in the tissue of highest expression
[b]: In the different organs (PK-Sim expression database profile)
CYP2D6: cytochrome P450 2D6, EHC: enterohepatic circulation, RT-PCR: reverse transcription-polymerase chain reaction profile

Pharmaceutics ***2020***, *12*, 1200; doi.org/10.3390/pharmaceutics12121200

S5 Abbreviations

ρ_i ith observed plasma AUC_{last} or C_{max} value

$\hat{\rho}_i$ ith predicted plasma AUC_{last} or C_{max} value

ADME Absorption, distribution, metabolism and excretion

AS CYP2D6 activity score

AUC Area under the plasma concentration-time curve

AUC_{last} AUC from the time of the first concentration measurement to the last time point of concentration measurement

BA Bioavailability

bid Twice daily

BCS Biopharmaceutics Classification System

c_i ith observed plasma concentration

$\hat{c}_i$ ith predicted plasma concentration

CL Clearance

$CL_{hep,\ unsp.}$ Unspecific hepatic clearance

C_{max} Peak plasma concentration

CR Controlled release

Pharmaceutics ***2020***, *12*, 1200; doi.org/10.3390/pharmaceutics12121200

CYP2B6 Cytochrome P450 2B6

CYP2C9 Cytochrome P450 2C9

CYP2D6 Cytochrome P450 2D6

CYP3A4 Cytochrome P450 3A4

DDI Drug-drug interaction

DGI Drug-gene interaction

EHC Enterohepatic circulation

FDA U. S. Food and Drug Administration

f_u Fraction unbound

g- Genotyped

GFR Glomerular filtration rate

GMFE Geometric mean fold error

ICRP International Commission on Radiological Protection

IM Intermediate metabolizer

inf Infusion

iv Intravenous

k_{cat} Catalytic rate constant

Pharmaceutics ***2020***, *12*, 1200; doi.org/10.3390/pharmaceutics12121200

$k_{cat,\ rel}$ Catalytic rate constant relative to AS=2

K_m Michaelis-Menten constant

MRD Mean relative deviation

MW Molecular weight

NHANES Third National Health and Nutrition Examination Survey

NM Normal metabolizer

NR Normal release

p- Phenotyped

PBPK Physiologically based pharmacokinetic

pKa Acid dissociation constant

PM Poor metabolizer

po Oral

QSAR Quantitative structure-activity relationship

sd Single dose

sol Oral solution

tab Tablet

UM Ultrarapid metabolizer

v_{max} Maximum reaction velocity

Bibliography

1. Austin, R. P., Barton, P., Cockroft, S. L., Wenlock, M. C. & Riley, R. J. The influence of nonspecific microsomal binding on apparent intrinsic clearance, and its prediction from physicochemical properties. *Drug Metabolism and Disposition* **30,** 1497–1503 (2002).
2. Avdeef, A. & Berger, C. M. pH-metric solubility.: 3. Dissolution titration template method for solubility determination. *European Journal of Pharmaceutical Sciences* **14,** 281–291 (2001).
3. Bae, S. H., Lee, J. K., Cho, D.-Y. & Bae, S. K. Simultaneous determination of metoprolol and its metabolites, α-hydroxymetoprolol and O-desmethylmetoprolol, in human plasma by liquid chromatography with tandem mass spectrometry: Application to the pharmacokinetics of metoprolol associated with CYP2D6 g. *Journal of separation science* **37,** 1256–64 (June 2014).
4. Bennett, P. N., John, V. A. & Whitmarsh, V. B. Effect of rifampicin on metoprolol and antipyrine kinetics. *British journal of clinical pharmacology* **13,** 387–91 (Mar. 1982).
5. Berger, B., Bachmann, F., Duthaler, U., Krähenbühl, S. & Haschke, M. Cytochrome P450 enzymes involved in metoprolol metabolism and use of metoprolol as a CYP2D6 phenotyping probe drug. *Frontiers in Pharmacology* **9,** 1–11 (2018).
6. Boldhane, S. & Kuchekar, B. Development and optimization of metoprolol succinate gastroretentive drug delivery system. *Acta Pharmaceutica* **60,** 415–425 (2010).
7. Bozkurt, A., Başçi, N. B., Işimer, A., Sayal, A. & Kayaalp, S. O. Metabolic ratios of four probes of CYP2D6 in Turkish subjects: A cross-over study. *European Journal of Drug Metabolism and Pharmacokinetics* **21,** 309–314 (1996).
8. Cerqueira, P. M. *et al.* Enantioselectivity in the steady-state pharmacokinetics of metoprolol in hypertensive patients. *Chirality* **11,** 591–597.
9. Chellingsworth, M. C., Laugher, S., Akhlaghi, S., Jack, D. B. & Kendall, M. J. The effects of ranitidine and cimetidine on the pharmacokinetics and pharmacodynamics of metoprolol. *Alimentary pharmacology & therapeutics* **2,** 521–7 (Dec. 1988).
10. ClinCalc LLC. *ClinCalc DrugStats Database* `https://clincalc.com/Drugstats/` (2020).
11. Damy, T., Pousset, F., Caplain, H., Hulot, J.-S. S. & Lechat, P. Pharmacokinetic and pharmacodynamic interactions between metoprolol and dronedarone in extensive and poor CYP2D6 metabolizers healthy subjects. *Fundamental and Clinical Pharmacology* **18,** 113–123 (Feb. 2004).

12. Godbillon, J. *et al.* Investigation of drug absorption from the gastrointestinal tract of man. III. Metoprolol in the colon. *British journal of clinical pharmacology* **19 Suppl 2,** 113S–118S (Apr. 1985).
13. Guest, E. J., Aarons, L., Houston, J. B., Rostami-Hodjegan, A. & Galetin, A. Critique of the two-fold measure of prediction success for ratios: application for the assessment of drug-drug interactions. *Drug metabolism and disposition: the biological fate of chemicals* **39,** 170–3 (Feb. 2011).
14. Hamelin, B. A. *et al.* Significant interaction between the nonprescription antihistamine diphenhydramine and the CYP2D6 substrate metoprolol in healthy men with high or low CYP2D6 activity. *Clinical pharmacology and therapeutics* **67,** 466–77 (May 2000).
15. Hemeryck, A., Lefebvre, R. A., De Vriendt, C. & Belpaire, F. M. Paroxetine affects metoprolol pharmacokinetics and pharmacodynamics in healthy volunteers. *Clinical pharmacology and therapeutics* **67,** 283–91 (Mar. 2000).
16. Houtzagers, J. J., Streurman, O. & Regårdh, C. G. The effect of pretreatment with cimetidine on the bioavailability and disposition of atenolol and metoprolol. *British journal of clinical pharmacology* **14,** 67–72 (July 1982).
17. Huang, J., Chuang, S. K., Cheng, C. L. & Lai, M. L. Pharmacokinetics of metoprolol enantiomers in Chinese subjects of major CYP2D6 genotypes. *Clinical pharmacology and therapeutics* **65,** 402–7 (Apr. 1999).
18. Jack, D. B. *et al.* The effect of hydralazine on the pharmacokinetics of three different beta adrenoceptor antagonists: Metoprolol, nadolol, and acebutolol. *Biopharmaceutics & drug disposition* **3,** 47–54.
19. Jin, S. K. *et al.* Influence of CYP2D6*10 on the pharmacokinetics of metoprolol in healthy Korean volunteers. *Journal of clinical pharmacy and therapeutics* **33,** 567–73.
20. Johnson, J. A. & Burlew, B. S. Metoprolol metabolism via cytochrome P4502D6 in ethnic populations. *Drug metabolism and disposition: the biological fate of chemicals* **24,** 350–5 (Mar. 1996).
21. Johnson, J. A. & Burlew, B. S. Metoprolol metabolism via cytochrome P4502D6 in ethnic populations. *Drug metabolism and disposition: the biological fate of chemicals* **24,** 350–5 (Mar. 1996).
22. Johnsson, G., Regärdh, C.-G. & Sölvell, L. Combined pharmacokinetic and pharmacodynamic studies in man of the adrenergic β1-receptor antagonist metoprolol. *Acta Pharmacologica et Toxicologica* **36,** 31–44 (Mar. 1975).
23. Kelly, J. G., Salem, S. A., Kinney, C. D., Shanks, R. G. & McDevitt, D. G. Effects of ranitidine on the disposition of metoprolol. *British Journal of Clinical Pharmacology* **19,** 219–224 (Feb. 1985).
24. Kim, S. *et al.* PubChem 2019 update: Improved access to chemical data. *Nucleic Acids Research* **47,** D1102–D1109 (2019).

25. Kirchheiner, J. *et al.* Impact of the ultrarapid metabolizer genotype of cytochrome P450 2D6 on metoprolol pharmacokinetics and pharmacodynamics. *Clinical pharmacology and therapeutics* **76,** 302–12 (Oct. 2004).
26. Krauwinkel, W. *et al.* The effect of mirabegron, a potent and selective β3-adrenoceptor agonist, on the pharmacokinetics of CYP2D6 substrates desipramine and metoprolol. *European journal of drug metabolism and pharmacokinetics* **39,** 43–52 (Mar. 2014).
27. Krösser, S. *et al.* Investigation of sarizotan's impact on the pharmacokinetics of probe drugs for major cytochrome P450 isoenzymes: a combined cocktail trial. *European Journal of Clinical Pharmacology* **62,** 277–84.
28. Langenbucher, F. Linearization of dissolution rate curves by the Weibull distribution. *The Journal of pharmacy and pharmacology* **24,** 979–81. `http://www.ncbi.nlm.nih.gov/pubmed/4146531` (Dec. 1972).
29. Lennard, M. S., Tucker, G. T., Silas, J. H. & Woods, H. F. Debrisoquine polymorphism and the metabolism and action of metoprolol, timolol, propranolol and atenolol. *Xenobiotica* **16,** 435–447.
30. Luzier, A. B. *et al.* Gender-related effects on metoprolol pharmacokinetics and pharmacodynamics in healthy volunteers. *Clinical pharmacology and therapeutics* **66,** 594–601 (Dec. 1999).
31. Luzier, A. B. *et al.* Gender-related effects on metoprolol pharmacokinetics and pharmacodynamics in healthy volunteers. *Clinical pharmacology and therapeutics* **66,** 594–601 (Dec. 1999).
32. Mateus, A., Matsson, P. & Artursson, P. A high-throughput cell-based method to predict the unbound drug fraction in the brain. *Journal of Medicinal Chemistry* **57,** 3005–3010.
33. Mautz, D. S., Nelson, W. L. & Shen, D. D. Regioselective and stereoselective oxidation of metoprolol and bufuralol catalyzed by microsomes containing cDNA-expressed human P4502D6. *Drug metabolism and disposition: the biological fate of chemicals* **23,** 513–7 (Apr. 1995).
34. Nathanson, J. A. Stereospecificity of beta adrenergic antagonists: R-enantiomers show increased selectivity for beta-2 receptors in ciliary process. *The Journal of pharmacology and experimental therapeutics* **245,** 94–101 (Apr. 1988).
35. National Center for Health Statistics Hyattsville MD 20782. *Third National Health and Nutrition Examination Survey, (NHANES III)* tech. rep. (1997).
36. Novartis Pharmaceuticals Corporation. *Lopressor® tablet and injection - Prescribing information* `https://www.accessdata.fda.gov/drugsatfda%7B%5C_%7Ddocs/label/2008/017963s062,018704s021lbl.pdf` (2020).
37. Open Systems Pharmacology Suite Community. Open Systems Pharmacology Suite Manual, Version 7.4. `https://github.com/Open-Systems-Pharmacology/OSPSuite.Documentation/blob/master/Open%20Systems%20Pharmacology%20Suite.pdf` (2018).

38. Open Systems Pharmacology Suite Community. PK-Sim® Ontogeny Database Documentation, Version 7.3. https://github.com/Open-Systems-Pharmacology/OSPSuite.Documentation/blob/master/PK-Sim%20Ontogeny%20Database%20Version%207.3.pdf (2018).
39. Parker, R. B. & Soberman, J. E. Effects of paroxetine on the pharmacokinetics and pharmacodynamics of immediate-release and extended-release metoprolol. *Pharmacotherapy* **31,** 630–641 (2011).
40. Plosker, G. L. & Clissold, S. P. Controlled Release Metoprolol Formulations. *Drugs* **43,** 382–414 (Mar. 1992).
41. Regårdh, C. G., Borg, K. O., Johansson, R., Johnsson, G. & Palmer, L. Pharmacokinetic studies on the selective beta1-receptor antagonist metoprolol in man. *Journal of pharmacokinetics and biopharmaceutics* **2,** 347–64 (Aug. 1974).
42. Regårdh, C. G. & Johnsson, G. Clinical Pharmacokinetics of Metoprolol. *Clinical Pharmacokinetics* **5,** 557–569 (1980).
43. Rodgers, T., Leahy, D. & Rowland, M. Physiologically based pharmacokinetic modeling 1: predicting the tissue distribution of moderate-to-strong bases. *Journal of pharmaceutical sciences* **94,** 1259–76. http://www.ncbi.nlm.nih.gov/pubmed/15858854 (June 2005).
44. Rodgers, T. & Rowland, M. Physiologically based pharmacokinetic modelling 2: predicting the tissue distribution of acids, very weak bases, neutrals and zwitterions. *Journal of pharmaceutical sciences* **95,** 1238–57. arXiv: z0024 (June 2006).
45. Rodrigues, A. D. Integrated cytochrome P450 reaction phenotyping: attempting to bridge the gap between cDNA-expressed cytochromes P450 and native human liver microsomes. *Biochemical pharmacology* **57,** 465–80 (1999).
46. Seeringer, A., Brockmöller, J., Bauer, S. & Kirchheiner, J. Enantiospecific pharmacokinetics of metoprolol in CYP2D6 ultra-rapid metabolizers and correlation with exercise-induced heart rate. *European journal of clinical pharmacology* **64,** 883–8 (Sept. 2008).
47. Sharma, A. *et al.* Modulation of Metoprolol Pharmacokinetics and Hemodynamics by Diphenhydramine Coadministration during Exercise Testing in Healthy Premenopausal Women. *Journal of Pharmacology and Experimental Therapeutics* **313,** 1172–1181 (June 2005).
48. Stout, S. M. *et al.* Influence of metoprolol dosage release formulation on the pharmacokinetic drug interaction with paroxetine. *Journal of clinical pharmacology* **51,** 389–96 (Mar. 2011).
49. Tanaka, G. & Kawamura, H. Anatomical and physiological characteristics for Asian reference man: male and female of different ages: Tanaka model. Division of Radioecology, National Institute of Radiological Sciences. Hitachinaka 311-12 Japan. NIRS-M-115 (1996).

50. Thelen, K. *et al.* Evolution of a detailed physiological model to simulate the gastrointestinal transit and absorption process in humans, Part 1: Oral solutions. *Journal of Pharmaceutical Sciences* **100,** 5324–5345 (Dec. 2011).
51. U.S. Food and Drug Administration. *Drug Development and Drug Interactions: Table of Substrates, Inhibitors and Inducers | FDA* `https://www.fda.gov/drugs/drug-interactions-labeling/drug-development-and-drug-interactions-table-substrates-inhibitors-and-inducers` (2020).
52. Valentin, J. Basic anatomical and physiological data for use in radiological protection: reference values. A report of age- and gender-related differences in the anatomical and physiological characteristics of reference individuals. ICRP Publication 89. *Annals of the ICRP* **32,** 5–265 (2002).
53. Watanabe, R. *et al.* Predicting Fraction Unbound in Human Plasma from Chemical Structure: Improved Accuracy in the Low Value Ranges. *Molecular Pharmaceutics* **15,** 5302–5311 (2018).
54. Werner, U. *et al.* Celecoxib inhibits metabolism of cytochrome P450 2D6 substrate metoprolol in humans. *Clinical pharmacology and therapeutics* **74,** 130–137.
55. Wishart, D. S. *et al.* HMDB 4.0: the human metabolome database for 2018. *Nucleic Acids Research* **46,** D608–D617 (Jan. 2018).
56. Wojtyniak, J. G., Britz, H., Selzer, D., Schwab, M. & Lehr, T. Data Digitizing: Accurate and Precise Data Extraction for Quantitative Systems Pharmacology and Physiologically-Based Pharmacokinetic Modeling. *CPT: Pharmacometrics and Systems Pharmacology* **9,** 322–331 (2020).
57. Zhao, Y. *et al.* High-throughput logP measurement using parallel liquid chromatography/ultraviolet/mass spectrometry and sample-pooling. *Rapid communications in mass spectrometry : RCM* **16,** 1548–55 (2002).

B.2 PROJECT II: SUPPLEMENTARY MATERIALS

Physiologically Based Pharmacokinetic Modeling of Dextromethorphan to Investigate Interindividual Variability Within CYP2D6 Activity Score Groups

Supplement S1 - Model Information and Evaluation

Simeon Rüdesheim[1,2], Dominik Selzer[1], Uwe Fuhr[3], Matthias Schwab[2,4,5], Thorsten Lehr[1]

[1] Clinical Pharmacy, Saarland University, Saarbrücken, Germany
[2] Dr. Margarete Fischer-Bosch-Institute of Clinical Pharmacology, Stuttgart, Germany
[3] Department I of Pharmacology, Center for Pharmacology, Faculty of Medicine and University Hospital Cologne, University of Cologne, Germany
[4] Departments of Clinical Pharmacology, Pharmacy and Biochemistry, University of Tübingen, Tübingen, Germany
[5] Cluster of Excellence iFIT (EXC2180) "Image-guided and Functionally Instructed Tumor Therapies", University of Tübingen, Tübingen, Germany

Funding
M.S. was supported by the Robert Bosch Stiftung (Stuttgart, Germany), the European Commission Horizon 2020 UPGx grant 668353, a grant from the German Federal Ministry of Education and Research (BMBF 031L0188D), and the Deutsche Forschungsgemeinschaft (DFG, German Research Foundation) under Germany's Excellence Strategy—EXC 2180—390900677. T.L. was supported by the German Federal Ministry of Education and Research (BMBF, Horizon 2020 INSPIRATION grant 643271), under the frame of ERACoSysMed.

Disclosures
The authors declared no competing interest for this work.

Corresponding Author
Prof. Dr. Thorsten Lehr
Clinical Pharmacy, Saarland University
Campus C2 2, 66123 Saarbrücken
Phone: +49 681 302 70255
Email: thorsten.lehr@mx.uni-saarland.de
ORCID: 0000 0002 8372 1465

Contents

S1 Methods (Addendum)

S1.1 Cocktail Studies

Table S1.1.1: Phenotyping cocktails and respective drug doses

Study	Caffeine	Dextromethorphan	Digoxin	Mephenytoin	Midazolam	Omeprazole	Tolbutamide	Warfarin
Population studies								
Armani 2017 [1]	100 mg	30 mg	-	-	2 mg	20 mg	-	-
Dumond 2010 [8]	200 mg	30 mg	0.25 mg (po + iv)[a]	-	5 mg (po)[c] + 2 mg (iv)[c]	20 mg	-	10 mg[b]
Ermer 2015 [10]	200 mg	30 mg	-	-	0.025 mg/kg (iv)	40 mg	-	-
Kakuda 2014 [18]	15 mg	30 mg	0.5 mg (po)	-	1.5 mg (po)	40 mg	-	10 mg[b]
Khalilieh 2018 [21]	20 mg	30 mg	-	-	1.5 mg (po)	40 mg	-	10 mg[b]
Nyunt 2008 [28]	-	30 mg	-	-	5 mg (po)	-	-	-
Sager 2014 [31]	100 mg	30 mg	-	-	2 mg (po)	20 mg	-	-
Stage 2018 [35]	100 mg	30 mg	-	-	2.5 mg (buccal)	20 mg	-	-
DGI studies								
Gorski 2004 [14]	200 mg	30 mg	-	-	0.05 mg/kg (iv)	-	500 mg	-
Gazzaz 2018 [13]	150 mg	30 mg	-	-	2 mg (po)	20 mg	-	-
Frank 2009 [12]								
Study A	150 mg	30 mg	-	50 mg	2 mg (po) + 1 mg (iv)[c]	-	125 mg	-
Study B[d]	150 mg	30 mg	0.5 mg	50 mg	2 mg (po) + 1 mg (iv)[c]	-	125 mg	-
Study C	150 mg	30 mg	-	50 mg	2 mg (po) + 1 mg (iv)[c]	-	125 mg	-
Study D	-	30 mg	0.5 mg	50 mg	1.5 mg (po) + 1 mg (iv)[c]	-	-	-
Study E	-	30 mg	0.5 mg	50 mg	1.5 mg (po) + 1 mg (iv)[c]	-	-	-

-: not administered, [a]: doses were administered on the study days following the administration of the phenotyping cocktail, [b]: Study subjects received 10 mg vitamin K together with the warfarin dose, [b]: iv dose administered 240 min after administration of the cocktail, [d]: study excluded from modeling due to reasons described in Section S6.1, iv: intravenous, po: oral.

S1.2 Dextromethorphan Formulations

The Weibull function was implemented according to Eq. 1 and 2 [23] to describe the dissolution process for studies where dextromethorphan was administered in a cocktail capsule

$$m = 1 - \text{exp}\left(\frac{-(t - T_{lag})^{\beta}}{\alpha}\right) \tag{1}$$

$$\alpha = (T_d)^{\beta} \tag{2}$$

where m = fraction of dissolved drug at time t, T_{lag} = lag time before the onset of dissolution, α = scale parameter, β = shape parameter, T_d = time needed to dissolve 63% of the formulation.

The final Weibull shape parameters and Weibull time parameters (50% dissolved) for the cocktail formulation used in the dextromethorphan physiologically based pharmacokinetic (PBPK) model are given in Table S2.1.1.

S1.3 Virtual Individuals

The PBPK model was built based on data from healthy individuals, using the reported sex, ethnicity and mean values for age, weight and height from each study protocol. If no demographic information was provided, the following default values were substituted: male, European, 30 years of age, 73 kg body weight and 176 cm body height (characteristics from the PK-Sim® population database [27, 38, 41]. Cytochrome P450 2D6 (CYP2D6) was implemented in accordance with literature, using the PK-Sim® expression database to define their relative expression in the different organs of the body [29]. Details on the implementation of CYP2D6 are summarized in Section **??**.

S1.4 Virtual Populations

For population simulations, virtual populations of 1000 individuals were created based on the population characteristics stated in the respective publication. If no information was provided in the publication, populations based on European male individuals aged 20–50 years were assumed. Metrics were generated (depending on ethnicity) from one of the following databases; American: Third National Health and Nutrition Examination Survey (NHANES) [27] database, Asian: Tanaka model [38], European: International Commission on Radiological Protection (ICRP) database [41]. In the generated virtual populations, system-dependent parameters such as weight, height, organ volumes, blood flow rates, tissue compositions, etc. were varied by the implemented algorithm in PK-Sim® within the limits of the databases listed above [27, 38, 41]. Since study populations were grouped by their CYP2D6 activity score or phenotype, no variability in CYP2D6 reference concentrations was assumed for population simulations. Reference concentrations of implemented proteins as well as the relative expression are provided in Section **??**.

S1.5 Lysosomal Trapping in the Intestinal Mucosa

Although dextromethorphan is rapidly absorbed from the intestine, time to reach peak plasma concentration C_{max} (t_{max}) often occurs as late as 4h after oral administration [4]. This phenomenon likely occurs due to lysosomal trapping of dextromethorphan in the intestinal mucosa [4, 20]. However, other processes, such as renal excretion may also be affected by lysosomal trapping in the respective tissue. In short, lipophilic amines (logP > 1, acid dissociation constant (pKa) > 6) accumulate in

lysosomes due to rapid diffusion across the lysosomal membrane in unionized form. Subsequently, due to the acidic environment in lysosomes (pH 4–5), the amine is then ionized and thus unable to permeate back into the cytosol [20]. The information necessary to physiologically implement lysosomal trapping (i.e. relative abundances of lysosomes in relevant tissues and diffusion constants for permeation across lysosomal membranes) are not yet available in the literature. Hence, intestinal lysosomal trapping was implemented as follows: First, a surrogate protein binding partner was expressed in high abundances (500 µmol/L) in the relevant tissues (duodenum, upper jejunum, lower jejunum, upper ileum and lower ileum, each 100% of relative expression). Second, a corresponding protein binding process was implemented for dextromethorphan. Finally, the relevant parameters for the binding process - dissociation rate constant (k_{off}) and dissociation constant (K_D) - were informed by parameter optimization. For a comprehensive explanation on the process of lysosomal trapping under physiological circumstances, please refer to [20].

S1.6 PBPK Model Sensitivity Analysis

Sensitivity of the final models to single parameter changes (local sensitivity analysis) was calculated as relative change of the area under the plasma concentration-time curve $(AUC)_{0-24\,h}$. Sensitivity analysis was carried out using a relative perturbation of 1000% (variation range 10.0, maximum number of 9 steps). Parameters were included into the analysis if they have been optimized, if they are associated with optimized parameters or if they might have a strong impact due to calculation methods used in the model. Sensitivity to a parameter was calculated as the ratio of the relative change of the simulated $AUC_{0-24\,h}$ to the relative variation of the parameter according to Eq. 3:

$$S = \frac{\Delta AUC_{0-24\,h}}{\Delta p} \times \frac{p}{AUC_{0-24\,h}} \tag{3}$$

where S = sensitivity of the $AUC_{0-24\,h}$ to the examined model parameter, $\Delta AUC_{0-24\,h}$ = change of the $AUC_{0-24\,h}$, $AUC_{0-24\,h}$ = simulated $AUC_{0-24\,h}$ with the original parameter value, Δp = change of the examined parameter value, p = original parameter value.

A sensitivity of +0.5 signifies that a 100% increase of the examined parameter value causes a 50% increase of the simulated $AUC_{0-24\,h}$. The results of the sensitivity analysis are provided in Section S3.6.

S2 PBPK Base Model Building

S2.1 Drug-Dependent Parameters

Table S2.1.1: Dextromethorphan and dextrorphan drug-dependent parameters drug-dependent parameters

Parameter	Unit	Value	Source	Literature	Reference	Value	Source	Literature	Reference	Description
		Dextromethorphan				**Dextrorphan**				
MW	g/mol	271.41	Lit.	271.41	[2]	257.37	Lit.	257.37	[16, 43]	Molecular weight
pKa (strongest basic)	-	9.10	Lit.	9.10	[34]	9.10	Lit.	9.10	[34]	Acid dissociation constant
pKa (strongest acidic)	-	-	Lit.	-	-	10.10	Lit.	10.10	[34]	Acid dissociation constant
Solubility (base)	g/L	-	-	-	-	0.17	Lit.	0.17	[43]	Solubility at pH 7
Solubility (hydrobromide)	g/L	15.00	Lit.	15.00	[2]	-	-	-	-	Solubility at pH 7
logP	-	4.10	Lit.	4.10	[34]	2.90	Lit.	2.90	[22]	Lipophilicity
f_u	%	35.00	Lit.	35.00	[25]	42.00	Lit.	42.00	[42]	Fraction unbound
CYP2D6 $K_M \rightarrow$ dxt	µmol/L	4.65	Lit.	4.65[a]	[5]	-	-	-	-	Michaelis-Menten constant
CYP2D6 $k_{cat} \rightarrow$ dxt (EM)	1/min	90.89	Optim.	6.60	[5]	-	-	-	-	Catalytic rate constant
CYP2D6 $k_{cat} \rightarrow$ dxt (PM)	1/min	0.00	-	-	-	-	-	-	-	Catalytic rate constant
CYP3A4 K_M	µmol/L	176.80	Lit.	176.80[a]	[25]	910.00	Lit.	910.00[a]	[25]	Michaelis-Menten constant
CYP3A4 k_{cat}	1/min	7.94	Lit.	5.65	[25]	7.41	Lit.	7.41	[25]	Catalytic rate constant
UGT2B15 $K_M \rightarrow$ dxt-glu	µmol/L	-	-	-	-	184.80	Lit.	184.80[a]	[25]	Michaelis-Menten constant
UGT2B15 $k_{cat} \rightarrow$ dxt-glu	1/min	-	-	-	-	1137.98	Optim.	37.04	[25]	Catalytic rate constant
Lysosomal trapping K_D	µmol/L	74.21	-	-	-	-	-	-	-	Dissociation constant
Lysosomal trapping k_{off}	1/min	$7.10 \cdot 10^5$	-	-	-	-	-	-	-	Dissociation rate constant
GFR fraction	-	1.00	Asm.	-	-	1.00	Asm.	-	-	Filtered drug in the urine
EHC continuous fraction	-	1.00	Asm.	-	-	1.00	Asm.	-	-	Bile fraction cont. released
Intestinal perm.	cm/min	$2.48 \cdot 10^{-6}$	Optim.	$1.12 \cdot 10^{-3}$	Calc. [40]	$1.80 \cdot 10^{-5}$	Calc.	$1.80 \cdot 10^{-5}$	Calc. [40]	Transcellular intestinal perm.
Cellular permeability	cm/min	0.91	Calc.	PK-Sim	[19]	0.08	Calc.	PK-Sim	[19]	Perm. into the cellular space
Partition coefficients	-	Diverse	Calc.	Ber	[3]	Diverse	Calc.	Ber	[3]	Cell to plasma partitioning
Weibull time parameter	min	46.05	Optim.	[12]	-	-	-	-	-	Dissolution time (50%)
Weibull shape parameter	-	1.05	Optim.	[12]	-	-	-	-	-	Dissolution shape

-: not available, [a]: in vitro values corrected for binding in the assay (fu_{mic}) as given in the respective publications, asm.: assumed, Ber: Berezhkovskiy calculation method, calc.: calculated, cont.: continuously, CYP2D6: Cytochrome P450 2D6, CYP3A4: cytochrome P450 3A4, dxt: dextrorphan, dxt-glu: dextrorphan *O*-glucuronide, EHC: enterohepatic circulation, GFR: glomerular filtration rate, intest.: intestinal, lit: literature, EM: extensive metabolizer, optim.: optimized, perm.: permeability, PM: poor metabolizer, PK-Sim: PK-Sim standard calculation method, uridine 5'-diphospho-glucuronosyltransferase family 2 member B15 (UGT2B15): uridine 5'-diphospho-glucuronosyltransferase family 2 member B15.

Table S2.1.2: Dextrorphan *O*-glucuronide drug-dependent parameters

Parameter	Unit	Value	Source	Literature	Reference	Description
MW	g/mol	433.50	Lit.	433.50	[17, 43]	Molecular weight
pKa (strongest basic)	-	9.82	Lit.	9.82	[17, 43]	Acid dissociation constant
pKa (strongest acidic)	-	2.85	Lit.	2.85	[17, 43]	Acid dissociation constant
Solubility	g/L	1.20	Lit.	1.20	[17, 43]	Solubility
logP	-	0.29	Optim.	1.38	[17, 43]	Lipophilicity
f_u	%	37.00	Calc.	37.00	[42]	Fraction unbound
GFR fraction	-	4.92	Optim.	-	-	Filtered drug in the urine
EHC continuous fraction	-	1.00	Asm.	-	-	Bile fraction cont. released
Intestinal permeability	cm/min	$4.26 \cdot 10^{-6}$	Calc.	$4.26 \cdot 10^{-6}$	Calc. [40]	Transcellular intestinal perm.
Cellular permeability	cm/min	$8.51 \cdot 10^{-6}$	Calc.	CdS	[33]	Perm. into the cellular space
Partition coefficients	-	Diverse	Calc.	Ber	[3]	Cell to plasma partitioning

-: not available, asm: assumed, Ber: Berezhkovskiy calculation method, calc.: calculated, CdS: Charge dependent Schmitt, cont.: continuously, EHC: enterohepatic circulation, GFR: glomerular filtration rate, intest.: intestinal, lit.: literature, optim: optimized, perm.: permeability.

S2.2 Clinical Study Data

Table S2.2.3: Dextromethorphan study table

Route	Dose [mg]	n	Females [%]	Age [years]	Weight [kg]	Height [cm]	Metabolite measured	CYP2D6 P. Phenotype	Dataset	References
iv (inf, 30 min, sd)	0.5/kg	24	0	27 (21-35)	79 (55-110)	-	-	EM	training	Duedahl 2005 [7]
po (cap, sd)	80	36	0	26	73	-	dtt	EM	training	Tennezé 1999 [39]
po (-, sd)	60	17	41	67 (49-74)	80 (49-107)	173 (150-187)	dtt	EM	test	Feld 2013 [11]
po (cap, bid, 8 days)	60	10	0	-	-	-	dtt	EM	test	Antecip Bioventures [24]
po (cap, sd)	30	20	50	(27-42)	73	-	-	EM	test[a]	Armani 2017 [1]
po (cap, sd)	30	23	30	27	76	174	-	EM	test[a]	Dumond 2010 [8]
po (cap, sd)	30	48	35	33	76	171	-	EM	test	Edwards 2017 [9]
po (cap, sd)	30	30	40	(18-45)	78	172	dxt	EM	test[a]	Ermer 2015 [10]
po (-, sd)	30	14	0	(21-49)	-	-	-	EM	test[a]	Kakuda 2014 [18]
po (-, sd)	30	20	35	40 (22-63)	-	-	-	EM	test[a]	Khalilieh 2018 [21]
po (tab, sd)	50	24	0	25 (20-33)	64 (50-76)	-	dxt	EM	test	Nakashima 2007 [26]
po (-, sd)	30	12	25	40 (22-53)	-	-	-	EM	test[a]	Nyunt 2008 [28]
po (cap, sd)	30	10	50	20	72	172	dxt	EM	test[a]	Sager 2014 [31]
po (cap, sd)	30	5	80	26 (22-31)	-	-	dxt, dxt-glu	EM	training	Schadel 1995 [32]
po (cap, sd)	30	4	50	33 (22-46)	-	-	-	PM	training	Schadel 1995 [32]
po (cap, sd)	30	12	0	(21-29)	-	-	-	EM	test[a]	Stage 2018 [35]

Values for age, weight and height are given as mean (range), -: not given, [a]: cocktail study, AS: CYP2D6 activity score, bid: twice daily, cap: capsule, CYP2D6: Cytochrome P450 2D6, DGI: drug-gene interaction, dxt: dextrorphan, dxt-glu: dextrorphan *O*-glucuronide, dtt: total dextrorphan, EM: extensive metabolizer, inf: infusion, iv: intravenous, p.: projected, PM: poor metabolizer, po: oral, sd: single dose, sol: oral solution.

S2.3 Dextromethorphan model pathways

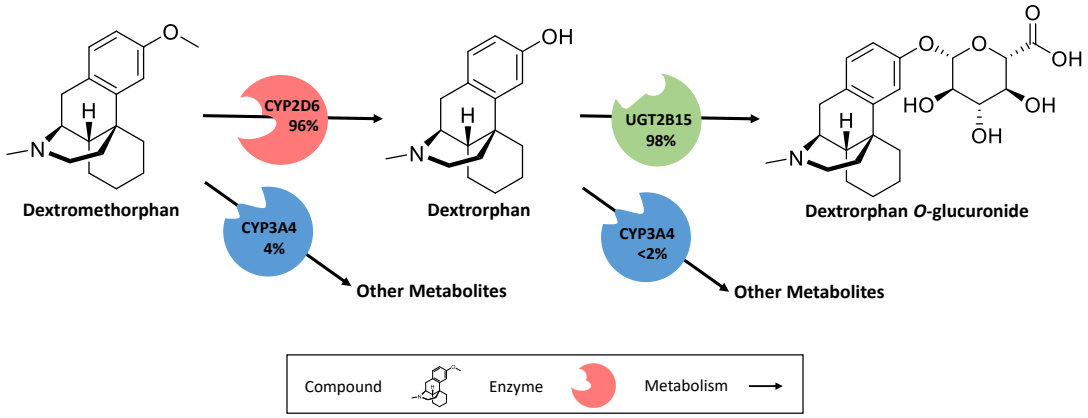

Figure S2.3.1: Implemented dextromethorphan metabolic pathways. Dextromethorphan is *O*-demethylated by CYP2D6 and *N*-demethylated by CYP3A4. The metabolite dextrorphan is further metabolized via CYP3A4 (*N*-demethylation) and UGT2B15 (*O*-glucuronidation). Dextrorphan *O*-glucuronide is excreted in the urine. Percentages shown refer to the fraction metabolized by the respective enzyme, calculated for extensive metabolizers of CYP2D6. CYP2D6: cytochrome P450 2D6, CYP3A4: cytochrome P450 3A4, UGT2B15: Uridine 5'-diphospho-glucuronosyltransferase 2B15.

S3 PBPK Base Model Evaluation

S3.1 Plasma Concentration-Time Profiles

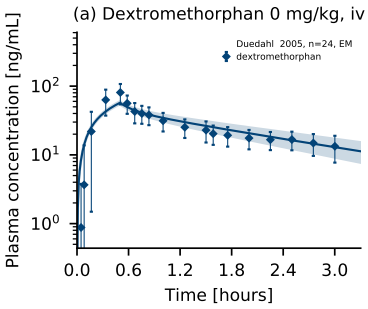

Figure S3.1.1: Dextromethorphan plasma concentration-time profile after intravenous administration of dextromethorphan (semilogarithmic representation). Population predictions (n=1000) are shown as lines with ribbons (arithmetic mean $\pm$ standard deviation (SD)), symbols represent the corresponding observed data $\pm$ SD. EM: extensive metabolizer, iv: intravenous.

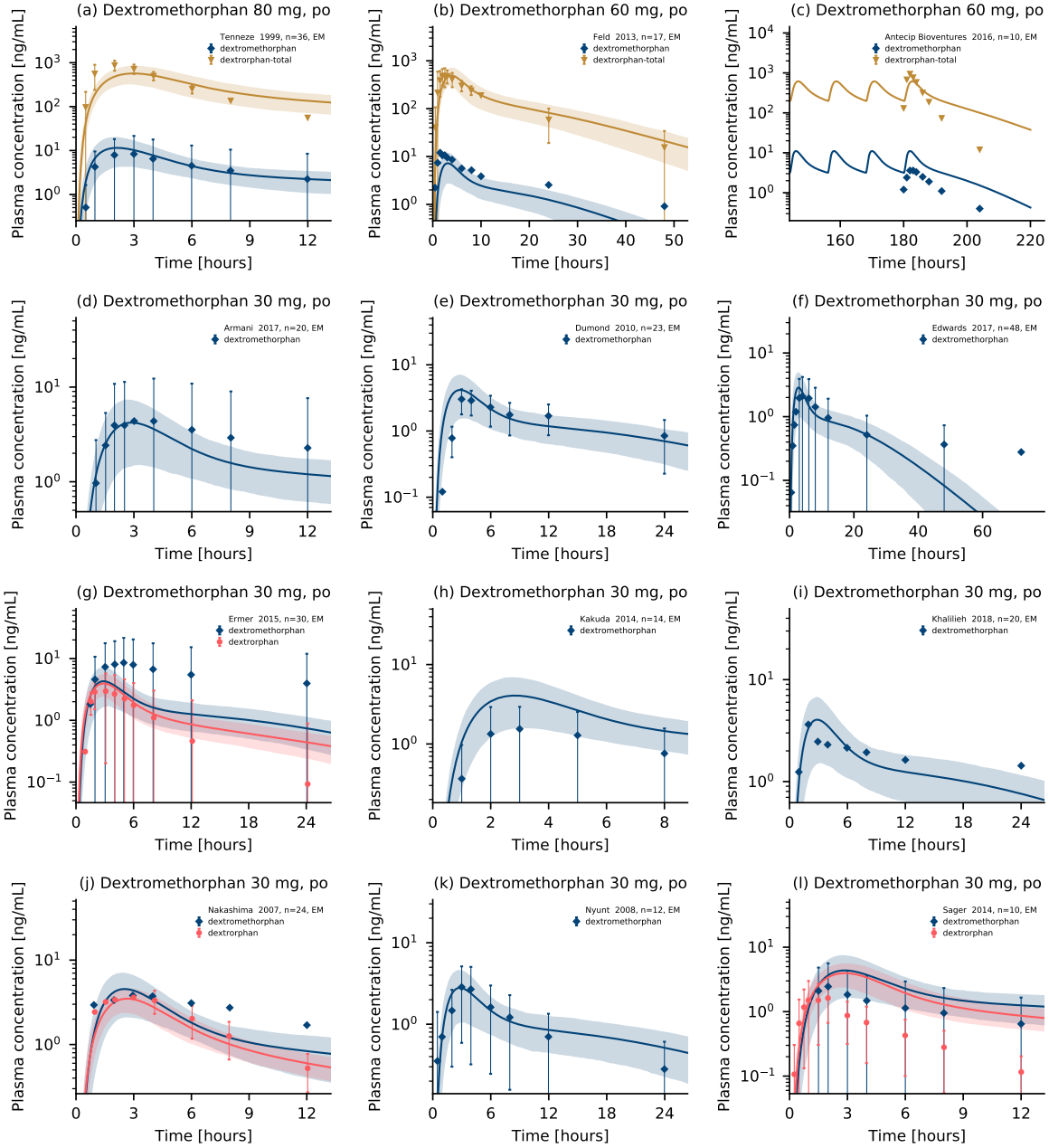

Figure S3.1.2: Dextromethorphan, dextrorphan and total dextrorphan (dextrorphan + dextrorphan *O*-glucuronide) plasma concentration-time profiles after oral administration of dextromethorphan (semilogarithmic representation). Population predictions (n=1000) are shown as lines with ribbons (arithmetic mean ± standard deviation (SD)), symbols represent the corresponding observed data ± SD. EM: extensive metabolizer, po: oral.

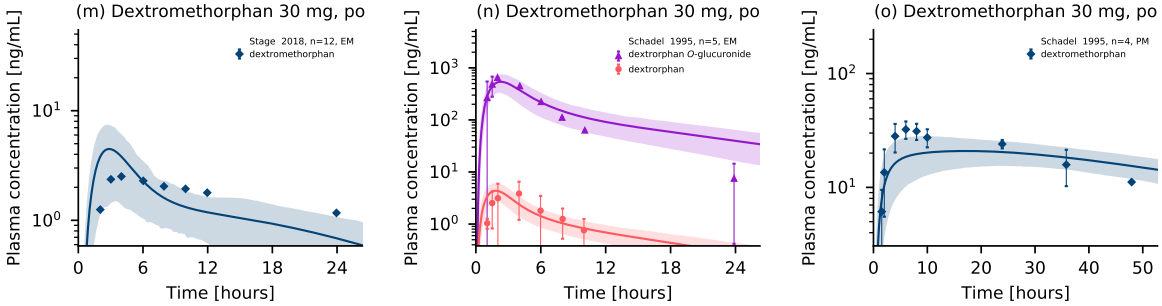

Figure S3.1.3: Dextromethorphan, dextrorphan, dextrorphan *O*-glucuronide and total dextrorphan (dextrorphan + dextrorphan *O*-glucuronide) plasma concentration-time profiles after oral administration of dextromethorphan (semilogarithmic representation). Population predictions (n=1000) are shown as lines with ribbons (arithmetic mean $\pm$ standard deviation (SD)), symbols represent the corresponding observed data $\pm$ SD. EM: extensive metabolizer, PM: poor metabolizer, po: oral.

S3.2 Goodness-of-Fit Plots: Plasma Concentrations

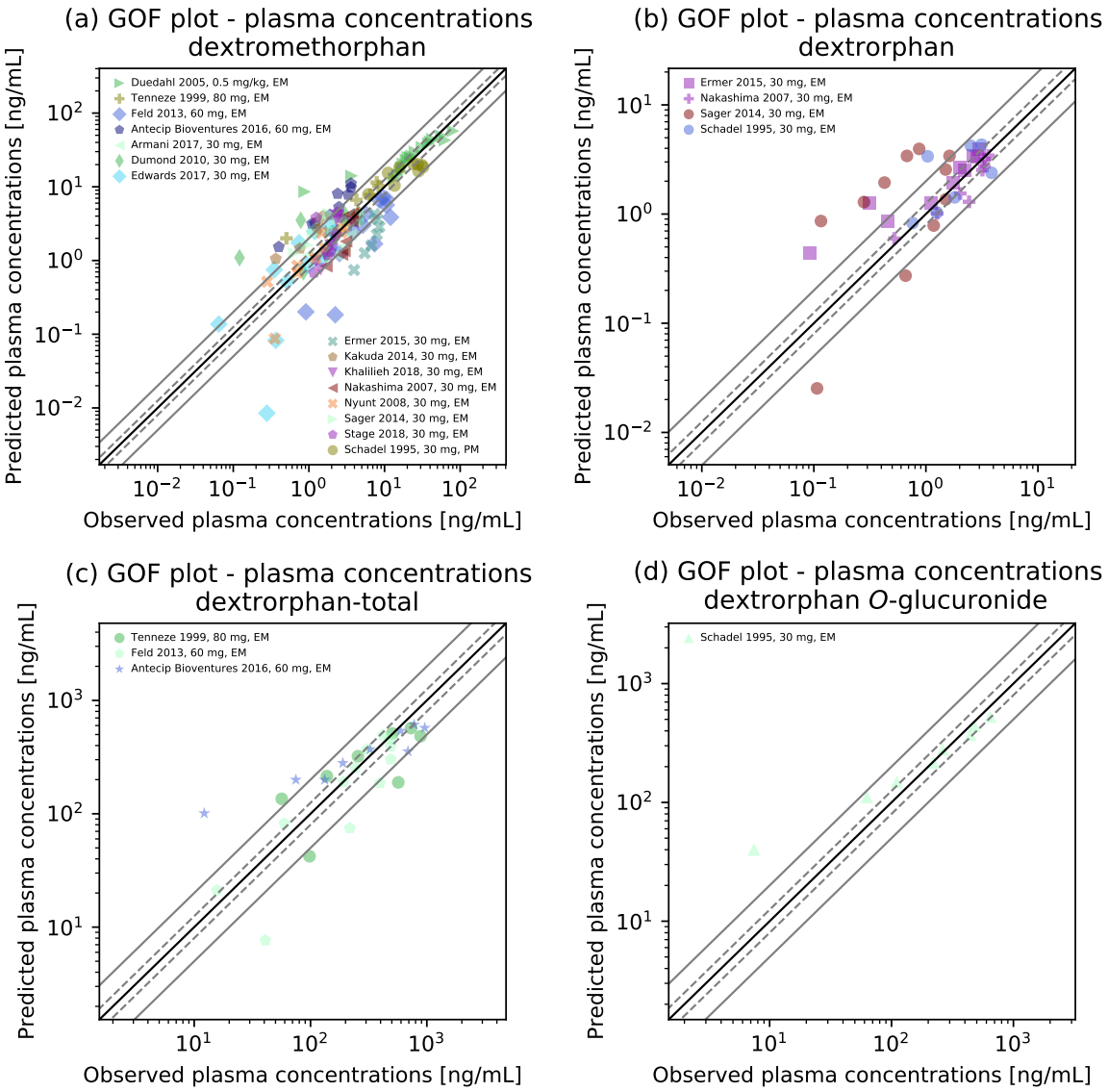

Figure S3.2.4: Goodness-of-fit plots. Predicted versus observed plasma concentration values for (a) dextromethorphan, (b) dextrorphan, (c) total dextrorphan (dextrorphan + dextrorphan *O*-glucuronide) and (d) dextrorphan *O*-glucuronide for all studies of the PBPK model building dataset. The solid black line marks the line of identity, the dashed gray lines mark the 0.8- to 1.25-fold range, the solid gray lines indicate the 0.5- to 2-fold range. Colored symbols represent the study population given in the legend. EM: extensive metabolizer, PM: poor metabolizer.

S3.3 MRD of Plasma Concentration Predictions

Table S3.3.1: Mean relative deviation of plasma concentration predictions

Dosing	Molecule	CYP2D6 status	MRD	Reference
iv, inf, 0.5 mg	dextromethorphan	EM	1.87	Duedahl et al. 2005 [7]
po, cap, 80 mg	dextromethorphan	EM	1.85	Tenneze et al. 1999 [39]
po, -, 60 mg	dextromethorphan	EM	3.19	Feld et al. 2013 [11]
po, tab, 60 mg	dextromethorphan	EM	2.73	Antecip Bioventures [24]
po, cap, 30 mg	dextromethorphan	EM	1.42	Armani et al. 2017 [1]
po, cap, 30 mg	dextromethorphan	EM	2.60	Dumond et al. 2010 [8]
po, cap, 30 mg	dextromethorphan	EM	3.32	Edwards et al. 2017 [9]
po, -, 30 mg	dextromethorphan	EM	2.96	Ermer et al. 2015 [10]
po, cap, 30 mg	dextromethorphan	EM	2.63	Kakuda et al. 2014 [18]
po, -, 30 mg	dextromethorphan	EM	1.46	Khalilieh et al. 2018 [21]
po, tab, 30 mg	dextromethorphan	EM	1.70	Nakashima et al. 2007 [26]
po, cap, 30 mg	dextromethorphan	EM	1.94	Nyunt et al. 2008 [28]
po, cap, 30 mg	dextromethorphan	EM	1.97	Sager et al. 2014 [31]
po, cap, 30 mg	dextromethorphan	PM	1.44	Schadel et al. 1995 [32]
po, cap, 30 mg	dextromethorphan	EM	1.74	Stage et al. 2018 [35]
MRD (dextromethorphan)			2.19 (1.42–3.32) 9/15 with MRD $\leq$ 2	
po, -, 30 mg	dextrorphan	EM	2.05	Ermer et al. 2015 [10]
po, tab, 30 mg	dextrorphan	EM	1.35	Nakashima et al. 2007 [26]
po, cap, 30 mg	dextrorphan	EM	3.56	Sager et al. 2014 [31]
po, cap, 30 mg	dextrorphan	EM	1.73	Schadel et al. 1995 [32]
MRD (dextrorphan)			2.17 (1.35–3.56) 2/4 with MRD $\leq$ 2	
po, cap, 30 mg	dextrorphan *O*-glucuronide	EM	2.01	Schadel et al. 1995 [32]
MRD (dextrorphan *O*-glucuronide)			2.01 0/1 with MRD $\leq$ 2	
po, cap, 80 mg	dextrorphan-total	EM	1.88	Tenneze et al. 1999 [39]
po, -, 60 mg	dextrorphan-total	EM	2.04	Feld et al. 2013 [11]
po, tab, 60 mg	dextrorphan-total	EM	3.40	Antecip Bioventures [24]
MRD (dextrorphan-total)			2.44 (1.88–3.40) 1/3 with MRD $\leq$ 2	
Overall MRD			2.21 (1.35–3.56) 12/23 with MRD $\leq$ 2	

-: not given, cap: capsule, CYP2D6: Cytochrome P450 2D6, EM: extensive metabolizer, inf: infusion, iv: intravenous, PM: poor metabolizer, po: oral.

S3.4 AUC_{last} and C_{max} Goodness-of-Fit Plots

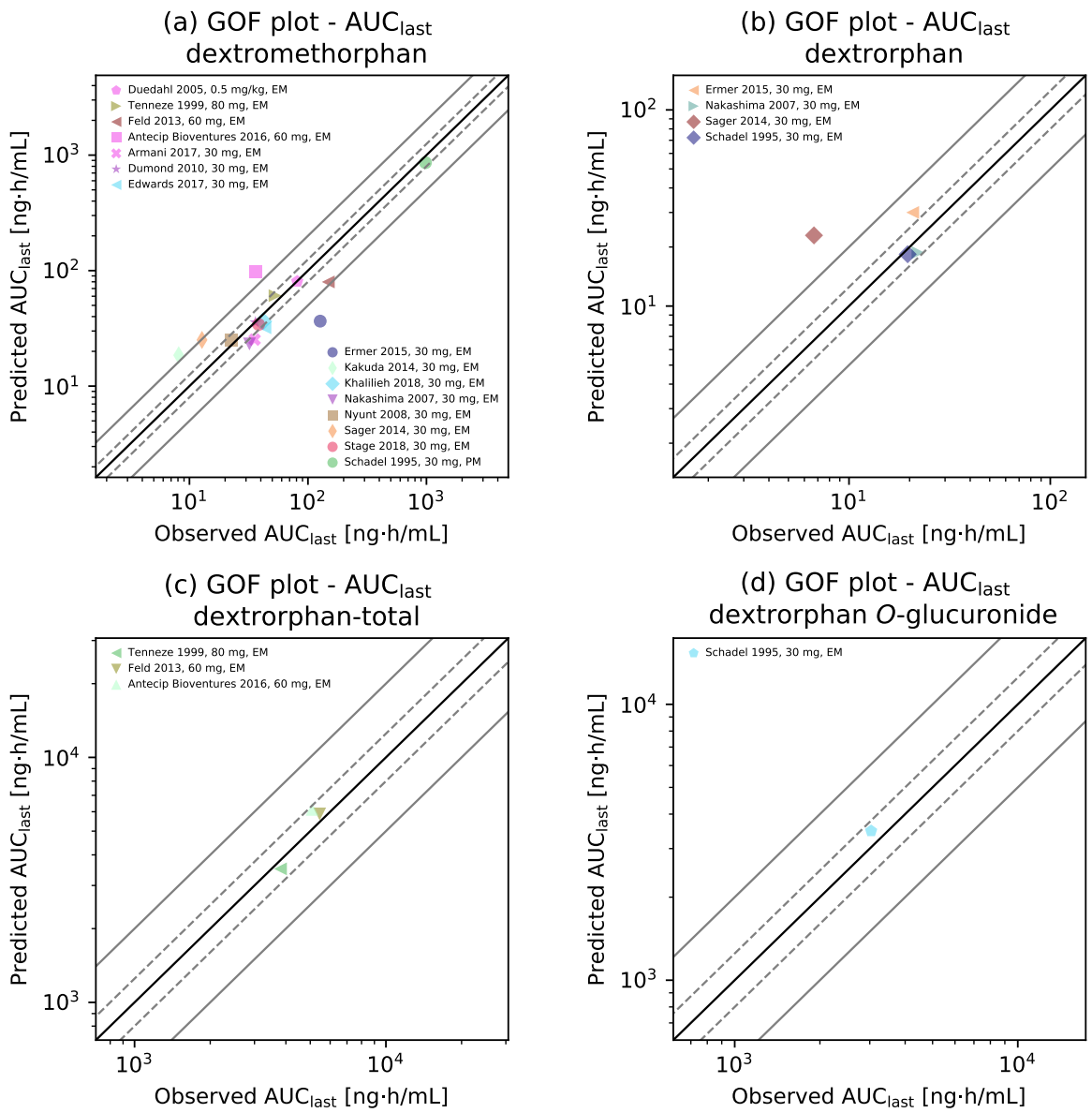

Figure S3.4.5: AUC from the time of the first concentration measurement to the last time point of concentration measurement (AUC_{last}) correlation plots. Predicted versus observed AUC_{last} for (a) dextromethorphan, (b) dextrorphan, (c) total dextrorphan (dextrorphan + dextrorphan *O*-glucuronide) and (d) dextrorphan *O*-glucuronide for all studies of the PBPK model building dataset. The solid black line marks the line of identity, the dashed gray lines mark the 0.8- to 1.25-fold range, the solid gray lines indicate the 0.5- to 2-fold range. Colored symbols represent the study population given in the legend. AUC_{last}: AUC from the time of the first concentration measurement to the last time point of concentration measurement, EM: extensive metabolizer, PM: poor metabolizer.

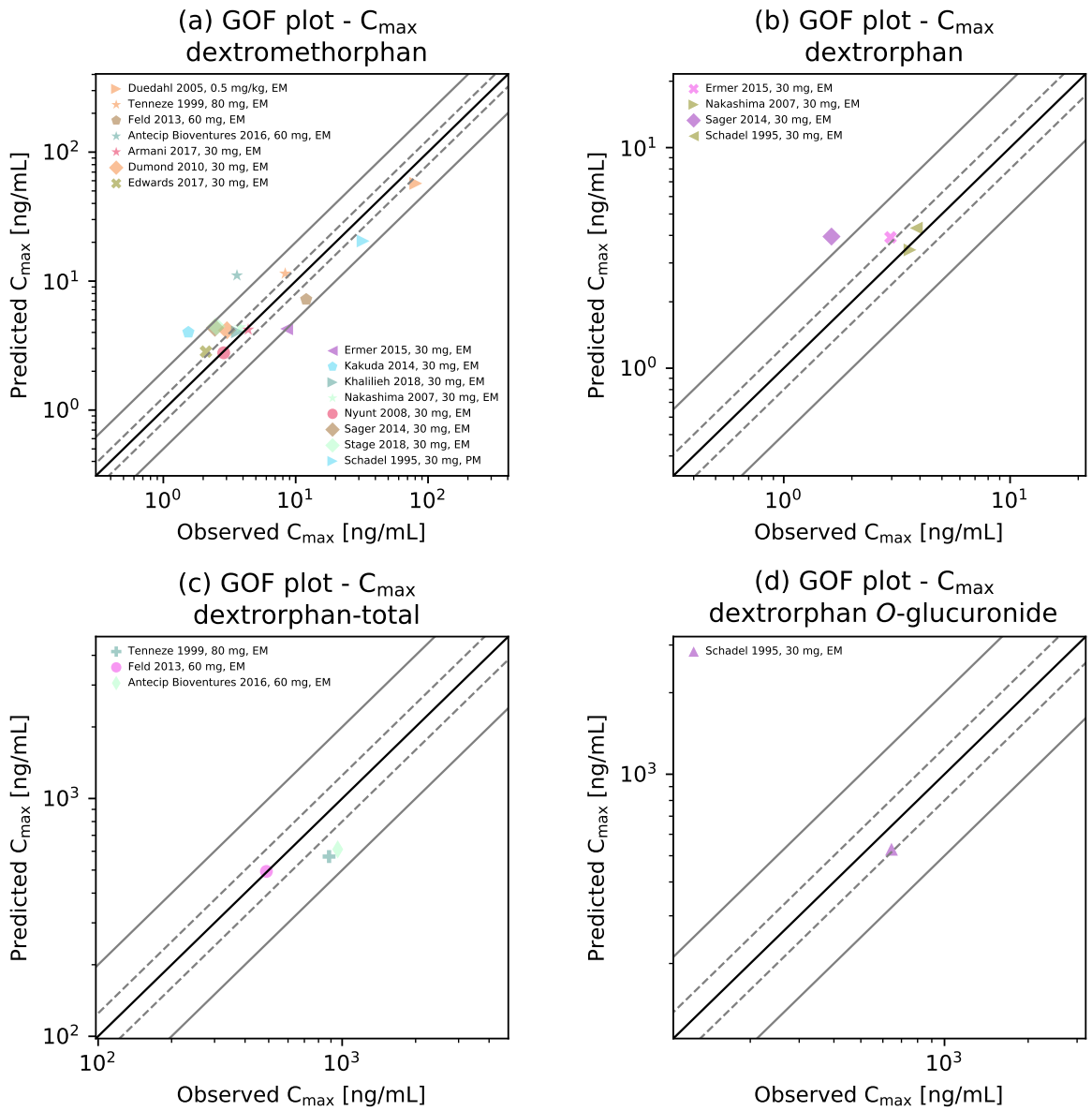

Figure S3.4.6: C_{max} correlation plots. Predicted versus observed C_{max} for (a) dextromethorphan, (b) dextrorphan, (c) total dextrorphan (dextrorphan + dextrorphan *O*-glucuronide) and (d) dextrorphan *O*-glucuronide for all studies of the PBPK model building dataset. The solid black line marks the line of identity, the dashed gray lines mark the 0.8- to 1.25-fold range, the solid gray lines indicate the 0.5- to 2-fold range. Colored symbols represent the study population given in the legend. C_{max}: peak plasma concentration, EM: extensive metabolizer, PM: poor metabolizer.

S3.5 GMFE of Predicted AUC_{last} and C_{max} Values

Table S3.5.2: Predicted and observed AUC_{last} and C_{max} values and geometric mean fold errors

Dosing	Molecule	CYP2D6 status	AUC_{last} [ng·h/mL] Pred	Obs	Pred/Obs	C_{max} [ng/mL] Pred	Obs	Pred/Obs	Reference
iv, inf, 0.5 mg/kg	dextromethorphan	EM	80.25	81.20	0.99	-	-	-	Duedahl et al. 2005 [7]
po, cap, 80 mg	dextromethorphan	EM	65.59	52.78	1.24	12.94	8.33	1.55	Tenneze et al. 1999 [39]
po, -, 60 mg	dextromethorphan	EM	83.31	148.40	0.56	6.73	12.01	0.56	Feld et al. 2013 [11]
po, tab, 60 mg	dextromethorphan	EM	95.57	36.14	2.64	10.69	3.60	2.97	Antecip Bioventures 2016 [24]
po, cap, 30 mg	dextromethorphan	EM	25.66	35.47	0.72	4.33	4.38	0.99	Armani et al. 2017 [1]
po, cap, 30 mg	dextromethorphan	EM	36.25	36.01	1.01	4.22	3.02	1.39	Dumond et al. 2010 [8]
po, cap, 30 mg	dextromethorphan	EM	31.61	43.32	0.73	2.95	2.10	1.41	Edwards et al. 2017 [9]
po, -, 30 mg	dextromethorphan	EM	36.87	126.85	0.29	3.85	8.55	0.45	Ermer et al. 2015 [10]
po, cap, 30 mg	dextromethorphan	EM	19.51	8.11	2.40	4.35	1.55	2.82	Kakuda et al. 2014 [18]
po, -, 30 mg	dextromethorphan	EM	36.97	41.89	0.88	4.27	3.63	1.18	Khalilieh et al. 2018 [21]
po, tab, 30 mg	dextromethorphan	EM	23.03	32.08	0.72	4.26	3.81	1.12	Nakashima et al. 2007 [26]
po, cap, 30 mg	dextromethorphan	EM	23.77	22.53	1.05	2.45	2.86	0.86	Nyunt et al. 2008 [28]
po, cap, 30 mg	dextromethorphan	EM	25.79	12.76	2.02	4.42	2.45	1.80	Sager et al. 2014 [31]
po, cap, 30 mg	dextromethorphan	PM	848.57	981.20	0.86	20.65	32.30	0.64	Schadel et al. 1995 [32]
po, cap, 30 mg	dextromethorphan	EM	34.17	38.36	0.89	4.48	2.51	1.78	Stage et al. 2018 [35]
GMFE (dextromethorphan)					1.61 (1.01–3.45) 10/14 with GMFE ≤ 2			1.70 (1.01–2.97) 10/14 with GMFE ≤ 2	
po, -, 30 mg	dextrorphan	EM	29.47	20.71	1.42	3.76	2.96	1.27	Ermer et al. 2015 [10]
po, tab, 30 mg	dextrorphan	EM	18.53	22.02	0.84	3.35	3.61	0.93	Nakashima et al. 2007 [26]
po, cap, 30 mg	dextrorphan	EM	23.10	6.70	3.45	3.94	1.63	2.42	Sager et al. 2014 [31]
po, cap, 30 mg	dextrorphan	EM	18.40	19.56	0.94	4.34	3.85	1.13	Schadel et al. 1995 [32]
GMFE (dextrorphan)					1.78 (1.06–3.45) 3/4 with GMFE ≤ 2			1.47 (1.08–2.42) 3/4 with GMFE ≤ 2	
po, cap, 30 mg	dextrorphan *O*-glucuronide	EM	3634.81	3033.65	1.20	536.57	644.52	0.83	Schadel et al. 1995 [32]
GMFE (dextrorphan *O*-glucuronide)					1.20			1.20	

-: not given, AUC_{last}: AUC from the time of the first concentration measurement to the last time point of concentration measurement, cap: capsule, C_{max}: peak plasma concentration, CYP2D6: Cytochrome P450 2D6, EM: extensive metabolizer, inf: infusion, iv: intravenous, obs.: observed, PM: poor metabolizer, po: oral, pred: predicted.

Table S3.5.2: Predicted and observed AUC_{last} and C_{max} values and geometric mean fold errors (continued)

Dosing	Molecule	CYP2D6 status	AUC_{last} [ng·h/mL] Pred	Obs	Pred/Obs	C_{max} [ng/mL] Pred	Obs	Pred/Obs	Reference
					1/1 with GMFE $\leq$ 2			1/1 with GMFE $\leq$ 2	
po, tab, 60 mg	dextrorphan-total	EM	8053.06	5085.21	1.58	465.71	959.10	0.49	Antecip Bioventures 2016 [24]
po, -, 60 mg	dextrorphan-total	EM	5902.53	5449.79	1.08	474.19	489.35	0.97	Feld et al. 2013 [11]
po, cap, 80 mg	dextrorphan-total	EM	3658.56	3805.82	0.96	595.96	883.78	0.67	Tenneze et al. 1999 [39]
GMFE (dextrorphan-total)					1.23 (1.04–1.58) 3/3 with GMFE $\leq$ 2			1.52 (1.03–2.04) 2/3 with GMFE $\leq$ 2	
Overall GMFE					1.57 (1.01–3.45) 18/23 with GMFE $\leq$ 2			1.61 (1.01–2.97) 17/22 with GMFE $\leq$ 2	

-: not given, AUC_{last}: AUC from the time of the first concentration measurement to the last time point of concentration measurement, cap: capsule, C_{max}: peak plasma concentration, CYP2D6: Cytochrome P450 2D6, EM: extensive metabolizer, inf: infusion, iv: intravenous, obs.: observed, PM: poor metabolizer, po: oral, pred: predicted.

S3.6 Sensitivity Analysis

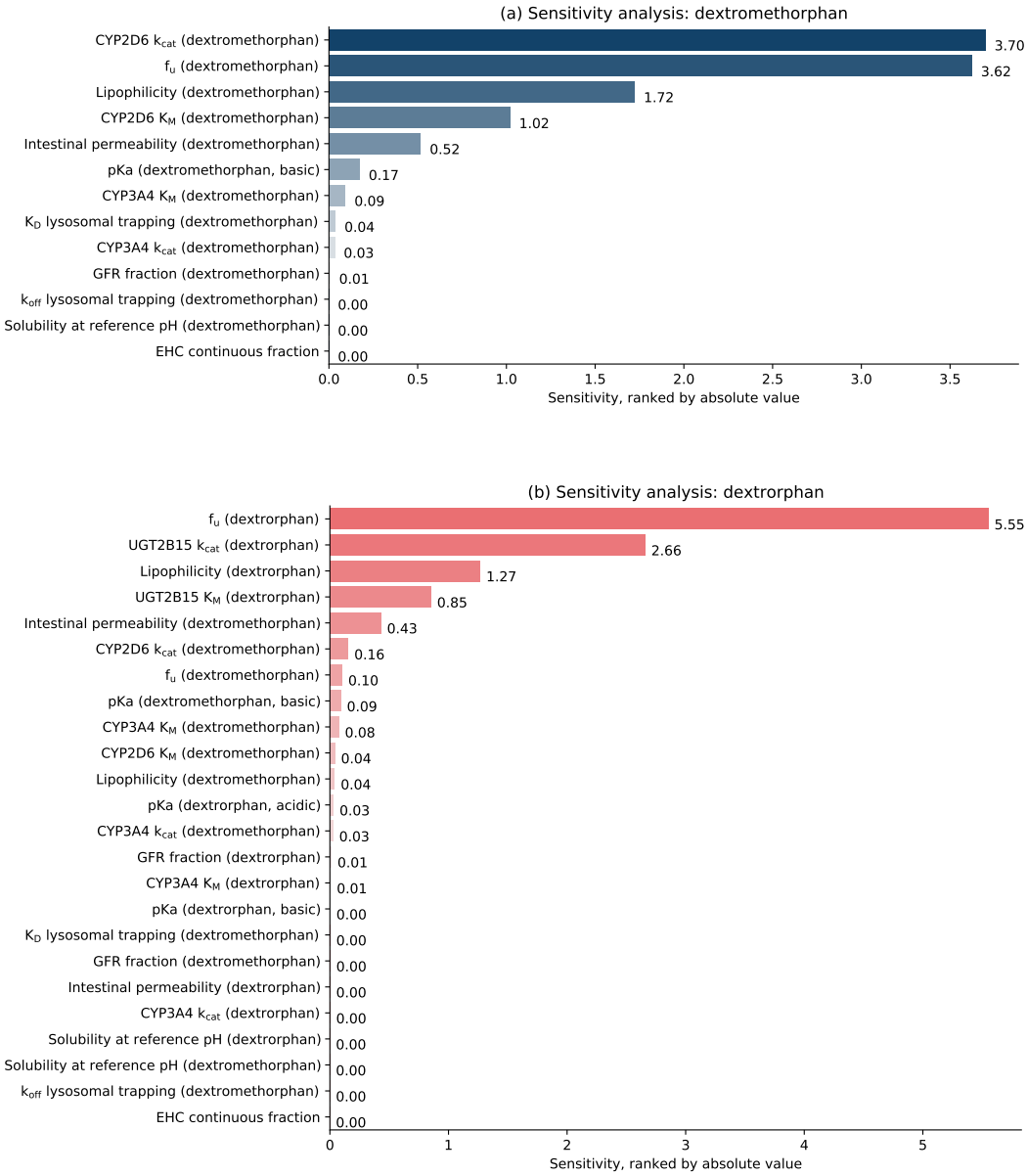

Figure S3.6.7: Sensitivity analysis of the dextromethorphan model. A sensitivity of +1.0 signifies that a 10% increase of the examined parameter value causes a 10% increase of the simulated $AUC_{0\text{-}24\,h}$. CYP2D6: Cytochrome P450 2D6, CYP3A4: cytochrome P450 3A4, f_u: fraction unbound, GFR: glomerular filtration rate, intest.: intestinal, k_{cat}: catalytic rate constant, K_D: dissociation constant, Michaelis-Menten constant (K_M): Michaelis-Menten constant, k_{off}: dissociation rate constant, pKa: acid dissociation constant.

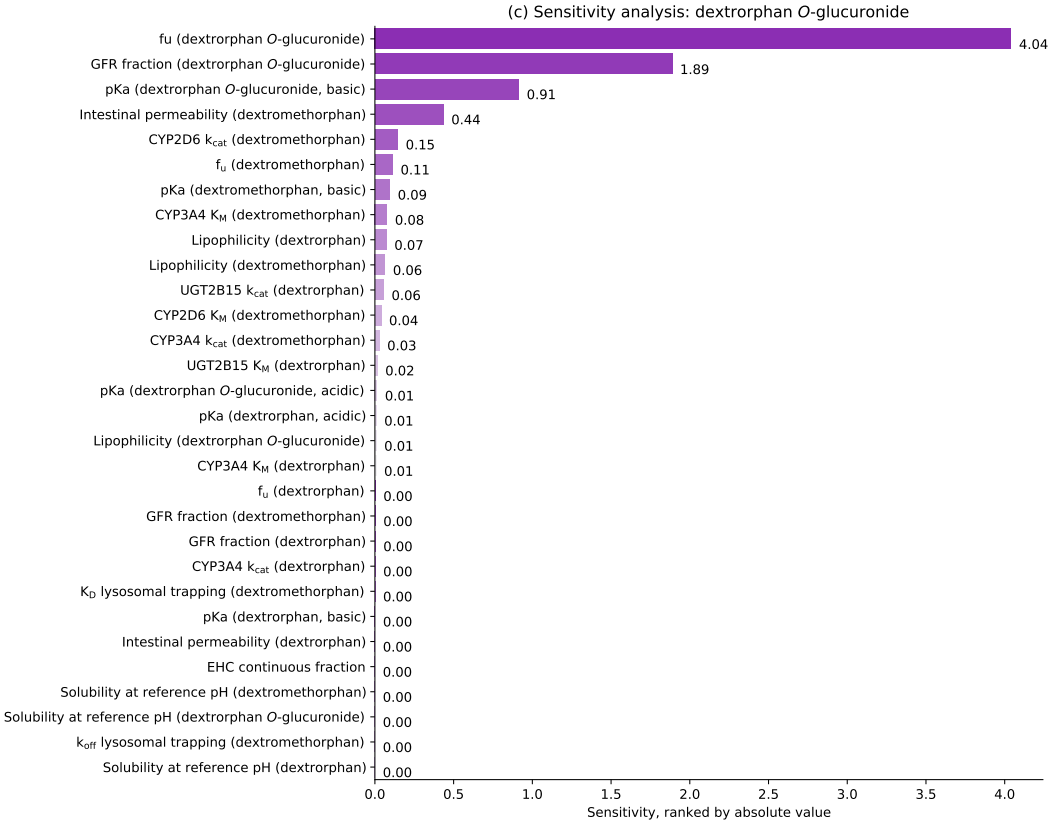

Figure S3.6.8: Sensitivity analysis of the dextromethorphan model. A sensitivity of +1.0 signifies that a 10% increase of the examined parameter value causes a 10% increase of the simulated $AUC_{0\text{-}24\,h}$. CYP2D6: Cytochrome P450 2D6, CYP3A4: cytochrome P450 3A4, f_u: fraction unbound, GFR: glomerular filtration rate, intest.: intestinal, k_{cat}: catalytic rate constant, K_D: dissociation constant, K_M: Michaelis-Menten constant, k_{off}: dissociation rate constant, pKa: acid dissociation constant.

S4 DGI Model Building

S4.1 Population k_{cat} Values

Table S4.1.1: Dextromethorphan population CYP2D6 k_{cat} values for CYP2D6 activity scores (ASs)

Activity Score	Projected Phenotype	$k_{cat} \rightarrow$ dxt [1/min]	k_{cat} Percentage of Reference (AS = 2) [%]
0	PM	0.0	0
0.25	IM	5.3	2
0.5		32.9	14
1		96.6	40
1.25	NM	115.2	48
1.5		151.8	63
2		242.5	100
3	UM	413.2	170

AS: CYP2D6 activity score, CYP2D6: Cytochrome P450 2D6, IM: intermediate metabolizer, k_{cat}: catalytic rate constant, NM: normal metabolizer, PM: poor metabolizer, UM: ultrarapid metabolizer.

S4.2 DGI Clinical Study Data

Table S4.2.2: Dextromethorphan DGI population study table

Route	Dose [mg]	n	Females [%]	Age [years]	Weight [kg]	Height [cm]	Metabolite measured	CYP2D6 Genotype	CYP2D6 AS	CYP2D6 P. Phenotype	Dataset	References
po (cap, sd)	30	6	33	22 (20-26)	-	-	dtt	-	-	EM	test	Capon 1996 [6]
po (cap, sd)	30	6	33	22 (20-26)	-	-	dtt	-	-	PM	test	Capon 1996 [6]
po (cap, sd)	30	16	50	34	73	175	-	†	1.25	NM	test[a]	Gazzaz 2018 [13]
po (-, sd)	30	11	55	31	79	-	dtt	-	-	EM	test[a]	Gorski 2004 [14]
po (-, sd)	30	1	0	31	79	-	dtt	-	-	PM	test[a]	Gorski 2004 [14]
po (cap, sd)	30	11	0	(18-55)	-	-	-	**1/*1*	2	NM	test	Yamazaki 2017 [44]
po (cap, sd)	30	12	0	(18-55)	-	-	-	**10/*10*	0.5	IM	test	Yamazaki 2017 [44]
po (tab, sd)	15	6	50	24 (22-26)	60	-	-	**1/*1*	2	NM	training	Qiu 2016 [30]
po (tab, sd)	15	6	50	24 (22-26)	60	-	-	**1/*10*	1.25	NM	training	Qiu 2016 [30]
po (tab, sd)	15	6	50	24 (22-26)	60	-	-	**10/*10*	0.5	IM	training	Qiu 2016 [30]
po (sol, sd)	5	17	53	27 (18-42)	-	-	dxt	†	2	NM	test	Storelli 2018 [36]
po (sol, sd)	5	16	75	24 (21-27)	-	-	dxt	†	1	IM	test	Storelli 2018 [36]
po (cap, sd)	3/kg	6	33	(21-34)	-	-	dxt, dtt	**1/*1*	2	NM	training	Zawertailo 2010 [45]

Values for age, weight and height are given as mean (range), -: not given, †: full genotype provided in publication, [a]: cocktail study, AS: CYP2D6 activity score, bid: twice daily, cap: capsule, CYP2D6: Cytochrome P450 2D6, DGI: drug-gene interaction, dxt: dextrorphan, dxt-glu: dextrorphan *O*-glucuronide, dtt: total dextrorphan, IM: intermediate metabolizer, inf: infusion, iv: intravenous, p.: projected, PM: poor metabolizer, po: oral, sd: single dose, sol: oral solution.

S5 DGI Model Evaluation

S5.1 Plasma Concentration-Time Profiles

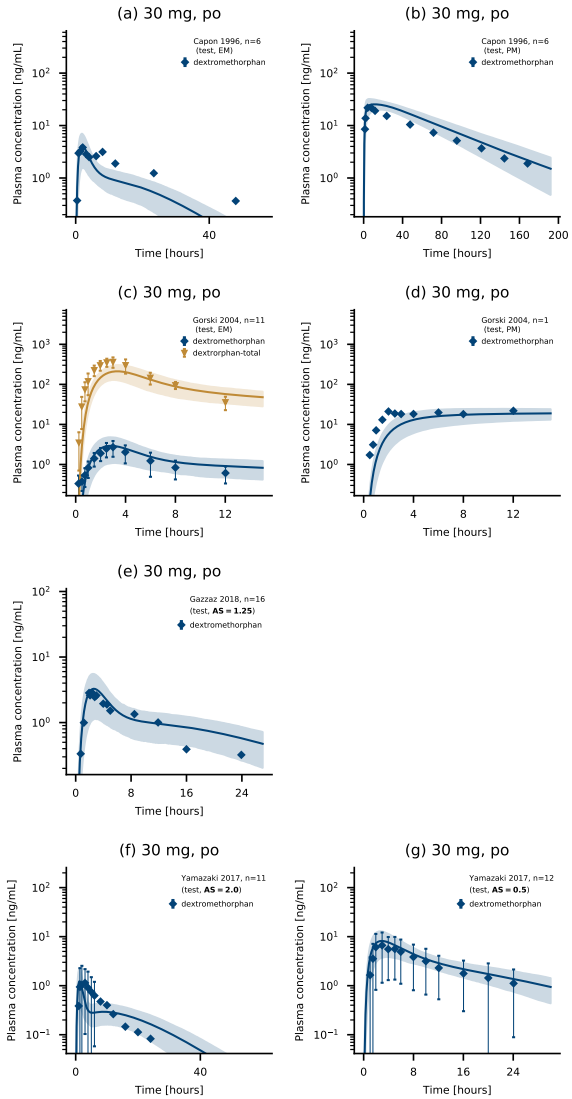

Figure S5.1.1: Dextromethorphan and total dextrorphan plasma concentrations of the modeled CYP2D6 drug-gene interaction. Predictions using the population k_{cat} of dextromethorphan and total dextrorphan (dextrorphan + dextrorphan *O*-glucuronide) plasma concentration-time profiles of the CYP2D6 drug-gene interaction (DGI) studies, compared to observed data (semilogarithmic representation). Population predictions (n=1000) are shown as lines with ribbons (arithmetic mean ± standard deviation (SD)), symbols represent the corresponding observed data ± SD. AS: activity score, EM: extensive metabolizer, PM: poor metabolizer, oral (po): oral.

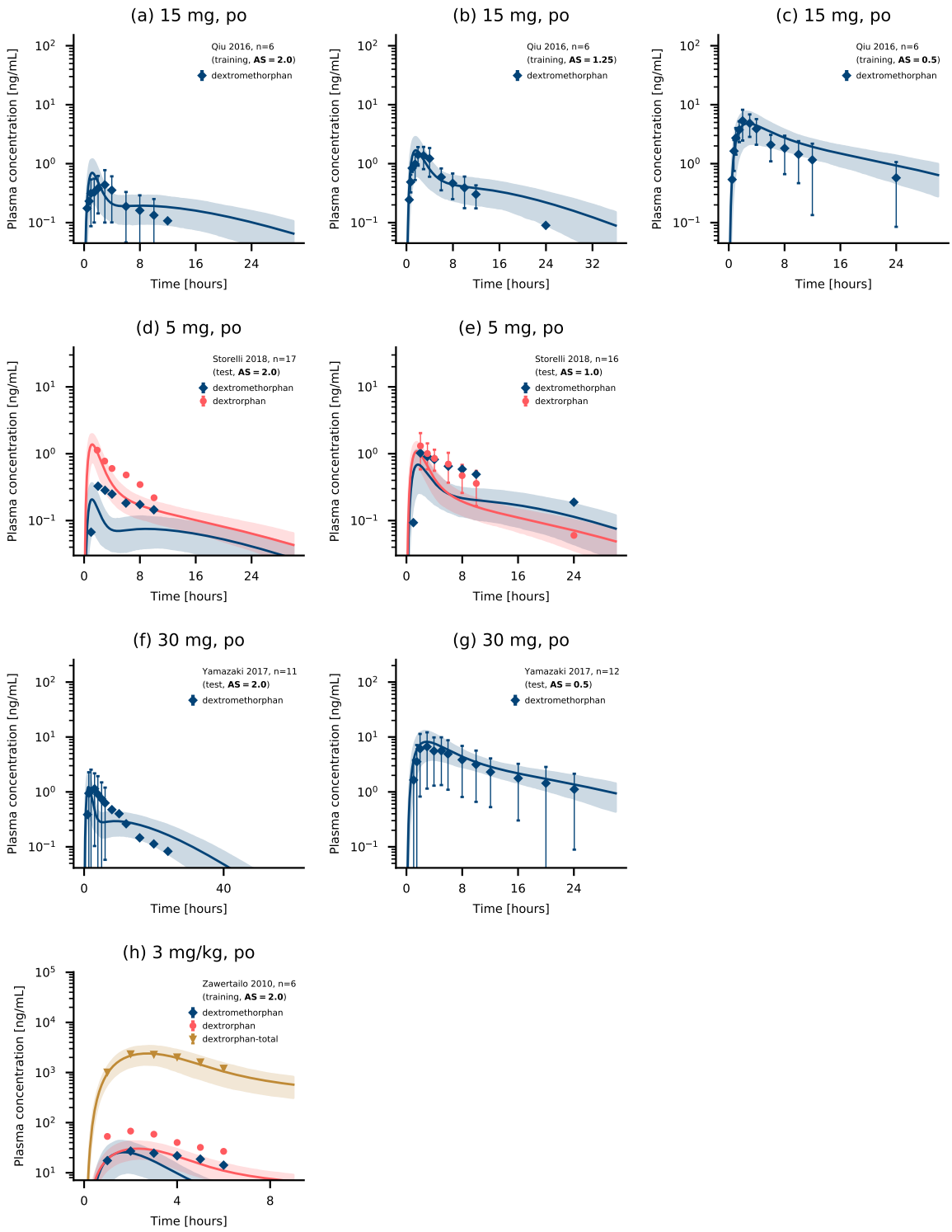

Figure S5.1.2: Dextromethorphan, dextrorphan and total dextrorphan plasma concentrations of the modeled CYP2D6 drug-gene interaction. Predictions using the population k_{cat} of dextromethorphan and total dextrorphan (dextrorphan + dextrorphan *O*-glucuronide) plasma concentration-time profiles of the CYP2D6 DGI studies, compared to observed data (semilogarithmic representation). Population predictions (n=1000) are shown as lines with ribbons (arithmetic mean $\pm$ standard deviation (SD)), symbols represent the corresponding observed data $\pm$ SD. AS: activity score, po: oral.

S5.2 Goodness-of-Fit Plots: Plasma Concentrations

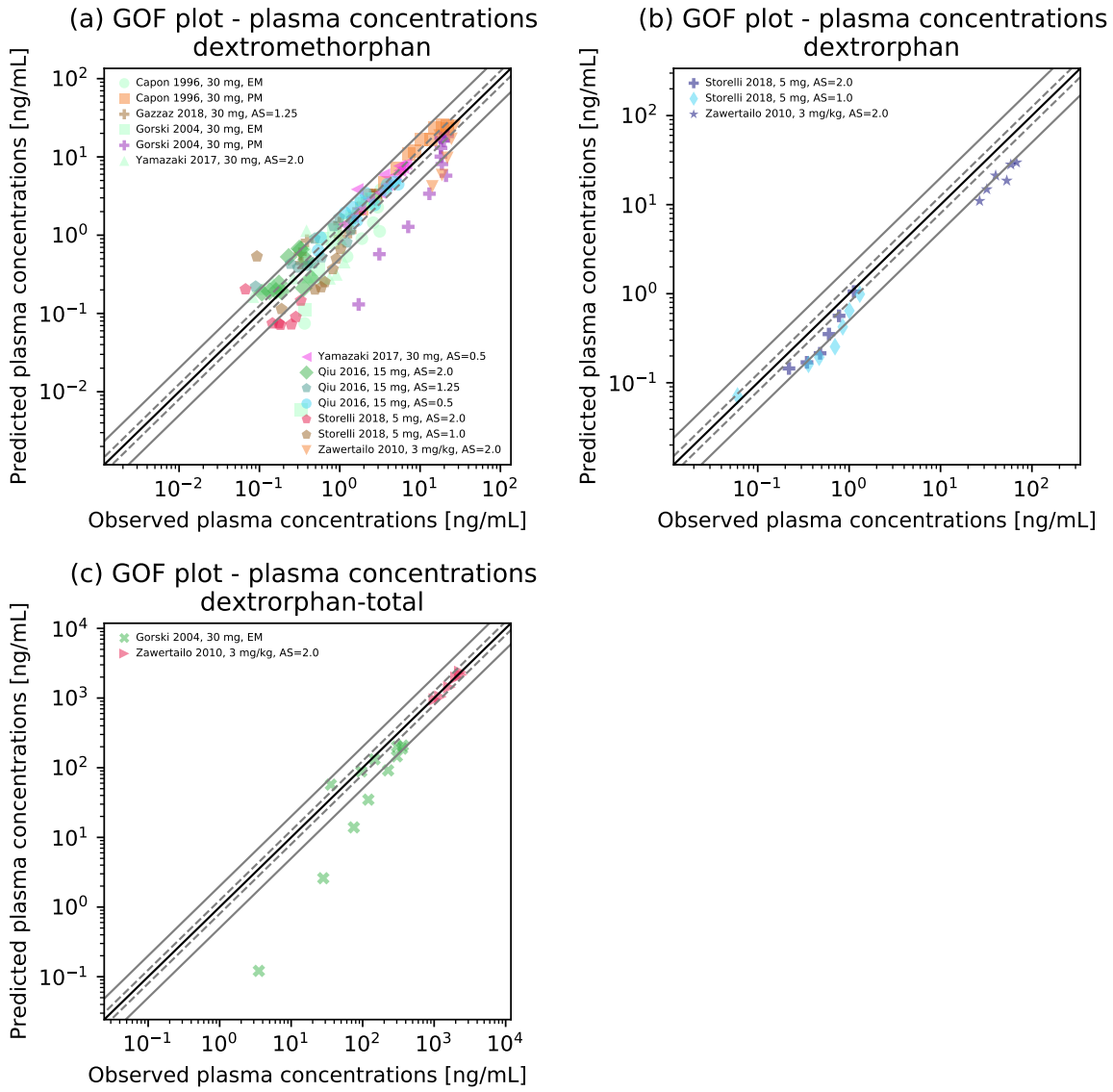

Figure S5.2.3: Goodness-of-fit plots. Predicted versus observed plasma concentration values for (a) dextromethorphan, (b) dextrorphan and (c) total dextrorphan (dextrorphan + dextrorphan *O*-glucuronide) for all studies of the DGI dataset. The solid black line marks the line of identity, the dashed gray lines mark the 0.8- to 1.25-fold range, the solid gray lines indicate the 0.5- to 2-fold range. Colored symbols represent the study population given in the legend. AS: CYP2D6 activity score, EM: extensive metabolizer, PM: poor metabolizer.

S5.3 MRD of Plasma Concentration Predictions

Table S5.3.1: Mean relative deviation of plasma concentration predictions

Dosing	Molecule	CYP2D6 status	MRD	Reference
po, cap, 30 mg	dextromethorphan	EM	2.00	Capon et al. 1996 [6]
po, cap, 30 mg	dextromethorphan	PM	1.34	Capon et al. 1996 [6]
po, cap, 30 mg	dextromethorphan	AS=1.25	1.40	Gazzaz et al. 2018 [13]
po, -, 30 mg	dextromethorphan	EM	3.68	Gorski et al. 2004 [14]
po, -, 30 mg	dextromethorphan	PM	3.36	Gorski et al. 2004 [14]
po, cap, 30 mg	dextromethorphan	AS=2.0	1.96	Yamazaki et al. 2017 [44]
po, cap, 30 mg	dextromethorphan	AS=0.5	1.46	Yamazaki et al. 2017 [44]
po, tab, 15 mg	dextromethorphan	AS=2.0	1.59	Qiu et al. 2016 [30]
po, tab, 15 mg	dextromethorphan	AS=1.25	1.59	Qiu et al. 2016 [30]
po, tab, 15 mg	dextromethorphan	AS=0.5	1.38	Qiu et al. 2016 [30]
po, sol, 5 mg	dextromethorphan	AS=2.0	2.68	Storelli et al. 2018 [37]
po, sol, 5 mg	dextromethorphan	AS=1.0	2.47	Storelli et al. 2018 [37]
po, cap, 3 mg/kg	dextromethorphan	AS=2.0	2.11	Zawertailo et al. 2010 [45]
MRD (dextromethorphan)			2.08 (1.34–3.68) 8/13 with MRD $\leq$ 2	
po, sol, 5 mg	dextrorphan	AS=2.0	1.69	Storelli et al. 2018 [37]
po, sol, 5 mg	dextrorphan	AS=1.0	1.98	Storelli et al. 2018 [37]
po, cap, 3 mg/kg	dextrorphan	AS=2.0	2.26	Zawertailo et al. 2010 [45]
MRD (dextrorphan)			1.98 (1.69–2.26) 2/3 with MRD $\leq$ 2	
po, -, 30 mg	dextrorphan-total	EM	4.26	Gorski et al. 2004 [14]
po, cap, 3 mg/kg	dextrorphan-total	AS=2.0	1.10	Zawertailo et al. 2010 [45]
MRD (dextrorphan-total)			2.68 (1.10–4.26) 1/2 with MRD $\leq$ 2	
Overall MRD			2.13 (1.10–4.26) 11/18 with MRD $\leq$ 2	

-: not given, AS: CYP2D6 activity score, cap: capsule, CYP2D6: Cytochrome P450 2D6, EM: extensive metabolizer, inf: infusion, iv: intravenous, PM: poor metabolizer, po: oral, sol: oral solution.

S5.4 AUC_{last} and C_{max} Goodness-of-Fit Plots

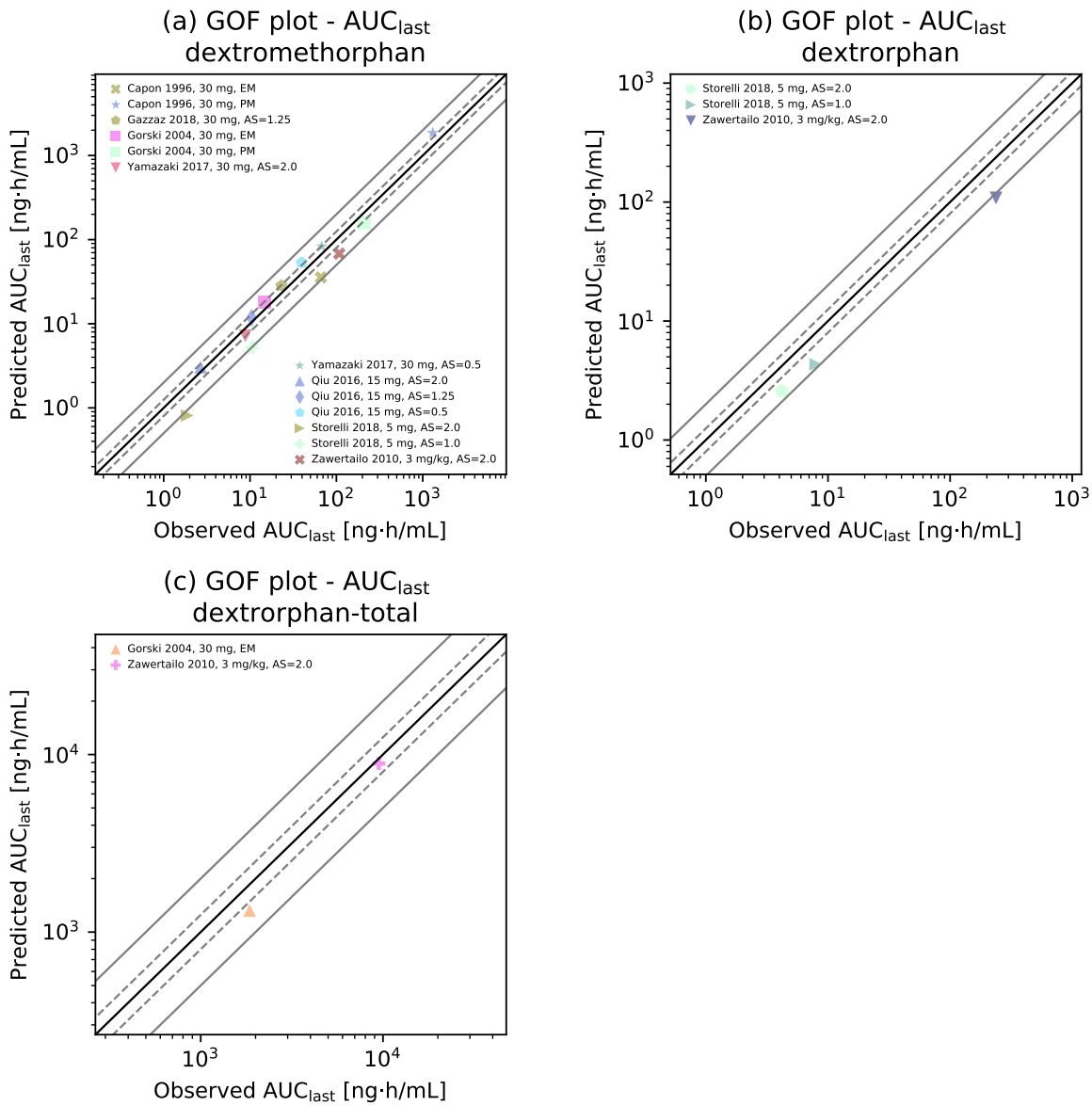

Figure S5.4.4: AUC correlation plots. Predicted versus observed AUC_{last} for (a) dextromethorphan, (b) dextrorphan and (c) total dextrorphan (dextrorphan + dextrorphan *O*-glucuronide) for all studies of the DGI dataset. The solid black line marks the line of identity, the dashed gray lines mark the 0.8- to 1.25-fold range, the solid gray lines indicate the 0.5- to 2-fold range. Colored symbols represent the study population given in the legend. AS: CYP2D6 activity score, AUC_{last}: AUC from the time of the first concentration measurement to the last time point of concentration measurement, EM: extensive metabolizer, PM: poor metabolizer.

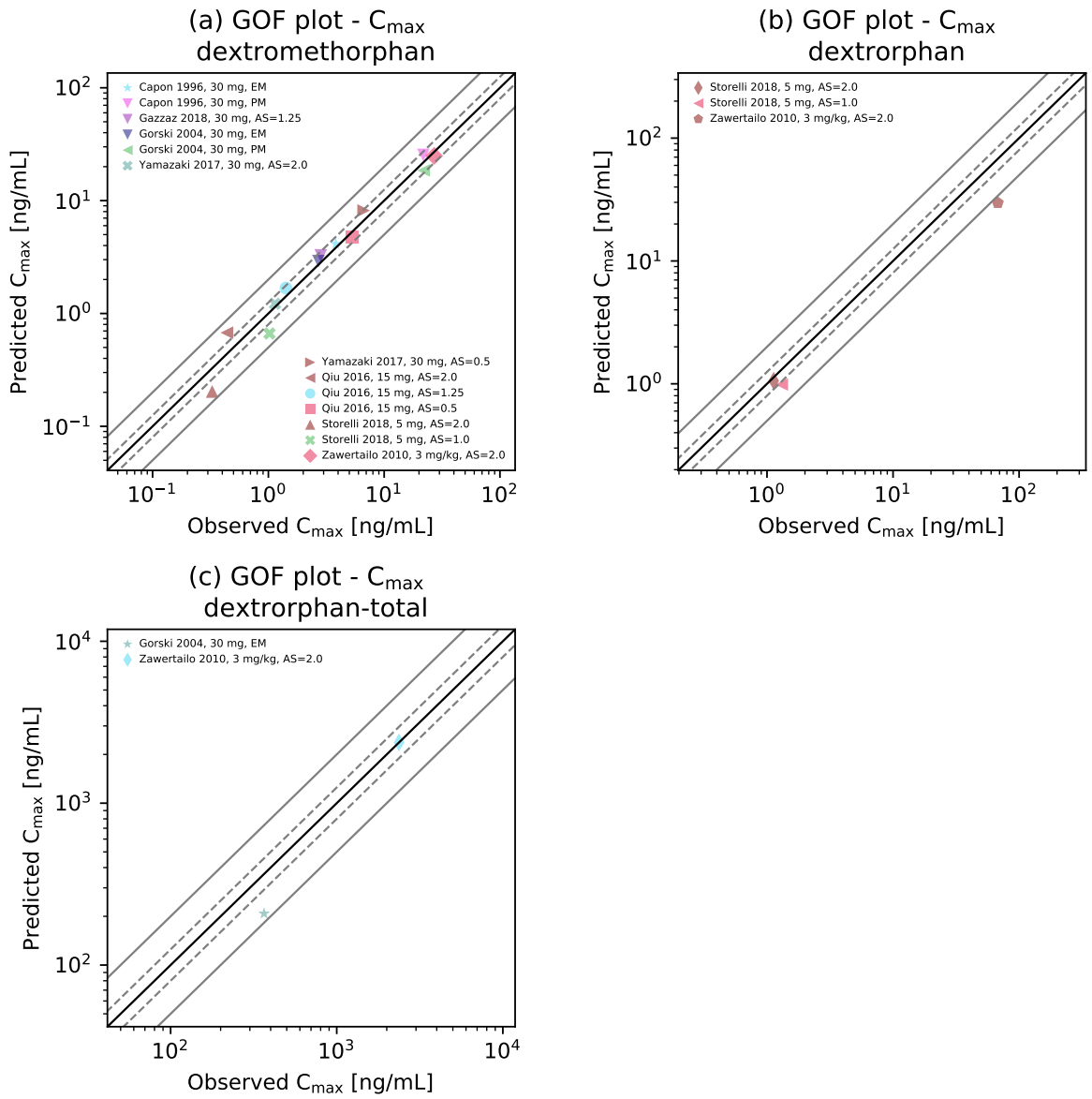

Figure S5.4.5: C_{max} correlation plots. Predicted versus observed C_{max} for (a) dextromethorphan, (b) dextrorphan and (c) total dextrorphan (dextrorphan + dextrorphan *O*-glucuronide) for all studies of the DGI dataset. The solid black line marks the line of identity, the dashed gray lines mark the 0.8- to 1.25-fold range, the solid gray lines indicate the 0.5- to 2-fold range. Colored symbols represent the study population given in the legend. AS: CYP2D6 activity score, C_{max}: peak plasma concentration, EM: extensive metabolizer, PM: poor metabolizer.

S5.5 GMFE of Predicted AUC_{last} and C_{max} Values

Table S5.5.2: Predicted and observed AUC_{last} and C_{max} values and geometric mean fold errors

Dosing	Molecule	CYP2D6 status	AUC_{last} [ng·h/ml] Pred	Obs	Pred/Obs	C_{max} [ng/ml] Pred	Obs	Pred/Obs	Reference
po, cap, 30 mg	dextromethorphan	EM	34.02	66.20	0.51	3.50	3.82	0.92	Capon et al. 1996 [6]
po, cap, 30 mg	dextromethorphan	PM	1840.48	1304.44	1.41	24.92	21.81	1.14	Capon et al. 1996 [6]
po, -, 30 mg	dextromethorphan	EM	17.77	14.62	1.22	2.98	2.70	1.10	Gorski et al. 2004 [14]
po, -, 30 mg	dextromethorphan	PM	171.48	208.95	0.82	20.09	21.93	0.92	Gorski et al. 2004 [14]
po, cap, 30 mg	dextromethorphan	AS=1.25	28.60	23.09	1.24	3.45	2.83	1.22	Gazzaz et al. 2018 [13]
po, cap, 30 mg	dextromethorphan	AS=2.0	7.34	8.83	0.83	1.13	1.14	0.99	Yamazaki et al. 2017 [44]
po, cap, 30 mg	dextromethorphan	AS=0.5	85.58	67.73	1.26	8.87	6.65	1.33	Yamazaki et al. 2017 [44]
po, tab, 15 mg	dextromethorphan	AS=2.0	2.91	2.68	1.08	0.62	0.44	1.41	Qiu et al. 2016 [30]
po, tab, 15 mg	dextromethorphan	AS=1.25	12.42	10.41	1.19	1.72	1.42	1.22	Qiu et al. 2016 [30]
po, tab, 15 mg	dextromethorphan	AS=0.5	54.16	39.65	1.37	5.12	5.33	0.96	Qiu et al. 2016 [30]
po, sol, 5 mg	dextromethorphan	AS=2.0	0.80	1.87	0.43	0.20	0.33	0.62	Storelli et al. 2018 [37]
po, sol, 5 mg	dextromethorphan	AS=1.0	5.42	10.59	0.51	0.65	1.02	0.63	Storelli et al. 2018 [37]
po, cap, 3 mg/kg	dextromethorphan	AS=2.0	69.64	107.81	0.65	25.94	27.04	0.96	Zawertailo et al. 2010 [45]
GMFE (dextromethorphan)					1.46 (1.08–2.33) 12/13 with GMFE ≤ 2			1.22 (1.01–1.61) 13/13 with GMFE ≤ 2	
po, sol, 5 mg	dextrorphan	AS=2.0	2.60	4.19	0.62	1.38	1.13	1.22	Storelli et al. 2018 [37]
po, sol, 5 mg	dextrorphan	AS=1.0	4.37	7.94	0.55	1.06	1.31	0.81	Storelli et al. 2018 [37]
po, cap, 3 mg/kg	dextrorphan	AS=2.0	109.82	237.65	0.46	30.63	67.77	0.45	Zawertailo et al. 2010 [45]
GMFE (dextrorphan)					1.87 (1.61–2.17) 2/3 with GMFE ≤ 2			1.52 (1.08–2.22) 2/3 with GMFE ≤ 2	
po, -, 30 mg	dextrorphan-total	EM	1307.35	1854.58	0.70	214.79	365.28	0.59	Gorski et al. 2004 [14]

-: not given, AS: CYP2D6 activity score, AUC_{last}: AUC from the time of the first concentration measurement to the last time point of concentration measurement, cap: capsule, C_{max}: peak plasma concentration, CYP2D6: Cytochrome P450 2D6, EM: extensive metabolizer, inf: infusion, iv: intravenous, obs.: observed, PM: poor metabolizer, po: oral, pred: predicted.

Table S5.5.2: Predicted and observed AUC_{last} and C_{max} values and geometric mean fold errors (continued)

Dosing	Molecule	CYP2D6 status	AUC_{last} [ng·h/ml]			C_{max} [ng/ml]			Reference
			Pred	Obs	Pred/Obs	Pred	Obs	Pred/Obs	
cap, 3 mg/kg	dextrorphan-total	AS=2.0	8998.15	9490.66	0.95	2427.95	2370.93	1.02	Zawertailo et al. 2010 [45]
GMFE (dextrorphan-total)					1.24 (1.05–1.43) 2/2 with GMFE $\leq$ 2			1.36 (1.02–1.69) 2/2 with GMFE $\leq$ 2	
Overall GMFE					1.50 (1.05–2.33) 16/18 with GMFE $\leq$ 2			1.28 (1.01–2.22) 17/18 with GMFE $\leq$ 2	

-: not given, AS: CYP2D6 activity score, AUC_{last}: AUC from the time of the first concentration measurement to the last time point of concentration measurement, cap: capsule, C_{max}: peak plasma concentration, CYP2D6: Cytochrome P450 2D6, EM: extensive metabolizer, inf: infusion, iv: intravenous, obs.: observed, PM: poor metabolizer, po: oral, pred: predicted.

S5.6 DGI AUC_{last} and C_{max} Ratio Plots

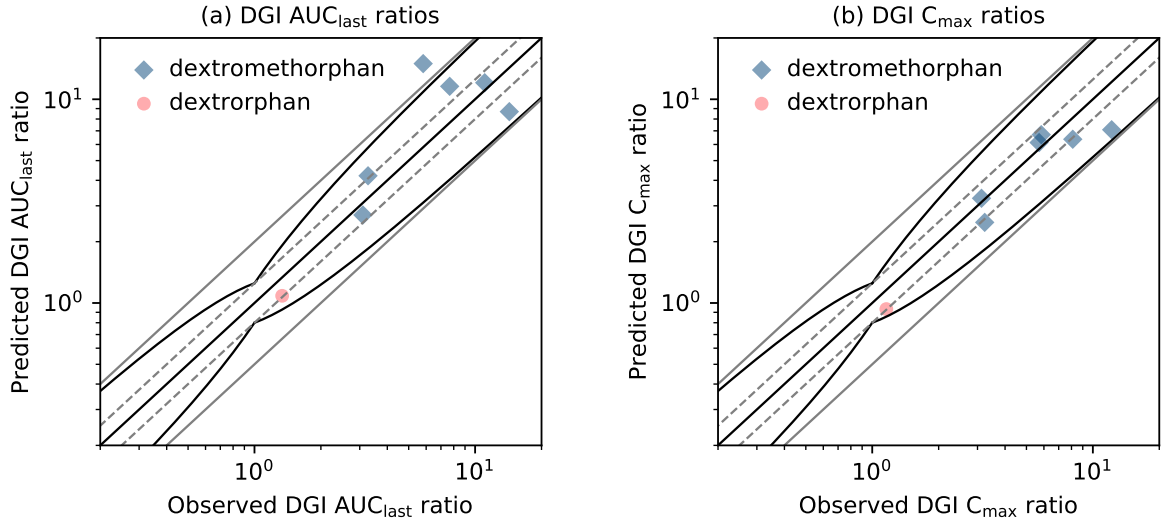

Figure S5.6.6: Predicted versus observed dextromethorphan DGI ratios. Comparison of predicted versus observed (a) AUC_{last} ratios and (b) C_{max} ratios for dextromethorphan CYP2D6 DGI-studies. The straight black line indicates the line of identity, curved black lines show prediction success limits proposed by Guest et al. including 1.25-fold variability [15]. Solid light gray lines indicate 2-fold deviation, dashed light gray lines show 1.25-fold deviation. AUC_{last}: AUC from the time of the first concentration measurement to the last time point of concentration measurement, C_{max}: peak plasma concentration, DGI: drug-gene interaction

S5.7 GMFE of Predicted DGI AUC_{last} and C_{last} Ratios

Table S5.7.3: Geometric mean fold error of predicted DGI AUC_{last} and C_{max} ratios

		CYP2D6			AUC_{last} ratio			C_{max} ratio			
Molecule	Dosing	AS	Genotype	p. Phenotype	Pred	Obs	Pred/Obs	Pred	Obs	Pred/Obs	Reference
dextromethorphan	30 mg, cap, sd	-	-	PM	16.55	5.82	2.84	7.2	5.71	1.26	Capon et al. 1996 [6]
dextromethorphan	30 mg, -, sd	-	-	PM	10.67	14.29	0.75	7.02	8.11	0.87	Gorski et al. 2004 [14]
dextromethorphan	5 mg, sol, sd	1.0	†	IM	4.37	3.27	1.34	3.2	3.13	1.02	Storelli et al. 2018 [37]
dextrorphan	5 mg, sol, sd	1.0	†	IM	1.07	1.33	0.8	0.92	1.16	0.8	Storelli et al. 2018 [37]
dextromethorphan	15 mg, tab, sd	1.25	**1/*10*	NM	2.97	3.1	0.96	2.94	3.23	0.91	Qiu et al. 2016 [30]
dextromethorphan	15 mg, tab, sd	0.5	**10/*10*	IM	14.01	11.06	1.27	8.94	12.17	0.73	Qiu et al. 2016 [30]
dextromethorphan	30 mg, cap, sd	0.5	**10/*10*	IM	12.07	7.67	1.57	8.17	5.84	1.4	Yamazaki et al. 2017 [44]
Overall GMFE						1.45 (1.04–2.84)				1.21 (1.02–1.40)	
						6/7 with GMFE $\leq$ 2				7/7 with GMFE $\leq$ 2	
Ratios within the limits of *Guest et al.* [15] (including 1.25-fold deviation)						6/7				7/7	

-: not available, †: full genotype provided in publication, AS: CYP2D6 activity score, AUC_{last}: AUC from the time of the first concentration measurement to the last time point of concentration measurement, cap: capsule, C_{max}: peak plasma concentration, CYP2D6: Cytochrome P450 2D6, obs: observed, IM: intermediate metabolizer, NM: normal metabolizer, p.: projected, PM: poor metabolizer, pred: predicted, sol: oral solution, sd: single dose.

S6 Interindividual Variability Within Activity Score Groups

S6.1 Exploratory Analysis of Reported Individual Plasma Concentration-Time Profiles

In the PhD thesis by Frank [12], plasma concentration-time profiles for dextromethorphan, dextrorphan and total dextrorphan were reported for five cocktail studies (A–E) for a total of 84 individuals. To assess the plausibility of the reported individual profiles, AUC_{last} and C_{max} values were calculated for all observed dextromethorphan profiles. The authors assumed that AUC_{last} and C_{max} values would generally decrease with increasing CYP2D6 activity scores. This was true for four (A, C, D and E) of the five studies, as depicted in Figure S6.1.1. As AUC_{last} and C_{max} values clearly violated this assumption, study B was excluded from the subsequent modeling steps and analyses.

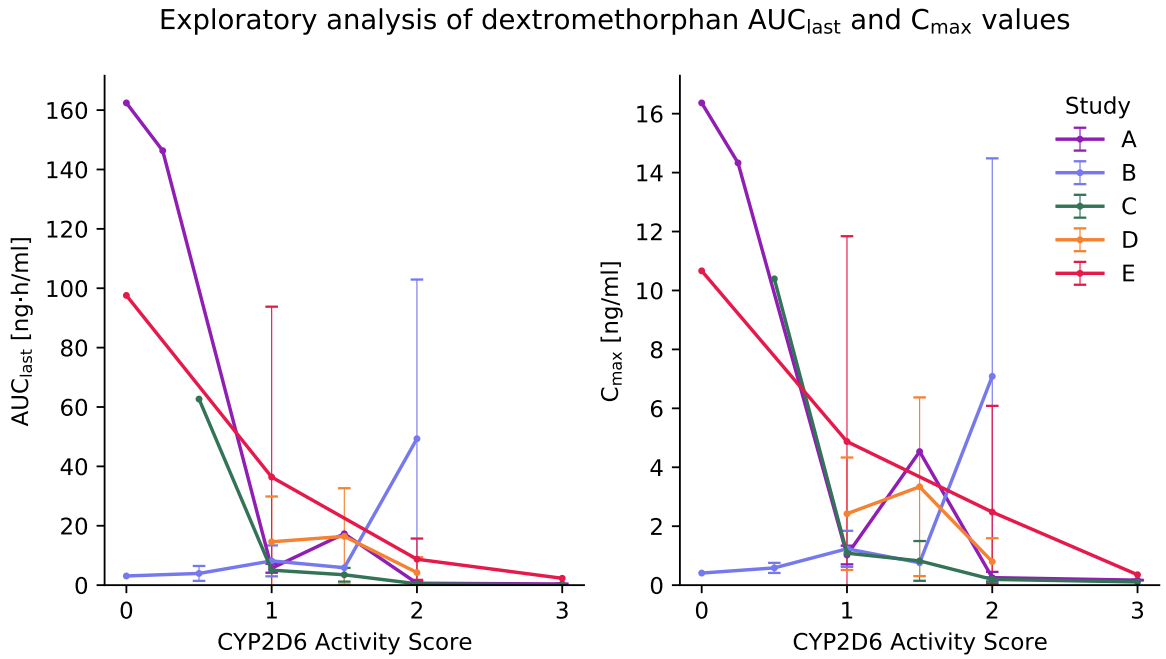

Figure S6.1.1: Exploratory analysis of dextromethorphan AUC_{last} and C_{max} values. Observed AUC_{last} (left) and C_{max} values (right panel) for dextromethorphan for individual profiles. Lines and symbols represent the observed AUC_{last} and C_{max} data points per activity score AUC_{last}: AUC from the time of the first concentration measurement to the last time point of concentration measurement, C_{max}: peak plasma concentration.

S6.2 Mean Individual k_{cat} Values

Table S6.2.1: CYP2D6 activity scores in the DGI study population with population k_{cat} values and mean individual optimized k_{cat} values.

Activity Score	Projected Phenotype	Individuals (n)	Population k_{cat} [1/min]	Mean Individual k_{cat} [1/min]
0	PM	2	0.0	-
0.25	IM	1	5.3	-
0.5		1	32.9	-
1		25	96.6	106.3 (2.5)
1.25	NM	0	115.2	-
1.5		7	151.8	168.5 (1.9)
2		26	242.5	260.0 (2.1)
3	UM	4	413.2	462 (1.3)

Individual optimized k_{cat} values are given as mean (SD), IM: intermediate metabolizer, k_{cat}: catalytic rate constant, NM: normal metabolizer, PM: poor metabolizer, n: number of individuals, UM: ultrarapid metabolizer.

S6.3 Clinical Study Data

Table S6.3.2: Dextromethorphan cocktail study table [12]

Subject ID	Sex	Age [years]	Weight [kg]	Height [cm]	Ethnicity	CYP2D6 genotype	CYP2D6 AS	CYP2D6 p. phenotype	Dataset
A01	male	42	84	188	caucasian	*4/*10	0.25	IM	training
A02	male	27	65	171	caucasian	*1/*41	1.5	NM	test
A03	male	34	77	189	caucasian	*1/*1	2	NM	test
A04	male	24	78	183	caucasian	*1/*4	1	IM	test
A05	male	27	69	176	caucasian	*1/*4	1	IM	test
A06	male	24	86	181	caucasian	*1/*1	2	NM	test
A07	male	27	74	173	caucasian	*1/*4	1	IM	training
A08	male	23	71	180	caucasian	*4/*4	0	PM	training
A09	male	27	90	190	caucasian	*1/*2	2	NM	training
A10	male	38	80	185	caucasian	*2/*4	1	IM	test
A11	male	34	101	195	caucasian	*1/*4	1	IM	test
A12	male	34	65	174	caucasian	*2/*2x2	3	UM	test
A13	male	31	83	189	caucasian	*1/*4	1	IM	training
A14	male	25	79	180	caucasian	*1/*2	2	NM	test
A15	male	23	69	175	caucasian	*1x2/*2	3	UM	test
A16	male	29	86	188	caucasian	*1/*4	1	IM	test
C01	male	25	80	178	caucasian	*1/*1	2	NM	test
C02	male	24	71	173	caucasian	*1/*1	2	NM	training
C03	male	37	66	178	caucasian	*1/*1	2	NM	training
C04	male	27	92	185	caucasian	*2x2/*3	2	NM	test
C05	male	21	79	190	caucasian	-	-	-	test
C06	male	29	76	176	caucasian	*1/*1x2	3	UM	training
C07	male	31	84	185	caucasian	-	-	-	test
C08	male	26	83	182	caucasian	*4/*41	0.5	IM	training
C09	male	25	77	184	caucasian	-	-	-	test
C10	male	26	69	184	caucasian	*2/*9	1.5	NM	training
C11	male	33	91	194	caucasian	*1/*41	1.5	NM	test
C12	male	43	71	177	caucasian	*1/*41	1.5	NM	test
C13	male	29	79	179	caucasian	-	-	-	test
C14	male	30	89	187	caucasian	*1/*41	1.5	NM	test
C15	male	22	74	176	caucasian	*1/*4	1	IM	training
C16	male	29	99	189	caucasian	-	-	-	test
D01	male	44	60	171	caucasian	*1/*2	2	NM	test
D02	male	25	75	185	caucasian	*2/*41	1.5	NM	training
D03	male	23	82	183	caucasian	*1/*1	2	NM	training
D04	male	18	74	186	caucasian	*2/*2	2	NM	test
D05	male	46	69	178	caucasian	-	-	-	test
D06	male	48	73	179	caucasian	*2/*4	1	IM	test
D07	male	30	69	173	caucasian	*1/*2	2	NM	test
D08	male	27	70	180	caucasian	*2/*4	1	IM	training
D09	male	42	74	173	caucasian	*2/*2	2	NM	test
D10	male	26	73	184	caucasian	*1/*41	1.5	NM	test

Studies A, C and D were performed in healthy subjects, whereas participants of study E were HIV-infected patients, which did not yet receive any antiretroviral treatment.
-: not given, AS: CYP2D6 activity score, CYP2D6: Cytochrome P450 2D6, IM: intermediate metabolizer, NM: normal metabolizer, p.: projected, PM: poor metabolizer, UM: ultrarapid metabolizer.

Table S6.3.2: Dextromethorphan cocktail study table [12] *(continued)*

Subject ID	Sex	Age [years]	Weight [kg]	Height [cm]	Ethnicity	CYP2D6 genotype	CYP2D6 AS	CYP2D6 p. phenotype	Dataset
D11	male	26	70	175	caucasian	*2/*4	1	IM	training
D12	male	27	73	190	caucasian	*2/*4x2	1	IM	test
E01	male	33	56	185	caucasian	*1/*4	1	IM	test
E02	male	51	106	170	caucasian	*1/*4	1	IM	test
E03	male	39	75	175	caucasian	*1/*4	1	IM	test
E04	male	48	73	173	caucasian	*1/*1	2	NM	training
E05	male	33	85	190	caucasian	*1/*1	2	NM	test
E06	male	35	72	175	caucasian	*1/*3	1	IM	test
E07	female	32	73	164	african american	*1/*1	2	NM	test
E08	male	43	76	172	african american	*1/*1	2	NM	test
E09	male	57	62	174	caucasian	*1/*1	2	NM	test
E10	male	30	49	171	caucasian	*1/*5	1	IM	training
E11	male	41	86	184	caucasian	*1/*4	1	IM	test
E12	male	38	69	176	caucasian	*1/*1	2	NM	training
E13	male	43	66	167	african american	*1/*1	2	NM	test
E14	male	30	75	180	caucasian	*1/*4	1	IM	test
E15	female	27	55	164	caucasian	*1/*1	2	NM	training
E16	male	59	87	183	caucasian	*1/*4	1	IM	training
E17	female	28	50	167	african american	*1/2x*4	1	IM	test
E18	female	39	63	178	caucasian	*1/*1	2	NM	test
E20	male	34	73	176	caucasian	*1/*1	2	NM	training
E21	female	36	54	156	african american	*1/*5	1	IM	training
E22	male	42	94	169	caucasian	*4/*6	0	PM	test
E23	male	60	64	178	caucasian	*1x2/*1	3	UM	training
E24	male	33	70	180	caucasian	*1/*1	2	NM	training
E25	female	60	73	180	caucasian	*1/*1	2	NM	training
E26	male	25	83	166	caucasian	*1/*3	1	IM	training
E27	male	40	70	176	caucasian	*1/*1	2	NM	test
E28	male	48	80	172	caucasian	*1/*4	1	IM	training
E30	female	38	67	173	caucasian	*1/*4	1	IM	test

Studies A, C and D were performed in healthy subjects, whereas participants of study E were HIV-infected patients, which did not yet receive any antiretroviral treatment.
-: not given, AS: CYP2D6 activity score, CYP2D6: Cytochrome P450 2D6, IM: intermediate metabolizer, NM: normal metabolizer, p.: projected, PM: poor metabolizer, UM: ultrarapid metabolizer.

S6.4 Plasma Concentration-Time Profiles

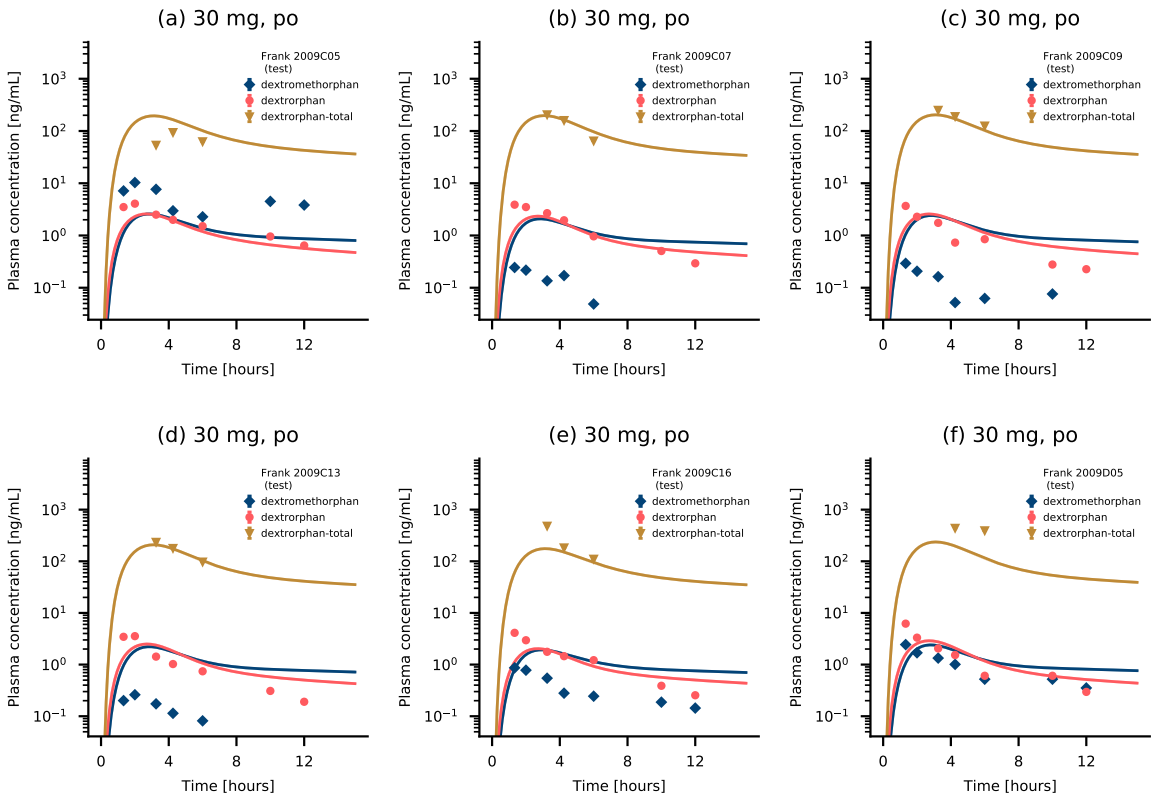

Figure S6.4.2: Dextromethorphan plasma concentrations for individuals where no genotype was provided. The simulations were performed using the model CYP2D6 k_{cat} value for normal metabolizers (see Section S2.1). Predictions of dextromethorphan and dextrorphan profiles, compared to observed data [12] (semilogarithmic representation). Predictions using the population k_{cat} are shown as solid lines, individual predictions are shown as dotted lines. Symbols represent the corresponding observed data. po: oral.

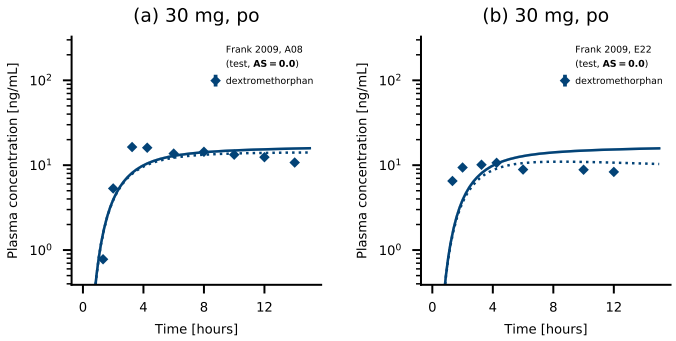

Figure S6.4.3: Dextromethorphan plasma concentrations for individuals with a CYP2D6 AS = 0 (poor metabolizer (PM)). Predictions of dextromethorphan plasma concentration-time profiles, compared to observed data [12] (semilogarithmic representation). Predictions using the population k_{cat} are shown as solid lines, individual predictions are shown as dotted lines. Symbols represent the corresponding observed data. AS: activity score, po: oral.

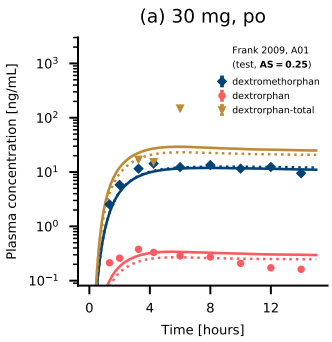

Figure S6.4.4: Dextromethorphan, dextrorphan and total dextrorphan plasma concentrations for individuals with a CYP2D6 AS = 0.25. Predictions of dextromethorphan plasma concentration-time profiles, compared to observed data [12] (semilogarithmic representation). Predictions using the population k_{cat} are shown as solid lines, individual predictions are shown as dotted lines. Symbols represent the corresponding observed data. AS: activity score, po: oral.

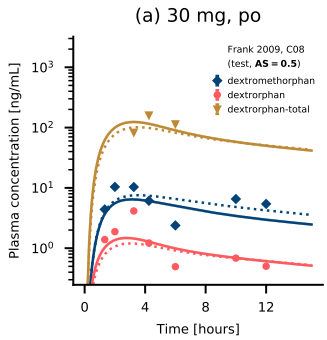

Figure S6.4.5: Dextromethorphan, dextrorphan and total dextrorphan plasma concentrations for individuals with a CYP2D6 AS = 0.5. Predictions of dextromethorphan plasma concentration-time profiles, compared to observed data [12] (semilogarithmic representation). Predictions using the population k_{cat} are shown as solid lines, individual predictions are shown as dotted lines. Symbols represent the corresponding observed data. AS: activity score, po: oral.

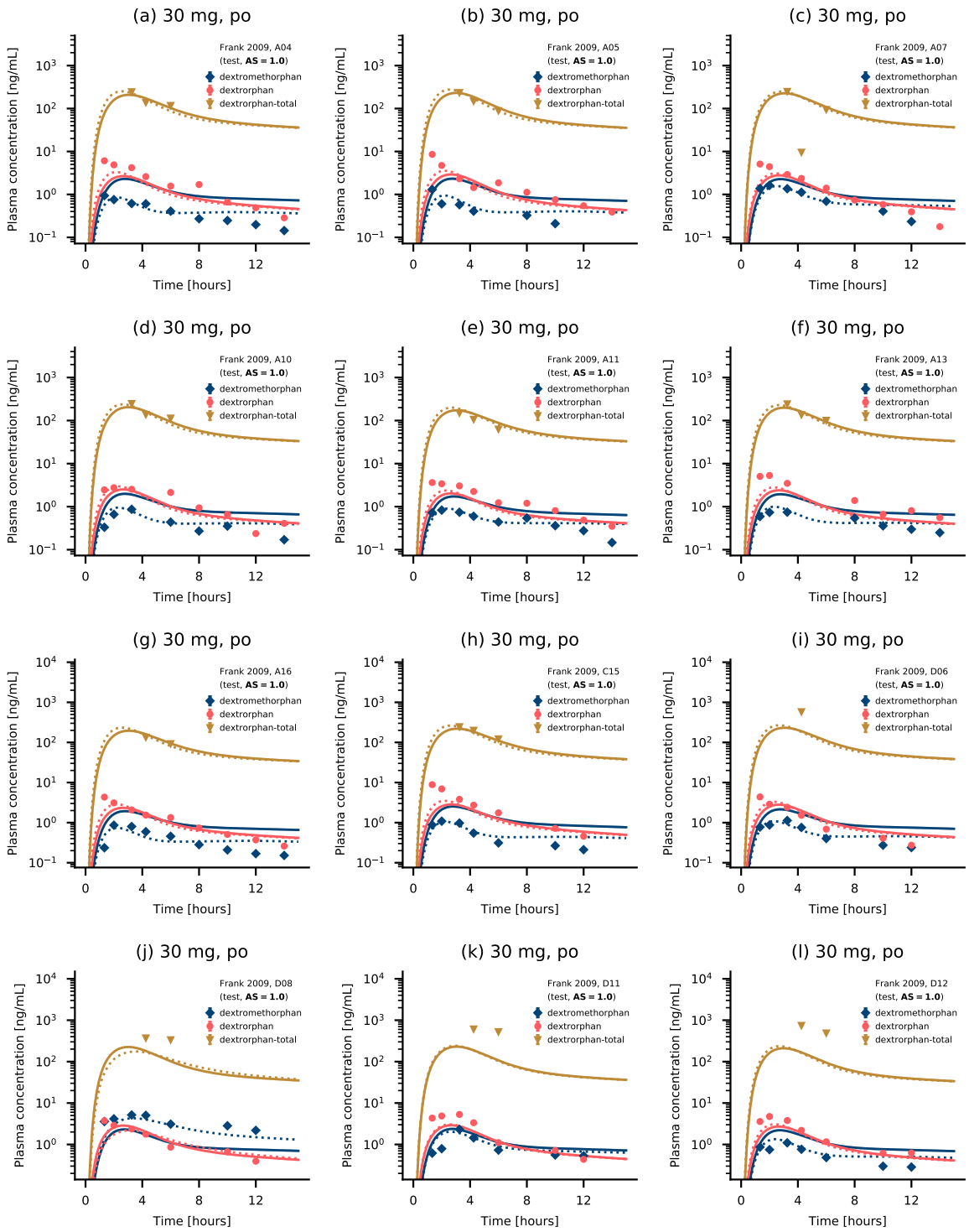

Figure S6.4.6: Dextromethorphan, dextrorphan and total dextrorphan plasma concentrations for individuals with a CYP2D6 AS = 1. Predictions of dextromethorphan plasma concentration-time profiles, compared to observed data [12] (semilogarithmic representation). Predictions using the population k_{cat} are shown as solid lines, individual predictions are shown as dotted lines. Symbols represent the corresponding observed data. AS: activity score, po: oral.

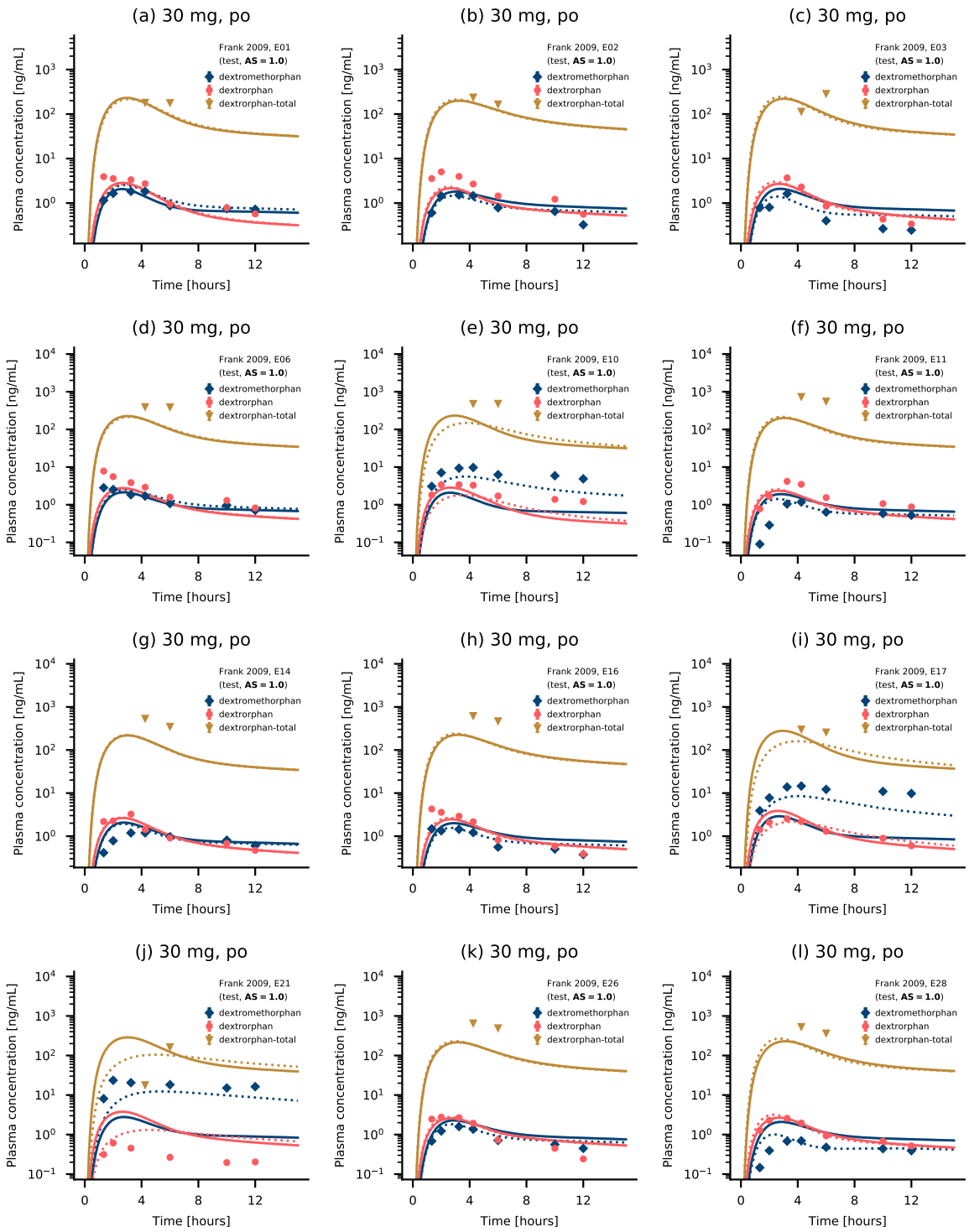

Figure S6.4.7: Dextromethorphan, dextrorphan and total dextrorphan plasma concentrations for individuals with a CYP2D6 AS = 1. Predictions of dextromethorphan plasma concentration-time profiles, compared to observed data [12] (semilogarithmic representation). Predictions using the population k_{cat} are shown as solid lines, individual predictions are shown as dotted lines. Symbols represent the corresponding observed data. AS: activity score, po: oral.

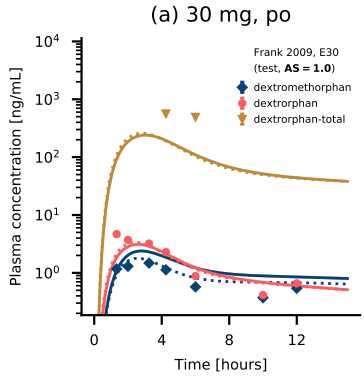

Figure S6.4.8: Dextromethorphan, dextrorphan and total dextrorphan plasma concentrations for individuals with a CYP2D6 AS = 1. Predictions of dextromethorphan plasma concentration-time profiles, compared to observed data [12] (semilogarithmic representation). Predictions using the population k_{cat} are shown as solid lines, individual predictions are shown as dotted lines. Symbols represent the corresponding observed data. AS: activity score, po: oral.

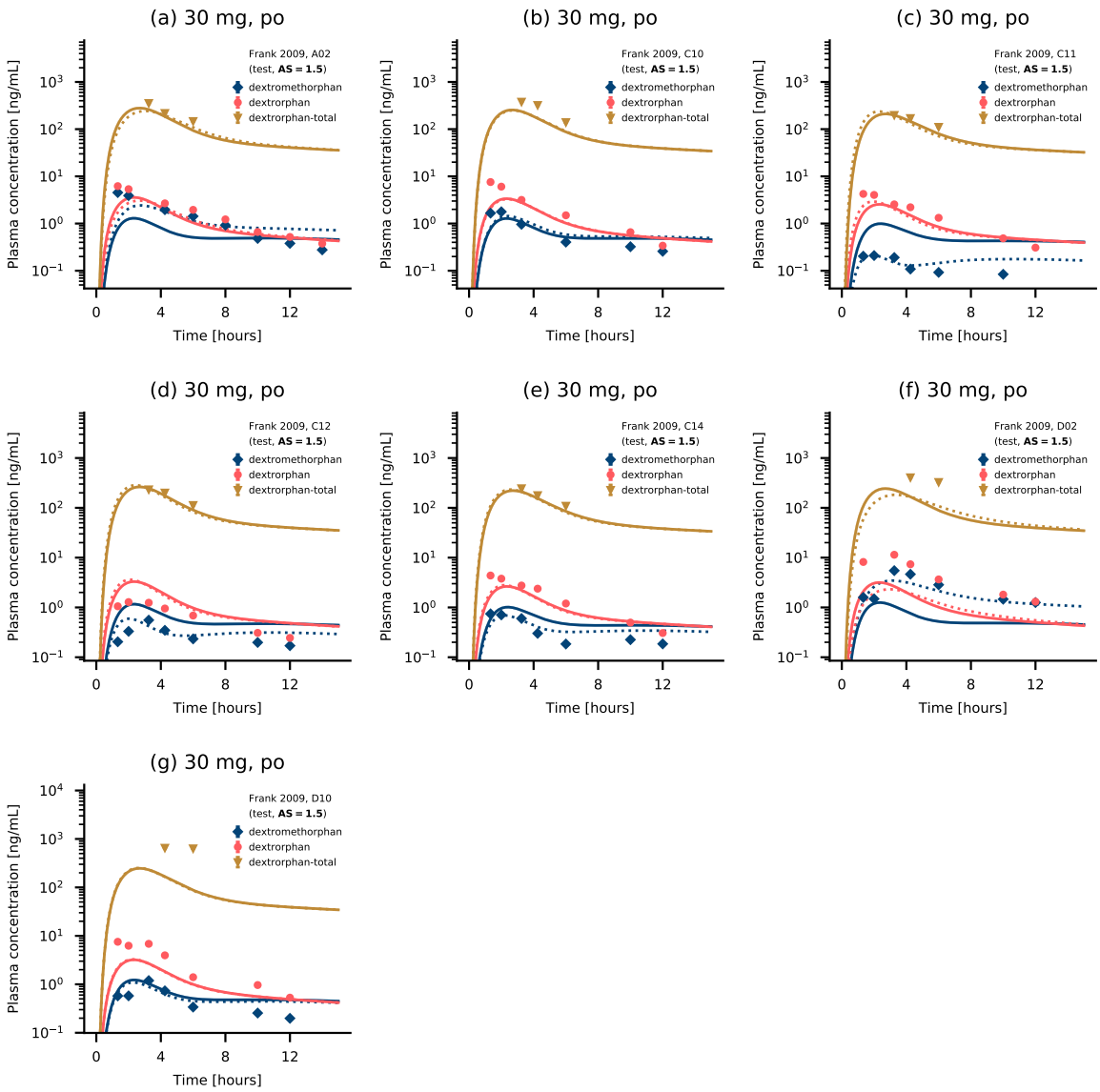

Figure S6.4.9: Dextromethorphan, dextrorphan and total dextrorphan plasma concentrations for individuals with a CYP2D6 AS = 1.5. Predictions of dextromethorphan plasma concentration-time profiles, compared to observed data [12] (semilogarithmic representation). Predictions using the population k_{cat} are shown as solid lines, individual predictions are shown as dotted lines. Symbols represent the corresponding observed data. AS: activity score, po: oral.

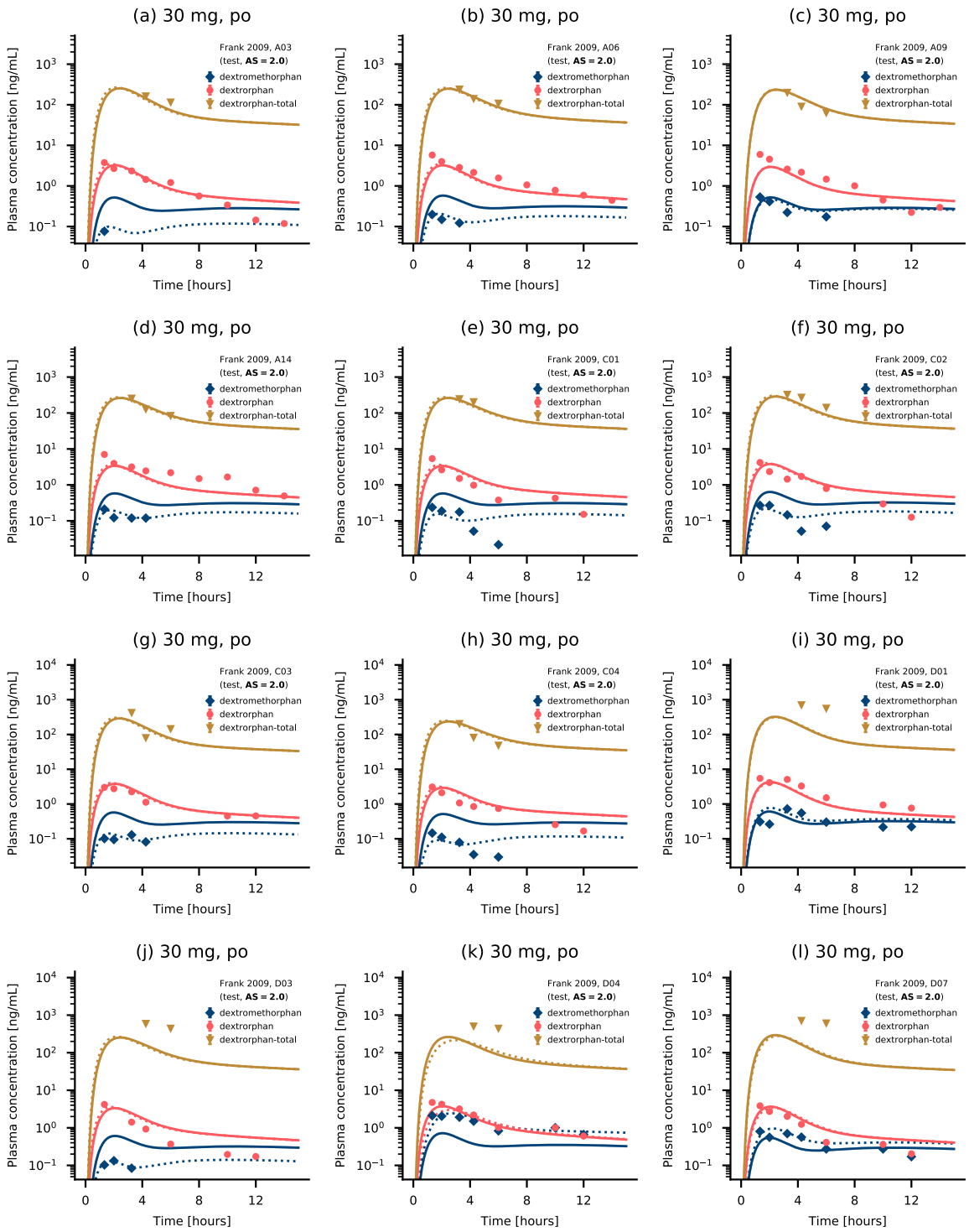

Figure S6.4.10: Dextromethorphan, dextrorphan and total dextrorphan plasma concentrations for individuals with a CYP2D6 AS = 2. Predictions of dextromethorphan plasma concentration-time profiles, compared to observed data [12] (semilogarithmic representation). Predictions using the population k_{cat} are shown as solid lines, individual predictions are shown as dotted lines. Symbols represent the corresponding observed data. AS: activity score, po: oral.

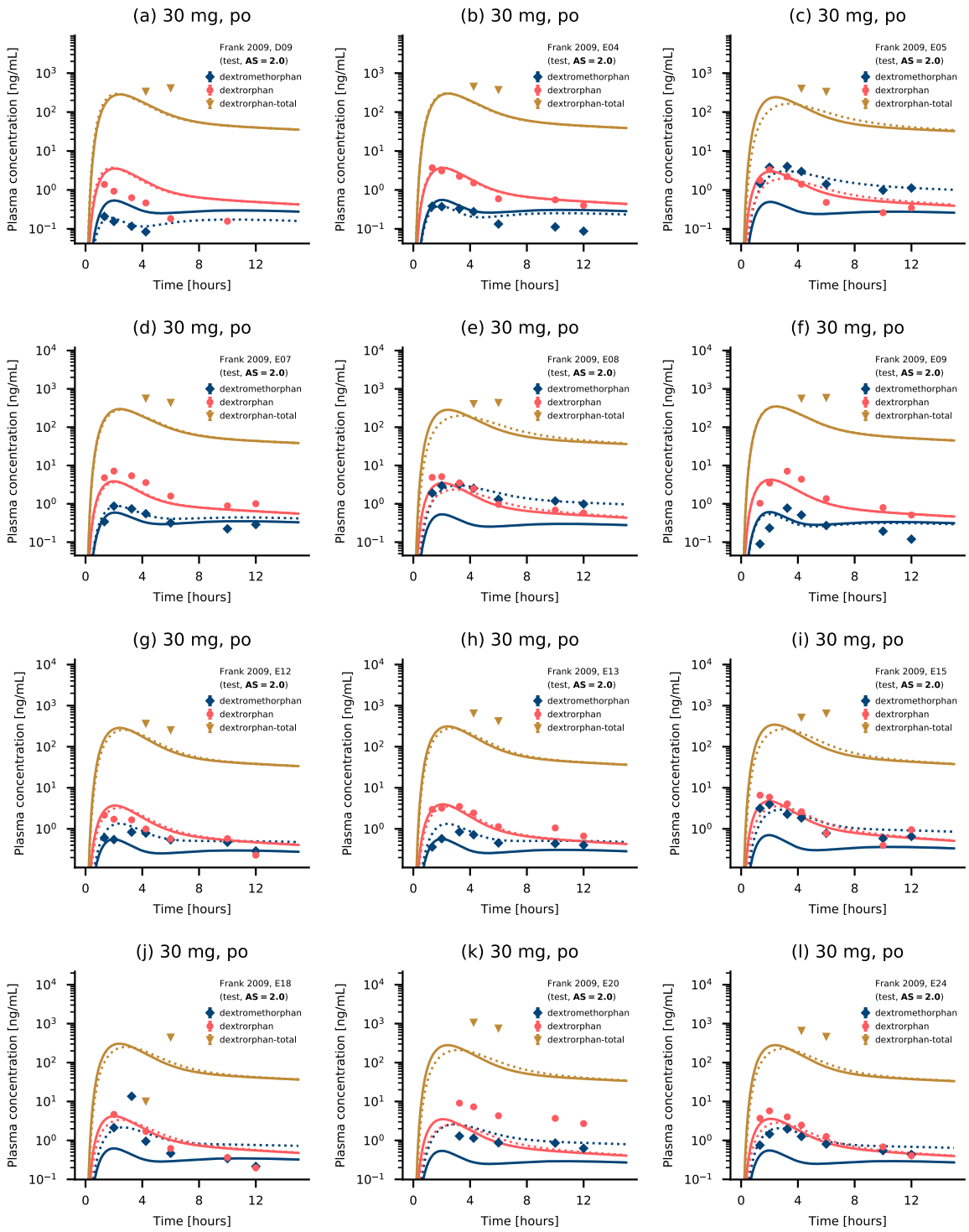

Figure S6.4.11: Dextromethorphan, dextrorphan and total dextrorphan plasma concentrations for individuals with a CYP2D6 AS = 2. Predictions of dextromethorphan plasma concentration-time profiles, compared to observed data [12] (semilogarithmic representation). Predictions using the population k_{cat} are shown as solid lines, individual predictions are shown as dotted lines. Symbols represent the corresponding observed data. AS: activity score, po: oral.

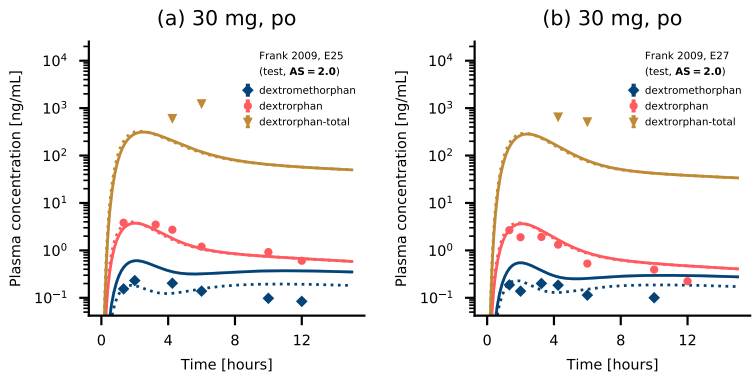

Figure S6.4.12: Dextromethorphan, dextrorphan and total dextrorphan plasma concentrations for individuals with a CYP2D6 AS = 2. Predictions of dextromethorphan plasma concentration-time profiles, compared to observed data [12] (semilogarithmic representation). Predictions using the population k_{cat} are shown as solid lines, individual predictions are shown as dotted lines. Symbols represent the corresponding observed data. AS: activity score, po: oral.

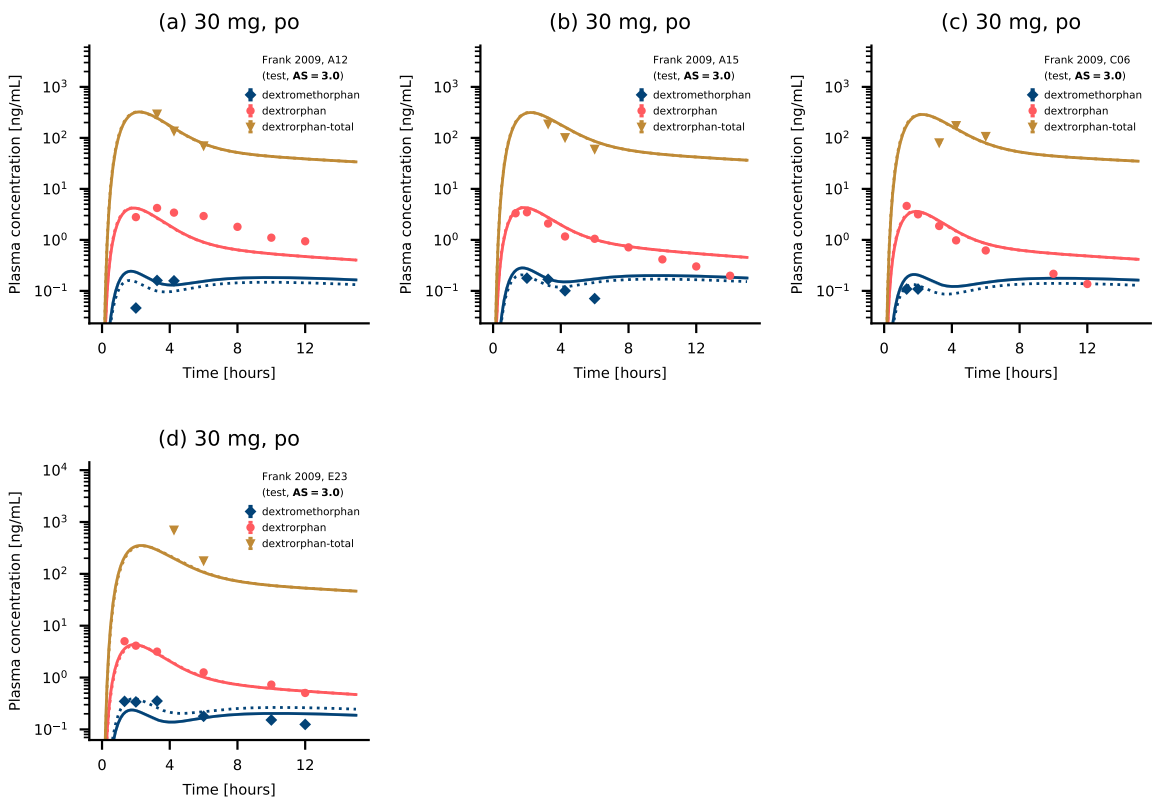

Figure S6.4.13: Dextromethorphan, dextrorphan and total dextrorphan plasma concentrations for individuals with a CYP2D6 AS = 3. Predictions of dextromethorphan plasma concentration-time profiles, compared to observed data [12] (semilogarithmic representation). Predictions using the population k_{cat} are shown as solid lines, individual predictions are shown as dotted lines. Symbols represent the corresponding observed data. AS: activity score, po: oral.

S6.5 MRD of Plasma Concentration Predictions

Table S6.5.3: Mean relative deviation of plasma concentration predictions

Dosing	Molecule	CYP2D6 status	MRD		Subject ID
			population k_{cat}	optim. ind. k_{cat}	
po, cap, 30 mg	dextromethorphan	AS=0.25	1.27	1.26	A01
po, cap, 30 mg	dextromethorphan	AS=1.5	2.59	2.06	A02
po, cap, 30 mg	dextromethorphan	AS=2.0	5.08	1.21	A03
po, cap, 30 mg	dextromethorphan	AS=1.0	3.22	1.60	A04
po, cap, 30 mg	dextromethorphan	AS=1.0	3.19	1.59	A05
po, cap, 30 mg	dextromethorphan	AS=2.0	2.70	1.20	A06
po, cap, 30 mg	dextromethorphan	AS=1.0	1.77	1.47	A07
po, cap, 30 mg	dextromethorphan	AS=0.0	1.50	1.49	A08
po, cap, 30 mg	dextromethorphan	AS=2.0	1.50	1.43	A09
po, cap, 30 mg	dextromethorphan	AS=1.0	2.68	1.55	A10
po, cap, 30 mg	dextromethorphan	AS=1.0	2.26	1.48	A11
po, cap, 30 mg	dextromethorphan	AS=3.0	2.26	1.97	A12
po, cap, 30 mg	dextromethorphan	AS=1.0	2.12	1.32	A13
po, cap, 30 mg	dextromethorphan	AS=2.0	3.19	1.29	A14
po, cap, 30 mg	dextromethorphan	AS=3.0	1.61	1.43	A15
po, cap, 30 mg	dextromethorphan	AS=1.0	3.06	1.67	A16
po, cap, 30 mg	dextromethorphan	AS=2.0	4.73	2.51	C01
po, cap, 30 mg	dextromethorphan	AS=2.0	3.43	1.76	C02
po, cap, 30 mg	dextromethorphan	AS=2.0	4.14	1.33	C03
po, cap, 30 mg	dextromethorphan	AS=2.0	5.65	1.97	C04
po, cap, 30 mg	dextromethorphan	-	3.75	3.75	C05
po, cap, 30 mg	dextromethorphan	AS=3.0	1.79	1.15	C06
po, cap, 30 mg	dextromethorphan	-	10.79	10.79	C07
po, cap, 30 mg	dextromethorphan	AS=0.5	1.70	1.61	C08
po, cap, 30 mg	dextromethorphan	-	14.00	14.00	C09
po, cap, 30 mg	dextromethorphan	AS=1.5	1.61	1.65	C10
po, cap, 30 mg	dextromethorphan	AS=1.5	4.60	1.46	C11
po, cap, 30 mg	dextromethorphan	AS=1.5	2.53	1.62	C12
po, cap, 30 mg	dextromethorphan	-	10.29	10.29	C13
po, cap, 30 mg	dextromethorphan	AS=1.5	1.91	1.51	C14
po, cap, 30 mg	dextromethorphan	AS=1.0	2.96	1.46	C15
po, cap, 30 mg	dextromethorphan	-	3.78	3.78	C16
po, cap, 30 mg	dextromethorphan	AS=2.0	1.68	1.77	D01
po, cap, 30 mg	dextromethorphan	AS=1.5	3.64	1.42	D02
po, cap, 30 mg	dextromethorphan	AS=2.0	4.70	1.10	D03
po, cap, 30 mg	dextromethorphan	AS=2.0	3.13	1.35	D04
po, cap, 30 mg	dextromethorphan	-	1.94	1.94	D05
po, cap, 30 mg	dextromethorphan	AS=1.0	2.31	1.41	D06
po, cap, 30 mg	dextromethorphan	AS=2.0	1.63	1.56	D07
po, cap, 30 mg	dextromethorphan	AS=1.0	2.86	1.57	D08
po, cap, 30 mg	dextromethorphan	AS=2.0	2.97	1.24	D09
po, cap, 30 mg	dextromethorphan	AS=1.5	1.69	1.60	D10
po, cap, 30 mg	dextromethorphan	AS=1.0	1.64	1.49	D11
po, cap, 30 mg	dextromethorphan	AS=1.0	2.20	1.44	D12
po, cap, 30 mg	dextromethorphan	AS=1.0	1.15	1.20	E01
po, cap, 30 mg	dextromethorphan	AS=1.0	1.49	1.34	E02
po, cap, 30 mg	dextromethorphan	AS=1.0	2.23	1.67	E03
po, cap, 30 mg	dextromethorphan	AS=2.0	1.98	1.75	E04

-: not given, AS: CYP2D6 activity score, cap: capsule, CYP2D6: Cytochrome P450 2D6, ind.: individual, optim.: optimized, po: oral.

Table S6.5.3: Mean relative deviation of plasma concentration predictions (continued)

Dosing	Molecule	CYP2D6 status	MRD population k_{cat}	MRD optim. ind. k_{cat}	Subject ID
po, cap, 30 mg	dextromethorphan	AS=2.0	6.49	1.35	E05
po, cap, 30 mg	dextromethorphan	AS=1.0	1.54	1.51	E06
po, cap, 30 mg	dextromethorphan	AS=2.0	1.46	1.45	E07
po, cap, 30 mg	dextromethorphan	AS=2.0	5.64	1.30	E08
po, cap, 30 mg	dextromethorphan	AS=2.0	2.44	2.37	E09
po, cap, 30 mg	dextromethorphan	AS=1.0	5.90	1.94	E10
po, cap, 30 mg	dextromethorphan	AS=1.0	3.07	2.65	E11
po, cap, 30 mg	dextromethorphan	AS=2.0	1.84	1.51	E12
po, cap, 30 mg	dextromethorphan	AS=2.0	1.71	1.56	E13
po, cap, 30 mg	dextromethorphan	AS=1.0	1.64	1.58	E14
po, cap, 30 mg	dextromethorphan	AS=2.0	3.91	1.63	E15
po, cap, 30 mg	dextromethorphan	AS=1.0	1.68	1.45	E16
po, cap, 30 mg	dextromethorphan	AS=1.0	6.78	1.95	E17
po, cap, 30 mg	dextromethorphan	AS=2.0	4.89	2.89	E18
po, cap, 30 mg	dextromethorphan	AS=2.0	3.23	1.63	E20
po, cap, 30 mg	dextromethorphan	AS=1.0	11.61	2.48	E21
po, cap, 30 mg	dextromethorphan	AS=0.0	2.06	2.00	E22
po, cap, 30 mg	dextromethorphan	AS=3.0	1.63	1.51	E23
po, cap, 30 mg	dextromethorphan	AS=2.0	2.96	1.29	E24
po, cap, 30 mg	dextromethorphan	AS=2.0	2.94	1.65	E25
po, cap, 30 mg	dextromethorphan	AS=1.0	1.56	1.27	E26
po, cap, 30 mg	dextromethorphan	AS=2.0	2.31	1.45	E27
po, cap, 30 mg	dextromethorphan	AS=1.0	3.12	1.90	E28
po, cap, 30 mg	dextromethorphan	AS=1.0	1.75	1.36	E30
MRD (dextromethorphan)			3.29 (1.15–14.00) 26/72	2.09 (1.10–14.00) 61/72 with MRD $\leq$ 2	
po, cap, 30 mg	dextrorphan	AS=0.25	1.54	1.62	A01
po, cap, 30 mg	dextrorphan	AS=1.5	1.65	1.78	A02
po, cap, 30 mg	dextrorphan	AS=2.0	1.83	1.81	A03
po, cap, 30 mg	dextrorphan	AS=1.0	1.91	1.73	A04
po, cap, 30 mg	dextrorphan	AS=1.0	1.90	1.70	A05
po, cap, 30 mg	dextrorphan	AS=2.0	1.48	1.44	A06
po, cap, 30 mg	dextrorphan	AS=1.0	1.76	1.66	A07
po, cap, 30 mg	dextrorphan	AS=2.0	1.73	1.72	A09
po, cap, 30 mg	dextrorphan	AS=1.0	1.55	1.54	A10
po, cap, 30 mg	dextrorphan	AS=1.0	1.76	1.64	A11
po, cap, 30 mg	dextrorphan	AS=3.0	2.09	2.10	A12
po, cap, 30 mg	dextrorphan	AS=1.0	2.07	1.88	A13
po, cap, 30 mg	dextrorphan	AS=2.0	1.91	1.88	A14
po, cap, 30 mg	dextrorphan	AS=3.0	1.52	1.52	A15
po, cap, 30 mg	dextrorphan	AS=1.0	1.61	1.43	A16
po, cap, 30 mg	dextrorphan	AS=2.0	2.05	1.97	C01
po, cap, 30 mg	dextrorphan	AS=2.0	2.02	1.99	C02
po, cap, 30 mg	dextrorphan	AS=2.0	1.28	1.26	C03
po, cap, 30 mg	dextrorphan	AS=2.0	1.90	1.85	C04
po, cap, 30 mg	dextrorphan	-	1.54	1.54	C05
po, cap, 30 mg	dextrorphan	AS=3.0	1.92	1.90	C06

-: not given, AS: CYP2D6 activity score, cap: capsule, CYP2D6: Cytochrome P450 2D6, ind.: individual, optim.: optimized, po: oral.

Table S6.5.3: Mean relative deviation of plasma concentration predictions (continued)

Dosing	Molecule	CYP2D6 status	MRD		Subject ID
			population k_{cat}	optim. ind. k_{cat}	
po, cap, 30 mg	dextrorphan	-	1.66	1.66	C07
po, cap, 30 mg	dextrorphan	AS=0.5	1.67	1.84	C08
po, cap, 30 mg	dextrorphan	-	2.00	2.00	C09
po, cap, 30 mg	dextrorphan	AS=1.5	1.84	1.87	C10
po, cap, 30 mg	dextrorphan	AS=1.5	1.63	1.51	C11
po, cap, 30 mg	dextrorphan	AS=1.5	1.99	2.06	C12
po, cap, 30 mg	dextrorphan	-	1.95	1.95	C13
po, cap, 30 mg	dextrorphan	AS=1.5	1.61	1.55	C14
po, cap, 30 mg	dextrorphan	AS=1.0	2.18	1.86	C15
po, cap, 30 mg	dextrorphan	-	1.84	1.84	C16
po, cap, 30 mg	dextrorphan	AS=2.0	1.59	1.59	D01
po, cap, 30 mg	dextrorphan	AS=1.5	3.60	3.91	D02
po, cap, 30 mg	dextrorphan	AS=2.0	2.37	2.27	D03
po, cap, 30 mg	dextrorphan	AS=2.0	1.31	1.55	D04
po, cap, 30 mg	dextrorphan	-	1.89	1.89	D05
po, cap, 30 mg	dextrorphan	AS=1.0	1.68	1.49	D06
po, cap, 30 mg	dextrorphan	AS=2.0	1.66	1.72	D07
po, cap, 30 mg	dextrorphan	AS=1.0	1.43	1.76	D08
po, cap, 30 mg	dextrorphan	AS=2.0	3.27	3.26	D09
po, cap, 30 mg	dextrorphan	AS=1.5	2.14	2.11	D10
po, cap, 30 mg	dextrorphan	AS=1.0	1.72	1.66	D11
po, cap, 30 mg	dextrorphan	AS=1.0	1.57	1.43	D12
po, cap, 30 mg	dextrorphan	AS=1.0	1.63	1.69	E01
po, cap, 30 mg	dextrorphan	AS=1.0	2.00	1.91	E02
po, cap, 30 mg	dextrorphan	AS=1.0	1.35	1.32	E03
po, cap, 30 mg	dextrorphan	AS=2.0	1.27	1.25	E04
po, cap, 30 mg	dextrorphan	AS=2.0	1.41	1.79	E05
po, cap, 30 mg	dextrorphan	AS=1.0	2.27	2.35	E06
po, cap, 30 mg	dextrorphan	AS=2.0	1.73	1.74	E07
po, cap, 30 mg	dextrorphan	AS=2.0	1.43	1.97	E08
po, cap, 30 mg	dextrorphan	AS=2.0	1.88	1.90	E09
po, cap, 30 mg	dextrorphan	AS=1.0	2.03	2.19	E10
po, cap, 30 mg	dextrorphan	AS=1.0	1.77	1.85	E11
po, cap, 30 mg	dextrorphan	AS=2.0	1.68	1.69	E12
po, cap, 30 mg	dextrorphan	AS=2.0	1.38	1.35	E13
po, cap, 30 mg	dextrorphan	AS=1.0	1.26	1.24	E14
po, cap, 30 mg	dextrorphan	AS=2.0	1.49	1.83	E15
po, cap, 30 mg	dextrorphan	AS=1.0	1.67	1.57	E16
po, cap, 30 mg	dextrorphan	AS=1.0	1.38	1.27	E17
po, cap, 30 mg	dextrorphan	AS=2.0	1.76	1.92	E18
po, cap, 30 mg	dextrorphan	AS=2.0	5.10	4.55	E20
po, cap, 30 mg	dextrorphan	AS=1.0	5.33	3.11	E21
po, cap, 30 mg	dextrorphan	AS=3.0	1.20	1.22	E23
po, cap, 30 mg	dextrorphan	AS=2.0	1.43	1.62	E24
po, cap, 30 mg	dextrorphan	AS=2.0	1.29	1.30	E25
po, cap, 30 mg	dextrorphan	AS=1.0	1.61	1.56	E26
po, cap, 30 mg	dextrorphan	AS=2.0	1.59	1.59	E27
po, cap, 30 mg	dextrorphan	AS=1.0	1.10	1.27	E28
po, cap, 30 mg	dextrorphan	AS=1.0	1.55	1.45	E30

-: not given, AS: CYP2D6 activity score, cap: capsule, CYP2D6: Cytochrome P450 2D6, ind.: individual, optim.: optimized, po: oral.

Table S6.5.3: Mean relative deviation of plasma concentration predictions (continued)

Dosing	Molecule	CYP2D6 status	MRD population k_{cat}	MRD optim. ind. k_{cat}	Subject ID
MRD (dextrorphan)			1.85 (1.10–5.33)	1.82 (1.22–4.55)	
			57/72	60/70 with MRD ≤ 2	
po, cap, 30 mg	dextrorphan-total	AS=0.25	2.75	2.99	A01
po, cap, 30 mg	dextrorphan-total	AS=1.5	1.40	1.35	A02
po, cap, 30 mg	dextrorphan-total	AS=2.0	1.41	1.50	A03
po, cap, 30 mg	dextrorphan-total	AS=1.0	1.20	1.22	A04
po, cap, 30 mg	dextrorphan-total	AS=1.0	1.17	1.09	A05
po, cap, 30 mg	dextrorphan-total	AS=2.0	1.17	1.20	A06
po, cap, 30 mg	dextrorphan-total	AS=1.0	5.56	5.48	A07
po, cap, 30 mg	dextrorphan-total	AS=2.0	1.33	1.33	A09
po, cap, 30 mg	dextrorphan-total	AS=1.0	1.21	1.25	A10
po, cap, 30 mg	dextrorphan-total	AS=1.0	1.30	1.27	A11
po, cap, 30 mg	dextrorphan-total	AS=3.0	1.15	1.15	A12
po, cap, 30 mg	dextrorphan-total	AS=1.0	1.18	1.17	A13
po, cap, 30 mg	dextrorphan-total	AS=2.0	1.14	1.14	A14
po, cap, 30 mg	dextrorphan-total	AS=3.0	1.44	1.42	A15
po, cap, 30 mg	dextrorphan-total	AS=1.0	1.13	1.14	A16
po, cap, 30 mg	dextrorphan-total	AS=2.0	1.17	1.23	C01
po, cap, 30 mg	dextrorphan-total	AS=2.0	1.54	1.63	C02
po, cap, 30 mg	dextrorphan-total	AS=2.0	1.88	1.90	C03
po, cap, 30 mg	dextrorphan-total	AS=2.0	1.56	1.48	C04
po, cap, 30 mg	dextrorphan-total	-	2.33	2.33	C05
po, cap, 30 mg	dextrorphan-total	AS=3.0	1.88	1.87	C06
po, cap, 30 mg	dextrorphan-total	-	1.25	1.25	C07
po, cap, 30 mg	dextrorphan-total	AS=0.5	1.39	1.43	C08
po, cap, 30 mg	dextrorphan-total	-	1.21	1.21	C09
po, cap, 30 mg	dextrorphan-total	AS=1.5	1.72	1.70	C10
po, cap, 30 mg	dextrorphan-total	AS=1.5	1.24	1.36	C11
po, cap, 30 mg	dextrorphan-total	AS=1.5	1.17	1.25	C12
po, cap, 30 mg	dextrorphan-total	-	1.08	1.08	C13
po, cap, 30 mg	dextrorphan-total	AS=1.5	1.22	1.25	C14
po, cap, 30 mg	dextrorphan-total	AS=1.0	1.11	1.19	C15
po, cap, 30 mg	dextrorphan-total	-	1.84	1.84	C16
po, cap, 30 mg	dextrorphan-total	AS=2.0	5.36	5.22	D01
po, cap, 30 mg	dextrorphan-total	AS=1.5	3.08	2.76	D02
po, cap, 30 mg	dextrorphan-total	AS=2.0	4.53	4.83	D03
po, cap, 30 mg	dextrorphan-total	AS=2.0	4.14	3.61	D04
po, cap, 30 mg	dextrorphan-total	-	2.85	2.85	D05
po, cap, 30 mg	dextrorphan-total	AS=1.0	3.06	3.21	D06
po, cap, 30 mg	dextrorphan-total	AS=2.0	5.92	5.56	D07
po, cap, 30 mg	dextrorphan-total	AS=1.0	2.70	2.60	D08
po, cap, 30 mg	dextrorphan-total	AS=2.0	3.52	3.70	D09
po, cap, 30 mg	dextrorphan-total	AS=1.5	5.51	5.60	D10
po, cap, 30 mg	dextrorphan-total	AS=1.0	4.09	4.19	D11
po, cap, 30 mg	dextrorphan-total	AS=1.0	4.84	5.20	D12
po, cap, 30 mg	dextrorphan-total	AS=1.0	1.62	1.55	E01
po, cap, 30 mg	dextrorphan-total	AS=1.0	1.38	1.38	E02
po, cap, 30 mg	dextrorphan-total	AS=1.0	2.26	2.38	E03

-: not given, AS: CYP2D6 activity score, cap: capsule, CYP2D6: Cytochrome P450 2D6, ind.: individual, optim.: optimized, po: oral.

Table S6.5.3: Mean relative deviation of plasma concentration predictions (continued)

Dosing	Molecule	CYP2D6 status	MRD		Subject ID
			population k_{cat}	optim. ind. k_{cat}	
po, cap, 30 mg	dextrorphan-total	AS=2.0	3.32	3.40	E04
po, cap, 30 mg	dextrorphan-total	AS=2.0	3.73	3.12	E05
po, cap, 30 mg	dextrorphan-total	AS=1.0	3.07	3.00	E06
po, cap, 30 mg	dextrorphan-total	AS=2.0	4.03	3.88	E07
po, cap, 30 mg	dextrorphan-total	AS=2.0	3.75	3.04	E08
po, cap, 30 mg	dextrorphan-total	AS=2.0	4.07	4.11	E09
po, cap, 30 mg	dextrorphan-total	AS=1.0	4.00	3.89	E10
po, cap, 30 mg	dextrorphan-total	AS=1.0	5.17	5.36	E11
po, cap, 30 mg	dextrorphan-total	AS=2.0	2.84	2.54	E12
po, cap, 30 mg	dextrorphan-total	AS=2.0	4.36	3.92	E13
po, cap, 30 mg	dextrorphan-total	AS=1.0	3.34	3.37	E14
po, cap, 30 mg	dextrorphan-total	AS=2.0	4.95	3.96	E15
po, cap, 30 mg	dextrorphan-total	AS=1.0	3.48	3.53	E16
po, cap, 30 mg	dextrorphan-total	AS=1.0	1.95	1.97	E17
po, cap, 30 mg	dextrorphan-total	AS=2.0	9.98	10.14	E18
po, cap, 30 mg	dextrorphan-total	AS=2.0	8.25	6.70	E20
po, cap, 30 mg	dextrorphan-total	AS=1.0	6.08	3.55	E21
po, cap, 30 mg	dextrorphan-total	AS=3.0	2.67	2.61	E23
po, cap, 30 mg	dextrorphan-total	AS=2.0	5.23	4.36	E24
po, cap, 30 mg	dextrorphan-total	AS=2.0	6.30	6.58	E25
po, cap, 30 mg	dextrorphan-total	AS=1.0	3.94	4.02	E26
po, cap, 30 mg	dextrorphan-total	AS=2.0	5.41	5.70	E27
po, cap, 30 mg	dextrorphan-total	AS=1.0	2.98	3.24	E28
po, cap, 30 mg	dextrorphan-total	AS=1.0	3.71	3.88	E30
MRD (dextrorphan-total)			2.99 (1.08–9.98) 31/70	2.90 (1.08–10.14) 31/70 with MRD $\leq$ 2	
Overall MRD			2.72 (1.08–14.00) 114/212	2.27 (1.08–14.00) 152/212 with MRD $\leq$ 2	

-: not given, AS: CYP2D6 activity score, cap: capsule, CYP2D6: Cytochrome P450 2D6, ind.: individual, optim.: optimized, po: oral.

S6.6 Goodness-of-Fit Plots

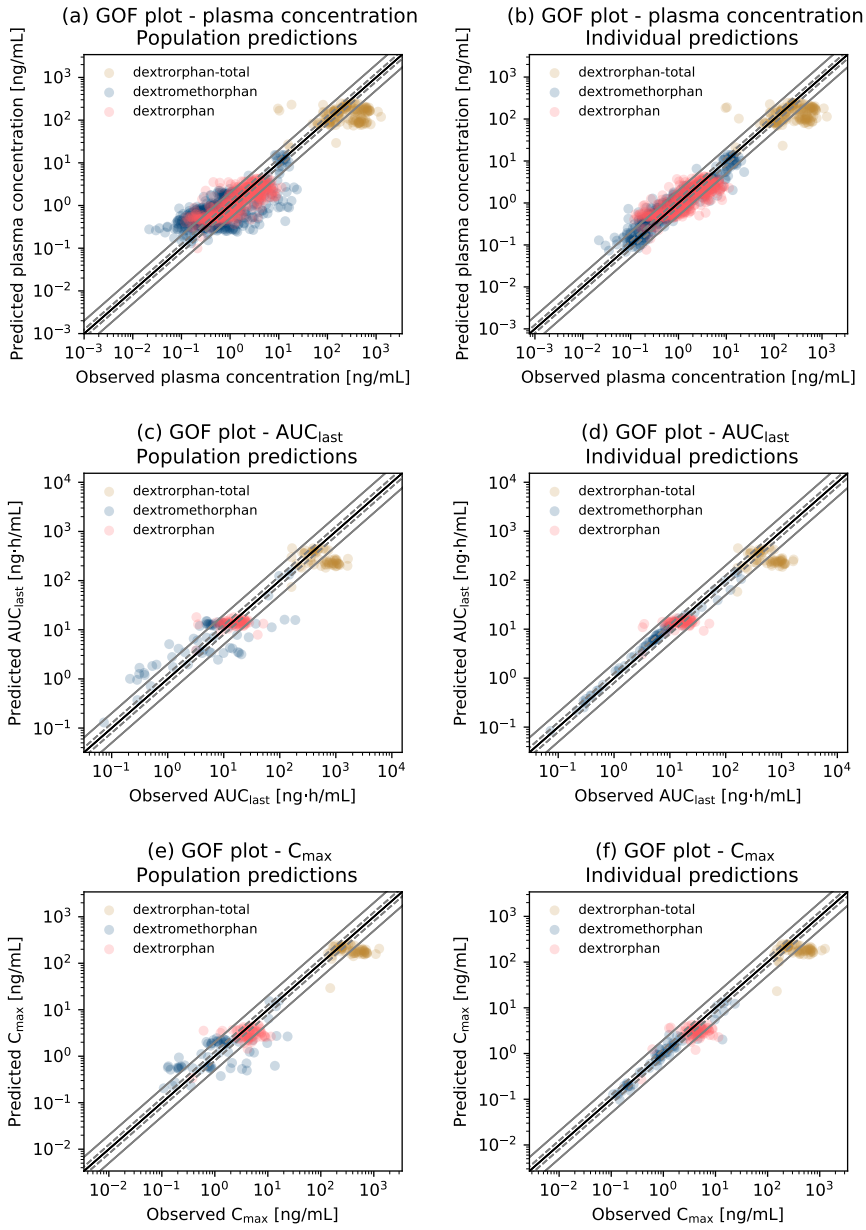

Figure S6.6.14: Goodness-of-fit plots for plasma concentrations, AUC_{last} and C_{max} values comparing predictions using the population k_{cat} (left column) to individual predictions (right column). Predicted versus observed (a, b) plasma concentrations, (c, d) AUC_{last} and (e, f) C_{max} values for dextromethorphan, dextrorphan and total dextrorphan (dextrorphan + dextrorphan *O*-glucuronide) for all individuals. The solid black line marks the line of identity, the dashed gray lines mark the 0.8- to 1.25-fold range, the solid gray lines indicate the 0.5- to 2-fold range. Colored symbols show the predicted compared to observed values for an individual study participant. AUC_{last}: AUC from the time of the first concentration measurement to the last time point of concentration measurement, C_{max}: peak plasma concentration.

S6.7 GMFE of Predicted AUC_{last} and C_{max} Values

Table S6.7.4: Predicted and observed AUC_{last} and C_{max} values and geometric mean fold errors

Molecule	CYP2D6 status	AUC_{last} [ng·h/mL]					C_{max} [ng/mL]					Subject ID
		Pred		Obs	Pred/Obs		Pred		Obs	Pred/Obs		
		population k_{cat}	ind. optim. k_{cat}		population k_{cat}	ind. optim. k_{cat}	population k_{cat}	ind. optim. k_{cat}		population k_{cat}	ind. optim. k_{cat}	
dextromethorphan	AS=0.25	131.51	138.87	146.34	0.90	0.95	11.92	12.59	14.33	0.83	0.88	A01
dextromethorphan	AS=1.5	7.84	14.67	17.31	0.45	0.85	1.30	2.07	4.53	0.29	0.46	A02
dextromethorphan	AS=2.0	*	*	*	*	*	0.52	0.09	0.08	6.80	1.21	A03
dextromethorphan	AS=1.0	15.04	5.75	4.87	3.09	1.18	2.30	0.85	0.94	2.46	0.90	A04
dextromethorphan	AS=1.0	11.94	4.62	3.72	3.21	1.24	2.33	0.93	1.30	1.79	0.72	A05
dextromethorphan	AS=2.0	1.33	0.34	0.28	4.67	1.20	0.58	0.20	0.20	2.92	1.03	A06
dextromethorphan	AS=1.0	13.19	8.83	6.68	1.97	1.05	2.28	1.43	1.62	1.41	0.89	A07
dextromethorphan	AS=0.0	156.79	146.08	162.42	0.97	0.90	15.85	14.08	16.37	0.97	0.86	A08
dextromethorphan	AS=2.0	1.75	1.60	1.24	1.41	1.29	0.52	0.48	0.53	0.98	0.90	A09
dextromethorphan	AS=1.0	13.16	6.41	5.34	2.46	1.20	1.99	0.92	0.87	2.29	1.06	A10
dextromethorphan	AS=1.0	12.28	6.40	5.99	2.05	1.07	1.73	0.85	0.83	2.08	1.03	A11
dextromethorphan	AS=3.0	0.52	0.25	0.30	1.72	0.88	0.24	0.15	0.16	1.52	0.94	A12
dextromethorphan	AS=1.0	13.27	7.01	6.49	2.04	1.08	1.95	0.96	0.74	2.62	1.29	A13
dextromethorphan	AS=2.0	1.32	0.45	0.38	3.47	1.18	0.58	0.19	0.21	2.75	0.91	A14
dextromethorphan	AS=3.0	0.89	0.56	0.56	1.61	1.12	0.28	0.20	0.18	1.59	1.10	A15
dextromethorphan	AS=1.0	13.05	5.18	4.92	2.65	1.05	1.94	0.73	0.86	2.24	0.84	A16
dextromethorphan	AS=2.0	1.83	0.56	0.53	3.45	1.06	0.58	0.15	0.24	2.45	0.64	C01
dextromethorphan	AS=2.0	1.95	0.73	0.63	3.09	1.16	0.64	0.21	0.27	2.36	0.78	C02
dextromethorphan	AS=2.0	1.26	0.32	0.31	4.07	1.03	0.57	0.13	0.13	4.41	1.04	C03
dextromethorphan	AS=2.0	1.68	0.38	0.31	5.37	1.20	0.52	0.10	0.15	3.54	0.66	C04
dextromethorphan	-	15.57	15.57	48.37	0.32	0.32	2.58	2.58	10.31	0.25	0.25	C05
dextromethorphan	AS=3.0	0.13	0.08	0.07	1.79	1.15	0.21	0.13	0.11	1.93	1.18	C06
dextromethorphan	-	7.47	7.47	0.69	10.74	10.74	2.08	2.08	0.24	8.53	8.53	C07
dextromethorphan	AS=0.5	49.56	63.17	62.68	0.79	1.01	6.45	7.53	10.39	0.62	0.72	C08
dextromethorphan	-	12.79	12.79	0.87	14.70	14.70	2.41	2.41	0.29	8.23	8.23	C09
dextromethorphan	AS=1.5	7.15	8.02	6.61	1.08	1.21	1.28	1.36	1.78	0.72	0.77	C10
dextromethorphan	AS=1.5	5.10	1.38	1.06	4.80	1.30	0.99	0.21	0.21	4.74	1.02	C11
dextromethorphan	AS=1.5	6.59	3.64	2.91	2.27	1.25	1.16	0.59	0.56	2.09	1.07	C12
dextromethorphan	-	7.90	7.90	0.73	10.77	10.77	2.22	2.22	0.26	8.51	8.51	C13
dextromethorphan	AS=1.5	6.07	4.27	3.38	1.79	1.26	1.01	0.68	0.74	1.36	0.92	C14
dextromethorphan	AS=1.0	14.86	6.01	5.05	2.94	1.19	2.53	1.03	1.09	2.33	0.95	C15
dextromethorphan	-	12.49	12.49	3.41	3.66	3.66	1.93	1.93	0.87	2.23	2.23	C16

*: no AUC_{last} calculated due to insufficient amount of observed data points, -: not available, †: AUC_{last} and C_{max} values as well as corresponding ratios were calculated based on a small number of observed data points (n = 3 for studies A and B, n = 2 for studies D and E) and should be interpreted with caution, AS: CYP2D6 activity score, AUC: area under the plasma concentration-time curve, AUC_{last}: AUC from the time of the first concentration measurement to the last time of concentration measurement, C_{max}: peak plasma concentration, CYP2D6: Cytochrome P450 2D6, obs: observed, po: oral, ind.: individual, optim.: optimized, pred: predicted.

Table S6.7.4: Predicted and observed AUC_{last} and C_{max} values and geometric mean fold errors (continued)

Molecule	CYP2D6 status	AUC_{last} [ng·h/mL]					C_{max} [ng/mL]					Subject ID
		Pred		Obs	Pred/Obs		Pred		Obs	Pred/Obs		
		population k_{cat}	ind. optim. k_{cat}		population k_{cat}	ind. optim. k_{cat}	population k_{cat}	ind. optim. k_{cat}		population k_{cat}	ind. optim. k_{cat}	
dextromethorphan	AS=2.0	3.66	4.46	3.63	1.01	1.23	0.61	0.77	0.72	0.84	1.07	D01
dextromethorphan	AS=1.5	7.04	22.06	27.89	0.25	0.79	1.25	3.46	5.48	0.23	0.63	D02
dextromethorphan	AS=2.0	1.00	0.22	0.21	4.73	1.02	0.61	0.13	0.13	4.58	0.95	D03
dextromethorphan	AS=2.0	4.27	14.10	12.89	0.33	1.09	0.72	2.31	2.11	0.34	1.09	D04
dextromethorphan	-	14.27	14.27	8.66	1.65	1.65	2.40	2.40	2.44	0.98	0.98	D05
dextromethorphan	AS=1.0	12.76	6.27	5.56	2.30	1.13	2.15	1.05	1.13	1.90	0.93	D06
dextromethorphan	AS=2.0	3.36	5.41	4.11	0.82	1.32	0.55	0.94	0.80	0.68	1.17	D07
dextromethorphan	AS=1.0	13.28	28.47	37.31	0.36	0.76	2.31	4.29	5.16	0.45	0.83	D08
dextromethorphan	AS=2.0	1.20	0.43	0.39	3.09	1.12	0.54	0.19	0.21	2.56	0.90	D09
dextromethorphan	AS=1.5	6.90	6.15	4.96	1.39	1.24	1.23	1.06	1.19	1.03	0.89	D10
dextromethorphan	AS=1.0	13.70	11.47	9.73	1.41	1.18	2.38	1.89	2.31	1.03	0.82	D11
dextromethorphan	AS=1.0	12.84	7.53	5.80	2.21	1.30	2.21	1.27	1.10	2.01	1.16	D12
dextromethorphan	AS=1.0	11.15	14.17	11.92	0.94	1.19	2.07	2.44	1.83	1.13	1.33	E01
dextromethorphan	AS=1.0	12.49	9.83	9.76	1.28	1.01	1.81	1.42	1.53	1.19	0.93	E02
dextromethorphan	AS=1.0	12.37	8.14	6.28	1.97	1.30	2.09	1.30	1.62	1.29	0.80	E03
dextromethorphan	AS=2.0	3.48	2.66	2.03	1.72	1.31	0.55	0.39	0.38	1.45	1.01	E04
dextromethorphan	AS=2.0	3.16	20.19	20.65	0.15	0.98	0.49	3.04	4.02	0.12	0.76	E05
dextromethorphan	AS=1.0	12.47	14.99	14.40	0.87	1.04	2.14	2.45	2.82	0.76	0.87	E06
dextromethorphan	AS=2.0	3.90	5.44	4.37	0.89	1.25	0.59	0.86	0.87	0.68	0.99	E07
dextromethorphan	AS=2.0	3.38	19.53	18.81	0.18	1.04	0.53	3.04	3.26	0.16	0.93	E08
dextromethorphan	AS=2.0	3.80	3.46	3.25	1.17	1.06	0.61	0.54	0.77	0.79	0.70	E09
dextromethorphan	AS=1.0	11.23	39.11	71.91	0.16	0.54	2.09	5.50	9.74	0.21	0.56	E10
dextromethorphan	AS=1.0	11.70	8.43	7.14	1.64	1.18	1.91	1.30	1.18	1.63	1.11	E11
dextromethorphan	AS=2.0	3.40	7.48	5.98	0.57	1.25	0.56	1.27	0.83	0.67	1.53	E12
dextromethorphan	AS=2.0	3.48	7.37	5.61	0.62	1.31	0.57	1.26	0.84	0.68	1.49	E13
dextromethorphan	AS=1.0	12.15	11.29	9.66	1.26	1.17	2.07	1.83	1.19	1.73	1.54	E14
dextromethorphan	AS=2.0	4.16	16.56	14.35	0.29	1.15	0.70	2.80	3.96	0.18	0.71	E15
dextromethorphan	AS=1.0	12.90	9.78	8.47	1.52	1.15	2.00	1.47	1.48	1.35	1.00	E16
dextromethorphan	AS=1.0	16.05	63.43	121.81	0.13	0.52	2.91	8.47	14.57	0.20	0.58	E17
dextromethorphan	AS=2.0	3.51	11.55	17.93	0.20	0.64	0.62	2.02	13.60	0.05	0.15	E18
dextromethorphan	AS=2.0	2.45	11.75	7.90	0.31	1.49	0.54	2.56	1.29	0.42	1.98	E20
dextromethorphan	AS=1.0	15.78	105.27	189.37	0.08	0.56	2.79	12.25	23.61	0.12	0.52	E21
dextromethorphan	AS=0.0	124.38	98.69	97.59	1.27	1.01	15.80	10.94	10.67	1.48	1.03	E22
dextromethorphan	AS=3.0	1.97	2.79	2.30	0.85	1.21	0.24	0.39	0.35	0.67	1.10	E23
dextromethorphan	AS=2.0	3.36	11.76	9.91	0.34	1.19	0.55	1.93	1.97	0.28	0.98	E24

*: no AUC_{last} calculated due to insufficient amount of observed data points, -: not available, †: AUC_{last} and C_{max} values as well as corresponding ratios were calculated based on a small number of observed data points (n = 3 for studies A and B, n = 2 for studies D and E) and should be interpreted with caution, AS: CYP2D6 activity score, AUC: area under the plasma concentration-time curve, AUC_{last}: AUC from the time of the first concentration measurement to the last time of concentration measurement, C_{max}: peak plasma concentration, CYP2D6: Cytochrome P450 2D6, obs: observed, po: oral, ind.: individual, optim.: optimized, pred: predicted.

Table S6.7.4: Predicted and observed AUC_{last} and C_{max} values and geometric mean fold errors (continued)

Molecule	CYP2D6 status	AUC_{last} [ng·h/mL]					C_{max} [ng/mL]					Subject ID
		Pred		Obs	Pred/Obs		Pred		Obs	Pred/Obs		
		population k_{cat}	ind. optim. k_{cat}		population k_{cat}	ind. optim. k_{cat}	population k_{cat}	ind. optim. k_{cat}		population k_{cat}	ind. optim. k_{cat}	
dextromethorphan	AS=2.0	4.11	1.78	1.56	2.63	1.14	0.61	0.19	0.23	2.62	0.84	E25
dextromethorphan	AS=1.0	14.14	11.00	9.18	1.54	1.20	2.29	1.74	1.60	1.43	1.09	E26
dextromethorphan	AS=2.0	3.38	1.44	1.20	2.82	1.20	0.55	0.22	0.20	2.73	1.12	E27
dextromethorphan	AS=1.0	12.84	6.00	5.22	2.46	1.15	2.09	0.97	0.69	3.01	1.39	E28
dextromethorphan	AS=1.0	14.37	10.44	8.06	1.78	1.30	2.39	1.63	1.48	1.62	1.11	E30
GMFE (dextromethorphan)		population k_{cat}			3.14 (1.01–14.70) 31/71 with GMFE $\leq$ 2					3.04 (1.02–20.00) 33/72 with GMFE $\leq$ 2		
		ind. optim. k_{cat}				1.75 (1.01–14.70) 66/71 with GMFE $\leq$ 2					1.67 (1.00–8.53) 65/72 with GMFE $\leq$ 2	
dextrorphan	AS=0.25	3.80	3.05	3.20	1.19	0.95	0.34	0.27	0.38	0.90	0.71	A01
dextrorphan	AS=1.5	15.45	15.23	23.58	0.66	0.65	3.59	2.73	6.20	0.58	0.44	A02
dextrorphan	AS=2.0	13.63	13.54	12.74	1.07	1.06	3.24	3.42	3.76	0.86	0.91	A03
dextrorphan	AS=1.0	14.70	15.01	23.58	0.62	0.64	2.67	3.27	6.07	0.44	0.54	A04
dextrorphan	AS=1.0	15.18	15.39	20.28	0.75	0.76	2.92	3.50	8.57	0.34	0.41	A05
dextrorphan	AS=2.0	14.62	14.61	19.99	0.73	0.73	3.22	3.39	5.77	0.56	0.59	A06
dextrorphan	AS=1.0	14.91	15.08	18.44	0.81	0.82	2.79	2.91	5.10	0.55	0.57	A07
dextrorphan	AS=2.0	13.28	13.28	18.38	0.72	0.72	2.95	2.97	5.97	0.49	0.50	A09
dextrorphan	AS=1.0	13.31	13.66	17.41	0.76	0.78	2.51	2.89	2.75	0.91	1.05	A10
dextrorphan	AS=1.0	11.58	11.85	18.45	0.63	0.64	2.03	2.30	3.63	0.56	0.63	A11
dextrorphan	AS=3.0	14.86	12.17	24.21	0.61	0.52	4.21	4.20	4.22	1.00	1.00	A12
dextrorphan	AS=1.0	13.19	13.71	24.45	0.54	0.56	2.40	2.71	5.30	0.45	0.51	A13
dextrorphan	AS=2.0	14.82	14.78	25.10	0.59	0.59	3.39	3.56	7.03	0.48	0.51	A14
dextrorphan	AS=3.0	16.86	16.83	13.25	1.27	1.27	4.30	4.27	3.47	1.24	1.23	A15
dextrorphan	AS=1.0	12.84	13.11	14.73	0.87	0.89	2.34	2.83	4.32	0.54	0.65	A16
dextrorphan	AS=2.0	13.95	13.88	9.57	1.46	1.45	3.37	3.56	5.38	0.63	0.66	C01
dextrorphan	AS=2.0	15.21	15.12	10.55	1.44	1.43	3.81	4.00	4.20	0.91	0.95	C02
dextrorphan	AS=2.0	15.28	15.08	11.83	1.29	1.28	3.80	4.00	3.01	1.26	1.33	C03
dextrorphan	AS=2.0	12.47	12.42	8.22	1.52	1.51	2.93	3.11	3.09	0.95	1.01	C04
dextrorphan	-	13.91	13.91	18.28	0.76	0.76	2.59	2.59	4.07	0.64	0.64	C05
dextrorphan	AS=3.0	13.53	13.49	10.29	1.31	1.31	3.61	3.61	4.63	0.78	0.78	C06
dextrorphan	-	12.14	12.41	14.67	0.83	0.83	2.34	2.34	3.89	0.60	0.60	C07

*: no AUC_{last} calculated due to insufficient amount of observed data points, -: not available, †: AUC_{last} and C_{max} values as well as corresponding ratios were calculated based on a small number of observed data points (n = 3 for studies A and B, n = 2 for studies D and E) and should be interpreted with caution, AS: CYP2D6 activity score, AUC: area under the plasma concentration-time curve, AUC_{last}: AUC from the time of the first concentration measurement to the last time of concentration measurement, C_{max}: peak plasma concentration, CYP2D6: Cytochrome P450 2D6, obs: observed, po: oral, ind.: individual, optim.: optimized, pred: predicted.

Table S6.7.4: Predicted and observed AUC_{last} and C_{max} values and geometric mean fold errors (continued)

Molecule	CYP2D6 status	AUC_{last} [ng·h/mL]					C_{max} [ng/mL]					Subject ID
		Pred		Obs	Pred/Obs		Pred		Obs	Pred/Obs		
		population k_{cat}	ind. optim. k_{cat}		population k_{cat}	ind. optim. k_{cat}	population k_{cat}	ind. optim. k_{cat}		population k_{cat}	ind. optim. k_{cat}	
dextrorphan	AS=0.5	10.52	9.41	12.19	0.86	0.77	1.48	1.20	4.14	0.36	0.29	C08
dextrorphan	-	13.49	13.49	9.56	1.41	1.41	2.58	2.58	3.68	0.70	0.70	C09
dextrorphan	AS=1.5	14.54	14.50	21.27	0.68	0.68	3.36	3.15	7.57	0.44	0.42	C10
dextrorphan	AS=1.5	11.63	11.67	16.35	0.71	0.71	2.55	2.93	4.25	0.60	0.69	C11
dextrorphan	AS=1.5	14.11	14.13	7.32	1.93	1.93	3.30	3.59	1.28	2.58	2.80	C12
dextrorphan	-	12.88	12.88	10.47	1.23	1.23	2.50	2.50	3.55	0.70	0.70	C13
dextrorphan	AS=1.5	11.98	12.03	16.33	0.73	0.74	2.65	2.76	4.38	0.60	0.63	C14
dextrorphan	AS=1.0	14.89	15.25	24.67	0.60	0.62	2.85	3.44	8.85	0.32	0.39	C15
dextrorphan	-	11.09	11.09	12.72	0.87	0.87	2.03	2.03	4.12	0.49	0.49	C16
dextrorphan	AS=2.0	15.91	15.93	23.63	0.67	0.67	4.28	4.15	5.46	0.78	0.76	D01
dextrorphan	AS=1.5	13.31	12.96	50.92	0.26	0.25	3.17	2.29	11.43	0.28	0.20	D02
dextrorphan	AS=2.0	13.33	13.40	8.58	1.55	1.56	3.35	3.17	4.20	0.80	0.76	D03
dextrorphan	AS=2.0	15.79	15.44	18.62	0.85	0.83	3.77	2.78	4.74	0.80	0.59	D04
dextrorphan	-	14.40	14.40	13.21	1.09	1.09	2.89	2.89	6.20	0.47	0.47	D05
dextrorphan	AS=1.0	13.87	14.10	12.29	1.13	1.15	2.81	3.19	4.38	0.64	0.73	D06
dextrorphan	AS=2.0	14.10	14.11	10.13	1.39	1.39	3.67	3.36	3.86	0.95	0.87	D07
dextrorphan	AS=1.0	14.11	13.25	13.82	1.02	0.96	2.86	2.19	3.73	0.77	0.59	D08
dextrorphan	AS=2.0	13.91	12.80	3.47	4.00	3.68	3.55	3.72	1.39	2.56	2.68	D09
dextrorphan	AS=1.5	14.03	14.04	28.51	0.49	0.49	3.21	3.19	7.54	0.43	0.42	D10
dextrorphan	AS=1.0	14.49	14.59	21.95	0.66	0.66	2.91	2.80	5.30	0.55	0.53	D11
dextrorphan	AS=1.0	13.43	13.63	18.50	0.73	0.74	2.71	2.94	4.74	0.57	0.62	D12
dextrorphan	AS=1.0	12.86	12.76	17.56	0.73	0.73	2.85	2.57	3.91	0.73	0.66	E01
dextrorphan	AS=1.0	11.89	12.08	22.24	0.53	0.54	2.16	2.15	5.02	0.43	0.43	E02
dextrorphan	AS=1.0	9.00	8.60	8.75	1.03	0.98	2.70	2.63	3.68	0.73	0.71	E03
dextrorphan	AS=2.0	14.42	14.40	12.37	1.17	1.16	3.69	3.78	3.71	0.99	1.02	E04
dextrorphan	AS=2.0	12.22	11.43	10.42	1.17	1.10	2.99	1.93	3.32	0.90	0.58	E05
dextrorphan	AS=1.0	13.61	13.49	25.24	0.54	0.53	2.77	2.53	7.80	0.36	0.32	E06
dextrorphan	AS=2.0	15.58	15.56	27.20	0.57	0.57	3.87	3.66	7.16	0.54	0.51	E07
dextrorphan	AS=2.0	13.86	13.23	19.02	0.73	0.70	3.51	2.33	5.12	0.69	0.45	E08
dextrorphan	AS=2.0	16.43	16.42	23.77	0.69	0.69	4.26	4.29	7.10	0.60	0.60	E09
dextrorphan	AS=1.0	12.90	11.48	22.31	0.58	0.51	2.86	1.79	3.40	0.84	0.53	E10
dextrorphan	AS=1.0	12.05	12.20	19.52	0.62	0.63	2.35	2.39	4.17	0.56	0.57	E11
dextrorphan	AS=2.0	14.21	14.20	9.07	1.57	1.56	3.70	3.12	2.16	1.71	1.44	E12
dextrorphan	AS=2.0	15.01	15.01	18.21	0.82	0.82	3.96	3.36	3.50	1.13	0.96	E13
dextrorphan	AS=1.0	13.05	13.09	13.44	0.97	0.97	2.64	2.51	3.24	0.81	0.77	E14

*: no AUC_{last} calculated due to insufficient amount of observed data points, -: not available, †: AUC_{last} and C_{max} values as well as corresponding ratios were calculated based on a small number of observed data points (n = 3 for studies A and B, n = 2 for studies D and E) and should be interpreted with caution, AS: CYP2D6 activity score, AUC: area under the plasma concentration-time curve, AUC_{last}: AUC from the time of the first concentration measurement to the last time of concentration measurement, C_{max}: peak plasma concentration, CYP2D6: Cytochrome P450 2D6, obs: observed, po: oral, ind.: individual, optim.: optimized, pred: predicted.

Table S6.7.4: Predicted and observed AUC_{last} and C_{max} values and geometric mean fold errors (continued)

Molecule	CYP2D6 status	AUC_{last} [ng·h/mL]					C_{max} [ng/mL]					Subject ID
		Pred		Obs	Pred/Obs		Pred		Obs	Pred/Obs		
		population k_{cat}	ind. optim. k_{cat}		population k_{cat}	ind. optim. k_{cat}	population k_{cat}	ind. optim. k_{cat}		population k_{cat}	ind. optim. k_{cat}	
dextrorphan	AS=2.0	17.65	17.41	19.88	0.89	0.88	4.75	3.33	6.59	0.72	0.51	E15
dextrorphan	AS=1.0	13.17	13.35	15.34	0.86	0.87	2.47	2.47	4.27	0.58	0.58	E16
dextrorphan	AS=1.0	18.06	15.15	15.19	1.19	1.00	3.87	2.14	2.54	1.52	0.84	E17
dextrorphan	AS=2.0	13.33	13.67	10.96	1.22	1.25	4.21	3.15	4.68	0.90	0.67	E18
dextrorphan	AS=2.0	7.91	9.23	40.37	0.20	0.23	3.51	2.48	9.09	0.39	0.27	E20
dextrorphan	AS=1.0	18.07	10.95	3.25	5.56	3.37	3.79	1.24	0.61	6.19	2.03	E21
dextrorphan	AS=3.0	16.36	16.40	18.37	0.89	0.89	4.32	4.24	5.02	0.86	0.84	E23
dextrorphan	AS=2.0	13.86	13.71	20.35	0.68	0.67	3.59	2.66	5.74	0.63	0.46	E24
dextrorphan	AS=2.0	15.06	15.15	19.11	0.79	0.79	3.76	3.51	3.83	0.98	0.91	E25
dextrorphan	AS=1.0	13.99	14.16	12.58	1.11	1.13	2.59	2.58	2.75	0.94	0.94	E26
dextrorphan	AS=2.0	14.10	14.03	9.45	1.49	1.48	3.65	3.81	2.67	1.37	1.43	E27
dextrorphan	AS=1.0	13.59	13.87	13.29	1.02	1.04	2.67	3.10	2.57	1.04	1.20	E28
dextrorphan	AS=1.0	15.52	15.70	15.96	0.97	0.98	3.11	3.21	4.68	0.66	0.69	E30
GMFE (dextrorphan)		population k_{cat}			1.56 (1.02–5.56) 65/71 with GMFE ≤ 2					1.74 (1.02–6.19) 52/70 with GMFE ≤ 2		
		ind. optim. k_{cat}				1.52 (1.00–4.35) 65/71 with GMFE ≤ 2					1.77 (1.00–5.00) 53/70 with GMFE ≤ 2	
dextrorphan-total†	AS=0.25	74.20	58.21	161.67	0.46	0.36	29.23	23.13	150.57	0.19	0.15	A01
dextrorphan-total†	AS=1.5	454.99	475.88	601.15	0.76	0.79	279.59	240.73	357.76	0.78	0.67	A02
dextrorphan-total†	AS=2.0	183.04	169.66	244.59	0.75	0.69	254.27	131.90	165.50	1.54	0.80	A03
dextrorphan-total†	AS=1.0	424.62	402.80	412.90	1.03	0.98	209.12	227.79	246.57	0.85	0.92	A04
dextrorphan-total†	AS=1.0	454.50	424.97	394.40	1.15	1.08	231.55	248.29	236.53	0.98	1.05	A05
dextrorphan-total†	AS=2.0	392.52	374.71	408.72	0.96	0.92	249.29	213.58	243.48	1.02	0.88	A06
dextrorphan-total†	AS=1.0	456.59	450.25	165.81	2.75	2.72	226.94	240.80	251.20	0.90	0.96	A07
dextrorphan-total†	AS=2.0	364.60	362.66	275.97	1.32	1.31	235.26	205.83	203.07	1.16	1.01	A09
dextrorphan-total†	AS=1.0	402.03	385.18	409.90	0.98	0.94	204.39	218.86	248.89	0.82	0.88	A10
dextrorphan-total†	AS=1.0	355.67	351.09	273.45	1.30	1.28	173.18	188.07	150.82	1.15	1.25	A11
dextrorphan-total†	AS=3.0	391.50	385.54	384.82	1.02	1.00	322.96	241.70	298.56	1.08	0.81	A12
dextrorphan-total†	AS=1.0	394.78	382.08	393.84	1.00	0.97	199.11	213.38	245.03	0.81	0.87	A13
dextrorphan-total†	AS=2.0	396.92	376.71	373.92	1.06	1.01	262.34	220.25	259.95	1.01	0.85	A14

*: no AUC_{last} calculated due to insufficient amount of observed data points, -: not available, †: AUC_{last} and C_{max} values as well as corresponding ratios were calculated based on a small number of observed data points (n = 3 for studies A and B, n = 2 for studies D and E) and should be interpreted with caution, AS: CYP2D6 activity score, AUC: area under the plasma concentration-time curve, AUC_{last}: AUC from the time of the first concentration measurement to the last time of concentration measurement, C_{max}: peak plasma concentration, CYP2D6: Cytochrome P450 2D6, obs: observed, po: oral, ind.: individual, optim.: optimized, pred: predicted.

Table S6.7.4: Predicted and observed AUC_{last} and C_{max} values and geometric mean fold errors (continued)

Molecule	CYP2D6 status	AUC_{last} [ng·h/mL]					C_{max} [ng/mL]					Subject ID
		Pred		Obs	Pred/Obs		Pred		Obs	Pred/Obs		
		population k_{cat}	ind. optim. k_{cat}		population k_{cat}	ind. optim. k_{cat}	population k_{cat}	ind. optim. k_{cat}		population k_{cat}	ind. optim. k_{cat}	
dextrorphan-total†	AS=3.0	412.59	408.01	282.20	1.46	1.45	314.56	244.64	189.69	1.66	1.29	A15
dextrorphan-total†	AS=1.0	217.90	196.43	197.95	1.10	0.99	195.69	150.81	135.38	1.45	1.11	A16
dextrorphan-total†	AS=2.0	401.27	182.30	227.89	1.76	0.80	262.48	220.11	249.92	1.05	0.88	C01
dextrorphan-total†	AS=2.0	424.15	400.81	658.17	0.64	0.61	288.64	238.43	332.02	0.87	0.72	C02
dextrorphan-total†	AS=2.0	390.84	363.31	409.76	0.95	0.89	289.88	227.44	429.82	0.67	0.53	C03
dextrorphan-total†	AS=2.0	373.50	351.28	249.66	1.50	1.41	236.62	200.55	207.19	1.14	0.97	C04
dextrorphan-total†	-	407.26	407.26	211.28	1.93	1.93	195.02	195.02	94.97	2.05	2.05	C05
dextrorphan-total†	AS=3.0	381.95	376.42	374.65	1.02	1.00	288.07	225.95	177.33	1.62	1.27	C06
dextrorphan-total†	-	401.92	401.92	369.49	1.09	1.09	196.93	196.93	207.71	0.95	0.95	C07
dextrorphan-total†	AS=0.5	298.66	257.64	361.64	0.83	0.71	123.96	100.89	161.12	0.77	0.63	C08
dextrorphan-total†	-	419.51	419.51	495.73	0.85	0.85	203.83	203.83	253.26	0.80	0.80	C09
dextrorphan-total†	AS=1.5	417.32	421.64	736.42	0.57	0.57	255.36	235.39	380.92	0.67	0.62	C10
dextrorphan-total†	AS=1.5	362.15	331.47	429.22	0.84	0.77	210.39	193.95	199.73	1.05	0.97	C11
dextrorphan-total†	AS=1.5	432.92	408.08	486.83	0.89	0.84	263.30	243.68	234.47	1.12	1.04	C12
dextrorphan-total†	-	427.02	427.02	444.12	0.96	0.96	208.64	208.64	237.05	0.88	0.88	C13
dextrorphan-total†	AS=1.5	384.85	374.74	459.39	0.84	0.82	221.79	210.97	246.57	0.90	0.86	C14
dextrorphan-total†	AS=1.0	453.27	434.50	501.42	0.90	0.87	220.11	241.79	247.34	0.89	0.98	C15
dextrorphan-total†	-	373.44	373.44	565.76	0.66	0.66	175.74	175.74	486.45	0.36	0.36	C16
dextrorphan-total†	AS=2.0	216.72	222.34	1118.88	0.19	0.20	322.59	178.02	715.52	0.45	0.25	D01
dextrorphan-total†	AS=1.5	215.92	235.93	643.82	0.34	0.37	243.57	166.09	409.23	0.60	0.41	D02
dextrorphan-total†	AS=2.0	206.22	192.90	916.72	0.22	0.21	253.66	145.40	604.84	0.42	0.24	D03
dextrorphan-total†	AS=2.0	210.91	239.27	843.28	0.25	0.28	263.27	175.27	514.76	0.51	0.34	D04
dextrorphan-total†	-	266.16	266.16	733.43	0.36	0.36	236.55	236.55	442.69	0.53	0.53	D05
dextrorphan-total†	AS=1.0	*	*	*	*	*	232.19	182.19	584.25	0.40	0.31	D06
dextrorphan-total†	AS=2.0	206.70	220.21	1175.42	0.18	0.19	294.37	174.40	725.81	0.41	0.24	D07
dextrorphan-total†	AS=1.0	240.53	242.27	621.04	0.39	0.39	225.72	166.26	373.20	0.60	0.45	D08
dextrorphan-total†	AS=2.0	209.00	197.10	671.12	0.31	0.29	284.35	153.37	422.10	0.67	0.36	D09
dextrorphan-total†	AS=1.5	215.12	211.81	1132.72	0.19	0.19	247.51	164.62	656.32	0.38	0.25	D10
dextrorphan-total†	AS=1.0	250.64	245.81	997.96	0.25	0.25	230.56	186.75	615.14	0.37	0.30	D11
dextrorphan-total†	AS=1.0	222.69	208.61	1069.74	0.21	0.20	210.41	161.69	748.98	0.28	0.22	D12
dextrorphan-total†	AS=1.0	226.73	233.80	319.11	0.71	0.73	231.23	178.23	183.51	1.26	0.97	E01
dextrorphan-total†	AS=1.0	258.72	257.99	355.20	0.73	0.73	199.71	181.42	241.42	0.83	0.75	E02
dextrorphan-total†	AS=1.0	237.66	225.35	355.60	0.67	0.63	221.17	174.50	290.84	0.76	0.60	E03
dextrorphan-total†	AS=2.0	230.12	224.43	736.33	0.31	0.30	299.18	173.57	463.28	0.65	0.37	E04

*: no AUC_{last} calculated due to insufficient amount of observed data points, -: not available, †: AUC_{last} and C_{max} values as well as corresponding ratios were calculated based on a small number of observed data points (n = 3 for studies A and B, n = 2 for studies D and E) and should be interpreted with caution, AS: CYP2D6 activity score, AUC: area under the plasma concentration-time curve, AUC_{last}: AUC from the time of the first concentration measurement to the last time of concentration measurement, C_{max}: peak plasma concentration, CYP2D6: Cytochrome P450 2D6, obs: observed, po: oral, ind.: individual, optim.: optimized, pred: predicted.

Table S6.7.4: Predicted and observed AUC_{last} and C_{max} values and geometric mean fold errors (continued)

Molecule	CYP2D6 status	AUC_{last} [ng·h/mL]					C_{max} [ng/mL]					Subject ID
		Pred		Obs	Pred/Obs		Pred		Obs	Pred/Obs		
		population k_{cat}	ind. optim. k_{cat}		population k_{cat}	ind. optim. k_{cat}	population k_{cat}	ind. optim. k_{cat}		population k_{cat}	ind. optim. k_{cat}	
dextrorphan-total†	AS=2.0	183.00	213.64	657.99	0.28	0.32	241.17	149.52	411.81	0.59	0.36	E05
dextrorphan-total†	AS=1.0	239.50	243.56	698.13	0.34	0.35	225.90	181.06	401.51	0.56	0.45	E06
dextrorphan-total†	AS=2.0	226.27	235.11	889.13	0.25	0.26	297.46	180.96	576.53	0.52	0.31	E07
dextrorphan-total†	AS=2.0	213.98	256.04	749.94	0.29	0.34	284.10	181.68	442.69	0.64	0.41	E08
dextrorphan-total†	AS=2.0	267.65	265.21	1026.95	0.26	0.26	346.78	205.39	599.70	0.58	0.34	E09
dextrorphan-total†	AS=1.0	227.56	222.95	858.04	0.27	0.26	232.09	146.24	491.60	0.47	0.30	E10
dextrorphan-total†	AS=1.0	223.13	216.46	1138.83	0.20	0.19	200.12	163.28	746.40	0.27	0.22	E11
dextrorphan-total†	AS=2.0	198.39	221.73	548.05	0.36	0.40	287.50	174.66	373.20	0.77	0.47	E12
dextrorphan-total†	AS=2.0	220.02	244.75	942.32	0.23	0.26	312.94	192.70	664.04	0.47	0.29	E13
dextrorphan-total†	AS=1.0	234.15	232.37	776.34	0.30	0.30	218.61	175.89	545.65	0.40	0.32	E14
dextrorphan-total†	AS=2.0	228.09	282.61	1038.21	0.22	0.27	344.89	215.69	661.47	0.52	0.33	E15
dextrorphan-total†	AS=1.0	278.20	275.00	962.07	0.29	0.29	225.93	198.00	630.58	0.36	0.31	E16
dextrorphan-total†	AS=1.0	273.00	252.19	496.73	0.55	0.51	278.85	160.19	306.28	0.91	0.52	E17
dextrorphan-total†	AS=2.0	211.63	249.18	405.37	0.52	0.61	304.65	191.00	452.99	0.67	0.42	E18
dextrorphan-total†	AS=2.0	199.98	243.32	1614.43	0.12	0.15	280.19	179.57	1091.29	0.26	0.16	E20
dextrorphan-total†	AS=1.0	299.53	178.71	161.92	1.85	1.10	288.46	102.34	166.78	1.73	0.61	E21
dextrorphan-total†	AS=3.0	257.95	263.62	677.83	0.38	0.39	352.78	201.86	710.37	0.50	0.28	E23
dextrorphan-total†	AS=2.0	194.69	231.92	994.10	0.20	0.23	280.43	177.47	674.34	0.42	0.26	E24
dextrorphan-total†	AS=2.0	277.88	264.65	1646.27	0.17	0.16	313.71	195.66	1263.74	0.25	0.15	E25
dextrorphan-total†	AS=1.0	260.20	256.00	1015.63	0.26	0.25	216.48	187.46	666.61	0.32	0.28	E26
dextrorphan-total†	AS=2.0	198.01	187.34	1035.70	0.19	0.18	284.61	147.60	664.04	0.43	0.22	E27
dextrorphan-total†	AS=1.0	266.46	246.65	787.91	0.34	0.31	229.73	187.15	540.50	0.43	0.35	E28
dextrorphan-total†	AS=1.0	258.77	249.21	930.94	0.28	0.27	240.65	191.07	568.81	0.42	0.34	E30
GMFE (dextrorphan-total†)		population k_{cat}			2.63 (1.00–8.33) 35/69 with GMFE $\leq$ 2					1.84 (1.01–5.26) 48/70 with GMFE $\leq$ 2		
		ind. optim. k_{cat}				2.58 (1.00–6.67) 35/69 with GMFE $\leq$ 2					2.41 (1.01–6.67) 34/70 with GMFE $\leq$ 2	
Overall GMFE		population k_{cat}			2.45 (1.00–14.70) 131/210 with GMFE $\leq$ 2					2.21 (1.00–20.00) 133/212 with GMFE $\leq$ 2		

*: no AUC_{last} calculated due to insufficient amount of observed data points, -: not available, †: AUC_{last} and C_{max} values as well as corresponding ratios were calculated based on a small number of observed data points (n = 3 for studies A and B, n = 2 for studies D and E) and should be interpreted with caution, AS: CYP2D6 activity score, AUC: area under the plasma concentration-time curve, AUC_{last}: AUC from the time of the first concentration measurement to the last time of concentration measurement, C_{max}: peak plasma concentration, CYP2D6: Cytochrome P450 2D6, obs: observed, po: oral, ind.: individual, optim.: optimized, pred: predicted.

Table S6.7.4: Predicted and observed AUC_{last} and C_{max} values and geometric mean fold errors (continued)

Molecule	CYP2D6 status	AUC_{last} [ng·h/mL]					C_{max} [ng/mL]					Subject ID
		Pred		Obs	Pred/Obs		Pred		Obs	Pred/Obs		
		population k_{cat}	ind. optim. k_{cat}		population k_{cat}	ind. optim. k_{cat}	population k_{cat}	ind. optim. k_{cat}		population k_{cat}	ind. optim. k_{cat}	
		ind. optim. k_{cat}				1.94 (1.00–14.70) 166/210 with GMFE $\leq$ 2					1.94 (1.00–8.53) 152/212 with GMFE $\leq$ 2	

*: no AUC_{last} calculated due to insufficient amount of observed data points, -: not available, †: AUC_{last} and C_{max} values as well as corresponding ratios were calculated based on a small number of observed data points (n = 3 for studies A and B, n = 2 for studies D and E) and should be interpreted with caution, AS: CYP2D6 activity score, AUC: area under the plasma concentration-time curve, AUC_{last}: AUC from the time of the first concentration measurement to the last time of concentration measurement, C_{max}: peak plasma concentration, CYP2D6: Cytochrome P450 2D6, obs: observed, po: oral, ind.: individual, optim.: optimized, pred: predicted.

S6.8 GMFE of Predicted AUC_{last} and C_{max} Values Grouped by Study and Activity Score

Table S6.8.5: Predicted and observed AUC_{last} and C_{max} values and geometric mean fold errors grouped by study and activity score

Study	Molecule	CYP2D6 Activity Score	n	AUC_{last} [ng·h/mL]					C_{max} [ng/mL]				
				Pred		Obs	Pred/Obs		Pred		Obs	Pred/Obs	
				population k_{cat}	ind. optim. k_{cat}		population k_{cat}	ind. optim. k_{cat}	population k_{cat}	ind. optim. k_{cat}		population k_{cat}	ind. optim. k_{cat}
A	dextromethorphan	0	1	156.79	146.08	162.42	0.97	0.9	15.85	14.08	16.37	0.97	0.86
		0.25	1	131.51	138.87	146.34	0.90	0.95	14.33	11.92	12.59	0.83	0.88
		1	7	13.15 (0.99)	6.32 (1.37)	5.68 (1.50)	2.44 (0.59)	1.12 (0.08)	1.02 (0.32)	2.07 (0.23)	0.95 (0.23)	2.13 (0.41)	0.96 (0.18)
		1.5	1	7.84	14.67	17.31	0.45	0.85	4.53	1.30	2.07	0.29	0.46
		2	3	1.34 (0.40)	0.79 (0.70)	0.64 (0.53)	2.74 (1.16)	1.22 (0.06)	0.25 (0.19)	0.55 (0.03)	0.24 (0.16)	3.36 (2.45)	1.01 (0.15)
		3	2	0.54 (0.24)	0.40 (0.22)	0.39 (0.15)	1.37 (0.11)	1 (0.17)	0.17 (0.01)	0.26 (0.03)	0.17 (0.03)	1.55 (0.05)	1.02 (0.12)
GMFE dextromethorphan, study A							2.16	1.13				2.32	1.17
A	dextrorphan	0.25	1	3.80	3.05	3.20	1.19	0.95	0.38	0.34	0.27	0.90	0.71
		1	7	13.67 (1.31)	13.97 (1.27)	19.62 (3.44)	0.71 (0.12)	0.73 (0.12)	5.11 (1.88)	2.52 (0.3)	2.92 (0.39)	0.54 (0.18)	0.62 (0.20)
		1.5	1	15.45	15.23	23.58	0.66	0.65	6.20	3.59	2.73	0.58	0.44
		2	4	14.09 (0.75)	14.05 (0.75)	19.05 (5.09)	0.78 (0.2)	0.78 (0.2)	5.63 (1.37)	3.2 (0.18)	3.33 (0.26)	0.6 (0.18)	0.63 (0.19)
		3	2	14.57 (3.25)	14.5 (3.29)	18.26 (7.09)	0.9 (0.53)	0.9 (0.53)	3.85 (0.53)	4.25 (0.06)	4.24 (0.05)	1.12 (0.17)	1.11 (0.17)
GMFE dextrorphan, study A							1.33	1.31				1.64	1.57
A	dextrorphan-total†	0.25	1	74.20	58.21	161.67	0.46	0.36	150.57	29.23	23.13	0.19	0.15
		1	7	386.58 (82.34)	370.4 (83.06)	321.18 (106.87)	1.33 (0.64)	1.28 (0.64)	216.35 (50.44)	205.71 (19.72)	212.57 (33.57)	0.99 (0.23)	1.01 (0.14)
		1.5	1	454.99	475.88	601.15	0.76	0.79	357.76	279.59	240.73	0.78	0.67
		2	4	334.27 (101.83)	320.94 (101.04)	325.8 (78.04)	1.02 (0.24)	0.98 (0.26)	218 (42.38)	250.29 (11.37)	192.89 (41.08)	1.18 (0.25)	0.88 (0.09)
		3	2	402.05 (14.91)	396.78 (15.89)	333.51 (72.56)	1.24 (0.31)	1.22 (0.31)	244.12 (76.98)	318.76 (5.94)	243.17 (2.08)	1.37 (0.41)	1.05 (0.34)
GMFE dextrorphan-total, study A							1.29	1.30				1.40	1.44
Overall GMFE, study A							1.59	1.24				1.80	1.31
C	dextromethorphan	0.5	1	49.56	63.17	62.68	0.79	1.01	10.39	6.45	7.53	0.62	0.72
		1	1	14.86	6.01	5.05	2.94	1.19	1.09	2.53	1.03	2.33	0.95
		1.5	4	6.23 (0.87)	4.33 (2.75)	3.49 (2.31)	2.49 (1.62)	1.26 (0.04)	0.82 (0.67)	1.11 (0.14)	0.71 (0.48)	2.23 (1.76)	0.94 (0.13)
		2	4	1.68 (0.30)	0.50 (0.19)	0.45 (0.16)	3.99 (1.00)	1.11 (0.08)	0.2 (0.07)	0.58 (0.05)	0.15 (0.05)	3.19 (0.97)	0.78 (0.18)
		3	1	0.13	0.08	0.07	1.79	1.15	0.11	0.21	0.13	1.93	1.18
GMFE dextromethorphan, study C							2.90	1.17				2.50	1.18
C	dextrorphan	0.5	1	10.52	9.41	12.19	0.86	0.77	4.14	1.48	1.20	0.36	0.29
		1	1	14.89	15.25	24.67	0.6	0.62	8.85	2.85	3.44	0.32	0.39
		1.5	4	13.07 (1.47)	13.08 (1.44)	15.32 (5.82)	1.01 (0.61)	1.02 (0.61)	4.37 (2.57)	2.97 (0.43)	3.11 (0.36)	1.06 (1.02)	1.14 (1.12)
		2	4	14.23 (1.32)	14.13 (1.27)	10.04 (1.53)	1.43 (0.1)	1.42 (0.1)	3.92 (1.11)	3.48 (0.42)	3.66 (0.43)	0.94 (0.26)	0.99 (0.27)
		3	1	13.53	13.49	10.29	1.31	1.31	4.63	3.61	3.61	0.78	0.78

All values are given as mean (SD). †: AUC_{last} and C_{max} values as well as corresponding ratios were calculated based on a small number of observed data points (n = 3 for studies A and B, n = 3 for studies D and E) and should be interpreted with caution, AUC: area under the plasma concentration-time curve, AUC_{last}: AUC from the time of the first concentration measurement to the last time of concentration measurement, C_{max}: peak plasma concentration, CYP2D6: Cytochrome P450 2D6 obs: observed, po: oral, ind.: individual, optim.: optimized, pred: predicted.

Table S6.8.5: Predicted and observed AUC_{last} and C_{max} values and geometric mean fold errors (continued)

Study	Molecule	CYP2D6 Activity Score	n	AUC_{last} [ng·h/mL] Pred population k_{cat}	AUC_{last} [ng·h/mL] Pred ind. optim. k_{cat}	AUC_{last} [ng·h/mL] Obs	AUC_{last} [ng·h/mL] Pred/Obs population k_{cat}	AUC_{last} [ng·h/mL] Pred/Obs ind. optim. k_{cat}	C_{max} [ng/mL] Pred population k_{cat}	C_{max} [ng/mL] Pred ind. optim. k_{cat}	C_{max} [ng/mL] Obs	C_{max} [ng/mL] Pred/Obs population k_{cat}	C_{max} [ng/mL] Pred/Obs ind. optim. k_{cat}
GMFE dextrorphan, study C							1.26	1.27				1.43	1.45
C	dextrorphan-total†	0.5	1	298.66	257.64	361.64	0.83	0.71	161.12	123.96	100.89	0.77	0.63
		1	1	453.27	434.5	501.42	0.9	0.87	247.34	220.11	241.79	0.89	0.98
		1.5	4	399.31 (31.86)	383.98 (40.17)	527.97 (140.95)	0.78 (0.15)	0.75 (0.12)	265.42 (79.52)	237.71 (25.6)	221 (22.76)	0.94 (0.20)	0.87 (0.18)
		2	4	345.18 (104.11)	324.43 (97.07)	386.37 (198.52)	0.98 (0.36)	0.93 (0.34)	304.74 (98.17)	269.41 (25.24)	221.63 (15.94)	0.93 (0.21)	0.77 (0.19)
		3	1	381.95	376.42	374.65	1.02	1.00	177.33	288.07	225.95	1.62	1.27
GMFE dextrorphan-total, study C							1.14	1.20				1.15	1.24
Overall GMFE, study C							1.77	1.21				1.69	1.29
D	dextromethorphan	1	4	13.15 (0.44)	13.44 (10.27)	14.60 (15.26)	1.57 (0.90)	1.09 (0.23)	2.42 (1.91)	2.26 (0.10)	2.12 (1.49)	1.35 (0.74)	0.93 (0.16)
		1.5	2	6.97 (0.10)	14.11 (11.25)	16.43 (16.21)	0.82 (0.80)	1.02 (0.32)	3.34 (3.03)	1.24 (0.02)	2.26 (1.7)	0.63 (0.57)	0.76 (0.18)
		2	5	2.70 (1.50)	4.92 (5.63)	4.25 (5.15)	1.99 (1.86)	1.15 (0.12)	0.8 (0.79)	0.6 (0.07)	0.87 (0.88)	1.8 (1.78)	1.04 (0.11)
GMFE dextromethorphan, study D							1.70	1.11				1.60	1.10
D	dextrorphan	1	4	13.98 (0.44)	13.89 (0.58)	16.64 (4.42)	0.88 (0.23)	0.88 (0.22)	4.54 (0.66)	2.82 (0.08)	2.78 (0.43)	0.63 (0.10)	0.62 (0.09)
		1.5	2	13.67 (0.50)	13.50 (0.76)	39.71 (15.84)	0.38 (0.16)	0.37 (0.17)	9.48 (2.75)	3.19 (0.03)	2.74 (0.64)	0.35 (0.10)	0.31 (0.16)
		2	5	14.40 (1.39)	14.34 (1.33)	12.89 (8.11)	1.63 (1.21)	1.63 (1.21)	3.93 (1.54)	3.72 (0.35)	3.43 (0.52)	1.18 (0.77)	1.13 (0.87)
GMFE dextrorphan, study D							1.64	1.64				1.63	1.69
D	dextrorphan-total†	1	3	237.95 (14.15)	232.23 (20.53)	896.25 (241.03)	0.28 (0.09)	0.28 (0.10)	580.39 (155.53)	224.72 (9.93)	174.22 (12.12)	0.41 (0.14)	0.32 (0.09)
		1.5	2	215.52 (0.56)	223.87 (17.05)	888.27 (345.7)	0.26 (0.1)	0.28 (0.13)	532.78 (174.72)	245.54 (2.79)	165.35 (1.04)	0.49 (0.15)	0.33 (0.11)
		2	5	209.91 (4.25)	214.36 (19.22)	945.08 (205.84)	0.23 (0.05)	0.23 (0.05)	596.61 (130.43)	283.65 (27.14)	165.29 (14.85)	0.49 (0.11)	0.29 (0.06)
GMFE dextrorphan-total, study D							3.99	3.93				2.17	3.28
Overall GMFE, study D							2.39	2.17				1.80	2.02
E	dextromethorphan	0	1	124.38	98.69	97.59	1.27	1.01	10.67	15.8	10.94	1.48	1.03
		1	13	13.05 (1.58)	23.99 (29.30)	36.4 (57.39)	1.2 (0.74)	1.02 (0.29)	4.87 (6.97)	2.2 (0.32)	3.29 (3.43)	1.21 (0.78)	0.99 (0.32)
		2	13	3.46 (0.48)	9.31 (6.53)	8.73 (6.96)	0.88 (0.84)	1.16 (0.20)	2.48 (3.61)	0.58 (0.05)	1.55 (1.08)	0.83 (0.9)	1.01 (0.45)
		3	1	1.97	2.79	2.30	0.85	1.21	0.35	0.24	0.39	0.67	1.10
GMFE dextromethorphan, study E							1.18	1.09				1.23	1.02
E	dextrorphan	1	13	13.67 (2.44)	12.84 (1.86)	15.74 (5.92)	1.21 (1.33)	1.02 (0.74)	3.74 (1.67)	2.83 (0.5)	2.41 (0.51)	1.18 (1.53)	0.79 (0.44)
		2	13	14.13 (2.32)	14.11 (2.09)	18.48 (8.75)	0.92 (0.38)	0.92 (0.38)	4.97 (2.05)	3.8 (0.43)	3.19 (0.67)	0.89 (0.36)	0.76 (0.37)

All values are given as mean (SD). †: AUC_{last} and C_{max} values as well as corresponding ratios were calculated based on a small number of observed data points (n = 3 for studies A and B, n = 3 for studies D and E) and should be interpreted with caution, AUC: area under the plasma concentration-time curve, AUC_{last}: AUC from the time of the first concentration measurement to the last time of concentration measurement, C_{max}: peak plasma concentration, CYP2D6: Cytochrome P450 2D6 obs: observed, po: oral, ind.: individual, optim.: optimized, pred: predicted.

Table S6.8.5: Predicted and observed AUC_{last} and C_{max} values and geometric mean fold errors (continued)

Study	Molecule	CYP2D6 Activity Score	n	AUC_{last} [ng·h/mL] Pred population k_{cat}	AUC_{last} [ng·h/mL] Pred ind. optim. k_{cat}	AUC_{last} [ng·h/mL] Obs	AUC_{last} [ng·h/mL] Pred/Obs population k_{cat}	AUC_{last} [ng·h/mL] Pred/Obs ind. optim. k_{cat}	C_{max} [ng/mL] Pred population k_{cat}	C_{max} [ng/mL] Pred ind. optim. k_{cat}	C_{max} [ng/mL] Obs	C_{max} [ng/mL] Pred/Obs population k_{cat}	C_{max} [ng/mL] Pred/Obs ind. optim. k_{cat}
		3	1	16.36	16.40	18.37	0.89	0.89	5.02	4.32	4.24	0.86	0.84
GMFE dextrorphan, study E							1.15	1.06				1.56	1.29
E	dextrorphan-total†	1	13	252.59 (23.27)	237.71 (24.05)	681.27 (311.13)	0.52 (0.44)	0.46 (0.27)	444.65 (192.2)	231.46 (26.03)	171.3 (24.94)	0.67 (0.43)	0.46 (0.22)
		2	13	219.21 (27.82)	239.99 (25.11)	944.98 (363.07)	0.26 (0.10)	0.29 (0.12)	641.47 (262.92)	298.28 (28.04)	181.96 (19.27)	0.52 (0.16)	0.32 (0.1)
		3	1	257.95	263.62	677.83	0.38	0.39	710.37	352.78	201.86	0.50	0.28
GMFE dextrorphan-total, study E							2.86	2.81				1.72	2.69
Overall GMFE, study E							1.72	1.65				1.36	1.66

All values are given as mean (SD). †: AUC_{last} and C_{max} values as well as corresponding ratios were calculated based on a small number of observed data points (n = 3 for studies A and B, n = 3 for studies D and E) and should be interpreted with caution, AUC: area under the plasma concentration-time curve, AUC_{last}: AUC from the time of the first concentration measurement to the last time of concentration measurement, C_{max}: peak plasma concentration, CYP2D6: Cytochrome P450 2D6 obs: observed, po: oral, ind.: individual, optim.: optimized, pred: predicted.

S7 Summary

In this supplementary file, the development process of a whole-body PBPK model of dextromethorphan and its metabolites dextrorphan and dextrorphan *O*-glucuronide is documented. The model has been thoroughly evaluated to predict the pharmacokinetics of the modeled analytes including a wide range of CYP2D6 DGI scenarios. Moreover, the model was applied to predict individual plasma concentration-time profiles using the model k_{cat} values obtained during the DGI model building process. These were then compared to predictions using individual optimized k_{cat} values. For a tabular summary of model geometric mean fold error (GMFE) and mean relative deviation (MRD) values, refer to Table S7.0.1.

Table S7.0.1: Summary of quantitative performance metrics for the different model subsets

	AUC_{last}		C_{max}		MRD (range)	MRD ≤ 2
	GMFE (range)	GMFE ≤ 2	GMFE (range)	GMFE ≤ 2		
Population studies						
PBPK base model	1.57 (1.01–3.45)	18/23	1.61 (1.01–2.97)	17/22	2.21 (1.35–3.56)	12/23
DGI model	1.50 (1.05–2.33)	16/18	1.28 (1.01–2.22)	17/18	2.13 (1.10–4.26)	11/18
Overall (populations)	1.54 (1.01–3.45)	34/41	1.47 (1.01–2.97)	34/40	2.17 (1.10–4.26)	23/41
Individual profiles						
Population predictions	2.45 (1.00–14.70)	131/210	2.21 (1.00–20.00)	133/212	2.72 (1.08–14.00)	114/212
Individual predictions	1.94 (1.00–14.70)	166/210	1.94 (1.00–8.53)	152/212	1.94 (1.08–14.00)	152/212

AUC_{last}: AUC from the time of the first concentration measurement to the last time point of concentration measurement, C_{max}: peak plasma concentration, DGI: drug-gene interaction, GMFE: geometric mean fold error, MRD: mean relative deviation, PBPK: physiologically based pharmacokinetic.

S8 Abbreviations

AS	CYP2D6 activity score
AUC	Area under the plasma concentration-time curve
AUC_{last}	AUC from the time of the first concentration measurement to the last time point of concentration measurement
cap	Capsule
C_{max}	Peak plasma concentration
CYP2D6	Cytochrome P450 2D6
CYP3A4	Cytochrome P450 3A4
DGI	Drug-gene interaction
EHC	Enterohepatic circulation
EM	Extensive metabolizer
f_u	Fraction unbound
GFR	Glomerular filtration rate
GMFE	Geometric mean fold error
ICRP	International Commission on Radiological Protection
IM	Intermediate metabolizer
inf	Infusion
iv	Intravenous
K_D	Dissociation constant
k_{cat}	Catalytic rate constant
K_M	Michaelis-Menten constant
k_{off}	Dissociation rate constant
MRD	Mean relative deviation
MW	Molecular weight
NHANES	Third National Health and Nutrition Examination Survey
NM	Normal metabolizer
PBPK	Physiologically based pharmacokinetic
pKa	Acid dissociation constant
PM	Poor metabolizer
po	Oral
sd	Single dose
sol	Oral solution
tab	Tablet
t_{max}	Time to reach Peak plasma concentration
UM	Ultrarapid metabolizer
UGT2B15	Uridine 5'-diphospho-glucuronosyltransferase family 2 member B15

Bibliography

1. Armani, S. *et al.* Drug Interaction Potential of Osilodrostat (LCI699) Based on Its Effect on the Pharmacokinetics of Probe Drugs of Cytochrome P450 Enzymes in Healthy Adults. *Clinical drug investigation* **37,** 465–472 (May 2017).
2. Benet, L. Z., Broccatelli, F. & Oprea, T. I. BDDCS Applied to Over 900 Drugs. *The AAPS Journal* **13,** 519–547 (Dec. 2011).
3. Berezhkovskiy, L. M. Volume of distribution at steady state for a linear pharmacokinetic system with peripheral elimination. *Journal of Pharmaceutical Sciences* **93,** 1628–1640 (2004).
4. Bolger, M. B., Macwan, J. S., Sarfraz, M., Almukainzi, M. & Löbenberg, R. The Irrelevance of In Vitro Dissolution in Setting Product Specifications for Drugs Like Dextromethorphan That are Subject to Lysosomal Trapping. *Journal of Pharmaceutical Sciences* **108,** 268–278 (2019).
5. Brown, H. S., Griffin, M. & Houston, J. B. Evaluation of cryopreserved human hepatocytes as an alternative in vitro system to microsomes for the prediction of metabolic clearance. *Drug Metabolism and Disposition* **35,** 293–301 (2007).
6. Capon, D. A. *et al.* The influence of CYP2D6 polymorphism and quinidine on the disposition and antitussive effect of dextromethorphan in humans. *Clinical pharmacology and therapeutics* **60,** 295–307 (Sept. 1996).
7. Duedahl, T. H. *et al.* Intravenous dextromethorphan to human volunteers: relationship between pharmacokinetics and anti-hyperalgesic effect. *Pain* **113,** 360–8 (Feb. 2005).
8. Dumond, J. B. *et al.* A phenotype-genotype approach to predicting CYP450 and P-glycoprotein drug interactions with the mixed inhibitor/inducer tipranavir/ritonavir. *Clinical pharmacology and therapeutics* **87,** 735–42 (June 2010).
9. Edwards, J. E., Eliot, L., Parkinson, A., Karan, S. & MacConell, L. Assessment of Pharmacokinetic Interactions Between Obeticholic Acid and Caffeine, Midazolam, Warfarin, Dextromethorphan, Omeprazole, Rosuvastatin, and Digoxin in Phase 1 Studies in Healthy Subjects. *Advances in therapy* **34,** 2120–2138 (2017).
10. Ermer, J., Corcoran, M. & Martin, P. Lisdexamfetamine dimesylate effects on the pharmacokinetics of cytochrome P450 substrates in healthy adults in an open-label, randomized, crossover study. *Drugs in R and D* **15,** 175–185 (2015).
11. Feld, R. *et al.* A clinical investigation of inhibitory effect of panobinostat on CYP2D6 substrate in patients with advanced cancer. *Cancer chemotherapy and pharmacology* **72,** 747–55 (Oct. 2013).
12. Frank, D. *Bewertung von pharmakokinetischen Parametern zur Phänotypisierung des menschlichen Cytochrom P450 Enzyms CYP2D6 mittels Dextromethorphan* PhD thesis (Rheinische Friedrich-Wilhelms-Universität Bonn, 2009).
13. Gazzaz, M. *et al.* Drinking Ethanol Has Few Acute Effects on CYP2C9, CYP2C19, NAT2, and P-Glycoprotein Activities but Somewhat Inhibits CYP1A2, CYP2D6, and Intestinal CYP3A: So What? *Clinical Pharmacology & Therapeutics* **104,** 1249–1259 (Dec. 2018).
14. Gorski, J. C. *et al.* The effect of echinacea (Echinacea purpurea root) on cytochrome P450 activity in vivo. *Clinical pharmacology and therapeutics* **75,** 89–100 (Jan. 2004).
15. Guest, E. J., Aarons, L., Houston, J. B., Rostami-Hodjegan, A. & Galetin, A. Critique of the two-fold measure of prediction success for ratios: application for the assessment of drug-drug interactions. *Drug metabolism and disposition: the biological fate of chemicals* **39,** 170–3 (Feb. 2011).

16. *Human Metabolome Database: Showing metabocard for Dextrorphan (HMDB0060552)*
17. *Human Metabolome Database: Showing metabocard for Dextrorphan O-glucuronide (HMDB0010341)*
18. Kakuda, T. N. *et al.* The effect of single- and multiple-dose etravirine on a drug cocktail of representative cytochrome P450 probes and digoxin in healthy subjects. *Journal of clinical pharmacology* **54,** 422–31 (Apr. 2014).
19. Kawai, R. *et al.* Physiologically based pharmacokinetic study on a cyclosporin derivative, SDZ IMM 125. *Journal of pharmacokinetics and biopharmaceutics* **22,** 327–65 (Oct. 1994).
20. Kazmi, F. *et al.* Lysosomal sequestration (trapping) of lipophilic amine (cationic amphiphilic) drugs in immortalized human hepatocytes (Fa2N-4 cells). *Drug Metabolism and Disposition* **41,** 897–905 (2013).
21. Khalilieh, S. *et al.* Effect of tildrakizumab (MK-3222), a high affinity, selective anti-IL23p19 monoclonal antibody, on cytochrome P450 metabolism in subjects with moderate to severe psoriasis. *British journal of clinical pharmacology* **84,** 2292–2302 (2018).
22. Kim, S. *et al.* PubChem 2019 update: Improved access to chemical data. *Nucleic Acids Research* **47,** D1102–D1109 (2019).
23. Langenbucher, F. Linearization of dissolution rate curves by the Weibull distribution. *The Journal of pharmacy and pharmacology* **24,** 979–81 (Dec. 1972).
24. LLC, A. B. I. *US9370513B2 - Compositions and methods for increasing the metabolic lifetime of dextromethorphan and related pharmacodynamic effects* 2016.
25. Lutz, J. D. & Isoherranen, N. Prediction of relative in vivo metabolite exposure from in vitro data using two model drugs: Dextromethorphan and omeprazole. *Drug Metabolism and Disposition* **40,** 159–168 (2012).
26. Nakashima, D. *et al.* Effect of cinacalcet hydrochloride, a new calcimimetic agent, on the pharmacokinetics of dextromethorphan: in vitro and clinical studies. *Journal of clinical pharmacology* **47,** 1311–9 (Oct. 2007).
27. National Center for Health Statistics Hyattsville MD 20782. *Third National Health and Nutrition Examination Survey, (NHANES III)* tech. rep. (1997).
28. Nyunt, M. M. *et al.* Pharmacokinetic effect of AMD070, an Oral CXCR4 antagonist, on CYP3A4 and CYP2D6 substrates midazolam and dextromethorphan in healthy volunteers. *Journal of acquired immune deficiency syndromes (1999)* **47,** 559–65 (Apr. 2008).
29. Open Systems Pharmacology Suite Community. PK-Sim® Ontogeny Database Documentation, Version 7.3 (2018).
30. Qiu, F. *et al.* Effects of the Chinese herbal formula "Zuojin Pill" on the pharmacokinetics of dextromethorphan in healthy Chinese volunteers with CYP2D6*10 genotype. *European Journal of Clinical Pharmacology* **72,** 689–695 (June 2016).
31. Sager, J. E. *et al.* Fluoxetine- and norfluoxetine-mediated complex drug-drug interactions: in vitro to in vivo correlation of effects on CYP2D6, CYP2C19, and CYP3A4. *Clinical pharmacology and therapeutics* **95,** 653–62. arXiv: NIHMS150003 (June 2014).
32. Schadel, M., Wu, D., Otton, S. V., Kalow, W. & Sellers, E. M. Pharmacokinetics of dextromethorphan and metabolites in humans: influence of the CYP2D6 phenotype and quinidine inhibition. *Journal of clinical psychopharmacology* **15,** 263–9 (Aug. 1995).
33. Schmitt, W. General approach for the calculation of tissue to plasma partition coefficients. *Toxicology in vitro : an international journal published in association with BIBRA* **22,** 457–67 (Mar. 2008).

34. Spaggiari, D. *et al.* Comparison of liquid chromatography and supercritical fluid chromatography coupled to compact single quadrupole mass spectrometer for targeted in vitro metabolism assay. *Journal of Chromatography A* **1371,** 244–256 (2014).

35. Stage, T. B. *et al.* Dicloxacillin induces CYP2C19, CYP2C9 and CYP3A4 in vivo and in vitro. *British journal of clinical pharmacology* **84,** 510–519 (Mar. 2018).

36. Storelli, F., Desmeules, J. & Daali, Y. Physiologically-Based Pharmacokinetic Modeling for the Prediction of CYP2D6-Mediated Gene–Drug–Drug Interactions. *CPT: Pharmacometrics & Systems Pharmacology,* psp4.12411 (2019).

37. Storelli, F. *et al.* Impact of CYP2D6 Functional Allelic Variations on Phenoconversion and Drug-Drug Interactions. *Clinical pharmacology and therapeutics* **104,** 148–157 (2018).

38. Tanaka, G. & Kawamura, H. Anatomical and physiological characteristics for Asian reference man: male and female of different ages: Tanaka model. Division of Radioecology, National Institute of Radiological Sciences. Hitachinaka 311-12 Japan. NIRS-M-115 (1996).

39. Tennezé, L. *et al.* Assessment of CYP2D6 and CYP2C19 activity in vivo in humans: a cocktail study with dextromethorphan and chloroguanide alone and in combination. *Clinical pharmacology and therapeutics* **66,** 582–8 (Dec. 1999).

40. Thelen, K. *et al.* Evolution of a detailed physiological model to simulate the gastrointestinal transit and absorption process in humans, Part 1: Oral solutions. *Journal of Pharmaceutical Sciences* **100,** 5324–5345 (Dec. 2011).

41. Valentin, J. Basic anatomical and physiological data for use in radiological protection: reference values. A report of age- and gender-related differences in the anatomical and physiological characteristics of reference individuals. ICRP Publication 89. *Annals of the ICRP* **32,** 5–265 (2002).

42. Watanabe, R. *et al.* Predicting Fraction Unbound in Human Plasma from Chemical Structure: Improved Accuracy in the Low Value Ranges. *Molecular Pharmaceutics* **15,** 5302–5311 (2018).

43. Wishart, D. S. *et al.* HMDB 4.0: the human metabolome database for 2018. *Nucleic Acids Research* **46,** D608–D617 (Jan. 2018).

44. Yamazaki, T. *et al.* Pharmacokinetic Effects of Isavuconazole Coadministration With the Cytochrome P450 Enzyme Substrates Bupropion, Repaglinide, Caffeine, Dextromethorphan, and Methadone in Healthy Subjects. *Clinical Pharmacology in Drug Development* **6,** 54–65 (2017).

45. Zawertailo, L. A., Tyndale, R. F., Busto, U. & Sellers, E. M. Effect of metabolic blockade on the psychoactive effects of dextromethorphan. *Human psychopharmacology* **25,** 71–9 (Jan. 2010).

B.3 PROJECT III: SUPPLEMENTARY MATERIALS

pharmaceutics

MDPI

Supplementary Materials

Physiologically Based Pharmacokinetic Modeling to Describe the CYP2D6 Activity Score-Dependent Metabolism of Paroxetine, Atomoxetine and Risperidone

Simeon Rüdesheim[1,2], Dominik Selzer[1], Thomas Mürdter[2], Svetlana Igel[2], Reinhold Kerb[2], Matthias Schwab[2,3,4] and Thorsten Lehr[1,*]

[1] Department of Clinical Pharmacy, Saarland University, 66123 Saarbrücken, Germany

[2] Dr. Margarete Fischer-Bosch-Institute of Clinical Pharmacology, 70376 Stuttgart, Germany

[3] Departments of Clinical Pharmacology, Pharmacy and Biochemistry, University Tübingen, 72076 Tübingen, Germany

[4] Cluster of Excellence iFIT (EXC2180) "Image-Guided and Functionally Instructed Tumor Therapies", University of Tübingen, 72076 Tübingen, Germany

[*] Correspondence: thorsten.lehr@mx.uni-saarland.de; Tel.: +49-681-302-70255

Received: 11 July 2022; Accepted: 17 August; Published: 18 August 2022

Corresponding Author Prof. Dr. Thorsten Lehr
Clinical Pharmacy, Saarland University
Campus C5 3, 66123 Saarbrücken
Phone: +49 681 302 70255
Email: thorsten.lehr@mx.uni-saarland.de
ORCID: 0000 0002 8372 1465

Pharmaceutics **2022**, *14*, 1734. https://doi.org/10.3390/pharmaceutics14081734

Contents

Pharmaceutics **2022**, *14*, 1734. https://doi.org/10.3390/pharmaceutics14081734

S1 Methods (Addendum)

S1.1 Virtual Individuals

The PBPK model was built based on data from healthy individuals, using the reported sex, ethnicity and mean values for age, weight and height from each study protocol. If no demographic information was provided, the following default values were substituted: male, European, 30 years of age, 73 kg body weight and 176 cm body height (characteristics from the PK-Sim® population database [34, 48, 50]. CYP2D6 was implemented in accordance with literature, using the PK-Sim® expression database to define their relative expression in the different organs of the body [37]. Details on the implementation of CYP2D6 are summarized in Section S1.3.

S1.2 Virtual Populations

For population simulations, virtual populations of 1000 individuals were created based on the population characteristics stated in the respective publication. If no information was provided in the publication, populations based on European male individuals aged 20–50 years were assumed. Metrics were generated (depending on ethnicity) from one of the following databases; American: NHANES [34] database, Asian: Tanaka model [48], European: ICRP database [50]. In the generated virtual populations, system-dependent parameters such as weight, height, organ volumes, blood flow rates, tissue compositions, etc. were varied by the implemented algorithm in PK-Sim® within the limits of the databases listed above [34, 48, 50]. Since study populations were grouped by their AS or phenotype, no variability in CYP2D6 reference concentrations was assumed for population simulations. Reference concentrations of implemented proteins as well as the relative expression are provided in Section S1.3.

Pharmaceutics **2022**, *14*, 1734. https://doi.org/10.3390/pharmaceutics14081734

S1.3 System-Dependent Parameters

Table S1.3.1: System-dependent parameters

	Reference concentration			Localization	Half-life	
	Mean[†]	GSD[*]	Relative expression[a]		Liver [h]	Intestine [h]
Enzymes						
CYP2C19	0.76 [41]	1.79 [37]	RT-PCR [37]	Intracellular	26 [37]	23 [37]
CYP2D6	0.40 [41]	0[b]	RT-PCR [37]	Intracellular	51 [37]	23 [37]
CYP3A4	4.32 [41]	1.18 [37]	RT-PCR [37]	Intracellular	36 [42]	23 [13]
Transporters						
P-gp	1.41[15]	1.60 [38]	RT-PCR [35]	Apical (Efflux)	36 [37]	23 [37]

[†]: µmol protein/l in the tissue of highest expression, [*]: Geometric standard deviation of the reference concentration, [a]: In the different organs (PK-Sim expression database profile), [b]: Variability for Cytochrome P450 2D6 (CYP2D6) was set to 0, as study populations were stratified by CYP2D6 activity,

S1.4 PBPK Model Sensitivity Analysis

Sensitivity of the final models to single parameter changes (local sensitivity analysis) was calculated as relative change of the $AUC_{0\text{–}24\ h}$. Sensitivity analysis was carried out using a relative perturbation of 1000% (variation range 10.0, maximum number of 9 steps). Parameters were included into the analysis if they have been optimized, if they are associated with optimized parameters or if they might have a strong impact due to calculation methods used in the model. Sensitivity to a parameter was calculated as the ratio of the relative change of the simulated area under the plasma concentration-time curve (AUC) from the time of the drug administration extrapolated to infinity ($AUC_{0\text{–inf}}$) to the relative variation of the parameter according to Eq. S1:

$$S = \frac{\Delta AUC_{0--inf}}{\Delta p} \times \frac{p}{AUC_{0--inf}} \tag{S1}$$

where S = sensitivity of the $AUC_{0-24\ h}$ to the examined model parameter, ΔAUC_{0--inf} = change of the $AUC_{0\text{–inf}}$, $AUC_{0-24\ h}$ = simulated $AUC_{0\text{–inf}}$ with the original parameter value, Δp = change of the examined parameter value, p = original parameter value.

A sensitivity of +0.5 signifies that a 100% increase of the examined parameter value causes a 50% increase of the simulated $AUC_{0\text{–}24\ h}$.

Pharmaceutics **2022**, *14*, 1734. https://doi.org/10.3390/pharmaceutics14081734

S2 Paroxetine

S2.1 Paroxetine PBPK Base Model Building

S2.1.1 Paroxetine Drug-Dependent Parameters

Table S2.1.1: Drug-dependent parameters for the final paroxetine PBPK model

Parameter	Unit	Value	Source	Literature	Reference
MW	g/mol	329.37	Literature	329.37	[57]
pKa (base)	-	9.90	Literature	9.90	[1]
Solubility (pH 4.5)	mg/mL	7.31	Literature	7.31	[20]
logP	-	3.95	Literature	3.95	[1]
f_u	%	5.00	Literature	5.00	[19]
CYP3A4 K_M	µmol/L	4.70	Literature	$4.70^{\dagger}$	[17]
CYP3A4 k_{cat}	1/min	1.01	Optimized	5.32	[17]
CYP2D6 K_M	µmol/L	0.03	Literature	$0.03^{\dagger}$	[17]
CYP2D6 k_{cat} ^{EM}	1/min	1.37	Optimized	9.70	[17]
CYP2D6 k_{cat} ^{PM}	1/min	0.00	Assumed	-	[17]
Unspecific CL_{hep}	1/min	1.37	Optimized	-	[17]
CYP2D6 K_i	µmol/L	0.17	Optimized	0.32	[52]
CYP2D6 k_{inact}	1/min	0.17	Literature	0.17	[52]
CYP3A4 K_i	µmol/L	4.48	Literature	$4.48^{\dagger}$	[5]
CYP3A4 k_{inact}	1/min	0.01	Literature	0.01	[5]
GFR fraction	-	1.00	Assumed	-	-
CR Weibull shape	-	7.17	Optimized	-	-
CR Weibull time	min	276.35	Optimized	-	[9, 21]
Partition coefficients	-	Diverse	Calculated	R&R	[40]
Cellular permeabilities	cm/min	0.28	Calculated	PK-Sim	[18]
Specific intestinal perm.	cm/min	3.93E-05	Calculated	4.89E-04	[18]

-: not given, †: in vitro values corrected for binding in the assay fu_{mic} calculated according to [2].

Pharmaceutics **2022**, *14*, 1734. https://doi.org/10.3390/pharmaceutics14081734

S2.1.2 Paroxetine Clinical Studies

Table S2.1.2: Paroxetine study table

Route	Dose [mg]	n	Females [%]	Age [years]	Weight [kg]	CYP2D6 activity	Dataset	References
PBPK base model building and evaluation								
iv (inf, sd)	28	1	0	28	75	-	training	Lund 1982 [25]
iv (inf, sd)	28	1	0	24	66	-	training	Lund 1982 [25]
iv (inf, sd)	28	1	0	26	88	-	training	Lund 1982 [25]
iv (inf, sd)	23	1	0	29	72	-	training	Lund 1982 [25]
po (tab, qd)	20	22	23	38 (20-49)	-	g-EM	training	Belle 2002 [3]
po (-, qd)	20	25	64	26	64	-	test	Calvo 2004 [8]
po (po, sd)	45	1	0	28	75	-	training	Lund 1982 [25]
po (po, sd)	45	1	0	24	66	-	training	Lund 1982 [25]
po (po, sd)	45	1	0	26	88	-	training	Lund 1982 [25]
po (po, sd)	45	1	0	29	72	-	training	Lund 1982 [25]
po (tab, sd)	20	28	0	28 (18-42)	72 (57-87)	-	training	Massaroti 2005 [29]
po (-, sd)	70	5	0	31 (22-44)	-	-	test	McClelland 1984 [30]
po (-, qd)	20	14	14	34 (19-55)	75	-	test	Schoedel 2012 [44]
po (tab, qd)	20	7	0	23	65	p-EM	test	Segura 2005 [45]
po (tab, qd)	20	26	69	44 (18-64)	69 (51-89)	g-EM	test	van der Lee 2007 [51]
po (-, sd)	20	12	25	25 (20-35)	58 (46-75)	AS = 1.25*	test	Yasui-Furukori 2006 [54]
po (-, sd)	20	13	23	24 (21-35)	57 (45-67)	-	test	Yasui-Furukori 2007 [53]
DGI model building and evaluation								
po (CR, sd)	25	4	25	26 (19–45)	64	AS = 0.5*	test	Chen 2015 [9]
po (CR, sd)	25	11	45	26 (19–45)	61	AS = 1.0*	test	Chen 2015 [9]
po (CR, sd)	25	5	60	22 (19–45)	58	AS = 1.5*	test	Chen 2015 [9]
po (CR, sd)	25	4	25	28 (19–45)	61	AS = 2*	test	Chen 2015 [9]
po (tab, sd)	40	3	100	25 (22–26)	62 (50–70)	AS = 0*	test	Mürdter 2016 [12, 16, 31]
po (tab, sd)	40	4	100	24 (21–20)	59 (56–64)	AS = 0.5*	test	Mürdter 2016 [12, 16, 31]
po (tab, sd)	40	1	100	25	68	AS = 0.75*	test	Mürdter 2016 [12, 16, 31]
po (tab, sd)	40	2	100	26 (23–28)	67 (64–74)	AS = 1*	test	Mürdter 2016 [12, 16, 31]
po (tab, sd)	40	3	100	32 (26–43)	57 (48–64)	AS = 2*	training	Mürdter 2016 [12, 16, 31]
po (tab, sd)	40	3	100	26 (22–28)	62 (54–73)	AS = 3*	test	Mürdter 2016 [12, 16, 31]
po (tab, qd)	30	8	0	27 (23–39)	82 (68–95)	p-PM	training	Sindrup 1992 [46]
po (tab, qd)	30	9	0	24 (20–30)	73 (65–81)	p-EM	training	Sindrup 1992 [46]
po (tab, sd)	40	1	100	21	58	AS = 0*	test	Yoon 2000 [55]
po (tab, sd)	40	3	0	22	68	AS = 0.5*	test	Yoon 2000 [55]
po (tab, sd)	40	6	0	22	67	AS = 1.25*	test	Yoon 2000 [55]
po (tab, sd)	40	6	17	23	59	AS = 2*	training	Yoon 2000 [55]

-: not given, *: full genotype provided in publication.

Pharmaceutics **2022**, *14*, 1734. https://doi.org/10.3390/pharmaceutics14081734

S2.2 Paroxetine PBPK Base Model Evaluation

S2.2.1 Plasma Concentration-Time Profiles

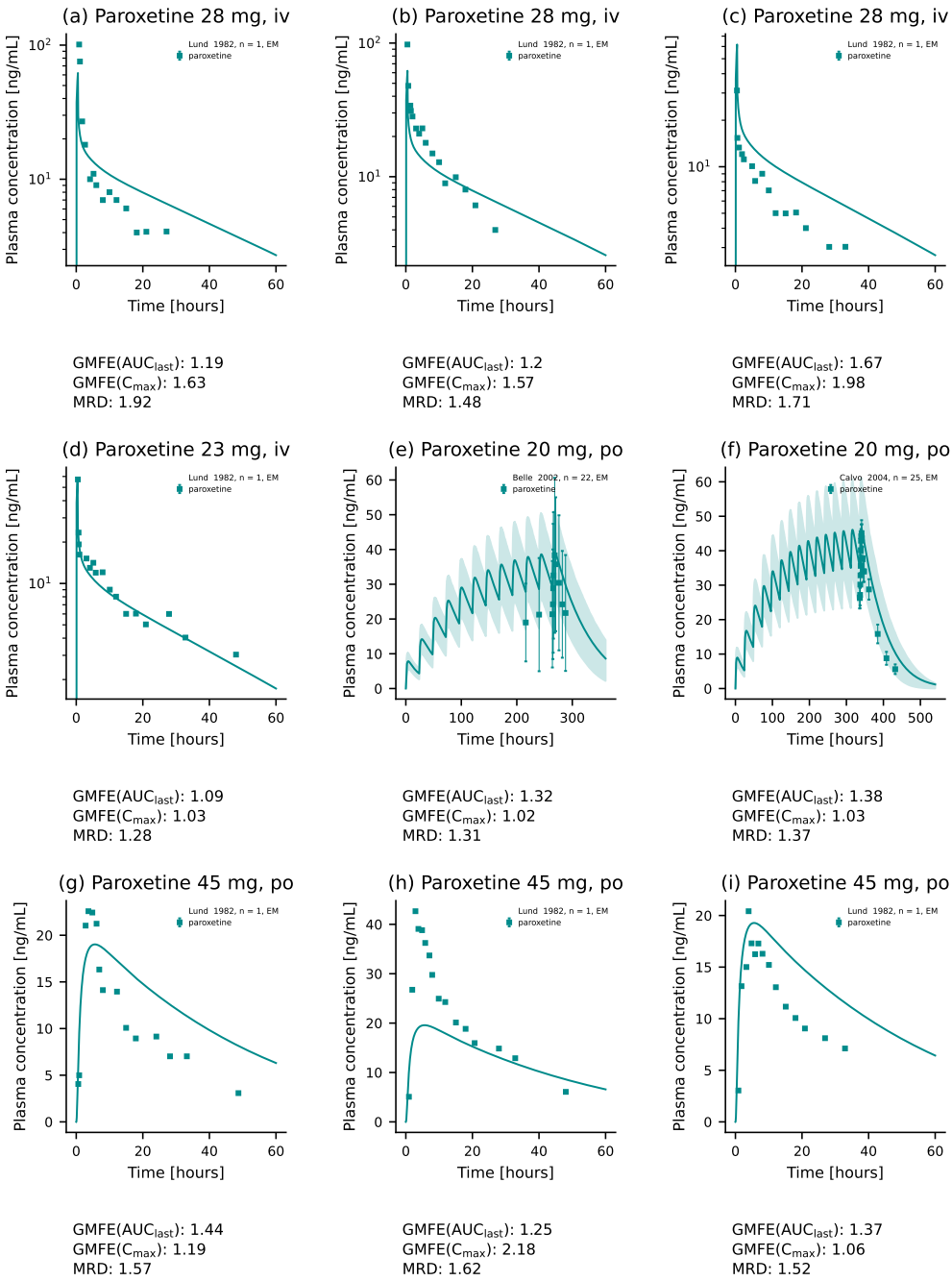

Figure S2.2.1: Paroxetine plasma concentration-time profiles. Population predictions (n=1000) are shown as lines with ribbons (arithmetic mean ± SD). Individual predictions (n=1) are shown as lines. Symbols represent the corresponding observed data ± SD if provided.

Pharmaceutics **2022**, *14*, 1734. https://doi.org/10.3390/pharmaceutics14081734

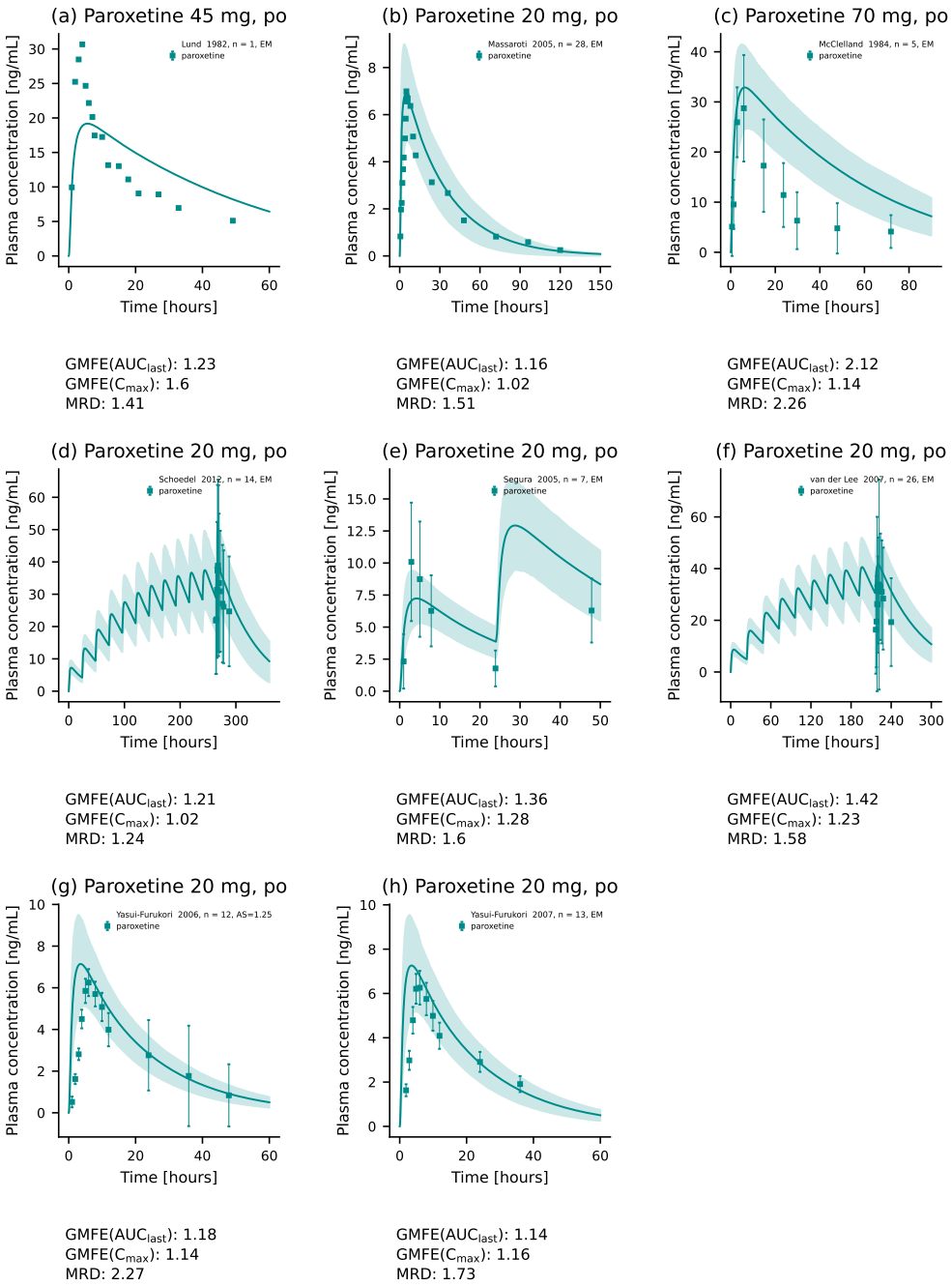

Figure S2.2.2: Paroxetine plasma concentration-time profiles. Population predictions (n=1000) are shown as lines with ribbons (arithmetic mean ± SD). Individual predictions (n=1) are shown as lines. Symbols represent the corresponding observed data ± SD if provided.

Pharmaceutics **2022**, *14*, 1734. https://doi.org/10.3390/pharmaceutics14081734

S2.2.2 Goodness-of-Fit Plots

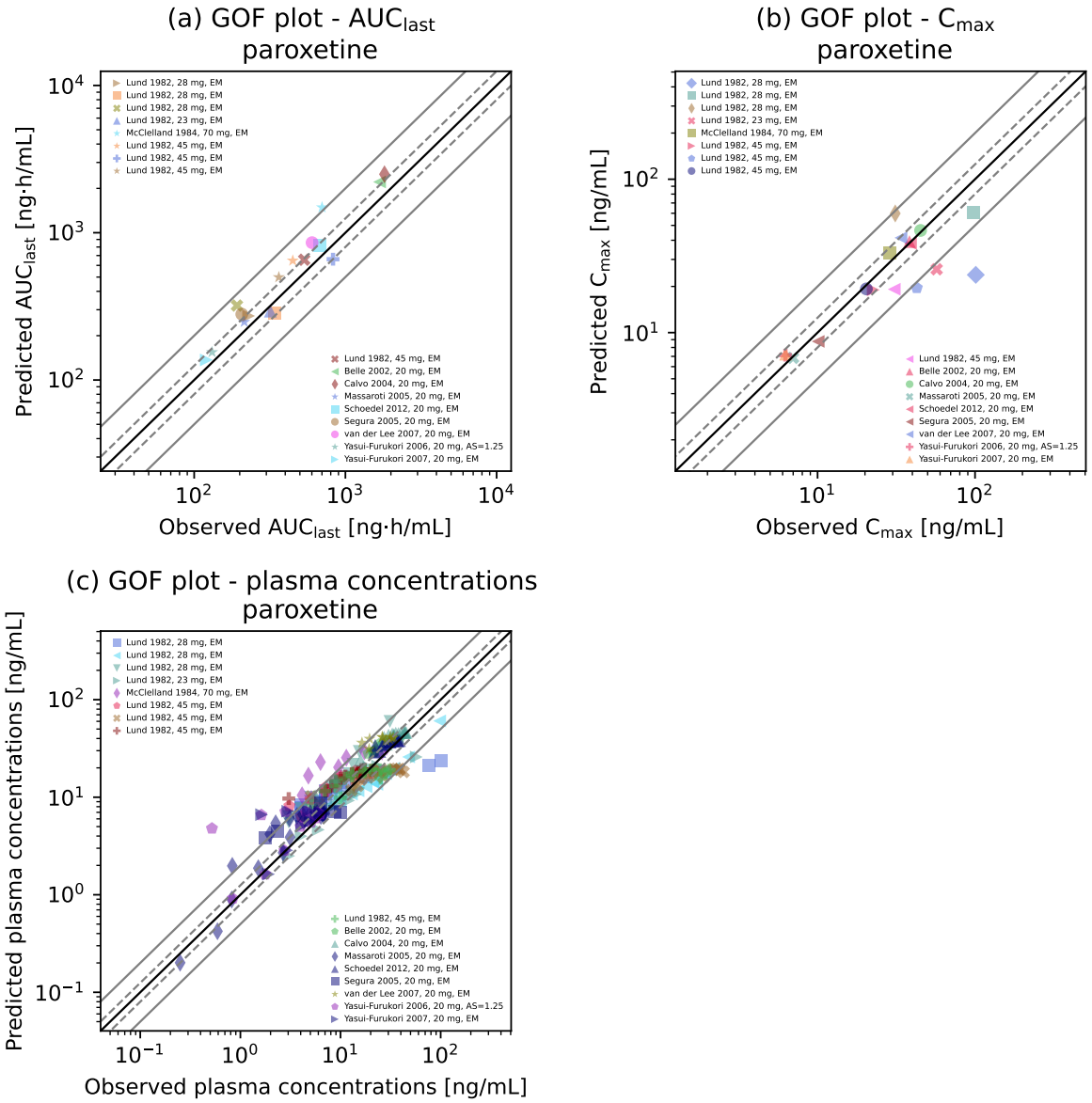

Figure S2.2.3: Goodness of fit plots. Predicted versus observed (a) AUC_{last}, (b) C_{max} and (c) plasma concentration values for all studies. The solid black line marks the line of identity, the dashed grey lines mark the 0.8- to 1.25-fold range, the solid grey lines indicate the 0.5- to 2-fold range. Colored symbols represent the study population given in the legend.

Pharmaceutics **2022**, *14*, 1734. https://doi.org/10.3390/pharmaceutics14081734

S2.2.3 Sensitivity Analysis

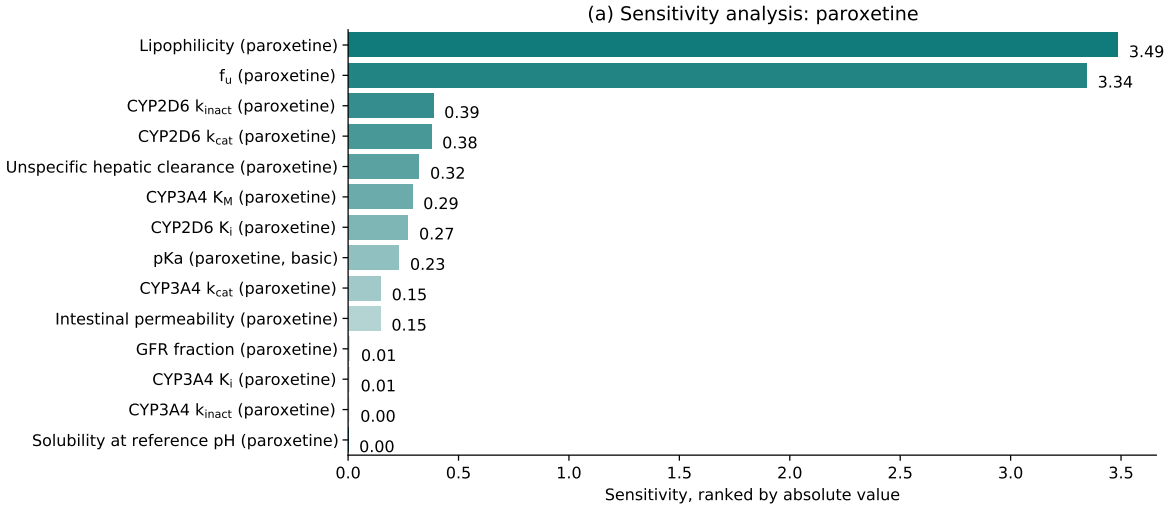

Figure S2.2.4: Sensitivity analysis of the paroxetine model. Sensitivity of the model to single parameters, determined as change of the simulated AUC from time of the administration extrapolated to infinity of a single oral administration of 20 mg paroxetine hydrochloride.

Pharmaceutics **2022**, *14*, 1734. https://doi.org/10.3390/pharmaceutics14081734

S2.3 Paroxetine DGI Model Evaluation

S2.3.1 Plasma Concentration-Time Profiles

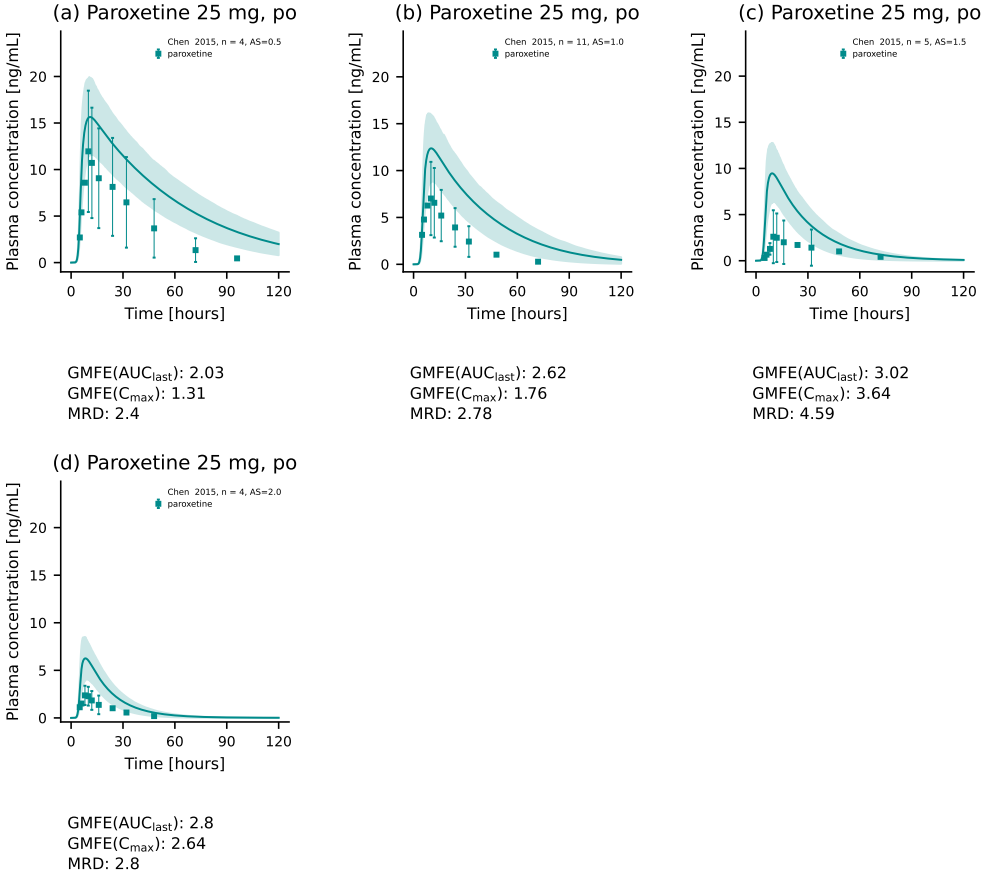

Figure S2.3.5: Paroxetine plasma concentration-time profiles [9]. Population predictions (n=1000) are shown as lines with ribbons (arithmetic mean ± SD). Symbols represent the corresponding observed data ± SD if provided.

Pharmaceutics **2022**, *14*, 1734. https://doi.org/10.3390/pharmaceutics14081734

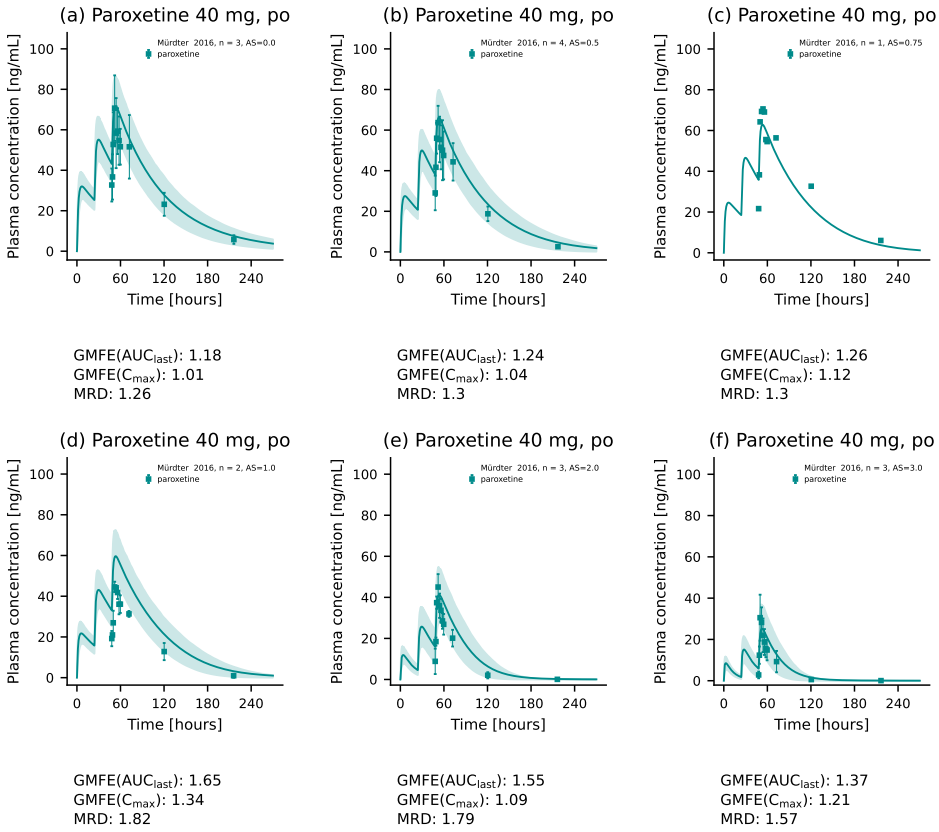

Figure S2.3.6: Paroxetine plasma concentration-time profiles [12]. Population predictions (n=1000) are shown as lines with ribbons (arithmetic mean ± SD). Individual predictions (n=1) are shown as lines. Symbols represent the corresponding observed data ± SD if provided.

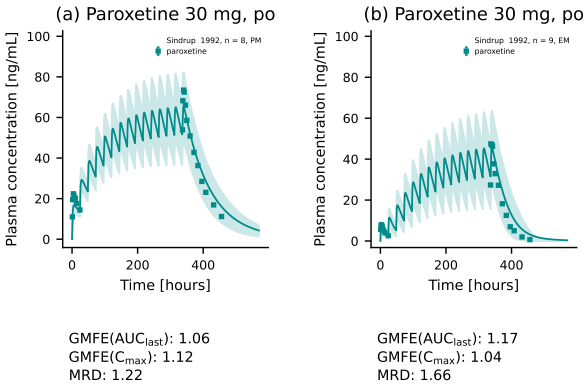

Figure S2.3.7: Paroxetine plasma concentration-time profiles [46]. Population predictions (n=1000) are shown as lines with ribbons (arithmetic mean ± SD). Symbols represent the corresponding observed data ± SD if provided.

Pharmaceutics **2022**, *14*, 1734. https://doi.org/10.3390/pharmaceutics14081734

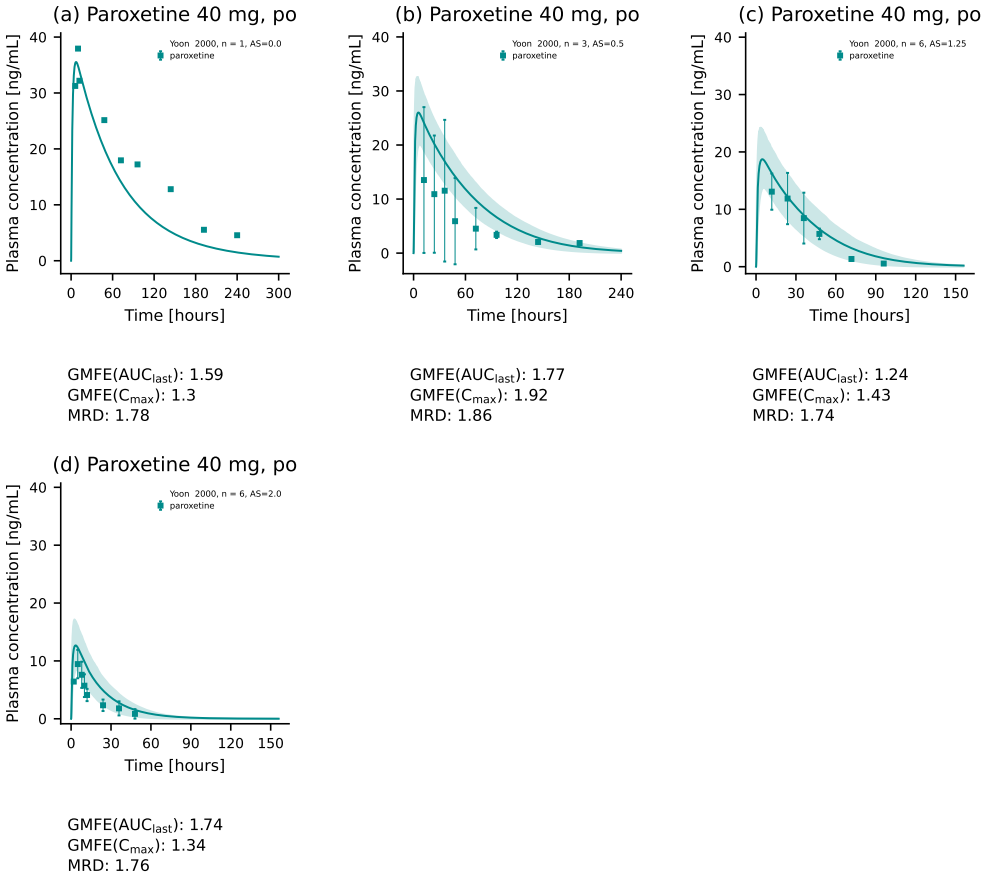

Figure S2.3.8: Paroxetine plasma concentration-time profiles [55]. Population predictions (n=1000) are shown as lines with ribbons (arithmetic mean ± SD). Individual predictions (n=1) are shown as lines. Symbols represent the corresponding observed data ± SD if provided.

Pharmaceutics **2022**, *14*, 1734. https://doi.org/10.3390/pharmaceutics14081734

S2.3.2 Goodness-of-Fit Plots

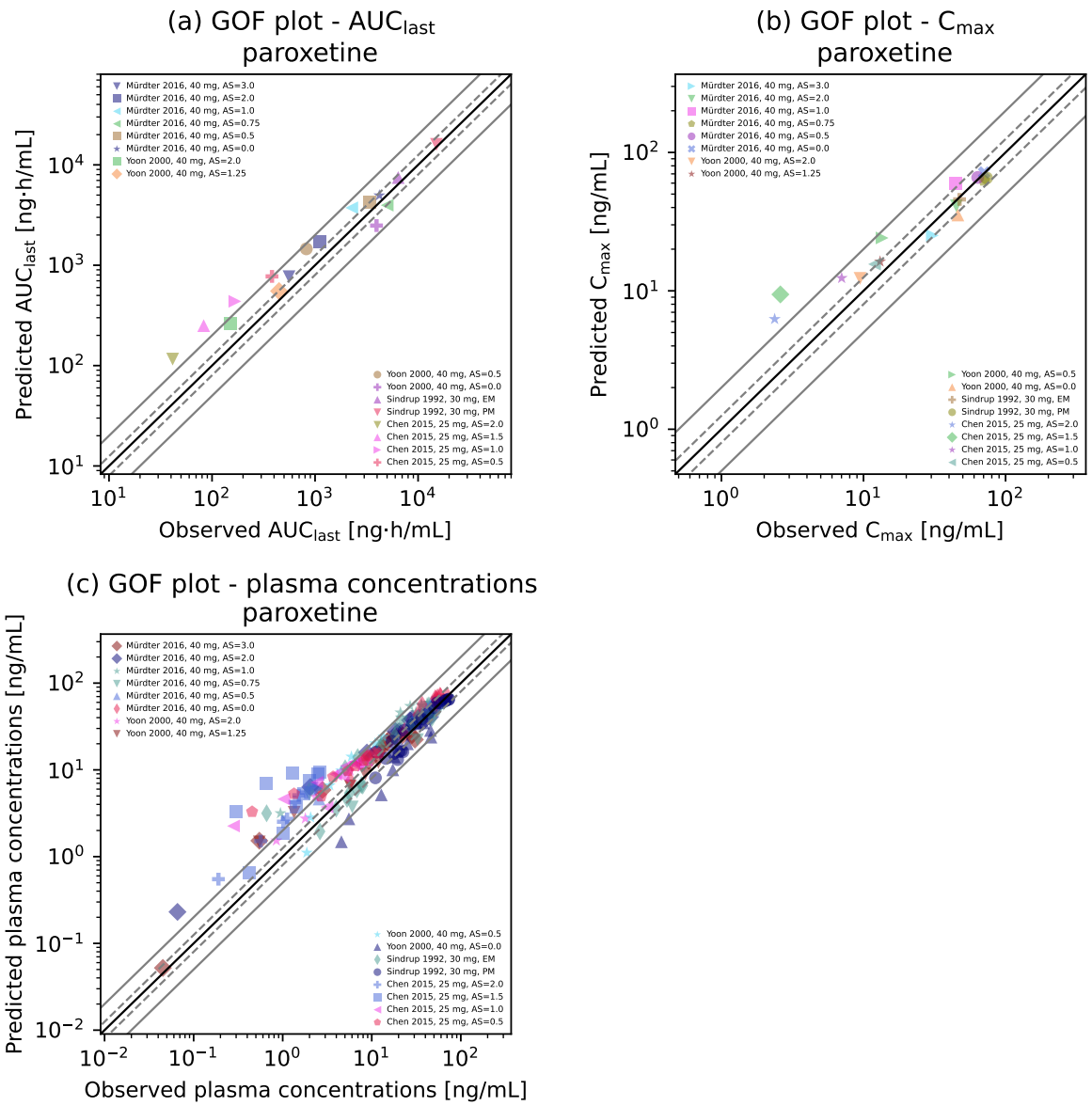

Figure S2.3.9: Goodness of fit plots. Predicted versus observed (a) AUC_{last}, (b) C_{max} and (c) plasma concentration values for all DGI studies. The solid black line marks the line of identity, the dashed grey lines mark the 0.8- to 1.25-fold range, the solid grey lines indicate the 0.5- to 2-fold range. Colored symbols represent the study population given in the legend.

Pharmaceutics **2022**, *14*, 1734. https://doi.org/10.3390/pharmaceutics14081734

S2.3.3 DGI Ratios

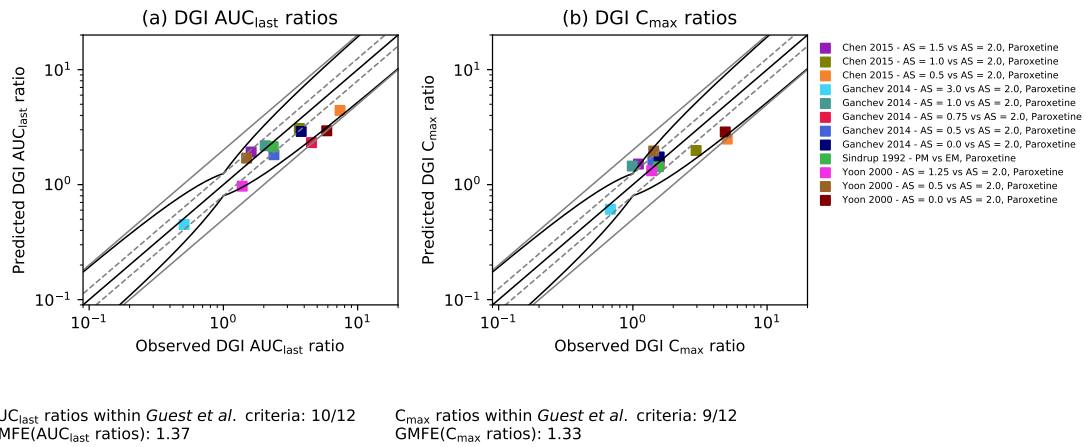

Figure S2.3.10: DGI ratio plot. Predicted versus observed (a) DGI AUC_{last} and (b) C_{max} ratios for all DGI studies. The solid straight black line marks the line of identity, the solid curved black line shows the prediction success limits proposed by *Guest et al.* [14], the dashed grey lines mark the 0.8- to 1.25-fold range, the solid grey lines indicate the 0.5- to 2-fold range. Colored symbols represent the study population given in the legend.

Pharmaceutics **2022**, *14*, 1734. https://doi.org/10.3390/pharmaceutics14081734

S3 Atomoxetine

S3.1 Atomoxetine PBPK Base Model Building

S3.1.1 Drug-dependent Parameters

Table S3.1.1: Drug-dependent parameters for the final atomoxetine PBPK model

Parameter	Unit	Value	Source	Literature	Reference
MW	g/mol	255.35	Literature	255.35	[57]
pKa (base)	-	9.80	Literature	9.80	[47]
Solubility (pH 7.4)	mg/mL	10.29	Literature	10.29	[47]
logP	-	3.49	Optimized	3.81	[47]
f_u	%	1.30	Literature	1.30	[56]
CYP2C19 K_M	µmol/L	83.00	Literature	83.00	[39]
CYP2C19 k_{cat}	1/min	165.23	Optimized	5.11	[39]
CYP2D6 K_M	µmol/L	2.30	Literature	2.30	[39]
CYP2D6 k_{cat} ^{EM}	1/min	37.44	Optimized	11.50	[39]
CYP2D6 k_{cat} ^{PM}	1/min	0.00	Assumed	-	[39]
GFR fraction	-	1.00	Assumed	-	-
EHC continuous fraction	-	1.00	Assumed	-	-
Partition coefficients	-	Diverse	Calculated	Be	[4]
Cellular permeabilities	-	0.32	Calculated	PK-Sim	[18]
Specific intestinal perm.	cm/min	5.23E-5	Optimized	7.23E-04	[18]

-: not given, perm.: permeability.

Pharmaceutics **2022**, *14*, 1734. https://doi.org/10.3390/pharmaceutics14081734

S3.1.2 Clinical studies

Table S3.1.2: Atomoxetine study table

Route	Dose [mg]	n	Females [%]	Age [years]	Weight [kg]	CYP2D6 activity	Dataset	References
PBPK base model building and evaluation								
po (tab, qd)	20	22	23	38 (20-49)	-	g-EM	test	Belle 2002 [3]
po (cap, sd)	40	16	33	(20-29)	(53-72)	AS = 1*	test	Cui 2007 [10]
po (cap, qd)	80	16	33	(20-29)	(53-72)	AS = 1*	test	Cui 2007 [10]
po (sol, sd)	50	42	0	23 (20-37)	62 (52-76)	g-EM	training	Nakano 2016 [33]
po (cap, sd)	50	42	0	23 (20-37)	62 (52-76)	g-EM	training	Nakano 2016 [33]
DGI model building and evaluation								
po (cap, sd)	40	18	0	23	68	AS = 0.5*	test	Byeon 2015 [7]
po (cap, sd)	40	22	0	23	65	AS = 1.25*	test	Byeon 2015 [7]
po (cap, sd)	40	22	0	23	67	AS = 2*	training	Byeon 2015 [7]
po (cap, sd)	20	8	0	(19-25)	(52-72)	AS = 0.5*	test	Kim 2018 [23]
po (cap, sd)	20	11	0	(19-25)	(49-73)	AS = 2*	training	Kim 2018 [23]
po (cap, qd)	20	3	0	35 (19-49)	-	g-PM	training	Sauer 2003 [43]
po (cap, qd)	20	4	0	45 (38-54)	-	g-EM	training	Sauer 2003 [43]
po (cap, sd)	40	12	0	(18-55)	-	g-PM	test	Todor 2016 [49]
po (cap, sd)	40	18	0	(18-55)	-	g-EM	test	Todor 2016 [49]

-: not given, *: full genotype provided in publication.

Pharmaceutics **2022**, *14*, 1734. https://doi.org/10.3390/pharmaceutics14081734

S3.2 Atomoxetine PBPK Base Model Evaluation

S3.2.1 Plasma Concentration-Time Profiles

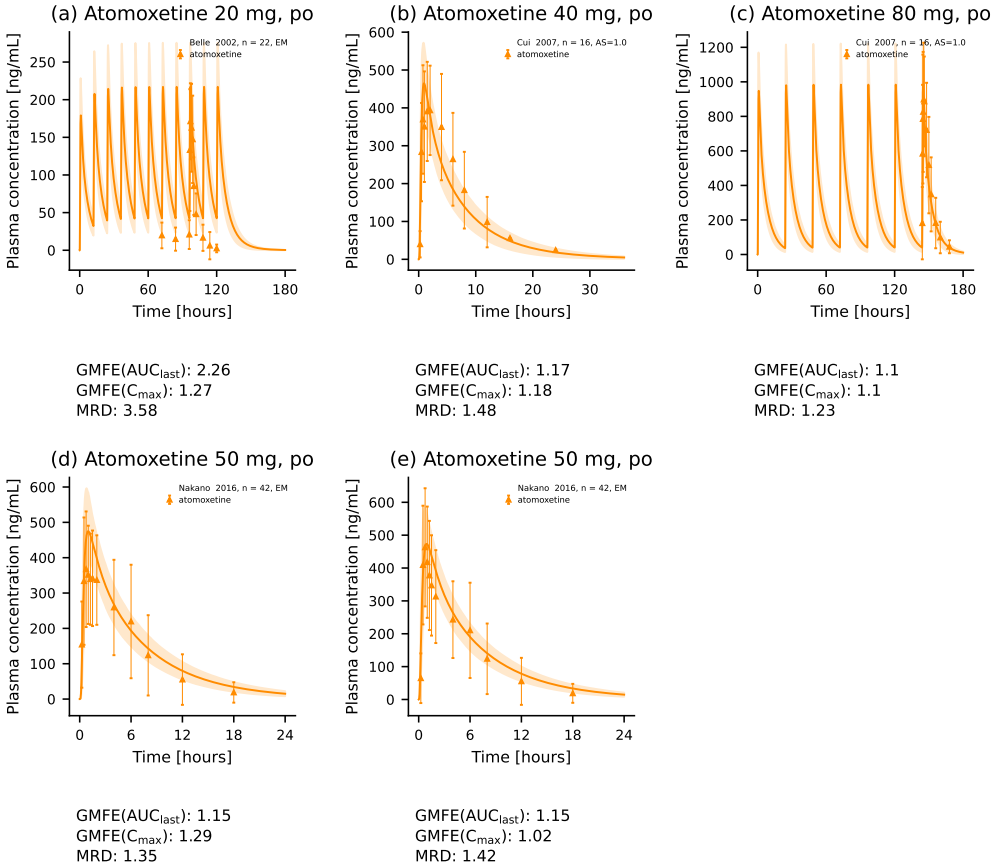

Figure S3.2.1: Atomoxetine plasma concentration-time profiles. Population predictions (n=1000) are shown as lines with ribbons (arithmetic mean ± standard deviation (SD)). Symbols represent the corresponding observed data ± SD if provided.

Pharmaceutics **2022**, *14*, 1734. https://doi.org/10.3390/pharmaceutics14081734

S3.2.2 Goodness-of-Fit Plots

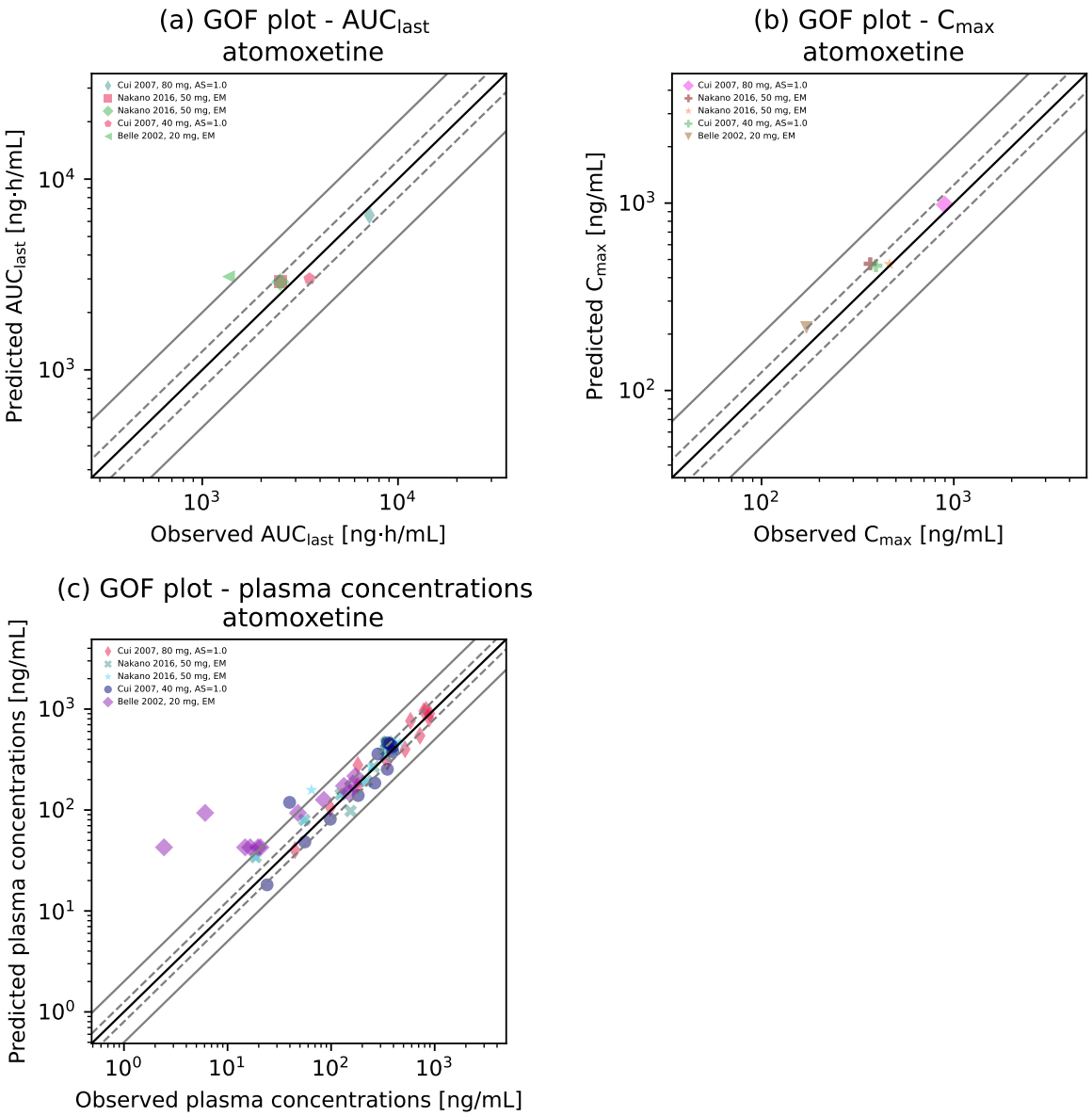

Figure S3.2.2: Goodness of fit plots. Predicted versus observed (a) AUC_{last}, (b) C_{max} and (c) plasma concentration values for all studies. The solid black line marks the line of identity, the dashed grey lines mark the 0.8- to 1.25-fold range, the solid grey lines indicate the 0.5- to 2-fold range. Colored symbols represent the study population given in the legend.

Pharmaceutics **2022**, *14*, 1734. https://doi.org/10.3390/pharmaceutics14081734

S3.2.3 Sensitivity Analysis

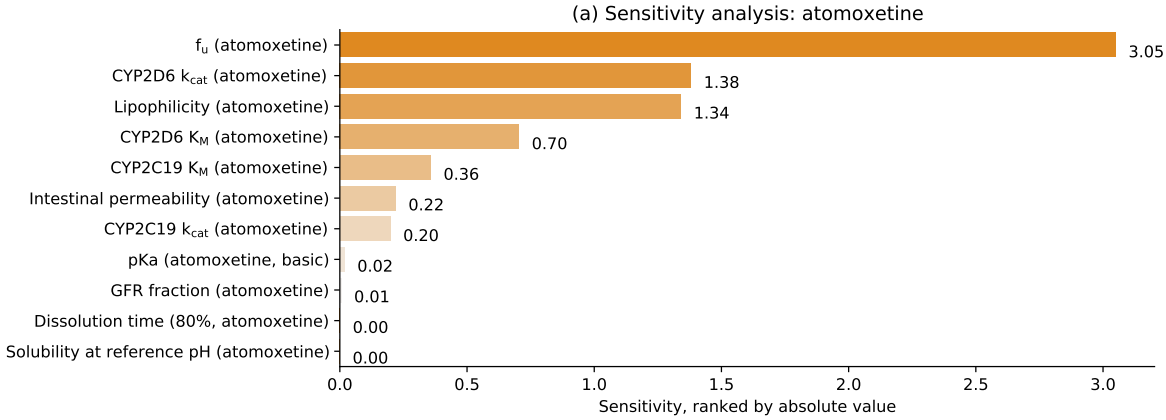

Figure S3.2.3: Sensitivity analysis of the atomoxetine model. Sensitivity of the model to single parameters, determined as change of the simulated AUC from time of the drug administration extrapolated to infinity of a single oral administration of 20 mg atomoxetine.

S3.3 Atomoxetine DGI Model Evaluation

S3.3.1 Plasma Concentration-Time Profiles

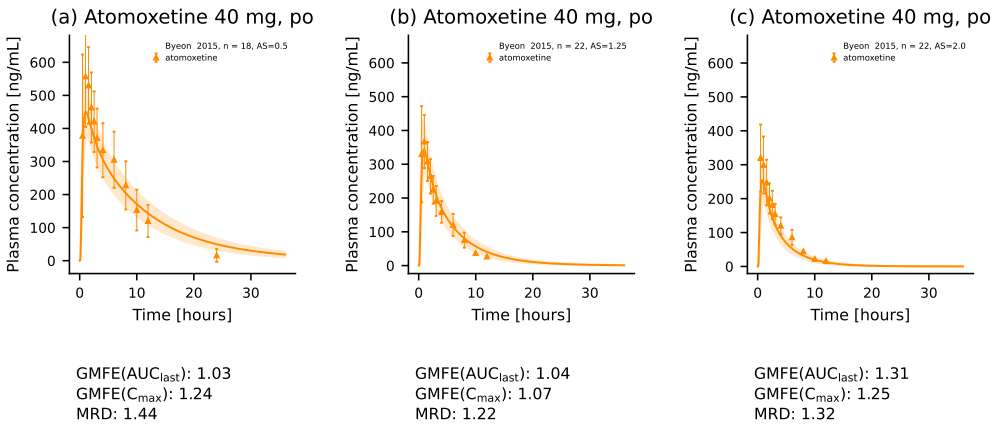

Figure S3.3.4: Atomoxetine plasma concentration-time profiles. Population predictions (n=1000) are shown as lines with ribbons (arithmetic mean ± SD). Symbols represent the corresponding observed data ± SD if provided.

Pharmaceutics **2022**, *14*, 1734. https://doi.org/10.3390/pharmaceutics14081734

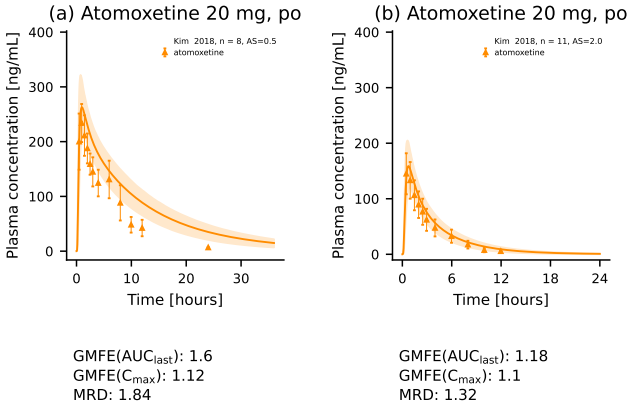

Figure S3.3.5: Atomoxetine plasma concentration-time profiles. Population predictions (n=1000) are shown as lines with ribbons (arithmetic mean ± SD). Symbols represent the corresponding observed data ± SD if provided.

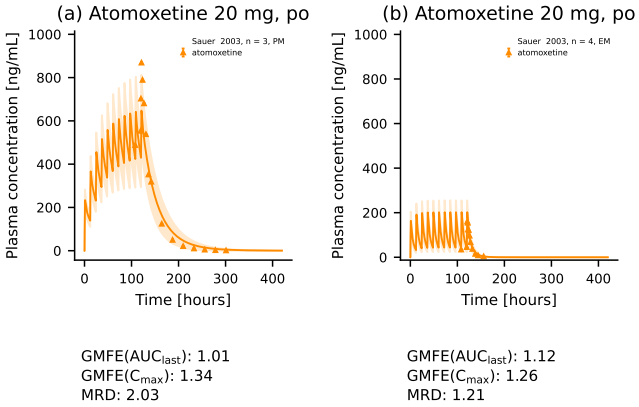

Figure S3.3.6: Atomoxetine plasma concentration-time profiles. Population predictions (n=1000) are shown as lines with ribbons (arithmetic mean ± SD). Symbols represent the corresponding observed data ± SD if provided.

Pharmaceutics ***2022***, *14*, 1734. https://doi.org/10.3390/pharmaceutics14081734

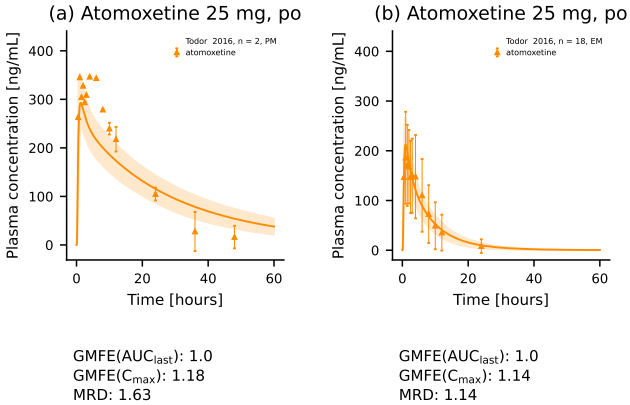

Figure S3.3.7: Atomoxetine plasma concentration-time profiles. Population predictions (n=1000) are shown as lines with ribbons (arithmetic mean ± SD). Symbols represent the corresponding observed data ± SD if provided.

Pharmaceutics **2022**, *14*, 1734. https://doi.org/10.3390/pharmaceutics14081734

S3.3.2 Goodness-of-Fit Plots

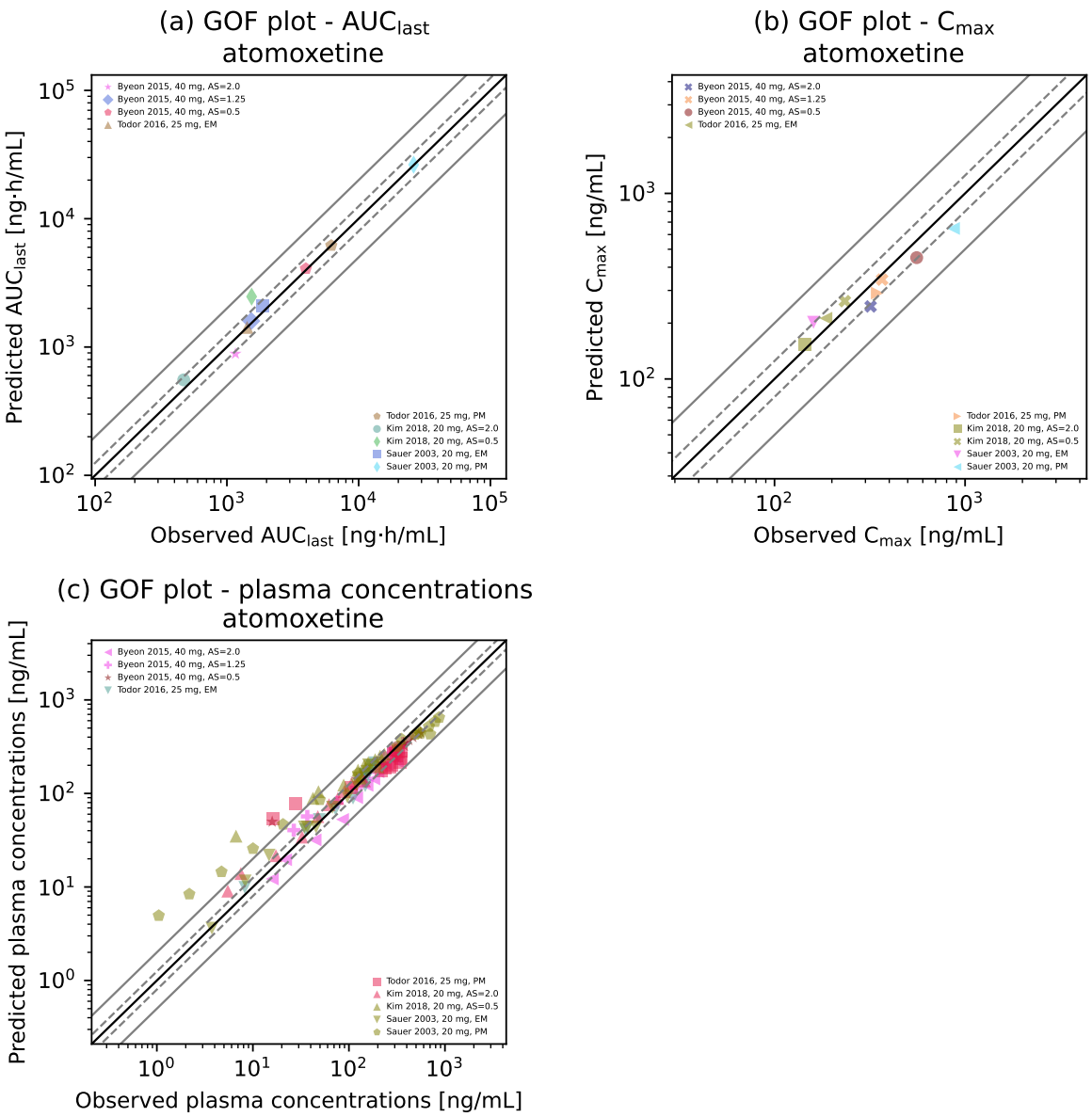

Figure S3.3.8: Goodness of fit plots. Predicted versus observed (a) AUC_{last}, (b) C_{max} and (c) plasma concentration values for all DGI studies. The solid black line marks the line of identity, the dashed grey lines mark the 0.8- to 1.25-fold range, the solid grey lines indicate the 0.5- to 2-fold range. Colored symbols represent the study population given in the legend.

Pharmaceutics **2022**, *14*, 1734. https://doi.org/10.3390/pharmaceutics14081734

S3.3.3 DGI ratios

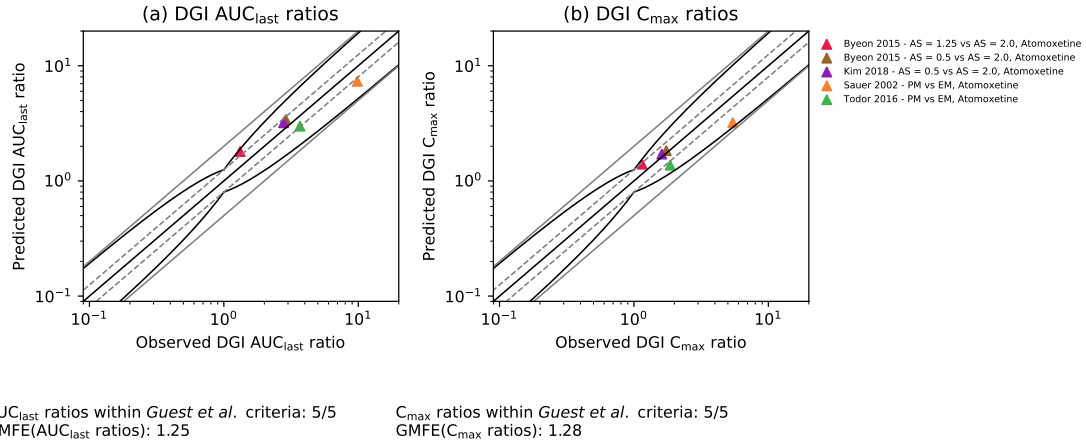

Figure S3.3.9: DGI ratio plot. Predicted versus observed DGI (a) AUC_{last} and (b) C_{max} ratios for all DGI studies. The solid straight black line marks the line of identity, the solid curved black line shows the prediction success limits proposed by *Guest et al.* [14], the dashed grey lines mark the 0.8- to 1.25-fold range, the solid grey lines indicate the 0.5- to 2-fold range. Colored symbols represent the study population given in the legend.

Pharmaceutics **2022**, *14*, 1734. https://doi.org/10.3390/pharmaceutics14081734

S4 Risperidone

For the risperidone PBPK model, a published model by Kneller et al. [24] was used. Here, most model parameters were used unchanged from the initial model. However, as the intestinal permeability for risperidone as well as system-dependent parameters were not reported in the article, and the model could not be reproduced entirely from the reported values, minor refinements were made.

S4.1 Risperidone PBPK Base Model Building

S4.1.1 Drug-dependent parameters

Table S4.1.1: Drug-dependent parameters for the final risperidone PBPK model

Parameter	Unit	Value	Source	Literature	Reference
Risperidone					
MW	g/mol	410.48	Literature	410.48	[24]
pKa (base)	-	8.76	Literature	8.76	[24]
pKa (acid)	-	3.11	Literature	3.11	[24]
Solubility (pH 7.3)	mg/mL	0.17	Literature	0.17	[24]
logP	-	2.40	Literature	2.40	[24]
f_u	%	17.50	Literature	17.50	[24]
CYP3A4 $K_M \rightarrow$ 9-HR	µmol/L	61.00	Literature	61.00	[24]
CYP3A4 $k_{cat} \rightarrow$ 9-HR	1/min	0.70	Literature	0.70	[24]
CYP3A4 $K_M \rightarrow$ sink	µmol/L	61.00	Literature	61.00	[24]
CYP3A4 $k_{cat} \rightarrow$ sink	1/min	0.15	Literature	0.15	[24]
CYP2D6 $K_M \rightarrow$ 9-HR	µmol/L	1.10	Literature	1.10	[24]
CYP2D6 ${k_{cat}}^{EM} \rightarrow$ 9-HR	1/min	1.07	Optimized	2.30	[24]
CYP2D6 ${k_{cat}}^{PM} \rightarrow$ 9-HR	1/min	0.00	Literature	0.00	[24]
CYP2D6 $K_M \rightarrow$ sink	µmol/L	1.10	Literature	1.10	[24]
CYP2D6 ${k_{cat}}^{EM} \rightarrow$ sink	1/min	0.67	Optimized	1.40	[24]
CYP2D6 ${k_{cat}}^{PM} \rightarrow$ sink	1/min	0.00	Literature	0.00	[24]
P-gp K_M	µmol/L	26.30	Literature	26.30	[24]
P-gp k_{cat}	1/min	12.72	Optimized	0.20	[24]
GFR fraction	-	1.00	Assumed	-	-
Partition coefficients	-	Diverse	Calculated	R&R	[40]
Cell permeabilities	cm/min	1.95E-03	Calculated	PK-Sim	[18]
Specific intestinal perm.	cm/min	8.04E-06	Optimized	-	[18]
9-Hydroxyrisperidone					
MW	g/mol	426.48	Literature	426.48	[24]
pKa (base)	-	8.76	Literature	8.76	[24]
pKa (acid)	-	3.11	Literature	3.11	[24]
Solubility (pH 6.5)	mg/mL	0.17	Literature	0.17	[24]

-: not available, 9-HR: 9-hydroxyrisperidone, perm.: permeabilities.

Pharmaceutics **2022**, *14*, 1734. https://doi.org/10.3390/pharmaceutics14081734

Table S4.1.1: Drug-dependent parameters for the final risperidone PBPK model

Parameter	Unit	Value	Source	Literature	Reference
logP	-	2.10	Literature	2.10	[24]
f_u	%	29.00	Literature	29.00	[24]
Unspecific CL_{hep}	1/min	0.08	Optimized	0.04	[24]
P-gp K_M	µmol/L	26.30	Literature	26.30	[24]
P-gp k_{cat}	1/min	5.70E-03	Optimized	9.64E-03	[24]
GFR fraction	-	1.00	Assumed	-	-
Partition coefficients	-	Diverse	Calculated	R&R	[40]
Cell permeabilities	cm/min	7.69E-04	Calculated	PK-Sim	[18]
Specific intestinal perm.	cm/min	3.53E-06	Calculated	3.53E-06	[18]

-: not available, 9-HR: 9-hydroxyrisperidone, perm.: permeabilities.

Pharmaceutics **2022**, *14*, 1734. https://doi.org/10.3390/pharmaceutics14081734

S4.1.2 Clinical studies

Table S4.1.2: Risperidone study table

Route	Dose [mg]	n	Females [%]	Age [years]	Weight [kg]	CYP2D6 activity	Metabolite measured	Dataset	References
PBPK base model building and evaluation									
po (tab sd)	2	36	33	32	79	-	no	training	Darwish 2015 [11]
po (tab, sd)	1	10	0	(23-38)	(65-80)	AS = 1.25*	yes	test	Kim 2008 [22]
po (tab, sd)	1	11	21	28 (22-42)	-	-	no	training	Markowitz 2002 [28]
po (tab, sd)	2	10	0	33 (23-44)	64 (55-76)	-	yes	training	Mahatthanatrakul 2012 [27]
po (tab, sd)	4	10	0	31	(55-76)	-	no	test	Mahatthanatrakul 2007 [26]
po (tab, sd)	1	12	0	24 (20-28)	65 (53-86)	AS = 1*	yes	test	Nakagami 2005 [32]
DGI model building and evaluation									
po (tab, qd)	2	8	27	43 (18-63)	-	g-EM	no	training	Bondolfi 2001 [6]
po (tab, qd)	2	3	27	43 (18-63)	-	g-PM	no	training	Bondolfi 2001 [6]
po (tab, sd)	1	6	33	24 (19-27)	67 (51-86)	AS = 0*	yes	test	Novalbos 2010 [36]
po (tab, sd)	1	26	58	23 (19-27)	65 (43-106)	AS = 1*	yes	test	Novalbos 2010 [36]
po (tab, sd)	1	33	55	23 (19-27)	66 (46-89)	AS = 2*	yes	training	Novalbos 2010 [36]
po (tab, sd)	1	6	17	23 (19-34)	73 (56-81)	AS = 3*	yes	test	Novalbos 2010 [36]

-: not given, *: full genotype provided in publication.

Pharmaceutics **2022**, *14*, 1734. https://doi.org/10.3390/pharmaceutics14081734

S4.2 Risperidone PBPK Base Model Evaluation

S4.2.1 Plasma Concentration-Time Profiles

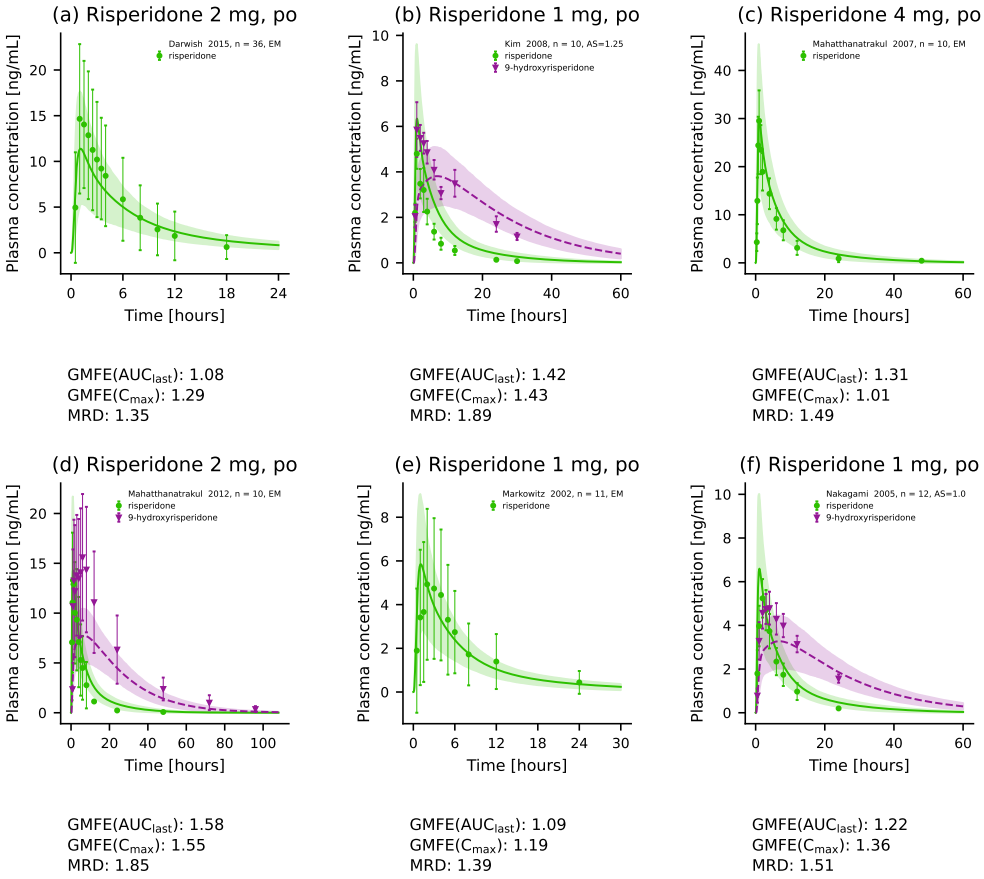

Figure S4.2.1: Risperidone and 9-hydroxyrisperidone plasma concentration-time profiles. Population predictions (n=1000) are shown as lines with ribbons (arithmetic mean ± SD) Individual predictions (n=1) are shown as lines. Symbols represent the corresponding observed data ± SD if provided.

Pharmaceutics **2022**, *14*, 1734. https://doi.org/10.3390/pharmaceutics14081734

S4.2.2 Goodness-of-Fit Plots

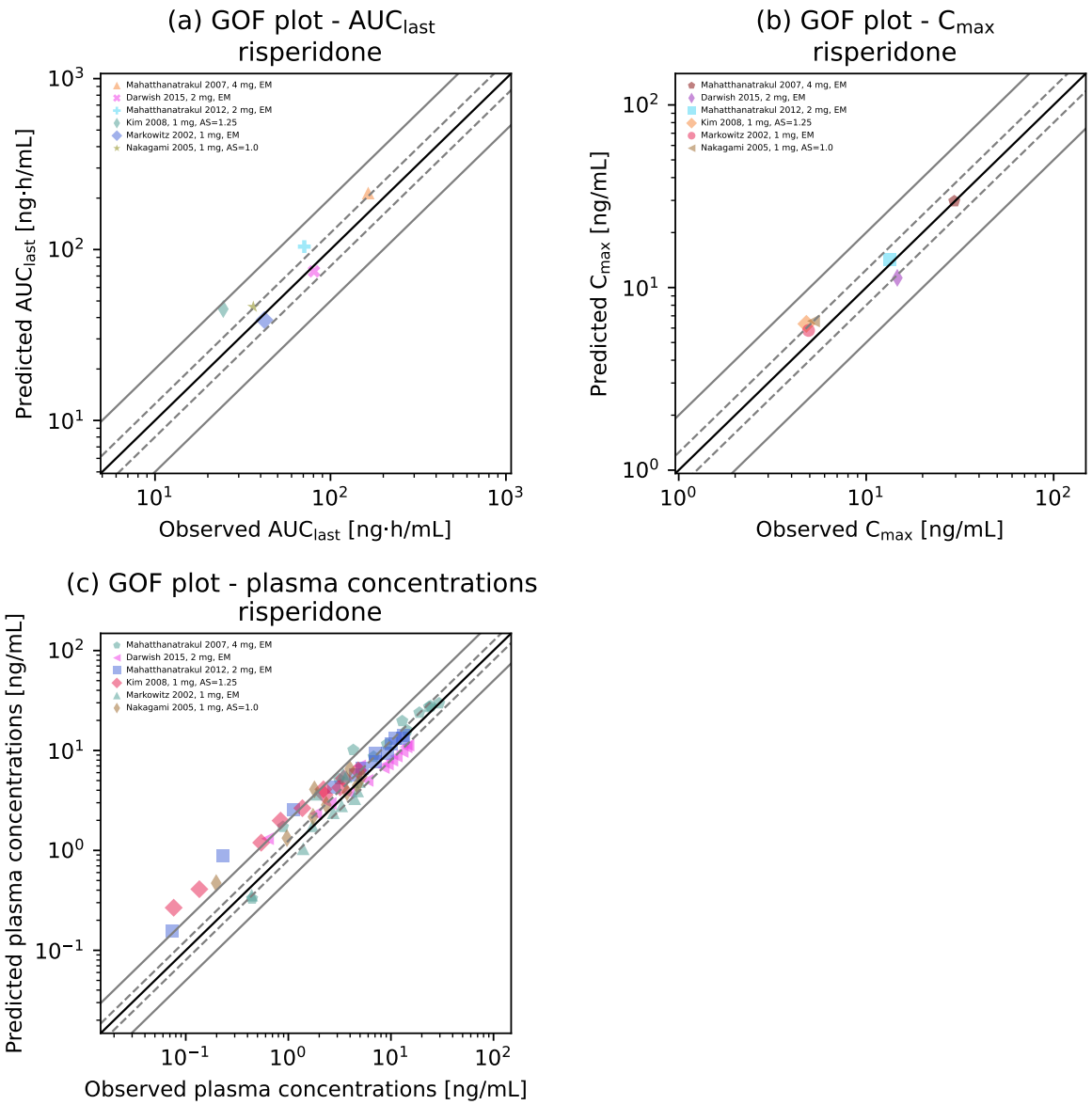

Figure S4.2.2: Goodness of fit plots. Predicted versus observed (a) AUC_{last}, (b) C_{max} and (c) plasma concentration values for all studies. The solid black line marks the line of identity, the dashed grey lines mark the 0.8- to 1.25-fold range, the solid grey lines indicate the 0.5- to 2-fold range. Colored symbols represent the study population given in the legend.

Pharmaceutics **2022**, *14*, 1734. https://doi.org/10.3390/pharmaceutics14081734

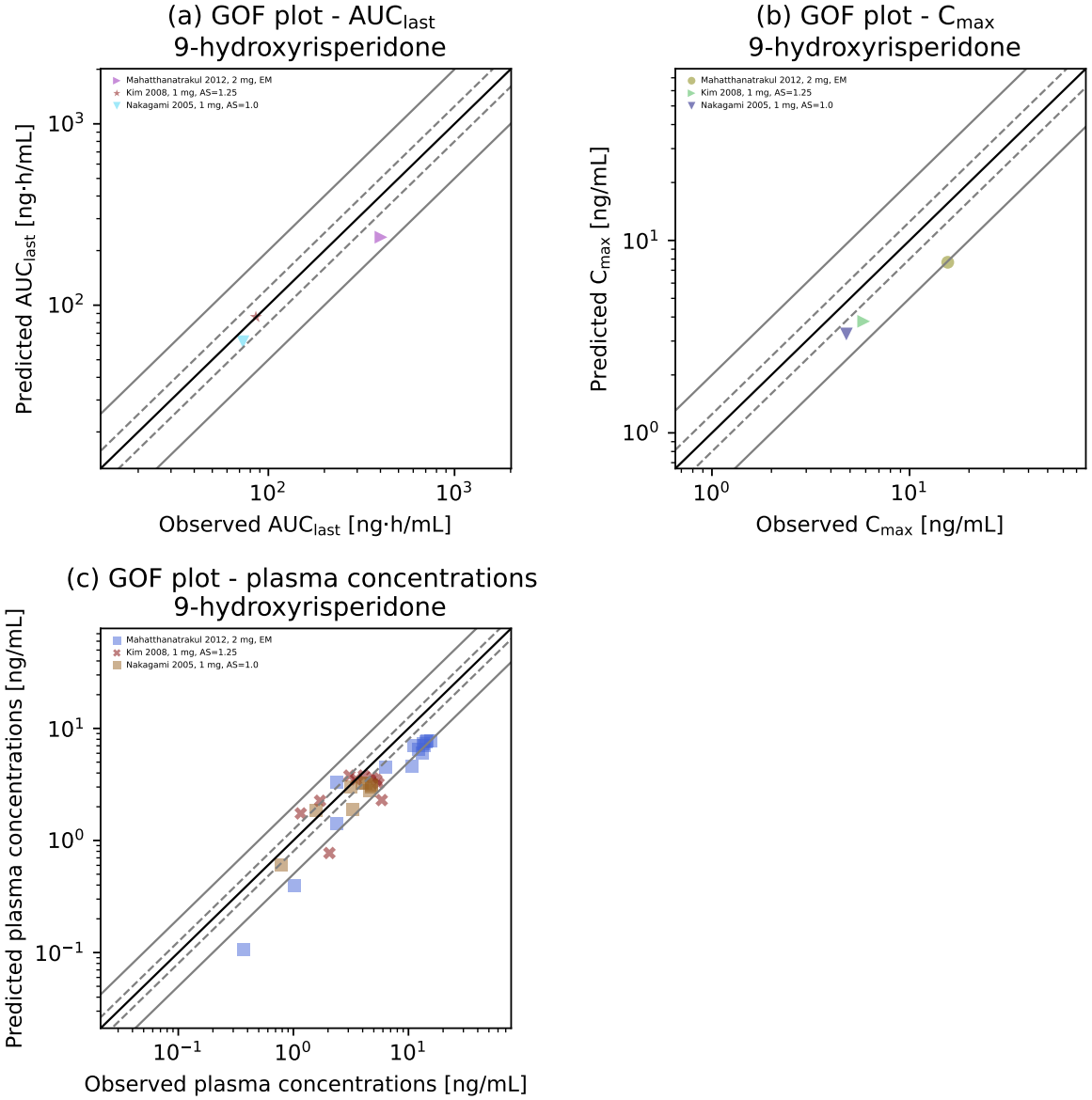

Figure S4.2.3: Goodness of fit plots. Predicted versus observed (a) AUC_{last}, (b) C_{max} and (c) plasma concentration values for all studies. The solid black line marks the line of identity, the dashed grey lines mark the 0.8- to 1.25-fold range, the solid grey lines indicate the 0.5- to 2-fold range. Colored symbols represent the study population given in the legend.

Pharmaceutics **2022**, *14*, 1734. https://doi.org/10.3390/pharmaceutics14081734

S4.2.3 Sensitivity Analysis

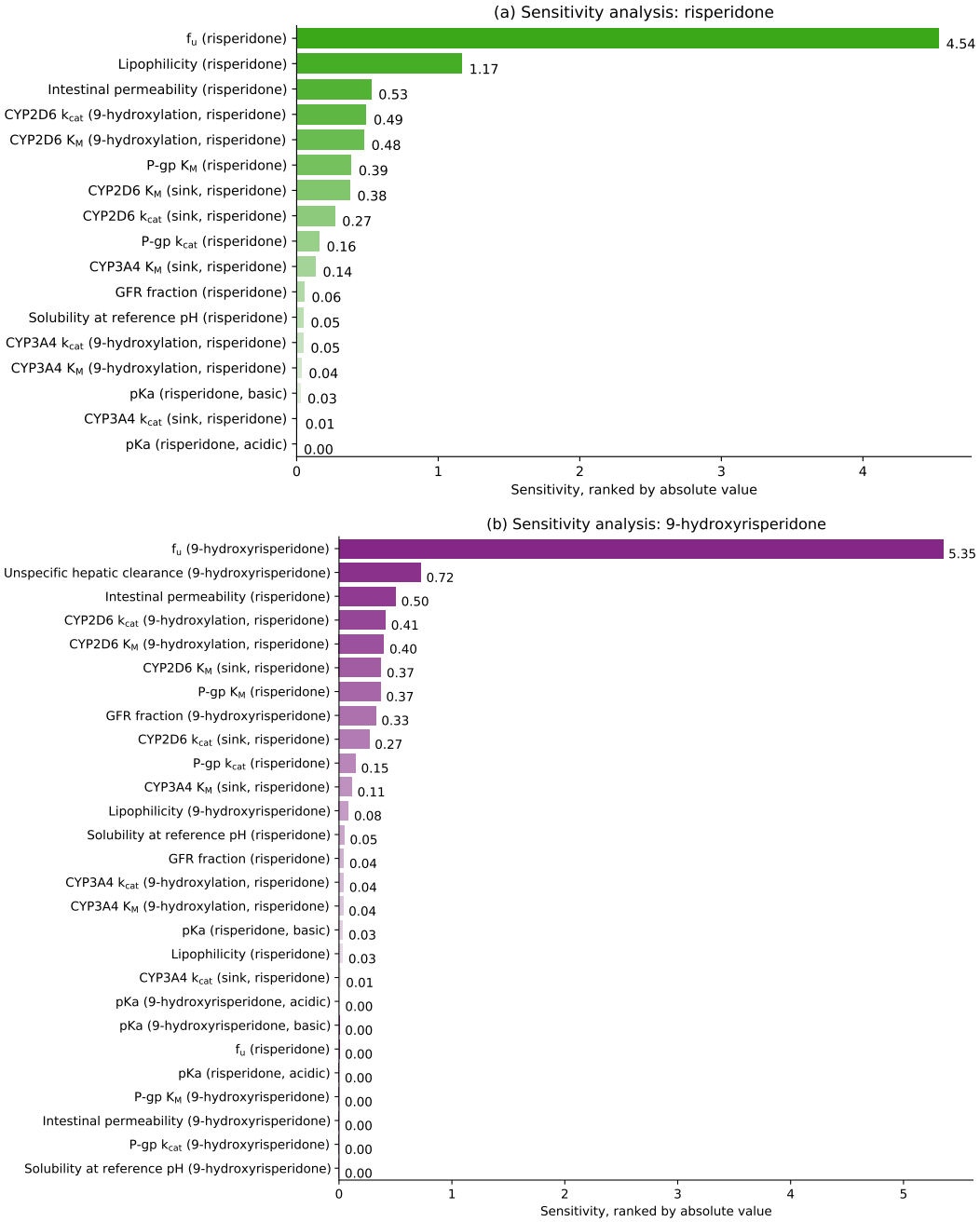

Figure S4.2.4: Sensitivity analysis of the risperidone (a) and 9-hydroxyrisperidone (b) model. Sensitivity of the model to single parameters, determined as change of the simulated AUC from time of the drug adminstration extrapolated to infinity of a single oral administration of 2 mg risperidone.

Pharmaceutics **2022**, *14*, 1734. https://doi.org/10.3390/pharmaceutics14081734

S4.3 Risperidone DGI Model Evaluation

S4.3.1 Plasma Concentration-Time Profiles

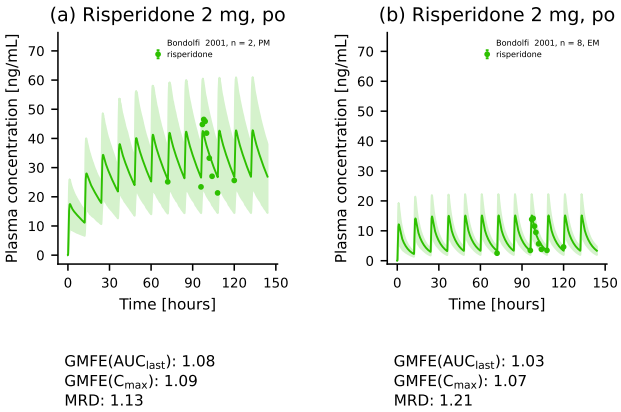

Figure S4.3.5: Risperidone plasma concentration-time profiles [9]. Population predictions (n=1000) are shown as lines with ribbons (arithmetic mean ± SD) Symbols represent the corresponding observed data ± SD if provided.

Pharmaceutics **2022**, *14*, 1734. https://doi.org/10.3390/pharmaceutics14081734

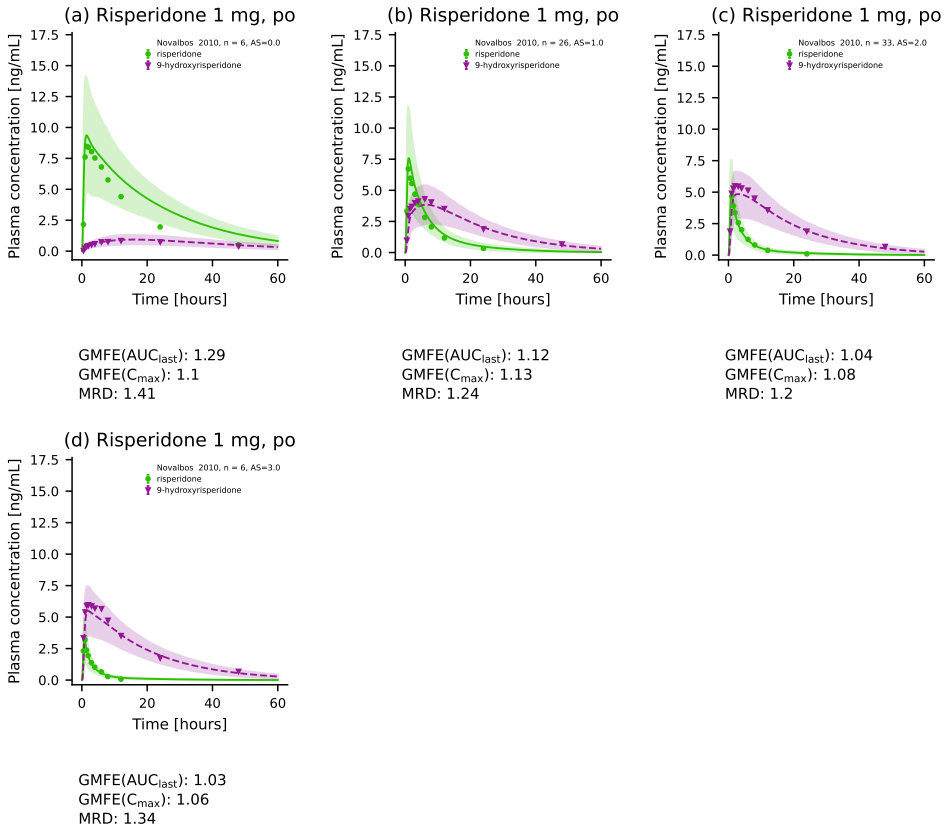

Figure S4.3.6: Risperidone plasma concentration-time profiles [12]. Population predictions (n=1000) are shown as lines with ribbons (arithmetic mean ± SD) Individual predictions (n=1) are shown as lines. Symbols represent the corresponding observed data ± SD if provided.

Pharmaceutics **2022**, *14*, 1734. https://doi.org/10.3390/pharmaceutics14081734

S4.3.2 Goodness-of-Fit Plots

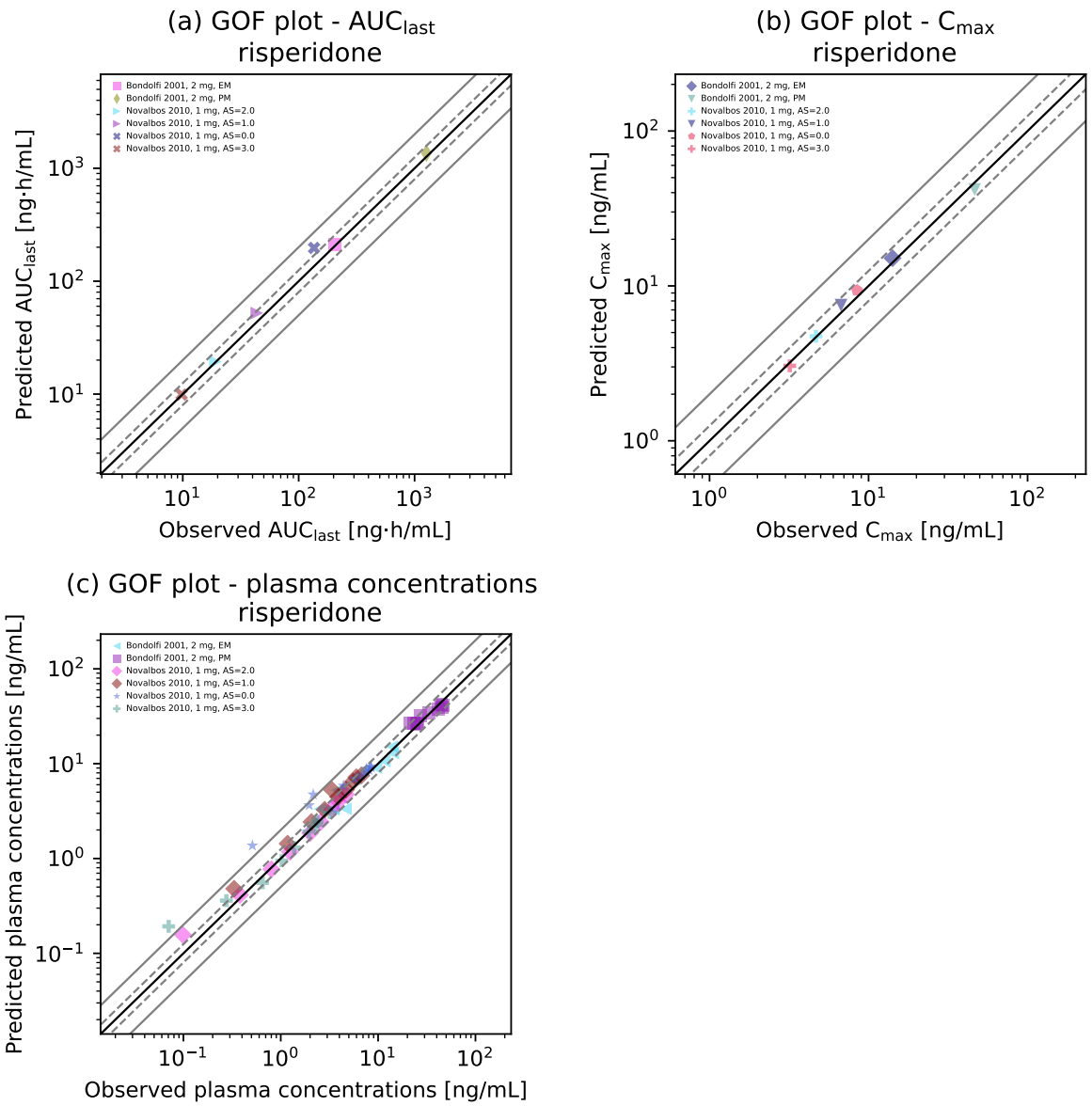

Figure S4.3.7: Goodness of fit plots. Predicted versus observed (a) AUC_{last}, (b) C_{max} and (c) plasma concentration values for all DGI studies. The solid black line marks the line of identity, the dashed grey lines mark the 0.8- to 1.25-fold range, the solid grey lines indicate the 0.5- to 2-fold range. Colored symbols represent the study population given in the legend.

Pharmaceutics **2022**, *14*, 1734. https://doi.org/10.3390/pharmaceutics14081734

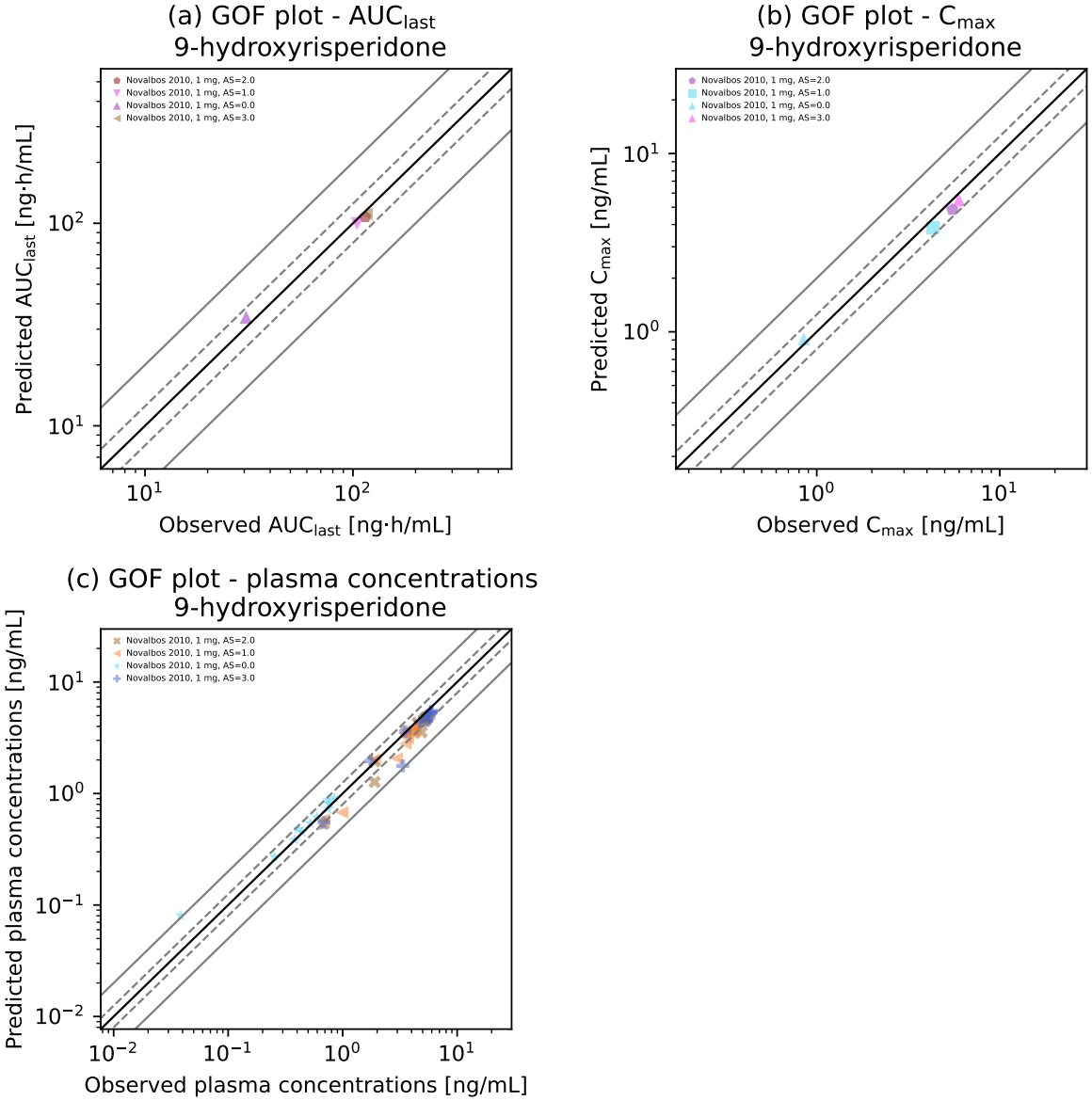

Figure S4.3.8: Goodness of fit plots. Predicted versus observed (a) AUC_{last}, (b) C_{max} and (c) plasma concentration values for all DGI studies. The solid black line marks the line of identity, the dashed grey lines mark the 0.8- to 1.25-fold range, the solid grey lines indicate the 0.5- to 2-fold range. Colored symbols represent the study population given in the legend.

Pharmaceutics **2022**, *14*, 1734. https://doi.org/10.3390/pharmaceutics14081734

S4.3.3 DGI Ratios

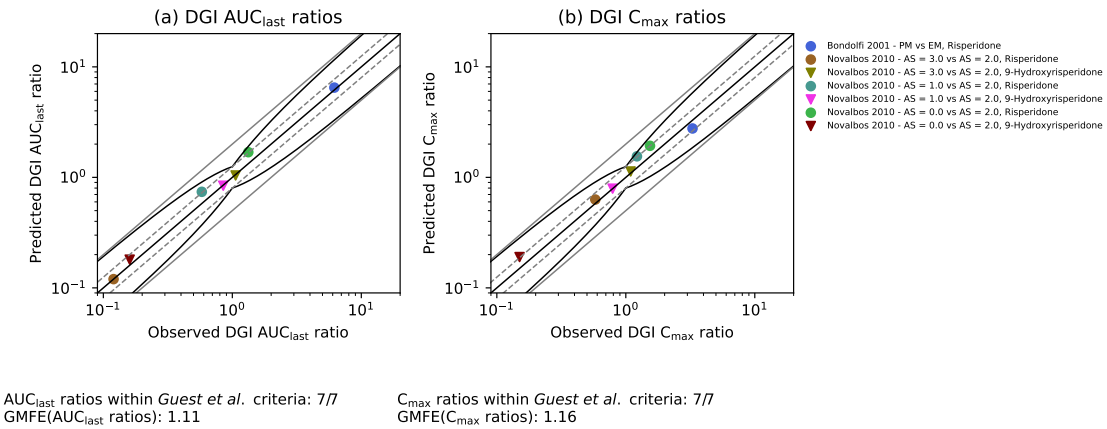

Figure S4.3.9: DGI ratio plot. Predicted versus observed (a) AUC_{last} and (b) C_{max} DGI ratios for all DGI studies. The solid straight black line marks the line of identity, the solid curved black line shows the prediction success limits proposed by *Guest et al.* [14], the dashed grey lines mark the 0.8- to 1.25-fold range, the solid grey lines indicate the 0.5- to 2-fold range. Colored symbols represent the study population given in the legend.

Pharmaceutics **2022**, *14*, 1734. https://doi.org/10.3390/pharmaceutics14081734

S5 Abbreviations

AS	CYP2D6 activity score
AUC	Area under the plasma concentration-time curve
AUC_{last}	AUC from the time of the first concentration measurement to the last time point of concentration measurement
Be	Berezhkovskiy calculation method [4]
cap	Capsule
CL_{hep}	Hepatic clearance
C_{max}	Peak plasma concentration
CR	Controlled release
CYP2C19	Cytochrome P450 2C19
CYP2D6	Cytochrome P450 2D6
CYP3A4	Cytochrome P450 3A4
DGI	Drug-gene interaction
EHC	Enterohepatic circulation
EM	Extensive metabolizer
fu_{mic}	Free fraction of compound in microsomal incubation
f_u	Fraction unbound
g-	Genotyped
GFR	Glomerular filtration rate
ICRP	International Commission on Radiological Protection
inf	Infusion
iv	Intravenous
k_{cat}	Catalytic rate constant
K_i	Dissociation constant of the inhibitor-enzyme complex
k_{inact}	Maximum inactivation rate constant
K_M	Michaelis-Menten constant
logP	Partition coefficient
MW	Molecular weight
NHANES	Third National Health and Nutrition Examination Survey
p-	Phenotyped
P-gp	P-glycoprotein
PBPK	Physiologically based pharmacokinetic
pKa	Acid dissociation constant
perm.	Permeability
PM	Poor metabolizer
po	Oral

Pharmaceutics ***2022***, 1734. https://doi.org/10.3390/pharmaceutics14081734

qd	Once daily
R&R	Rodgers and Rowland calculation method [40]
RT-PCR	Reverse transcription polymerase chain reaction
sd	Single dose
SD	Standard deviation
sol	Oral solution
tab	Tablet

Pharmaceutics ***2022***, *14*, 1734. https://doi.org/10.3390/pharmaceutics14081734

Bibliography

1. Agrawal, N. Determination of Paroxetine in Pharmaceutical Preparations Using HPLC with Electrochemical Detection. *The Open Analytical Chemistry Journal* **7,** 1–5 (2013).
2. Austin, R. P., Barton, P., Cockroft, S. L., Wenlock, M. C. & Riley, R. J. The influence of nonspecific microsomal binding on apparent intrinsic clearance, and its prediction from physicochemical properties. *Drug Metabolism and Disposition* **30,** 1497–1503 (2002).
3. Belle, D. J. *et al.* Effect of potent CYP2D6 inhibition by paroxetine on atomoxetine pharmacokinetics. *Journal of clinical pharmacology* **42,** 1219–27.
4. Berezhkovskiy, L. M. Volume of distribution at steady state for a linear pharmacokinetic system with peripheral elimination. *Journal of Pharmaceutical Sciences* **93,** 1628–1640 (2004).
5. Bertelsen, K. M., Venkatakrishnan, K., Von Moltke, L. L., Obach, R. S. & Greenblatt, D. J. Apparent mechanism-based inhibition of human CYP2D6 in vitro by paroxetine: Comparison with fluoxetine and quinidine. *Drug Metabolism and Disposition* **31,** 289–293.
6. Bondolfi, G. *et al.* The effect of fluoxetine on the pharmacokinetics and safety of risperidone in psychotic patients. *Pharmacopsychiatry* **35,** 50–56 (2002).
7. Byeon, J. Y. *et al.* Effects of the CYP2* allele on the pharmacokinetics of atomoxetine and its metabolites. *Archives of Pharmacal Research* **38,** 2083–2091 (2015).
8. Calvo, G. *et al.* Lack of pharmacologic interaction between paroxetine and alprazolam at steady state in healthy volunteers. *Journal of clinical psychopharmacology* **24,** 268–76 (June 2004).
9. Chen, R., Wang, H., Shi, J., Shen, K. & Hu, P. Cytochrome P450 2D6 genotype affects the pharmacokinetics of controlled-release paroxetine in healthy Chinese subjects: Comparison of traditional phenotype and activity score systems. *European Journal of Clinical Pharmacology* **71,** 835–841.
10. Cui, Y. M. *et al.* Atomoxetine pharmacokinetics in healthy Chinese subjects and effect of the CYP2D6*10 allele. *British Journal of Clinical Pharmacology* **64,** 445–449 (2007).
11. Darwish, M., Bond, M., Yang, R., Hellriegel, E. T. & Robertson, P. Evaluation of Potential Pharmacokinetic Drug-Drug Interaction Between Armodafinil and Risperidone in Healthy Adults. *Clinical Drug Investigation* **35,** 725–733 (2015).
12. Ganchev, B. *Charakterisierung der metabolischen Bioaktivierung des Clomifens unter besonderer Berücksichtigung genetischer Polymorphismen* PhD thesis (Tübingen, 2014), 149.
13. Greenblatt, D. J. *et al.* Time course of recovery of cytochrome P450 3A function after single doses of grapefruit juice. *Clinical Pharmacology and Therapeutics* **74,** 121–29 (2003).
14. Guest, E. J., Aarons, L., Houston, J. B., Rostami-Hodjegan, A. & Galetin, A. Critique of the two-fold measure of prediction success for ratios: application for the assessment of drug-drug interactions. *Drug metabolism and disposition: the biological fate of chemicals* **39,** 170–3 (Feb. 2011).
15. Hanke, N. *et al.* PBPK models for CYP3A4 and P-gp DDI prediction: a modeling network of rifampicin, itraconazole, clarithromycin, midazolam, alfentanil and digoxin. *CPT: pharmacometrics & systems pharmacology,* Supplementary document (Aug. 2018).
16. *Influence of Pharmacogenetic Factors, Paroxetine and Clarithromycin on Pharmacokinetics of Clomiphene - EudraCT 2009-014531-20.*

Pharmaceutics **2022**, *14*, 1734. https://doi.org/10.3390/pharmaceutics14081734

17. Jornil, J., Jensen, K. G., Larsen, F. & Linnet, K. Identification of cytochrome P450 isoforms involved in the metabolism of paroxetine and estimation of their importance for human paroxetine metabolism using a population-based simulator. *Drug Metabolism and Disposition* **38,** 376–385.
18. Kawai, R. *et al.* Physiologically based pharmacokinetic study on a cyclosporin derivative, SDZ IMM 125. *Journal of pharmacokinetics and biopharmaceutics* **22,** 327–65 (Oct. 1994).
19. Kaye, C. M. *et al.* A review of the metabolism and pharmacokinetics of paroxetine in man. *Acta Psychiatrica Scandinavica* **80,** 60–75 (1989).
20. Khatavkar, U. N., Jayaram Kumar, K. & Shimpi, S. L. Novel approaches for development of oral controlled release compositions of galantamine hydrobromide and paroxetine hydrochloride hemihydrate: A review. *International Journal of Applied Pharmaceutics* **8,** 1–6 (2016).
21. Khatavkar, U. N., Shimpi, S. L., Jayaram Kumar, K. & Deo, K. D. Development and comparative evaluation of in vitro, in vivo properties of novel controlled release compositions of paroxetine hydrochloride hemihydrate as against Geomatrix™ platform technology. *Drug Development and Industrial Pharmacy* **39,** 1175–1186.
22. Kim, K. A. *et al.* Effect of rifampin, an inducer of CYP3A and P-glycoprotein, on the pharmacokinetics of risperidone. *Journal of Clinical Pharmacology* **48,** 66–72 (2008).
23. Kim, S. H. *et al.* Physiologically based pharmacokinetic modelling of atomoxetine with regard to CYP2D6 genotypes. *Scientific Reports* **8,** 1–9 (2018).
24. Kneller, L. A., Abad-Santos, F. & Hempel, G. Physiologically Based Pharmacokinetic Modelling to Describe the Pharmacokinetics of Risperidone and 9-Hydroxyrisperidone According to Cytochrome P450 2D6 Phenotypes. *Clinical Pharmacokinetics* **59,** 51–65 (Jan. 2020).
25. Lund, J. *et al.* Paroxetine: Pharmacokinetics and Cardiovascular Effects after Oral and Intravenous Single Doses in Man. *Acta Pharmacologica et Toxicologica* **51,** 351–357.
26. Mahatthanatrakul, W., Nontaput, T., Ridtitid, W., Wongnawa, M. & Sunbhanich, M. Rifampin, a cytochrome P450 3A inducer, decreases plasma concentrations of antipsychotic risperidone in healthy volunteers. *Journal of Clinical Pharmacy and Therapeutics* **32,** 161–167 (2007).
27. Mahatthanatrakul, W. *et al.* Effect of cytochrome P450 3A4 inhibitor ketoconazole on risperidone pharmacokinetics in healthy volunteers. *Journal of Clinical Pharmacy and Therapeutics* **37,** 221–225 (2012).
28. Markowitz, J. S., DeVane, C. L., Liston, H. L., Boulton, D. W. & Risch, S. C. The effects of probenecid on the disposition of risperidone and olanzapine in healthy volunteers. *Clinical Pharmacology and Therapeutics* **71,** 30–38 (2002).
29. Massaroti, P. *et al.* Validation of a selective method for determination of paroxetine in human plasma by LC-MS/MS. *Journal of pharmacy & pharmaceutical sciences : a publication of the Canadian Society for Pharmaceutical Sciences, Societe canadienne des sciences pharmaceutiques* **8,** 340–7 (Aug. 2005).
30. McClelland, G. R. & Raptopoulos, P. EEG and blood level of the potential antidepressant paroxetine after a single oral dose to normal volunteers. *Psychopharmacology* **83,** 327–9 (1984).
31. Mürdter, T. *et al.* Impact of CYP2D6 genotype and co-medication with paroxetine and clarithromycin on clomiphene metabolism in vivo. *Abstracts of the 82nd Annual Meeting of the German Society for Experimental and Clinical Pharmacology and Toxicology (DGPT) in Naunyn-Schmiedeberg's Archives of Pharmacology* **389,** 8 (Feb. 2016).
32. Nakagami, T., Yasui-Furukori, N., Saito, M., Tateishi, T. & Kaneo, S. Effect of verapamil on pharmacokinetics and pharmacodynamics of risperidone: In vivo evidence of involvement of P-glycoprotein in risperidone disposition. *Clinical Pharmacology and Therapeutics* **78,** 43–51 (2005).

Pharmaceutics **2022**, *14*, 1734. https://doi.org/10.3390/pharmaceutics14081734

33. Nakano, M., Witcher, J., Satoi, Y. & Goto, T. Pharmacokinetic Profile and Palatability of Atomoxetine Oral Solution in Healthy Japanese Male Adults. *Clinical Drug Investigation* **36,** 903–911 (2016).
34. National Center for Health Statistics Hyattsville MD 20782. *Third National Health and Nutrition Examination Survey, (NHANES III)* tech. rep. (1997).
35. Nishimura, M. & Naito, S. Tissue-specific mRNA expression profiles of human ATP-binding cassette and solute carrier transporter superfamilies. *Drug metabolism and pharmacokinetics* **20,** 452–77 (2005).
36. Novalbos, J. *et al.* Effects of CYP2D6 genotype on the pharmacokinetics, pharmacodynamics, and safety of risperidone in healthy volunteers. *Journal of Clinical Psychopharmacology* **30,** 504–511 (2010).
37. Open Systems Pharmacology Suite Community. PK-Sim® Ontogeny Database Documentation, Version 7.3 (2018).
38. Prasad, B. *et al.* Interindividual variability in hepatic organic anion - transporting polypeptides and P-glycoprotein (ABCB1) protein expression: quantification by liquid chromatography tandem mass spectroscopy and influence of genotype, age, and sex. *Drug metabolism and disposition: the biological fate of chemicals* **42,** 78–88 (2014).
39. Ring, B. J., Gillespie, J. S., Eckstein, J. A. & Wrighton, S. A. Identification of the human cytochromes P450 responsible for atomoxetine metabolism. *Drug Metabolism and Disposition* **30,** 319–323 (2002).
40. Rodgers, T. & Rowland, M. Mechanistic approaches to volume of distribution predictions: understanding the processes. *Pharmaceutical research* **24,** 918–33 (May 2007).
41. Rodrigues, A. D. Integrated cytochrome P450 reaction phenotyping: attempting to bridge the gap between cDNA-expressed cytochromes P450 and native human liver microsomes. *Biochemical pharmacology* **57,** 465–80 (1999).
42. Rowland Yeo, K., Walsky, R. L., Jamei, M., Rostami-Hodjegan, A. & Tucker, G. T. Prediction of time-dependent CYP3A4 drug-drug interactions by physiologically based pharmacokinetic modelling: Impact of inactivation parameters and enzyme turnover. *European Journal of Pharmaceutical Sciences* **43,** 160–73 (2011).
43. Sauer, J. M. *et al.* Disposition and metabolic fate of atomoxetine hydrochloride: The role of CYP2D6 in human disposition and metabolism. *Drug Metabolism and Disposition* **31,** 98–107 (2003).
44. Schoedel, K. A., Pope, L. E. & Sellers, E. M. Randomized open-label drug-drug interaction trial of dextromethorphan/quinidine and paroxetine in healthy volunteers. *Clinical drug investigation* **32,** 157–69 (Mar. 2012).
45. Segura, M. *et al.* Contribution of cytochrome P450 2D6 to 3,4-methylenedioxymethamphetamine disposition in humans: Use of paroxetine as a metabolic inhibitor probe. *Clinical Pharmacokinetics* **44,** 649–660 (2005).
46. Sindrup, S. H. *et al.* The relationship between paroxetine and the sparteine oxidation polymorphism. *Clinical pharmacology and therapeutics* **51,** 278–87 (Mar. 1992).
47. Swain, M. chemicalize.org. *Journal of Chemical Information and Modeling* **52,** 613–615 (Feb. 2012).
48. Tanaka, G. & Kawamura, H. Anatomical and physiological characteristics for Asian reference man: male and female of different ages: Tanaka model. Division of Radioecology, National Institute of Radiological Sciences. Hitachinaka 311-12 Japan. NIRS-M-115 (1996).

Pharmaceutics ***2022***, *14*, 1734. https://doi.org/10.3390/pharmaceutics14081734

49. Todor, I. *et al.* Evaluation of a potential metabolism-mediated drug-drug interaction between atomoxetine and bupropion in healthy volunteers. *Journal of Pharmacy and Pharmaceutical Sciences* **19,** 198–207 (2016).
50. Valentin, J. Basic anatomical and physiological data for use in radiological protection: reference values. A report of age- and gender-related differences in the anatomical and physiological characteristics of reference individuals. ICRP Publication 89. *Annals of the ICRP* **32,** 5–265 (2002).
51. Van der Lee, M. J. *et al.* Interaction study of the combined use of paroxetine and fosamprenavir-ritonavir in healthy subjects. *Antimicrobial agents and chemotherapy* **51,** 4098–104 (Nov. 2007).
52. Venkatakrishnan, K. & Obach, R. S. In vitro-in vivo extrapolation of CYP2D6 inactivation by paroxetine: prediction of nonstationary pharmacokinetics and drug interaction magnitude. *Drug metabolism and disposition: the biological fate of chemicals* **33,** 845–52 (June 2005).
53. Yasui-Furukori, N. *et al.* Effect of itraconazole on pharmacokinetics of paroxetine: the role of gut transporters. *Therapeutic drug monitoring* **29,** 45–8 (Feb. 2007).
54. Yasui-Furukori, N. *et al.* Terbinafine increases the plasma concentration of paroxetine after a single oral administration of paroxetine in healthy subjects. *European Journal of Clinical Pharmacology* **63,** 51–56 (2007).
55. Yoon, Y. R. *et al.* Relationship of paroxetine disposition to metoprolol metabolic ratio and CYP2D6*10 genotype of Korean subjects. *Clinical Pharmacology and Therapeutics* **67,** 567–576 (2000).
56. Yu, G., Li, G. F. & Markowitz, J. S. Atomoxetine: A Review of Its Pharmacokinetics and Pharmacogenomics Relative to Drug Disposition. *Journal of Child and Adolescent Psychopharmacology* **26,** 314–326 (2016).
57. Zhong, H., Mashinson, V., Woolman, T. & Zha, M. Understanding the Molecular Properties and Metabolism of Top Prescribed Drugs. *Current Topics in Medicinal Chemistry* **13,** 1290–1307 (2013).

B.4 PROJECT IV: SUPPLEMENTARY MATERIALS

Pharmaceutics

Supplementary Materials: Prediction of Drug-Drug-Gene Interaction Scenarios of (*E*)-Clomiphene and its Metabolites Using Physiologically Based Pharmacokinetic Modeling

Christina Kovar [1,2], Lukas Kovar [1], Simeon Rüdesheim [1,2], Dominik Selzer [1], Boian Ganchev [2], Patrick Kröner [2], Svitlana Igel [2], Reinhold Kerb [2], Elke Schaeffeler [2], Thomas E. Mürdter [2], Matthias Schwab [2,3] and Thorsten Lehr [1,*]

[1] Clinical Pharmacy, Saarland University, 66123 Saarbrücken, Germany

[2] Dr. Margarete Fischer-Bosch Institute of Clinical Pharmacology, University of Tübingen, 70376 Stuttgart, Germany

[3] Departments of Clinical Pharmacology, Pharmacy and Biochemistry, University of Tübingen, 72076 Tübingen, Germany

* Correspondence: thorsten.lehr@mx.uni-saarland.de; Tel.: +49-681-302-70255

Contents

S1. PBPK Model Building

S1.1. Clinical Studies

Plasma and renal excretion profiles of (*E*)-clomiphene ((*E*)-Clom) and its metabolites from a pharmacokinetic panel study with 20 healthy female volunteers, that were assigned to six different cytochrome P450 (CYP) 2D6 activity scores (AS), were available for model building and evaluation (see Table 1 in the main manuscript for demographic information). The pharmacokinetic panel study was complemented with digitized data from published clinical studies (study search criteria were (a) studies with intravenous or oral (*E*)-Clom administration and (b) reported pharmacokinetic data of (*E*)-Clom and/or its metabolites (*E*)-4-hydroxyclomiphene ((*E*)-4-OH-Clom), (*E*)-N-desethylclomiphene ((*E*)-DE-Clom) and (*E*)-4-hydroxy-N-desethylclomiphene ((*E*)-4-OH-DE-Clom). Data originating from two single dose and two multiple dose studies with oral (*E*)-Clom administration could be integrated. To the best of our knowledge, plasma profiles of (*E*)-Clom and its metabolites after intravenous administration were not publicly available. Information on the identified and integrated published clinical studies are listed in Table S2. As CYP2D6 AS and phenotype of corresponding study participants were not reported, CYP2D6 catalytic rate constants (k_{cat}) values in the PBPK model were estimated (see Table S1).

Table S1. Optimized CYP2D6 k_{cat} values for each study.

CYP2D6 k_{cat} values	**Mikkelson et al. 1986 [1]**	**Study Ratioph. 1991 [2]**	**Wiehle et al. 2013 (a) [3]**	**Wiehle et al. 2013 (b)[3]**	**Wiehle et al. 2013 (c) [3]**	**Miller et al. 2018 [4]**
(*E*)-Clom → (*E*)-4-OH-Clom	213.0	283.1	87.7	124.1	43.3	18.1
(*E*)-Clom → undef.	90.6	120.5	37.3	52.8	18.4	7.7
(*E*)-Clom → (*E*)-DE-Clom	84.4	112.1	34.8	49.1	17.1	7.2

CYP: cytochrome P450, **(*E*)-4-OH-Clom**: (*E*)-4-hydroxyclomiphene, **(*E*)-Clom**: (*E*)-clomiphene, **(*E*)-DE-Clom**: (*E*)-N-desethylclomiphene, **k_{cat}**: catalytic rate constant, **Ratioph.**: Ratiopharm® GmbH, **undef.**: undefined metabolite

Of note, in the pharmacokinetic panel study, two study participants with the *CYP2D6* genotypes $^*9/^*10$ and $^*9/^*41$ had been classified as AS=0.75. Here, a high interindividual variability in the plasma profiles could be observed. The study participant genotyped as $^*9/^*41$ showed unexpectedly high (*E*)-Clom plasma concentrations for an AS=0.75 individual with (*E*)-Clom levels comparable with those of poor metabolizers (PM). Since the allele haplotype ^{*41} has shown a high dispersion in CYP2D6 enzyme activity, the respective individual was excluded from the dataset [5].

Table S2. Overview of clinical study data from literature used for model evaluation.

Clinical study	**Route**	**Dose [mg]**[a]	***E/Z* ratio**	**n**	**Females [%]**	**Age [years]**[b]	**Weight [kg]**[b]	**BMI [kg/m²]**[b]	**Metabolites measured**	***CYP2D6* genotyped**
Mikkelson et al. 1986 [1]	po, tab, s.d.	50	-[c]	23	100	32	62.4	-	no	no
Study Ratioph. 1991 [2]	po, tab, s.d.	50	62/38	18	-	-	-	-	no	no
Wiehle et al. 2013 (a) [3]	po, caps, m.d.	6.25	100/0	16	0	53.3±10.2	-	34.7±7.2	no	no
Wiehle et al. 2013 (b) [3]	po, caps, m.d.	12.5	100/0	14	0	53.3±10.2	-	34.7±7.2	no	no
Wiehle et al. 2013 (c) [3]	po, caps, m.d.	25	100/0	16	0	53.3±10.2	-	34.7±7.2	no	no
Miller et al. 2018 [4]	po, tab, m.d.	50	62/38	12	0	31.5±3.6	77.9±8.2	24.4±2.4	no	no

BMI: body mass index, **caps**: capsule, **CYP**: cytochrome P450, ***E/Z***: (*E*)-/(*Z*)-clomiphene, **m.d.**: multiple dose, **n**: number of subjects, **po**: per oral, **Ratioph.**: Ratiopharm® GmbH, **s.d.**: single dose, **tab**: tablet

[a] (E)-/(Z)-clomiphene citrate

[b] mean (±SD) if applicable

[c] E/Z-ratio of 62/38 was assumed

S1.2. System-dependent Parameters and Virtual Populations

Virtual individuals were created in PK-Sim®, using the published information on the respective study population, including mode of ethnicity and gender as well as mean values of age, weight and height. For the study population in the study from Ratiopharm® GmbH [2], demographic information were not provided. Here, the default values of a 30-year-old male European individual with body weight of 73 kg and height of 176 cm according to the International Commission on Radiological Protection (ICRP) reference values were used [6]. Distribution and abundance of enzymes in the different tissues was implemented according to the PK-Sim® expression database [7]. For the generation of virtual populations, 1000 individuals were created according to the respective study population demographics. Demographic characteristics of virtual individuals were varied within the ICRP [6] and the third National Health and Nutrition Examination Survey (NHANES) [8] limits by an implemented algorithm in PK-Sim®. The corresponding algorithms for the generation of virtual populations have been reported by Willmann and coworkers [9]. For the study by Mikkelson et al. [1] and the study from Ratiopharm® GmbH [2] an age range of 20 to 50 years was assumed.
Variabilities for CYP2B6 and CYP3A4 enzyme abundances in the virtual populations were integrated and variability in CYP2D6 abundance was allowed for study populations that were not genotyped and thus not stratified by CYP2D6 AS. For the pharmacokinetic panel study, CYP2D6 k_{cat} values differ across CYP2D6 AS groups, already accounting for varying CYP2D6 abundance and/or activity. Thus, CYP2D6 expression variability was set to 0 for the respective population simulations.
System-dependent parameters including reference concentrations and enzyme expression variabilities are listed in Table S3.

Table S3. System-dependent parameters and expression of relevant enzymes.

Enzyme / Processes	Mean reference concentration [µmol/L][a]	GeoSD of the reference concentration	Relative expression in different organs[b]	Half-life liver [hours]	Half-life intestine [hours]
Enzymes					
CYP2B6	1.56 [10]	1.40[c]	RT-PCR [11]	32	23
CYP2D6	0.40 [10]	0[d]	RT-PCR [11]	51	23
CYP3A4	4.32 [10]	1.18 (liver)[7] 1.45 (duodenum)[7]	RT-PCR [11]	36 [12]	23 [13]
Processes					
Unspec. hep. CL of (*E*)-4-OH-Clom	-	1.40[c]			
Unspec. hep. CL of (*E*)-4-OH-DE-Clom	-	1.40[c]			

CYP: cytochrome P450, **(*E*)-4-OH-Clom**: (*E*)-4-hydroxyclomiphene, **(*E*)-4-OH-DE-Clom**: (*E*)-4-hydroxy-N-desethylclomiphene, **GeoSD**: geometric standard deviation, **RT-PCR**: reverse transcription polymerase chain reaction, **unspec. hep. CL**: unspecific hepatic clearance

[a] [µmol protein/L] in the tissue of the highest expression

[b] PK-Sim® expression database profile

[c] geometric standard deviation with coefficient of variation (CV) of 35 % assumed

[d] as described in Section 1.2

S1.3. Supplementary Information on (*E*)-clomiphene PBPK Model Building

The parent-metabolite PBPK model of (*E*)-Clom was developed using a middle-out approach, combining information on drug- and system-specific parameters from literature with a parameter estimation step based on clinical trial data [14]. *In vitro*, *in silico* and clinical *in vivo* data were combined to inform model input parameters [14]. Information about absorption, distribution, metabolism and excretion (ADME) processes were used to incorporate relevant enzymes.
Metabolism via CYP enzymes was implemented as Michaelis-Menten kinetic processes. To account for nonspecific binding in *in vitro* assays, apparent Michaelis-Menten constant (K_m) values informed from literature were adjusted by the free fraction of drug compound as suggested by Obach and Austin et al. [15, 16]. K_m and v_{max} values were available only for composite metabolic pathway reactions, while parameters for each specific CYP enzyme involved in the respective pathway were not reported. When multiple CYP enzymes were incorporated in one metabolic pathway (see Figure 2 in the main manuscript), identical K_m values were allocated to each CYP enzyme and the corresponding k_{cat} estimated with a fixed ratio based on *in vitro* results on the metabolic enzyme activities [17, 18].
In the PBPK model, three metabolic pathways were implemented for the parent compound (*E*)-Clom: metabolism to (*E*)-DE-Clom, metabolism to (*E*)-4-OH-Clom and metabolism to (*Z*)-3-hydroxyclomiphene (implemented as an undefined metabolite). The latter enzymatic pathway, mediated via CYP2D6, was estimated with a 1.8-fold higher intrinsic clearance compared to the formation of (*E*)-4-OH-Clom in the PBPK model according to literature [19]. Further, the formation of (*E*)-DE-Clom is primarily catalyzed by CYP3A4 and to some extent by CYP2D6 [17, 18]. This was integrated by accounting for the 80:20 metabolic ratio of CYP3A4 to CYP2D6 reported by Mazzarino and coworkers [20]. (*E*)-DE-CLOM itself is also metabolized via CYP3A4 and CYP2D6 to (*E*)-N,N-didesethylclomiphene (implemented as an undefined metabolite) [17, 18]. As previously described, the ratio of the corresponding measured *in vitro* metabolic enzyme activities was used during the parameter estimation step for optimization of k_{cat} values ($k_{cat,\ CYP3A4} = 0.13 * k_{cat,\ CYP2D6}$) [17, 18].

S1.4. Drug-dependent Parameter Tables

Table S4. Drug-dependent parameters for (*E*)-clomiphene.

Parameter	Value	Unit	Source	Literature	Reference	Description
MW	405.96	g/mol	Literature	405.96	[22]	Molecular weight
pK_a (base)	9.31	-	Literature	9.31	[23]	Acid dissociation constant
Solubility (pH 6.8)	0.0138	mg/ml	Literature	0.0138	[24]	Solubility
logP	5.67	-	Optimized	5.18, 6.08, 6.48, 6.65	[23, 25–27]	Lipophilicity
f_u	0.08	%	Optimized	1.42[a]	[21]	Fraction unbound
CYP2D6 K_m → (*E*)-4-OH-Clom	0.13	µmol/l	Literature	0.13[b]	[19]	Michaelis-Menten constant
CYP2D6 k_{cat} → (*E*)-4-OH-Clom	306.4[c]	1/min	Optimized	-	-	Catalytic rate constant
CYP2D6 K_m → undef.	0.03	µmol/l	Literature	0.03[b]	[19]	Michaelis-Menten constant
CYP2D6 k_{cat} → undef.	130.4[c]	1/min	Optimized	-	-	Catalytic rate constant
CYP2B6 K_m → (*E*)-4-OH-Clom	0.60	µmol/l	Literature	0.60[b]	[17, 18]	Michaelis-Menten constant
CYP2B6 k_{cat} → (*E*)-4-OH-Clom	7.5	1/min	Optimized	-	-	Catalytic rate constant
CYP2D6 K_m → (*E*)-DE-Clom	0.78	µmol/l	Literature	0.78[b]	[17, 18]	Michaelis-Menten constant
CYP2D6 k_{cat} → (*E*)-DE-Clom	121.4[c]	1/min	Optimized	-	-	Catalytic rate constant
CYP3A4 K_m → (*E*)-DE-Clom	0.78	µmol/l	Literature	0.78[b]	[17, 18]	Michaelis-Menten constant
CYP3A4 k_{cat} → (*E*)-DE-Clom	45.0	1/min	Optimized	-	-	Catalytic rate constant
GFR fraction	0.92	-	Optimized	-	-	Fraction of filtered drug in the urine
EHC continuous fraction	1.00	-	Assumed	-	-	Fraction of bile continually released
Partition coefficients	Diverse[d]	-	Calculated	Schmitt	[28]	Cell to plasma partition coefficients
Cellular permeability	Diverse[d]	cm/min	Calculated	Ch. dep. Schmitt	[29]	Permeability into the cellular space
Intestinal permeability	0.08	cm/min	Optimized	-	-	Transcellular intestinal permeability
Tablet Weibull time	6.80	min	Assumed	-	[e]	Dissolution time (50 % dissolved)
Tablet Weibull shape	0.47	-	Assumed	-	[e]	Dissolution profile shape

Ch. dep. Schmitt: Charge dependent Schmitt calculation method, **CYP**: cytochrome P450, **(*E*)-4-OH-Clom**: (*E*)-4-hydroxyclomiphene, **(*E*)-DE-Clom**: (*E*)-N-desethylclomiphene, **EHC**: enterohepatic circulation, **GFR**: glomerular filtration rate, **IM**: intermediate metabolizers, **IVSF**: *in vitro* scaling factor, **NM**: normal metabolizers, **UM**: ultrarapid metabolizers, **undef.**: undefined metabolite

[a] f_u was estimated with the classification model by Watanabe et al. [21]

[b] K_m values from literature were adapted with the calculated $f_{u,inc}$=0.024, considering nonspecific binding in *in vitro* assays according to [15, 16]

[c] Only CYP2D6 k_{cat} values of NM are shown while IM- and UM-k_{cat} values were extrapolated according to Equation 1 in the main manuscript (IVSFs represented in Table S8)

[d] values differ across the organs

[e] see Section 1.6

Table S5. Drug-dependent parameters for (*E*)-N-desethylclomiphene.

Parameter	Value	Unit	Source	Literature	Reference	Description
MW	377.91	g/mol	Literature	377.91	[30]	Molecular weight
pK_a (base)	8.14	-	Optimized	9.59	[30]	Acid dissociation constant
Solubility (pH 6.5)	0.46	mg/ml	Literature	0.46	[30]	Solubility
logP	4.17	-	Optimized	5.74, 6.4	[30, 31]	Lipophilicity
f_u	0.86	%	Optimized	1.37[a]	[21]	Fraction unbound
CYP2D6 K_m → (*E*)-4-OH-DE-Clom	0.49	µmol/l	Literature	0.49[b]	[17, 18]	Michaelis-Menten constant
CYP2D6 k_{cat} → (*E*)-4-OH-DE-Clom	64.5[c]	1/min	Optimized	-	-	Catalytic rate conbstant
CYP2D6 K_m → undef.	0.97	µmol/l	Literature	0.97[b]	[17, 18]	Michaelis-Menten constant
CYP2D6 k_{cat} → undef.	5.8[c]	1/min	Optimized	-	-	Catalytic rate constant
CYP3A4 K_m → undef.	0.97	µmol/l	Literature	0.97[b]	[17, 18]	Michaelis-Menten constant
CYP3A4 k_{cat} → undef.	0.8	1/min	Optimized	-	-	Catalytic rate constant
GFR fraction	0.10	-	Optimized	-	-	Fraction of filtered drug in the urine
EHC continuous fraction	1.00	-	Assumed	-	-	Fraction of bile continually released
Partition coefficients	Diverse[d]	-	Calculated	R&R	[32, 33]	Cell to plasma partition coefficients
Cellular permeability	Diverse[d]	cm/min	Calculated	Ch. dep. Schmitt	[29]	Permeability into the cellular space

Ch. dep. Schmitt: Charge dependent Schmitt caclulation method, **CYP**: cytochrome P450,
(*E*)-4-OH-DE-Clom: (*E*)-4-hydroxy-N-desethylclomiphene, **EHC**: enterohepatic circulation, **GFR**: glomerular filtration rate,
IM: intermediate metabolizers, **IVSF**: *in vitro* scaling factor, **NM**: normal metabolizers, **R&R**: Rodgers and Rowland calculation method,
UM: ultrarapid metabolizers, **undef.**: undefined metabolite

[a] f_u was estimated with the classification model by Watanabe et al. [21]

[b] K_m values from literature were adapted with the calculated $f_{u,inc}$=0.059, considering nonspecific binding in *in vitro* assays according to [15, 16]

[c] Only CYP2D6 k_{cat} values of NM are shown while IM- and UM-k_{cat} values were extrapolated according to Equation 1 in the main manuscript (IVSFs represented in Table S8)

[d] values differ across the organs

Table S6. Drug-dependent parameters for (*E*)-4-hydroxyclomiphene.

Parameter	Value	Unit	Source	Literature	Reference	Description
MW	421.97	g/mol	Literature	421.97	[34]	Molecular weight
pK_a (acid)	8.64	-	Literature	8.64	[34]	Acid dissociation constant
pK_a (base)	7.90	-	Optimized	9.41	[34]	Acid dissociation constant
Solubility (pH 6.5)	0.06	mg/ml	Literature	0.06	[34]	Solubility
logP	5.50	-	Optimized	5.31, 5.64	[25, 34]	Lipophilicity
f_u	0.45	%	Optimized	0.6, 1.33[a]	[21, 35]	Fraction unbound
CYP2D6 K_m → undef.	3.60	µmol/l	Literature	3.60[b]	[19]	Michaelis-Menten constant
CYP2D6 k_{cat} → undef.	855.2[c]	1/min	Optimized	-	-	Catalytic rate constant
CYP3A4 K_m → (*E*)-4-OH-DE-Clom	3.40	µmol/l	Literature	3.40[b]	[17, 18]	Michaelis-Menten constant
CYP3A4 k_{cat} → (*E*)-4-OH-DE-Clom	19.5	1/min	Optimized	-	-	Catalytic rate constant
Unspec. hep. CL → undef.	23.78	1/min	Optimized	-	-	Elimination from plasma (first-order process in the liver)
GFR fraction	0.24	-	Optimized	-	-	Fraction of filtered drug in the urine
EHC continuous fraction	1.00	-	Assumed	-	-	Fraction of bile continually released
Partition coefficients	Diverse[d]	-	Calculated	Berez.	[36]	Cell to plasma partition coefficients
Cellular permeability	2.23	cm/min	Calculated	PK-Sim	[37]	Permeability into the cellular space

Berez.: Berezhkovskiy calculation method, **CYP**: cytochrome P450, **(*E*)-4-OH-DE-Clom**: (*E*)-4-hydroxy-N-desethylclomiphene, **EHC**: enterohepatic circulation, **GFR**: glomerular filtration rate, **IM**: intermediate metabolizers, **IVSF**: *in vitro* scaling factor, **NM**: normal metabolizers, **PK-Sim**: PK-Sim standard calculation method, **UM**: ultrarapid metabolizers, **undef.**: undefined metabolite, **unspec. hep. CL**: unspecific hepatic clearance

[a] f_u was estimated with the classification model by Watanabe et al. [21]

[b] K_m values from literature were adapted with the calculated $f_{u,inc}$=0.099, considering nonspecific binding in *in vitro* assays according to [15, 16]

[c] Only CYP2D6 k_{cat} values of NM are shown while IM- and UM-k_{cat} values were extrapolated according to Equation 1 in the main manuscript (IVSFs represented in Table S8)

[d] values differ across the organs

Table S7. Drug-dependent parameters for (*E*)-4-hydroxy-N-desethyl-clomiphene.

Parameter	Value	Unit	Source	Literature	Reference	Description
MW	393.91	g/mol	Literature	393.91	[38]	Molecular weight
pK_a (acid)	8.69	-	Literature	8.69	[38]	Acid dissociation constant
pK_a (base)	9.65	-	Literature	9.65	[38]	Acid dissociation constant
Solubility (pH 6.5)	0.17	mg/ml	Literature	0.17	[38]	Solubility
logP	3.71	-	Optimized	4.47	[38]	Lipophilicity
f_u	1.32	%	Calculated	1.32[a]	[21]	Fraction unbound
CYP2D6 K_m → undef.	8.86	µmol/l	Assumed	8.86[b,c]	-	Michaelis-Menten constant
CYP2D6 k_{cat} → undef.	211.7[d]	1/min	Optimized	-	-	Catalytic rate constant
Unsp. hep. CL → undef.	8.50	1/min	Optimized	-	-	Elimination from plasma (first-order process in the liver)
GFR fraction	0.13	-	Optimized	-	-	Fraction of filtered drug in the urine
EHC continuous fraction	1.00	-	Assumed	-	-	Fraction of bile continually released
Partition coefficients	Diverse[e]	-	Calculated	Schmitt	[28]	Cell to plasma partition coefficients
Cellular permeability	Diverse[e]	cm/min	Calculated	Ch. dep. Schmitt	[29]	Permeability into the cellular space

Ch. dep. Schmitt: Charge dependent Schmitt calculation method, **CYP**: cytochrome P450, **(*E*)-4-OH-Clom**: (*E*)-4-hydroxyclomiphene, **(*E*)-4-OH-DE-Clom**: (*E*)-4-hydroxy-N-desethylclomiphene, **EHC**: enterohepatic circulation, **GFR**: glomerular filtration rate, **IM**: intermediate metabolizers, **IVSF**: *in vitro* scaling factor, **NM**: normal metabolizers, **UM**: ultrarapid metabolizers, **undef.**: undefined metabolite, **unsp. hep. CL**: unspecific hepatic clearance

[a] f_u was estimated with the classification model by Watanabe et al. [21]

[b] K_m values from literature were adapted with the calculated $f_{u,inc}$=0.243, considering nonspecific binding in *in vitro* assays according to [15, 16]

[c] K_m value for CYP2D6-mediated hydroxylation of (*E*)-4-OH-DE-Clom was assumed to be equal to K_m value of the CYP2D6-mediated hydroxylation of (*E*)-4-OH-Clom

[d] Only CYP2D6 k_{cat} values of NM are shown while IM- and UM-k_{cat} values were extrapolated according to Equation 1 in the main manuscript (IVSFs represented in Table S8)

[e] values differ across the organs

S1.5. Calculation of Fractions Metabolized

The fraction metabolized (f_m) of (*E*)-Clom via CYP2D6 was calculated according to Equation S1, using the observed relative AUC_{last} increase between the PM population and the control group (normal metabolizers (NM)) [39]. Calculation yielded a CYP2D6 f_m of ~90%. In addition, data from the CYP2D6 NM population in the clarithromycin DDI scenario (CYP3A4 inhibition) was used to estimate f_m of (*E*)-Clom via CYP3A4 to inform model development regarding CYP3A4-dependent (*E*)-Clom degradation. For this, the observed relative AUC_{last} increase in the NM population between the DDI scenario with CYP3A4 inhibition and the control scenario without inhibition was used, yielding a CYP3A4 f_m of about 13%. Of note, a complete CYP3A4 inhibition through clarithromycin was assumed, given the strong and mechanism-based inhibition through clarithromycin, which was administered twice a day for four days before the victim drug, (*E*)-Clom, was administered.

$$\frac{1}{1-f_m} = \frac{AUC_{last,effect,\,AS=i}}{AUC_{last,control}} \tag{S1}$$

In case of CYP2D6 f_m calculation, $AUC_{last,\ effect}$ represents the AUC_{last} of (*E*)-Clom for the PM population, while $AUC_{last,\ control}$ represents the AUC_{last} of (*E*)-Clom for the NM population. For

calculation of the CYP3A4 f_m, $AUC_{last,\ effect}$ represents the AUC_{last} of (*E*)-Clom for the NM population in the DDI scenario with clarithromycin, while $AUC_{last,\ control}$ represents the AUC_{last} of (*E*)-Clom for the NM population without concomitant clarithromycin administration.

S1.6. Formulations

Dissolution profiles for clomiphene citrate tablets and (*E*)-Clom citrate capsules were not publicly available. However, according to the U.S. pharmacopoeia, the dissolution rate within the first 30 minutes of clomiphene citrate tablets is required to be at least 75% [40]. This information was used to inform the dissolution shape and time (50% dissolved) parameters of a Weibull function, which was employed as the formulation in PK-Sim® (mathematical implementation see Equation S2 and Equation S3). The respective parameter values are represented in Table S4.

$$m = 1 - exp\left(\frac{-(t - T_{lag})^{\beta}}{\alpha}\right) \tag{S2}$$

$$with\ \alpha = (T_d)^{\beta} \tag{S3}$$

Here, m represents the fraction of dissolved drug at time t, T_{lag} is the lag time before onset of dissolution, α is the scaling parameter, β the shape parameter and T_d the time needed to dissolve 63% of the formulation [37].

S1.7. Handling Data Below the Lower Limit of Quantification (LLOQ)

In the pharmacokinetic panel study used for model building and evaluation, 9% of measured concentrations fell below the lower limit of quantification (LLOQ). For handling lower limit of quantification (LLOQ) data, a combination of the M5 and M6 method [41] was used. Below limit of quantification (BLQ) individual plasma concentrations were substituted by LLOQ/2. Subsequently, mean concentrations were calculated for each CYP2D6 activity score (AS) and only the first BLQ data was used for model building and evaluation, while subsequent concentrations were excluded. During the initial period of metabolite formation, BLQ data also appeared in the ascending branch of the plasma profiles. In this case, the last BLQ concentration was included in the data, while BLQ concentrations before this time point were discarded.

S2. Drug-Gene-Interaction (DGI) Modeling

S2.1. CYP2D6 *in vitro* Scaling Factors

The estimated CYP2D6 k_{cat} values for the NM population were extrapolated to the intermediate metabolizers (IM) (AS=0.5, AS=0.75 and AS=1) and ultrarapid metabolizers (UM) populations according to Equation 1 in the main manuscript, using *in vitro* scaling factors (IVSFs). Determination of IVSFs were based on AS-specific *in vitro* metabolite formation rates relative to the corresponding formation rate in NM as a reference. The respective IVSFs for each CYP2D6-dependent pathway are depicted in Table S8. Measured *in vitro* data for (*E*)-4-OH-Clom and (*E*)-4-OH-DE-Clom AS-specific formation rates were available, while mean values were assumed for the remaining CYP2D6-dependent metabolic pathways [17].

Table S8. Employed *in vitro* scaling factors (IVSFs) for individual CYP2D6 activity scores.

CYP2D6-mediated metabolic pathways	AS=0	AS=0.5	AS=0.75	AS=1	AS=2	AS=3
(*E*)-Clom → (*E*)-4-OH-Clom	0	0.19	0.27	0.57	1	1.52
(*E*)-Clom → (*E*)-DE-Clom	0	0.17	0.23	0.51	1	1.41
(*E*)-Clom → undef.	0	0.17	0.23	0.51	1	1.41
(*E*)-4-OH-Clom → undef.	0	0.17	0.23	0.51	1	1.41
(*E*)-4-OH-DE-Clom → undef.	0	0.17	0.23	0.51	1	1.41
(*E*)-DE-Clom → (*E*)-4-OH-DE-Clom	0	0.16	0.19	0.44	1	1.30
(*E*)-DE-Clom → undef.	0	0.17	0.23	0.51	1	1.41

AS: CYP2D6 activity score, **CYP**: cytochrome P450, ***(E)*-4-OH-Clom**: (*E*)-4-hydroxyclomiphene, ***(E)*-4-OH-DE-Clom**: (*E*)-4-hydroxy-N-desethylclomiphene, ***(E)*-Clom**: (*E*)-clomiphene, ***(E)*-DE-Clom**: (*E*)-N-desethylclomiphene, **undef.**: undefined metabolite

S3. Drug-Drug-(Gene)-Interaction (DD(G)I) Modeling

S3.1. Clarithromycin and Paroxetine

Clarithromycin acts as a mechanism-based inhibitor of CYP3A4, while paroxetine inhibits CYP2D6 and to a minor extent CYP3A4 [42]. Inhibition mechanisms of CYP3A4 and CYP2D6 were implemented according to the PK-Sim® manual [37]. Two previously published PBPK models of clarithromycin [43] and paroxetine [44] were applied and coupled with the developed parent-metabolite PBPK model of (*E*)-Clom to assess the model prediction performance in the DD(G)I setting. Interaction parameters were used as published in the respective perpetrator PBPK models.

S4. PBPK Model Evaluation

S4.1. Evaluation of the DGI Model

S4.1.1. Plasma Profiles (Linear Scale)

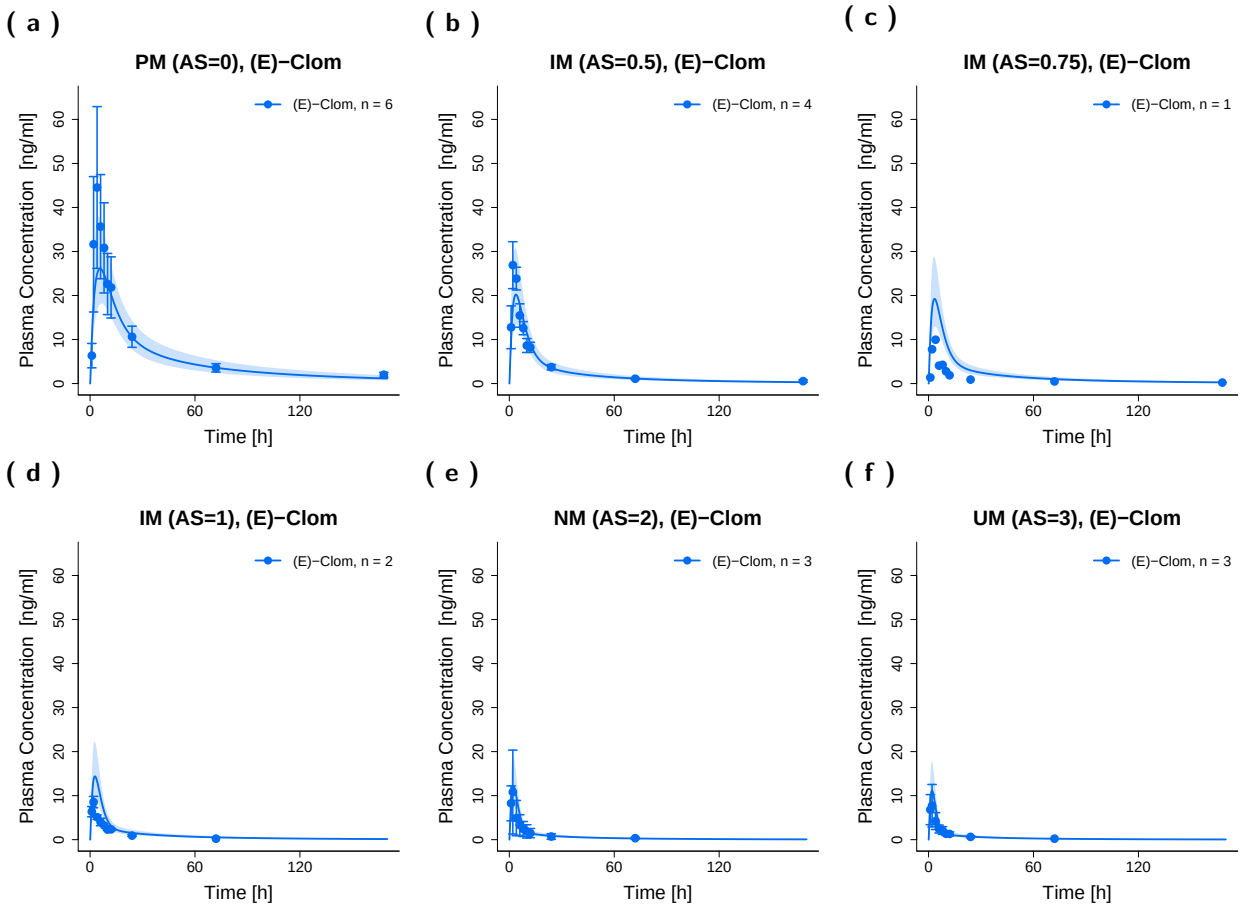

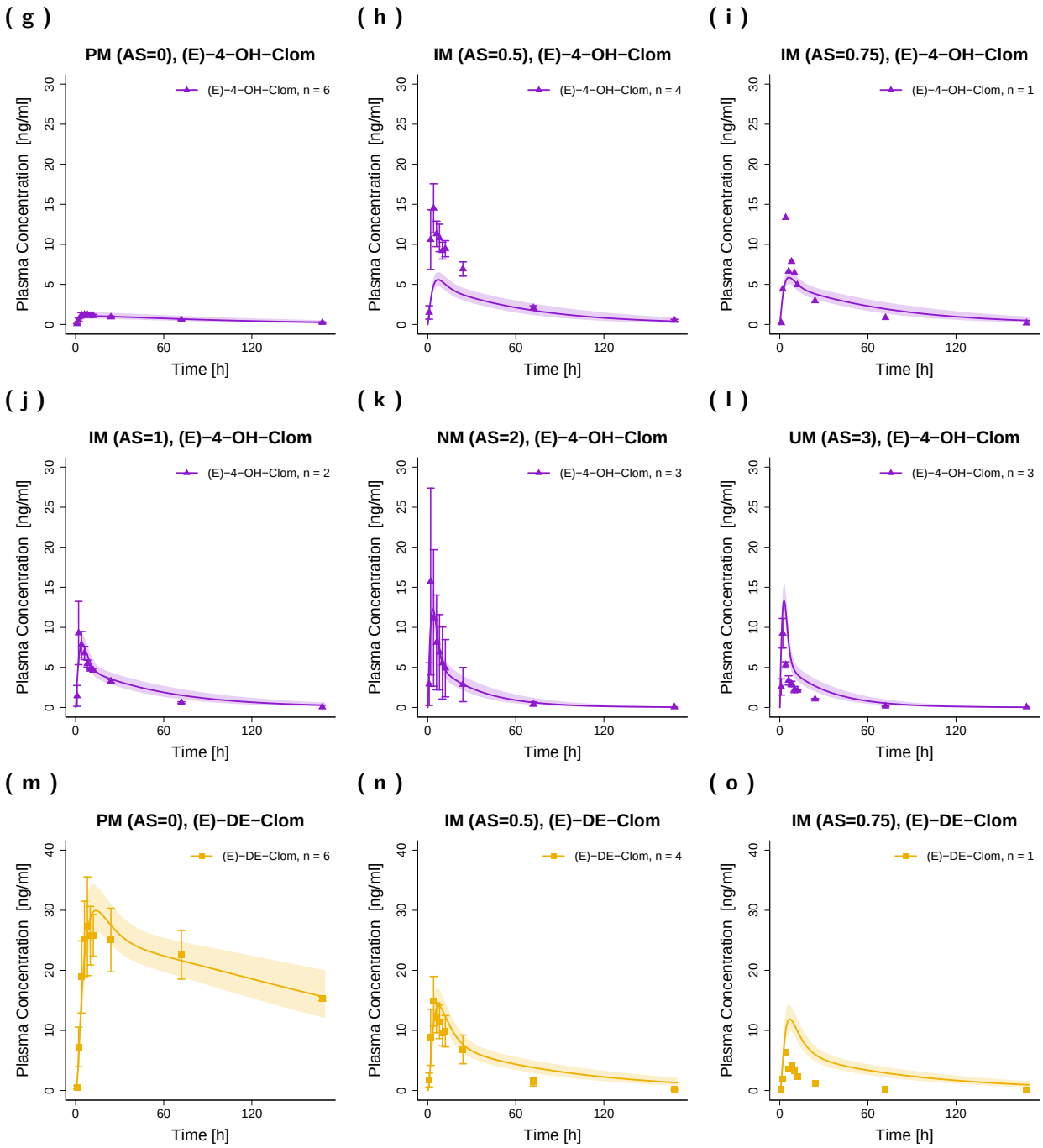
(g)
PM (AS=0), (E)−4−OH−Clom
(E)−4−OH−Clom, n = 6
(h)
IM (AS=0.5), (E)−4−OH−Clom
(E)−4−OH−Clom, n = 4
(i)
IM (AS=0.75), (E)−4−OH−Clom
(E)−4−OH−Clom, n = 1
(j)
IM (AS=1), (E)−4−OH−Clom
(E)−4−OH−Clom, n = 2
(k)
NM (AS=2), (E)−4−OH−Clom
(E)−4−OH−Clom, n = 3
(l)
UM (AS=3), (E)−4−OH−Clom
(E)−4−OH−Clom, n = 3
(m)
PM (AS=0), (E)−DE−Clom
(E)−DE−Clom, n = 6
(n)
IM (AS=0.5), (E)−DE−Clom
(E)−DE−Clom, n = 4
(o)
IM (AS=0.75), (E)−DE−Clom
(E)−DE−Clom, n = 1
Plasma Concentration [ng/ml]
Time [h]

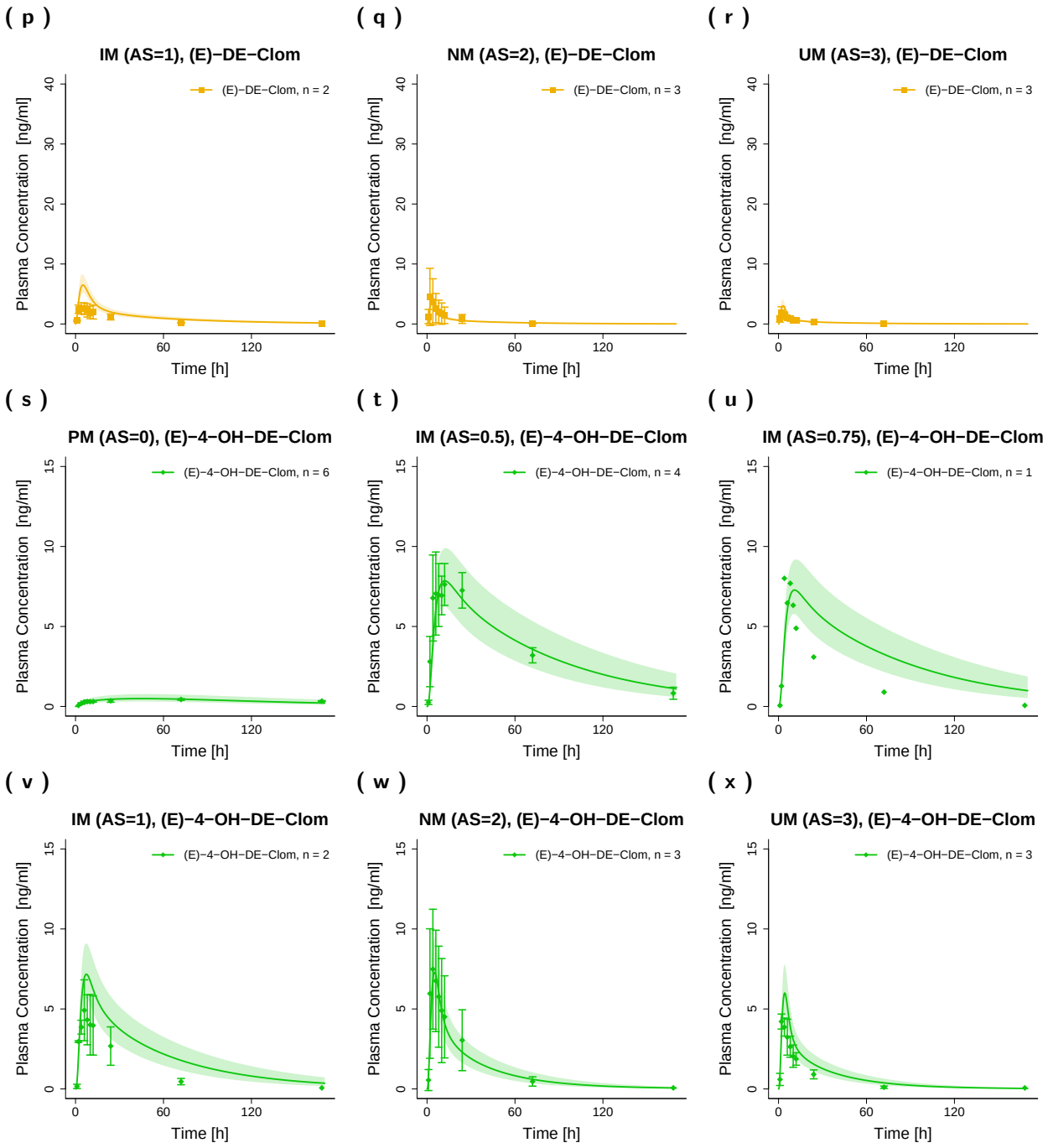

Figure S1. Predicted and observed plasma concentration-time profiles (linear scale) of (E)-Clom (a–f), (*E*)-4-OH-Clom (g–l), (*E*)-DE-Clom (m–r) and (*E*)-4-OH-DE-Clom (s–x) for DGI scenarios. Solid lines de-pict predicted geometric mean concentration-time profiles in PM, IM, NM and UM. The respective semitranspar-ent areas show the geometric standard deviation of the population simulations (n=1000). Mean observed data are shown as symbols with the corresponding standard deviation. **AS**, CYP2D6 activity score; **DGI**, drug-gene inter-action; **(*E*)-4-OH-Clom**, (*E*)-4-hydroxyclomiphene; **(*E*)-4-OH-DE-Clom**, (*E*)-4-hydroxy-N-desethylclomiphene;**(*E*)-Clom**, (*E*)-clomiphene; **(*E*)-DE-Clom**, (*E*)-N-desethylclomiphene; **IM**, intermediate metabolizers; **n**, num-ber of subjects; **NM**, normal metabolizers; **PM**, poor metabolizers; **UM**, ultrarapid metabolizers.

S4.1.2. Plasma Profiles (Semilogarithmic Scale)

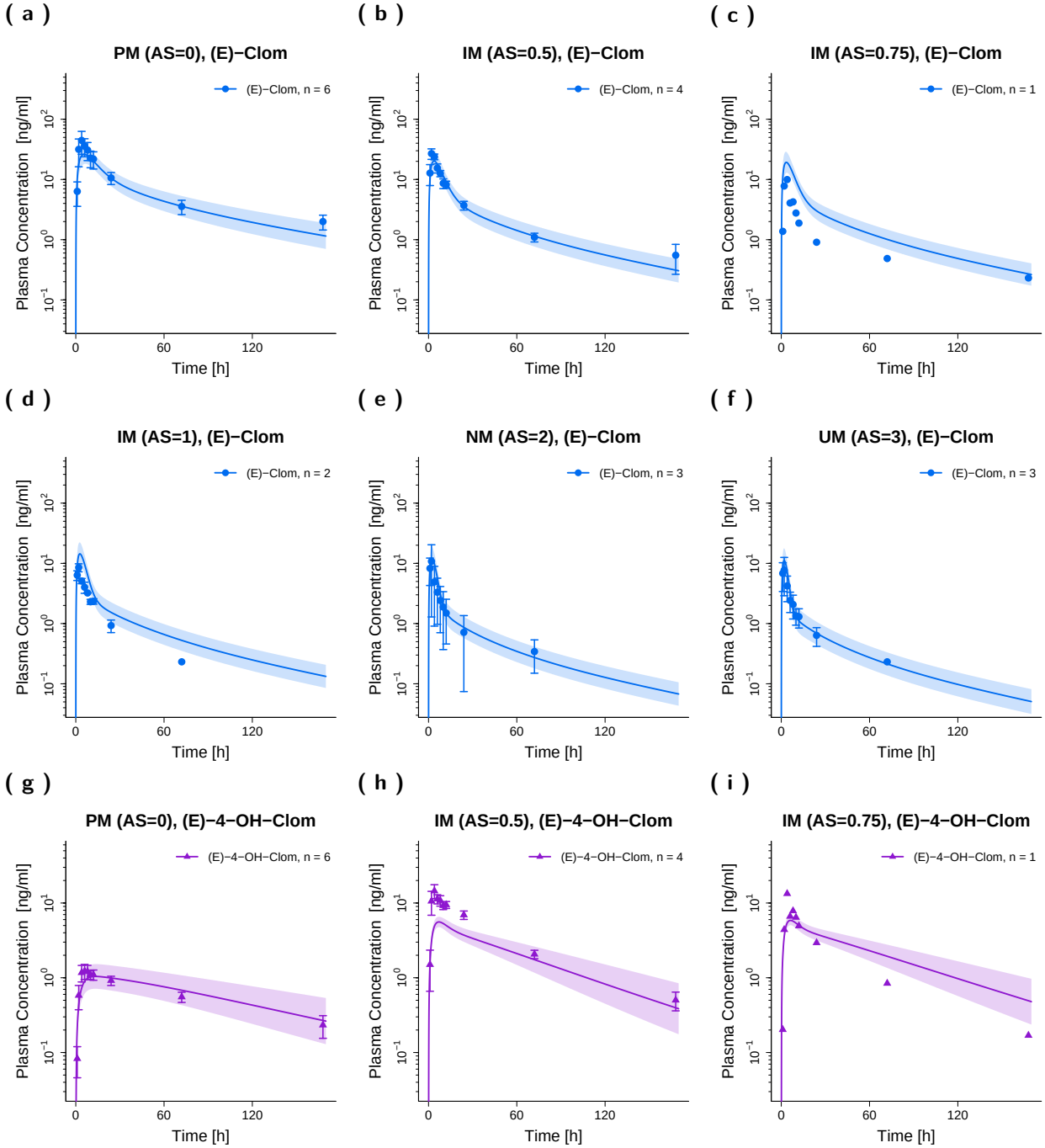

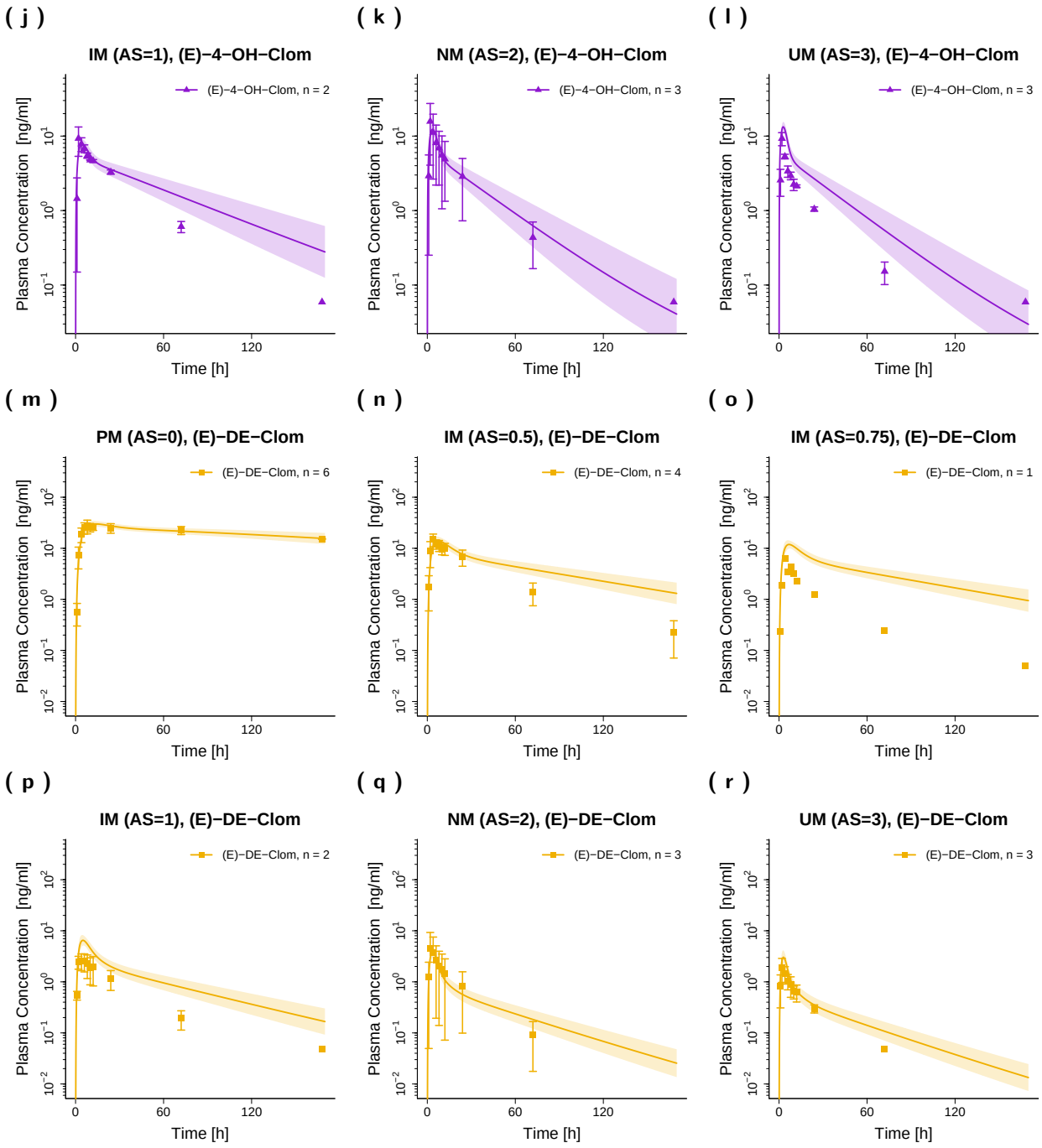
(j)
IM (AS=1), (E)−4−OH−Clom
(E)−4−OH−Clom, n = 2
(k)
NM (AS=2), (E)−4−OH−Clom
(E)−4−OH−Clom, n = 3
(l)
UM (AS=3), (E)−4−OH−Clom
(E)−4−OH−Clom, n = 3
(m)
PM (AS=0), (E)−DE−Clom
(E)−DE−Clom, n = 6
(n)
IM (AS=0.5), (E)−DE−Clom
(E)−DE−Clom, n = 4
(o)
IM (AS=0.75), (E)−DE−Clom
(E)−DE−Clom, n = 1
(p)
IM (AS=1), (E)−DE−Clom
(E)−DE−Clom, n = 2
(q)
NM (AS=2), (E)−DE−Clom
(E)−DE−Clom, n = 3
(r)
UM (AS=3), (E)−DE−Clom
(E)−DE−Clom, n = 3
Plasma Concentration [ng/ml]
Time [h]

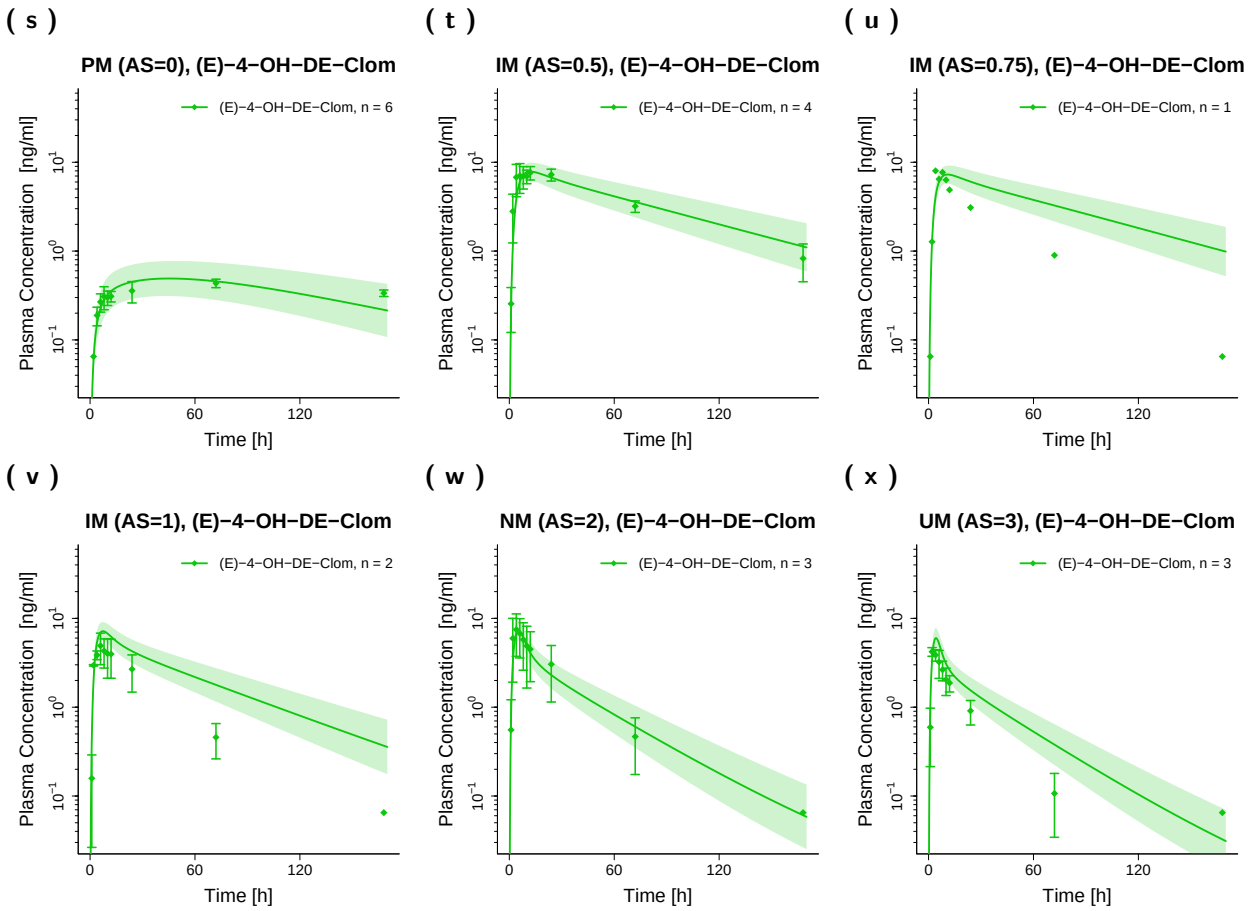

Figure S2. Predicted and observed plasma concentration-time profiles (semilogarithmic scale) of (*E*)-Clom (a–f), (*E*)-4-OH-Clom (g–l), (*E*)-DE-Clom (m–r) and (*E*)-4-OH-DE-Clom (s–x) for DGI scenarios. Solid lines depict predicted geometric mean concentration-time profiles in the PM, IM, NM and UM populations. The respective semitransparent areas show the geometric standard deviation of the population simulations (n=1000). Mean observed data are shown as symbols with the corresponding standard deviation. **AS**, CYP2D6 activity score; **DGI**, drug-gene interaction; **(*E*)-4-OH-Clom**, (*E*)-4-hydroxyclomiphene; **(*E*)-4-OH-DE-Clom**, (*E*)-4-hydroxy-N-desethylclomiphene; (E)-Clom, (E)-clomiphene; (E)-DE-Clom, (E)-N-desethylclomiphene; IM, intermediate metabolizers; n, number of subjects; NM, normal metabolizers; PM, poor metabolizers; UM, ultrarapid metab-olizers.

S4.1.3. Goodness-of-Fit Plots

(a) AUC_{last}

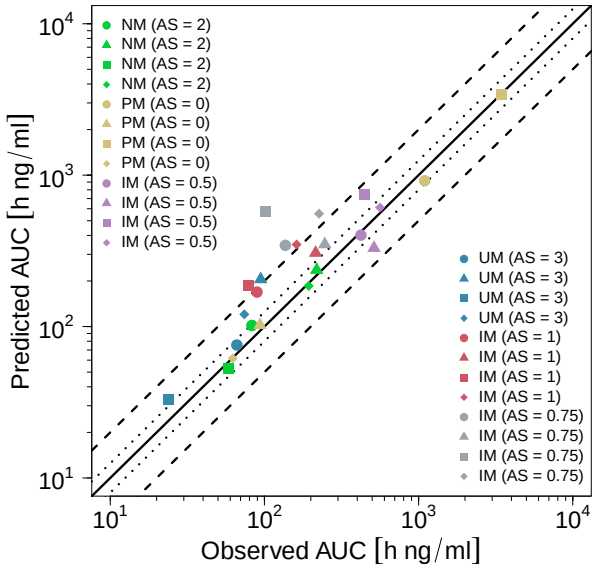

(b) C_{max}

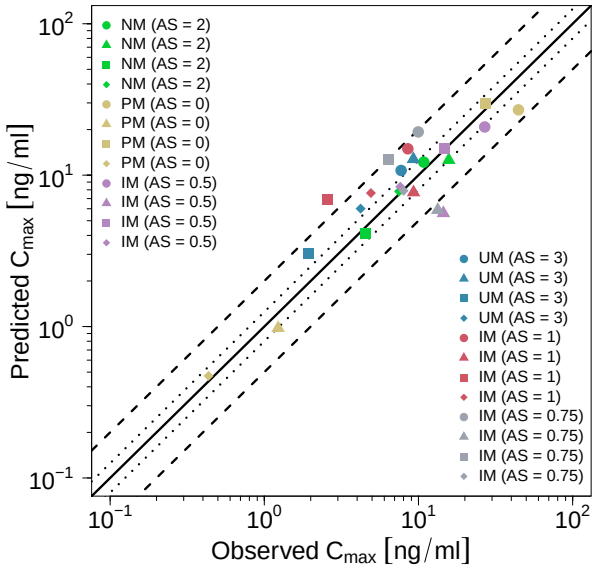

(c) Plasma concentrations

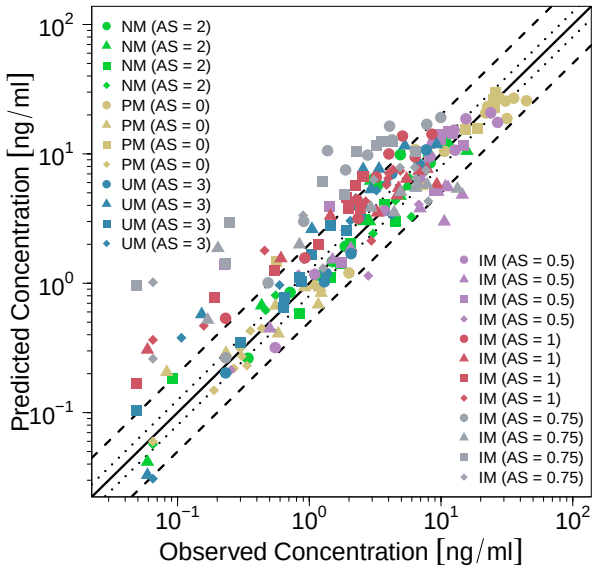

Figure S3. Predicted versus observed AUClast (a), Cmax (b) and plasma concentrations (c) of (E)-Clom (circles), (*E*)-4-OH-Clom (triangles), (*E*)-DE-Clom (squares) and (*E*)-4-OH-DE-Clom (diamonds) in PM, IM, NM and UM (DGI scenarios). The black solid lines mark the lines of identity. Black dotted lines indicate 1.25-fold, black dashed lines indicate 2-fold deviation. **AS**, CYP2D6 activity score; **DGI**, drug-gene interaction;**(*E*)-4-OH-Clom**, (*E*)-4-hydroxyclomiphene; **(*E*)-4-OH-DE-Clom**, (*E*)-4-hydroxy-N-desethylclomiphene; **(*E*)-Clom**, (*E*)-clomiphene; **(*E*)-DE-Clom**, (*E*)-N-desethylclomiphene; **IM**, intermediate metabolizers; **NM**, normal metabolizers; **PM**, poor metabolizers; **UM**, ultrarapid metabolizers.

(a) AUC_{last}

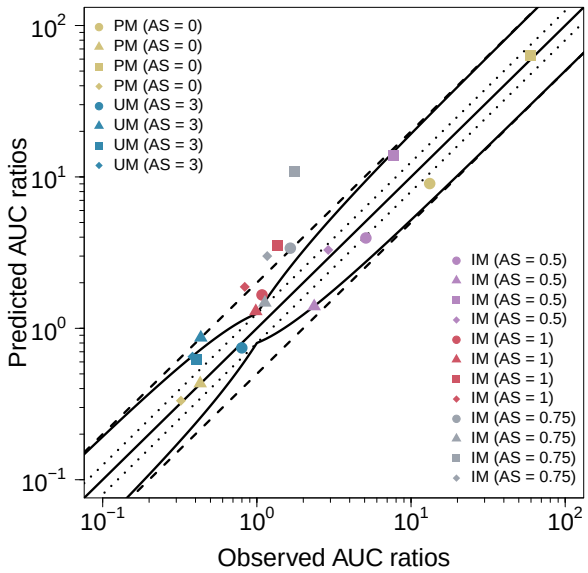

(b) C_{max}

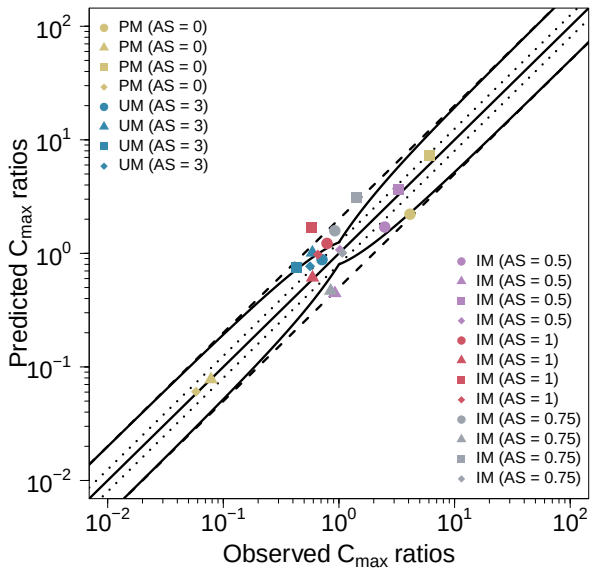

Figure S4. Predicted versus observed DGI AUC_{last} (a) and C_{max} (b) ratios of (*E*)-Clom (circles), (*E*)-4-OH-Clom (tri-angles), (*E*)-DE-Clom (squares) and (*E*)-4-OH-DE-Clom (diamonds) in PM, IM and UM. The straight black lines mark the lines of identity, the curved solid black lines show the limits of the predictive measure proposed by Guest et al. with 1.25-fold variability [46]. Black dotted lines indicate 1.25-fold, black dashed lines indicate 2-fold deviation. **AS**, CYP2D6 activity score; **(*E*)-4-OH-Clom**, (*E*)-4-hydroxyclomiphene; **(*E*)-4-OH-DE-Clom**, (*E*)-4-hydroxy-N-desethylclomiphene; (*E*)-**Clom**, (*E*)-clomiphene; (*E*)-**DE-Clom**, (E)-N-desethylclomiphene; **IM**, intermediate metabolizers; **PM**, poor metabolizers; **UM**, ultrarapid metabolizers.

S4.1.4. Renal Excretion Profiles (Linear Scale)

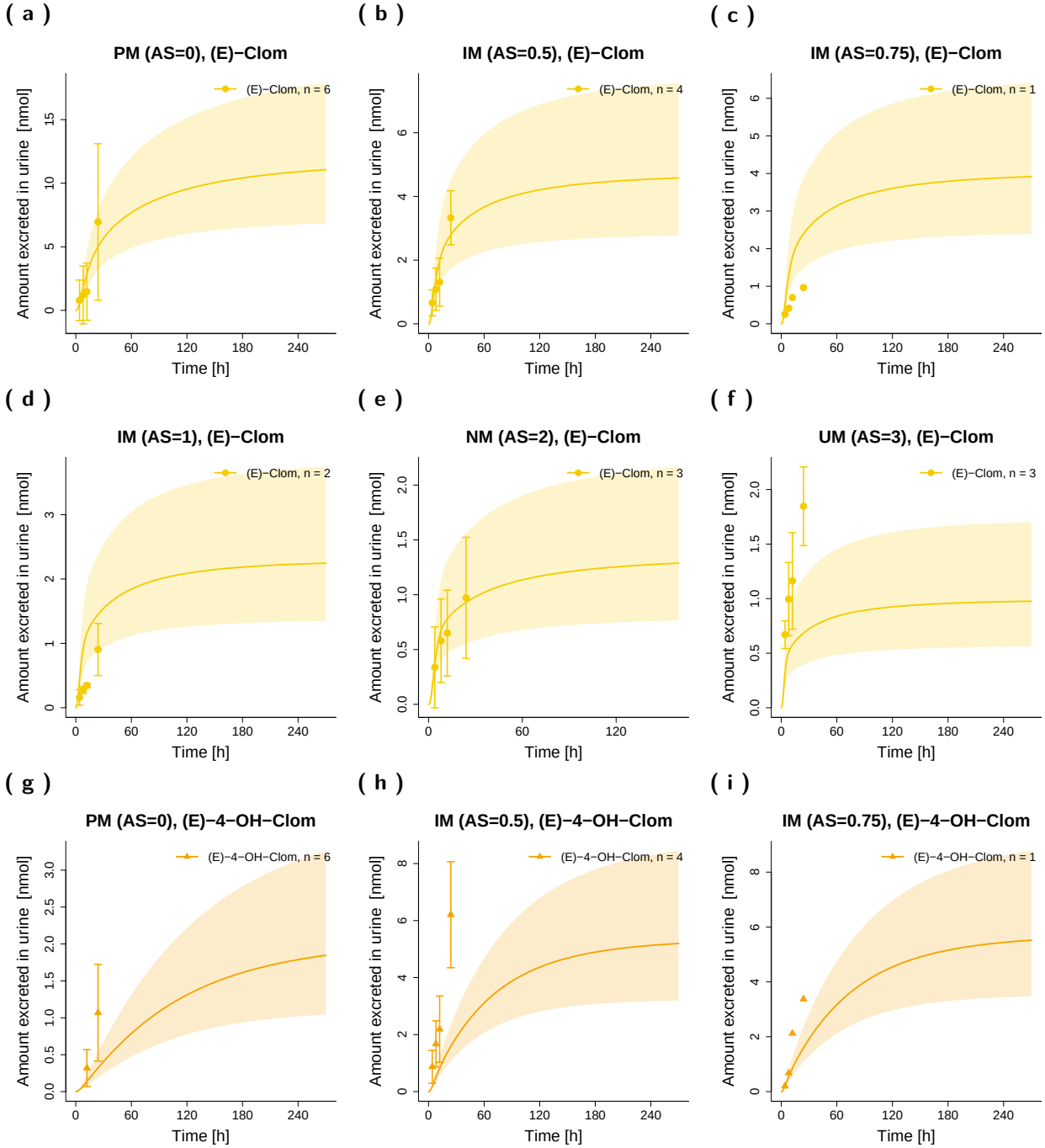

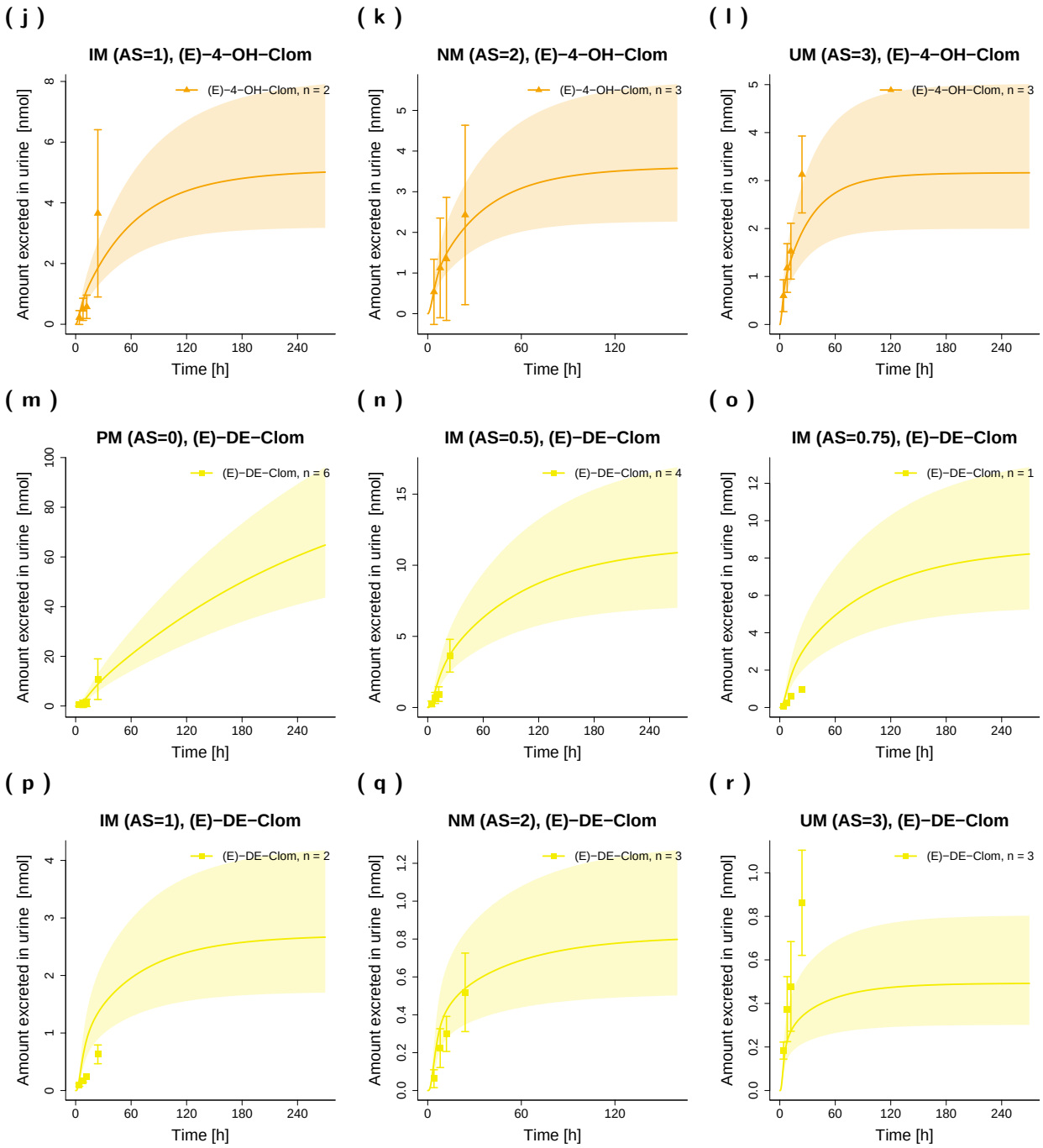
(j)
IM (AS=1), (E)−4−OH−Clom
(E)−4−OH−Clom, n = 2
(k)
NM (AS=2), (E)−4−OH−Clom
(E)−4−OH−Clom, n = 3
(l)
UM (AS=3), (E)−4−OH−Clom
(E)−4−OH−Clom, n = 3
(m)
PM (AS=0), (E)−DE−Clom
(E)−DE−Clom, n = 6
(n)
IM (AS=0.5), (E)−DE−Clom
(E)−DE−Clom, n = 4
(o)
IM (AS=0.75), (E)−DE−Clom
(E)−DE−Clom, n = 1
(p)
IM (AS=1), (E)−DE−Clom
(E)−DE−Clom, n = 2
(q)
NM (AS=2), (E)−DE−Clom
(E)−DE−Clom, n = 3
(r)
UM (AS=3), (E)−DE−Clom
(E)−DE−Clom, n = 3
Amount excreted in urine [nmol]
Time [h]

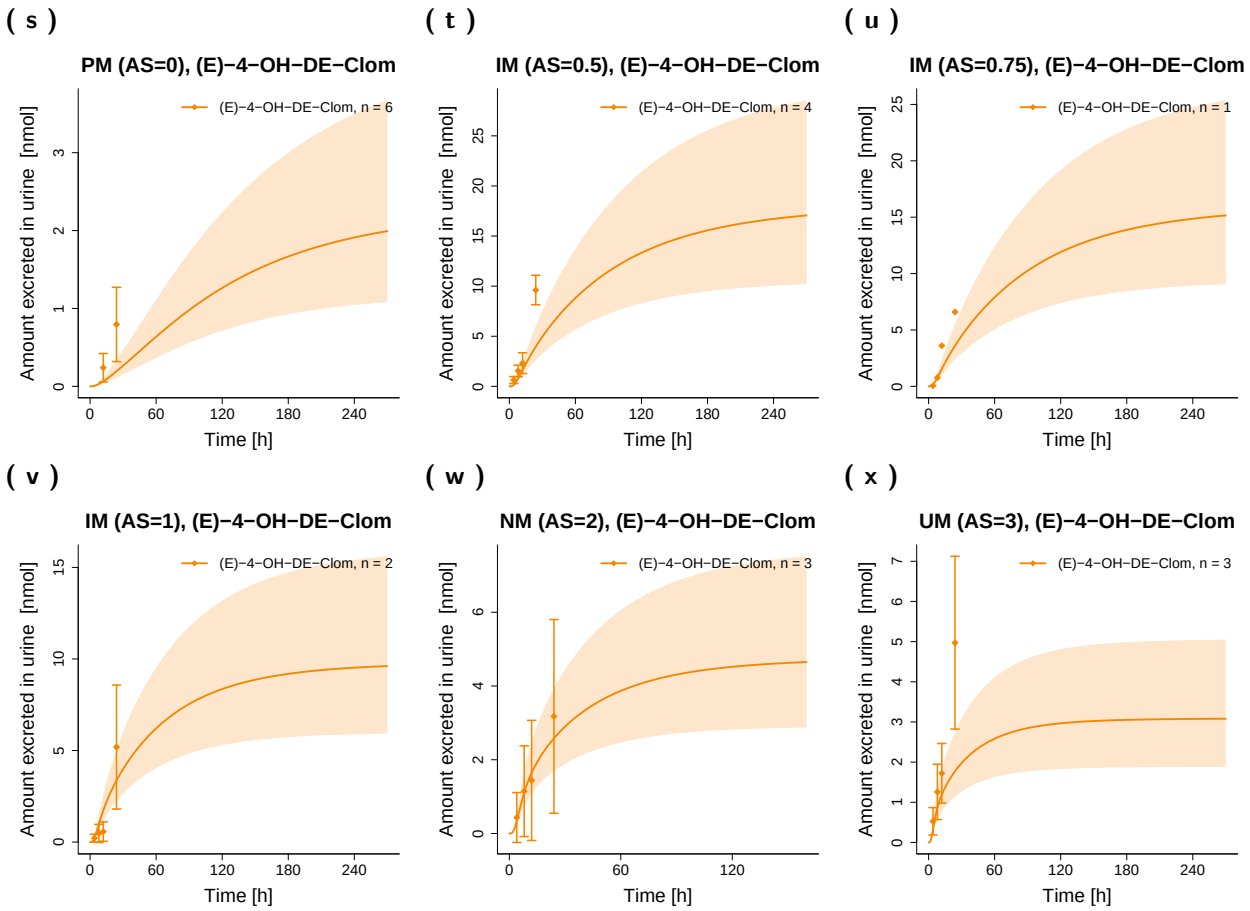

Figure S5. Predicted and observed renal excretion profiles (linear scale) of (E)-Clom (a–f), (E)-4-OH-Clom (g–l), (*E*)-DE-Clom (m–r) and (*E*)-4-OH-DE-Clom (s–x) for DGI scenarios. Solid lines depict predicted geometric mean profiles in PM, IM, NM and UM. The respective semitransparent areas show the geometric standard deviation of the population simulations (n=1000). Mean observed data are shown as symbols with the corresponding standard deviation. **AS**, CYP2D6 activity score; **DGI**, drug-gene interaction; **(*E*)-4-OH-Clom**, (*E*)-4-hydroxyclomiphene; **(*E*)-4-OH-DE-Clom**, (*E*)-4-hydroxy-N-desethylclomiphene; **(*E*)-Clom**, (*E*)-clomiphene; **(*E*)-DE-Clom**, (*E*)-N-desethylclomiphene; **IM**, intermediate metabolizers; **n**, number of subjects; **NM**, normal metabolizers, **PM**, poor metabolizers; **UM**, ultrarapid metabolizers.

S4.1.5. Plasma Profiles from Literature (Linear Scale)

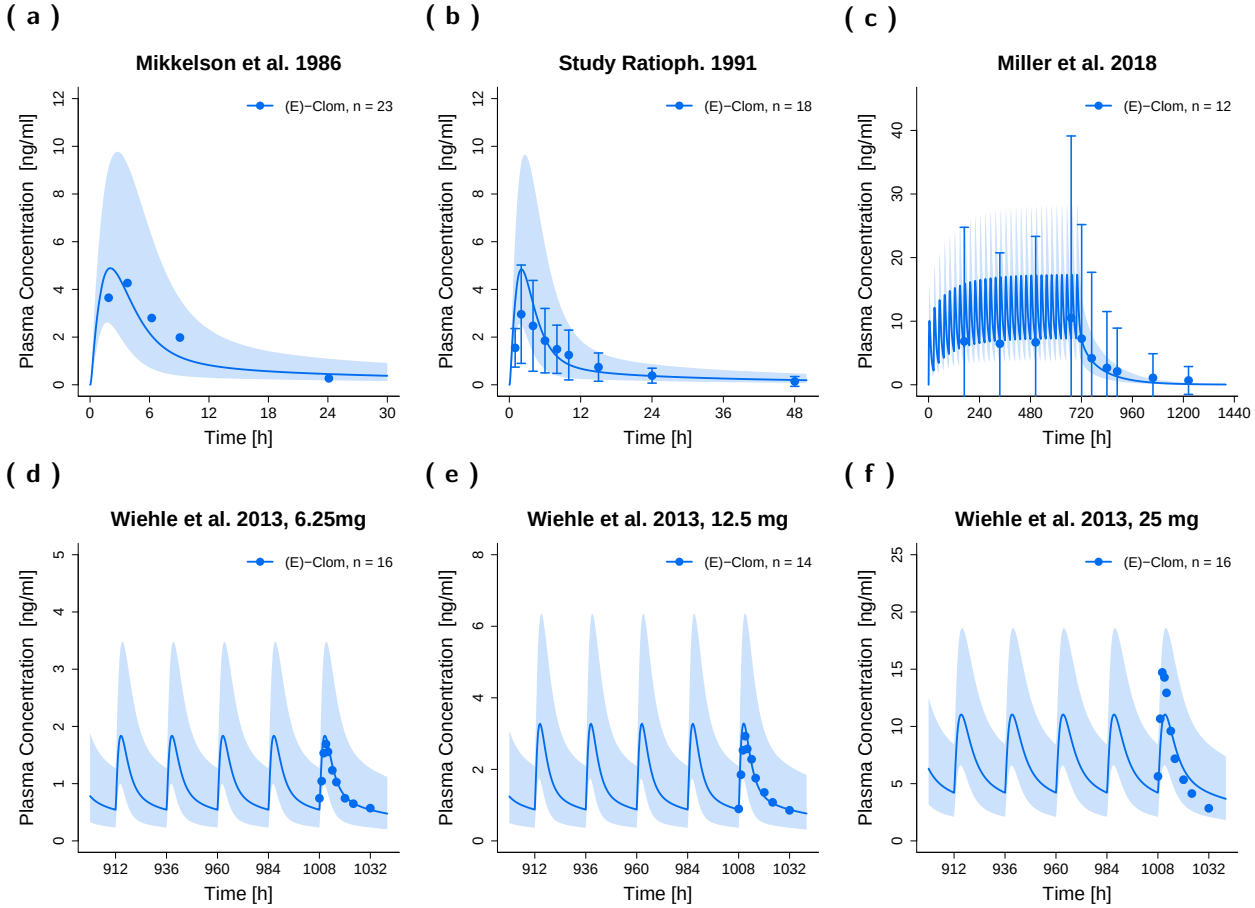

Figure S6. Predicted and observed plasma concentration-time profiles (linear scale) of digitized studies from literature after single (a,b) and multiple (c–f) dosing. Solid lines depict predicted geometric mean concentration-time profiles of (*E*)-Clom. The respective semitransparent areas show the geometric standard deviation of the population simulations (n=1000). Mean observed data are shown as symbols with the corresponding standard deviation. **(*E*)-Clom**, (*E*)-clomiphene; **n**, number of subjects; **Ratioph.**, Ratiopharm® GmbH.

S4.1.6. Plasma Profiles from Literature (Semilogarithmic Scale)

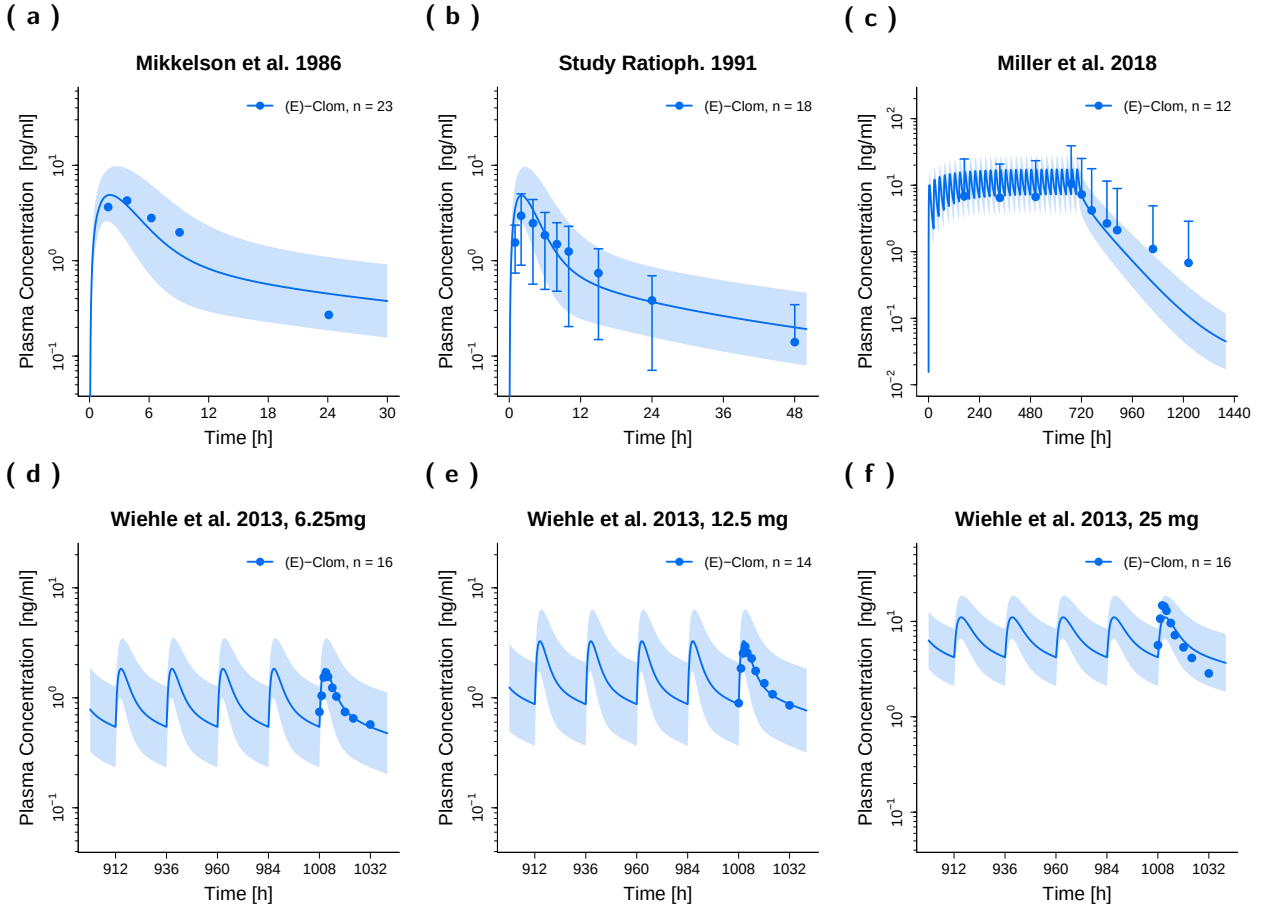

Figure S7. Predicted and observed plasma concentration-time profiles (semilogarithmic scale) of digitized studies from literature after single (a,b) and multiple (c–f) dosing. Solid lines depict predicted geometric mean concentration-time profiles o f (*E*) -Clom. T he r espective s emitransparent a reas s how t he g eometric standard deviation of the population simulations (n=1000). Mean observed data are shown as symbols with the corresponding standard deviation. **(*E*)-Clom**, (*E*)-clomiphene; **n**, number of subjects; **Ratioph.**, Ratiopharm® GmbH.

S4.1.7. Goodness-of-Fit Plots (from Literature)

(a) AUC_{last}

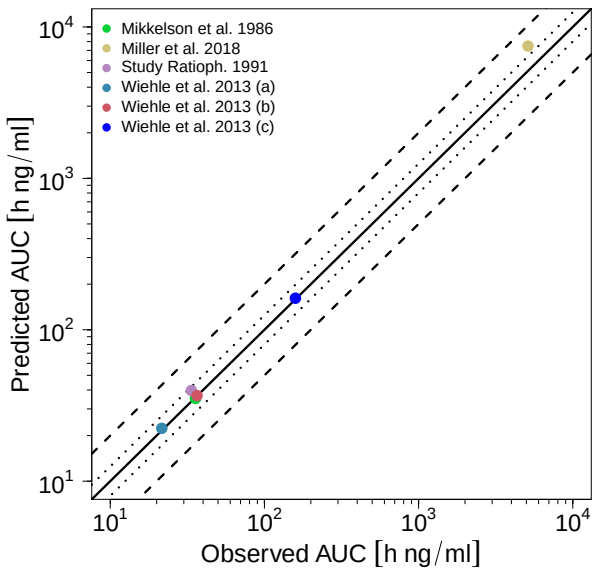

(b) C_{max}

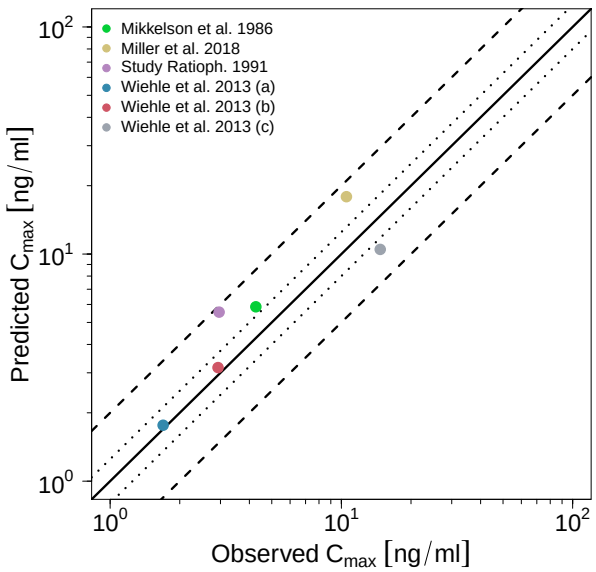

(c) Plasma concentrations

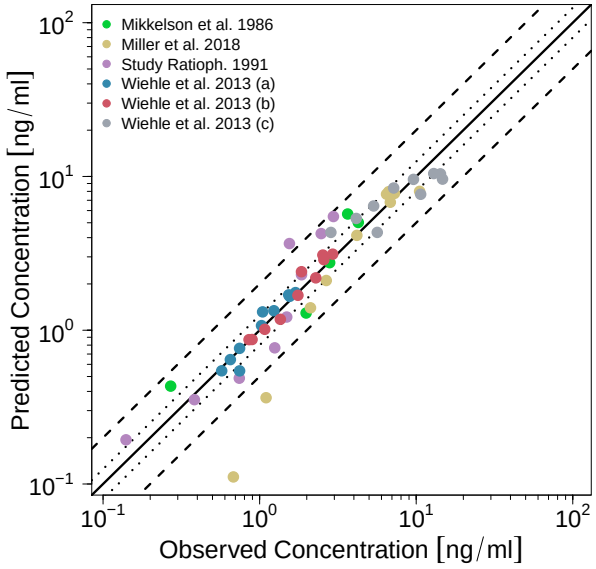

Figure S8. Predicted versus observed (a) AUC_{last}, (b) C_{max} and (c) plasma concentrations of (*E*)-Clom. The black solid lines mark the lines of identity. Black dotted lines indicate 1.25-fold, black dashed lines indicate 2-fold deviation. **Ratioph.**, Ratiopharm® GmbH.

S4.2. Evaluation of the DD(G)I Model

S4.2.1. Plasma Profiles (Linear Scale)

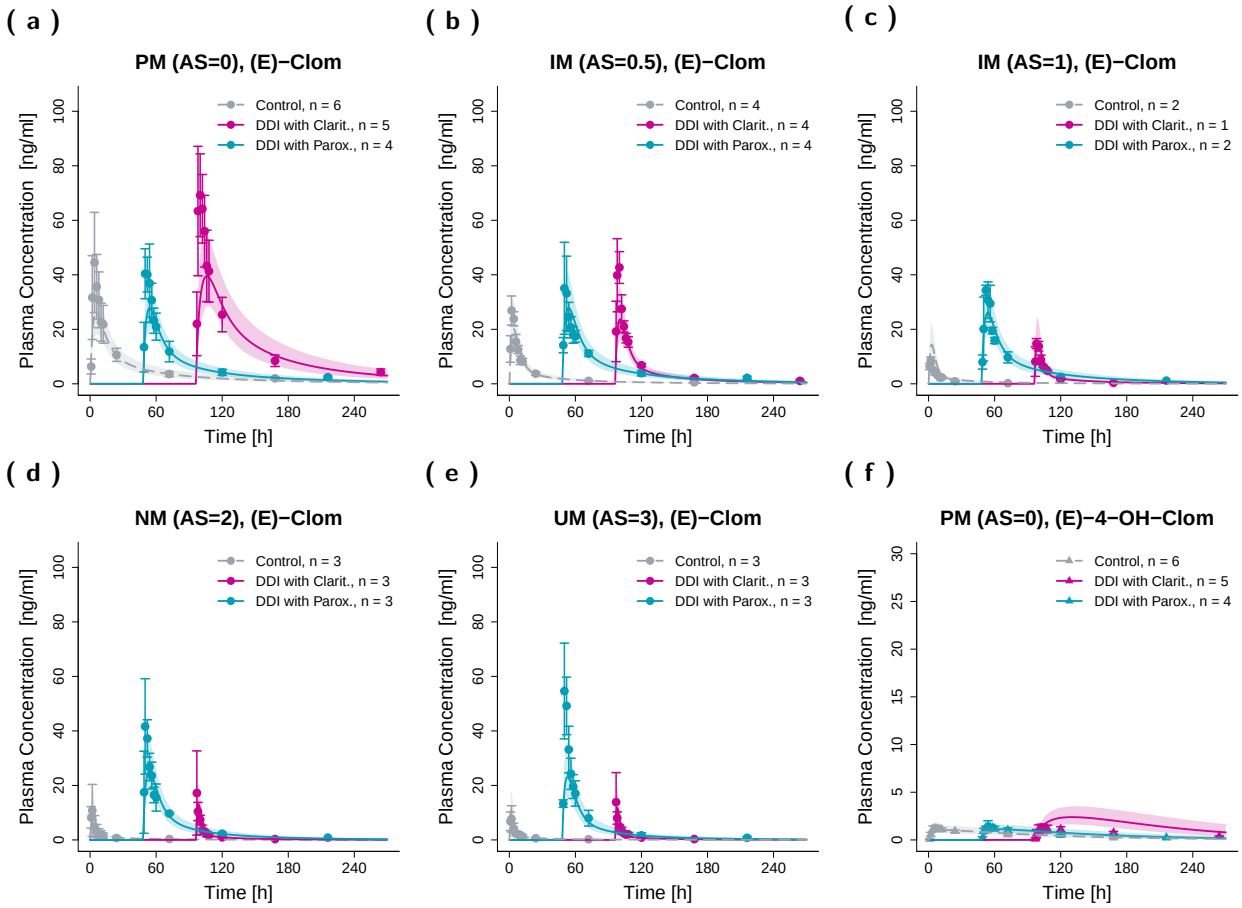

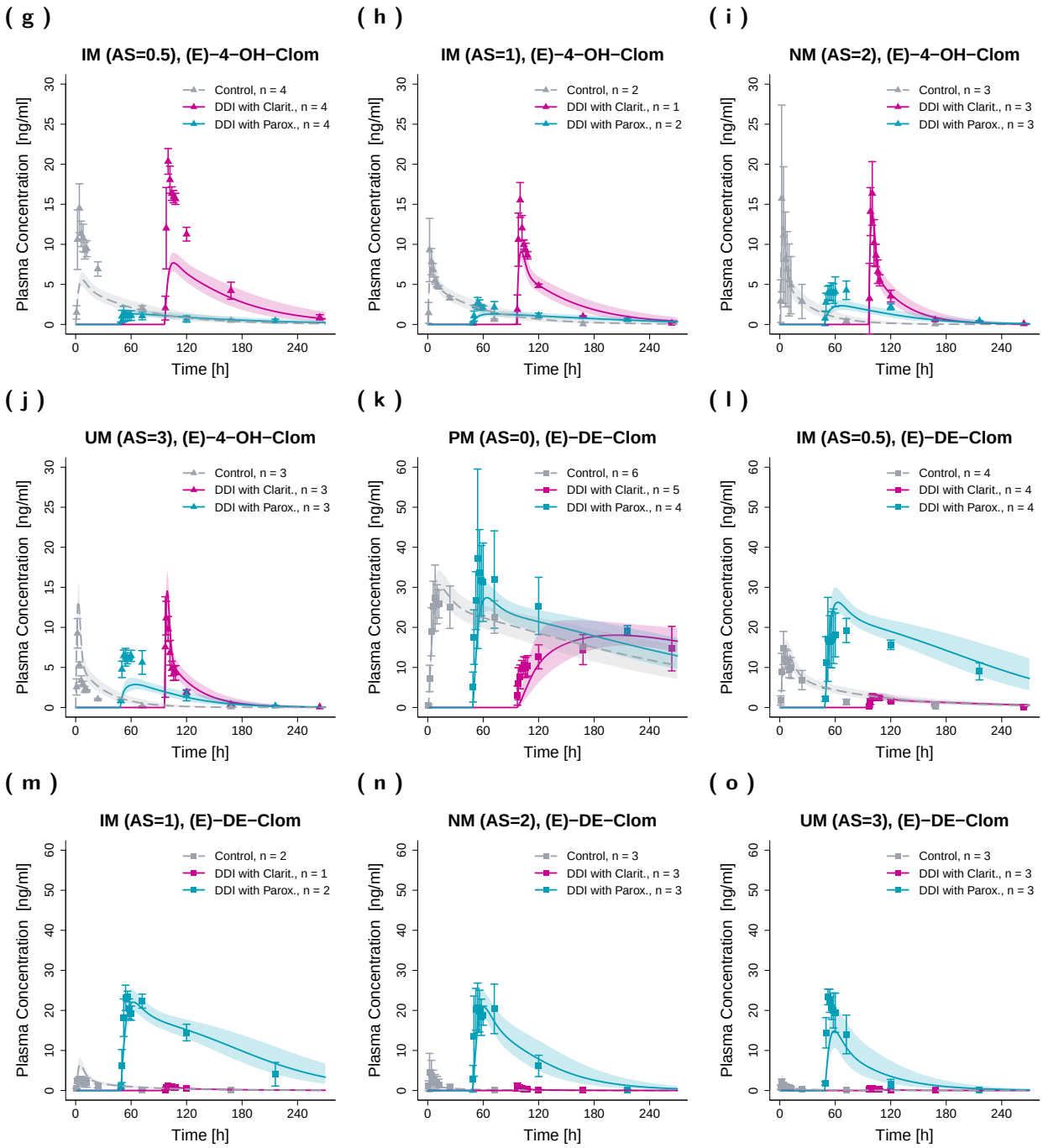
(g)
IM (AS=0.5), (E)−4−OH−Clom
Control, n = 4
DDI with Clarit., n = 4
DDI with Parox., n = 4
(h)
IM (AS=1), (E)−4−OH−Clom
Control, n = 2
DDI with Clarit., n = 1
DDI with Parox., n = 2
(i)
NM (AS=2), (E)−4−OH−Clom
Control, n = 3
DDI with Clarit., n = 3
DDI with Parox., n = 3
(j)
UM (AS=3), (E)−4−OH−Clom
Control, n = 3
DDI with Clarit., n = 3
DDI with Parox., n = 3
(k)
PM (AS=0), (E)−DE−Clom
Control, n = 6
DDI with Clarit., n = 5
DDI with Parox., n = 4
(l)
IM (AS=0.5), (E)−DE−Clom
Control, n = 4
DDI with Clarit., n = 4
DDI with Parox., n = 4
(m)
IM (AS=1), (E)−DE−Clom
Control, n = 2
DDI with Clarit., n = 1
DDI with Parox., n = 2
(n)
NM (AS=2), (E)−DE−Clom
Control, n = 3
DDI with Clarit., n = 3
DDI with Parox., n = 3
(o)
UM (AS=3), (E)−DE−Clom
Control, n = 3
DDI with Clarit., n = 3
DDI with Parox., n = 3
Plasma Concentration [ng/ml]
Time [h]

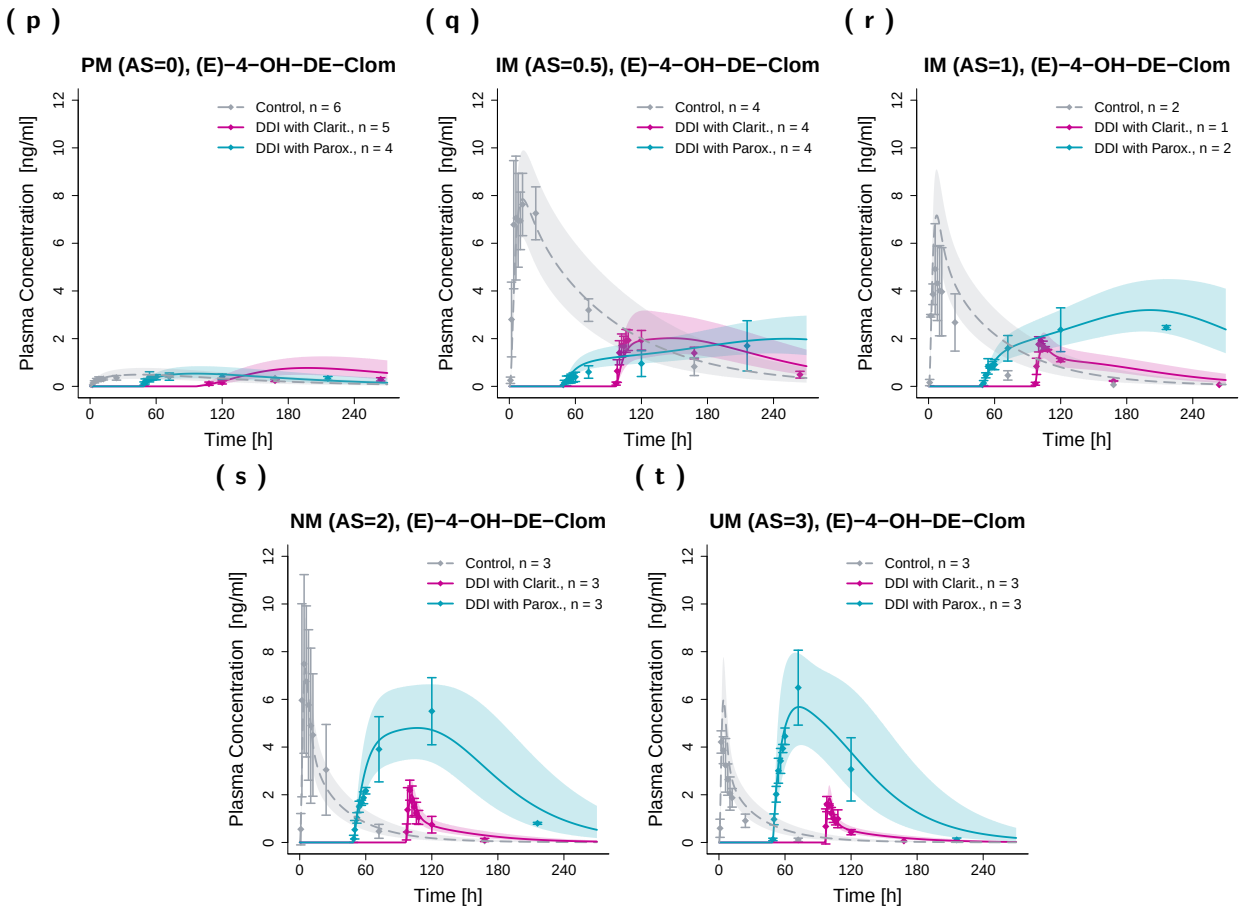

Figure S9. Predicted and observed plasma concentration-time profiles (linear scale) of (*E*)-Clom (a–e), (*E*)-4-OH-Clom (f–j), (*E*)-DE-Clom (k–o) and (*E*)-4-OH-DE-Clom (p–t) for DD(G)I scenarios in PM, IM, NM and UM. Grey dashed lines depict the predicted geometric mean concentration-time profiles without clarithromycin and paroxetine (control), turquoise lines represent the predicted geometric mean profiles in presence of paroxetine and pink lines the predicted geometric mean profiles in presence of clarithromycin (DD(G)I). The respective semitransparent areas show the geometric standard deviation of the population simulations (n=1000). Mean observed data are shown as symbols with the corresponding standard deviation. For a better visibility, DD(G)I scenarios were plotted with a time offset with t =0 at the first dose of the perpetrator drug. **AS**, CYP2D6 activity score; **Clarit.**, clarithromycin; **DD(G)I**, drug-drug and drug-drug-gene interactions; **(*E*)-4-OH-Clom**, (*E*)-4-hydroxyclomiphene; **(*E*)-4-OH-DE-Clom**, (*E*)-4-hydroxy-N-desethylclomiphene; **(*E*)-Clom**, (*E*)-clomiphene; **(*E*)-DE-Clom**, (*E*)-N-desethylclomiphene; **IM**, intermediate metabolizers; **n**, number of subjects; **NM**, normal metabolizers; **Parox.**, paroxetine; **PM**, poor metabolizers; **UM**, ultrarapid metabolizers.

S4.2.2. Plasma Profiles (Semilogarithmic Scale)

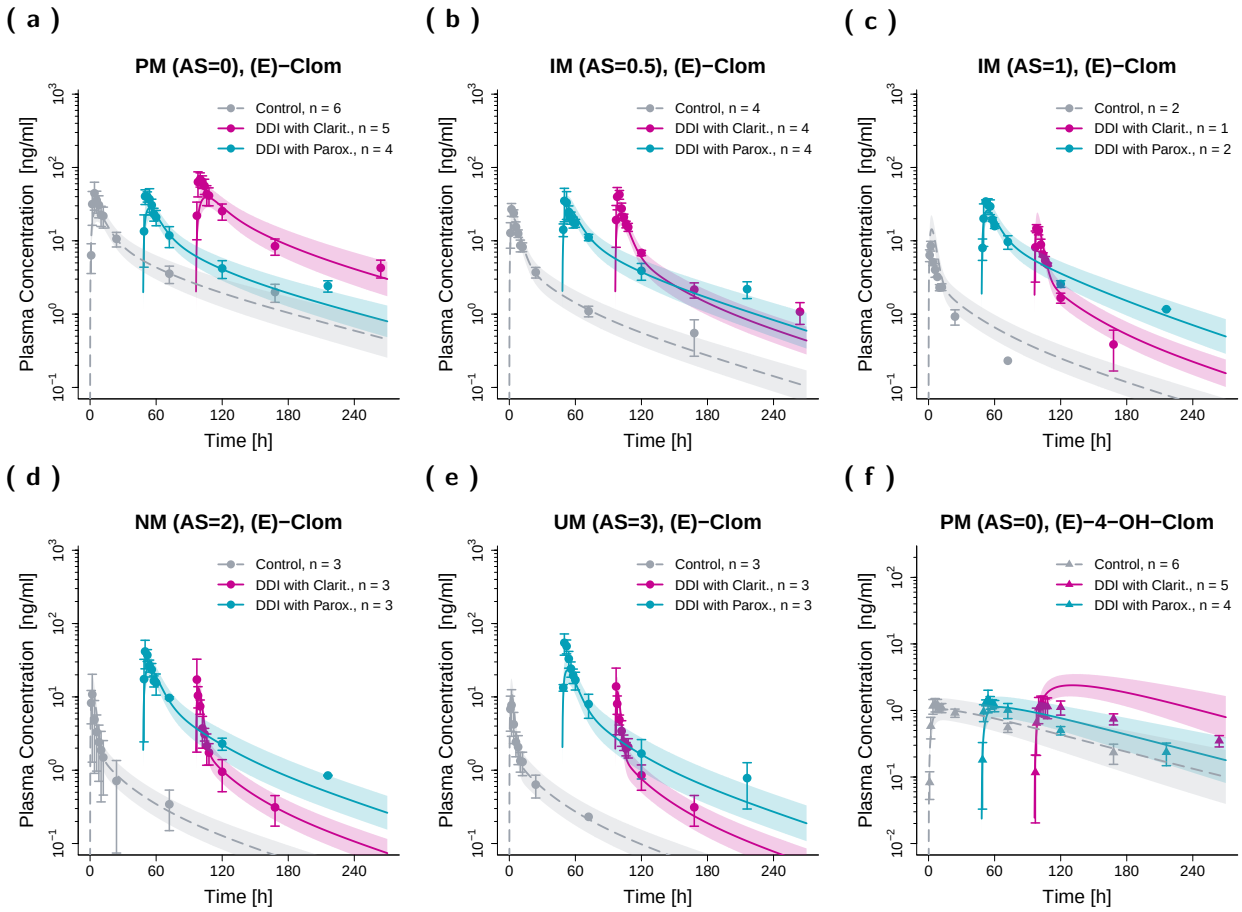

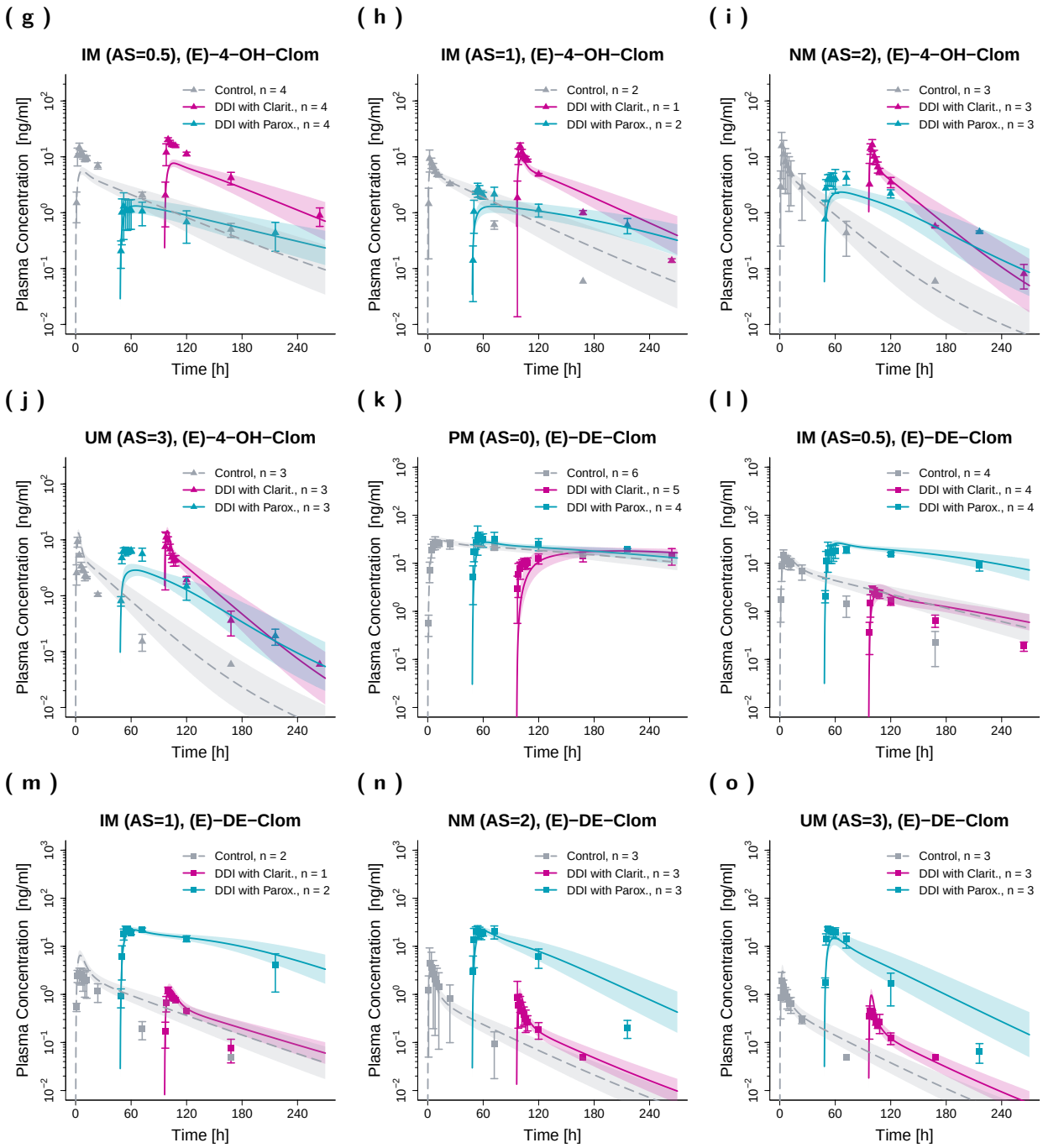
(g)
IM (AS=0.5), (E)−4−OH−Clom
Control, n = 4
DDI with Clarit., n = 4
DDI with Parox., n = 4
(h)
IM (AS=1), (E)−4−OH−Clom
Control, n = 2
DDI with Clarit., n = 1
DDI with Parox., n = 2
(i)
NM (AS=2), (E)−4−OH−Clom
Control, n = 3
DDI with Clarit., n = 3
DDI with Parox., n = 3
(j)
UM (AS=3), (E)−4−OH−Clom
Control, n = 3
DDI with Clarit., n = 3
DDI with Parox., n = 3
(k)
PM (AS=0), (E)−DE−Clom
Control, n = 6
DDI with Clarit., n = 5
DDI with Parox., n = 4
(l)
IM (AS=0.5), (E)−DE−Clom
Control, n = 4
DDI with Clarit., n = 4
DDI with Parox., n = 4
(m)
IM (AS=1), (E)−DE−Clom
Control, n = 2
DDI with Clarit., n = 1
DDI with Parox., n = 2
(n)
NM (AS=2), (E)−DE−Clom
Control, n = 3
DDI with Clarit., n = 3
DDI with Parox., n = 3
(o)
UM (AS=3), (E)−DE−Clom
Control, n = 3
DDI with Clarit., n = 3
DDI with Parox., n = 3
Plasma Concentration [ng/ml]
Time [h]

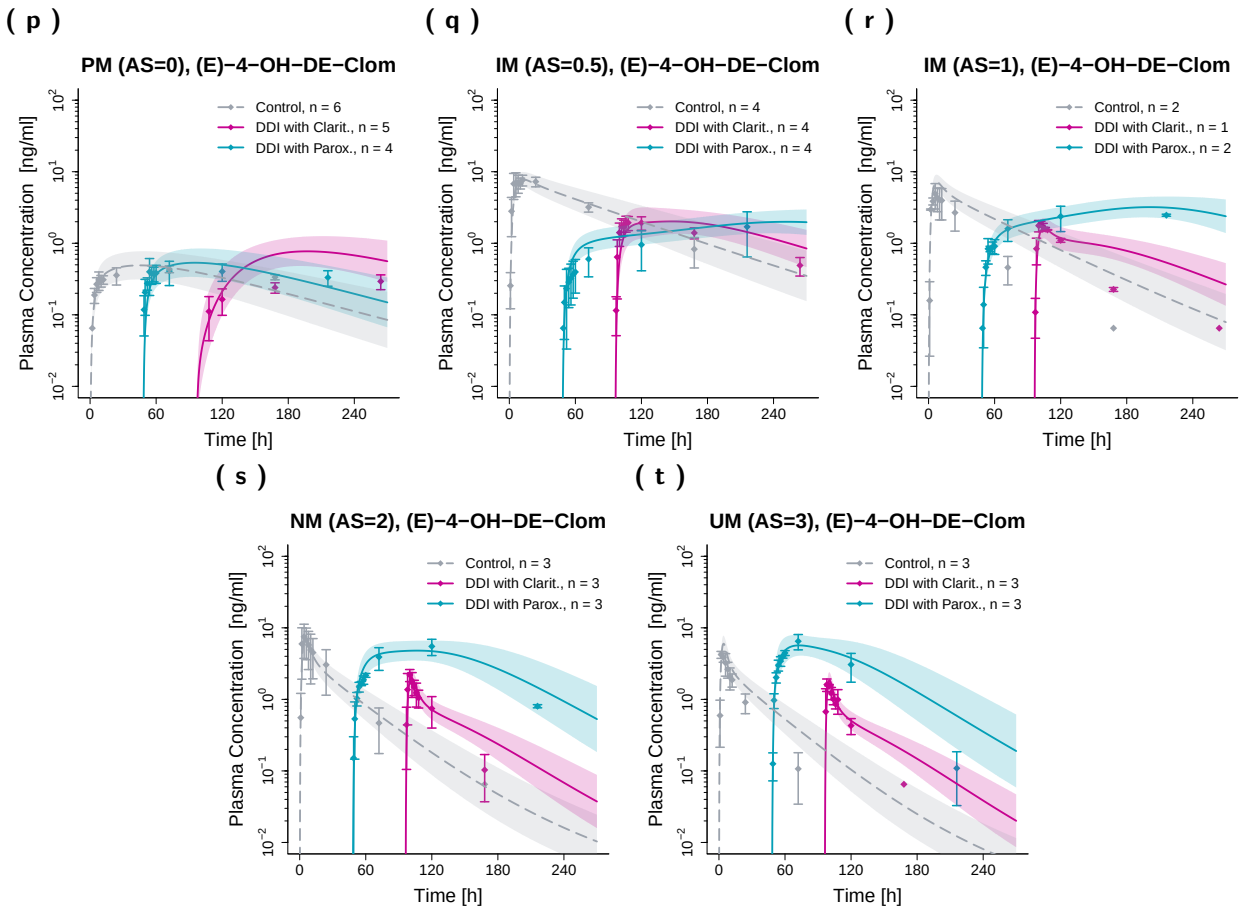

Figure S10. Predicted and observed plasma concentration-time profiles (semilogarithmic scale) of (*E*)-Clom (a–e), (*E*)-4-OH-Clom (f–j), (*E*)-DE-Clom (k–o) and (*E*)-4-OH-DE-Clom (p–t) for DD(G)I scenarios in PM, IM, NM and UM. Grey dashed lines depict the predicted geometric mean concentration-time profiles without clarithromycin and paroxetine (control), turquoise lines represent the predicted geometric mean profiles in presence of paroxetine and pink lines the predicted geometric mean profiles in presence of c larithromycin. The respective semitransparent areas show the geometric standard deviation of the population simulations (n=1000). Mean observed data are shown as symbols with the corresponding standard deviation. For a better visibility, DD(G)I scenarios were plotted with a time offset w ith t =0 a t t he fi rst do se of th e pe rpetrator dr ug. **AS**, CYP2D6 activity score; **Clarit.**, clarithromycin; **DD(G)I**, drug-drug and drug-drug-gene interactions; **(*E*)-4-OH-Clom**, (*E*)-4-hydroxyclomiphene; **(*E*)-4-OH-DE-Clom**, (*E*)-4-hydroxy-N-desethylclomiphene; **(*E*)-Clom**, (*E*)-clomiphene; **(*E*)-DE-Clom**, (*E*)-N-desethylclomiphene; **IM**, intermediate metabolizers; **n**, number of subjects; **NM**, normal metabolizers; **Parox.**, paroxetine; **PM**, poor metabolizers; **UM**, ultrarapid metabolizers.

S4.2.3. Goodness-of-Fit Plots

(a) AUC_{last}

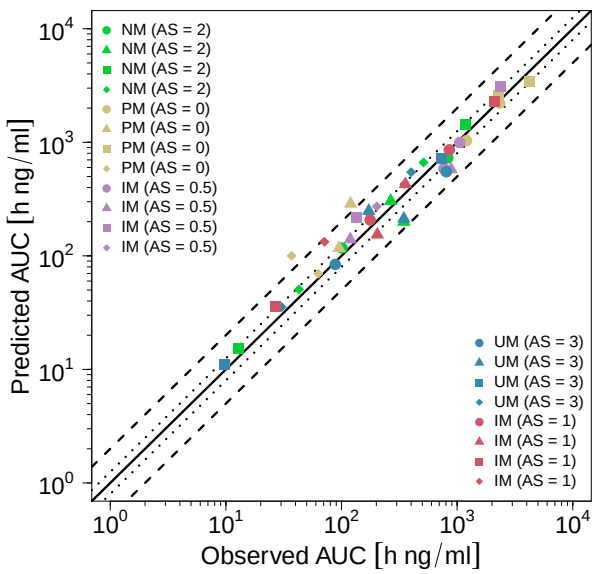

(b) C_{max}

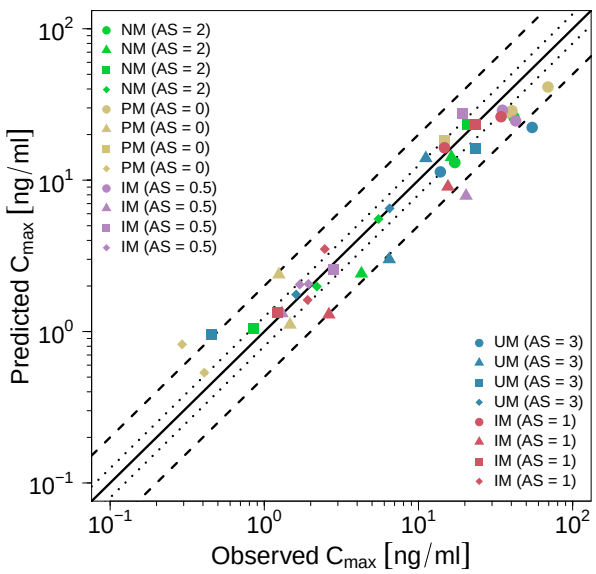

(c) Plasma concentrations

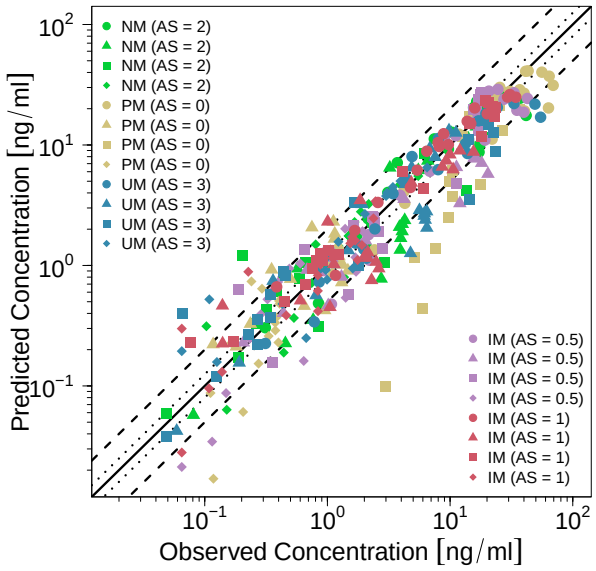

Figure S11. Predicted versus observed AUC_{last} (a), C_{max} (b) and plasma concentrations (c) of (*E*)-Clom (circles), (*E*)-4-OH-Clom (triangles), (*E*)-DE-Clom (squares) and (*E*)-4-OH-DE-Clom (diamonds) for DD(G)I scenarios with clarithromycin and paroxetine, respectively in PM, IM, NM and UM. The black solid lines mark the lines of identity. Black dotted lines indicate 1.25-fold, black dashed lines indicate 2-fold deviation. **AS**, CYP2D6 activity score; **DD(G)I**, drug-drug and drug-drug-gene interactions; **(*E*)-4-OH-Clom**, (*E*)-4-hydroxyclomiphene;**(*E*)-4-OH-DE-Clom**, (*E*)-4-hydroxy-N-desethylclomiphene; **(*E*)-Clom**, (*E*)-clomiphene; **(*E*)-DE-Clom**, (*E*)-N-desethylclomiphene; **IM**, intermediate metabolizers; **NM**, normal metabolizers, **PM**, poor metabolizers; **UM**, ultrarapid metabolizers.

(a) AUC

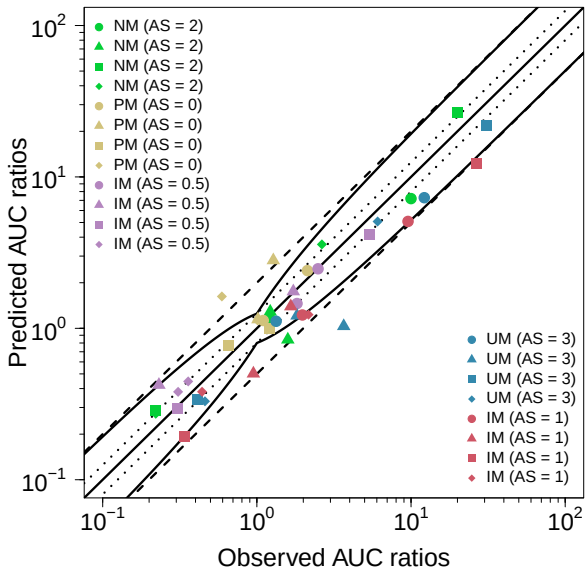

(b) C_{max}

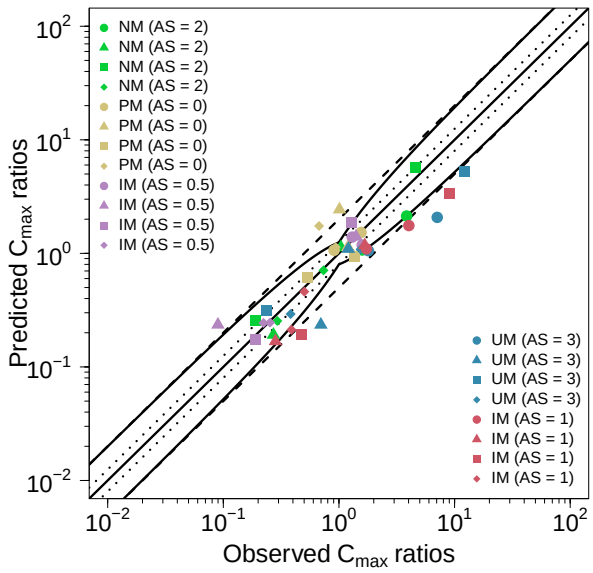

Figure S12. Predicted versus observed DD(G)I AUC_{last} (a) and C_{max} (b) ratios of (*E*)-Clom (circles), (*E*)-4-OH-Clom (triangles), (*E*)-DE-Clom (squares) and (*E*)-4-OH-DE-Clom (diamonds) in PM, IM, NM and UM. The straight black lines mark the lines of identity, the curved black lines show the limits of the predictive measure proposed by Guest et al. with 1.25-fold variability [46]. Black dotted lines indicate 1.25-fold, black dashed lines indicate 2-fold deviation. **AS**, CYP2D6 activity score; **DD(G)I**, drug-drug and drug-drug-gene interactions;**(*E*)-4-OH-Clom**, (*E*)-4-hydroxyclomiphene; **(*E*)-4-OH-DE-Clom**, (*E*)-4-hydroxy-N-desethylclomiphene; **(*E*)-Clom**, (*E*)-clomiphene; **(*E*)-DE-Clom**, (*E*)-N-desethylclomiphene; **IM**, intermediate metabolizers; **NM**, normal metabolizers, **PM**, poor metabolizers; **UM**, ultrarapid metabolizers.

S4.2.4. Renal Excretion Profiles (Linear Scale)

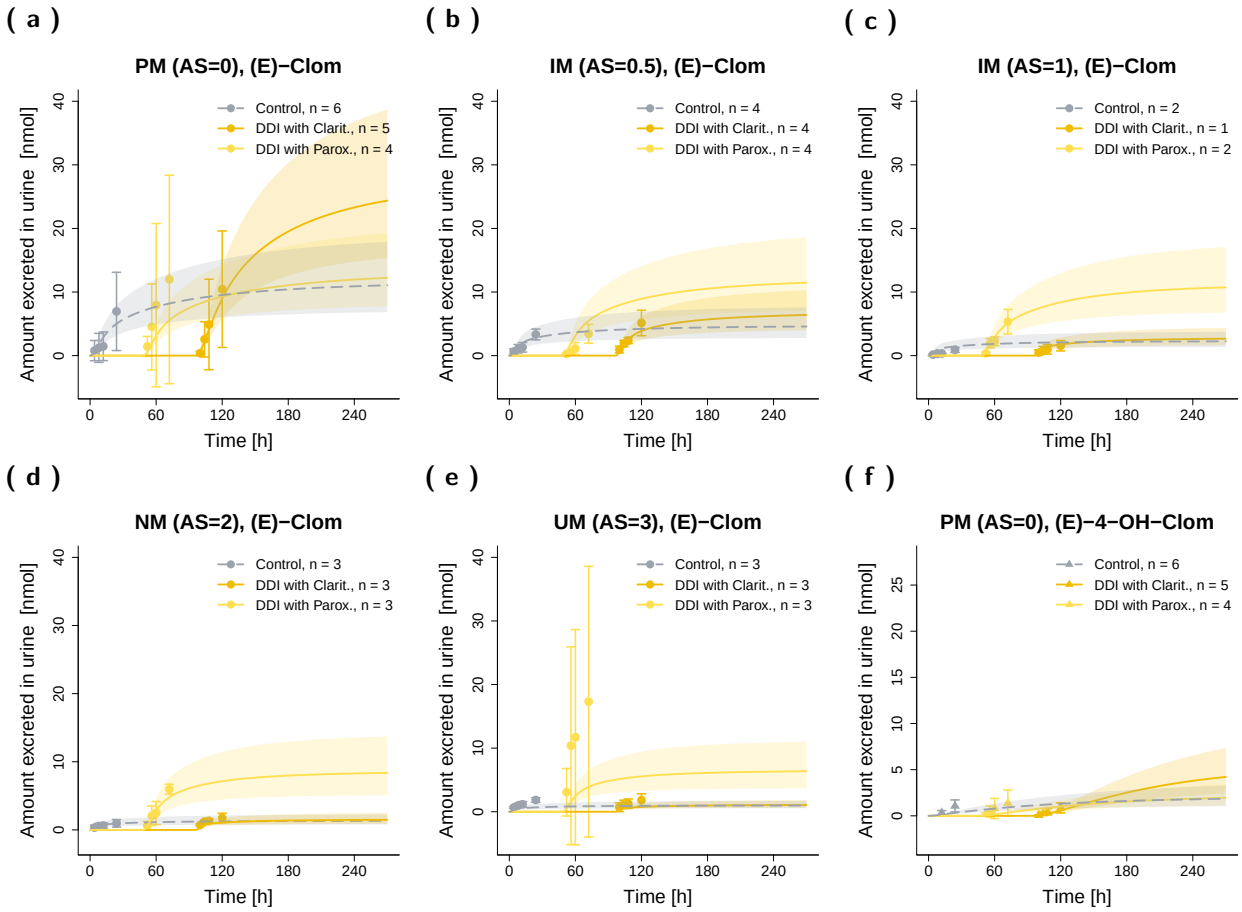

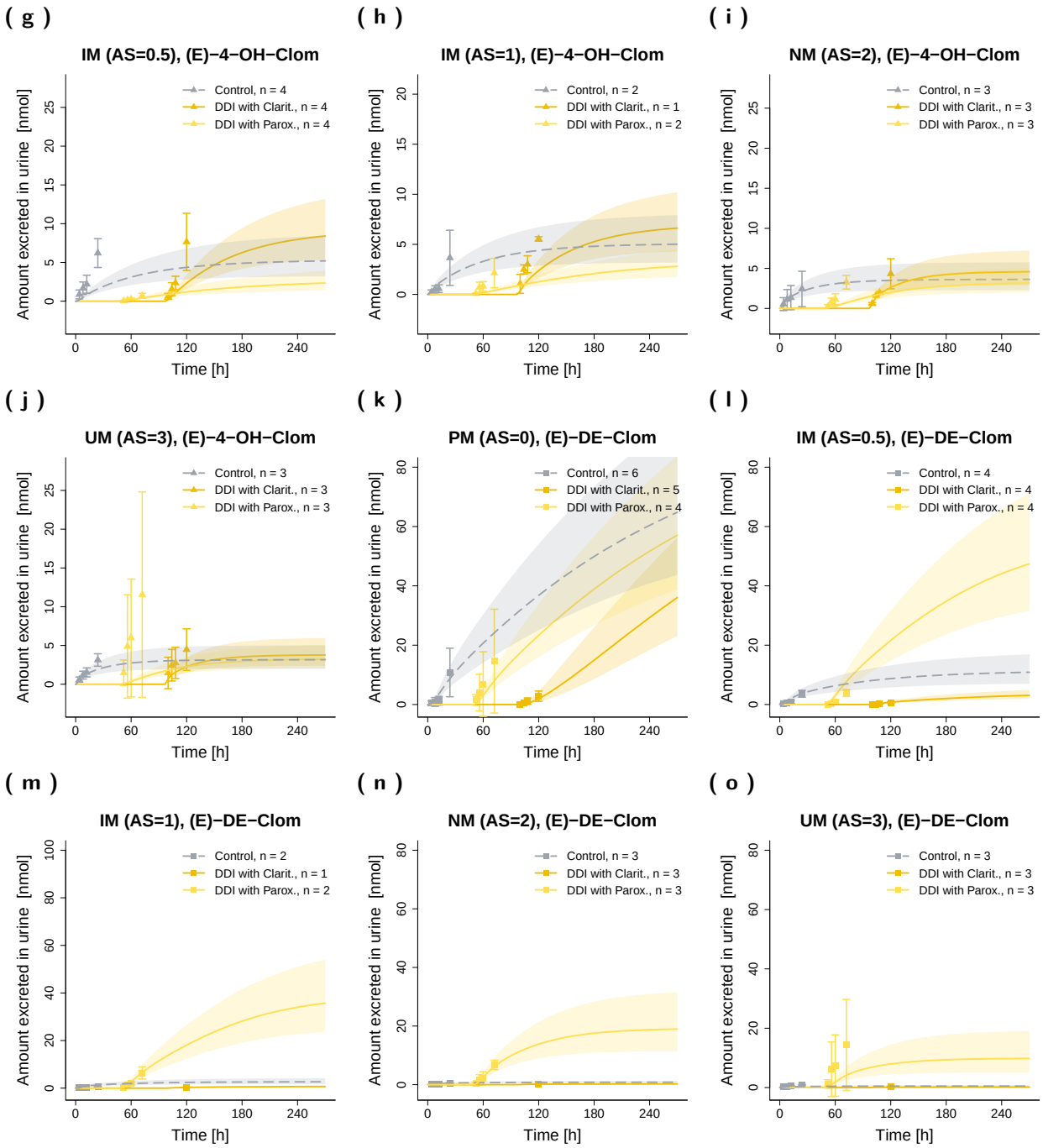
(g)
IM (AS=0.5), (E)−4−OH−Clom
Control, n = 4
DDI with Clarit., n = 4
DDI with Parox., n = 4
(h)
IM (AS=1), (E)−4−OH−Clom
Control, n = 2
DDI with Clarit., n = 1
DDI with Parox., n = 2
(i)
NM (AS=2), (E)−4−OH−Clom
Control, n = 3
DDI with Clarit., n = 3
DDI with Parox., n = 3
(j)
UM (AS=3), (E)−4−OH−Clom
Control, n = 3
DDI with Clarit., n = 3
DDI with Parox., n = 3
(k)
PM (AS=0), (E)−DE−Clom
Control, n = 6
DDI with Clarit., n = 5
DDI with Parox., n = 4
(l)
IM (AS=0.5), (E)−DE−Clom
Control, n = 4
DDI with Clarit., n = 4
DDI with Parox., n = 4
(m)
IM (AS=1), (E)−DE−Clom
Control, n = 2
DDI with Clarit., n = 1
DDI with Parox., n = 2
(n)
NM (AS=2), (E)−DE−Clom
Control, n = 3
DDI with Clarit., n = 3
DDI with Parox., n = 3
(o)
UM (AS=3), (E)−DE−Clom
Control, n = 3
DDI with Clarit., n = 3
DDI with Parox., n = 3
Amount excreted in urine [nmol]
Time [h]

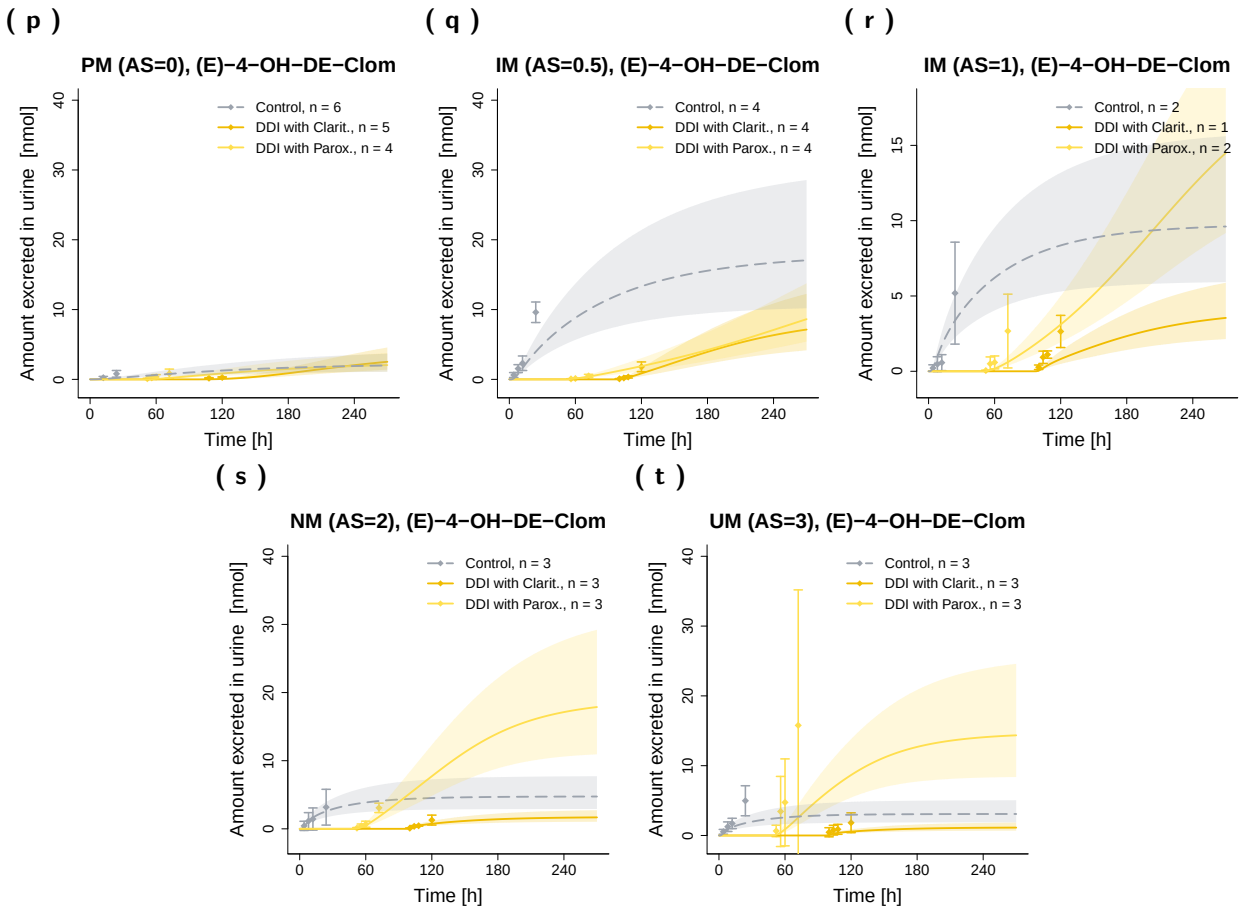

Figure S13. Predicted and observed renal excretion profiles (linear scale) of (*E*)-Clom (a–e), (*E*)-4-OH-Clom (f–j), (*E*)-DE-Clom (k–o) and (*E*)-4-OH-DE-Clom (p–t) for DD(G)I scenarios in PM, IM, NM and UM. Grey dashed lines depict the predicted geometric mean profiles in absence of clarithromycin and paroxetine (control), yellow solid lines represent the predicted geometric mean profiles in presence of paroxetine and orange solid lines represent the predicted geometric mean profiles in presence of clarithromycin (DD(G)I). The respective semitransparent areas show the geometric standard deviation of the population simulations (n=1000). Mean observed data are shown as symbols with the corresponding standard deviation. For a better visibility, DD(G)I scenarios were plotted with a time offset with t=0 at the first dose of the perpetrator drug. **AS**, CYP2D6 activity score; **Clarit.**, clarithromycin; **DD(G)I**, drug-drug and drug-drug-gene interactions; **(*E*)-4-OH-Clom**, (*E*)-4-hydroxyclomiphene; **(E)-4-OH-DE-Clom**, (*E*)-4-hydroxy-N-desethylclomiphene; **(*E*)-Clom**, (*E*)-clomiphene; **(*E*)-DE-Clom**, (*E*)-N-desethylclomiphene; **IM**, intermediate metabolizers; **n**, number of subjects; **NM**, normal metabolizers; **Parox.**, paroxetine; **PM**, poor metabolizers; **UM**, ultrarapid metabolizers.

S4.3. Quantitative PBPK Model Evaluation

S4.3.1. Mean Relative Deviation (MRD)

Table S9. Mean relative deviation (MRD) values of DGI plasma concentration predictions.

Study	Compound	MRD	Reference
PK Panel Study, PM (AS = 0)	(*E*)-4-OH-Clom	1.49	[19]
PK Panel Study, PM (AS = 0)	(*E*)-4-OH-DE-Clom	1.20	[19]
PK Panel Study, PM (AS = 0)	(*E*)-Clom	1.42	[19]
PK Panel Study, PM (AS = 0)	(*E*)-DE-Clom	1.38	[19]
PK Panel Study, IM (AS = 0.5)	(*E*)-4-OH-Clom	2.00	[19]
PK Panel Study, IM (AS = 0.5)	(*E*)-4-OH-DE-Clom	1.44	[19]
PK Panel Study, IM (AS = 0.5)	(*E*)-Clom	1.31	[19]
PK Panel Study, IM (AS = 0.5)	(*E*)-DE-Clom	2.04	[19]
PK Panel Study, IM (AS = 0.75)	(*E*)-4-OH-Clom	2.45	[19]
PK Panel Study, IM (AS = 0.75)	(*E*)-4-OH-DE-Clom	3.04	[19]
PK Panel Study, IM (AS = 0.75)	(*E*)-Clom	3.24	[19]
PK Panel Study, IM (AS = 0.75)	(*E*)-DE-Clom	5.42	[19]
PK Panel Study, IM (AS = 1)	(*E*)-4-OH-Clom	1.96	[19]
PK Panel Study, IM (AS = 1)	(*E*)-4-OH-DE-Clom	2.38	[19]
PK Panel Study, IM (AS = 1)	(*E*)-Clom	1.99	[19]
PK Panel Study, IM (AS = 1)	(*E*)-DE-Clom	2.52	[19]
PK Panel Study, NM (AS = 2)	(*E*)-4-OH-Clom	1.40	[19]
PK Panel Study, NM (AS = 2)	(*E*)-4-OH-DE-Clom	1.30	[19]
PK Panel Study, NM (AS = 2)	(*E*)-Clom	1.39	[19]
PK Panel Study, NM (AS = 2)	(*E*)-DE-Clom	1.38	[19]
PK Panel Study, UM (AS = 3)	(*E*)-4-OH-Clom	2.26	[19]
PK Panel Study, UM (AS = 3)	(*E*)-4-OH-DE-Clom	1.81	[19]
PK Panel Study, UM (AS = 3)	(*E*)-Clom	1.30	[19]
PK Panel Study, UM (AS = 3)	(*E*)-DE-Clom	1.50	[19]
Mikkelson et al. 1986	(*E*)-Clom	1.43	[1]
Miller et al. 2018	(*E*)-Clom	2.01	[4]
Study Ratioph. 1991	(*E*)-Clom	1.61	[2]
Wiehle et al. 2013 (a)	(*E*)-Clom	1.14	[3]
Wiehle et al. 2013 (b)	(*E*)-Clom	1.13	[3]
Wiehle et al. 2013 (c)	(*E*)-Clom	1.33	[3]
Overall MRD: 1.95 (1.13–5.42)			
21/30 MRD ≤ 2			

AS: CYP2D6 acitivity score, **DGI**: drug-gene interaction, **(*E*)-4-OH-Clom**: (*E*)-4-hydroxyclomiphene, **(*E*)-4-OH-DE-Clom**: (*E*)-4-hydroxy-N-desethylclomiphene, **(*E*)-Clom**: (*E*)-clomiphene, **(*E*)-DE-Clom**: (*E*)-N-desethylclomiphene, **IM**: intermediate metabolizers, **NM**: normal metabolizers, **PK**: pharmacokinetic, **PM**: poor metabolizers, **UM**: ultrarapid metabolizers, **Ratioph.**: Ratiopharm® GmbH

Table S10. Mean relative deviation (MRD) values of DD(G)I plasma concentration predictions.

Study	Compound	Perpetrator	MRD	Reference
PK Panel Study, PM (AS = 0)	(*E*)-4-OH-Clom	Clarithromycin	1.80	[19]
PK Panel Study, PM (AS = 0)	(*E*)-4-OH-Clom	Paroxetine	1.50	[19]
PK Panel Study, PM (AS = 0)	(*E*)-4-OH-DE-Clom	Clarithromycin	2.04	[19]
PK Panel Study, PM (AS = 0)	(*E*)-4-OH-DE-Clom	Paroxetine	2.18	[19]
PK Panel Study, PM (AS = 0)	(*E*)-Clom	Clarithromycin	1.72	[19]
PK Panel Study, PM (AS = 0)	(*E*)-Clom	Paroxetine	1.41	[19]
PK Panel Study, PM (AS = 0)	(*E*)-DE-Clom	Clarithromycin	4.87	[19]
PK Panel Study, PM (AS = 0)	(*E*)-DE-Clom	Paroxetine	2.04	[19]
PK Panel Study, IM (AS = 0.5)	(*E*)-4-OH-Clom	Clarithromycin	2.18	[19]
PK Panel Study, IM (AS = 0.5)	(*E*)-4-OH-Clom	Paroxetine	1.38	[19]
PK Panel Study, IM (AS = 0.5)	(*E*)-4-OH-DE-Clom	Clarithromycin	2.11	[19]
PK Panel Study, IM (AS = 0.5)	(*E*)-4-OH-DE-Clom	Paroxetine	1.73	[19]
PK Panel Study, IM (AS = 0.5)	(*E*)-Clom	Clarithromycin	1.55	[19]
PK Panel Study, IM (AS = 0.5)	(*E*)-Clom	Paroxetine	1.43	[19]
PK Panel Study, IM (AS = 0.5)	(*E*)-DE-Clom	Clarithromycin	1.92	[19]
PK Panel Study, IM (AS = 0.5)	(*E*)-DE-Clom	Paroxetine	1.53	[19]
PK Panel Study, IM (AS = 1)	(*E*)-4-OH-Clom	Clarithromycin	1.79	[19]
PK Panel Study, IM (AS = 1)	(*E*)-4-OH-Clom	Paroxetine	2.01	[19]
PK Panel Study, IM (AS = 1)	(*E*)-4-OH-DE-Clom	Clarithromycin	2.03	[19]
PK Panel Study, IM (AS = 1)	(*E*)-4-OH-DE-Clom	Paroxetine	1.38	[19]
PK Panel Study, IM (AS = 1)	(*E*)-Clom	Clarithromycin	1.30	[19]
PK Panel Study, IM (AS = 1)	(*E*)-Clom	Paroxetine	1.25	[19]
PK Panel Study, IM (AS = 1)	(*E*)-DE-Clom	Clarithromycin	1.53	[19]
PK Panel Study, IM (AS = 1)	(*E*)-DE-Clom	Paroxetine	1.29	[19]
PK Panel Study, NM (AS = 2)	(*E*)-4-OH-Clom	Clarithromycin	1.38	[19]
PK Panel Study, NM (AS = 2)	(*E*)-4-OH-Clom	Paroxetine	2.23	[19]
PK Panel Study, NM (AS = 2)	(*E*)-4-OH-DE-Clom	Clarithromycin	1.67	[19]
PK Panel Study, NM (AS = 2)	(*E*)-4-OH-DE-Clom	Paroxetine	1.52	[19]
PK Panel Study, NM (AS = 2)	(*E*)-Clom	Clarithromycin	1.44	[19]
PK Panel Study, NM (AS = 2)	(*E*)-Clom	Paroxetine	1.51	[19]
PK Panel Study, NM (AS = 2)	(*E*)-DE-Clom	Clarithromycin	1.62	[19]
PK Panel Study, NM (AS = 2)	(*E*)-DE-Clom	Paroxetine	2.19	[19]
PK Panel Study, UM (AS = 3)	(*E*)-4-OH-Clom	Clarithromycin	1.42	[19]
PK Panel Study, UM (AS = 3)	(*E*)-4-OH-Clom	Paroxetine	2.28	[19]
PK Panel Study, UM (AS = 3)	(*E*)-4-OH-DE-Clom	Clarithromycin	1.72	[19]
PK Panel Study, UM (AS = 3)	(*E*)-4-OH-DE-Clom	Paroxetine	1.71	[19]
PK Panel Study, UM (AS = 3)	(*E*)-Clom	Clarithromycin	1.46	[19]
PK Panel Study, UM (AS = 3)	(*E*)-Clom	Paroxetine	1.74	[19]
PK Panel Study, UM (AS = 3)	(*E*)-DE-Clom	Clarithromycin	1.47	[19]
PK Panel Study, UM (AS = 3)	(*E*)-DE-Clom	Paroxetine	2.38	[19]

Overall MRD: 1.83 (1.25–4.87)
28/40 MRD ≤ 2

AS: CYP2D6 acitivity score, **DD(G)I**: drug-drug and drug-drug-gene interactions, **(*E*)-4-OH-Clom**: (*E*)-4-hydroxyclomiphene, **(*E*)-4-OH-DE-Clom**: (*E*)-4-hydroxy-N-desethylclomiphene, **(*E*)-Clom**: (*E*)-clomiphene, **(*E*)-DE-Clom**: (*E*)-N-desethylclomiphene, **IM**: intermediate metabolizers, **NM**: normal metabolizers, **PK**: pharmacokinetic, **PM**: poor metabolizers, **UM**: ultrarapid metabolizers

S4.3.2. Geometric Mean Fold Error (GMFE)

Table S11. Geometric Mean Fold Error (GMFE) of AUC_{last} and C_{max} DGI Predictions.

		$\mathbf{AUC_{last}}$			$\mathbf{C_{max}}$			
Study	Compound	Pred $\left[\frac{ng \cdot h}{ml}\right]$	Obs $\left[\frac{ng \cdot h}{ml}\right]$	Pred/Obs	Pred $\left[\frac{ng}{ml}\right]$	Obs $\left[\frac{ng}{ml}\right]$	Pred/Obs	Reference
PK Panel Study, PM (AS = 0)	(*E*)-Clom	919.01	1095.56	0.84	27.00	44.53	0.61	[19]
PK Panel Study, PM (AS = 0)	(*E*)-4-OH-Clom	102.28	93.66	1.09	0.98	1.23	0.79	[19]
PK Panel Study, PM (AS = 0)	(*E*)-DE-Clom	3389.54	3473.88	0.98	29.59	27.34	1.08	[19]
PK Panel Study, PM (AS = 0)	(*E*)-4-OH-DE-Clom	61.68	62.33	0.99	0.47	0.44	1.09	[19]
PK Panel Study, IM (AS = 0.5)	(*E*)-Clom	401.77	422.50	0.95	20.81	26.89	0.77	[19]
PK Panel Study, IM (AS = 0.5)	(*E*)-4-OH-Clom	330.20	513.99	0.64	5.61	14.50	0.39	[19]
PK Panel Study, IM (AS = 0.5)	(*E*)-DE-Clom	741.34	446.69	1.66	14.89	14.86	1.00	[19]
PK Panel Study, IM (AS = 0.5)	(*E*)-4-OH-DE-Clom	610.91	562.68	1.09	8.39	7.63	1.10	[19]
PK Panel Study, IM (AS = 0.75)	(*E*)-Clom	344.04	136.73	2.52	19.30	9.96	1.94	[19]
PK Panel Study, IM (AS = 0.75)	(*E*)-4-OH-Clom	349.10	246.20	1.42	5.89	13.33	0.44	[19]
PK Panel Study, IM (AS = 0.75)	(*E*)-DE-Clom	575.65	102.23	5.63	12.62	6.39	1.98	[19]
PK Panel Study, IM (AS = 0.75)	(*E*)-4-OH-DE-Clom	556.31	226.19	2.46	7.89	8.01	0.98	[19]
PK Panel Study, IM (AS = 1)	(*E*)-Clom	168.98	89.54	1.89	14.93	8.53	1.75	[19]
PK Panel Study, IM (AS = 1)	(*E*)-4-OH-Clom	306.54	214.87	1.43	7.69	9.29	0.83	[19]
PK Panel Study, IM (AS = 1)	(*E*)-DE-Clom	187.42	79.09	2.37	6.88	2.59	2.66	[19]
PK Panel Study, IM (AS = 1)	(*E*)-4-OH-DE-Clom	348.35	161.70	2.15	7.62	4.92	1.55	[19]
PK Panel Study, NM (AS = 2)	(*E*)-Clom	101.66	82.93	1.23	12.20	10.82	1.13	[19]
PK Panel Study, NM (AS = 2)	(*E*)-4-OH-Clom	236.46	218.30	1.08	12.59	15.72	0.80	[19]
PK Panel Study, NM (AS = 2)	(*E*)-DE-Clom	53.16	58.47	0.91	4.09	4.50	0.91	[19]
PK Panel Study, NM (AS = 2)	(*E*)-4-OH-DE-Clom	185.45	193.74	0.96	7.81	7.49	1.04	[19]
PK Panel Study, UM (AS = 3)	(*E*)-Clom	75.53	66.21	1.14	10.74	7.72	1.39	[19]
PK Panel Study, UM (AS = 3)	(*E*)-4-OH-Clom	205.20	94.52	2.17	12.76	9.26	1.38	[19]
PK Panel Study, UM (AS = 3)	(*E*)-DE-Clom	32.98	23.91	1.38	3.05	1.93	1.58	[19]
PK Panel Study, UM (AS = 3)	(*E*)-4-OH-DE-Clom	120.44	74.07	1.63	6.01	4.21	1.43	[19]
Mikkelson et al. 1986	(*E*)-Clom	35.20	35.70	0.99	5.86	4.27	1.37	[1]
Miller et al. 2018	(*E*)-Clom	7484.01	5121.29	1.46	17.89	10.51	1.70	[4]
Study Ratioph. 1991	(*E*)-Clom	39.73	33.60	1.18	5.55	2.96	1.88	[2]
Wiehle et al. 2013 (a)	(*E*)-Clom	22.34	21.59	1.03	1.76	1.69	1.04	[3]
Wiehle et al. 2013 (b)	(*E*)-Clom	36.73	36.53	1.01	3.16	2.93	1.08	[3]
Wiehle et al. 2013 (c)	(*E*)-Clom	161.63	158.86	1.02	10.49	14.72	0.71	[3]
			GMFE: 1.43 (1.01–5.63)			**GMFE: 1.41 (1.00–2.66)**		

(continued)

Table S11. *continued*

Study	Compound	Pred $\left[\frac{\text{ng}\cdot\text{h}}{\text{ml}}\right]$	Obs $\left[\frac{\text{ng}\cdot\text{h}}{\text{ml}}\right]$	Pred/Obs	Pred $\left[\frac{\text{ng}}{\text{ml}}\right]$	Obs $\left[\frac{\text{ng}}{\text{ml}}\right]$	Pred/Obs	Reference
			GMFE ≤ 2: 24/30			**GMFE ≤ 2: 27/30**		

AS: CYP2D6 acitivity score, **DGI**: drug-gene interaction, **(*E*)-4-OH-Clom**: (*E*)-4-hydroxyclomiphene, **(*E*)-4-OH-DE-Clom**: (*E*)-4-hydroxy-N-desethylclomiphene, **(*E*)-Clom**: (*E*)-clomiphene, **(*E*)-DE-Clom**: (*E*)-N-desethylclomiphene, **IM**: intermediate metabolizers, **NM**: normal metabolizers, **Obs**: observed, **PK**: pharmacokinetic, **PM**: poor metabolizers, **Pred**: predicted, **UM**: ultrarapid metabolizers, **Ratioph.**: Ratiopharm® GmbH

Table S12. Geometric Mean Fold Error (GMFE) of DGI AUC_{last} and C_{max} ratios.

		AUC_{last} Ratio			**C_{max} Ratio**			
Study	Compound	Pred [1]	Obs [1]	Pred/Obs	Pred [1]	Obs [1]	Pred/Obs	Reference
PK Panel Study, PM (AS = 0)	(*E*)-Clom	9.04	13.21	0.68	2.21	4.12	0.54	[19]
PK Panel Study, PM (AS = 0)	(*E*)-4-OH-Clom	0.43	0.43	1.01	0.08	0.08	0.99	[19]
PK Panel Study, PM (AS = 0)	(*E*)-DE-Clom	63.77	59.41	1.07	7.23	6.07	1.19	[19]
PK Panel Study, PM (AS = 0)	(*E*)-4-OH-DE-Clom	0.33	0.32	1.03	0.06	0.06	1.04	[19]
PK Panel Study, IM (AS = 0.5)	(*E*)-Clom	3.95	5.09	0.78	1.71	2.49	0.69	[19]
PK Panel Study, IM (AS = 0.5)	(*E*)-4-OH-Clom	1.40	2.35	0.59	0.45	0.92	0.48	[19]
PK Panel Study, IM (AS = 0.5)	(*E*)-DE-Clom	13.95	7.64	1.83	3.64	3.30	1.10	[19]
PK Panel Study, IM (AS = 0.5)	(*E*)-4-OH-DE-Clom	3.29	2.90	1.13	1.07	1.02	1.05	[19]
PK Panel Study, IM (AS = 0.75)	(*E*)-Clom	3.38	1.65	2.05	1.58	0.92	1.72	[19]
PK Panel Study, IM (AS = 0.75)	(*E*)-4-OH-Clom	1.48	1.13	1.31	0.47	0.85	0.55	[19]
PK Panel Study, IM (AS = 0.75)	(*E*)-DE-Clom	10.83	1.75	6.19	3.08	1.42	2.17	[19]
PK Panel Study, IM (AS = 0.75)	(*E*)-4-OH-DE-Clom	3.00	1.17	2.57	1.01	1.07	0.94	[19]
PK Panel Study, IM (AS = 1)	(*E*)-Clom	1.66	1.08	1.54	1.22	0.79	1.55	[19]
PK Panel Study, IM (AS = 1)	(*E*)-4-OH-Clom	1.30	0.98	1.32	0.61	0.59	1.03	[19]
PK Panel Study, IM (AS = 1)	(*E*)-DE-Clom	3.53	1.35	2.61	1.68	0.57	2.92	[19]
PK Panel Study, IM (AS = 1)	(*E*)-4-OH-DE-Clom	1.88	0.83	2.25	0.98	0.66	1.49	[19]
PK Panel Study, UM (AS = 3)	(*E*)-Clom	0.74	0.80	0.93	0.88	0.71	1.23	[19]
PK Panel Study, UM (AS = 3)	(*E*)-4-OH-Clom	0.87	0.43	2.00	1.01	0.59	1.72	[19]
PK Panel Study, UM (AS = 3)	(*E*)-DE-Clom	0.62	0.41	1.52	0.75	0.43	1.74	[19]
PK Panel Study, UM (AS = 3)	(*E*)-4-OH-DE-Clom	0.65	0.38	1.70	0.77	0.56	1.37	[19]
		GMFE: 1.65 (1.00–6.19)			**GMFE: 1.46 (1.00–2.95)**			
		GMFE ≤ 2: 14/20			**GMFE ≤ 2: 17/20**			
		Guest limits: 12/20			**Guest limits: 10/20**			

AS: CYP2D6 acitivity score, **DGI**: drug-gene interaction, **(*E*)-4-OH-Clom**: (*E*)-4-hydroxyclomiphene, **(*E*)-4-OH-DE-Clom**: (*E*)-4-hydroxy-N-desethylclomiphene, **(*E*)-Clom**: (*E*)-clomiphene, **(*E*)-DE-Clom**: (*E*)-N-desethylclomiphene, **IM**: intermediate metabolizers, **NM**: normal metabolizers, **Obs**: observed, **PK**: pharmacokinetic, **PM**: poor metabolizers, **Pred**: predicted, **UM**: ultrarapid metabolizers

Table S13. Geometric Mean Fold Error (GMFE) of AUC_{last} and C_{max} DD(G)I Predictions.

			$\mathbf{AUC_{last}}$			$\mathbf{C_{max}}$			
Study	Compound	Perpetrator	Pred $\left[\frac{ng \cdot h}{ml}\right]$	Obs $\left[\frac{ng \cdot h}{ml}\right]$	Pred/Obs	Pred $\left[\frac{ng}{ml}\right]$	Obs $\left[\frac{ng}{ml}\right]$	Pred/Obs	Reference
PK Panel Study, PM (AS = 0)	(*E*)-Clom	Clarithromycin	2211.99	2332.83	0.95	41.25	69.18	0.60	[19]
PK Panel Study, PM (AS = 0)	(*E*)-4-OH-Clom	Clarithromycin	287.69	119.75	2.40	2.38	1.24	1.91	[19]
PK Panel Study, PM (AS = 0)	(*E*)-DE-Clom	Clarithromycin	2592.38	2282.03	1.14	18.17	14.69	1.24	[19]
PK Panel Study, PM (AS = 0)	(*E*)-4-OH-DE-Clom	Clarithromycin	100.11	36.96	2.71	0.82	0.29	2.81	[19]
PK Panel Study, IM (AS = 0.5)	(*E*)-Clom	Clarithromycin	585.91	769.47	0.76	24.64	42.67	0.58	[19]
PK Panel Study, IM (AS = 0.5)	(*E*)-4-OH-Clom	Clarithromycin	578.95	885.93	0.65	7.88	20.35	0.39	[19]
PK Panel Study, IM (AS = 0.5)	(*E*)-DE-Clom	Clarithromycin	219.84	135.87	1.62	2.58	2.79	0.92	[19]
PK Panel Study, IM (AS = 0.5)	(*E*)-4-OH-DE-Clom	Clarithromycin	272.46	201.78	1.35	2.06	1.93	1.07	[19]
PK Panel Study, IM (AS = 1)	(*E*)-Clom	Clarithromycin	207.03	176.77	1.17	16.37	14.74	1.11	[19]
PK Panel Study, IM (AS = 1)	(*E*)-4-OH-Clom	Clarithromycin	427.82	356.60	1.20	9.05	15.53	0.58	[19]
PK Panel Study, IM (AS = 1)	(*E*)-DE-Clom	Clarithromycin	35.98	26.96	1.33	1.33	1.22	1.09	[19]
PK Panel Study, IM (AS = 1)	(*E*)-4-OH-DE-Clom	Clarithromycin	132.72	71.32	1.86	1.62	1.91	0.85	[19]
PK Panel Study, NM (AS = 2)	(*E*)-Clom	Clarithromycin	117.25	100.98	1.16	13.07	17.22	0.76	[19]
PK Panel Study, NM (AS = 2)	(*E*)-4-OH-Clom	Clarithromycin	304.50	266.53	1.14	14.21	16.36	0.87	[19]
PK Panel Study, NM (AS = 2)	(*E*)-DE-Clom	Clarithromycin	15.33	12.85	1.19	1.05	0.85	1.23	[19]
PK Panel Study, NM (AS = 2)	(*E*)-4-OH-DE-Clom	Clarithromycin	50.59	42.79	1.18	1.98	2.19	0.91	[19]
PK Panel Study, UM (AS = 3)	(*E*)-Clom	Clarithromycin	84.09	88.29	0.95	11.34	13.87	0.82	[19]
PK Panel Study, UM (AS = 3)	(*E*)-4-OH-Clom	Clarithromycin	248.86	172.19	1.45	13.96	11.16	1.25	[19]
PK Panel Study, UM (AS = 3)	(*E*)-DE-Clom	Clarithromycin	11.10	9.79	1.13	0.96	0.45	2.11	[19]
PK Panel Study, UM (AS = 3)	(*E*)-4-OH-DE-Clom	Clarithromycin	35.43	30.40	1.17	1.76	1.61	1.09	[19]
PK Panel Study, PM (AS = 0)	(*E*)-Clom	Paroxetine	1035.07	1204.78	0.86	28.75	40.39	0.71	[19]
PK Panel Study, PM (AS = 0)	(*E*)-4-OH-Clom	Paroxetine	117.15	95.18	1.23	1.11	1.47	0.76	[19]
PK Panel Study, PM (AS = 0)	(*E*)-DE-Clom	Paroxetine	3405.95	4195.92	0.81	27.95	37.12	0.75	[19]
PK Panel Study, PM (AS = 0)	(*E*)-4-OH-DE-Clom	Paroxetine	69.53	63.01	1.10	0.54	0.41	1.31	[19]
PK Panel Study, IM (AS = 0.5)	(*E*)-Clom	Paroxetine	993.64	1053.60	0.94	28.98	35.05	0.83	[19]
PK Panel Study, IM (AS = 0.5)	(*E*)-4-OH-Clom	Paroxetine	139.64	119.04	1.17	1.32	1.30	1.01	[19]
PK Panel Study, IM (AS = 0.5)	(*E*)-DE-Clom	Paroxetine	3094.26	2384.31	1.30	27.70	19.23	1.44	[19]
PK Panel Study, IM (AS = 0.5)	(*E*)-4-OH-DE-Clom	Paroxetine	232.51	173.56	1.34	2.05	1.70	1.20	[19]
PK Panel Study, IM (AS = 1)	(*E*)-Clom	Paroxetine	858.97	855.99	1.00	26.24	34.32	0.76	[19]
PK Panel Study, IM (AS = 1)	(*E*)-4-OH-Clom	Paroxetine	153.97	204.03	0.75	1.30	2.62	0.49	[19]
PK Panel Study, IM (AS = 1)	(*E*)-DE-Clom	Paroxetine	2288.71	2104.81	1.09	23.38	23.47	1.00	[19]
PK Panel Study, IM (AS = 1)	(*E*)-4-OH-DE-Clom	Paroxetine	428.74	349.83	1.23	3.51	2.47	1.42	[19]
PK Panel Study, NM (AS = 2)	(*E*)-Clom	Paroxetine	731.17	828.75	0.88	26.03	41.65	0.63	[19]

(continued)

Table S13. *continued*

Study	Compound	Perpetrator	Pred $\left[\frac{\text{ng}\cdot\text{h}}{\text{ml}}\right]$	Obs $\left[\frac{\text{ng}\cdot\text{h}}{\text{ml}}\right]$	Pred/Obs	Pred $\left[\frac{\text{ng}}{\text{ml}}\right]$	Obs $\left[\frac{\text{ng}}{\text{ml}}\right]$	Pred/Obs	Reference
PK Panel Study, NM (AS = 2)	(*E*)-4-OH-Clom	Paroxetine	199.16	346.58	0.57	2.41	4.27	0.57	[19]
PK Panel Study, NM (AS = 2)	(*E*)-DE-Clom	Paroxetine	1421.08	1170.81	1.21	23.33	20.66	1.13	[19]
PK Panel Study, NM (AS = 2)	(*E*)-4-OH-DE-Clom	Paroxetine	664.56	511.87	1.30	5.53	5.50	1.01	[19]
PK Panel Study, UM (AS = 3)	(*E*)-Clom	Paroxetine	550.74	806.88	0.68	22.29	54.63	0.41	[19]
PK Panel Study, UM (AS = 3)	(*E*)-4-OH-Clom	Paroxetine	212.08	345.90	0.61	3.00	6.46	0.46	[19]
PK Panel Study, UM (AS = 3)	(*E*)-DE-Clom	Paroxetine	722.15	739.59	0.98	16.09	23.37	0.69	[19]
PK Panel Study, UM (AS = 3)	(*E*)-4-OH-DE-Clom	Paroxetine	545.59	400.60	1.36	6.51	6.49	1.00	[19]
				GMFE: 1.30 (1.00–2.71)			**GMFE: 1.40 (1.00–2.83)**		
				GMFE ≤ 2: 38/40			**GMFE ≤ 2: 34/40**		

AS: CYP2D6 acitivity score, **DD(G)I**: drug-drug and drug-drug-gene interactions, **(*E*)-4-OH-Clom**: (*E*)-4-hydroxyclomiphene, **(*E*)-4-OH-DE-Clom**: (*E*)-4-hydroxy-N-desethylclomiphene, **(*E*)-Clom**: (*E*)-clomiphene, **(*E*)-DE-Clom**: (*E*)-N-desethylclomiphene, **IM**: intermediate metabolizers, **NM**: normal metabolizers, **Obs**: observed, **PK**: pharmacokinetic, **PM**: poor metabolizers, **Pred**: predicted, **UM**: ultrarapid metabolizers

Table S14. Geometric Mean Fold Error (GMFE) of DD(G)I AUC_{last} and C_{max} ratios.

			AUC_{last} Ratio			C_{max} Ratio			
Study	Compound	Perpetrator	Pred [1]	Obs [1]	Pred/Obs	Pred [1]	Obs [1]	Pred/Obs	Reference
PK Panel Study, PM (AS = 0)	(*E*)-Clom	Clarithromycin	2.41	2.13	1.13	1.53	1.55	0.98	[19]
PK Panel Study, PM (AS = 0)	(*E*)-4-OH-Clom	Clarithromycin	2.81	1.28	2.20	2.44	1.01	2.41	[19]
PK Panel Study, PM (AS = 0)	(*E*)-DE-Clom	Clarithromycin	0.76	0.66	1.16	0.61	0.54	1.14	[19]
PK Panel Study, PM (AS = 0)	(*E*)-4-OH-DE-Clom	Clarithromycin	1.62	0.59	2.74	1.74	0.67	2.59	[19]
PK Panel Study, IM (AS = 0.5)	(*E*)-Clom	Clarithromycin	1.46	1.82	0.80	1.18	1.59	0.75	[19]
PK Panel Study, IM (AS = 0.5)	(*E*)-4-OH-Clom	Clarithromycin	1.75	1.72	1.02	1.41	1.40	1.00	[19]
PK Panel Study, IM (AS = 0.5)	(*E*)-DE-Clom	Clarithromycin	0.30	0.30	0.97	0.17	0.19	0.92	[19]
PK Panel Study, IM (AS = 0.5)	(*E*)-4-OH-DE-Clom	Clarithromycin	0.45	0.36	1.24	0.25	0.25	0.97	[19]
PK Panel Study, IM (AS = 1)	(*E*)-Clom	Clarithromycin	1.23	1.97	0.62	1.10	1.73	0.63	[19]
PK Panel Study, IM (AS = 1)	(*E*)-4-OH-Clom	Clarithromycin	1.40	1.66	0.84	1.18	1.67	0.70	[19]
PK Panel Study, IM (AS = 1)	(*E*)-DE-Clom	Clarithromycin	0.19	0.34	0.56	0.19	0.47	0.41	[19]
PK Panel Study, IM (AS = 1)	(*E*)-4-OH-DE-Clom	Clarithromycin	0.38	0.44	0.86	0.21	0.39	0.55	[19]
PK Panel Study, NM (AS = 2)	(*E*)-Clom	Clarithromycin	1.15	1.22	0.95	1.07	1.59	0.67	[19]
PK Panel Study, NM (AS = 2)	(*E*)-4-OH-Clom	Clarithromycin	1.29	1.22	1.05	1.13	1.04	1.08	[19]
PK Panel Study, NM (AS = 2)	(*E*)-DE-Clom	Clarithromycin	0.29	0.22	1.31	0.26	0.19	1.36	[19]
PK Panel Study, NM (AS = 2)	(*E*)-4-OH-DE-Clom	Clarithromycin	0.27	0.22	1.24	0.25	0.29	0.87	[19]
PK Panel Study, UM (AS = 3)	(*E*)-Clom	Clarithromycin	1.11	1.33	0.84	1.06	1.80	0.59	[19]
PK Panel Study, UM (AS = 3)	(*E*)-4-OH-Clom	Clarithromycin	1.21	1.82	0.67	1.09	1.20	0.91	[19]
PK Panel Study, UM (AS = 3)	(*E*)-DE-Clom	Clarithromycin	0.34	0.41	0.82	0.31	0.23	1.33	[19]
PK Panel Study, UM (AS = 3)	(*E*)-4-OH-DE-Clom	Clarithromycin	0.33	0.46	0.72	0.29	0.38	0.77	[19]
PK Panel Study, PM (AS = 0)	(*E*)-Clom	Paroxetine	1.13	1.10	1.02	1.07	0.91	1.17	[19]
PK Panel Study, PM (AS = 0)	(*E*)-4-OH-Clom	Paroxetine	1.15	1.02	1.13	1.13	1.19	0.95	[19]
PK Panel Study, PM (AS = 0)	(*E*)-DE-Clom	Paroxetine	1.00	1.21	0.83	0.94	1.36	0.70	[19]
PK Panel Study, PM (AS = 0)	(*E*)-4-OH-DE-Clom	Paroxetine	1.13	1.01	1.12	1.13	0.94	1.21	[19]
PK Panel Study, IM (AS = 0.5)	(*E*)-Clom	Paroxetine	2.47	2.49	0.99	1.39	1.30	1.07	[19]
PK Panel Study, IM (AS = 0.5)	(*E*)-4-OH-Clom	Paroxetine	0.42	0.23	1.83	0.24	0.09	2.62	[19]
PK Panel Study, IM (AS = 0.5)	(*E*)-DE-Clom	Paroxetine	4.17	5.34	0.78	1.86	1.29	1.44	[19]
PK Panel Study, IM (AS = 0.5)	(*E*)-4-OH-DE-Clom	Paroxetine	0.38	0.31	1.23	0.24	0.22	1.10	[19]
PK Panel Study, IM (AS = 1)	(*E*)-Clom	Paroxetine	5.08	9.56	0.53	1.76	4.02	0.44	[19]
PK Panel Study, IM (AS = 1)	(*E*)-4-OH-Clom	Paroxetine	0.50	0.95	0.53	0.17	0.28	0.60	[19]
PK Panel Study, IM (AS = 1)	(*E*)-DE-Clom	Paroxetine	12.21	26.61	0.46	3.40	9.07	0.37	[19]
PK Panel Study, IM (AS = 1)	(*E*)-4-OH-DE-Clom	Paroxetine	1.23	2.16	0.57	0.46	0.50	0.92	[19]
PK Panel Study, NM (AS = 2)	(*E*)-Clom	Paroxetine	7.19	9.99	0.72	2.13	3.85	0.55	[19]

(continued)

Table S14. *continued*

Study	Compound	Perpetrator	Pred [1]	Obs [1]	Pred/Obs	Pred [1]	Obs [1]	Pred/Obs	Reference
PK Panel Study, NM (AS = 2)	(*E*)-4-OH-Clom	Paroxetine	0.84	1.59	0.53	0.19	0.27	0.71	[19]
PK Panel Study, NM (AS = 2)	(*E*)-DE-Clom	Paroxetine	26.73	20.02	1.34	5.70	4.59	1.24	[19]
PK Panel Study, NM (AS = 2)	(*E*)-4-OH-DE-Clom	Paroxetine	3.58	2.64	1.36	0.71	0.74	0.96	[19]
PK Panel Study, UM (AS = 3)	(*E*)-Clom	Paroxetine	7.29	12.19	0.60	2.08	7.08	0.29	[19]
PK Panel Study, UM (AS = 3)	(*E*)-4-OH-Clom	Paroxetine	1.03	3.66	0.28	0.24	0.70	0.34	[19]
PK Panel Study, UM (AS = 3)	(*E*)-DE-Clom	Paroxetine	21.90	30.93	0.71	5.27	12.14	0.43	[19]
PK Panel Study, UM (AS = 3)	(*E*)-4-OH-DE-Clom	Paroxetine	5.08	6.07	0.84	1.08	1.54	0.70	[19]
				GMFE: 1.40 (1.00–3.55)		**GMFE: 1.50 (1.00–3.40)**			
				GMFE ≤ 2: 36/40		**GMFE ≤ 2: 31/40**			
				Guest limits: 29/40		**Guest limits: 23/40**			

AS: CYP2D6 acitivity score, **DD(G)I**: drug-drug and drug-drug-gene interactions, **(*E*)-4-OH-Clom**: (*E*)-4-hydroxyclomiphene, **(*E*)-4-OH-DE-Clom**: (*E*)-4-hydroxy-N-desethylclomiphene, **(*E*)-Clom**: (*E*)-clomiphene, **(*E*)-DE-Clom**: (*E*)-N-desethylclomiphene, **IM**: intermediate metabolizers, **NM**: normal metabolizers, **Obs**: observed, **PK**: pharmacokinetic, **PM**: poor metabolizers, **Pred**: predicted, **UM**: ultrarapid metabolizers

S4.4. Local Sensitivity Analysis

S4.4.1. Mathematical Implementation

A sensitivity analysis of the developed model was conducted to explore the impact of single parameter changes (local sensitivity analysis) on the predicted AUC_{inf}. According to Equation S4, the relative change of AUC_{inf} after oral application of a single dose of 100 mg clomiphene citrate to the relative variation of model input parameters was calculated. All optimized parameters as well as parameters that might have a strong impact because of calculation methods employed in the model (e.g., lipophilicity) were integrated in the sensitivity analysis and a relative perturbation of 10% was used.

$$S = \frac{\Delta AUC_{inf}}{\Delta p} \cdot \frac{p}{AUC_{inf}} \tag{S4}$$

S is the sensitivity of the AUC_{inf} to the examined model parameter, ΔAUC_{inf} is the change of the AUC_{inf}, AUC_{inf} represents the simulated AUC_{inf} with the original parameter value, p is the original model parameter value and Δp the variation of the model parameter value. A sensitivity value of +1.0 signifies that a 10% increase of the examined parameter causes a 10% increase of the simulated AUC_{inf}.

S4.4.2. Results of the Sensitivity Analysis

(a) Sensitivity Analysis (*E*)-Clom

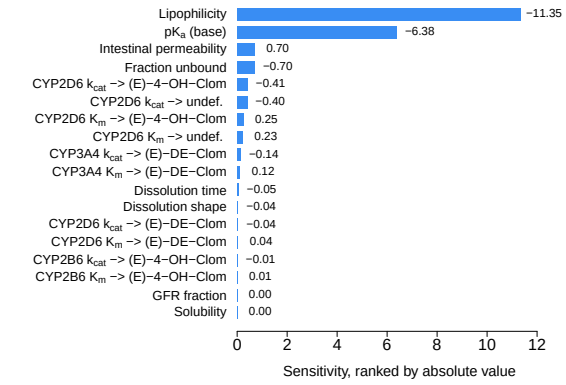

(b) Sensitivity Analysis (*E*)-4-OH-Clom

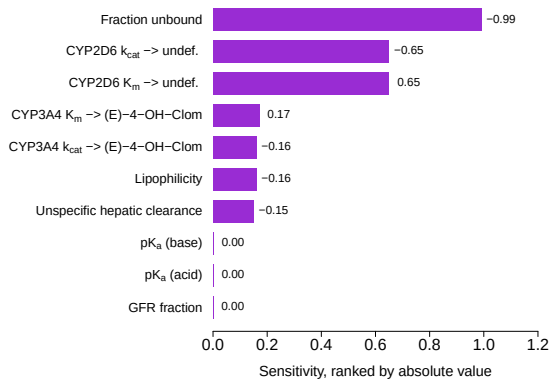

(c) Sensitivity Analysis (*E*)-Clom

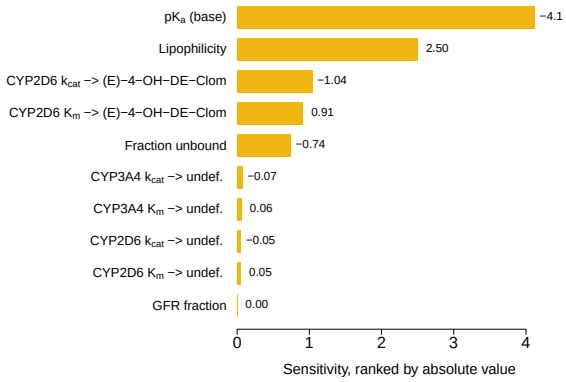

(d) Sensitivity Analysis (*E*)-4-OH-Clom

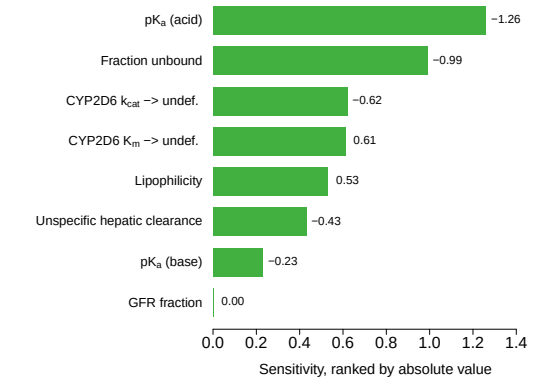

Figure S14. Sensitivity analysis of the PBPK model for (*E*)-Clom, (*E*)-4-OH-Clom, (*E*)-DE-Clom and (*E*)-4-OH-DE-Clom. CYP, cytochrome P450; **(*E*)-4-OH-Clom**, (*E*)-4-hydroxyclomiphene; **(*E*)-4-OH-DE-Clom**, (*E*)-4-hydroxy-N-desethylclomiphene; **(*E*)-Clom**, (*E*)-clomiphene; **(*E*)-DE-Clom**, (*E*)-N-desethylclomiphene; **GFR**, glomerular filtration rate; $\mathbf{k_{cat}}$, catalytic rate constant; $\mathbf{K_m}$, Michaelis Menten constant; $\mathbf{pK_a}$, acid dissociation constant; **undef.**, undefined metabolite.

S5. Molecular Structures

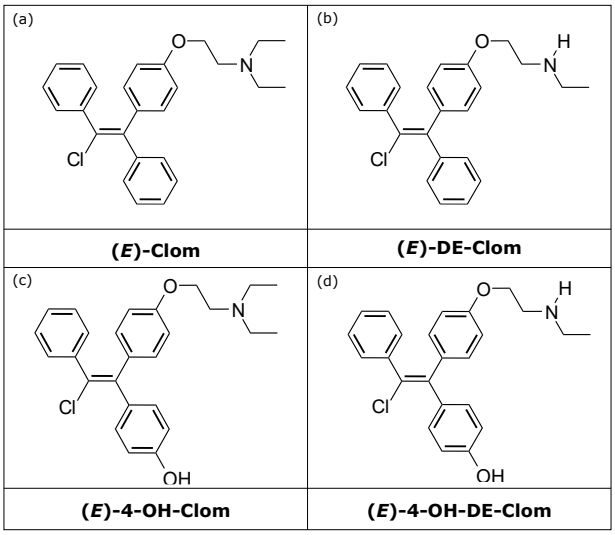

Figure S15. Molecular structures of (*E*)-Clom (a) and its metabolites (*E*)-DE-Clom (b), (*E*)-4-OH-Clom (c) and (*E*)-4-OH-DE-Clom (d). (*E*)-4-OH-Clom, (*E*)-4-hydroxyclomiphene; **(*E*)-4-OH-DE-Clom**, (*E*)-4-hydroxy-N-desethylclomiphene; **(*E*)-Clom**, (*E*)-clomiphene; **(*E*)-DE-Clom**, (*E*)-N-desethylclomiphene.

References

[1] Mikkelson TJ, Kroboth PD, Cameron WJ, Dittert LW, Chungi V, Manberg PJ (1986) Single-dose pharmacokinetics of clomiphene citrate in normal volunteers**Supported by a grant from Serono Laboratories, Inc., Randolph, Massachusetts. Fertility and Sterility 46(3):392–396

[2] Ratiopharm® GmbH (2016) Clomifen-ratiopharm® 50 mg Tabletten (Study 1991). https://www.ratiopharm.de/produkte/details/praeparate/praeparatedaten/detail/pzn-3884844.html, available online (accessed: 2021-11-23)

[3] Wiehle R, Cunningham GR, Pitteloud N, Wike J, Hsu K, Fontenot GK, Rosner M, Dwyer A, Podolski J (2013) Testosterone Restoration by Enclomiphene Citrate in Men with Secondary Hypogonadism: Pharmacodynamics and Pharmacokinetics. BJU international 112(8):1188–1200

[4] Miller GD, Moore C, Nair V, Hill B, Willick SE, Rogol AD, Eichner D (2019) Hypothalamic-Pituitary-Testicular Axis Effects and Urinary Detection Following Clomiphene Administration in Males. The Journal of clinical endocrinology and metabolism 104(3):906–914

[5] van der Lee M, Allard WG, Vossen RHAM, Baak-Pablo RF, Menafra R, Deiman BALM, Deenen MJ, Neven P, Johansson I, Gastaldello S, Ingelman-Sundberg M, Guchelaar HJ, Swen JJ, Anvar SY (2021) Toward predicting CYP2D6-mediated variable drug response from CYP2D6 gene sequencing data. Science translational medicine 13(603)

[6] Valentin J (2002) Basic anatomical and physiological data for use in radiological protection: reference values. A report of age- and gender-related differences in the anatomical and physiological characteristics of reference individuals. ICRP Publication 89. Annals of the ICRP 32(3-4):5–265

[7] Open Systems Pharmacology Suite Community (2018) PK-Sim® Ontogeny Database Documentation, Version 7.3. https://github.com/Open-Systems-Pharmacology/OSPSuite.Documentation/blob/master/PK-SimOntogenyDatabaseVersion7.3.pdf, available online (accessed: 2020-03-25)

[8] National Center for Health Statistics (1997) Third National Health and Nutrition Examination Survey (NHANES III). Tech. rep., Hyattsville, MD 20782

[9] Willmann S, Höhn K, Edginton A, Sevestre M, Solodenko J, Weiss W, Lippert J, Schmitt W (2007) Development of a physiology-based whole-body population model for assessing the influence of individual variability on the pharmacokinetics of drugs. Journal of pharmacokinetics and pharmacodynamics 34(3):401–31

[10] Rodrigues AD (1999) Integrated cytochrome P450 reaction phenotyping: attempting to bridge the gap between cDNA-expressed cytochromes P450 and native human liver microsomes. Biochemical pharmacology 57(5):465–80

[11] Nishimura M, Yaguti H, Yoshitsugu H, Naito S, Satoh T (2003) Tissue distribution of mRNA expression of human cytochrome P450 isoforms assessed by high-sensitivity real-time reverse transcription PCR. Yakugaku zasshi : Journal of the Pharmaceutical Society of Japan 123(5):369–75

[12] Rowland Yeo K, Walsky RL, Jamei M, Rostami-Hodjegan A, Tucker GT (2011) Prediction of time-dependent CYP3A4 drug-drug interactions by physiologically based pharmacokinetic modelling: impact of inactivation parameters and enzyme turnover. European journal of pharmaceutical sciences : official journal of the European Federation for Pharmaceutical Sciences 43(3):160–73

[13] Greenblatt DJ, von Moltke LL, Harmatz JS, Chen G, Weemhoff JL, Jen C, Kelley CJ, LeDuc BW, Zinny MA (2003) Time course of recovery of cytochrome p450 3A function after single doses of grapefruit juice. Clinical pharmacology and therapeutics 74(2):121–9

[14] Tsamandouras N, Rostami-Hodjegan A, Aarons L (2015) Combining the 'bottom up' and 'top down' approaches in pharmacokinetic modelling: fitting PBPK models to observed clinical data. British journal of clinical pharmacology 79(1):48–55

[15] Austin RP, Barton P, Cockroft SL, Wenlock MC, Riley RJ (2002) The influence of nonspecific microsomal binding on apparent intrinsic clearance, and its prediction from physicochemical properties. Drug metabolism and disposition: the biological fate of chemicals 30(12):1497–503

[16] Obach RS (1997) Nonspecific binding to microsomes: impact on scale-up of in vitro intrinsic clearance to hepatic clearance as assessed through examination of warfarin, imipramine, and propranolol. Drug metabolism and disposition: the biological fate of chemicals 25(12):1359–69

[17] Mürdter TE, Kerb R, Turpeinen M, Schroth W, Ganchev B, Böhmer GM, Igel S, Schaeffeler E, Zanger U, Brauch H, Schwab M (2012) Genetic polymorphism of cytochrome P450 2D6 determines oestrogen receptor activity of the major infertility drug clomiphene via its active metabolites. Human molecular genetics 21(5):1145–54

[18] Ganchev B (2014) Charakterisierung der metabolischen Bioaktivierung des Clomifens unter besonderer Berücksichtigung genetischer Polymorphismen. PhD thesis, Eberhard Karls University Tübingen

[19] Kröner P (2018) Hydroxylierte Metaboliten des Clomifens : in vitro und in vivo Untersuchungen zur Bildung, Aktivität und Konjugation. PhD thesis, Eberhard-Karls-University Tübingen

[20] Mazzarino M, Biava M, de la Torre X, Fiacco I, Botrè F (2013) Characterization of the biotransformation pathways of clomiphene, tamoxifen and toremifene as assessed by LC-MS/(MS) following in vitro and excretion studies. Analytical and bioanalytical chemistry 405(16):5467–87

[21] Watanabe R, Esaki T, Kawashima H, Natsume-Kitatani Y, Nagao C, Ohashi R, Mizuguchi K (2018) Predicting Fraction Unbound in Human Plasma from Chemical Structure: Improved Accuracy in the Low Value Ranges. Molecular pharmaceutics 15(11):5302–5311

[22] Siramshetty VB, Grishagin I, Nguyen cT, Peryea T, Skovpen Y, Stroganov O, Katzel D, Sheils T, Jadhav A, Mathé EA, Southall NT (2022) NCATS Inxight Drugs: a comprehensive and curated portal for translational research. Nucleic acids research 50(D1):D1307–D1316

[23] Developed by ChemAxon (2009) (http://www.chemaxon.com), chemicalize was used for prediction of (E)-clomiphene properties. https://chemicalize.com/, available online (accessed: 2021-08-09)

[24] Das P, Prajapati M, Maity A (2020) Study of equilibrium solubility of Clomiphene Citrate as model compound by Saturation orbital shake flask method 3(4):843–847

[25] Smith DA, Dalvie D (2012) Why do metabolites circulate? Xenobiotica; the fate of foreign compounds in biological systems 42(1):107–26

[26] Wishart DS, Knox C, Guo AC, Shrivastava S, Hassanali M, Stothard P, Chang Z, Woolsey J (2006) DrugBank: a comprehensive resource for in silico drug discovery and exploration. Nucleic acids research 34(Database issue):D668–72

[27] Güngör S, Delgado-Charro MB, Masini-Etévé V, Potts RO, Guy RH (2013) Transdermal flux predictions for selected selective oestrogen receptor modulators (SERMs): comparison with experimental results. Journal of controlled release : official journal of the Controlled Release Society 172(3):601–6

[28] Schmitt W (2008) General approach for the calculation of tissue to plasma partition coefficients. Toxicology in vitro : an international journal published in association with BIBRA 22(2):457–67

[29] Kawai R, Lemaire M, Steimer JL, Bruelisauer A, Niederberger W, Rowland M (1994) Physiologically based pharmacokinetic study on a cyclosporin derivative, SDZ IMM 125. Journal of pharmacokinetics and biopharmaceutics 22(5):327–65

[30] Developed by ChemAxon (2009) (http://www.chemaxon.com), chemicalize was used for prediction of (E)-N-desethylclomiphene properties. https://chemicalize.com/, available online (accessed: 2021-08-09)

[31] Kim S, Chen J, Cheng T, Gindulyte A, He J, He S, Li Q, Shoemaker BA, Thiessen PA, Yu B, Zaslavsky L, Zhang J, Bolton EE (2021) PubChem in 2021: new data content and improved web interfaces. Nucleic acids research 49(D1):D1388–D1395

[32] Rodgers T, Leahy D, Rowland M (2005) Physiologically based pharmacokinetic modeling 1: predicting the tissue distribution of moderate-to-strong bases. Journal of pharmaceutical sciences 94(6):1259–76

[33] Rodgers T, Rowland M (2006) Physiologically based pharmacokinetic modelling 2: predicting the tissue distribution of acids, very weak bases, neutrals and zwitterions. Journal of pharmaceutical sciences 95(6):1238–57

[34] Developed by ChemAxon (2009) (http://www.chemaxon.com), chemicalize was used for prediction of (E)-4-hydroxyclomiphene properties. https://chemicalize.com/, available online (accessed: 2021-08-09)

[35] European Medicines Agency (2018) Assessment Report EnCyzix. https://www.ema.europa.eu/en/documents/assessment-report/encyzix-epar-public-assessment-report_en.pdf, available online (accessed: 2021-08-12)

[36] Berezhkovskiy LM (2004) Volume of distribution at steady state for a linear pharmacokinetic system with peripheral elimination. Journal of pharmaceutical sciences 93(6):1628–40

[37] Open Systems Pharmacology Suite Community (2021) Open Systems Pharmacology Suite Manual. https://raw.githubusercontent.com/Open-Systems-Pharmacology/OSPSuite.Documentation/master/OpenSystemsPharmacologySuite.pdf, available online (accessed: 2022-02-19)

[38] Developed by ChemAxon (2009) (http://www.chemaxon.com), chemicalize was used for prediction of (E)-4-hydroxy-N-desethylclomiphene properties. https://chemicalize.com/, available online (accessed: 2021-08-09)

[39] T'jollyn H, Snoeys J, Vermeulen A, Michelet R, Cuyckens F, Mannens G, Van Peer A, Annaert P, Allegaert K, Van Bocxlaer J, Boussery K (2015) Physiologically Based Pharmacokinetic Predictions of Tramadol Exposure Throughout Pediatric Life: an Analysis of the Different Clearance Contributors with Emphasis on CYP2D6 Maturation. The AAPS journal 17(6):1376–87

[40] United States Pharmacopeial Convention (2006) United States Pharmacopeia and National Formulary (USP 29-NF 24). p 553, http://www.pharmacopeia.cn/v29240/usp29nf24s0_m18490.html, available online (accessed: 2021-08-24)

[41] Beal SL (2001) Ways to fit a PK model with some data below the quantification limit. Journal of pharmacokinetics and pharmacodynamics 28(5):481–504

[42] Obach RS, Walsky RL, Venkatakrishnan K (2007) Mechanism-based inactivation of human cytochrome p450 enzymes and the prediction of drug-drug interactions. Drug metabolism and disposition: the biological fate of chemicals 35(2):246–55

[43] Hanke N, Frechen S, Moj D, Britz H, Eissing T, Wendl T, Lehr T (2018) PBPK Models for CYP3A4 and P-gp DDI Prediction: A Modeling Network of Rifampicin, Itraconazole, Clarithromycin, Midazolam, Alfentanil, and Digoxin. CPT: pharmacometrics & systems pharmacology 7(10):647–659

[44] Rüdesheim S, Selzer D, Mürdter T, Igel S, Kerb R, Schwab M, Lehr T (2022) Physiologically Based Pharmacokinetic Modeling to Describe the CYP2D6 Activity Score-Dependent Metabolism of Paroxetine, Atomoxetine and Risperidone. Pharmaceutics 14(8):1734

[45] Guest EJ, Aarons L, Houston JB, Rostami-Hodjegan A, Galetin A (2011) Critique of the two-fold measure of prediction success for ratios: application for the assessment of drug-drug interactions. Drug metabolism and disposition: the biological fate of chemicals 39(2):170–3

B.5 PROJECT V: SUPPLEMENTARY MATERIALS

CPT:PSP

Physiologically Based Pharmacokinetic Modeling of Quinidine to Establish a CYP3A4, P-gp and CYP2D6 Drug-Drug-Gene Interaction Network

Supplement S1 - Model Information and Evaluation

Denise Feick[1], Simeon Rüdesheim[1,2], Fatima Zahra Marok[1], Dominik Selzer [1], Helena Leonie Hanae Loer[1], Donato Teutonico[3], Sebastian Frechen[4], Maaike van der Lee [5], Dirk Jan A. R. Moes[5], Jesse J. Swen[5], Matthias Schwab[2,6,7], and Thorsten Lehr[1]

[1]Clinical Pharmacy, Saarland University, Saarbrücken, Germany
[2]Dr. Margarete Fischer-Bosch-Institute of Clinical Pharmacology, Stuttgart, Germany
[3]Translational Medicine & Early Development, Sanofi-Aventis R&D, Chilly-Mazarin, France
[4]Bayer AG, Pharmaceuticals, Research & Development, Systems Pharmacology & Medicine, Leverkusen, Germany
[5]Department of Clinical Pharmacy & Toxicology, Leiden University Medical Center, Leiden, The Netherlands
[6]Departments of Clinical Pharmacology, Pharmacy and Biochemistry, University of Tübingen, Tübingen, Germany
[7]Cluster of Excellence iFIT (EXC2180) "Image-guided and Functionally Instructed Tumor Therapies", University of Tübingen, Tübingen, Germany

Funding:

This work is part of the Horizon 2020 INSPIRATION (Qualified Open Systems Pharmacology Modeling Network of Drug-Drug-Gene-Interactions) project. The INSPIRATION project (FKZ 031L0241) is supported by the German Federal Ministry of Education and Research under the framework of ERACoSysMed. Matthias Schwab was supported in parts by the Robert Bosch Stiftung Stuttgart, Germany, and the Deutsche Forschungsgemeinschaft (DFG) under Germany's Excellence Strategy-EXC 2180-390900677.

Conflict of Interest:

Donato Teutonico is an employee of Sanofi. Donato Teutonico uses Open Systems Pharmacology software, tools, or models in his professional role. Donato Teutonico and Thorsten Lehr are members of the Open Systems Pharmacology Management Team. Sebastian Frechen uses Open Systems Pharmacology software, tools, or models in his professional role. Sebastian Frechen is a member of the Open Systems Pharmacology Sounding Board. All other authors declared no competing interest for this work.

Corresponding Author:

Prof. Dr. Thorsten Lehr, Clinical Pharmacy, Saarland University, Campus C5 3, 66123 Saarbrücken, Germany, Phone: +49 681 302 70255, Email: thorsten.lehr@mx.uni-saarland.de

Contents

S1 PBPK Model Building

S1.1 System-Dependent Parameters

Table S1: Relevant enzymes, transporters and binding proteins

			Reference concentration [µmol/L]	
Protein	**Relevant model**	**Highest expression**	**Mean[a]**	**GSD**
Enzymes				
AADAC	Rifampicin	Liver [1]	1.00[b] [2]	1.40[c]
CYP1A2	Fluvoxamine, Mexiletine	Liver [3]	1.80 [4]	1.63 [5]
CYP2B6	Carbamazepine	Liver [1]	1.56 [4]	1.56 [5]
CYP2C8	Carbamazepine	Liver [3]	2.56 [4]	2.05 [5]
CYP2C19	R-/S-Omeprazole	Liver [3]	0.76 [4]	1.80 [5]
CYP2D6	Dextromethorphan, Fluvoxamine, R-/S-Metoprolol, Mexiletine, Paroxetine	Liver [3]	0.40 [4]	2.49 [5]
CYP3A4	Carbamazepine, Dextromethorphan, Dextrorphan, Itraconazole (+ metabolites), R-/S-Omeprazole, Paroxetine, Quinidine, 3-Hydroxyquinidine, R-/S-Verapamil (+ metabolites)	Liver [3]	4.32 [4]	1.18 liver, 1.46 int. [5]
EPHX1	Carbamazepine 10,11-epoxide	Liver [1]	1.00[b] [2]	1.40[c]
UGT2B7	Carbamazepine	Kidney [6]	2.78 [7]	1.60 [5]
UGT2B15	Dextrorphan	Liver [1]	2.48[d] [8, 9]	1.26 [8]
Transporters				
MATE1	Cimetidine	Kidney [10, 11]	0.13[e] [9, 12]	1.53 [12]
OAT3	Cimetidine	Kidney [13]	0.09[e] [9, 12]	1.53 [12]
OATP1B1	Rifampicin	Liver [13]	0.07[f] [14]	1.54 [14]
OCT1	Cimetidine	Liver [15]	0.16[f] [14, 16]	1.50 [16]
P-gp	Digoxin, Quinidine, Rifampicin, R-/S-Verapamil (+ metabolites)	Duodenum mucusa, Upper jejunum mucosa, Lower jejunum mucosa, Upper ileum mucosa Lower ileum mucosa [13]	1.41[g] [17]	1.60 [14]
Binding proteins				
ATP1A2	Digoxin	Brain [15]	0.48[g] [17]	1.40[c]

AADAC: arylacetamide deacetylase, ATP1A2: ATPase Na^+/K^+ transporting subunit alpha 2, CYP: cytochrome P450, EPHX: epoxide hydrolase, GSD: geometric standard deviation, int: intestine, MATE: multidrug and toxin extrusion protein, OAT: organic anion transporter, OATP: organic anion transporting polypeptide, OCT: organic cation transporter, P-gp: P-glycoprotein, UGT: uridine 5'-diphospho-glucuronosyltransferase. [a] In the tissue of highest expression. [b] If no information was available, the mean reference concentration was set to 1.00 µmol/L and the catalytic rate constant was optimized according to [2]. [c] If no information was available, a moderate variability of 35% CV was assumed (= 1.40 GSD). [d] Calculated from protein per mg microsomal protein x 40 mg microsomal protein per g liver [9]. [e] Calculated from transporter per mg membrane protein x 26.2 mg human kidney microsomal protein per g kidney [9]. [f] Calculated from transporter per mg membrane protein x 37.0 mg membrane protein per g liver [14]. [g] Previously optimized by Hanke et al [17].

Table S2: Expression data of relevant enzymes

	AADAC	CYP1A2	CYP2B6	CYP2C8	CYP2C19	CYP2D6	CYP3A4	EPHX1	UGT2B7	UGT2B15
Properties										
Localization	Intracellular	Intracellular	Intracellular	Intracellular	Intracellular	Intracellular	Intracellular	Intracellular	Intracellular	Intracellular
Half-life liver/intestine [h][a]	36/23	39/23	32/23	23/23	26/23	51/23	36/23 [18, 19]	36/23	36/23	36/23
Relative expression in various organs and tissues [%]										
Data source	RT-PCR [1]	RT-PCR [3]	RT-PCR [1]	RT-PCR [3]	RT-PCR [3, 20]	RT-PCR [3]	RT-PCR [3]	RT-PCR [1]	EST [6]	RT-PCR [1]
Blood Cells	0	0	0	0	0	0	0	1	0	0
Plasma	0	0	0	0	0	0	0	1	0	0
Bone	0	0	0	0	0	0	0	2	0	0
Brain	0	0	0	0	0	1	0	4	8	0
Fat	0	0	0	0	0	0	0	0	0	0
Gonads	0	0	1	1	0	77	0	18	13	0
Heart	0	0	0	0	0	0	0	12	0	0
Kidney	0	0	10	0	0	2	1	15	100	0
Liver Periportal	100	100	100	100	100	100	100	100	23	100
Liver Pericentral	100	100	100	100	100	100	100	100	23	100
Lung	3	0	60	0	0	2	0	14	0	0
Muscle	0	0	0	0	0	0	0	36	0	0
Pancreas	15	0	0	0	0	0	0	10	0	2
Skin	0	0	0	0	0	0	0	0	3	0
Spleen	0	0	0	0	0	0	0	6	0	0
Duodenum mucosa	25	0	7	0	2	9	7	6	4	0
Upper jejunum musoca	25	0	7	0	1	9	7	6	4	0
Lower jejunum mucosa	25	0	7	0	1	9	7	6	4	0
Upper ileum mucosa	25	0	7	0	1	9	7	6	4	0
Lower ileum mucosa	25	0	7	0	1	9	7	6	4	0
Colon ascendens mucosa	0	0	0	0	0	0	0	4	0	0
Colon transversum mucosa	0	0	0	0	0	0	0	4	0	0
Colon descendens mucosa	0	0	0	0	0	0	0	4	0	0
Colon sigmoid mucosa	0	0	0	0	0	0	0	4	0	0
Stomach non-muc. tissue	8	0	0	0	0	0	0	5	13	3
Small intestine non-muc. tissue	25	0	7	0	1	9	7	6	4	0
Large intestine non-muc. tissue	0	0	0	0	0	0	0	4	0	0

AADAC: arylacetamide deacetylase, CYP: cytochrome P450, EPHX: epoxide hydrolase, EST: expressed sequence tag, non-muc.: non-mucosal, RT-PCR: reverse transcription-polymerase chain reaction measured expression profile, UGT: uridine 5'-diphospho-glucuronosyltransferase. [a] Information from PK-Sim® expression database.

Table S3: Expression data of relevant transporters and binding proteins

	MATE1	OAT3	OATP1B1	OCT1	P-gp	ATP1A2
Properties						
Localization	Cell membrane	Cell membrane	Cell membrane	Cell membrane	Cell membrane	Interstitial
Direction	Efflux	Influx	Influx	Influx	Efflux	n.a.
Half-life liver/intestine [h][a]	n.a./n.a.	n.a./n.a.	36/23	36/23	36/23	36/23
Relative expression in various organs and tissues [%]						
Data source	[10, 11]	RT-PCR [13]	RT-PCR [13]	Array [15]	RT-PCR [13, 17]	Array [15]
Blood Cells	0	0	0	0	0	0
Plasma	0	0	0	0	0	0
Bone	0	0	0	2	2	1
Brain	0	0	0	1 (blood-brain barrier)	8 (blood-brain barrier)	100
Fat	0	0	0	0	0	0
Gonads	0	0	1	0	2	5
Heart	0	0	0	1	4	32
Kidney	100 (apical)	100 (basolateral)	0	3 (basolateral)	71 (apical)	2
Liver Periportal	0	0	100 (basolateral)	100 (basolateral)	19 (apical)	2
Liver Pericentral	0	0	100 (basolateral)	100 (basolateral)	19 (apical)	2
Lung	0	0	0	1	7	3
Muscle	0	0	0	4	1	70
Pancreas	0	0	0	1	1	1
Skin	0	0	0	1	0	4
Spleen	0	0	0	0	7	1
Duodenum mucosa	0	0	0	2 (apical)	100 (apical)	5
Upper jejunum musoca	0	0	0	2 (apical)	100 (apical)	5
Lower jejunum mucosa	0	0	0	2 (apical)	100 (apical)	5
Upper ileum mucosa	0	0	0	2 (apical)	100 (apical)	5
Lower ileum mucosa	0	0	0	2 (apical)	100 (apical)	5
Colon ascendens mucosa	0	0	0	0	40 (apical)	8
Colon transversum mucosa	0	0	0	0	40 (apical)	8
Colon descendens mucosa	0	0	0	0	40 (apical)	8
Colon sigmoid mucosa	0	0	0	0	40 (apical)	8
Stomach non-mucosal tissue	0	0	0	1	3	3
Small intestine non-mucosal tissue	0	0	0	2	28	5
Large intestine non-mucosal tissue	0	0	0	3	11	8

Array: microarray expression profile, ATP1A2: ATPase Na^+/K^+ transporting subunit alpha 2, MATE: multidrug and toxin extrusion, protein, n.a.: not applicable, OAT: organic anion transporter, OATP: organic anion transporting polypeptide, OCT: organic cation transporter, P-gp: P-glycoprotein, RT-PCR: reverse transcription-polymerase chain reaction measured expression profile. [a] Information from PK-Sim® expression database.

S1.2 Michaelis-Menten Kinetics

$$v = \frac{v_{max} * [S]}{K_M + [S]} = \frac{k_{cat} * [E] * [S]}{K_M + [S]} \tag{S1}$$

v = reaction velocity, v_{max} = maximum reaction velocity, $[S]$ = free substrate concentration, K_M = Michaelis-Menten constant, k_{cat} = catalytic or transporter rate constant and $[E]$ = enzyme concentration.

S1.3 Quinidine – Clinical studies

Table S4: Clinical study data used for quinidine model development

Quinidine administration											
Dose salt [mg]	**Dose base [mg]**	**Route**	**n**	**Population[a]**	**Fem. [%]**	**Age [years]**	**Weight [kg]**	**BMI [kg/m²]**	**Molecule**	**Dataset**	**Reference**
260.3[b]	162.2	s.d. iv 60 min inf	7	European [21]	-	-	-	-	QUI	te	Fremstad 1979 [22]
300[b]	187.5	s.d. iv 30 min inf	9	American [23]	0	28.6 (22-37)	68.4	-	QUI	te	Darbar 1997[c] [24]
300[b]	187.5	s.d. iv 30 min inf	9	American [23]	0	28.6 (22-37)	71.5	-	QUI	te	Darbar 1997[d] [24]
6/kg[b]	3.74/kg	s.d. iv 25 min inf	1	American [23]	0	32	82	-	QUI	te	Guentert 1979 [25]
6/kg[b]	3.74/kg	s.d. iv 25 min inf	1	American [23]	0	23	70.4	-	QUI	te	Guentert 1979 [25]
6/kg[b]	3.74/kg	s.d. iv 25 min inf	1	American [23]	0	23	72.2	-	QUI	te	Guentert 1979 [25]
6.42/kg[b]	4.00/kg	s.d. iv 20 min inf	12	Asian [26]	0	22.1	66.5	-	QUI	te	Shin 2007 [27]
6.42/kg[b]	4.00/kg	s.d. iv 20 min inf	7	American [23]	0	26.2	69.8	-	QUI	te	Shin 2007 [27]
6.42/kg[b]	4.00/kg	s.d. iv 20 min inf	12	Asian [26]	100	22.7	53.4	-	QUI	te	Shin 2007 [27]
6.42/kg[b]	4.00/kg	s.d. iv 20 min inf	6	American [23]	100	27.7	60.7	-	QUI	te	Shin 2007 [27]
481.4[b]	300	s.d. iv 15 min inf	1	European [21]	0	27	60	-	QUI, QUB	tr	Ochs 1980 [28]
481.4[b]	300	s.d. iv 15 min inf	1	European [21]	0	23	80	-	QUI, QUB	tr	Ochs 1980 [28]
520.6[b]	324.4	s.d. iv 60 min inf	6	European [21]	-	-	-	-	QUI	te	Fremstad 1979 [22]
0.1[e]	0.08	s.d. po sol	7	Japanese [29]	0	27	-	21.8	QUI, OHQ	tr	Maeda 2011 [30]
1[e]	0.83	s.d. po sol	7	Japanese [29]	0	27	-	21.8	QUI, OHQ	tr	Maeda 2011 [30]
10[e]	8.29	s.d. po sol	7	Japanese [29]	0	27	-	21.8	QUI, OHQ	tr	Maeda 2011 [30]
100[e]	82.87	s.d. po sol	7	Japanese [29]	0	27	-	21.8	QUI, OHQ	tr	Maeda 2011 [30]
100[e]	82.87	s.d. po tab	9	European [21]	56	25 (21-32)	64 (41-80)	-	QUI	te	Kaukonen 1997 [31]
200[e]	165.7	s.d. po cap	10	European [21]	0	(21-26)	(62-85)	(19-26)	QUI, OHQ	tr	Andreasen 2007 [32]
200[e]	165.7	s.d. po tab	6	European [21]	0	-	-	-	QUI, OHQ	te	Damkier 1999 [33]
200[e]	165.7	s.d. po tab	6	European [21]	0	-	-	-	QUI, OHQ	te	Damkier 1999a [34]
200[e]	165.7	s.d. po tab	12	European [21]	0	24 (19-37)	75 (65-101)	-	QUI	te	Laganière 1996 [35]
200[e]	165.7	s.d. po sol	13	American [23]	11	(22-40)	-	-	QUI	te	Mason 1976 [36]
200[e]	165.7	s.d. po cap	13	American [23]	11	(22-40)	-	-	QUI	te	Mason 1976 [36]
200[e]	165.7	s.d. po tab	13	American [23]	11	(22-40)	-	-	QUI	te	Mason 1976 [36]
250[e]	207.2	s.d. po cap	8	European [21]	0	(18-26)	(48-62)	(162.5-180)[f]	QUI	te	Rao 1995 [37]
400[e]	331.5	s.d. po tab	8	European [21]	0	(22-34)	-	-	QUI	te	Bleske 1990 [38]
400[e]	331.5	s.d. po tab	8	European [21]	0	(22-29)	(60-94)	-	QUI, OHQ	te	Ching 1991 [39]
400[e]	331.5	s.d. po tab	6	European [21]	0	(23-34)	-	-	QUI	te	Edwards 1987 [40]
400[e]	331.5	s.d. po tab	6	American [23]	0	(25-38)	-	-	QUI	te	Hardy 1983 [41]
400[e]	331.5	s.d. po tab	9	American [23]	0	(21-35)	-	-	QUI	te	Kolb 1984 [42]
400[e]	331.5	s.d. po tab	7	European [21]	43	28.9 (27-31)	68.4 (57.7-79.5)	-	QUI	te	Ochs 1978 [43]
400[e]	331.5	s.d. po tab	11	American [23]	0	(20-37)	-	-	-	te	Strum 1977[g] [44]
600[e]	497.2	s.d. po tab	9	American [23]	0	28.6 (22-27)	68.4	-	QUI	tr/te	Darbar 1997[c] [24]
600[e]	497.2	s.d. po tab	9	American [23]	0	28.6 (22-37)	71.5	-	QUI	te	Darbar 1997[d] [24]
600[e]	497.2	s.d. po tab	8	European [21]	0	26.4 (23-37))	67.1 (60-76)	1.74 (1.60-1.83)[f]	QUI	te	Frigo 1977 [45]

BMI: body mass index, calc: calculated, cap: capsule, fem: females, inf: infusion, iv: intravenous, n: number of study participants, OHQ: 3-hydroxyquinidine, po: oral, q.i.d.: four times daily, QUB: quinidine unbound, QUI: quinidine, s.d.: single dose, sol: solution, tab: tablet, te: test dataset, t.i.d.: three times daily, tr: training dataset, -: not available. Values are given as mean (range). Respective doses of quinidine base were calculated and incorporated in simulations. [a] Population used in simulations. [b] Quinidine glucunate dose. [c] Low-salt diet. [d] High-salt diet. [e] Quinidine sulfate dose. [f] Height of subjects [cm]. [g] Administration of four immediate-release formulations (Treatment A-D).

Table S4: Clinical study data used for quinidine model development *(continued)*

Quinidine administration											
Dose salt [mg]	**Dose base [mg]**	**Route**	**n**	**Population[a]**	**Fem. [%]**	**Age [years]**	**Weight [kg]**	**BMI [kg/m²]**	**Molecule**	**Dataset**	**Reference**
200[e]	165.7	t.i.d. po tab	5	European [21]	0	(26-33)	73.4 (62-90)		QUI	te	Bolme 1977 [46]
300[e]	248.6	t.i.d. po tab	5	European [21]	0	(26-33)	73.4 (62-90)	-	QUI	te	Bolme 1977 [46]
400[e]	331.5	t.i.d. po tab	3	European [21]	0	(26-33)	68 (62-75)	-	QUI	te	Bolme 1977 [46]
400 + 200[e]	331.5 +165.7	s.d. + q.i.d. po tab	7	European [21]	43	28.9 (27-31)	68.4 (57.7-79.5)	-	QUI	tr	Ochs 1978 [43]

BMI: body mass index, calc: calculated, cap: capsule, fem: females, inf: infusion, iv: intravenous, n: number of study participants, OHQ: 3-hydroxyquinidine, po: oral, q.i.d.: four times daily, QUB: quinidine unbound, QUI: quinidine, s.d.: single dose, sol: solution, tab: tablet, te: test dataset, t.i.d.: three times daily, tr: training dataset, -: not available. Values are given as mean (range). Respective doses of quinidine base were calculated and incorporated in simulations. [a] Population used in simulations. [b] Quinidine glucunate dose. [c] Low-salt diet. [d] High-salt diet. [e] Quinidine sulfate dose. [f] Height of subjects [cm]. [g] Administration of four immediate-release formulations (Treatment A-D).

S1.4 Quinidine – Drug-dependent parameters

Table S5: Drug-dependent parameters of the quinidine model

	Quinidine			3-Hydoxyquinidine			
Parameter	**Value or 95% CI[a]**	**Source**	**Literature**	**Value or 95% CI[a]**	**Source**	**Literature**	**Description**
MW [g/mol]	324.42	Lit.	324.42 [47, 48]	340.42	Lit.	340.42 [47, 49]	Molecular weight of quinidine base
pK_a (base 1)	4.02	Lit.	4.02 [50]	4.03	Lit.	4.03 [51]	Acid dissociation constant
pK_a (base 2)	9.05	Lit.	9.05 [47, 48]	8.63	Lit.	8.63 [47, 49]	Acid dissociation constant
pK_a (acid)	13.89	Lit.	13.89 [47, 48]	13.55	Lit.	13.55 [47, 49]	Acid dissociation constant
Solubility (pH 7.0) [g/L]	11.11	Lit.	11.11 (quinidine sulfate) [52]	12.57	Lit.	12.57 [51]	Solubility
Lipophilicity	2.51	Lit.	2.51 (logP) [47, 48]	1.66	Lit.	1.66 (logP) [51]	Lipophilicity
$f_{u,p}$ [%]	21	Lit.	21[b] [53]	31	Lit.	31[b] [53]	Fraction unbound plasma
P-gp K_M [µmol/L]	0.23	Lit.	0.23 [54]	-	-	-	Michaelis-Menten constant
P-gp k_{cat} [1/min]	0.77 ± 0.08	Opt.	-	-	-	-	Transport rate constant
CYP3A4 (QUI → OHQ) K_M [µmol/L]	51.8	Lit.	74.0 × 0.70[c] [55, 56]	-	-	-	Michaelis-Menten constant
CYP3A4 (QUI → OHQ) k_{cat} [1/min]	2.21 ± 1.02	Opt.	-	-	-	-	Catalytic rate constant
CYP3A4 (QUI → sink) K_M [µmol/L]	65.03	Lit.	92.9 × 0.70[c] [55, 56]	-	-	-	Michaelis-Menten constant
CYP3A4 (QUI → sink) k_{cat} [1/min]	3.84 ± 1.39	Opt.	-	-	-	-	Catalytic rate constant
CYP3A4 CL [1/min]	-	-	-	0.08 ± 0.06	Opt.	-	First-order clearance
CL_{hep} [1/min]	-	-	-	0.45 ± 0.39	Opt.	-	Hepatic metabolic clearance
GFR fraction	1	Asm.	-	1	Asm.	-	Fraction of filtered drug in the urine
EHC continuous fraction	1	Asm.	-	1	Asm.	-	Fraction of bile continually released
P-gp K_i [µmol/L]	0.10	Lit.	0.10 [57]	-	-	-	Conc. for 50% inhibition (comp.)
CYP2D6 K_i [µmol/L]	0.017	Lit.	0.017[d] [58]	2.30	Lit.	2.30 [59]	Conc. for 50% inhibition (comp.)
Partition coefficients	Diverse	Calc.	Berezhkovskiy [60]	Diverse	Calc.	Berezhkovskiy [60]	Cell to plasma partition coefficients
Cell. perm. [cm/min]	$7.99 \cdot 10^{-3}$	Calc.	PK-Sim [61]	$8.45 \cdot 10^{-4}$	Calc.	PK-Sim [61]	Permeability into the cellular space
Intest. perm. [cm/min]	$6.47 \cdot 10^{-6} \pm 5.78 \cdot 10^{-7}$	Opt.	$2.59 \cdot 10^{-5}$ (calc.)	$2.94 \cdot 10^{-6}$	Calc	$2.94 \cdot 10^{-6}$	Transcellular intestinal permeability
Formulation	Weibull[e]	Lit.	[62, 63]	-	-	-	Formulation used in predictions

asm.: assumed, Berezhkovskiy: Berezhkovskiy calculation method, calc.: calculated, cell.: cellular, CI: confidence interval, CL: clearance, comp.: competitive, conc.: concentration, CYP: cytochrome P450, EHC: enterohepatic circulation, GFR: glomerular filtration rate, intest.: intestinal, lit.: literature, OHQ: 3-hydroxyquinidine, opt.: optimized, P-gp: P-glycoprotein, PK-Sim: PK-Sim standard calculation method, QUI: quinidine, -: not implemented/not available. [a] 95% confidence interval calculated for optimized parameters, [b] Calculated with $f_{u,p}$ predictor [53]. [c] Reported K_M values adjusted for fraction unbound in the incubation (fu_{inc}) = 70% (calculated) [56]. [d] Estimated *in vivo* K_i value reported [58]. [e] Weibull function [64] with a dissolution time of 8.76 min (50% dissolved) and a dissolution shape of 0.42 for immediate release quinidine sulfate formulations (calculated with DDSolver) [62, 63].

S2 Quinidine – PBPK Model Evaluation

S2.1 Plasma concentration-time profiles (semilogarithmic representation)

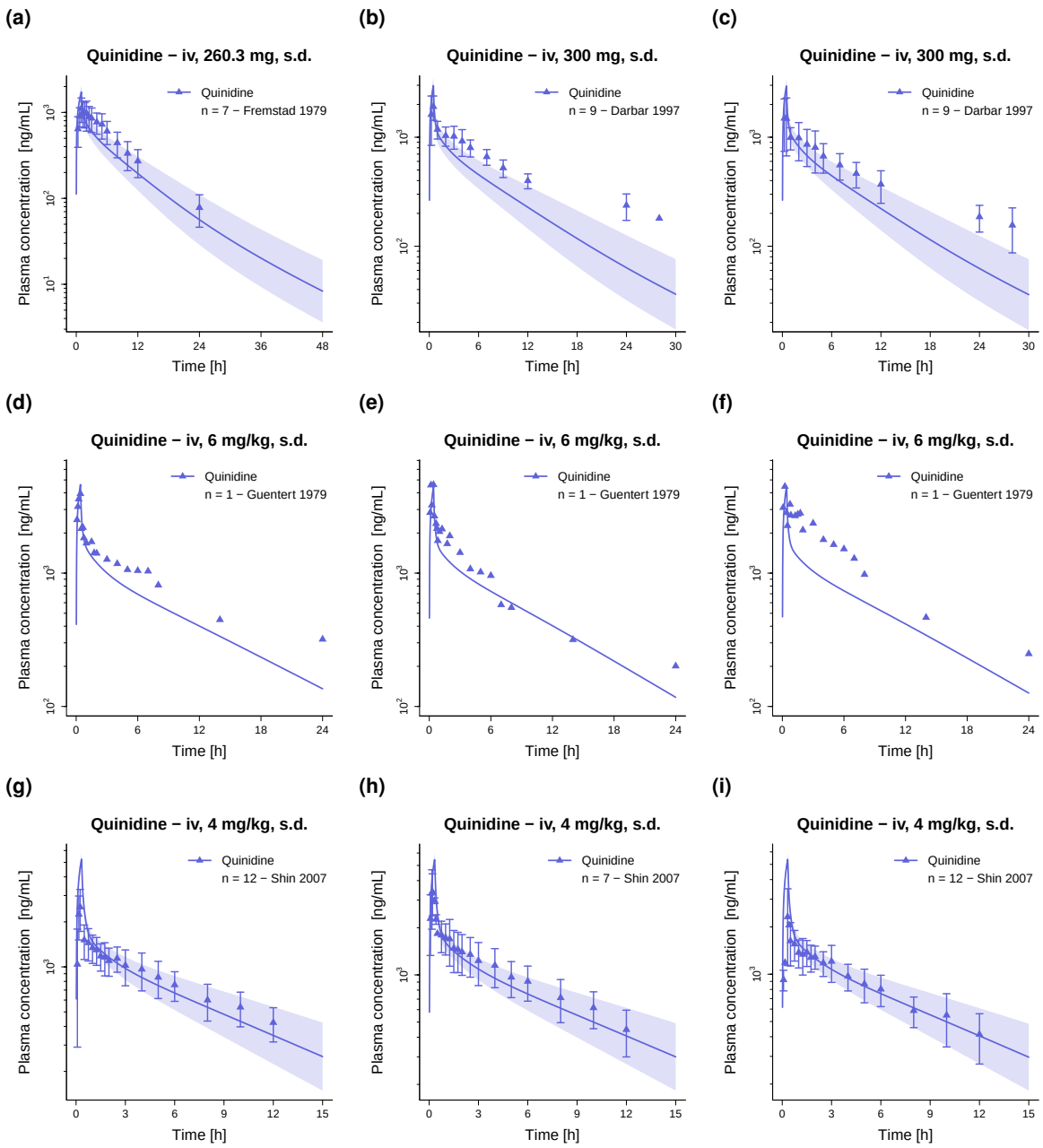

Figure S1: Quinidine plasma concentration-time profiles (semilogarithmic representation). Population predicted geometric means and individual predictions are shown as lines, corresponding geometric standard deviations are shown as shaded areas and observed data are shown as dots (training dataset) and triangles (test dataset) (± standard deviation, if reported). Doses indicate quinidine gluconate administration. Respective doses of quinidine base were calculated and incorporated in simulations. iv: intravenous, n: number of study participants,s.d.: single dose.

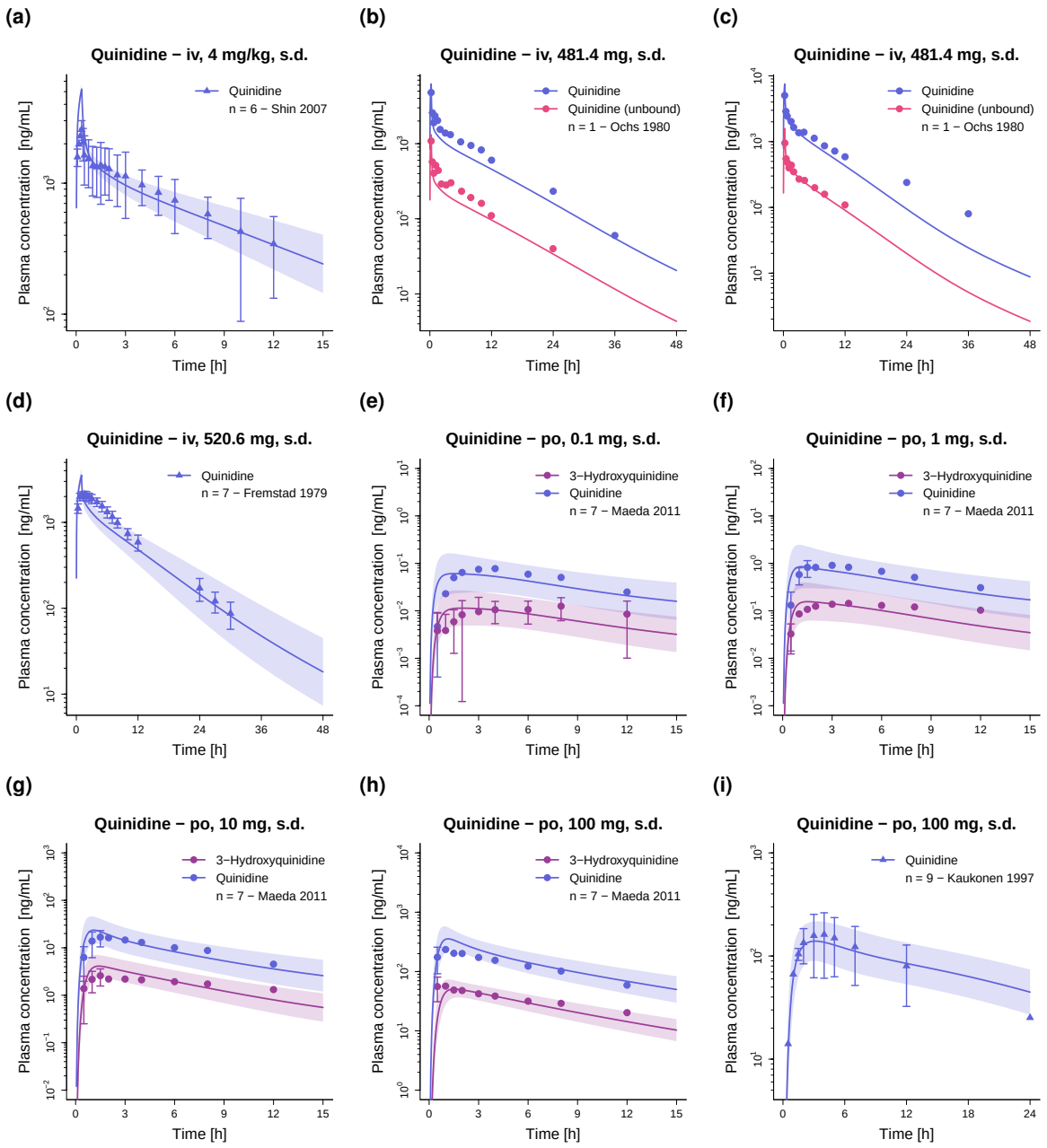

Figure S2: Quinidine plasma concentration-time profiles (semilogarithmic representation). Population predicted geometric means and individual predictions are shown as lines, corresponding geometric standard deviations are shown as shaded areas and observed data are shown as dots (training dataset) and triangles (test dataset) (± standard deviation, if reported). Doses indicate (a–d) quinidine gluconate and (e–i) quinidine sulfate administration. Respective doses of quinidine base were calculated and incorporated in simulations. iv: intravenous, n: number of study participants, po: oral, s.d.: single dose.

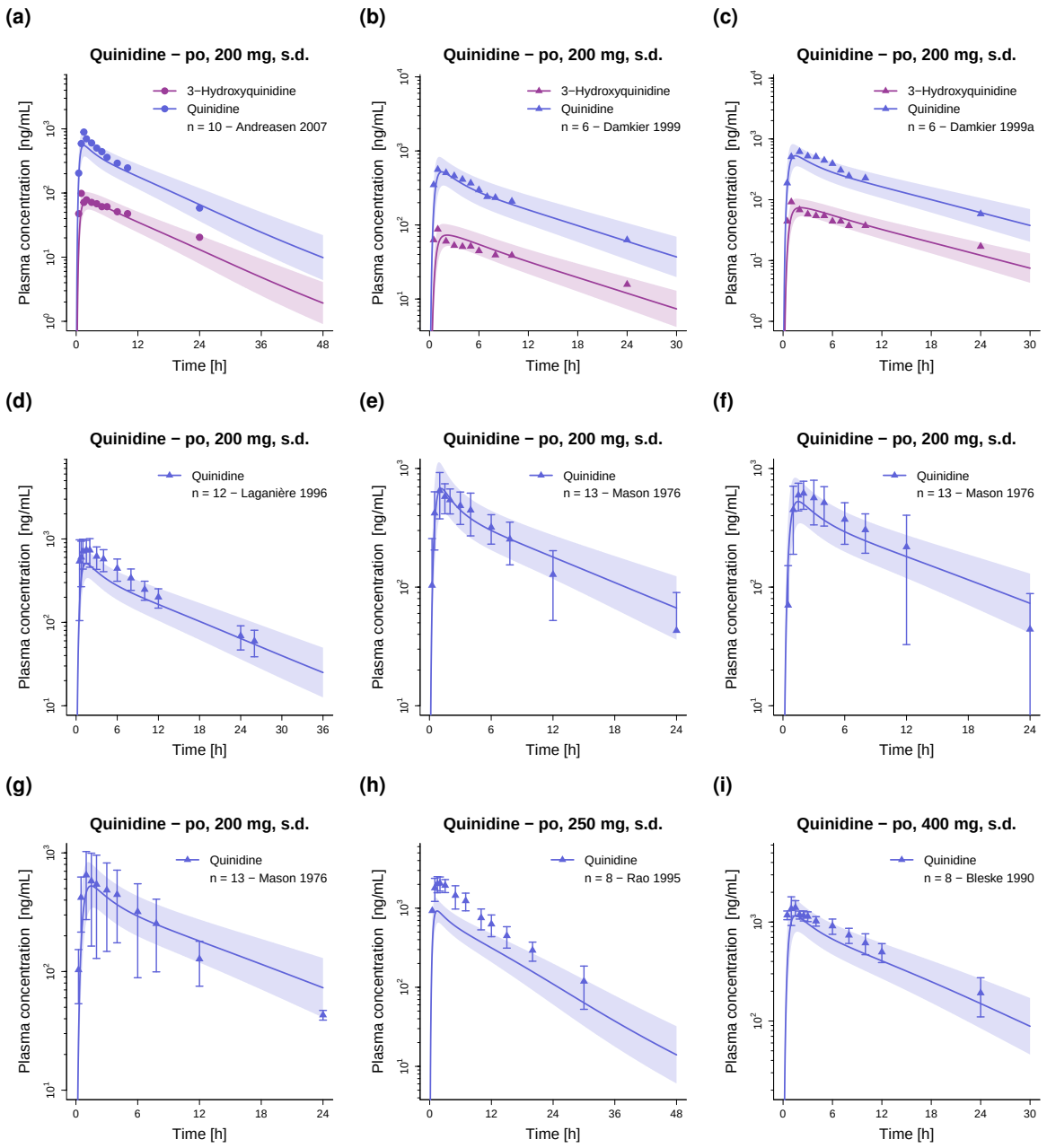

Figure S3: Quinidine plasma concentration-time profiles (semilogarithmic representation). Population predicted geometric means are shown as lines, corresponding geometric standard deviations are shown as shaded areas and observed data are shown as dots (training dataset) and triangles (test dataset) (± standard deviation, if reported). Doses indicate quinidine sulfate administration. Respective doses of quinidine base were calculated and incorporated in simulations. n: number of study participants, po: oral, s.d.: single dose.

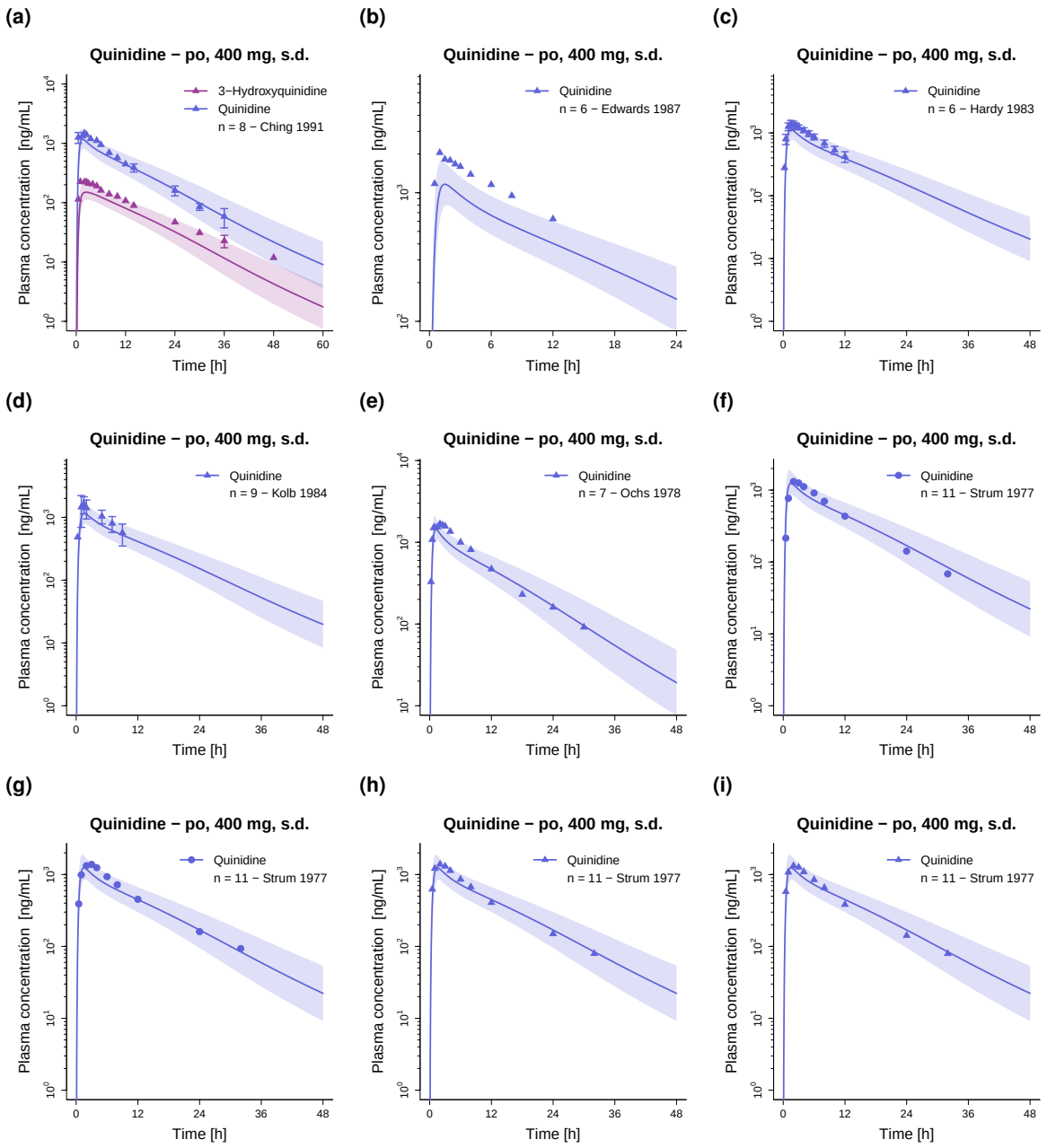

Figure S4: Quinidine plasma concentration-time profiles (semilogarithmic representation). Population predicted geometric means are shown as lines, corresponding geometric standard deviations are shown as shaded areas and observed data are shown as dots (training dataset) and triangles (test dataset) (± standard deviation, if reported). Doses indicate quinidine sulfate administration. Respective doses of quinidine base were calculated and incorporated in simulations. n: number of study participants, po: oral, s.d.: single dose.

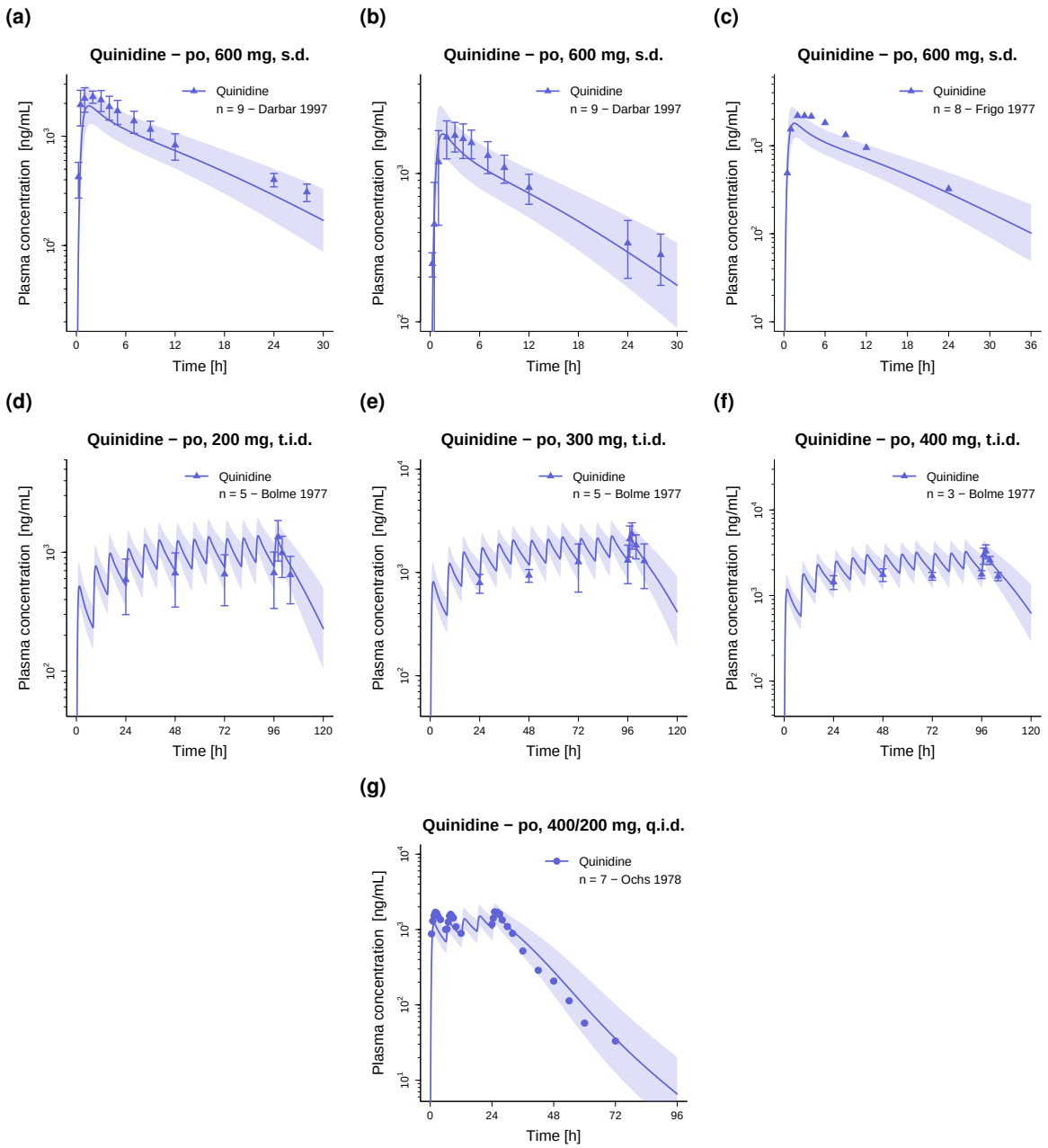

Figure S5: Quinidine plasma concentration-time profiles (semilogarithmic representation). Population predicted geometric means are shown as lines, corresponding geometric standard deviations are shown as shaded areas and observed data are shown as dots (training dataset) and triangles (test dataset) (± standard deviation, if reported). Doses indicate quinidine sulfate administration. Respective doses of quinidine base were calculated and incorporated in simulations. n: number of study participants, po: oral, q.i.d.: four times daily, s.d.: single dose, t.i.d.: three times daily.

S2.2 Amount excreted unchanged in urine profiles (semilogarithmic representation)

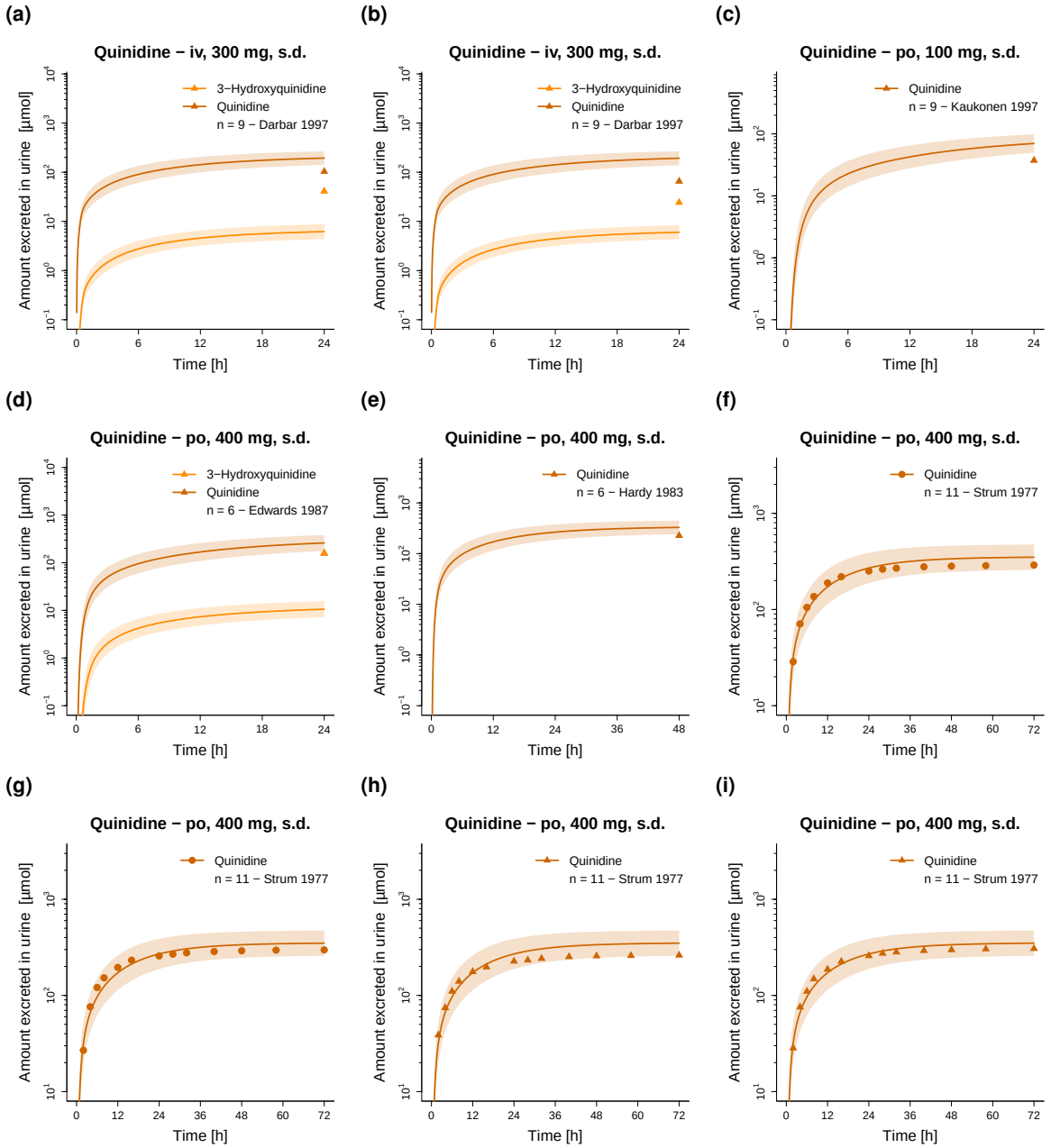

Figure S6: Quinidine amount excreted unchanged in urine profiles (semilogarithmic representation). Population predicted geometric means are shown as lines, corresponding geometric standard deviations are shown as shaded areas and observed data are shown as dots (training dataset) and triangles (test dataset). Doses indicate (a–b) quinidine gluconate and (c–i) quinidine sulfate administration. Respective doses of quinidine base were calculated and incorporated in simulations. iv: intravenous, n: number of study participants, po: oral, s.d.: single dose.

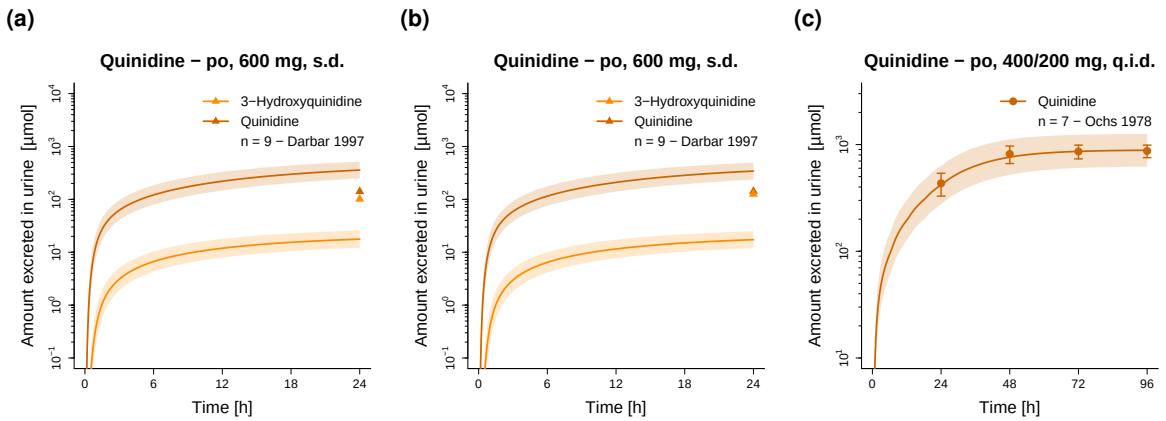

Figure S7: Quinidine amount excreted unchanged in urine profiles (semilogarithmic representation). Population predicted geometric means are shown as lines, corresponding geometric standard deviations are shown as shaded areas and observed data are shown as dots (training dataset) and triangles (test dataset) (± standard deviation, if reported). Doses indicate quinidine sulfate administration. Respective doses of quinidine base were calculated and incorporated in simulations. n: number of study participants, po: oral, q.i.d.: four times daily, s.d.: single dose.

S2.3 Plasma concentration-time profiles (linear representation)

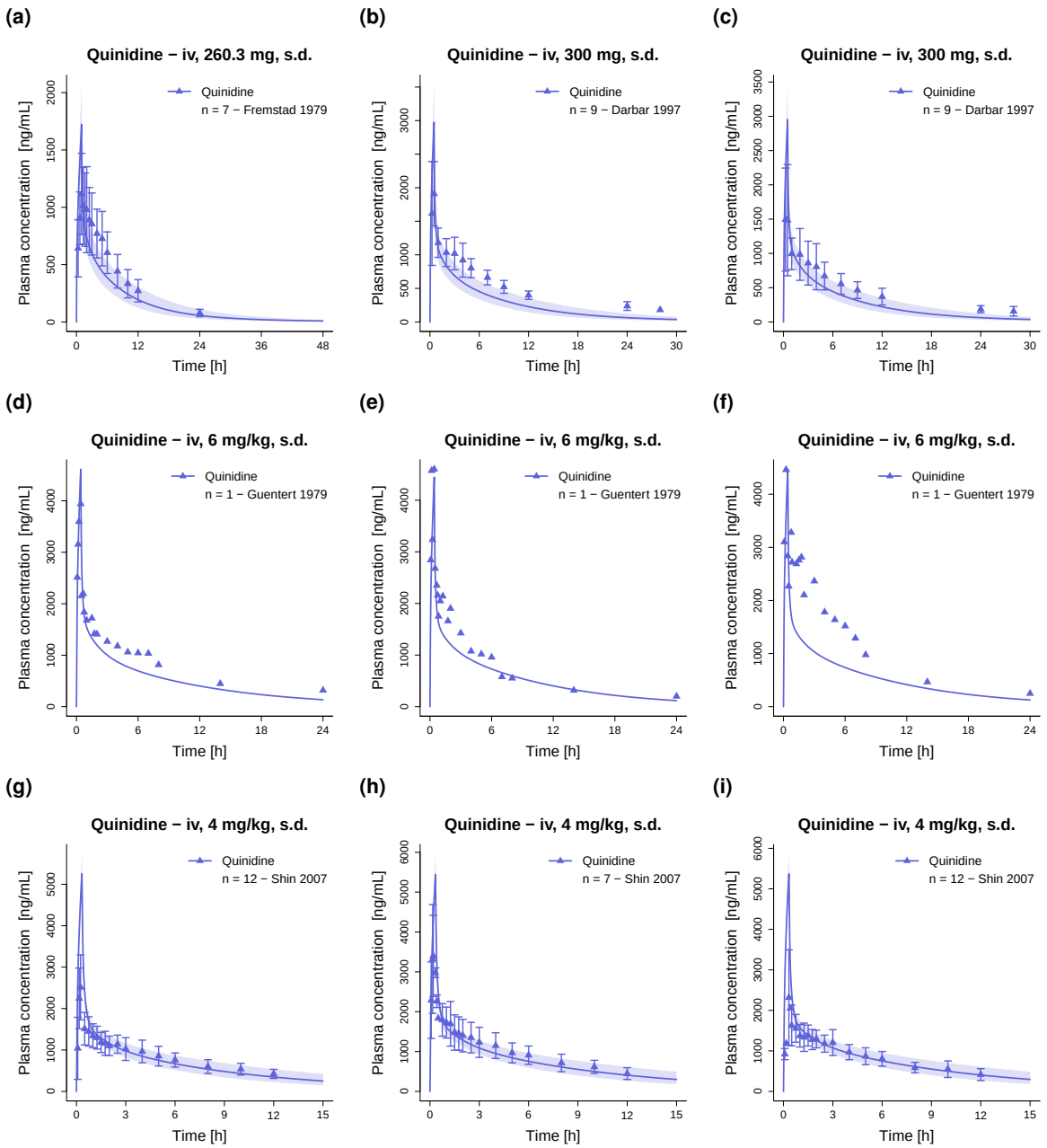

Figure S8: Quinidine plasma concentration-time profiles (linear representation). Population predicted geometric means and individual predictions are shown as lines, corresponding geometric standard deviations are shown as shaded areas and observed data are shown as dots (training dataset) and triangles (test dataset) (± standard deviation, if reported). Doses indicate quinidine gluconate administration. Respective doses of quinidine base were calculated and incorporated in simulations. iv: intravenous, n: number of study participants, s.d.: single dose.

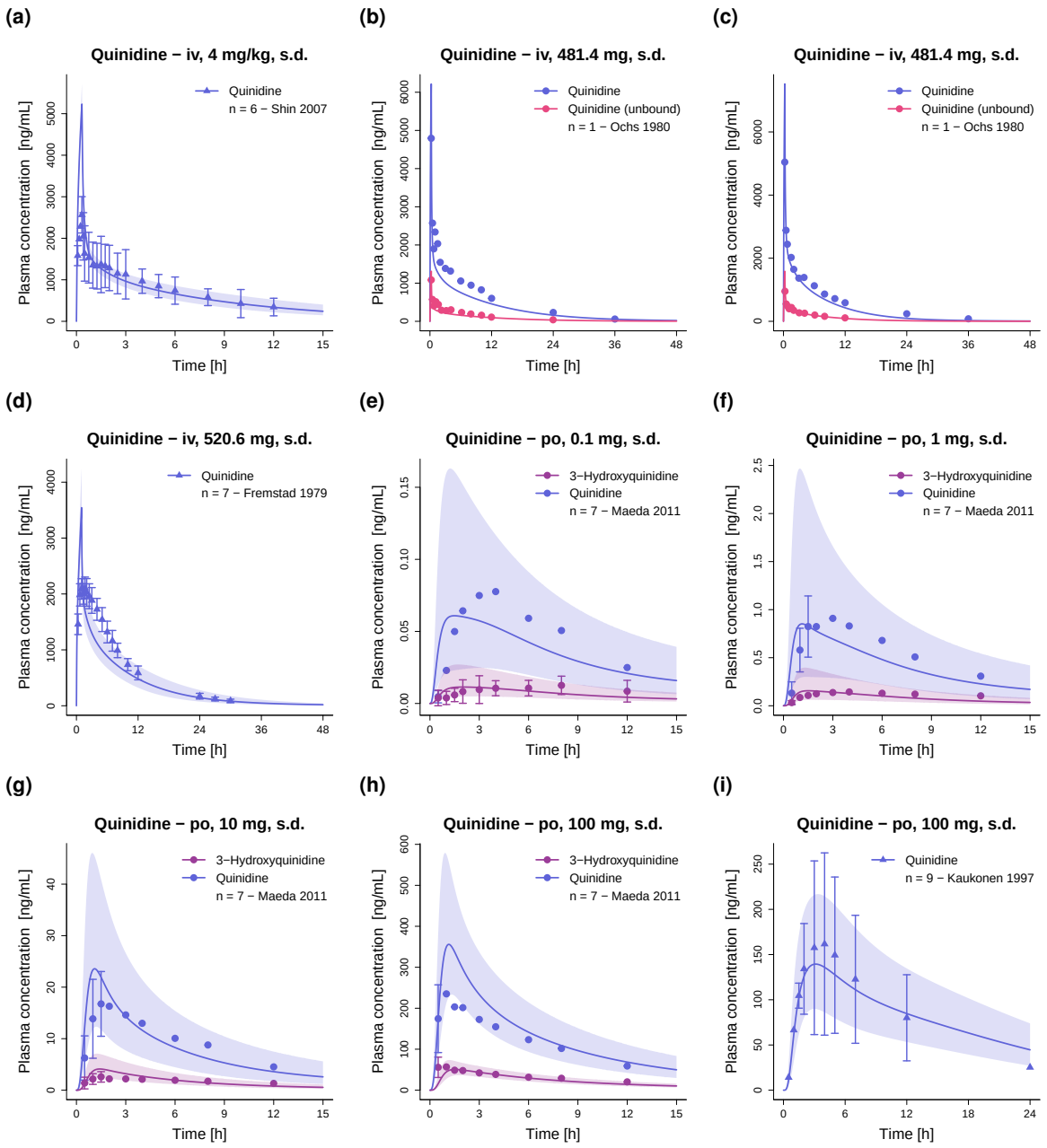

Figure S9: Quinidine plasma concentration-time profiles (linear representation). Population predicted geometric means and individual predictions are shown as lines, corresponding geometric standard deviations are shown as shaded areas and observed data are shown as dots (training dataset) and triangles (test dataset) (± standard deviation, if reported). Doses indicate (a–d) quinidine gluconate and (e–i) quinidine sulfate administration. Respective doses of quinidine base were calculated and incorporated in simulations. iv: intravenous, n: number of study participants, po: oral, s.d.: single dose.

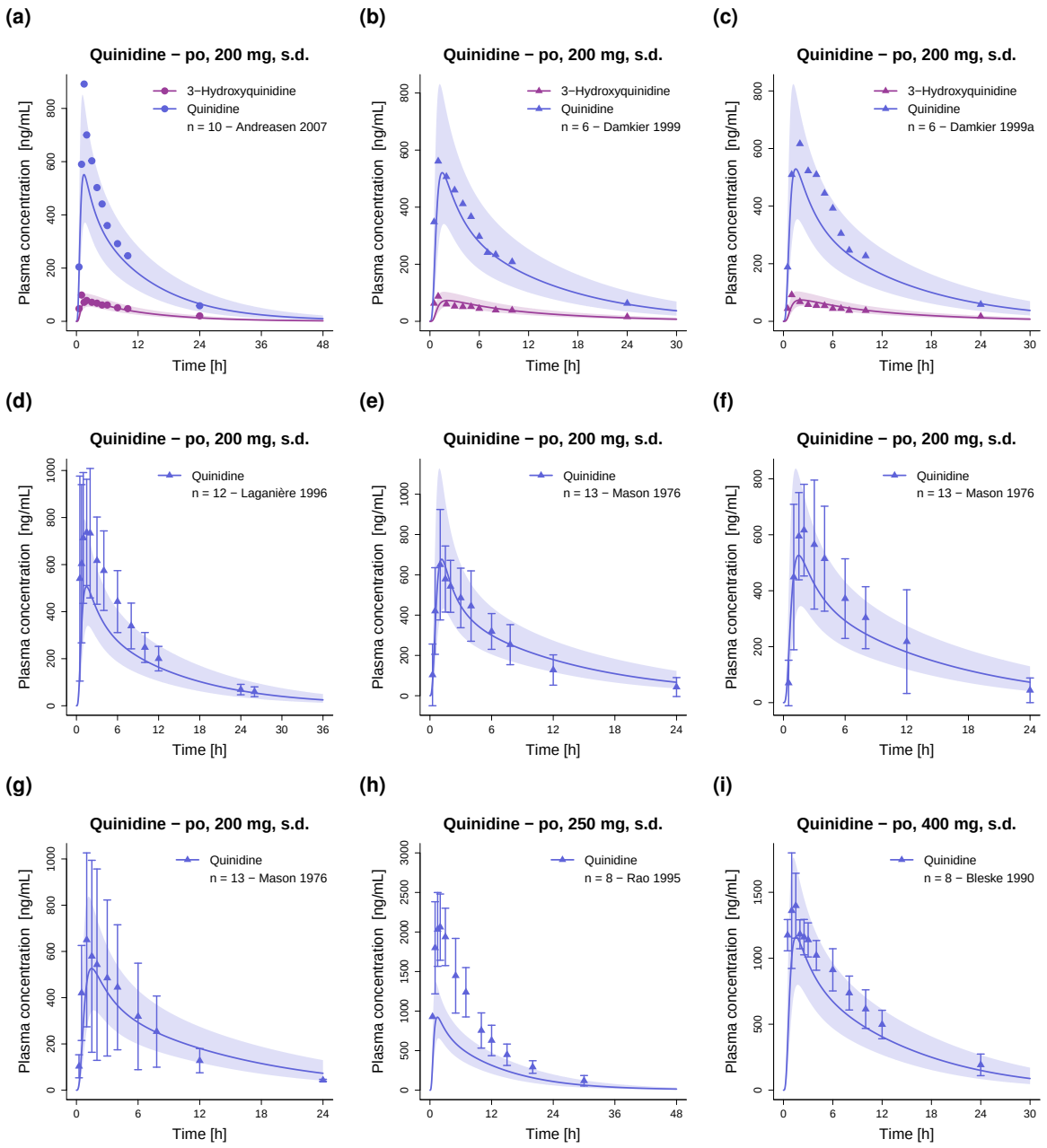

Figure S10: Quinidine plasma concentration-time profiles (linear representation). Population predicted geometric means are shown as lines, corresponding geometric standard deviations are shown as shaded areas and observed data are shown as dots (training dataset) and triangles (test dataset) (± standard deviation, if reported). Respective doses of quinidine base were calculated and incorporated in simulations. n: number of study participants, po: oral, s.d.: single dose.

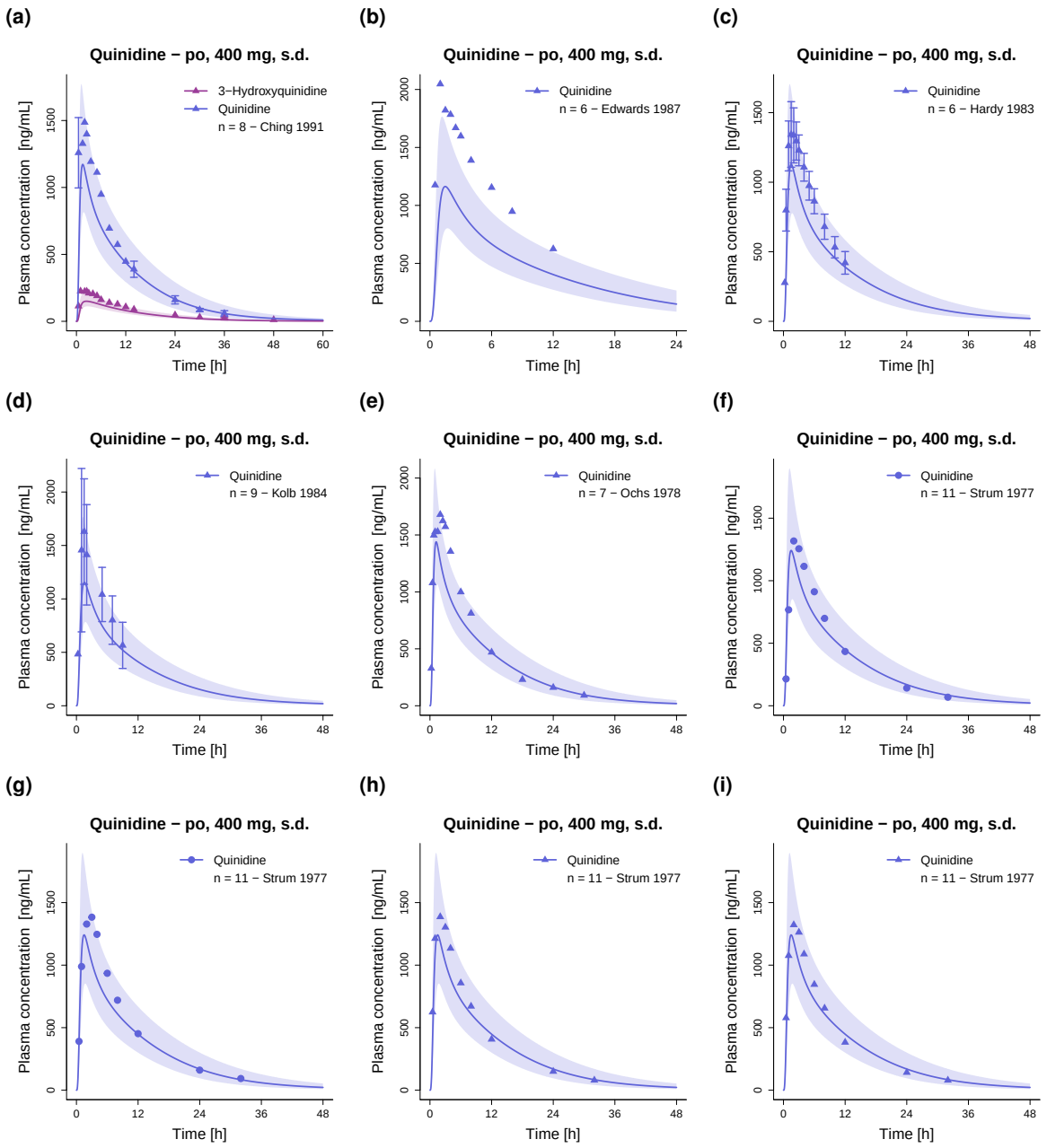

Figure S11: Quinidine plasma concentration-time profiles (linear representation). Population predicted geometric means are shown as lines, corresponding geometric standard deviations are shown as shaded areas and observed data are shown as dots (training dataset) and triangles (test dataset) (± standard deviation, if reported). Respective doses of quinidine base were calculated and incorporated in simulations. n: number of study participants, po: oral, s.d.: single dose.

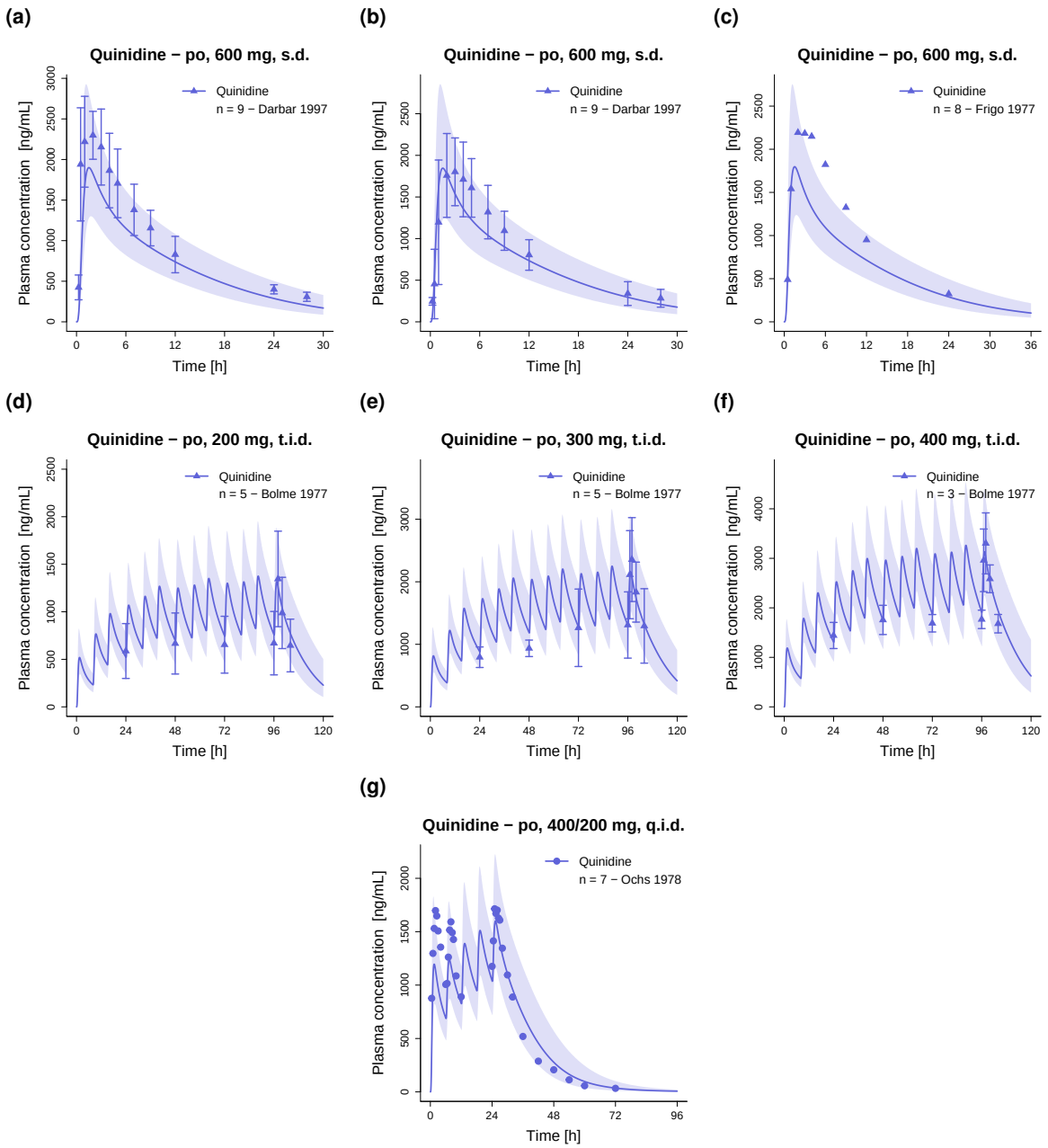

Figure S12: Quinidine plasma concentration-time profiles (linear representation). Population predicted geometric means are shown as lines, corresponding geometric standard deviations are shown as shaded areas and observed data are shown as dots (training dataset) and triangles (test dataset) (± standard deviation, if reported). Respective doses of quinidine base were calculated and incorporated in simulations. n: number of study participants, po: oral, q.i.d.: four times daily, s.d.: single dose.

S2.4 Amount excreted unchanged in urine profiles (linear representation)

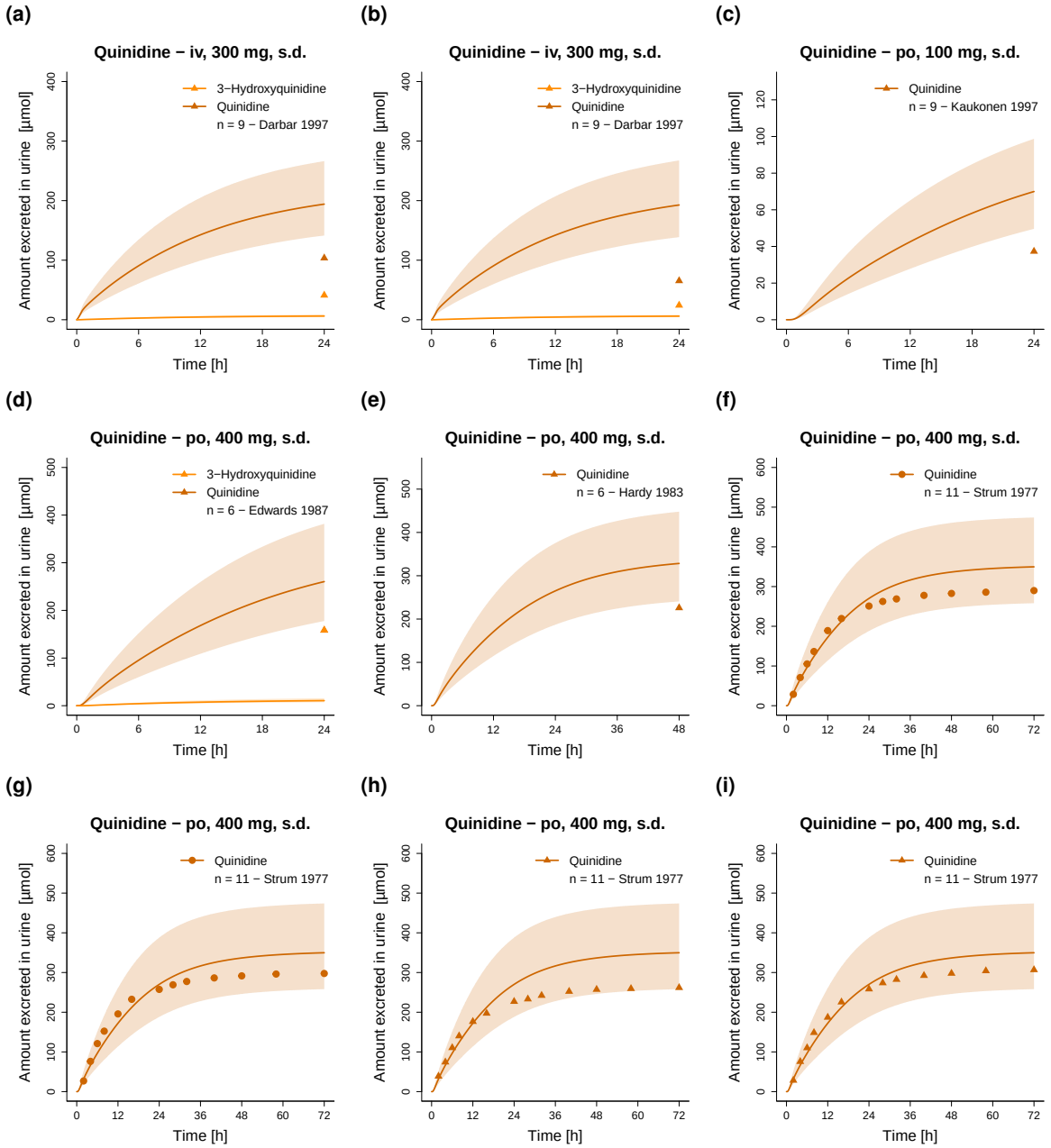

Figure S13: Quinidine amount excreted unchanged in urine profiles (linear representation). Population predicted geometric means are shown as lines, corresponding geometric standard deviations are shown as shaded areas and observed data are shown as dots (training dataset) and triangles (test dataset). Doses indicate (a–b) quinidine gluconate and (c–i) quinidine sulfate administration. Respective doses of quinidine base were calculated and incorporated in simulations. iv: intravenous, n: number of study participants, po: oral, s.d.: single dose.

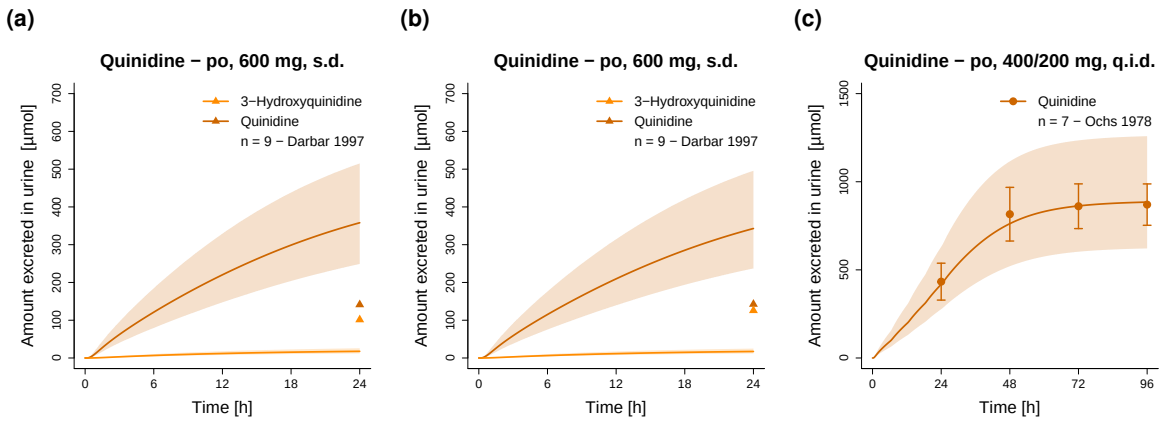

Figure S14: Quinidine amount excreted unchanged in urine profiles (linear representation). Population predicted geometric means are shown as lines, corresponding geometric standard deviations are shown as shaded areas and observed data are shown as dots (training dataset) and triangles (test dataset) (± standard deviation, if reported). Doses indicate quinidine sulfate administration. Respective doses of quinidine base were calculated and incorporated in simulations. n: number of study participants, po: oral, q.i.d.: four times daily, s.d.: single dose.

S2.5 Predicted compared to observed concentrations

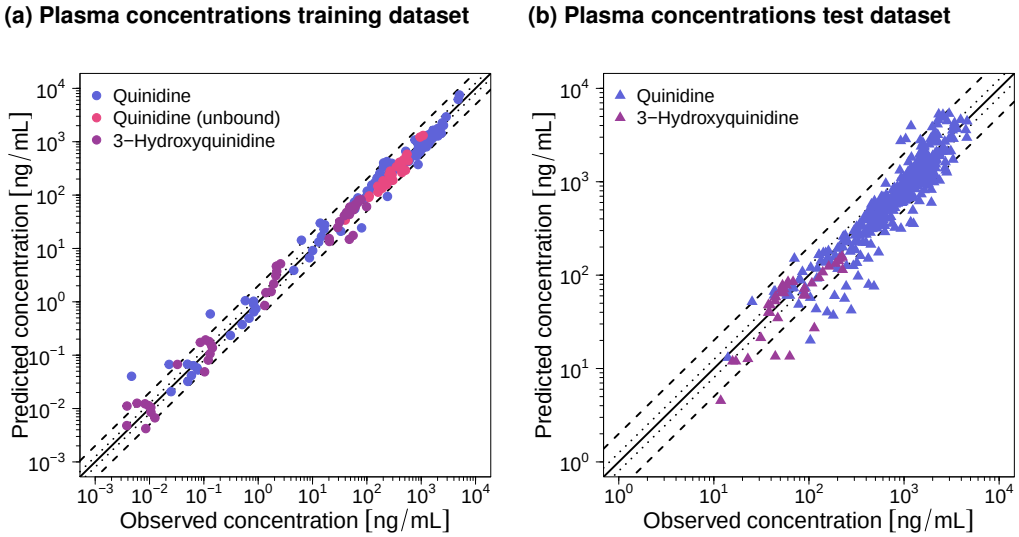

Figure S15: Goodness-of-fit plots comparing predicted and observed plasma concentration values. The solid line marks the line of identity. Dotted lines indicate 1.25-fold, dashed lines indicate 2-fold deviation.

S2.6 Mean relative deviation of plasma concentration predictions

Table S6: MRD values of quinidine plasma concentration predictions

Quinidine administration						
Dose salt [mg]	**Dose base [mg]**	**Route**	**Molecule**	**Dataset**	**MRD**	**Reference**
Quinidine						
260.3[a]	162.2	s.d. iv 60 min inf	QUI	te	1.48	Fremstad 1979 [22]
300[a]	187.5	s.d. iv 30 min inf	QUI	te	2.05	Darbar 1997[b] [24]
300[a]	187.5	s.d. iv 30 min inf	QUI	te	1.83	Darbar 1997[c] [24]
6/kg[a]	3.74/kg	s.d. iv 25 min inf	QUI	te	1.37	Guentert 1979 [25]
6/kg[a]	3.74/kg	s.d. iv 25 min inf	QUI	te	1.32	Guentert 1979 [25]
6/kg[a]	3.74/kg	s.d. iv 25 min inf	QUI	te	1.81	Guentert 1979 [25]
6.42/kg[a]	4.00/kg	s.d. iv 20 min inf	QUI	te	1.42	Shin 2007 [27]
6.42/kg[a]	4.00/kg	s.d. iv 20 min inf	QUI	te	1.24	Shin 2007 [27]
6.42/kg[a]	4.00/kg	s.d. iv 20 min inf	QUI	te	1.56	Shin 2007 [27]
6.42/kg[a]	4.00/kg	s.d. iv 20 min inf	QUI	te	1.38	Shin 2007 [27]
481.4[a]	300	s.d. iv 15 min inf	QUI	tr	1.40	Ochs 1980 [28]
481.4[a]	300	s.d. iv 15 min inf	QUI	tr	1.59	Ochs 1980 [28]
520.6[a]	324.4	s.d. iv 60 min inf	QUI	te	1.42	Fremstad 1979 [22]
0.1[d]	0.08	s.d. po sol	QUI	tr	2.33	Maeda 2011 [30]
1[d]	0.83	s.d. po sol	QUI	tr	1.79	Maeda 2011 [30]
10[d]	8.29	s.d. po sol	QUI	tr	1.56	Maeda 2011 [30]
100[d]	82.87	s.d. po sol	QUI	tr	1.49	Maeda 2011 [30]
100[d]	82.87	s.d. po tab	QUI	te	1.28	Kaukonen 1997 [31]
200[d]	165.7	s.d. po cap	QUI	tr	1.21	Andreasen 2007 [32]
200[d]	165.7	s.d. po tab	QUI	te	1.27	Damkier 1999 [33]
200[d]	165.7	s.d. po tab	QUI	te	1.18	Damkier 1999a [34]
200[d]	165.7	s.d. po tab	QUI	te	1.49	Laganière 1996 [35]
200[d]	165.7	s.d. po sol	QUI	te	1.30	Mason 1976 [36]
200[d]	165.7	s.d. po cap	QUI	te	1.43	Mason 1976 [36]
200[d]	165.7	s.d. po tab	QUI	te	1.85	Mason 1976 [36]
250[d]	207.2	s.d. po cap	QUI	te	2.29	Rao 1995 [37]
400[d]	331.5	s.d. po tab	QUI	te	1.44	Bleske 1990 [38]
400[d]	331.5	s.d. po tab	QUI	te	1.49	Ching 1991 [39]
400[d]	331.5	s.d. po tab	QUI	te	1.73	Edwards 1987 [40]
400[d]	331.5	s.d. po tab	QUI	te	1.86	Hardy 1983 [41]
400[d]	331.5	s.d. po tab	QUI	te	2.12	Kolb 1984 [42]
400[d]	331.5	s.d. po tab	QUI	te	1.47	Ochs 1978 [43]
400[d]	331.5	s.d. po tab	QUI	tr	1.33	Strum 1977 (A) [44]
400[d]	331.5	s.d. po tab	QUI	tr	1.28	Strum 1977 (B) [44]
400[d]	331.5	s.d. po tab	QUI	te	1.33	Strum 1977 (C) [44]
400[d]	331.5	s.d. po tab	QUI	te	1.29	Strum 1977 (D) [44]
600[d]	497.2	s.d. po tab	QUI	te	1.90	Darbar 1997[b] [24]
600[d]	497.2	s.d. po tab	QUI	te	1.50	Darbar 1997[c] [24]
600[d]	497.2	s.d. po tab	QUI	te	1.28	Frigo 1977 [45]
200[d]	165.7	t.i.d. po tab	QUI	te	1.07	Bolme 1977 [46]
300[d]	248.6	t.i.d. po tab	QUI	te	1.12	Bolme 1977 [46]
400[d]	331.5	t.i.d. po tab	QUI	te	1.09	Bolme 1977 [46]
400 + 200[d]	331.5 + 165.7	s.d. + q.i.d. po tab	QUI	tr	1.28	Ochs 1978 [43]
Mean QUI MRD training dataset (range):				**1.53 (1.21 – 2.33), 9/10 with MRD $\leq$ 2**		
Mean QUI MRD test dataset (range):				**1.51 (1.07 – 2.29), 30/33 with MRD $\leq$ 2**		
Overall QUI MRD (range):				**1.51 (1.07 – 2.33), 39/43 with MRD $\leq$ 2**		

cap: capsule, inf: infusion, iv: intravenous, MRD: mean relative deviation, OHQ: 3-hydroxyquinidine, po: oral, q.i.d.: four times daily, QUB: quinidine unbound, QUI: quinidine, s.d.: single dose, sol: solution, tab: tablet, te: test dataset, t.i.d.: three times daily, tr: training dataset. Respective doses of quinidine base were calculated and incorporated in simulations. [a] Quinidine gluconate dose. [b] Low-salt diet. [c] High-salt diet. [d] Quinidine sulfate dose.

Table S6: MRD values of quinidine plasma concentration predictions (*continued*)

Quinidine administration						
Dose salt [mg]	**Dose base [mg]**	**Route**	**Molecule**	**Dataset**	**MRD**	**Reference**
Quinidine (unbound)						
481.4[a]	300	s.d. iv 15 min inf	QUB	tr		Ochs 1980 [28]
481.4[a]	300	s.d. iv 15 min inf	QUB	tr		Ochs 1980 [28]
Mean QUB MRD (range):				**1.27 (1.12 – 1.41), 2/2 with MRD $\leq$ 2**		
3-Hydroxyquinidine						
0.1[b]	0.08	s.d. po sol	OHQ	tr	1.76	Maeda 2011 [30]
1[d]	0.83	s.d. po sol	OHQ	tr	1.65	Maeda 2011 [30]
10[d]	8.29	s.d. po sol	OHQ	tr	1.65	Maeda 2011 [30]
100[d]	82.87	s.d. po sol	OHQ	tr	1.65	Maeda 2011 [30]
200[d]	82.87	s.d. po cap	OHQ	tr	1.50	Andreasen 2007 [32]
200[d]	82.87	s.d. po tab	OHQ	te	1.75	Damkier 1999 [33]
200[d]	82.87	s.d. po tab	OHQ	te	1.55	Damkier 1999a [34]
400[d]	331.5	s.d. po tab	OHQ	te	1.75	Ching 1991 [39]
Mean OHQ MRD training dataset (range):				**1.62 (1.50 – 1.76), 5/5 with MRD $\leq$ 2**		
Mean OHQ MRD test dataset (range):				**1.68 (1.55 – 1.75), 3/3 with MRD $\leq$ 2**		
Overall OHQ MRD (range):				**1.64 (1.50 – 1.76), 8/8 with MRD $\leq$ 2**		
Overall MRD training dataset (range):				**1.52 (1.12 – 2.33), 16/17 with MRD $\leq$ 2**		
Overall MRD test dataset (range):				**1.52 (1.07 – 2.29), 33/36 with MRD $\leq$ 2**		
Overall MRD (range):				**1.52 (1.07 – 2.33), 49/53 with MRD $\leq$ 2**		

cap: capsule, inf: infusion, iv: intravenous, MRD: mean relative deviation, OHQ: 3-hydroxyquinidine, po: oral, q.i.d.: four times daily, QUB: quinidine unbound, QUI: quinidine, s.d.: single dose, sol: solution, tab: tablet, te: test dataset, t.i.d.: three times daily, tr: training dataset. Respective doses of quinidine base were calculated and incorporated in simulations. [a] Quinidine gluconate dose. [b] Low-salt diet. [c] High-salt diet. [d] Quinidine sulfate dose.

S2.7 Predicted compared to observed AUC_{last} and C_{max} values

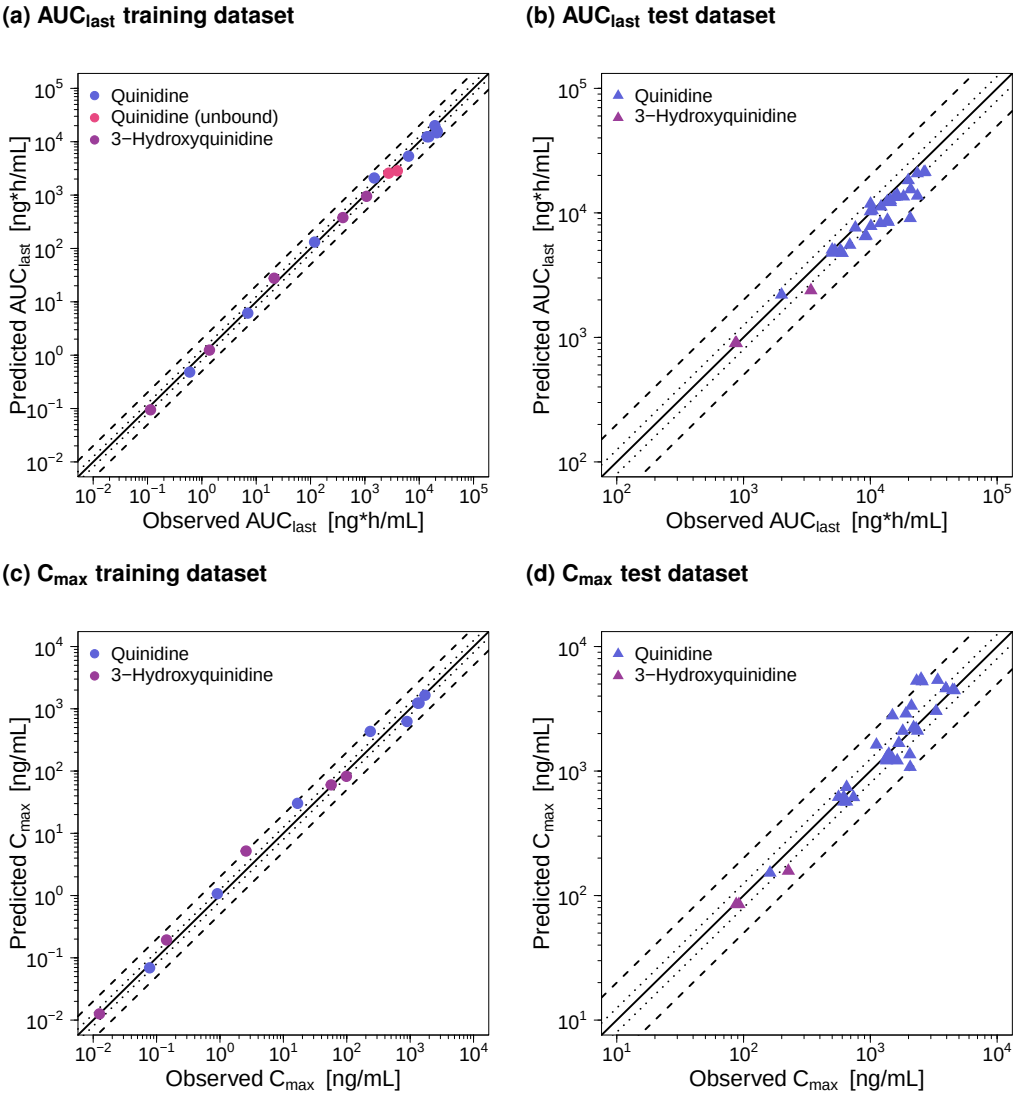

Figure S16: Goodness-of-fit plots comparing predicted and observed AUC_{last} and C_{max} values. The solid line marks the line of identity. Dotted lines indicate 1.25-fold, dashed lines indicate 2-fold deviation. AUC_{last}: area under the plasma concentration-time curve calculated between the first and last concentration measurement, C_{max}: maximum plasma concentration.

S2.8 Geometric mean fold errors of predicted AUC_{last} and C_{max} values

Table S7: Predicted and observed quinidine AUC_{last} and C_{max} values

Quinidine administration				AUC_{last}			C_{max}					
Dose salt [mg]	Dose base [mg]	Route	t_{last} [h]	Pred [ng*h/mL]	Obs [ng*h/mL]	Pred/Obs	Pred [ng/mL]	Obs [ng/mL]	Pred/Obs	Molecule	Dataset	Reference
Quinidine												
260.3[a]	162.2	s.d. iv 60 min inf	24	6554.71	9263.44	0.71	1626.43	1116.94	1.46	QUI	te	Fremstad 1979 [22]
300[a]	187.5	s.d. iv 30 min inf	28	8445.88	13853.58	0.61	2892.69	1909.17	1.52	QUI	te	Darbar 1997[b] [24]
300[a]	187.5	s.d. iv 30 min inf	28	8265.50	11985.68	0.96	2794.84	1493.54	1.87	QUI	te	Darbar 1997[c] [24]
6/kg[a]	3.74/kg	s.d. iv 25 min inf	24	13513.46	18270.86	0.74	4613.41	3940.06	1.17	QUI	te	Guentert 1979 [25]
6/kg[a]	3.74/kg	s.d. iv 25 min inf	24	13502.09	16073.67	0.84	4447.58	4601.00	0.97	QUI	te	Guentert 1979 [25]
6/kg[a]	3.74/kg	s.d. iv 25 min inf	24	13715.93	23533.78	0.58	4470.83	4461.40	1.00	QUI	te	Guentert 1979 [25]
6.42/kg[a]	4.00/kg	s.d. iv 20 min inf	12	11820.90	10039.30	1.18	5497.46	2512.40	2.19	QUI	te	Shin 2007 [27]
6.42/kg[a]	4.00/kg	s.d. iv 20 min inf	12	11235.57	12146.47	0.93	5384.97	3399.50	1.58	QUI	te	Shin 2007 [27]
6.42/kg[a]	4.00/kg	s.d. iv 20 min inf	12	10488.80	10356.78	1.01	5302.10	2315.80	2.29	QUI	te	Shin 2007 [27]
6.42/kg[a]	4.00/kg	s.d. iv 20 min inf	12	10277.00	10002.75	1.03	5245.17	2564.50	2.05	QUI	te	Shin 2007 [27]
481.4[a]	300	s.d. iv 15 min inf	38	14741.64	21152.33	0.70	-	-	-	QUI	tr	Ochs 1980 [28]
481.4[a]	300	s.d. iv 15 min inf	36	15818.56	21417.30	0.74	-	-	-	QUI	tr	Ochs 1980 [28]
520.6[a]	324.4	s.d. iv 60 min inf	24	15437.76	20807.88	0.74	3340.12	2108.70	1.58	QUI	te	Fremstad 1979 [22]
0.1[d]	0.08	s.d. po sol	12	0.48	0.60	0.81	0.07	0.08	0.89	QUI	tr	Maeda 2011 [30]
1[d]	0.83	s.d. po sol	12	6.14	7.01	0.88	1.07	0.91	1.18	QUI	tr	Maeda 2011 [30]
10[d]	8.29	s.d. po sol	12	131.72	118.68	1.11	30.29	16.75	1.81	QUI	tr	Maeda 2011 [30]
100[d]	82.87	s.d. po sol	12	2090.94	1488.69	1.40	433.41	235.06	1.84	QUI	tr	Maeda 2011 [30]
100[d]	82.87	s.d. po tab	24	2201.88	1994.05	1.10	152.36	161.66	0.94	QUI	te	Kaukonen 1997 [31]
200[d]	165.7	s.d. po cap	24	5360.72	6367.26	0.84	625.51	891.66	0.70	QUI	tr	Andreasen 2007 [32]
200[d]	165.7	s.d. po tab	24	4991.73	5248.11	0.95	618.73	561.00	1.10	QUI	te	Damkier 1999 [33]
200[d]	165.7	s.d. po tab	24	4991.74	5814.42	0.86	618.73	616.40	1.00	QUI	te	Damkier 1999a [34]
200[d]	165.7	s.d. po tab	26	5529.71	6884.07	0.80	615.87	736.73	0.84	QUI	te	Laganière 1996 [35]
200[d]	165.7	s.d. po sol	24	5057.62	5002.61	1.01	743.71	650.10	1.14	QUI	te	Mason 1976 [36]
200[d]	165.7	s.d. po cap	24	4755.30	6002.45	0.79	566.99	616.57	0.92	QUI	te	Mason 1976 [36]
200[d]	165.7	s.d. po tab	24	4774.21	5002.61	0.95	566.99	650.10	0.87	QUI	te	Mason 1976 [36]
250[d]	207.2	s.d. po cap	30	9063.63	20629.28	0.48	1076.40	2061.28	0.52	QUI	te	Rao 1995 [37]
400[d]	331.5	s.d. po tab	24	12181.74	14392.00	0.85	1372.09	1398.30	0.98	QUI	te	Bleske 1990 [38]
400[d]	331.5	s.d. po tab	48	13381.59	15453.90	0.87	1271.53	1486.31	0.86	QUI	te	Ching 1991 [39]
400[d]	331.5	s.d. po tab	12	8759.10	13634.29	0.64	1359.68	2046.99	0.66	QUI	te	Edwards 1987 [40]
400[d]	331.5	s.d. po tab	12	7831.41	10096.53	0.78	1214.62	1343.16	0.90	QUI	te	Hardy 1983 [41]
400[d]	331.5	s.d. po tab	9	6486.18	9100.55	0.71	1214.56	1629.89	0.75	QUI	te	Kolb 1984 [42]
400[d]	331.5	s.d. po tab	30	13958.36	16286.56	0.86	1676.78	1679.06	1.00	QUI	te	Ochs 1978 [43]
400[d]	331.5	s.d. po tab	32	12395.93	13954.84	0.89	1234.30	1317.65	0.94	QUI	tr	Strum 1977 (A) [44]
400[d]	331.5	s.d. po tab	32	12395.93	15040.31	0.82	1234.30	1383.33	0.89	QUI	tr	Strum 1977 (B) [44]
400[d]	331.5	s.d. po tab	32	12395.93	14253.64	0.87	1234.30	1386.25	0.89	QUI	te	Strum 1977 (C) [44]
400[d]	331.5	s.d. po tab	32	12395.93	13617.59	0.91	1234.30	1322.02	0.93	QUI	te	Strum 1977 (D) [44]
600[d]	497.2	s.d. po tab	28	21298.05	27000.85	0.79	2190.62	2297.91	0.95	QUI	te	Darbar 1997[b] [24]
600[d]	497.2	s.d. po tab	28	20762.60	23458.79	0.89	2099.90	1802.24	1.17	QUI	te	Darbar 1997[c] [24]
600[d]	497.2	s.d. po tab	24	21174.82	26466.89	0.80	2243.14	2193.19	1.02	QUI	te	Frigo 1977 [45]
200[d]	165.7	t.i.d. po tab	8	7608.27	7615.63	1.00	1292.21	1345.63	0.96	QUI	te	Bolme 1977 [46]
300[d]	248.6	t.i.d. po tab	8	12648.11	14391.95	0.88	2103.04	2354.96	0.89	QUI	te	Bolme 1977 [46]
400[d]	331.5	t.i.d. po tab	8	18276.65	19912.52	0.92	3033.61	3301.62	0.92	QUI	te	Bolme 1977 [46]
400 + 200[d]	331.5 + 165.7	s.d. + q.i.d. po tab	72	20002.91	19396.58	1.03	1650.11	1714.69	0.96	QUI	tr	Ochs 1978 [43]
Mean QUI GMFE training dataset (range):				**1.22 (1.03 – 1.43), 10/10 with GMFE $\leq$ 2**			**1.33 (1.04 – 1.84), 8/8 with GMFE $\leq$ 2**					
Mean QUI GMFE test dataset (range):				**1.26 (1.00 – 2.28), 32/33 with GMFE $\leq$ 2**			**1.31 (1.00 – 2.29), 30/33 with GMFE $\leq$ 2**					
Overall QUI GMFE (range):				**1.25 (1.00 – 2.28), 42/43 with GMFE $\leq$ 2**			**1.31 (1.00 – 2.29), 38/41 with GMFE $\leq$ 2**					

AUC_{last}: area under the plasma concentration-time curve calculated between the first and last concentration measurement, cap: capsule, C_{max}: maximum plasma concentration, GMFE: geometric mean fold error, inf: infusion, iv: intravenous, obs: observed, OHQ: 3-hydroxyquinidine, po: oral, q.i.d.: four times daily, QUB: quinidine unbound, QUI: quinidine, s.d.: single dose, tab: tablet, te: test dataset, t.i.d.: three times daily, t_{last}: time of the last concentration measurement, tr: training dataset, -: not available. Respective doses of quinidine base were calculated and incorporated in simulations. [a] Quinidine gluconate dose. [b] Low-salt diet. [c] High-salt diet. [d] Quinidine sulfate dose.

Table S7: Predicted and observed quinidine AUC_{last} and C_{max} values *(continued)*

Quinidine administration				AUC_{last}			C_{max}					
Dose salt [mg]	**Dose base [mg]**	**Route**	**t_{last} [h]**	**Pred [ng*h/mL]**	**Obs [ng*h/mL]**	**Pred/Obs**	**Pred [ng/mL]**	**Obs [ng/mL]**	**Pred/Obs**	**Molecule**	**Dataset**	**Reference**
Quinidine (unbound)												
481.4[a]	300	s.d. iv 15 min inf	24	2853.55	3956.09	0.72	-	-	-	QUB	tr	Ochs 1980 [28]
481.4[a]	300	s.d. iv 15 min inf	12	2577.23	2748.57	0.94	-	-	-	QUB	tr	Ochs 1980 [28]
Mean QUB GMFE (range):				**1.23 (1.07 – 1.39), 2/2 with GMFE $\leq$ 2**					**-**			
3-Hydroxyquinidine												
0.1[d]	0.08	s.d. po sol	12	0.09	0.11	0.83	0.01	0.01	1.00	OHQ	tr	Maeda 2011 [30]
1[d]	0.83	s.d. po sol	12	1.25	1.38	0.90	0.19	0.14	1.35	OHQ	tr	Maeda 2011 [30]
10[d]	8.29	s.d. po sol	12	27.66	21.42	1.29	5.19	2.58	2.01	OHQ	tr	Maeda 2011 [30]
100[d]	82.87	s.d. po sol	12	379.09	393.81	0.96	59.94	56.77	1.06	OHQ	tr	Maeda 2011 [30]
200[d]	165.7	s.d. po cap	24	948.78	1074.81	0.88	82.29	98.72	0.83	OHQ	tr	Andreasen 2007 [32]
200[d]	165.7	s.d. po tab	24	898.21	862.40	1.04	85.22	87.51	0.97	OHQ	te	Damkier 1999 [33]
200[d]	165.7	s.d. po tab	24	898.21	878.23	1.02	85.22	91.91	0.93	OHQ	te	Damkier 1999a [34]
400[d]	331.5	s.d. po tab	48	2385.10	3397.45	0.70	157.86	225.59	0.70	OHQ	te	Ching 1991 [39]
Mean OHQ GMFE training dataset (range):				**1.15 (1.04 – 1.29), 5/5 with GMFE $\leq$ 2**			**1.32 (1.00 – 2.01), 4/5 with GMFE $\leq$ 2**					
Mean OHQ GMFE test dataset (range):				**1.16 (1.02 – 1.42), 3/3 with GMFE $\leq$ 2**			**1.18 (1.03 – 1.43), 3/3 with GMFE $\leq$ 2**					
Overall OHQ GMFE (range):				**1.16 (1.02 – 1.42), 8/8 with GMFE $\leq$ 2**			**1.27 (1.00 – 2.07), 7/8 with GMFE $\leq$ 2**					
Mean GMFE training dataset (range):				**1.20 (1.03 – 1.43), 17/17 with GMFE $\leq$ 2**			**1.32 (1.00 – 2.01), 12/13 with GMFE $\leq$ 2**					
Mean GMFE test dataset (range):				**1.25 (1.00 – 2.28), 35/36 with GMFE $\leq$ 2**			**1.30 (1.00 – 2.29), 33/36 with GMFE $\leq$ 2**					
Overall GMFE (range):				**1.23 (1.00 – 2.28), 52/53 with GMFE $\leq$ 2**			**1.31 (1.00 – 2.29), 45/49 with GMFE $\leq$ 2**					

AUC_{last}: area under the plasma concentration-time curve calculated between the first and last concentration measurement, cap: capsule, C_{max}: maximum plasma concentration, GMFE: geometric mean fold error, inf: infusion, iv: intravenous, obs: observed, OHQ: 3-hydroxyquinidine, po: oral, q.i.d.: four times daily, QUB: quinidine unbound, QUI: quinidine, s.d.: single dose, tab: tablet, te: test dataset, t.i.d.: three times daily, t_{last}: time of the last concentration measurement, tr: training dataset, -: not available. Respective doses of quinidine base were calculated and incorporated in simulations. [a] Quinidine gluconate dose. [b] Low-salt diet. [c] High-salt diet. [d] Quinidine sulfate dose.

S2.9 Geometric mean fold errors of predicted V_d and half-life values

Table S8: Predicted and observed quinidine V_d values

Quinidine administration			V_d					
Dose salt [mg]	**Dose base [mg]**	**Route**	**Pred [L/kg]**	**Obs [L/kg]**	**Pred/Obs**	**Molecule**	**Dataset**	**Reference**
Quinidine								
260.3[a]	162.2	s.d. iv 60 min inf	3.03	2.27	1.33	QUI	te	Fremstad 1979 [22]
6/kg[a]	3.74/kg	s.d. iv 25 min inf	2.72	2.04	1.33	QUI	te	Guentert 1979 [25]
6/kg[a]	3.74/kg	s.d. iv 25 min inf	2.44	1.6	1.39	QUI	te	Guentert 1979 [25]
6/kg[a]	3.74/kg	s.d. iv 25 min inf	2.46	1.27	1.94	QUI	te	Guentert 1979 [25]
6.42/kg[a]	4.00/kg	s.d. iv 20 min inf	2.36[b]	2.85[b]	0.83	QUI	te	Shin 2007 [27]
6.42/kg[a]	4.00/kg	s.d. iv 20 min inf	2.20[b]	2.18[b]	1.01	QUI	te	Shin 2007 [27]
6.42/kg[a]	4.00/kg	s.d. iv 20 min inf	2.44[b]	2.70[b]	0.91	QUI	te	Shin 2007 [27]
6.42/kg[a]	4.00/kg	s.d. iv 20 min inf	2.36[b]	2.66[b]	0.89	QUI	te	Shin 2007 [27]
481.4[a]	300	s.d. iv 15 min inf	2.65	1.84	1.44	QUI	tr	Ochs 1980 [28]
481.4[a]	300	s.d. iv 15 min inf	2.97	2.55	1.16	QUI	tr	Ochs 1980 [28]
520.6[a]	324.4	s.d. iv 60 min inf	2.64	2.27	1.16	QUI	te	Fremstad 1979 [22]
Mean QUI GMFE training dataset (range):			**1.30 (1.16 – 1.44), 2/2 with GMFE $\leq$ 2**					
Mean QUI GMFE test dataset (range):			**1.27 (1.01 – 1.94), 9/9 with GMFE $\leq$ 2**					
Overall QUI GMFE (range):			**1.27 (1.01 – 1.94), 11/11 with GMFE $\leq$ 2**					

GMFE: geometric mean fold error, inf: infusion, iv: intravenous, obs: observed, pred: predicted, QUI: quinidine, s.d.: single dose, te: test dataset, tr: training dataset, V_d: apparent volume of distribution. Respective doses of quinidine base were calculated and incorporated in simulations. [a] Quinidine gluconate dose. [b] volume of distribution at steady state (V_{ss}).

Table S9: Predicted and observed quinidine half-life values

Quinidine administration			Half-life					
Dose salt [mg]	**Dose base [mg]**	**Route**	**Pred [h]**	**Obs [h]**	**Pred/Obs**	**Molecule**	**Dataset**	**Reference**
Quinidine								
260.3[a]	162.2	s.d. iv 60 min inf	6.84	6.42	1.07	QUI	te	Fremstad 1979 [22]
300[a]	187.5	s.d. iv 30 min inf	6.92	10.20	0.68	QUI	te	Darbar 1997[b] [24]
300[a]	187.5	s.d. iv 30 min inf	7.11	9.67	0.74	QUI	te	Darbar 1997[c] [24]
481.4[a]	300	s.d. iv 15 min inf	8.04	7.52	1.07	QUI	tr	Ochs 1980 [28]
481.4[a]	300	s.d. iv 15 min inf	7.10	7.88	0.90	QUI	tr	Ochs 1980 [28]
520.6[a]	324.4	s.d. iv 60 min inf	6.80	6.42	1.06	QUI	te	Fremstad 1979 [22]
0.1[d]	0.08	s.d. po sol	7.29	5.07	1.44	QUI	tr	Maeda 2011 [30]
1[d]	0.83	s.d. po sol	6.82	5.73	1.19	QUI	tr	Maeda 2011 [30]
10[d]	8.29	s.d. po sol	5.79	5.24	1.10	QUI	tr	Maeda 2011 [30]
100[d]	82.87	s.d. po sol	6.06	5.59	1.08	QUI	tr	Maeda 2011 [30]
100[d]	82.87	s.d. po tab	11.38	7.40	1.54	QUI	te	Kaukonen 1997 [31]
200[d]	165.7	s.d. po cap	7.92	6.88	1.15	QUI	tr	Andreasen 2007 [32]
200[d]	165.7	s.d. po tab	8.03	7.90	1.02	QUI	te	Damkier 1999 [33]
200[d]	165.7	s.d. po tab	8.03	8.10	0.99	QUI	te	Damkier 1999a [34]
200[d]	165.7	s.d. po tab	8.19	6.80	1.20	QUI	te	Laganière 1996 [35]
200[d]	165.7	s.d. po sol	8.23	5.68	1.45	QUI	te	Mason 1976 [36]
200[d]	165.7	s.d. po cap	8.84	5.74	1.54	QUI	te	Mason 1976 [36]
200[d]	165.7	s.d. po tab	8.84	7.35	1.20	QUI	te	Mason 1976 [36]
250[d]	207.2	s.d. po cap	6.67	7.00	0.95	QUI	te	Rao 1995 [37]
400[d]	331.5	s.d. po tab	7.51	7.90	0.95	QUI	te	Bleske 1990 [38]
400[d]	331.5	s.d. po tab	8.71	7.91	1.10	QUI	te	Ching 1991 [39]
400[d]	331.5	s.d. po tab	8.72	6.90	1.26	QUI	te	Edwards 1987 [40]
400[d]	331.5	s.d. po tab	10.14	5.80	1.75	QUI	te	Hardy 1983 [41]
400[d]	331.5	s.d. po tab	9.61	14.91	0.64	QUI	te	Kolb 1984 [42]
400[d]	331.5	s.d. po tab	6.38	6.10	1.05	QUI	te	Ochs 1978 [43]
400[d]	331.5	s.d. po tab	8.09	5.36	1.51	QUI	tr	Strum 1977 (A) [44]
400[d]	331.5	s.d. po tab	8.09	5.36	1.51	QUI	tr	Strum 1977 (B) [44]
400[d]	331.5	s.d. po tab	8.09	5.36	1.51	QUI	te	Strum 1977 (C) [44]
400[d]	331.5	s.d. po tab	8.09	5.36	1.51	QUI	te	Strum 1977 (D) [44]
600[d]	497.2	s.d. po tab	7.08	7.93	0.89	QUI	te	Darbar 1997[b] [24]
600[d]	497.2	s.d. po tab	7.41	8.12	0.91	QUI	te	Darbar 1997[c] [24]
600[d]	497.2	s.d. po tab	7.32	7.87	0.93	QUI	te	Frigo 1977 [45]
Mean QUI GMFE training dataset (range):			**1.23 (1.07 – 1.51), 9/9 with GMFE $\leq$ 2**					
Mean QUI GMFE test dataset (range):			**1.24 (1.01 – 1.75), 23/23 with GMFE $\leq$ 2**					
Overall QUI GMFE (range):			**1.24 (1.01 – 1.75), 32/32 with GMFE $\leq$ 2**					

cap: capsule, GMFE: geometric mean fold error, inf: infusion, iv: intravenous, obs: observed, po: oral, pred: predicted, q.i.d.: four times daily, QUI: quinidine, s.d.: single dose, tab: tablet, te: test dataset, t.i.d.: three times daily, tr: training dataset. Respective doses of quinidine base were calculated and incorporated in simulations. [a] Quinidine gluconate dose. [b] Low-salt diet. [c] High-salt diet. [d] Quinidine sulfate dose.

S2.10 Sensitivity Analyses

Sensitivity of the quinidine and 3-hydroxyquinidine models to single model parameters was calculated, determined as relative change of $AUC_{0\text{-}6h}$ at steady state in a four-times daily regimen of 200 mg (first dose 400 mg) quinidine (sulfate) according to Equation S2. A relative perturbation of 1000% (variation range 10.0, maximum number of 2 steps) was applied. Parameters were included into the analysis if (i) they have been optimized, (ii) they are associated with optimized parameters or (iii) they could have a strong impact due to their use in the calculation of permeabilities or partition coefficients (Table S10).

$$S = \frac{\Delta AUC}{AUC} \cdot \frac{p}{\Delta p} \tag{S2}$$

S = sensitivity of the AUC to the examined model parameter, ΔAUC = change of the AUC, AUC = simulated AUC with the original parameter value, Δp = change of the examined parameter value and p = original parameter value. Parameters were considered sensitive, if their sensitivity value was equal or greater than 0.5.

Table S10: Parameters evaluated during quinidine and 3-hydroxyquinidine sensitivity analyses

	Quinidine		**3-Hydoxyquinidine**	
Parameter	**Value**	**Source**	**Value**	**Source**
Solubility (pH 7.0) [g/L]	11.11	Literature	12.57	Literature
Lipophilicity	2.51	Literature	1.66	Literature
$f_{u,p}$ [%]	21	Literature	31	Literature
P-gp K_M [µmol/L]	0.23	Literature	-	-
P-gp k_{cat} [1/min]	0.77	Optimized	-	-
CYP3A4 (QUI $\rightarrow$ OHQ) K_M [µmol/L]	51.8	Literature	-	-
CYP3A4 (QUI $\rightarrow$ OHQ) k_{cat} [1/min]	2.21	Optimized	-	-
CYP3A4 (QUI $\rightarrow$ sink) K_M [µmol/L]	65.03	Literature	-	-
CYP3A4 (QUI $\rightarrow$ sink) k_{cat} [1/min]	3.84	Optimized	-	-
CYP3A4 CL [1/min]	-	-	0.08	Optimized
CL_{hep} [1/min]	-	-	0.45	Optimized
P-gp K_i [µmol/L]	0.10	Literature	-	-
Intestinal permeability [cm/min]	$6.47 \cdot 10^{-6}$	Optimized	-	-
Weibull dissolution time (50% dissolved) [min]	8.76	Literature	-	-
Weibull dissolution shape	0.42	Literature	-	-

CL: clearance, CL_{hep}: hepatic metabolic clearance, CYP: cytochrome P450, $f_{u,p}$: fraction unbound plasma, k_{cat}: catalytic or transport rate constant, K_i: concentration for 50% inhibition (competitive), K_M: Michaelis-Menten constant, OHQ: 3-hydroxyquinidine, P-gp: P-glycoprotein, QUI: quinidine, -: not available.

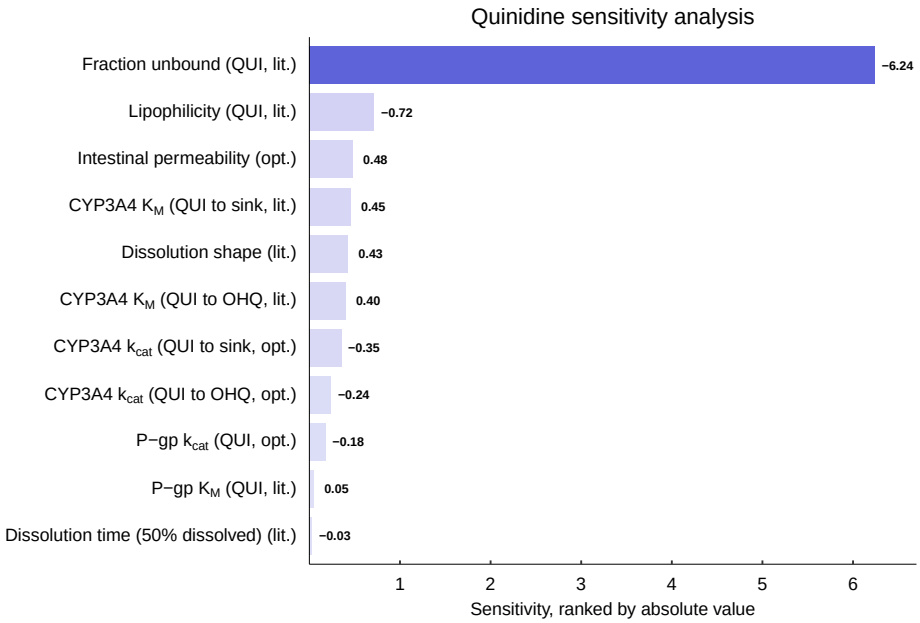

Figure S17: Local sensitivity analysis results of the quinidine PBPK model (parent quinidine), determined as relative change of $AUC_{0\text{-}6h}$ at steady state in a four-times daily regimen of 200 mg (first dose 400 mg) quinidine (sulfate). CYP: cytochrome P450, k_{cat}: catalytic or transport rate constant, K_M: Michaelis-Menten constant, lit.: literature value, OHQ: 3-hydroxyquinidine, opt.: optimized, P-gp: P-glycoprotein, QUI: quinidine.

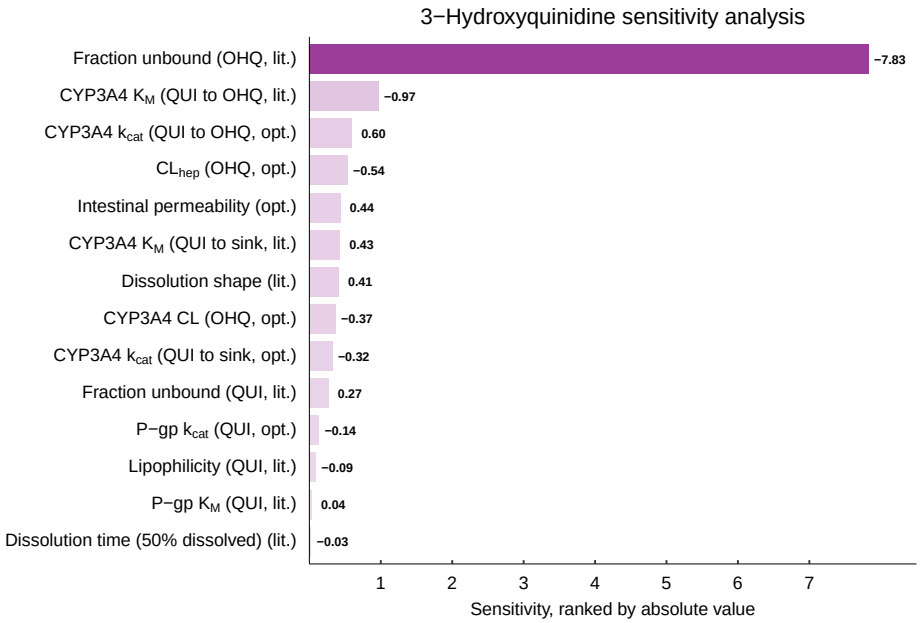

Figure S18: Local sensitivity analysis results of the quinidine PBPK model (metabolite 3-hydroxyquinidine), determined as relative change of $AUC_{0\text{-}6h}$ at steady state in a four-times daily regimen of 200 mg (first dose 400 mg) quinidine (sulfate). CL: clearance, CL_{hep}: hepatic metabolic clearance, CYP: cytochrome P450, k_{cat}: catalytic or transport rate constant, K_M: Michaelis-Menten constant, lit.: literature value, OHQ: 3-hydroxyquinidine, opt.: optimized, P-gp: P-glycoprotein, QUI: quinidine.

S3 DD(G)I Modeling

S3.1 Types of Interaction

S3.1.1 Competitive inhibition

$$K_{M,app} = K_M * (1 + \frac{[I]}{K_i}) \tag{S3}$$

$$v = \frac{v_{max} * [S]}{K_{M,app} + [S]} = \frac{k_{cat} * [E] * [S]}{K_{M,app} + [S]} \tag{S4}$$

$K_{M,app}$ = Michaelis-Menten constant in the presence of inhibitor, K_M = Michaelis-Menten constant, $[I]$ = free inhibitor concentration, K_i = dissociation constant of the inhibitor-enzyme/transporter complex, v = reaction velocity, $[S]$ = free substrate concentration, k_{cat} = catalytic or transport rate constant and $[E]$ = enzyme concentration.

S3.1.2 Non-competitive inhibition

$$v_{max,app} = \frac{v_{max}}{1 + \frac{[I]}{K_i}} \tag{S5}$$

$$v = \frac{v_{max,app} \cdot [S]}{K_M + [S]} \tag{S6}$$

$v_{max,app}$ = maximum reaction velocity in the presence of inhibitor, v_{max} = maximum reaction velocity, $[I]$ = free inhibitor concentration, K_i = dissociation constant of the inhibitor-enzyme/transporter complex, v = reaction velocity, $[S]$ = free substrate concentration and K_M = Michaelis-Menten constant.

S3.1.3 Mechanism-based inactivation

$$\frac{d[E]}{dt} = k_{deg} * E_0 - \frac{k_{deg} + k_{inact} * [I]}{K_I + [I]} * [E] \tag{S7}$$

$\frac{d[E]}{dt}$ = enzyme turnover, k_{deg} = degradation rate constant, E_0 = enzyme concentration at time 0, $[I]$ = free mechanism-based inactivator concentration, k_{inact} = maximum inactivation rate constant, K_I = concentration for half-maximal inactivation and $[E]$ = enzyme concentration.

S3.1.4 Induction

$$\frac{d[E]}{dt} = k_{deg} * E_0 * \frac{1 + (E_{max} * [Ind])}{EC50 + [Ind]} \tag{S8}$$

$\frac{d[E]}{dt}$ = enzyme turnover, k_{deg} = degradation rate constant, E_0 = enzyme concentration at time 0, E_{max} = maximal induction effect *in vivo*, $[Ind]$ = free inducer concentration and $EC50$ = concentration for half maximal induction *in vivo*.

S3.2 Published PBPK DDI models

Table S11: Published perpetrator models and included relevant interaction constants

Model (PK-Sim® Version)	Mechanism	Parameter	Value	Publication	Model repository
Carbamazepine (V11)				Fuhr et al. 2021 [65]	Carbamazepine-Model (OSP, v1.0)[a]
Carbamazepine	Induction	CYP3A4 E_{max}	6.00		
	Induction	CYP3A4 EC_{50} [µmol/L]	20.00		
Carbamazepine-10,11-epoxide	-	-	-		
Cimetidine (V11)				Hanke et al. 2020 [66]	Cimetidine-Model (OSP, v1.1)[a]
Cimetidine	Competitive inhibition	CYP3A4 K_i [µmol/L]	268.00		
Fluvoxamine (V11)				Britz et al. 2019 [67]	Fluvoxamine-Model (OSP, v1.2)[a]
Fluvoxamine	Competitive inhibition	CYP3A4 K_i [µmol/L]	1.60		
Itraconazole (V11)				Hanke et al. 2018 [17]	Itraconazole-Model (OSP, v1.3)[a]
Itraconazole	Competitive inhibition	CYP3A4 K_i [nmol/L]	1.30		
	Competitive inhibition	P-gp K_i [nmol/L]	8.00		
Hydroxy-itraconazole	Competitive inhibition	CYP3A4 K_i [nmol/L]	14.40		
Keto-itraconazole	Competitive inhibition	CYP3A4 K_i [nmol/L]	5.12		
N-Desalkyl-itraconazole	Competitive inhibition	CYP3A4 K_i [nmol/L]	0.32		
Omeprazole (V11)				Kanacher et al. 2020 [20]	Omeprazole-Model (OSP, v1.1)[a]
R-Omeprazole	Competitive inhibiton	CYP3A4 K_i [µmol/L]	44.50 [68]		
S-Omeprazole	Competitive inhibiton	CYP3A4 K_i [µmol/L]	46.60 [68]		
Rifampicin (V11)				Hanke et al. 2018 [17]	Rifampicin-Model (OSP, v1.2)[a]
Rifampicin	Induction	CYP3A4 E_{max}	9.00		
	Induction	CYP3A4 EC_{50} [µmol/L]	0.34		
	Competitive inhibition	CYP3A4 K_i [µmol/L]	18.50		
	Induction	P-gp E_{max}	2.50		
	Induction	P-gp EC_{50} [µmol/L]	0.34		
	Competitive inhibition	P-gp K_i [µmol/L]	169.00		
Verapamil (V11)				Hanke et al. 2020a [69]	Verapamil-Norverapamil-Model
R-Verapamil	Mechanism-based inactivation	CYP3A4 KI	27.63		
	Mechanism-based inactivation	CYP3A4 k_{inact} [µmol/L]	0.038		
	Non-competitive inhibition	P-gp K_i [µmol/L]	0.038		
S-Verapamil	Mechanism-based inactivation	CYP3A4 KI	3.85		
	Mechanism-based inactivation	CYP3A4 k_{inact} [µmol/L]	0.034		
	Non-competitive inhibition	P-gp K_i [µmol/L]	0.038		
R-Norverapamil	Mechanism-based inactivation	CYP3A4 KI	6.10		
	Mechanism-based inactivation	CYP3A4 k_{inact} [µmol/L]	0.048		
	Non-competitive inhibition	P-gp K_i [µmol/L]	0.038		

CYP: cytochrome P450, EC_{50}: concentration for half maximal induction, E_{max}: maximal induction effect, K_i: dissociation constant of the inhibitor-enzyme/transporter (competitive) and inhibitor-enzyme/transporter(-substrate) complex (non-competitive), KI: concentration for 50% inactivation (mechanism-based inactivation), k_{inact}: maximum inactivation rate (mechanism-based inactivation), OSP: Open Systems Pharmacology, P-gp: P-glycoprotein. If not otherwise indicated, interaction constants were adopted from the respective published models. Hyperlinks refer to the respective model repositories. [a] Open Systems Pharmacology model repository (https://github.com/Open-Systems-Pharmacology).

Table S11: *(continued)*

Model (PK-Sim® Version)	Mechanism	Parameter	Value	Publication	Model repository
S-Norverapamil	Mechanism-based inactivation	CYP3A4 KI	2.90		
	Mechanism-based inactivation	CYP3A4 k_{inact} [µmol/L]	0.080		
	Non-competitive inhibition	P-gp K_i [µmol/L]	0.038		

CYP: cytochrome P450, EC_{50}: concentration for half maximal induction, E_{max}: maximal induction effect, K_i: dissociation constant of the inhibitor-enzyme/transporter (competitive) and inhibitor-enzyme/transporter(-substrate) complex (non-competitive), KI: concentration for 50% inactivation (mechanism-based inactivation), k_{inact}: maximum inactivation rate (mechanism-based inactivation), OSP: Open Systems Pharmacology, P-gp: P-glycoprotein. If not otherwise indicated, interaction constants were adopted from the respective published models. Hyperlinks refer to the respective model repositories. [a] Open Systems Pharmacology model repository (https://github.com/Open-Systems-Pharmacology).

Table S12: Published victim models and affected metabolism and transport pathways

Model (PK-Sim® Version)	Mechanism	Parameter	Value	Publication	Model repository
Dextromethorphan (V11)				Rüdesheim et al. 2022 [70]	Dextromethorphan-Model
Dextromethorphan	Metabolism to DXT	CYP2D6 K_M [µmol/L]	4.65		
	Metabolism to DXT	CYP2D6 k_{kat} [1/min] (*NM*)	90.89		
	Metabolism to DXT	CYP2D6 k_{kat} [1/min] (*PM*)	0.00		
Dextrorphan	-	-	-		
Dextrorphan-O-glucuronide	-	-	-		
Digoxin (V11)				Hanke et al. 2018 [17]	Digoxin-Model (OSP)[a]
Digoxin	Transport	P-gp K_M [µmol/L]	177.00		
	Transport	P-gp k_{cat} [1/min]	71.20		
Metoprolol (V11)				Rüdesheim et al. 2020 [71]	Metoprolol-Model
R-Metoprolol	Metabolism to αHM	CYP2D6 K_M [µmol/L]	10.08		
	Metabolism to αHM	CYP2D6 k_{cat} [1/min] (*NM*)	6.02		
	Metabolism to αHM	CYP2D6 k_{cat} [1/min] (*PM*)	0.00		
	Metabolism (ODM)	CYP2D6 K_M [µmol/L]	8.82		
	Metabolism (ODM)	CYP2D6 k_{cat} [1/min] (*NM*)	9.87		
	Metabolism (ODM)	CYP2D6 k_{cat} [1/min] (*PM*)	0.00		
S-Metoprolol	Metabolism to αHM	CYP2D6 K_M [µmol/L]	10.75		
	Metabolism to αHM	CYP2D6 k_{cat} [1/min] (*NM*)	6.55		
	Metabolism to αHM	CYP2D6 k_{cat} [1/min] (*PM*)	0.00		
	Metabolism (ODM)	CYP2D6 K_M [µmol/L]	12.43		
	Metabolism (ODM)	CYP2D6 k_{cat} [1/min] (*NM*)	8.21		
	Metabolism (ODM)	CYP2D6 k_{cat} [1/min] (*PM*)	0.00		
α-Hydroxymetoprolol	-	-	-		
Mexiletine (V11)				Kanacher et al. 2020 [20]	Mexiletine-Model (OSP, v1.1)[a]
Mexiletine	Metabolism	CYP2D6 clearance [1/min]	0.46		
Paroxetine (V11)				Rüdesheim et al. 2022 [72]	Paroxetine-Model
Paroxetine	Metabolism	CYP2D6 K_M [µmol/L]	0.03		
	Metabolism	CYP2D6 k_{cat} [1/min] (*NM*)	1.37		

αHM: α-hydroxymetoprolol, CYP: cytochrome P450, DXT: dextrorphan, *NM: normal metabolizer*, ODM: O-demethylation OSP: Open Systems Pharmacology, P-gp: P-glycoprotein, *PM: poor metabolizer*. Interaction constants were adopted from the respective published models. Hyperlinks refer to the respective model repositories. [a] Open Systems Pharmacology model repository (https://github.com/Open-Systems-Pharmacology).

S3.3 DD(G)I – Clinical studies

S3.3.1 Quinidine as victim

Table S13: Clinical study data used for DDI model development with quinidine as victim

Drug administration		Perpetrator									
Perpetrator	***Quinidine***	**$C_{max,u}$ [µmol/L][a]**	**n**	**Population[b]**	**Fem. [%]**	**Age [years]**	**Weight [kg]**	**BMI [kg/m²]**	**Molecule**	**Dataset**	**Reference**
Carbamazepine											
200/400 mg b.i.d. po	200 mg[c] s.d. po	13.88	10	European [21]	0	(21-26)	(62-85)	(19-26)	QUI, OHQ	tr	Andreasen 2007 [32]
Cimetidine											
300 mg q.d. po	400 mg[c] s.d. po	3.58	9	American [23]	0	(21-35)	-	-	QUI	te	Kolb 1984 [42]
300 mg q.i.d. po	400 mg[c] s.d. po	4.52	9	American [23]	0	(21-35)	-	-	QUI	te	Hardy 1983 [41]
Fluvoxamine											
100 mg q.d. po	200 mg[c] s.d. po	0.06	6	American [23]	0	-	-	-	QUI, OHQ	te	Damkier 1999a [34]
Itraconazole											
200 mg q.d. po	100 mg[c] s.d. po	$3.20 \cdot 10^{-3}$	9	European [21]	56	25 (21-32)	64 (41-80)	-	QUI	te	Kaukonen 1997 [31]
Omeprazole											
40 mg q.d. po	400 mg[c] s.d. po	0.02 (R-omep) 0.03 (S-omep)	8	European [21]	0	(22-29)	(60-94)	- -	QUI, OHQ	te	Ching 1991 [39]
Rifampicin											
600 mg q.d. po	200 mg[c] s.d. po	2.13	6	European [21]	0	-	-	-	QUI, OHQ	te	Damkier 1999 [33]
Verapamil											
80 mg t.i.d. po	400 mg[c] s.d. po	0.01 (R-vera) $8.69 \cdot 10^{-3}$ (S-vera)	6	European [21]	0	(23-34)	-	-	QUI	te	Edwards 1987 [40]
120 mg t.i.d. po	400 mg[c] s.d. po	0.03 (R-vera) 0.02 (S-vera)	6	European [21]	0	(23-34)	-	-	QUI	te	Edwards 1987 [40]

b.i.d.: twice daily, BMI: body mass index, cap: capsule, $C_{max,u}$: unbound maximum plasma concentration, DDI: drug-drug interaction, fem: females, inf: infusion, n: number of study participants, OHQ: 3-hydroxyquinidine, omep: omeprazole, po: oral, q.d.: once daily, q.i.d.: four times daily, QUI: quinidine, s.d: single dose, te: test dataset, t.i.d.: three times daily, tr: training dataset, vera: verapamil, -: not available. Values are given as mean (range). If perpetrator and victim drugs were applied in form of salts, the respective dose of bases were calculated and incorporated in simulations. [a] Calculated from model-predicted perpetrator concentrations in the respective DDI simulations. [b] Population used in simulations. [c] Quinidine sulfate dose.

S3.3.2 Quinidine as perpetrator

Table S14: Clinical study data used for DD(G)I model development with quinidine as perpetrator

Drug administration		Quinidine										
Quinidine	*Victim*	$C_{max,u}$ [µmol/L][a]	n	Population[b]	Fem. [%]	Age [years]	Weight [kg]	BMI [kg/m²]	Phenotype	Molecule	Dataset	Reference
	Dextromethorphan											
50 mg[c] s.d. po	30 mg s.d. po[d]	0.09	6	European [21]	33.3	22.4 (20-26)	70 (49-86)	-	*CYP2D6 NM*	DEX, DTT	te	Capon 1996 [73]
100 mg[c] s.d. po	30 mg s.d. po	0.20	5	American [23]	80	26.4 (22-31)	-	-	*CYP2D6 NM*	DEX, DXT, DXG	te	Schadel 1995 [74]
30 mg[c] b.i.d. po[e]	30 mg b.i.d. po[f]	0.07	13	American [23]	14.3	33.5 (23-50)	73.3	25.1	*CYP2D6 NM*	DEX	te	Schoedel 2012 [75]
	Digoxin											
200 mg[c] b.i.d. po	10 µg/kg s.d. iv[g]	0.52	6	European [21]	33	(21-28)	-	-	-	DIG	te	Steiness 1980 [76]
200 mg[c] q.i.d. po	1 mg s.d. iv	1.01	7	European [21]	-	-	-	-	-	DIG	te	Ochs 1981 [77]
	Metoprolol											
50 mg[c] s.d. po	20 mg s.d. iv	0.08	4	European [21]	0	(22-34)	(58-80)	-	*CYP2D6 NM*	MET	te	Leemann 1993 [78]
50 mg[c] s.d. po	20 mg s.d. iv[h]	0.08	3	European [21]	0	(25-38)	(65-86)	-	*CYP2D6 PM*	MET	te	Leemann 1993 [78]
250 mg[c] b.i.d. po	20 mg s.d. iv	0.81	4	European [21]	0	(22-34)	(58-80)	-	*CYP2D6 NM*	MET	te	Leemann 1993 [78]
250 mg[c] b.i.d. po	20 mg s.d. iv[h]	0.81	3	European [21]	0	(25-38)	(65-86)	-	*CYP2D6 PM*	MET	te	Leemann 1993 [78]
100 mg[c] q.d. po	200 mg s.d. po	0.20	10	American [23]	0	28.9 (24-40)	85.2	-	*CYP2D6 NM*	RME, SME	te	Johnson 1996 [79]
100 mg[c] q.d. po	200 mg s.d. po	0.20	10	American [23]	0	28.5 (24-36)	82.2	-	*CYP2D6 NM*	RME, SME	te	Johnson 1996 [79]
	Mexiletine											
50 mg[c] q.i.d. po	200 mg s.d. po	0.21	6	American [23]	33.3	22.4 (20-26)	71 (49-86)	-	*CYP2D6 NM*	MEX	te	Abolfathi 1993 [80]
50 mg[c] q.i.d. po	200 mg s.d. po	0.21	10	American [23]	7	26	74	-	*CYP2D6 PM*	MEX	te	Abolfathi 1993 [80]
	Paroxetine											
30 mg[c] b.i.d. po	20 mg q.d. po[i]	0.07	14	American [23]	14.3	33.6 (19-55)	75.3	25.3	*CYP2D6 NM*	PAR	te	Schoedel 2012 [75]

b.i.d.: twice daily, BMI: body mass index, $C_{max,u}$: unbound maximum plasma concentration, DD(G)I: drug-drug(-gene) interaction, DEX: dextromethorphan, DIG: digoxin, DTT: total dextrorphan, DXG: dextrorphan-O-glucuronide, fem: females, iv: intravenous, MET: metoprolol (racemate), MEX: mexiletine, n: number of study participants, *NM*: *normal metabolizer*, PAR: paroxetine, *PM*: *poor metabolizer*, po: oral, q.d.: once daily, q.i.d:, four times daily, RME: R-metoprolol, s.d.: single dose, SME: S-metoprolol, te: test dataset, -: not available. Values are given as mean (range). If perpetrator and victim drugs were applied in form of salts, the respective doses of bases were calculated and incorporated in simulations. [a] Calculated from model-predicted quinidine concentrations in the respective DDI simulations. [b] Population used in simulations. [c] Quinidine sulfate dose. [d] CYP2D6 catalytic rate constant estimated for control to account for unexplained interindividual variability in CYP2D6 activity (57% of original model value). [e] Plus paroxetine (20 mg q.d. po). [f] CYP2D6 catalytic rate constant estimated for control to account for unexplained interindividual variability in CYP2D6 activity (26% of original model value). [g] Digoxin dose of 15 µg/kg before DDI, normalized to 15 µg/kg for evaluation. [h] CYP2D6 catalytic rate constant estimated for control to account for unexplained interindividual variability in CYP2D6 activity (300% for sink metabolism and 200% for formation of α-hydroxymetoprolol of original model value). [i] Plus dextromethorphan (30 mg b.i.d. po).

S3.4 Plasma concentration-time profiles (semilogarithmic representation)

S3.4.1 Quinidine as victim

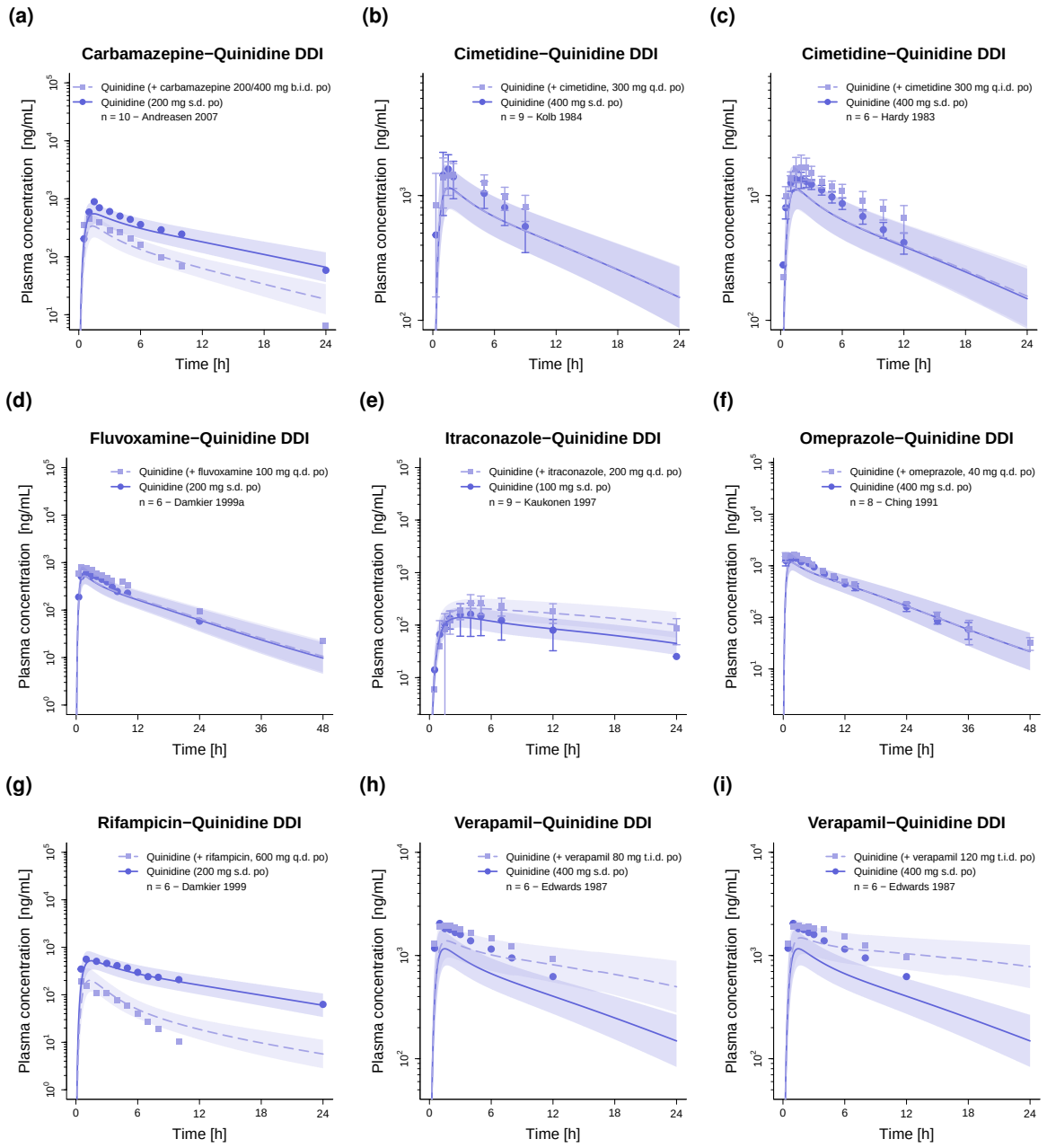

Figure S19: Predicted compared to observed plasma concentration-time profiles of quinidine alone and after pretreatment and/or concomitant administration of (a) carbamazepine, (b–c) cimetidine, (d) fluvoxamine, (e) itraconazole, (f) R-/S-omeprazole, (g) rifampicin and (h–i) R-/S-verapamil (semilogarithmic representation). Population predicted geometric means are shown as lines, corresponding geometric standard deviations are shown as shaded areas and observed data are shown as dots (control) and squares (DDI) (± standard deviation, if reported). b.i.d.: twice daily, DDI: drug-drug interaction, n: number of study participants, po: oral, q.d.: once daily, q.i.d.: four times daily, s.d.: single dose, t.i.d.: three times daily.

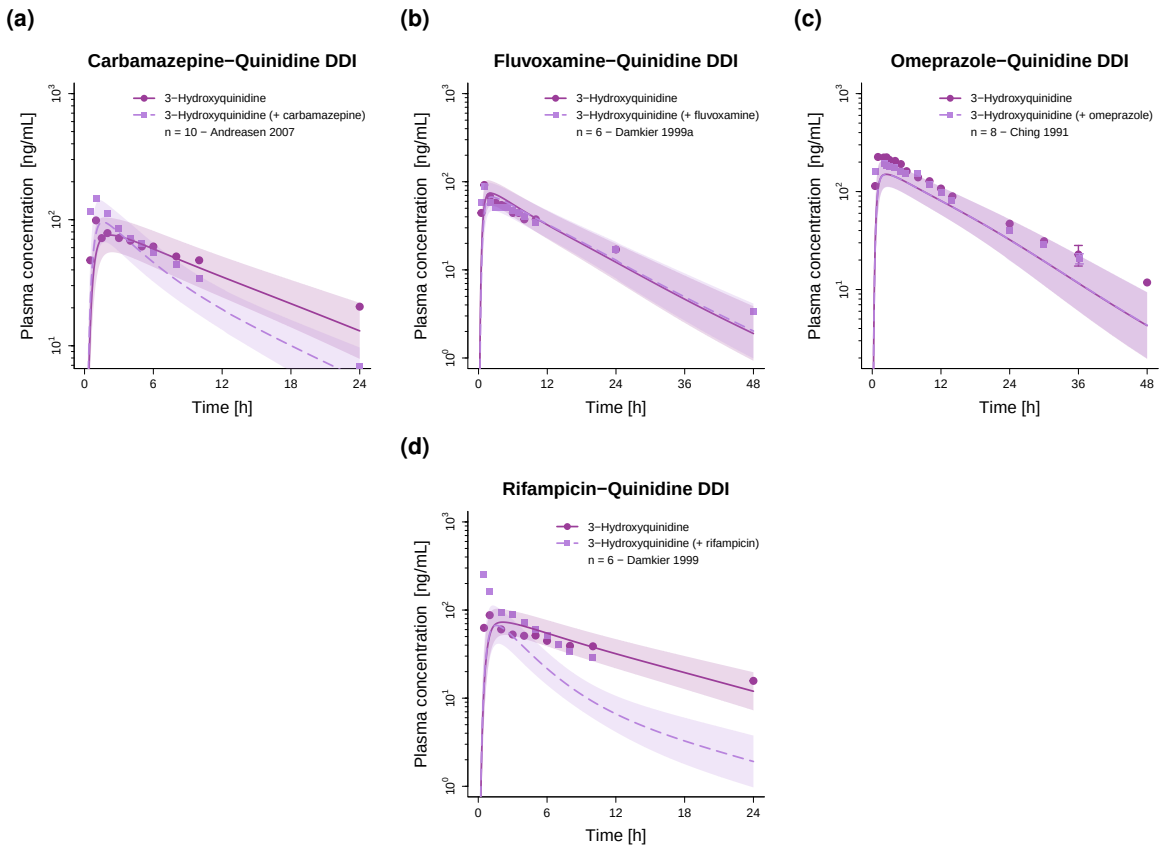

Figure S20: Predicted compared to observed plasma concentration-time profiles of 3-hydroxyquinidine alone and after pretreatment and/or concomitant administration of (a) carbamazepine, (b) fluvoxamine, (c) R-/S-omeprazole and (d) rifampicin (semilogarithmic representation). Population predicted geometric means are shown as lines, corresponding geometric standard deviations are shown as shaded areas and observed data are shown as dots (control) and squares (DDI). DDI: drug-drug interaction, n: number of study participants.

S3.4.2 Quinidine as perpetrator

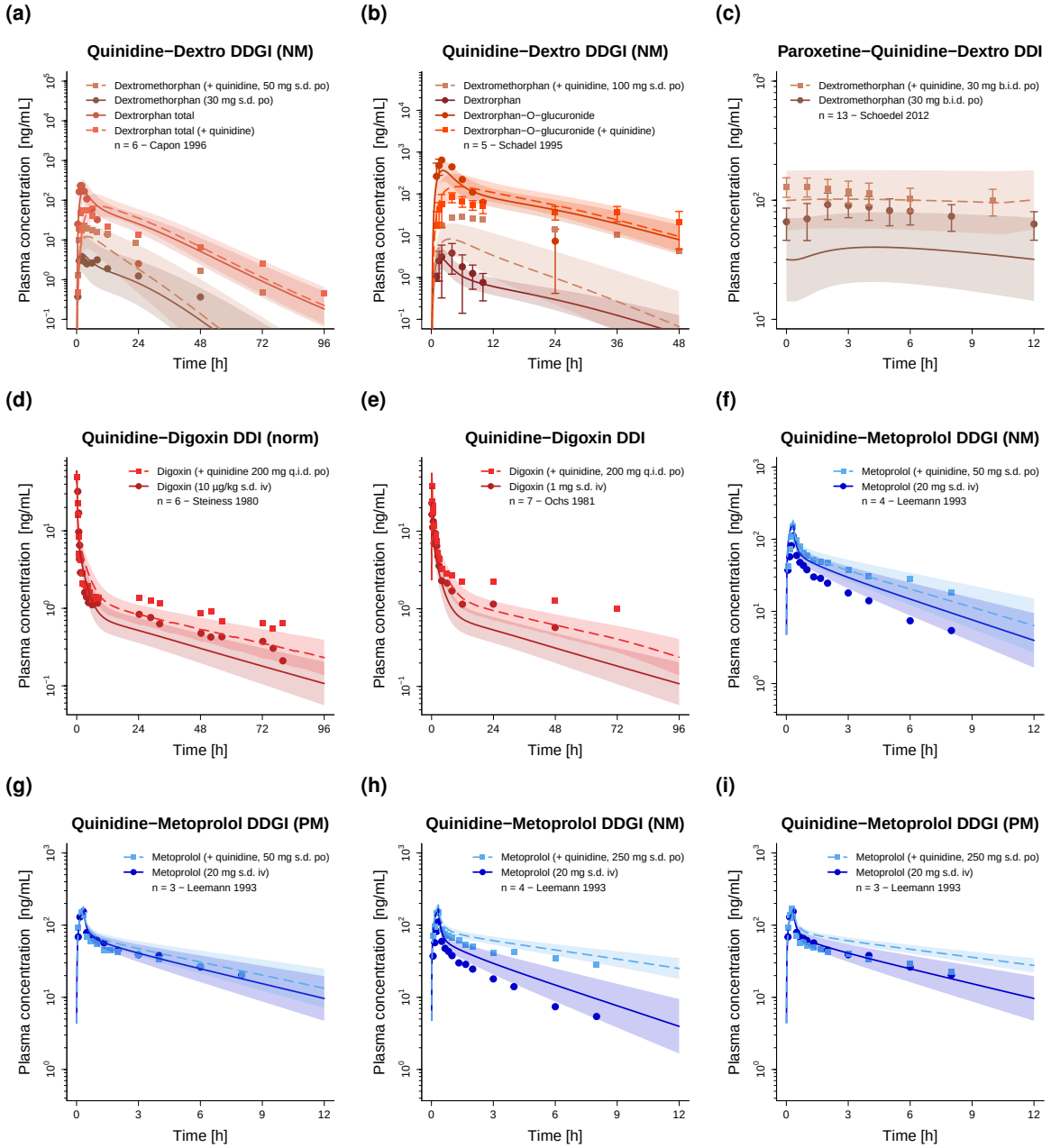

Figure S21: Predicted compared to observed plasma concentration-time profiles of (a–c) dextromethorphan (+ metabolites), (d–e) digoxin and (f–i) metoprolol alone and after pretreatment with and/or concomitant administration of quinidine (semilogarithmic representation). Population predicted geometric means are shown as lines, corresponding geometric standard deviations are shown as shaded areas and observed data are shown as dots (control) and squares (DDI) (± standard deviation, if reported). b.i.d.: twice daily, DDI: drug-drug interaction, DDGI: drug-drug-gene interaction, iv: intravenous, n: number of study participants, NM: CYP2D6 normal metabolizer, norm: dose-normalized, PM: CYP2D6 poor metabolizer, po: oral, q.i.d.: four times daily, s.d.: single dose.

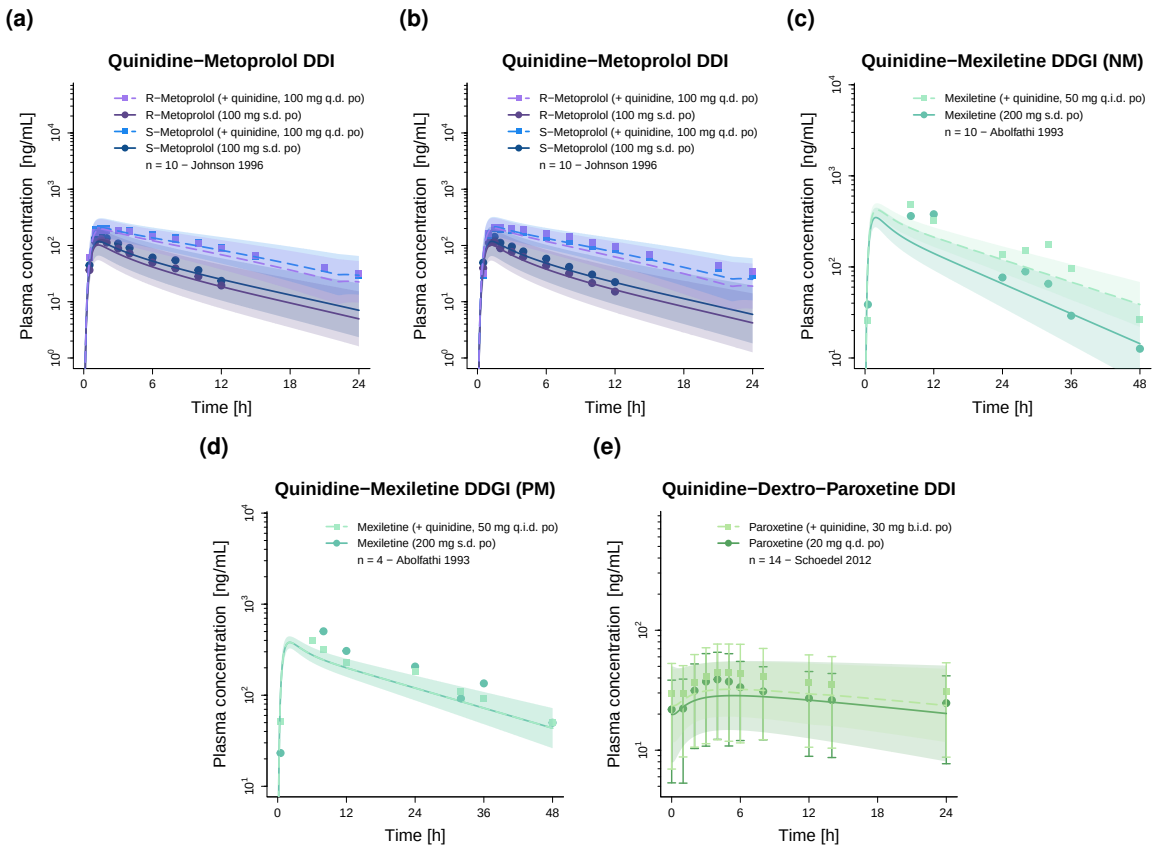

Figure S22: Predicted compared to observed plasma concentration-time profiles of (a–b) R-/S- metoprolol (comparison of different ethnic backgrounds), (c–d) mexiletine (observed data of representative subjects) and (e) paroxetine alone and after pretreatment with and/or concomitant administration of quinidine (semilogarithmic representation). Population predicted geometric means are shown as lines, corresponding geometric standard deviations are shown as shaded areas and observed data are shown as dots(control) and squares (DDI). b.i.d.: twice daily, DDI: drug-drug interaction, DDGI: drug-drug-gene interaction, n: number of study participants, NM: CYP2D6 normal metabolizer, PM: CYP2D6 poor metabolizer, po: oral, q.d.: once daily, q.i.d.: four times daily.

S3.5 Amount excreted unchnaged in urine profiles (semilogarithmic representation)

S3.5.1 Quinidine as victim

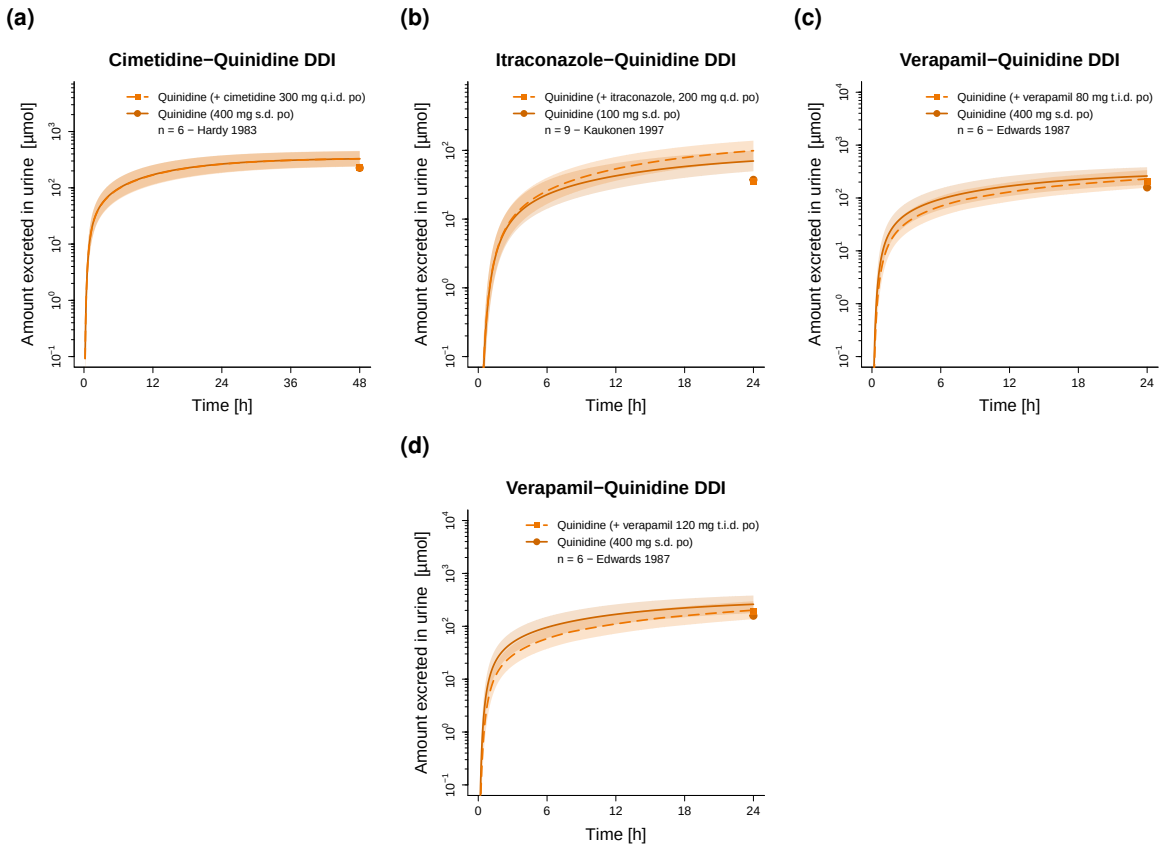

Figure S23: Predicted compared to observed plasma amount excreted unchanged in urine profiles of quinidine alone and after pretreatment and/or concomitant administration of (a) cimetidine, (b) itraconazole and (c–d) R-/S-verapamil (semilogarithmic representation). Population predicted geometric means are shown as lines, corresponding geometric standard deviations are shown as shaded areas and observed data are shown as dots (control) and squares (DDI). DDI: drug-drug interaction, n: number of study participants, po: oral, q.d.: once daily, q.i.d.: four times daily, s.d.: single dose, t.i.d.: three times daily.

S3.6 Plasma concentration-time profiles (linear representation)

S3.6.1 Quinidine as victim

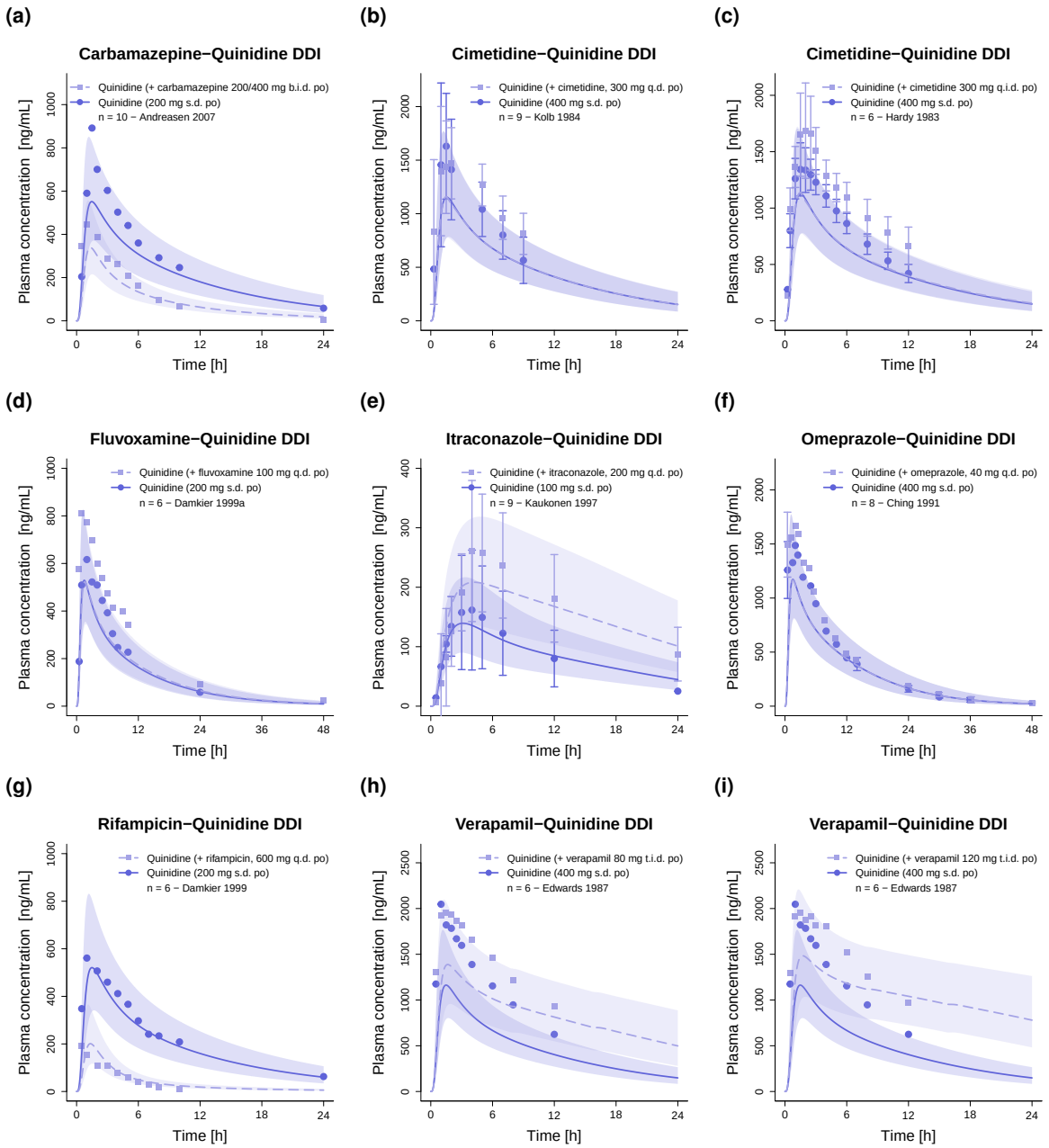

Figure S24: Predicted compared to observed plasma concentration-time profiles of quinidine and 3-hydroxyquinidine alone and after pretreatment and/or concomitant administration of (a) carbamazepine, (b–c) cimetidine, (d) fluvoxamine, (e) itraconazole, (f) R-/S-omeprazole, (g) rifampicin and (h–i) R-/S-verapamil (linear representation). Population predicted geometric means are shown as lines, corresponding geometric standard deviations are shown as shaded areas and observed data are shown as dots (± standard deviation, if reported). b.i.d.: twice daily, DDI: drug-drug interaction, n: number of study participants, po: oral, q.d.: once daily, q.i.d.: four times daily, s.d.: single dose, t.i.d.: three times daily.

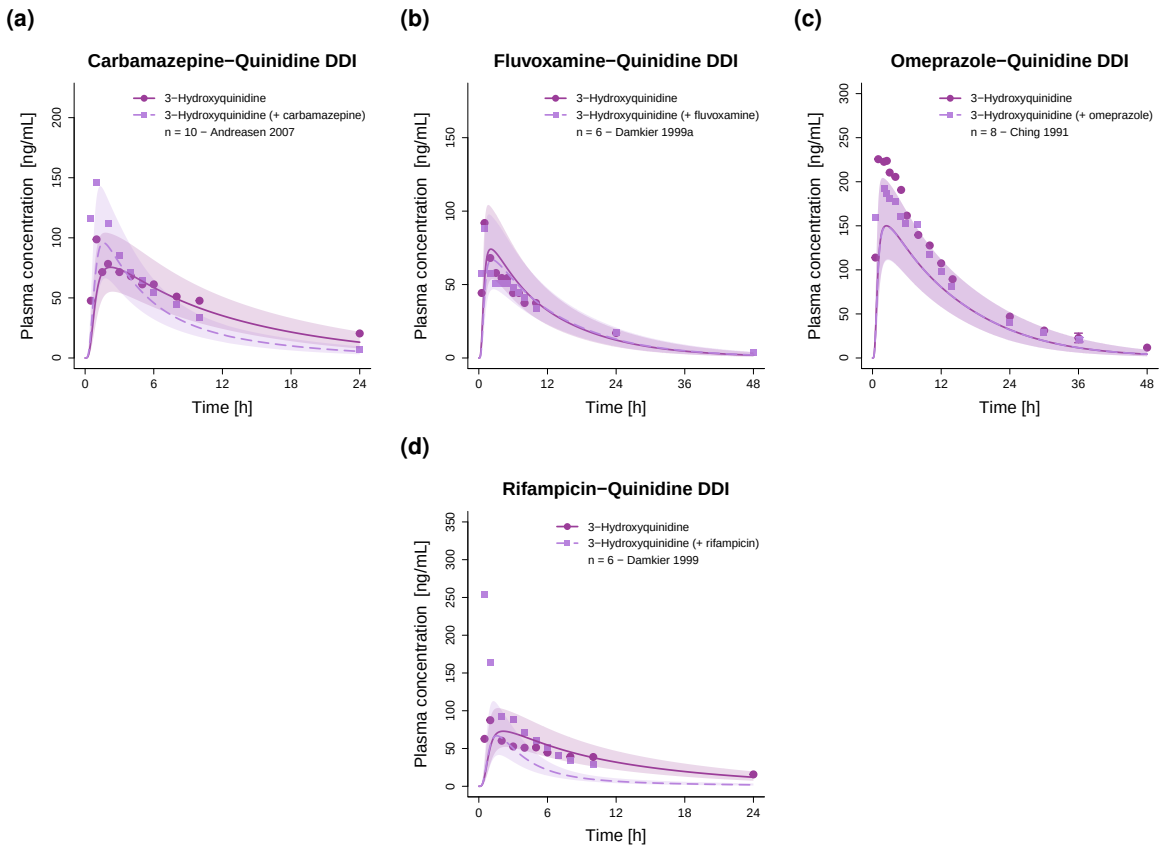

Figure S25: Predicted compared to observed plasma concentration-time profiles of 3-hydroxyquinidine alone and after pretreatment and/or concomitant administration of (a) carbamazepine, (b) fluvoxamine, (c) R-/S-omeprazole and (d) rifampicin (linear representation). Population predicted geometric means are shown as lines, corresponding geometric standard deviations are shown as shaded areas and observed data are shown as dots (± standard deviation, if reported). DDI: drug-drug interaction, n: number of study participants.

S3.6.2 Quinidine as perpetrator

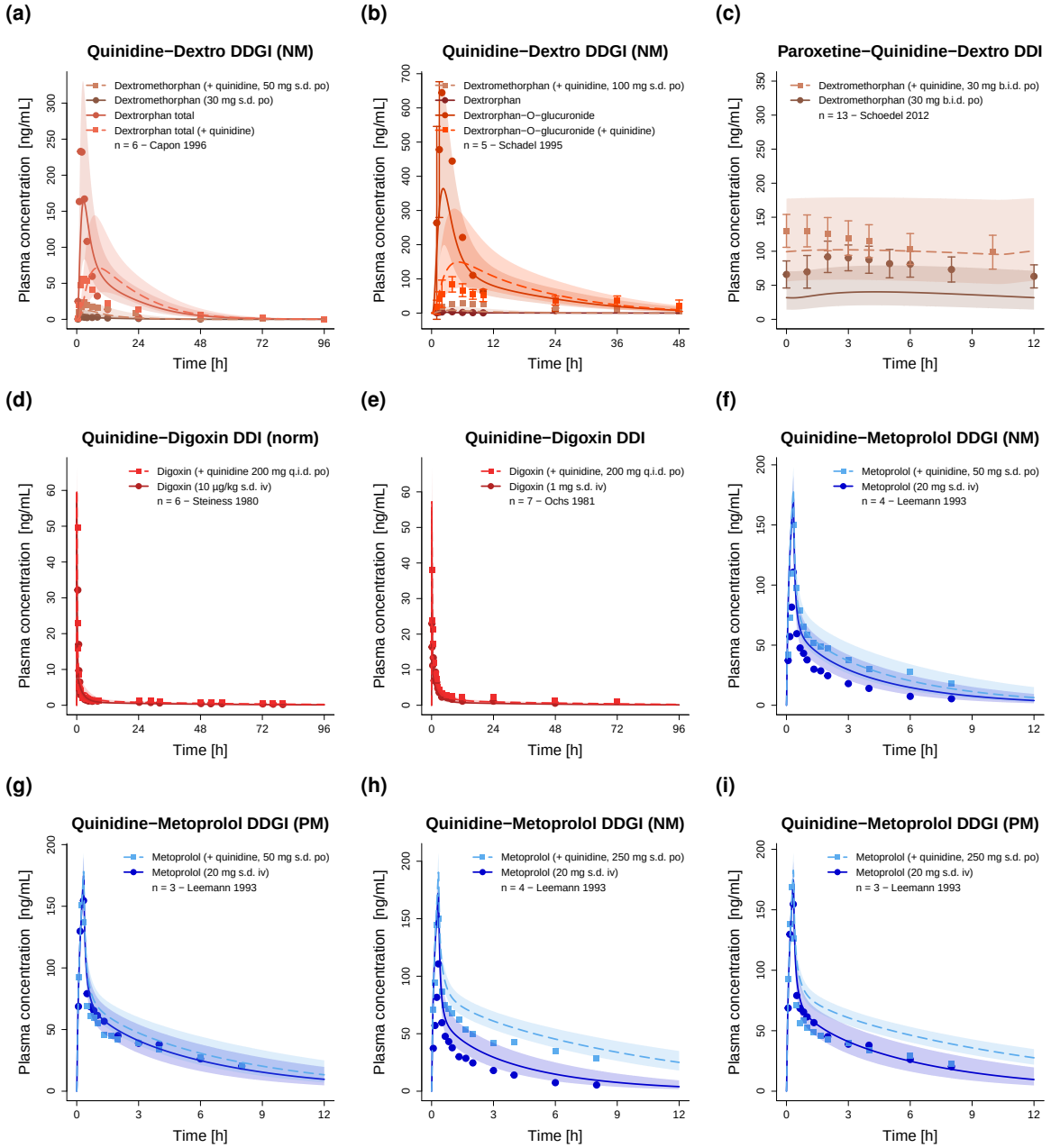

Figure S26: Predicted compared to observed plasma concentration-time profiles of (a–c) dextromethorphan (+ metabolites), (d–e) digoxin and (f–i) metoprolol alone and after pretreatment with and/or concomitant administration of quinidine (linear representation). Population predicted geometric means are shown as lines, corresponding geometric standard deviations are shown as shaded areas and observed data are shown as dots (± standard deviation, if reported). b.i.d.: twice daily, DDI: drug-drug interaction, DDGI: drug-drug-gene interaction, iv: intravenous, n: number of study participants, NM: CYP2D6 normal metabolizer, norm: dose-normalized, PM: CYP2D6 poor metabolizer, po: oral, q.i.d.: four times daily, s.d.: single dose.

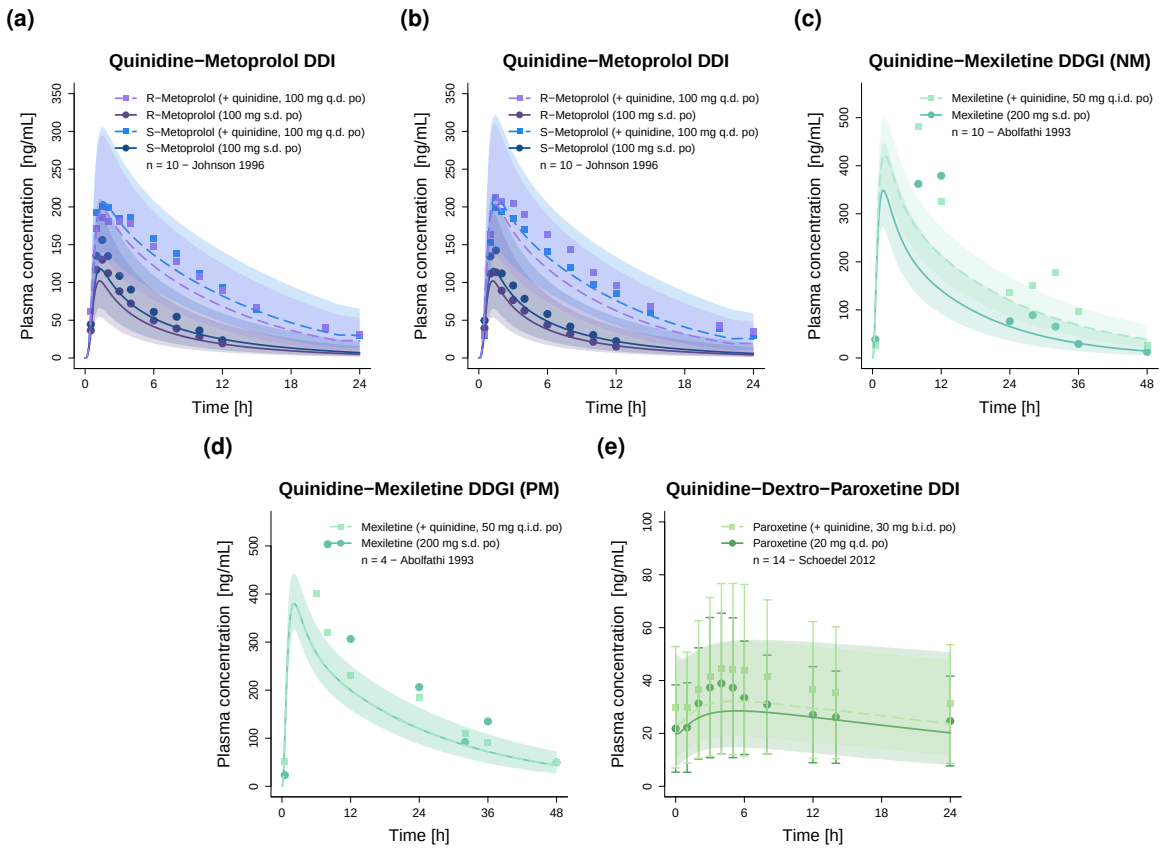

Figure S27: Predicted compared to observed plasma concentration-time profiles of (a–b) R-/S- metoprolol (comparison of different ethnic backgrounds), (c–d) mexiletine (observed data of representative subjects) and (e) paroxetine alone and after pretreatment with and/or concomitant administration of quinidine (linear representation). Population predicted geometric means are shown as lines, corresponding geometric standard deviations are shown as shaded areas and observed data are shown as dots (± standard deviation, if reported). b.i.d.: twice daily, DDI: drug-drug interaction, DDGI: drug-drug-gene interaction, n: number of study participants, NM: CYP2D6 normal metabolizer, PM: CYP2D6 poor metabolizer, po: oral, q.d.: once daily, q.i.d.: four times daily.

S3.7 Amount excreted unchnaged in urine profiles (linear representation)

S3.7.1 Quinidine as victim

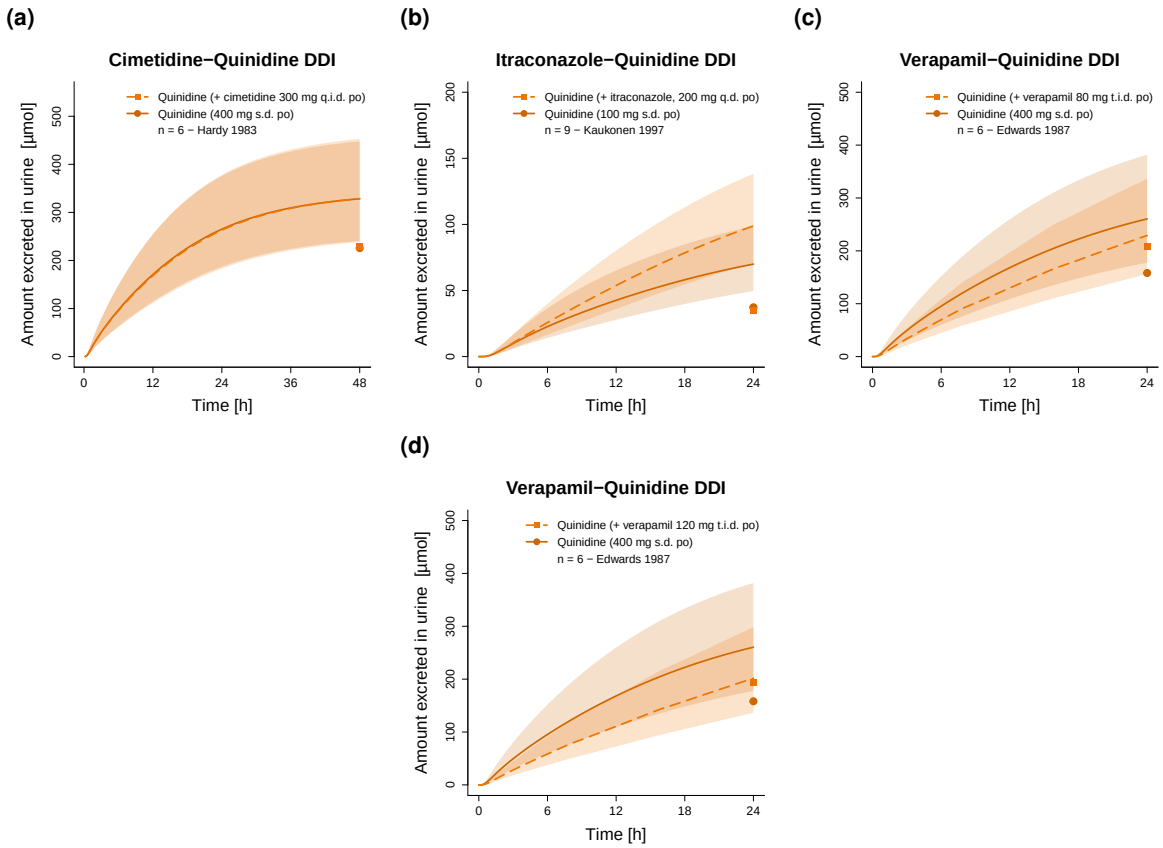

Figure S28: Predicted compared to observed plasma amount excreted unchanged in urine profiles of quinidine alone and after pretreatment and/or concomitant administration of (a) cimetidine, (b) itraconazole and (c–d) R-/S-verapamil (linear representation). Population predicted geometric means are shown as lines, corresponding geometric standard deviations are shown as shaded areas and observed data are shown as dots (control) and squares (DDI). DDI: drug-drug interaction, n: number of study participants, po: oral, q.d.: once daily, q.i.d.: four times daily, s.d.: single dose, t.i.d.: three times daily.

S3.8 DDI AUC_{last} and C_{max} ratios

S3.8.1 Quinidine as victim

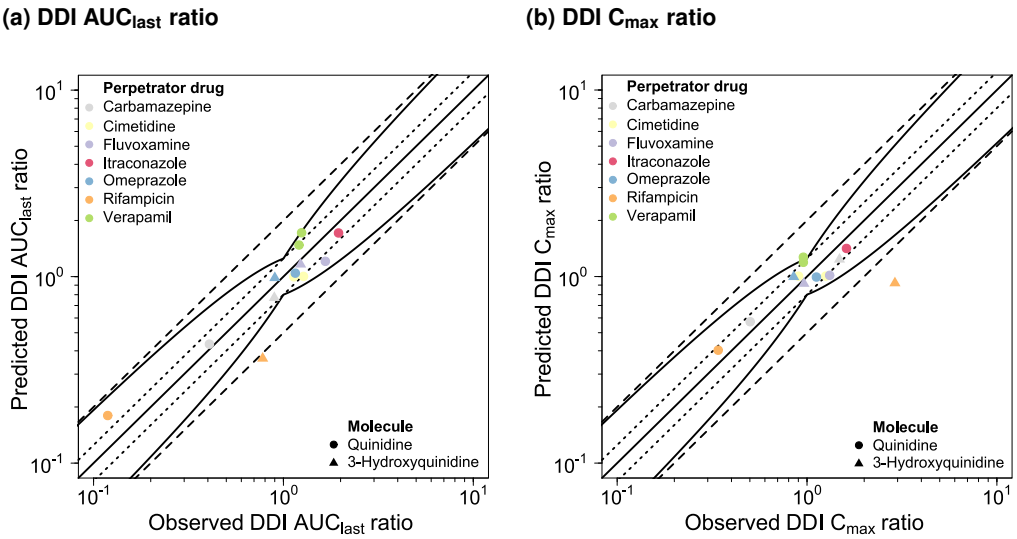

Figure S29: Goodness-of-fit plots comparing predicted and observed DDI AUC_{last} and C_{max} ratios. The solid line marks the line of identity. Dotted lines indicate 1.25-fold, dashed lines indicate 2-fold deviation. Prediction success limits proposed by Guest et al. [81] are shown as curved lines (including 20% variability). AUC_{last}: area under the plasma concentration-time curve calculated between the first and last concentration measurement, C_{max}: maximum plasma concentration, DDI: drug-drug interaction.

S3.8.2 Quinidine as perpetrator

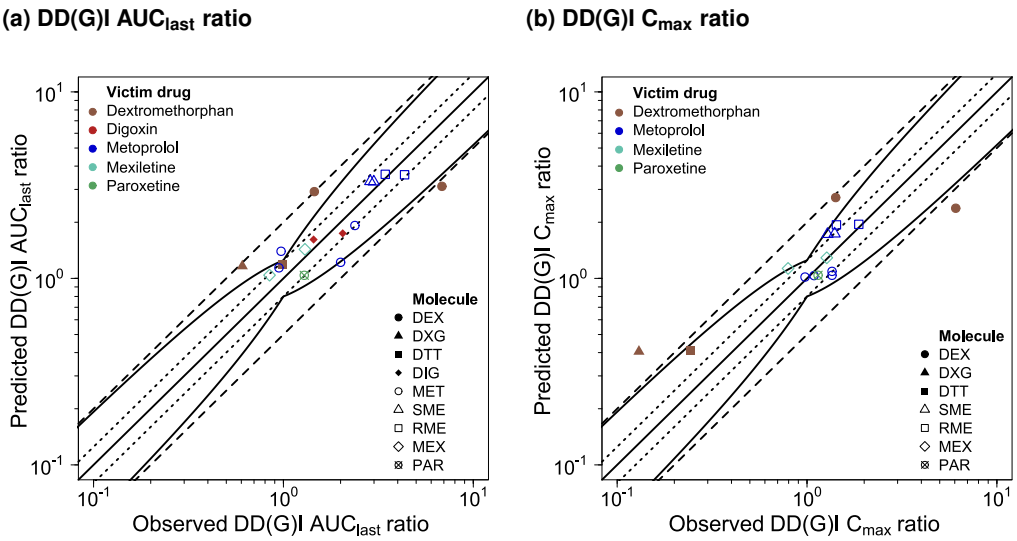

Figure S30: Goodness-of-fit plots comparing predicted and observed DD(G)I AUC$_{last}$ and C$_{max}$ ratios. The solid line marks the line of identity. Dotted lines indicate 1.25-fold, dashed lines indicate 2-fold deviation. Prediction success limits proposed by Guest et al. [81] are shown as curved lines (including 20% variability). AUC$_{last}$: area under the plasma concentration-time curve calculated between first and last concentration measurement, C$_{max}$: maximum plasma concentration, DD(G)I: drug-drug(-gene) interaction. DEX: dextromethorphan, DXG: dextrorphan-O-glucuronide, DTT: total dextrorphan, DIG: digoxin, MET: metoprolol, MEX: mexiletine, PAR: paroxetine, RME: R-metoprolol, SME: S-metoprolol.

S3.9 Geometric mean fold errors of predicted DD(G)I AUC_{last} and C_{max} ratios

S3.9.1 Quinidine as victim

Table S15: Predicted and observed DDI AUC_{last} and C_{max} ratios involving quinidine as victim drug

Drug administration			DDI AUC_{last} ratio			DDI C_{max} ratio					
Perpetrator	**Quinidine**	**t_{last} [h]**	**Pred**	**Obs**	**Pred/Obs**	**Pred**	**Obs**	**Pred/Obs**	**Molecule**	**Dataset**	**Reference**
Carbamazepine											
200/400 mg b.i.d. po	200 mg[a] s.d. po	24	0.43	0.41	1.07	0.57	0.50	1.14	QUI	tr	Andreasen 2007 [32]
200/400 mg b.i.d. po	200 mg[a] s.d. po	24	0.77	0.90	0.86	1.24	1.48	0.83	OHQ	tr	Andreasen 2007 [32]
Mean GMFE (range):			**1.11 (1.07 – 1.16), 2/2 with GMFE $\leq$ 2**			**1.17 (1.14 – 1.20), 2/2 with GMFE $\leq$ 2**					
Cimetidine											
300 mg q.d. po	400 mg[a] s.d. po	9	1.00	1.13	0.88	1.00	0.90	1.11	QUI	te	Kolb 1984 [42]
300 mg q.i.d. po	400 mg[a] s.d. po	12	1.00	1.28	0.79	1.01	1.26	0.80	QUI	te	Hardy 1983 [41]
Mean GMFE (range):			**1.20 (1.14 – 1.27), 2/2 with GMFE $\leq$ 2**			**1.18 (1.11 – 1.25), 2/2 with GMFE $\leq$ 2**					
Fluvoxamine											
100 mg q.d. po	200 mg[a] s.d. po	48	1.21	1.66	0.73	1.01	1.32	0.77	QUI	te	Damkier 1999a [34]
100 mg q.d. po	200 mg[a] s.d. po	48	1.16	1.23	0.94	0.92	0.96	0.95	OHQ	te	Damkier 1999a [34]
Mean GMFE (range):			**1.22 (1.06 – 1.38), 2/2 with GMFE $\leq$ 2**			**1.17 (1.05 – 1.30), 2/2 with GMFE $\leq$ 2**					
Itraconazole											
200 mg q.d. po	100 mg[a] s.d. po	24	1.71	1.95	0.88	1.41	1.61	0.88	QUI	te	Kaukonen 1997 [31]
Mean GMFE:			**1.14, 1/1 with GMFE $\leq$ 2**			**1.14, 1/1 with GMFE $\leq$ 2**					
Omeprazole											
40 mg q.d. po	400 mg[a] s.d. po	48	1.04	1.15	0.90	0.99	1.12	0.89	QUI	te	Ching 1991 [39]
40 mg q.d. po	400 mg[a] s.d. po	48	0.98	0.90	1.09	1.00	0.85	1.17	OHQ	te	Ching 1991 [39]
Mean GMFE (range):			**1.10 (1.09 – 1.11), 2/2 with GMFE $\leq$ 2**			**1.15 (1.13 – 1.17), 2/2 with GMFE $\leq$ 2**					
Rifampicin											
600 mg q.d. po	200 mg[a] s.d. po	10	0.18	0.12	1.52	0.40	0.34	1.18	QUI	te	Damkier 1999 [33]
600 mg q.d. po	200 mg[a] s.d. po	10	0.36	0.78	0.47	0.92	2.90	0.32	OHQ	te	Damkier 1999 [33]
Mean GMFE (range):			**1.83 (1.52 – 2.13), 1/2 with GMFE $\leq$ 2**			**2.17 (1.18 – 3.15), 1/2 with GMFE $\leq$ 2**					
Verapamil											
80 mg t.i.d. po	400 mg[a] s.d. po	12	1.48	1.21	1.22	1.19	0.96	1.25	QUI	te	Edwards 1987 [40]
120 mg t.i.d. po	400 mg[a] s.d. po	12	1.72	1.25	1.38	1.27	0.96	1.33	QUI	te	Edwards 1987 [40]
Mean GMFE (range):			**1.34 (1.30 – 1.38), 2/2 with GMFE $\leq$ 2**			**1.31 (1.29 – 1.33), 2/2 with GMFE $\leq$ 2**					
Overall GMFE (range):			**1.29 (1.06 – 2.19), 12/13 with GMFE $\leq$ 2**			**1.34 (1.05 – 3.15), 12/13 with GMFE $\leq$ 2**					

AUC_{last}: area under the plasma concentration-time curve calculated between the first and last concentration measurement, b.i.d.: twice daily, C_{max}: maximum plasma concentration, DDI: drug-drug interaction, GMFE: geometric mean fold error, obs: observed, OHQ: 3-hydroxyquinidine, po: oral, pred: predicted, q.d.: once daily, QUI: quinidine, s.d.: single dose, te: test dataset, t.i.d.: three times daily, t_{last}: time of the last concentration measurement, tr: training dataset. Respective doses of quinidine base were calculated and incorporated in simulations. [a] Quinidine sulfate dose.

S3.9.2 Quinidine as perpetrator

Table S16: Predicted and observed DD(G)I AUC_{last} and C_{max} ratios involving quinidine as perpetrator drug

Drug administration			DD(G)I AUC_{last} ratio			DD(G)I C_{max} ratio						
Quinidine	**Victim**	**t_{last} [h]**	**Pred**	**Obs**	**Pred/Obs**	**Pred**	**Obs**	**Pred/Obs**	**Phenotype**	**Molecule**	**Dataset**	**Reference**
	Dextromethorphan											
50 mg[a] s.d. po	30 mg s.d. po[b]	72	3.12	6.84	0.46	2.38	6.07	0.39	*CYP2D6 NM*	DEX	te	Capon 1996 [73]
50 mg[a] s.d. po	30 mg s.d. po	96	1.19	0.99	1.20	0.41	0.24	1.69	*CYP2D6 NM*	DTT	te	Capon 1996 [73]
100 mg[a] s.d. po	30 mg s.d. po	48	1.16	0.61	1.92	0.41	0.13	3.11	*CYP2D6 NM*	DXG	te	Schadel 1995 [74]
30 mg[a] b.i.d. po[c]	30 mg b.i.d. po[d]	12	2.92	1.45	2.01	2.71	1.42	1.92	*CYP2D6 NM*	DEX	te	Schoedel 2012 [75]
Mean GMFE (range):			**1.83 (1.20 – 2.19), 2/4 with GMFE $\leq$ 2**			**2.32 (1.69 – 3.11), 2/4 with GMFE $\leq$ 2**						
	Digoxin											
200 mg[a] q.i.d. po	10 µg/kg s.d. iv[e]	80	1.62	1.44	1.12	-	-	-	-	DIG	te	Steiness 1980 [76]
200 mg[a] q.i.d. po	1 mg s.d. iv	72	1.74	2.05	0.85	-	-	-	-	DIG	te	Ochs 1981 [77]
Mean GMFE (range):			**1.15 (1.12 – 1.18), 2/2 with GMFE $\leq$ 2**					**-**				
	Metoprolol											
50 mg[a] s.d. po	20 mg s.d. iv	8	1.22	2.00	0.61	1.04	1.35	0.77	*CYP2D6 NM*	MET	te	Leemann 1993 [78]
50 mg[a] s.d. po	20 mg s.d. iv[f]	8	1.14	0.95	1.20	1.02	0.98	1.04	*CYP2D6 PM*	MET	te	Leemann 1993 [78]
250 mg[a] b.i.d. po	20 mg s.d. iv	8	1.92	2.38	0.81	1.09	1.35	0.81	*CYP2D6 NM*	MET	te	Leemann 1993 [78]
250 mg[a] b.i.d. po	20 mg s.d. iv[f]	8	1.40	0.97	1.44	1.03	1.09	0.95	*CYP2D6 PM*	MET	te	Leemann 1993 [78]
100 mg[a] q.d. po	200 mg s.d. po	24	3.61	3.44	1.05	1.94	1.43	1.36	*CYP2D6 NM*	RME	te	Johnson 1996 [79]
100 mg[a] q.d. po	200 mg s.d. po	24	3.31	2.87	1.16	1.73	1.28	1.35	*CYP2D6 NM*	SME	te	Johnson 1996 [79]
100 mg[a] q.d. po	200 mg s.d. po	24	3.59	4.35	0.83	1.95	1.87	1.04	*CYP2D6 NM*	RME	te	Johnson 1996 [79]
100 mg[a] q.d. po	200 mg s.d. po	24	3.30	2.99	1.10	1.74	1.40	1.24	*CYP2D6 NM*	SME	te	Johnson 1996 [79]
Mean GMFE (range):			**1.24 (1.05 – 1.44), 8/8 with GMFE $\leq$ 2**			**1.20 (1.04 – 1.36), 8/8 with GMFE $\leq$ 2**						
	Mexiletine											
50 mg[a] q.i.d. po	200 mg s.d. po	48	1.43	1.30	1.10	1.29	1.27	1.01	*CYP2D6 NM*	MEX	te	Abolfathi 1993 [80]
50 mg[a] q.i.d. po	200 mg s.d. po	48	1.04	0.85	1.23	1.13	0.79	1.42	*CYP2D6 PM*	MEX	te	Abolfathi 1993 [80]
Mean GMFE (range):			**1.17 (1.10 – 1.23), 2/2 with GMFE $\leq$ 2**			**1.22 (1.01 – 1.42), 2/2 with GMFE $\leq$ 2**						
	Paroxetine											
30 mg[a] b.i.d. po	20 mg q.d. po[g]	24	1.04	1.29	0.81	1.04	1.14	0.91	*CYP2D6 NM*	PAR	te	Schoedel 2012 [75]
Mean GMFE:				**1.24, 1/1 with GMFE $\leq$ 2**			**1.10, 1/1 with GMFE $\leq$ 2**					
Overall GMFE (range):			**1.36 (1.05 – 2.19), 15/17 with GMFE $\leq$ 2**			**1.49 (1.01 – 3.11), 13/15 with GMFE $\leq$ 2**						

AUC_{last}: area under the plasma concentration-time curve calculated between the first and last concentration measurement, b.i.d.: twice daily, C_{max}: maximum plasma concentration, DD(G)I: drug-drug(-gene) interaction, DEX: dextromethorphan, DIG: digoxin, DTT: total dextrorphan, DXG: dextrorphan-O-glucuronide, GMFE: geometric mean fold error, iv: intravenous, MET: metoprolol (racemate), MEX: mexiletine, n: number of individuals studied, *NM*: *normal metabolizer*, *PM*: *poor metabolizer*, PAR: paroxetine, po: oral, pred: predicted, q.d.: once daily, q.i.d:, four times daily, RME: R-metoprolol, s.d.: single dose, SME: S-metoprolol, te: test dataset, t_{last}: time of the last concentration measurement. If perpetrator and victim drugs were applied in form of salts, the respective doses of bases were calculated and incorporated in simulations. [a] Quinidine sulfate dose. [b] CYP2D6 catalytic rate constant estimated for control to account for unexplained interindividual variability in CYP2D6 activity (57% of original model value). [c] Plus paroxetine (20 mg q.d. po). [d] CYP2D6 catalytic rate constant estimated for control to account for unexplained interindividual variability in CYP2D6 activity (26% of original model value). [e] Digoxin dose of 15 µg/kg before DDI, normalized to 15 µg/kg for evaluation. [f] CYP2D6 catalytic rate constant estimated for control to account for unexplained interindividual variability in CYP2D6 activity (300% for sink metabolism and 200% for formation of α-hydroxymetoprolol of original model value). [g] Plus dextromethorphan (30 mg b.i.d. po).

References

[1] M. Nishimura and S. Naito. Tissue-specific mRNA expression profiles of human phase I metabolizing enzymes except for cytochrome P450 and phase II metabolizing enzymes. *Drug metabolism and pharmacokinetics*, 21(5): 357–74, 2006. doi: 10.2133/dmpk.21.357.

[2] M. Meyer, S. Schneckener, B. Ludewig, L. Kuepfer, and J. Lippert. Using expression data for quantification of active processes in physiologically based pharmacokinetic modeling. *Drug metabolism and disposition: the biological fate of chemicals*, 40(5):892–901, 2012. doi: 10.1124/dmd.111.043174.

[3] M. Nishimura, H. Yaguti, H. Yoshitsugu, S. Naito, and T. Satoh. Tissue distribution of mRNA expression of human cytochrome P450 isoforms assessed by high-sensitivity real-time reverse transcription PCR. *Journal of the Pharmaceutical Society of Japan*, 123(5):369–75, 2003. doi: 10.1248/yakushi.123.369.

[4] A. D. Rodrigues. Integrated cytochrome P450 reaction phenotyping: attempting to bridge the gap between cDNA-expressed cytochromes P450 and native human liver microsomes. *Biochemical pharmacology*, 57(5):465–80, 1999. doi: 10.1016/S0006-2952(98)00268-8.

[5] Open Systems Pharmacology Suite Community. Open Systems Pharmacology Suite Manual, 2018. URL https://docs.open-systems-pharmacology.org/.

[6] National Center for Biotechnology Information (NCBI). Expressed Sequence Tags (EST) from UniGene, 2019.

[7] G. Margaillan, M. Rouleau, J. K. Fallon, P. Caron, L. Villeneuve, V. Turcotte, P. C. Smith, M. S. Joy, and C. Guillemette. Quantitative profiling of human renal UDP-glucuronosyltransferases and glucuronidation activity: A comparison of normal and tumoral kidney tissues. *Drug Metabolism and Disposition*, 43(4):611–19, 2015. doi: 10.1124/dmd.114.062877.

[8] B. Achour, M. R. Russell, J. Barber, and A. Rostami-Hodjegan. Simultaneous quantification of the abundance of several cytochrome P450 and uridine 5'-diphospho-glucuronosyltransferase enzymes in human liver microsomes using multiplexed targeted proteomics. *Drug metabolism and disposition: the biological fate of chemicals*, 42(4): 500–510, 2014. doi: 10.1124/dmd.113.055632.

[9] D. Scotcher, S. Billington, J. Brown, C. R. Jones, C. D. Brown, A. Rostami-Hodjegan, and A. Galetin. Microsomal and cytosolic scaling factors in dog and human kidney cortex and application for in vitro-in vivo extrapolation of renal metabolic clearance. *Drug Metabolism and Disposition*, 45(5):556–568, 2017. doi: 10.1124/dmd.117.075242.

[10] M. Otsuka, T. Matsumoto, R. Morimoto, S. Arioka, H. Omote, and Y. Moriyama. A human transporter protein that mediates the final excretion step for toxic organic cations. *Proceedings of the National Academy of Sciences of the United States of America*, 102(50):17923–8, 2005. doi: 10.1073/pnas.0506483102.

[11] S. Masuda, T. Terada, A. Yonezawa, Y. Tanihara, K. Kishimoto, T. Katsura, O. Ogawa, and K.-i. Inui. Identification and functional characterization of a new human kidney-specific H+/organic cation antiporter, kidney-specific multidrug and toxin extrusion 2. *Journal of the American Society of Nephrology : JASN*, 17(8):2127–35, 2006. doi: 10.1681/ASN.2006030205.

[12] B. Prasad, K. Johnson, S. Billington, C. Lee, G. W. Chung, C. D. Brown, E. J. Kelly, J. Himmelfarb, and J. D. Unadkat. Abundance of drug transporters in the human kidney cortex as quantified by quantitative targeted proteomics. *Drug Metabolism and Disposition*, 44(12):1920–1924, 2016. doi: 10.1124/dmd.116.072066.

[13] M. Nishimura and S. Naito. Tissue-specific mRNA expression profiles of human ATP-binding cassette and solute carrier transporter superfamilies. *Drug metabolism and pharmacokinetics*, 20(6):452–77, 2005. doi: 10.2133/dmpk.20.452.

[14] B. Prasad, R. Evers, A. Gupta, C. E. C. A. Hop, L. Salphati, S. Shukla, S. V. Ambudkar, and J. D. Unadkat. Interindividual variability in hepatic organic anion - transporting polypeptides and P-glycoprotein (ABCB1) protein expression: quantification by liquid chromatography tandem mass spectroscopy and influence of genotype, age, and sex. *Drug metabolism and disposition: the biological fate of chemicals*, 42(1):78–88, 2014. doi: 10.1124/dmd.113.053819.

[15] N. Kolesnikov, E. Hastings, M. Keays, O. Melnichuk, Y. A. Tang, E. Williams, M. Dylag, N. Kurbatova, M. Brandizi, T. Burdett, K. Megy, E. Pilicheva, G. Rustici, A. Tikhonov, H. Parkinson, R. Petryszak, U. Sarkans, and A. Brazma. ArrayExpress update-simplifying data submissions. *Nucleic Acids Research*, 43(D1):D1113–D1116, 2015. doi: 10.1093/nar/gku1057.

[16] L. Wang, B. Prasad, L. Salphati, X. Chu, A. Gupta, C. E. Hop, R. Evers, and J. D. Unadkat. Interspecies variability in expression of hepatobiliary transporters across human, dog, monkey, and rat as determined by quantitative proteomics. *Drug Metabolism and Disposition*, 43(3):367–74, 2015. doi: 10.1124/dmd.114.061580.

[17] N. Hanke, S. Frechen, D. Moj, H. Britz, T. Eissing, T. Wendl, and T. Lehr. PBPK models for CYP3A4 and P-gp DDI prediction: A modeling network of rifampicin, itraconazole, clarithromycin, midazolam, alfentanil, and digoxin. *CPT: Pharmacometrics & Systems Pharmacology*, 7(10):647–59, 2018. doi: 10.1002/psp4.12343.

[18] K. Rowland Yeo, R. L. Walsky, M. Jamei, A. Rostami-Hodjegan, and G. T. Tucker. Prediction of time-dependent CYP3A4 drug-drug interactions by physiologically based pharmacokinetic modelling: Impact of inactivation parameters and enzyme turnover. *European Journal of Pharmaceutical Sciences*, 43(3):160–73, 2011. doi: 10.1016/j.ejps.2011.04.008.

[19] D. J. Greenblatt, L. L. von Moltke, J. S. Harmatz, G. Chen, J. L. Weemhoff, C. Jen, C. J. Kelley, B. W. LeDuc, and M. A. Zinny. Time course of recovery of cytochrome P450 3A function after single doses of grapefruit juice. *Clinical Pharmacology and Therapeutics*, 74(2):121–29, 2003. doi: 10.1016/S0009-9236(03)00118-8.

[20] T. Kanacher, A. Lindauer, E. Mezzalana, I. Michon, C. Veau, J. D. G. Mantilla, V. Nock, and A. Fleury. A Physiologically-Based Pharmacokinetic (PBPK) Model Network for the Prediction of CYP1A2 and CYP2C19 Drug-Drug-Gene Interactions with Fluvoxamine, Omeprazole, S-mephenytoin, Moclobemide, Tizanidine, Mexiletine, Ethinylestradiol, and Caffeine. *Pharmaceutics*, 12(12):1–15, 2020. doi: 10.3390/pharmaceutics12121191.

[21] ICRP Publication 89. Third National Health and Nutrition Examination Survey (NHANES III). *Annals of the ICRP*, 3–4(32):5–265, 2014.

[22] D. Fremstad, O. G. Nilsen, L. Storstein, J. Amlie, and S. Jacobsen. Pharmacokinetics of quinidine related to plasma protein binding in man. *European journal of clinical pharmacology*, 15(3):187–92, 1979. doi: 10.1007/BF00563104.

[23] National Center for Health Statistics Hyattsville, MS 20782. Basic anatomical and physiological data for use in radiological protection: reference values. A report of age- and gender-related differences in the anatomical and physiological characteristics of reference individuals. 1997.

[24] D. Darbar, S. Dell'Orto, K. Mörike, G. R. Wilkinson, and D. M. Roden. Dietary salt increases first-pass elimination of oral quinidine. *Clinical pharmacology and therapeutics*, 61(3):292–300, 1997. doi: 10.1016/S0009-9236(97)90161-2.

[25] T. W. Guentert, N. H. Holford, P. E. Coates, R. A. Upton, and S. Riegelman. Quinidine pharmacokinetics in man: choice of a disposition model and absolute bioavailability studies. *Journal of pharmacokinetics and biopharmaceutics*, 7(4):315–30, 1979. doi: 10.1007/BF01062532.

[26] Tanaka, G and Kawamura, H. Anatomical and physiological characteristics for Asian reference man: Male and female of different ages: Tanaka model. *Division of Radioecology. National Institute of Radiological Sciences. Hitachinaka 311-12 Japan. Report Number NIRS-M-115.*, 1996.

[27] J.-G. Shin, W.-K. Kang, J.-H. Shon, M. Arefayene, Y.-R. Yoon, K.-A. Kim, D.-I. Kim, D.-S. Kim, K.-H. Cho, R. L. Woosley, and D. A. Flockhart. Possible interethnic differences in quinidine-induced QT prolongation between healthy Caucasian and Korean subjects. *British journal of clinical pharmacology*, 63(2):206–15, 2007. doi: 10.1111/j.1365-2125.2006.02793.x.

[28] H. R. Ochs, E. Grube, D. J. Greenblatt, E. Woo, and G. Bodem. Intravenous quinidine: pharmacokinetic properties and effects on left ventricular performance in humans. *American Heart Journal*, 99(4):468–475, 1980. doi: 10.1016/0002-8703(80)90381-6.

[29] O. S. Pharmacology. Japanese Population Report, 2019. URL https://github.com/Open-Systems-Pharmacology/OSPSuite.Documentation/blob/master/Japanese_Population/Report.md.

[30] K. Maeda, J. Takano, Y. Ikeda, T. Fujita, Y. Oyama, K. Nozawa, Y. Kumagai, and Y. Sugiyama. Nonlinear Pharmacokinetics of Oral Quinidine and Verapamil in Healthy Subjects: A Clinical Microdosing Study. *Clinical Pharmacology & Therapeutics*, 90(2):263–270, 2011. doi: 10.1038/clpt.2011.108.

[31] K. M. Kaukonen, K. T. Olkkola, and P. J. Neuvonen. Itraconazole increases plasma concentrations of quinidine. *Clinical pharmacology and therapeutics*, 62(5):510–7, 1997. doi: 10.1016/S0009-9236(97)90046-1.

[32] A.-H. Andreasen, K. Brøsen, and P. Damkier. A Comparative Pharmacokinetic Study in Healthy Volunteers of the Effect of Carbamazepine and Oxcarbazepine on Cyp3a4. *Epilepsia*, 48(3):490–496, 2007. doi: 10.1111/j.1528-1167.2007.00924.x.

[33] P. Damkier, L. L. Hansen, and K. Brøsen. Effect of fluvoxamine on the pharmacokinetics of quinidine. *European Journal of Clinical Pharmacology*, 55(6):451–456, 1999. doi: 10.1007/s002280050655.

[34] P. Damkier, L. L. Hansen, and K. Brøsen. Rifampicin treatment greatly increases the apparent oral clearance of quinidine. *Pharmacology and Toxicology*, 85(6):257–262, 1999. doi: 10.1111/j.1600-0773.1999.tb02019.x.

[35] S. Laganière, R. F. Davies, G. Carignan, K. Foris, L. Goernert, K. Carrier, C. Pereira, and I. McGilveray. Pharmacokinetic and pharmacodynamic interactions between diltiazem and quinidine. *Clinical pharmacology and therapeutics*, 60(3):255–64, 1996. doi: 10.1016/S0009-9236(96)90052-1.

[36] W. D. Mason, J. O. Covinsky, J. L. Valentine, K. L. Kelly, O. H. Weddle, and B. L. Martz. Comparative plasma concentrations of quinidine following administration of one intramuscular and three oral formulations to 13 human subjects. *Journal of pharmaceutical sciences*, 65(9):1325–9, 1976. doi: 10.1002/jps.2600650916.

[37] B. R. Rao and D. Rambhau. Absence of a pharmacokinetic interaction between quinidine and diazepam. *Drug Metabolism and Drug Interactions*, 12(1):45–52, 1995. doi: 10.1515/DMDI.1995.12.1.45.

[38] B. E. Bleske, P. L. Carver, T. M. Annesley, J. R. M. Bleske, and F. Morady. The Effect of Ciprofloxacin on the Pharmacokinetic and ECG Parameters of Quinidine. *The Journal of Clinical Pharmacology*, 30(10):911–915, 1990. doi: 10.1002/j.1552-4604.1990.tb03570.x.

[39] M. S. Ching, S. L. Elliott, C. K. Stead, R. T. Murdoch, S. Devenish-Meares, D. J. Morgan, and R. A. Smallwood. Quinidine single dose pharmacokinetics and pharmacodynamics are unaltered by omeprazole. *Alimentary pharmacology & therapeutics*, 5(5):523–31, 1991. doi: 10.1111/j.1365-2036.1991.tb00521.x.

[40] D. J. Edwards, R. Lavoie, H. Beckman, R. Blevins, and M. Rubenfire. The effect of coadministration of verapamil on the pharmacokinetics and metabolism of quinidine. *Clinical Pharmacology and Therapeutics*, 41(1):68–73, 1987. doi: 10.1038/clpt.1987.11.

[41] B. G. Hardy and J. J. Schentag. Lack of effect of cimetidine on the metabolism of quinidine: effect on renal clearance. *International journal of clinical pharmacology, therapy, and toxicology*, 26(8):388–91, 1983.

[42] K. W. Kolb, W. R. Garnett, R. E. Small, G. W. Vetrovec, B. J. Kline, and T. Fox. Effect of Cimetidine on Quinidine Clearance. *Therapeutic Drug Monitoring*, 6(3):306–312, 1984. doi: 10.1097/00007691-198409000-00009.

[43] H. R. Ochs, D. J. Greenblatt, E. Woo, K. Franke, H. J. Pfeifer, and T. W. Smith. Single and multiple dose pharmacokinetics of oral quinidine sulfate and gluconate. *The American journal of cardiology*, 41(4):770–7, 1978. doi: 10.1016/0002-9149(78)90830-5.

[44] J. D. Strum, J. L. Colaizzi, J. M. Jaffe, P. C. Martineau, and R. I. Poust. Comparative bioavaiability of four commercial quinidine sulfate tablets. *Journal of pharmaceutical sciences*, 66(4):539–42, 1977. doi: 10.1002/jps.2600660420.

[45] G. M. Frigo, E. Perucca, M. Teggia-Droghi, G. Gatti, A. Mussini, and J. Salerno. Comparison of quinidine plasma concentration curves following oral administration of some short- and long-acting formulations. *British journal of clinical pharmacology*, 4(4):449–54, 1977. doi: 10.1111/j.1365-2125.1977.tb00760.x.

[46] P. Bolme and U. Otto. Dose-dependence of the pharmacokinetics of quinidine. *European journal of clinical pharmacology*, 12(1):73–6, 1977. doi: 10.1007/BF00561409.

[47] D. S. Wishart, C. Knox, A. C. Guo, S. Shrivastava, M. Hassanali, P. Stothard, Z. Chang, and J. Woolsey. DrugBank: a comprehensive resource for in silico drug discovery and exploration. *Nucleic acids research*, 34(Database issue): D668–72, 2006. doi: 10.1093/nar/gkj067.

[48] Drugbank-online. Quinidine - Drugbank, 2022. URL https://go.drugbank.com/drugs/DB00908.

[49] Drugbank-online. 3-Hydroxyquinidine - Drugbank, 2022. URL https://go.drugbank.com/metabolites/DBMET00382.

[50] J. Takano, K. Maeda, M. B. Bolger, and Y. Sugiyama. The prediction of the relative importance of CYP3A/P-glycoprotein to the nonlinear intestinal absorption of drugs by advanced compartmental absorption and transit model. *Drug Metabolism and Disposition*, 44(11):1808–1818, 2016. doi: 10.1124/dmd.116.070011.

[51] ChemAxon. Chemicalize, 2020. URL https://chemicalize.com.

[52] S. Grube, P. Langguth, H. E. Junginger, S. Kopp, K. K. Midha, V. P. Shah, S. Stavchansky, J. B. Dressman, and D. M. Barends. Biowaiver monographs for immediate release solid oral dosage forms: quinidine sulfate. *Journal of pharmaceutical sciences*, 98(7):2238–51, 2009. doi: 10.1002/jps.21606.

[53] R. Watanabe, T. Esaki, H. Kawashima, Y. Natsume-Kitatani, C. Nagao, R. Ohashi, and K. Mizuguchi. Predicting Fraction Unbound in Human Plasma from Chemical Structure: Improved Accuracy in the Low Value Ranges. *Molecular Pharmaceutics*, 15(11):5302–5311, 2018. doi: 10.1021/acs.molpharmaceut.8b00785.

[54] T. Tachibana, S. Kitamura, M. Kato, T. Mitsui, Y. Shirasaka, S. Yamashita, and Y. Sugiyama. Model analysis of the concentration-dependent permeability of p-gp substrates. *Pharmaceutical Research*, 27(3):442–446, 2010. doi: 10.1007/s11095-009-0026-9.

[55] T. L. Nielsen, B. B. Rasmussen, J. P. Flinois, P. Beaune, and K. Brosen. In vitro metabolism of quinidine: the (3S)-3-hydroxylation of quinidine is a specific marker reaction for cytochrome P-4503A4 activity in human liver microsomes. *The Journal of pharmacology and experimental therapeutics*, 289(1):31–7, 1999.

[56] R. P. Austin, P. Barton, S. L. Cockroft, M. C. Wenlock, and R. J. Riley. The influence of nonspecific microsomal binding on apparent intrinsic clearance, and its prediction from physicochemical properties. *Drug Metabolism and Disposition*, 30(12):1497–1503, 2002. doi: 10.1124/dmd.30.12.1497.

[57] A. A. Lumen, P. Acharya, J. W. Polli, A. Ayrton, H. Ellens, and J. Bentz. If the K I Is Defined by the Free Energy of Binding to P-Glycoprotein, Which Kinetic Parameters Define the IC 50 for the Madin-Darby Canine Kidney II Cell Line Overexpressing Human Multidrug Resistance 1 Confluent Cell Monolayer? *Drug Metabolism and Disposition*, 38(2):260–269, 2010. doi: 10.1124/dmd.109.029843.

[58] A. A. Moghadamnia, A. Rostami-Hodjegan, R. Abdul-Manap, C. E. Wright, A. H. Morice, and G. T. Tucker. Physiologically based modelling of inhibition of metabolism and assessment of the relative potency of drug and metabolite: dextromethorphan vs . dextrorphan using quinidine inhibition. *British Journal of Clinical Pharmacology*, 56(1):57–67, 2003. doi: 10.1046/j.1365-2125.2003.01853.x.

[59] M. S. Ching, C. L. Blake, H. Ghabrial, S. W. Ellis, M. S. Lennard, G. T. Tucker, and R. A. Smallwood. Potent inhibition of yeast-expressed CYP2D6 by dihydroquinidine, quinidine, and its metabolites. *Biochemical pharmacology*, 50(6): 833–7, 1995. doi: 10.1016/0006-2952(95)00207-g.

[60] L. M. Berezhkovskiy. Volume of distribution at steady state for a linear pharmacokinetic system with peripheral elimination. *Journal of Pharmaceutical Sciences*, 93(6):1628–1640, 2004. doi: 10.1002/jps.20073.

[61] Open Systems Pharmacology Suite Community. Open Systems Pharmacology Documentation., 2018. URL https://docs.open-systems-pharmacology.org/working-with-pk-sim/pk-sim-documentation.

[62] C. A. Nguyen, Y. N. Konan-Kouakou, E. Allémann, E. Doelker, D. Quintanar-Guerrero, H. Fessi, and R. Gurny. Preparation of surfactant-free nanoparticles of methacrylic acid copolymers used for film coating. *AAPS PharmSciTech*, 7 (3):1–7, 2006. doi: 10.1208/pt070363.

[63] Y. Zhang, M. Huo, J. Zhou, A. Zou, W. Li, C. Yao, and S. Xie. DDSolver: An add-in program for modeling and comparison of drug dissolution profiles. *AAPS Journal*, 12(3):263–271, 2010. doi: 10.1208/s12248-010-9185-1.

[64] F. Langenbucher. Linearization of dissolution rate curves by the Weibull distribution. *The Journal of pharmacy and pharmacology*, 24(12):979–81, 1972. doi: 10.1111/j.2042-7158.1972.tb08930.x.

[65] L. M. Fuhr, F. Z. Marok, N. Hanke, D. Selzer, and T. Lehr. Pharmacokinetics of the CYP3A4 and CYP2B6 Inducer Carbamazepine and Its Drug-Drug Interaction Potential: A Physiologically Based Pharmacokinetic Modeling Approach. *Pharmaceutics*, 13(2), 2021. doi: 10.3390/pharmaceutics13020270.

[66] N. Hanke, D. Türk, D. Selzer, N. Ishiguro, T. Ebner, S. Wiebe, F. Müller, P. Stopfer, V. Nock, and T. Lehr. A Comprehensive Whole-Body Physiologically Based Pharmacokinetic Drug-Drug-Gene Interaction Model of Metformin and Cimetidine in Healthy Adults and Renally Impaired Individuals. *Clinical pharmacokinetics*, 59(11):1419–1431, 2020. doi: 10.1007/s40262-020-00896-w.

[67] H. Britz, N. Hanke, A.-K. Volz, O. Spigset, M. Schwab, T. Eissing, T. Wendl, S. Frechen, and T. Lehr. Physiologically-Based Pharmacokinetic Models for CYP1A2 Drug-Drug Interaction Prediction: A Modeling Network of Fluvoxamine, Theophylline, Caffeine, Rifampicin, and Midazolam. *CPT: pharmacometrics & systems pharmacology*, 8(5):296–307, 2019. doi: 10.1002/psp4.12397.

[68] X. Q. Li, T. B. Andersson, M. Ahlström, and L. Weidolf. Comparison of inhibitory effects of the proton pump-inhibiting drugs omeprazole, esomeprazole, lansoprazole, pantoprazole, and rabeprazole on human cytochrome P450 activities. *Drug Metabolism and Disposition*, 32(8):821–827, 2004. doi: 10.1124/dmd.32.8.821.

[69] N. Hanke, D. Türk, D. Selzer, S. Wiebe, É. Fernandez, P. Stopfer, V. Nock, and T. Lehr. A Mechanistic, Enantioselective, Physiologically Based Pharmacokinetic Model of Verapamil and Norverapamil, Built and Evaluated for Drug-Drug Interaction Studies. *Pharmaceutics*, 12(6), 2020. doi: 10.3390/pharmaceutics12060556.

[70] S. Rüdesheim, D. Selzer, U. Fuhr, M. Schwab, and T. Lehr. Physiologically-based pharmacokinetic modeling of dextromethorphan to investigate interindividual variability within CYP2D6 activity score groups. *CPT: pharmacometrics & systems pharmacology*, 11(4):494–511, 2022. doi: 10.1002/psp4.12776.

[71] S. Rüdesheim, J.-G. Wojtyniak, D. Selzer, N. Hanke, F. Mahfoud, M. Schwab, and T. Lehr. Physiologically Based Pharmacokinetic Modeling of Metoprolol Enantiomers and α-Hydroxymetoprolol to Describe CYP2D6 Drug-Gene Interactions. *Pharmaceutics*, 12(12), 2020. doi: 10.3390/pharmaceutics12121200.

[72] S. Rüdesheim, D. Selzer, T. Mürdter, S. Igel, R. Kerb, M. Schwab, and T. Lehr. Physiologically Based Pharmacokinetic Modeling to Describe the CYP2D6 Activity Score-Dependent Metabolism of Paroxetine, Atomoxetine and Risperidone. *Pharmaceutics*, 14(8), 2022. doi: 10.3390/pharmaceutics14081734.

[73] D. A. Capon, F. Bochner, N. Kerry, G. Mikus, C. Danz, and A. A. Somogyi. The influence of CYP2D6 polymorphism and quinidine on the disposition and antitussive effect of dextromethorphan in humans. *Clinical Pharmacology and Therapeutics*, 60(3):295–307, 1996. doi: 10.1016/S0009-9236(96)90056-9.

[74] M. Schadel, D. Wu, S. V. Otton, W. Kalow, and E. M. Sellers. Pharmacokinetics of Dextromethorphan and Metabolites in Humans. *Journal of Clinical Psychopharmacology*, 15(4):263–269, 1995. doi: 10.1097/00004714-199508000-00005.

[75] K. A. Schoedel, L. E. Pope, and E. M. Sellers. Randomized Open-Label Drug-Drug Interaction Trial of Dextromethorphan/Quinidine and Paroxetine in Healthy Volunteers. *Clinical Drug Investigation*, 32(3):157–169, 2012. doi: 10.2165/11599870-000000000-00000.

[76] E. Steiness, S. Waldorff, P. B. Hansen, H. Egebald, J. Buch, and H. Egeblad. Reduction of digoxin-induced inotropism during quinidine administration. *Clinical Pharmacology and Therapeutics*, 27(6):791–795, 1980. doi: 10.1038/clpt.1980.112.

[77] H. R. Ochs, G. Bodem, and D. J. Greenblatt. Impairment of digoxin clearance by coadministration of quinidine. *Journal of clinical pharmacology*, 21(10):396–400, 1981. doi: 10.1002/j.1552-4604.1981.tb01739.x.

[78] T. D. Leemann, K. P. Devi, and P. Dayer. Similar effect of oxidation deficiency (debrisoquine polymorphism) and quinidine on the apparent volume of distribution of (+/-)-metoprolol. *European journal of clinical pharmacology*, 45 (1):65–71, 1993. doi: 10.1007/BF00315352.

[79] J. A. Johnson and B. S. Burlew. Metoprolol metabolism via cytochrome P4502D6 in ethnic populations. *Drug metabolism and disposition: the biological fate of chemicals*, 24(3):350–5, 1996.

[80] Z. Abolfathi, C. Fiset, M. Gilbert, K. Moerike, P. M. Belanger, and J. Turgeon. Role of polymorphic debrisoquin 4-hydroxylase activity in the stereoselective disposition of mexiletine in humans. *Journal of Pharmacology and Experimental Therapeutics*, 266(3):1196–1201, 1993.

[81] E. J. Guest, L. Aarons, J. B. Houston, A. Rostami-Hodjegan, and A. Galetin. Critique of the two-fold measure of prediction success for ratios: application for the assessment of drug-drug interactions. *Drug metabolism and disposition: the biological fate of chemicals*, 39(2):170–3, 2011. doi: 10.1124/dmd.110.036103.

ACKNOWLEDGMENTS

Mit großer Dankbarkeit möchte ich die Gelegenheit nutzen, mich bei allen zu bedanken, die mich während meiner Doktorarbeit unterstützt haben. An erster Stelle möchte ich mich bei Herrn Prof. Dr. Thorsten Lehr für die Möglichkeit bedanken, meine Doktorarbeit in seiner Arbeitsgruppe durchzuführen. Nur Dank seiner Unterstützung, seinem wertvollen Input, aber letztlich auch seiner Geduld und seinem Vertrauen in meine Fähigkeiten konnte ich diese Arbeit erfolgreich abschließen. Nicht nur für die wissenschaftliche Unterstützung, sondern auch für die vielen Möglichkeiten und Freiräume, Dinge außerhalb der klassischen PBPK Modellierung zu lernen, bin ich sehr dankbar. Des Weiteren möchte ich mich bei Herrn Prof. Dr. Markus R. Meyer für die Übernahme des Zweitgutachtens und die wissenschaftliche Begleitung dieser Arbeit bedanken. Besonders möchte ich mich auch bei Herrn Prof. Dr. Matthias Schwab bedanken, dessen Ideenreichtum und Positivität mich immer wieder inspiriert haben. Herzlicher Dank gilt auch dem Team des Dr. Margarete Fischer-Bosch-Institut für Klinische Pharmakologie für die immer freundliche und hilfsbereite Unterstützung, sowie allen Partnern und Co-Autoren für die gute Zusammenarbeit in den verschiedenen Projekten dieser Arbeit.

Mein besonderer Dank gilt auch meinen Kolleginnen und Kollegen im Arbeitskreis Klinische Pharmazie, die mich während meiner Doktorarbeit begleitet haben. Zuerst möchte ich mich hier bei Herrn Dr. Dominik Selzer bedanken, der alle Projekte dieser Arbeit mit viel Geduld, Humor und wertvollen Ratschlägen begleitet hat. Großer Dank gilt Frau Dr. Nina Hanke und Herrn Dr. Jan-Georg Wojtyniak, die mich besonders vor und zu Beginn meiner Promotion mit ihrer Erfahrung, ihrem Wissen und ihrer Arbeitsweise sehr geprägt haben. Besonders bedanken möchte ich mich bei Frau Dr. Denise Feick für die immer angenehme Zusammenarbeit rund um das INSPIRATION Projekt, die vielen hilfreichen Diskussionen und dem aufmerksamen Korrekturlesen dieser Arbeit. Ich möchte mich zudem besonders bei all denjenigen bedanken, die aktiv, als Korrekturleser oder Autoren, zu dieser Arbeit beigetragen haben: Vielen Dank Fatima Marok, Laura Fuhr, Christina Kovar, Helena Loer und Dr. Lukas Kovar.

Abschließend möchte ich mich bei meiner Familie und meinen Freunden bedanken, die mich während meiner Doktorarbeit immer unterstützt haben. Besonders möchte ich mich bei meinen Eltern bedanken, die mich während meiner gesamten Bildungslaufbahn unterstützt haben und mir stets den Rücken freigehalten haben. Von ganzem Herzen möchte ich mich bei meiner Freundin Anna-Lena bedanken, für ihre aufopferungsvolle Unterstützung, ihre Geduld und ihre Liebe.

COLOPHON

This document was typeset using the typographical look-and-feel `classicthesis` developed by André Miede and Ivo Pletikosić. The style was inspired by Robert Bringhurst's seminal book on typography "*The Elements of Typographic Style*". `classicthesis` is available for both LaTeX and LyX:

https://bitbucket.org/amiede/classicthesis/

Happy users of `classicthesis` usually send a real postcard to the author, a collection of postcards received so far is featured here:

http://postcards.miede.de/

Thank you very much for your feedback and contribution.